FINAL DRAFT
OIL SPILL TRAJECTORY ANALYSIS
LOWER COOK INLET, ALASKA
BERING SEA-GULF OF ALASKA PROJECT OFFICE
OUTER CONTINENTAL SHELF ENVIRONMENTAL
ASSESSMENT PROGRAM
NATIONAL OCEANIC AND ATMOSPHERIC ADMINISTRATION

DAMES & MOORE JOB NO. 6797-011-02
LOS ANGELES, CALIFORNIA
MARCH 9, 1979

CONTENTS

	Page
EXECUTIVE SUMMARY	v
I. INTRODUCTION	1
II. OIL SPILL MODEL	3
III. INPUT DATA PREPARATION	6
A. OIL SPILL SCENARIOS	6
B. GRID SYSTEM	7
C. OCEANOGRAPHIC AND METEOROLOGIC INPUT DATA	8
D. MISCELLANEOUS DATA	18
IV. SIMULATION RESULTS	19
A. BASE CASES	19
B. SYSTEMATIC PERTURBATION ANALYSIS	25
C. RANDOM PERTURBATION ANALYSIS	33
V. RECOMMENDATIONS	37
BIBLIOGRAPHY	41
APPENDIX A OIL SPILL MODEL DOCUMENTATION	
APPENDIX B BASE CASE TRAJECTORIES AND RESULTS	
APPENDIX C PERTURBATION CASE TRAJECTORIES	
APPENDIX D INPUT DATA FILES	

LIST OF FIGURES

Figure No.

ES-1	Potential Boundary Contact Zones
ES-2	Annual Percent Probability of Exposure
1	Grid System
2	Postulated Oil Spill Sites
3	Wind Patterns 1 and 2
4	Wind Patterns 3 and 4
5	Wind Patterns 5 and 6
6	Wind Pattern 7
7	Wind Pattern 8
8	Current Meter Station Location
9	Net Current Pattern
10	Net Current Vector Pattern
11	Tidal Current Phase Distribution
12	Tidal Current Pattern at T = 0.00 Hrs
13	Tidal Current Pattern at T = 3.11 Hrs
14	Tidal Current Pattern at T = 6.21 Hrs
15	Tidal Current Pattern at T = 9.32 Hrs
16	Potential Boundary Contact Zones
17	Annual Percent Probability of Exposure
18	Net Current Standard Deviation Distribution
19	Example Trajectory for Time-Dependent Winds
A-1	Analytic Solution-Verification Runs
A-2	Computed Solution-Verification Runs, A_T = 0.1 Hrs
A-3	Computed Solution-Verification Runs, A_T = 0.4 Hrs
A-4	Verification Run - Net Current Only
A-5 through A-7	Verification Run - Wind only
B-1 through B-72	Base Case Trajectories
B-73 through B-81	Potential Boundary Contact Zones, Sites 1 to 8
B-82 through B-90	Annual Percent Probability of Exposure, Sites 1 to 8
c-1 through C-64	Systematic Perturbation Cases, Sites 1 and 7
c-65 through c-72	Systematic Perturbation Cases, Site 3
C-73 through C-78	Random Perturbation Cases, Site 7

LIST OF TABLES

Table No.	
1	Direction, Speed, and Frequency of Eight Wind Patterns
2	PMEL and NOS Net Current Data
3	PMEL and NOS Tidal Current Data
4	Comparison of Predicted Tidal Current with M2 Constituent
5	Comparison of Measured and Predicted M2 Tidal Current Components
6	Base Case Boundary Contact Cells
7	Systematic Perturbation Boundary Contact Cells
8	Variability Between Base Case and Systematic Perturbation Trajectories
A-1	Verification Data Files
A-2	Sample Program Output

EXECUTIVE SUMMARY

A. INTRODUCTION

As part of its ongoing program, the Outer Continental Shelf Environmental Assessment Program (OCSEAP) contracted with Dames & Moore for continuing studies of the behavior of spilled oil in Lower Cook Inlet, Alaska. The primary purpose of this study was to update existing wind and water current fields using recently available data and to analyze the transport of postulated surface oil slicks under these fields.

This Executive Summary highlights the results and conclusions arising out of this study. Details and supporting evidence as well as recommendations for further work are contained in the main body of the final project report.

B. SCOPE AND METHODOLOGY

Behavior of a surface oil slick was represented by the trajectory of the centroid of the slick neglecting mass-dependent phenomena such as spreading, evaporation, sinking, etc. The velocity of the centroid was modeled as the linear, vectorial addition of wind velocity coupled to centroidal velocity by a coefficient of 3 percent and the total surface current velocity. A Dames & Moore oil spill numerical model embodying these concepts was used to carry out the analyses.

Wind fields in the area of interest were defined by eight spatially dependent flow patterns assumed to be constant over the simulation period. These patterns represent wind conditions observed two-thirds of the time on an annual basis, and include six patterns with winds typically parallel to the main axis of Cook Inlet and two with the predominant flow across the Inlet.

Surface currents were divided into two components, a time-dependent tidal flow and a constant net surface circulation. The tidal flow field

was developed from harmonic analyses of current measurements in combination with an existing tidal flow hydrodynamic model. The net current field was derived from analyses of current measurements, published literature, and a previously developed net circulation pattern.

Using these data sets as input to the oil spill model, three types of spill scenarios were examined:

1. Base Cases

Trajectories, shoreline impact locations, times to impact and probabilities of impact were computed for spills occurring at nine postulated sites within Lower Cook Inlet. The environmental fields discussed above, in combination with other parameters, such as spill time in relation to tidal phase, were the key inputs to each scenario.

Results of these scenarios were synthesized into two summary figures showing the shoreline distribution of location of impact, time to impact, and probability of impact given that a spill could occur at any one of the sites.

2. **Systematic Perturbation Cases**

Systematic perturbation runs were made to investigate the sensitivity of the base case results to small changes in the environmental fields. Each field was independently altered so that speeds were changed ±25 percent from the base case while patterns (direction fields) were held constant. Spills driven by the perturbed fields were initiated at three of the nine base case sites.

Analyses of the perturbation results were based on a quantitative comparison of changes in the base case shoreline impact locations and times to impact. A qualitative analysis of the perturbation trajectories was also performed.

3. Random Perturbation Analysis

Using available information on the variability of the net current field, a stochastic analysis was performed to ascertain the effects of this variability on the base case results. Perturbation trajectories were computed in which base case net current vectors were augmented by vectors randomly drawn from a Gaussian distribution with zero mean and known standard deviations defined by field data.

Analysis of the random perturbation cases focused on the distribution of shoreline impact points about the base case result. In a subjective manner the behavior of the trajectories themselves were also analyzed.

C. RESULTS AND CONCLUSIONS

The results of this project include not only the predicted oil spill behavior, but also the input wind and current fields. The fields developed represent the most recent synthesis of current measurement and modeling results available in October 1978.

For purposes of oil spill simulation, the tidal current information is in the most satisfactory condition. . To a great extent, this is due to the availability of a hydrodynamic tidal current model, Mungall, 1973, and the excellent agreement between predicted and observed data. Based on the results discussed below, which show predominantly weak dependence of spill movement on tidal currents, it is concluded that further work on tidal currents should be deemphasized.

Review of the net current data yields a considerably different result . Considerable current meter data has been collected and analyzed to the extent that the general hydrodynamics of Lower Cook Inlet are reasonably well understood. Attempts to translate this knowledge into the level of detail necessary to perform meaningful spill modeling

uncovered certain deficiencies. In particular, the spatial and temporal coverage of processed data was found to be very uneven. No winter season current meter data had been processed though measurements have been taken. The results reflect only the summer season current data and should be interpreted in that light.

Equally as important, data collected in 1974 in the northern portion of the study area would have been invaluable in defining the net current pattern in the vicinity of Kalgin Island and southward along the western side of the Inlet. Without these data, there is uncertainty concerning the magnitude and direction of net flow in areas that the results of this study indicate are subject to considerable exposure to spilled oil. A satisfactory modeling effort cannot be completed until the 1974 data have been analyzed and interpreted.

The meteorologic data base remained essentially unchanged as a result of this project. However, further refinement and treatment of the meteorological input data is of primary importance for two reasons. First, as discussed below, the wind fields tend to dominate the surface spill movement. Even in the systematic perturbation cases with weak winds, the general area of shoreline impact is usually determined by the prevailing winds. Secondly, the simulation period limits the range of applicability of the trajectory impact results. While persistence of the wind fields can occur, it is more likely that a changing sequence of wind fields corresponding to the progression of passing weather fronts will be observed over a period equal to that used here. Hence, the results of this project indicate that the wind fields and their simulated behavior are the most limiting aspect of the environmental data base.

Results of the base case simulations are summarized in Figures ES-1 and ES-2. Shoreline impact location, time to impact, and probability of impact are presented. These are key parameters in evaluating the impact of potential oil spills. Areas subject to impact in a short period are critical in two senses:

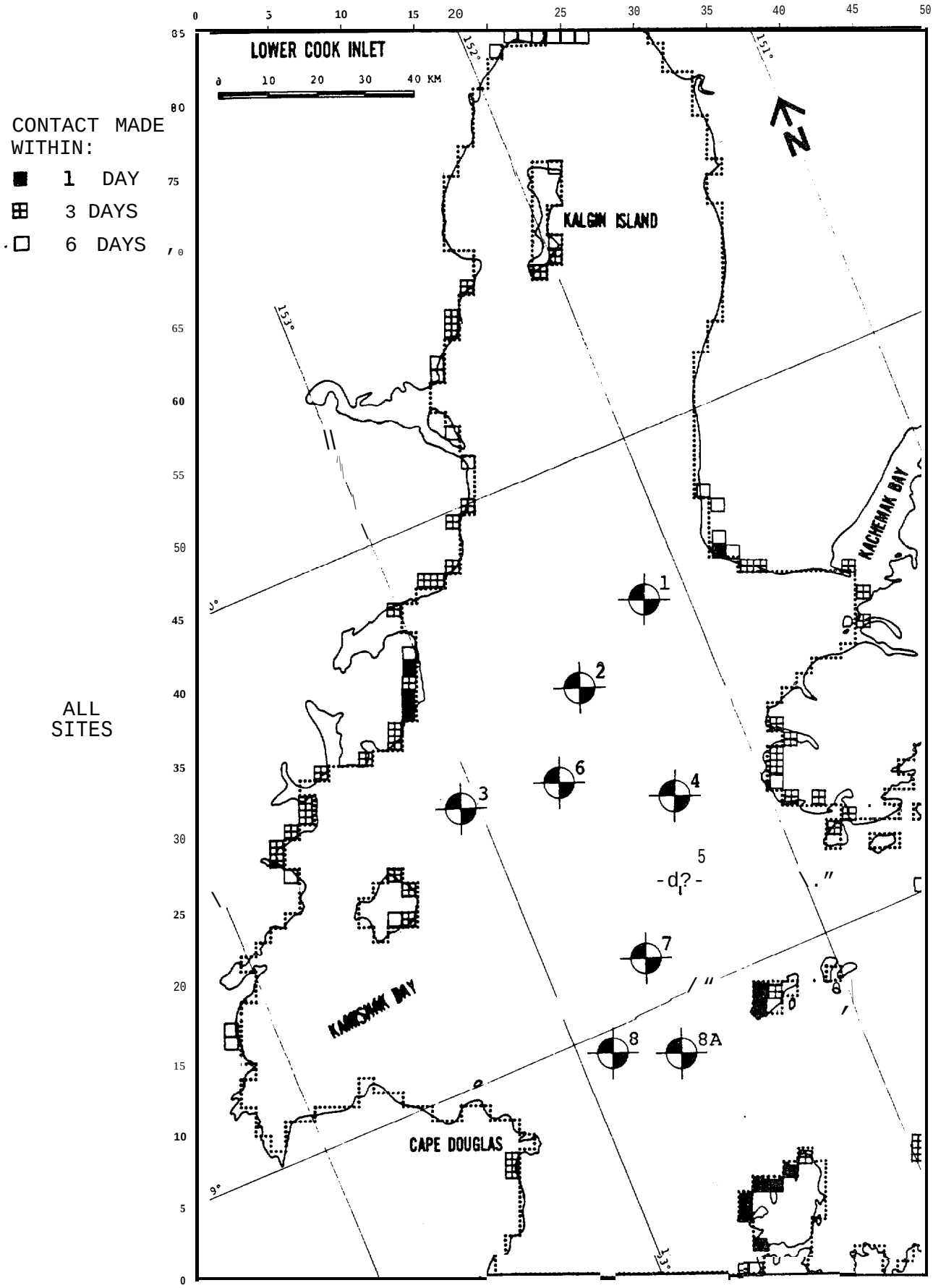

FIGURE ES-1: POTENTIAL BOUNDARY CONTACT ZONES

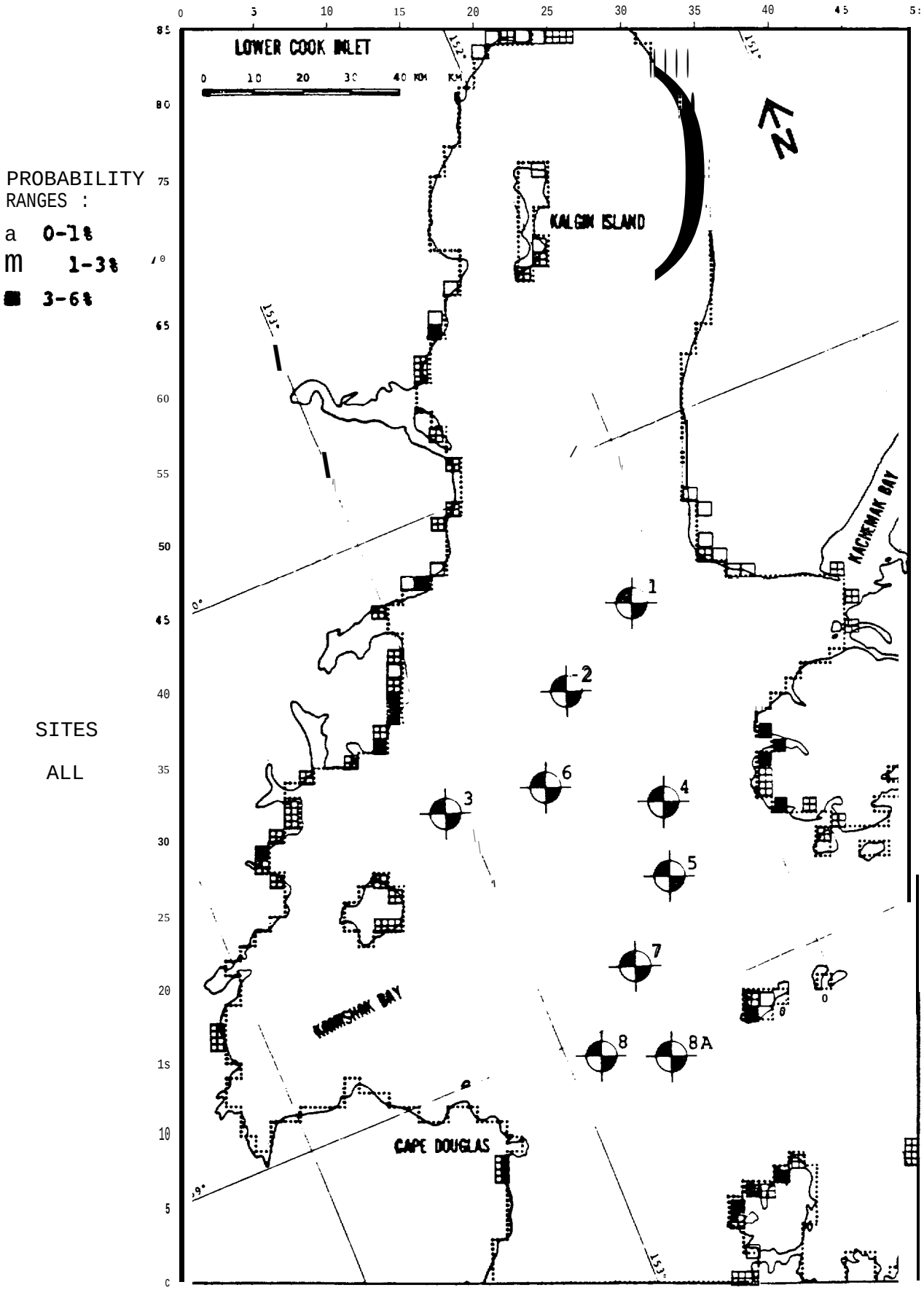

FIGURE ES-2: ANNUAL PERCENT PROBABILITY OF EXPOSURE

1) The rapid movement from spill site to shoreline impact makes containment and control difficult unless the necessary resources are in the immediate vicinity and are mobilized quickly once a spill release occurs.

2) For a given spill size, the shorter time to impact means that more oil is likely to be available for shoreline contamination and the more toxic constituents will have had less time to disperse.

The base case results show a broad area of shoreline impact points with two exceptions being the Cape Douglas and Cape Kasilof (east of Kalgin Island) areas. The most critical areas, both in terms of time to impact and probability of exposure are:

1) Iliamna Bay northward to Chinitna Bay on the west side of the Inlet.

2) Dangerous Cape to Cape Elizabeth

3) the Barren Islands

4) Shuyak Island at the northern end of Afognak Island.

To a lesser extent, Harriet Point, Anchor Point, and Augustine Island are also areas of concern.

These results are consistent with those presented in the Dames & Moore 1976 study. Two additional areas of exposure are suggested by the present study that were not apparent in the 1976 study:

1) The area north of the Forelands can be potentially exposed to spilled oil from Sites 1, 3, and 4 and to some extent from Sites 2 and 5, whereas the 1976 work showed no movement past the Forelands. This suggests that Upper Cook Inlet may also be an area of concern for oil impacts.

2) The Chugach Islands are impacted by trajectories from Site 5 and trajectories extend into the Gulf of Alaska from Sites 7 and 8A. These events, not seen in the 1976 study, suggest the possibility of exposure on the eastern side of the Kenai Peninsula as well as Kodiak Island,

The systematic perturbation analyses gave results that generally fall into two categories that can be defined by considering the shift in impact location resulting from the altered environmental conditions. One category, consisting of all perturbation trajectories impacting within 10 km of the corresponding base case, contains over 50 percent of all the perturbation case trajectories, This indicates that over half of the base case trajectory impact points would not be greatly affected by a 25 percent change in the environmental driving forces.

The remaining trajectories that had significantly different impact points from the base case generally correspond to cases where, for example, the base case trajectory impacted an island while the perturbation case did not and consequently took considerably longer to reach the shoreline. In these cases, the perturbation results should be interpreted to mean that the final impact point is sensitive to parameters defining the trajectory simulation case. These include not only the environmental forcing fields, but quantities such as the initial tidal current phase, wind drift angle, spill location, etc.

These results suggest that the spill scenarios investigated here can be evenly divided into two classes:

1) One class represents those cases where the simulation results are "stable," with respect to perturbations in the simulation parameters. Here, stable means small changes in the scenario result in small changes in the shoreline impact point.

2) The second class represents those "unstable" cases where small changes in the scenarios result in large changes in shoreline impact locations. These cases may require additional treatment of the environmental driving fields and advanced modeling methodologies to accurately predict the "real-world" behavior of an oil spill.

The random perturbation analyses generally reinforce the conclusions from the systematic analyses. That is, the random perturbations treated here do not significantly affect the base case results. However, there are cases where small, random deviations can lead to much larger changes in the shoreline impact distribution. These cases may require more sophisticated analysis to develop credible simulation results.

I. INTRODUCTION

PURPOSE

This study was initiated on request of the Outer Continental Shelf Environmental Assessment Program (OCSEAP) on behalf of the Bureau of Land Management. A previous oil spill trajectory analysis for Lower Cook Inlet was completed in March 1976 (Dames & Moore, 1976). That study provided information on probable shoreline impact areas and associated time to impact of hypothetical oil spills originating from 12 selected locations within Lower Cook Inlet. The results were based primarily on an oil spill trajectory model with winds, net, and tidal currents being the environmental driving forces.

The present study is an extension of the 1976 study in that the environmental data were updated to reflect more recent information and nine additional hypothetical spill locations in Lower Cook Inlet were investigated. This study also addressed certain questions regarding stochastic and deterministic aspects of the environmental data and their effects on the variability of the modeling results and conclusions drawn therefrom.

SCOPE

This study was conducted in accordance with the scope of work detailed in the Dames & Moore proposal, "Statement of Work, Oil Spill Analysis," RFx41-D&M-188, for National Oceanic and Atmospheric Administration, April 4, 1978 and "Revised Statement of Work, Oil Spill Trajectory Analysis," RFx41-D&M-346, June 1, 1978, and "Amendments to the Statement of Work, dated August 1, 1978, Oil Spill Trajectory Analysis," RFx41-D&M-346. In summary form,. the primary elements of the scope of work presented in the above documents were as follows:

2. Trajectory Simulation: Calculate "base case" trajectories using the same overall approach employed in the 1976 study. Simulate spill trajectories from eight hypothetical spill sites specified by Outer Continental Shelf Environmental Assessment Program (OCSEAP), using a basic set of selected wind and current fields. Provide the point at which the trajectory intersects the shoreline, the time to impact and the probability of exposure for each site individually and all sites combined,

3. Environmental Data: Update the environmental input data base used in the 1976 study with data made available since the 1976 study.

4. Sensitivity Analysis: Perform a perturbation analysis on a limited number of base case trajectories in order to assess the effects of systematic and random fluctuations of the environmental data on the predicted shoreline impact distributions.

Section II contains an overview of the oil spill model used in this study and provides the general framework of the analytic approach used to determine shoreline exposure due to postulated oil spills at selected sites; details on the model itself are contained in Appendix A, Model Documentation . Similarly, details of the environmental input data are presented in Section III and a discussion of the methodology and results of the trajectory simulations follow in Section "IV. Finally, based on the results of this study and their implications, recommendations for future studies are contained in Section V.

II. OIL SPILL MODEL

The physiochemical behavior and ultimate fate of oil spilled in the marine environment involve complex and, in most circumstances, poorly understood phenomena. In addition to the many oceanographic and meteorologic parameters of importance, characteristics of the oil itself play a major role in its transport and dispersion. In spite of the uncertainties associated with these parameters, several oil spill models have been developed that provide valuable information for contingency planning, environmental impact assessment, etc. The variety of simulation techniques and models that exist reflect, in part, the embryonic state-of-the-art and the range of modeling applications.

Reviews of generic approaches to oil spill modeling as well as selected oil spill models have been recently published (Fallah and Stark, 1976; Oceanographic Institute of Washington, 1977). These reviews focused on descriptions of the relevant physical processes, procedures for their simulation, and the uses and limitations of the various models. In general, these assessments indicate that present oil spill modeling efforts are limited by a meager understanding of the basic phenomena and the difficulties associated with accurately specifying the dominant environmental driving forces over a large area, such as Lower Cook Inlet.

For this study, trajectory simulation was used to track the centroid of a two-dimensional surface oil slick. Although the model has the capability to include surface spreading of a slick, this was not incorporated in the present study for several reasons. Since the ultimate extent of a surface slick depends strongly on spill volume, the absence of a comprehensive risk assessment defining appropriate spill sizes (most probable, maximum credible, worst-case, etc.) precluded the consideration of surface spreading. Secondly, the wind and current data bases available or anticipated at the outset of this effort were not sufficiently well defined to justify the use of more refined simulation techniques. These expectations have been fulfilled with a few notable exceptions; significant gaps in the environmental data bases do, in fact, remain to be filled. These are discussed in greater detail in Section III.

Consistent with the trajectory simulation approach, (neglecting the effects of spreading), other physiochemical processes affecting a marine oil spill have not been considered. These include evaporation, sinking, dissolution, emulsification, etc. While these processes may play important roles in determining the ultimate fate of an oil spill, they were assumed to be secondary to the primary surface transport mechanisms.

Movement of the spill centroid in the Dames & Moore model is considered to be governed by the independent effects of wind and water currents. Second-order forces such as waves and wind-wave-current interaction are neglected. The wind-induced velocity vector of the centroid is taken to be colinear with the wind vector and proportional to the wind speed. This "wind factor" has been experimentally found in the range from 1 to 5 percent (Oceanographic Institute of Washington, 1977) and is taken to be 3 percent for this study. There is some question as to whether the wind and slick vectors should be colinear due to the considerable scatter in relevant field data. However, the evidence is not conclusive on this issue and, hence, this study assumes collinearity.

The slick centroid is modeled to move at the same instantaneous velocity as the underlying current, neglecting the wind-driven component. As with the wind-driven component, there is no conclusive set of evidence which documents that this is the best approach. However, alternative schemes (i.e., Schwartzberg, 1971) have major flaws or have been subjected to limited validation.

For this study, the current field was divided into two components,' a net surface component and a tidal component. Hence, the centroidal velocity vector can be written as:

$$\bar{U}_{oil} = 0.03 \, U_{wind} + U_{tidal} + U_{net} \qquad (1)$$

Using this basic model, both deterministic and probabilistic simulations have been run. In both the base case and systematic perturbation

analyses, deterministic wind and current fields are used to describe unique trajectories from each postulated spill site. These deterministic trajectories provode time to shoreline impact and, when combined with the annual average probability of the wind patterns, yeild an average annual probability of exposure to an oil spill from any site.

The stochastic analyses were based on a knowledge of both the mean and standard deviation of the net surface current speeds at certain data measurement locations. Hence, a randomly selected vector was added to the deterministic net circulation field based on a Gaussian distribution with mean zero and known standard deviation. The resultant distribution of impact points provides a measure of the effect of variations in the net surface circulation field.

Operational implementation of the oil spill model is based on a grid system that overlaps the area of interest as illustrated in Figure 1. The grid system serves multiple purposes: 1) definition of the Cook Inlet geometry, 2) input of wind and current information, and 3) definition of shoreline impact locations. With the input available to the model, a trajectory is generated by evaluating Equation (1) over a sequence of finite time steps until the centroid reaches a boundary or exceeds an upper limit on time. Subsequent analyses are based on the trajectory termination point and, in a more subjective manner, on the nature of the trajectory itself.

NOTE
GRID
NETWORK
OUTLINED
FOR EVERY
FIFTH GRID
INTERVAL

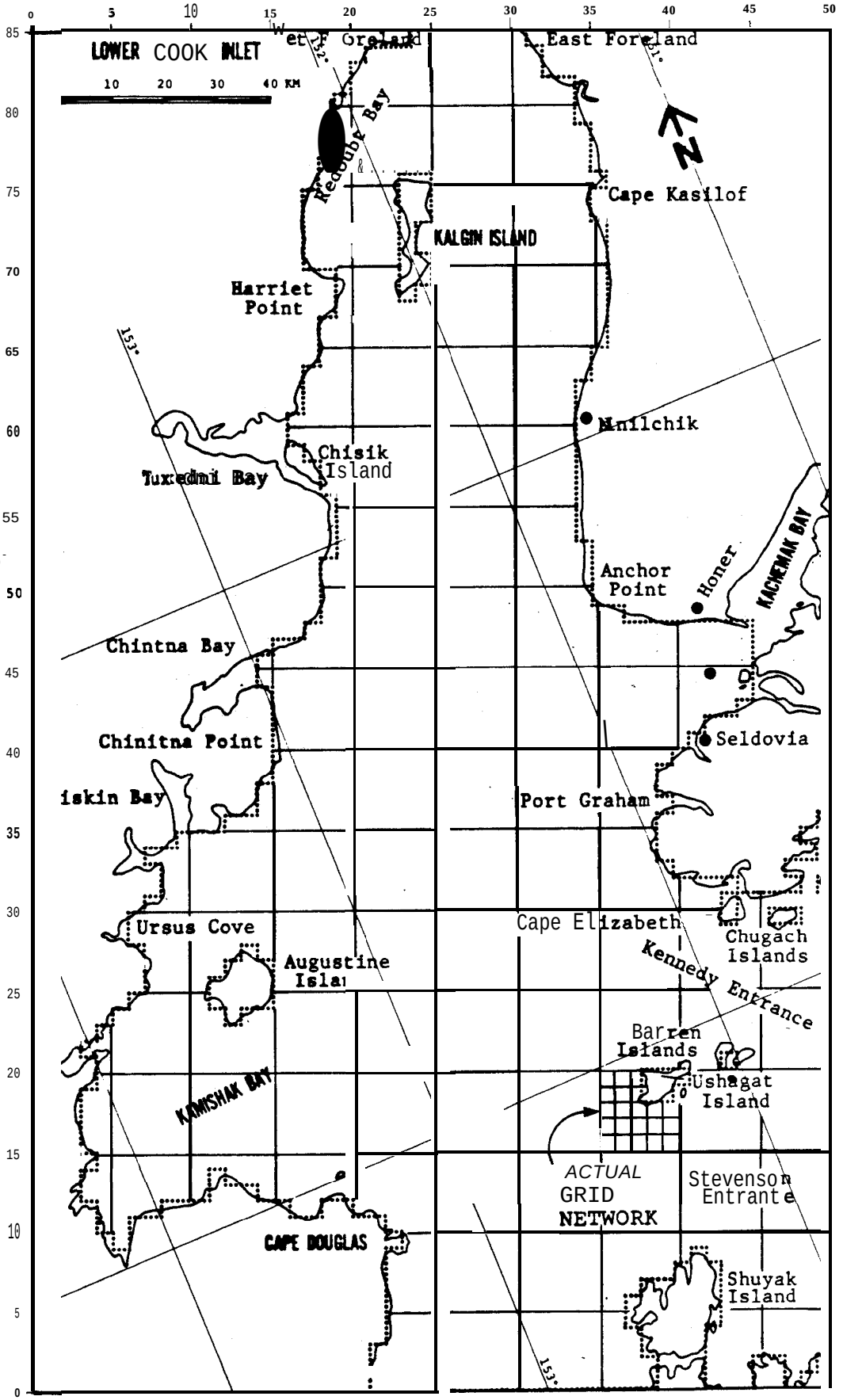

FIGURE 1: GRID SYSTEM

III. INPUT DATA PREPARATION

A. OIL SPILL SCENARIOS

The 1976 oil spill study evaluated the coastal exposure in terms of probabilities and times to impact from 12 postulated oil spill sites in Lower Cook Inlet. These 12 sites were selected as representative of areas where possible exploratory drilling would occur. In the present study, eight alternative sites were selected by the Bering Sea-Gulf of Alaska Project Office of OCSEAP to represent areas of more recently leased tracts and probable pipeline locations not evaluated in the 1976 study. Figure 2 shows the locations of the 12 hypothetical oil spill sites evaluated in the 1976 study and nine spill sites evaluated in the present study (one additional site was added by Dames & Moore to the original eight prescribed by OCSEAP).

Scenarios for potential oil spills at these locations were evaluated without consideration for volume or rate of release of oil. Further, all sites were treated independently, and the probability of a spill occurring at any location was considered equal. Based on these assumptions, the estimated time to impact and the probability of exposure for the coastal regions of Lower Cook Inlet were determined.

The 1976 study utilized existing information on the meteorologic and oceanographic conditions within Lower Cook Inlet. The present study has updated the meteorologic and oceanographic data using sources of information that have become available since the 1976 study. In addition, certain refinements were made to the analysis and interpolation of input data.

At each spill site, a separate centroidal trajectory was calculated for 32 postulated environmental events. These events were composed of eight wind patterns, a tidal current pattern (with spills occurring at four separate phases of the tide), and a net current pattern. Thus, the set of base case oil spill trajectories for the present study represented a

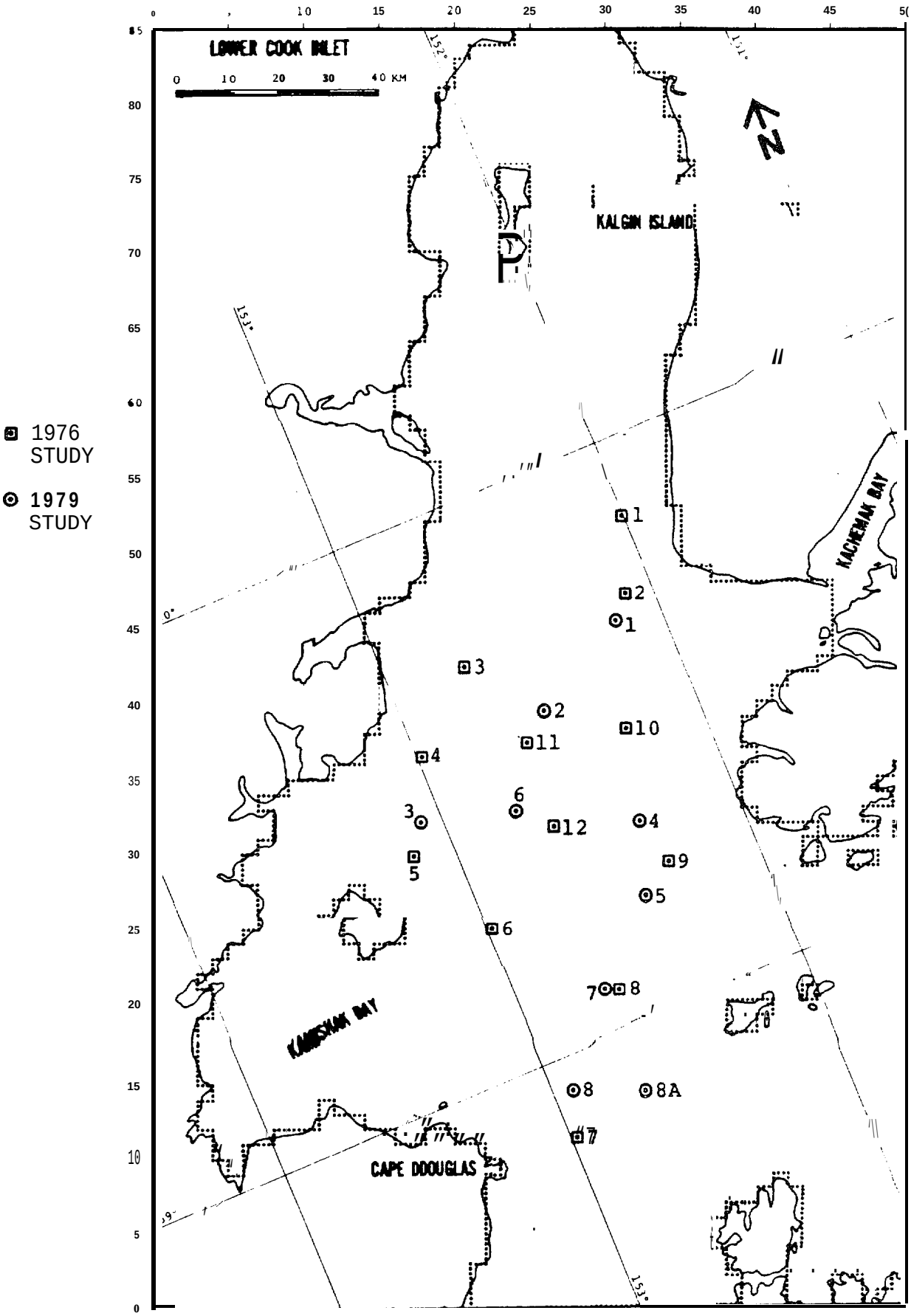

462 FIGURE 2: POSTULATED OIL SPILL SITES

total of 288 postulated spills. In addition, systematic variations on these base cases were run at Sites 1 and 7 for wind and net current fields having the same pattern (direction field) but with speeds ±25 percent of the base cases. Site 3 was also investigated for a single systematic variation of the wind fields with speeds reduced by 25 percent of the base cases. Since the perturbation trajectories were initiated at a single phase of the tidal current cycle, a total of 72 systematic perturbation runs were made. Finally, a set of random perturbation cases was run at Site 7 for wind fields Nos. 1, 2, and 7. A total of 18 individual trajectories were computed for each wind field at one phase of the tidal cycle; hence, 54 random perturbation runs were made.

B. GRID SYSTEM

The grid system illustrated in Figure 1 was used as the framework to input both wind and current data as well as to define the geometry of Lower Cook Inlet itself. This grid system was oriented along the main axis of Cook Inlet with each cell being 3 km on a side. Characteristic features of the Inlet required by the model such as land and water areas and open water boundaries, were prescribed by assigning to each cell an index that defines the predominant feature of that cell. Land boundaries were chosen to represent the "best" approximation of the geometric extent of the inlet. The input data file defining the land and water areas and the open water boundaries is presented in Appendix D.

Note in Figure 1 that several bays were delimited from the main body of water within Lower Cook Inlet by "water boundary" cells. Within these bays, the detailed nature of the wind and surface current fields are not sufficiently well known to permit an accurate simulation of spill movement. For those cases where the trajectory intersected one of these boundary cells, the trajectory was terminated and it was concluded that oil would have, in fact, entered the bay, but its subsequent behavior was not determined.

c. OCEANOGRAPHIC AND METEOROLOGIC INPUT DATA

GENERAL

The model used to simulate the centroidal trajectory of hypothetical oil spills in Lower Cook Inlet presumes that the oceanographic and meteorologic fields are the primary driving forces. The meteorologic inputs were surface wind speed and direction, and the oceanographic inputs were tidal and net surface currents. The primary effort in this phase of the study was to review and upgrade the data bases used in the 1976 study with data that had subsequently become available. During the review process several areas of improvement were made in the quality of the input data as well as the assumptions involved in deriving the spatial and temporal distributions of the input data fields. The improvements and results are discussed in the following sections.

METEOROLOGIC DATA

The meteorologic input data used in the 1976 study were representative surface wind patterns developed from historical data. Eight wind patterns were developed based on the work of Putnins (1966 and 1969) and used as input to the oil spill model. For a discussion of the development of the eight wind patterns see Dames & Moore, 1976. Each wind pattern represented a spatial distribution of wind speed and direction over Lower Cook Inlet and was held constant with time during the trajectory simulation. With respect to assumptions imposed on the modeling effort, the treatment of the wind fields as constant with time may be the most limiting factor in the input data. This is due to the fact that, based on the results from the 1976 study, the winds were the major driving force in the trajectory movement. While recognizing this limitation in the input data, it was agreed that a similar treatment of the wind fields would be followed in the present study.

A review of the wind fields utilized in the 1976 study was conducted by Dames & Moore's meteorologists in Anchorage. This review was partially

based on a comparison of the 1976 wind fields with data taken from the semi-submersible drilling platform Ocean Ranger operating in Lower Cook Inlet approximatley 40 miles southwest of Homer from June through September 1977. This information indicated that the wind speeds used in the 1976 study were essentially representative. However, the wind directions could not be refuted or confirmed by the 1977 data. In addition, a review of the literature available since 1976 did not uncover any significant additions to the knowledge of Lower Cook Inlet meteorology. Thus, based on this limited review, the wind patterns used in the 1976 study were retained for use in the present study.

Due to the extension of the grid system to cover the more southerly portion of Lower Cook Inlet, the wind fields were extended (manually) to provide the required coverage over this area. All wind fields were re-digitized to conform to the format of the shifted grid system with wind speed and direction specified at every third grid point. The input data files for all eight wind fields are presented in Appendix D.

The resulting wind fields are shown in Figures 3 to 7. Table 1 provides the frequency of occurrence for each of the eight wind patterns for the months of January, April, July, and October, plus the annual frequency.

OCEANOGRAPHIC DATA

Since the model simulates the centroidal trajectory of a surface oil spill, only those parameters that control and affect movement of the water surface were utilized in the simulation. As previously indicated in Section II, the simulation involved in this study neglects the effects of waves and wind-wave interaction directly, but assumes these mechanisms are included and represented in a simplified manner in the treatment of the wind-induced surface currents.

In the absence of any wind drift current component, surface currents in Lower Cook Inlet can be assumed to be comprised of two components: a net

WIND VECTOR MAGNITUDES:

PATTERN 1

10 M/S

PATTERN 2

10 M/S

WIND PATTERN ANNUAL PROBABILITY :

PATTERN 1
10%

PATTERN 2
3%

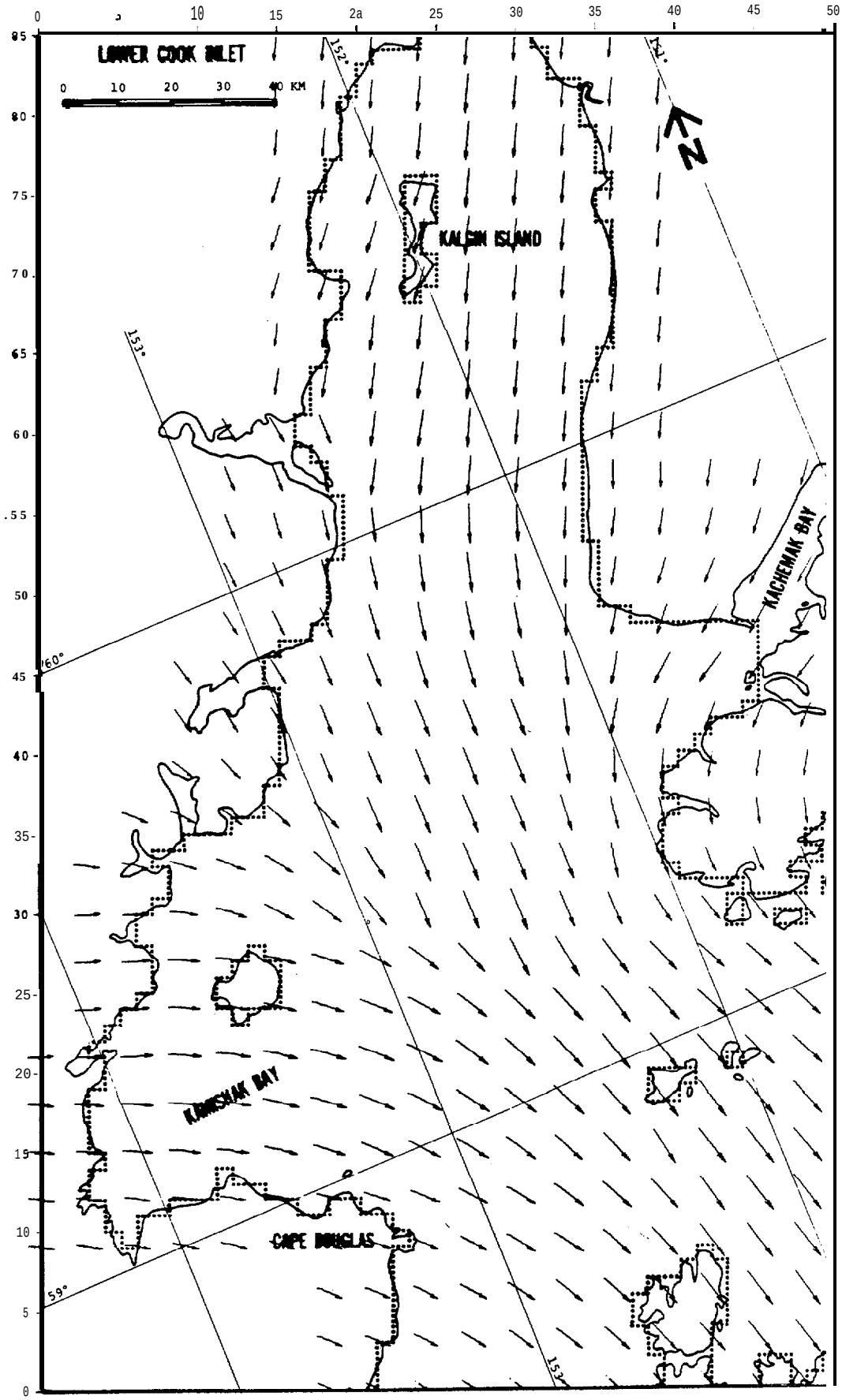

FIGURE 3: WIND PATTERNS 1 AND 2

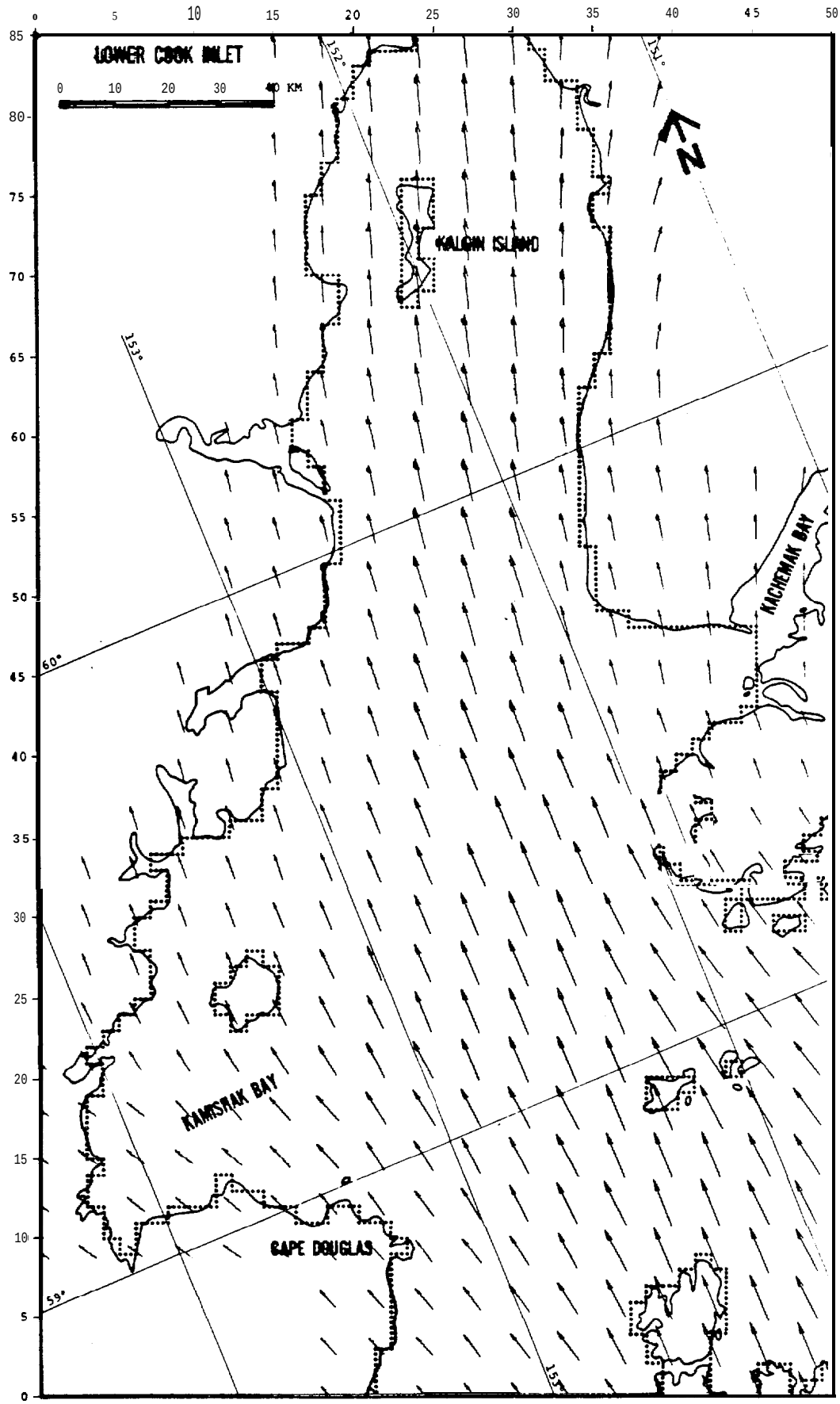

WIND VECTOR MAGNITUDES :

PATTERN 3

10 M/s

PATTERN 4

10 M/S

WIND PATTERN ANNUAL PROBABLIITY:

PATTERN 3
17%

PATTERN 4
6%

FIGURE 4: WIND PATTERNS 3 AND 4

WIND VECTOR MAGNITUDES:

PATTERN 5

10 M/S

PATTERN 6

10 M/S

WIND PATTERN ANNUAL PROBABILITY :

PATTERN 5
3%

PATTERN 6
1%

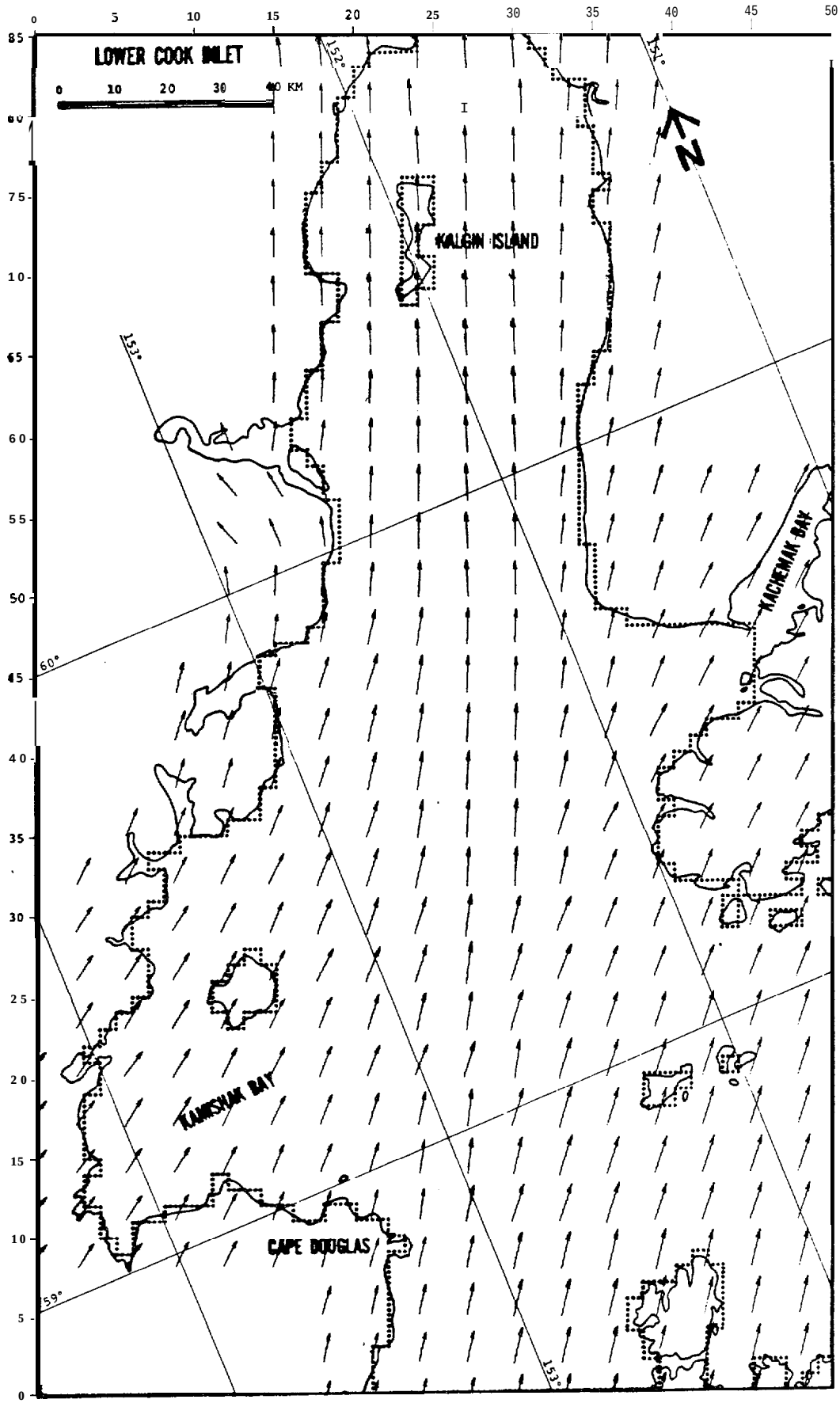

FIGURE 5: WIND PATTERNS 5 & 6

WIND VECTOR MAGNITUDE:

10 M/S

WIND PATTERN ANNUAL PROBABILITY:

13%

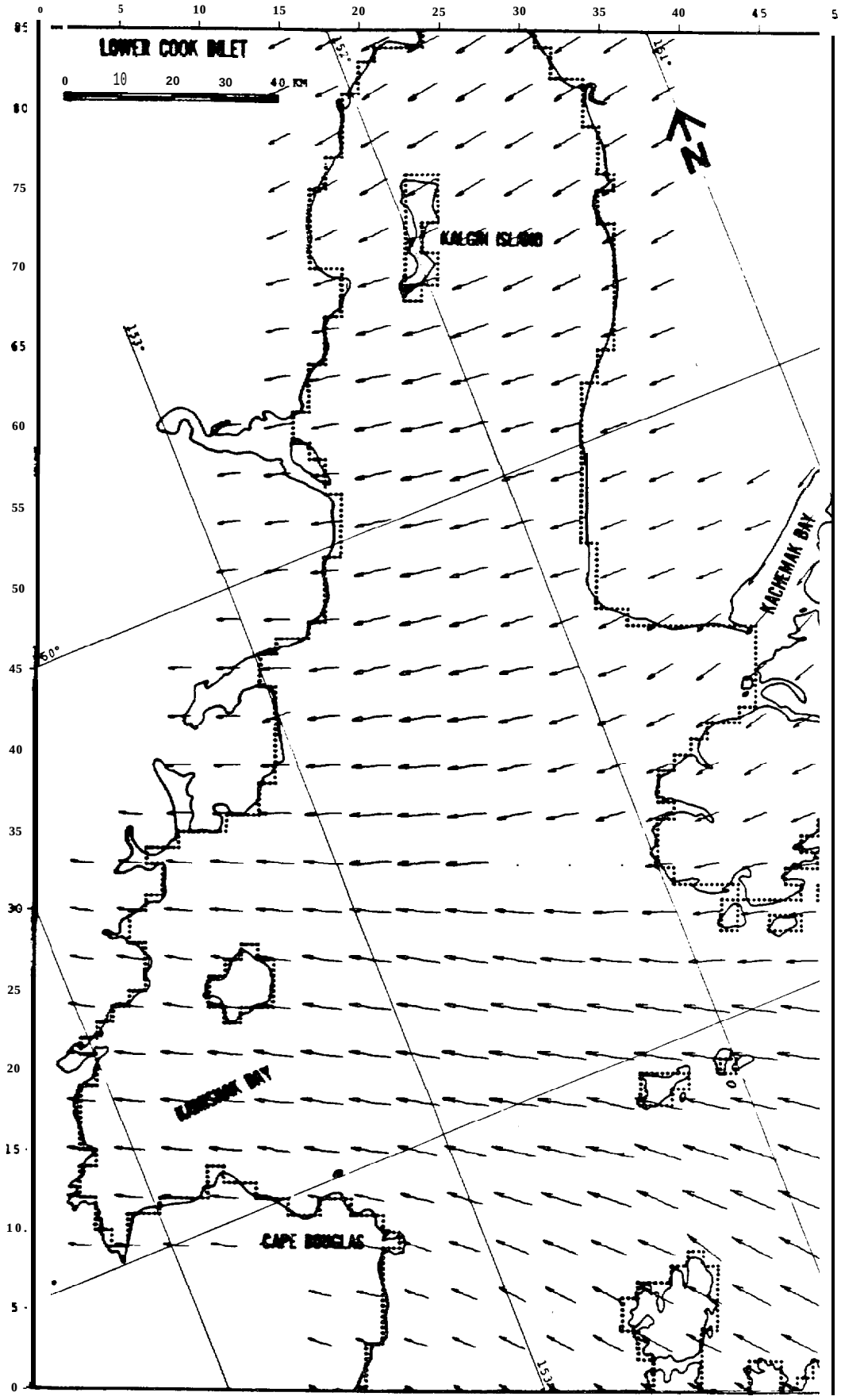

FIGURE 6: WIND PATTERN 7

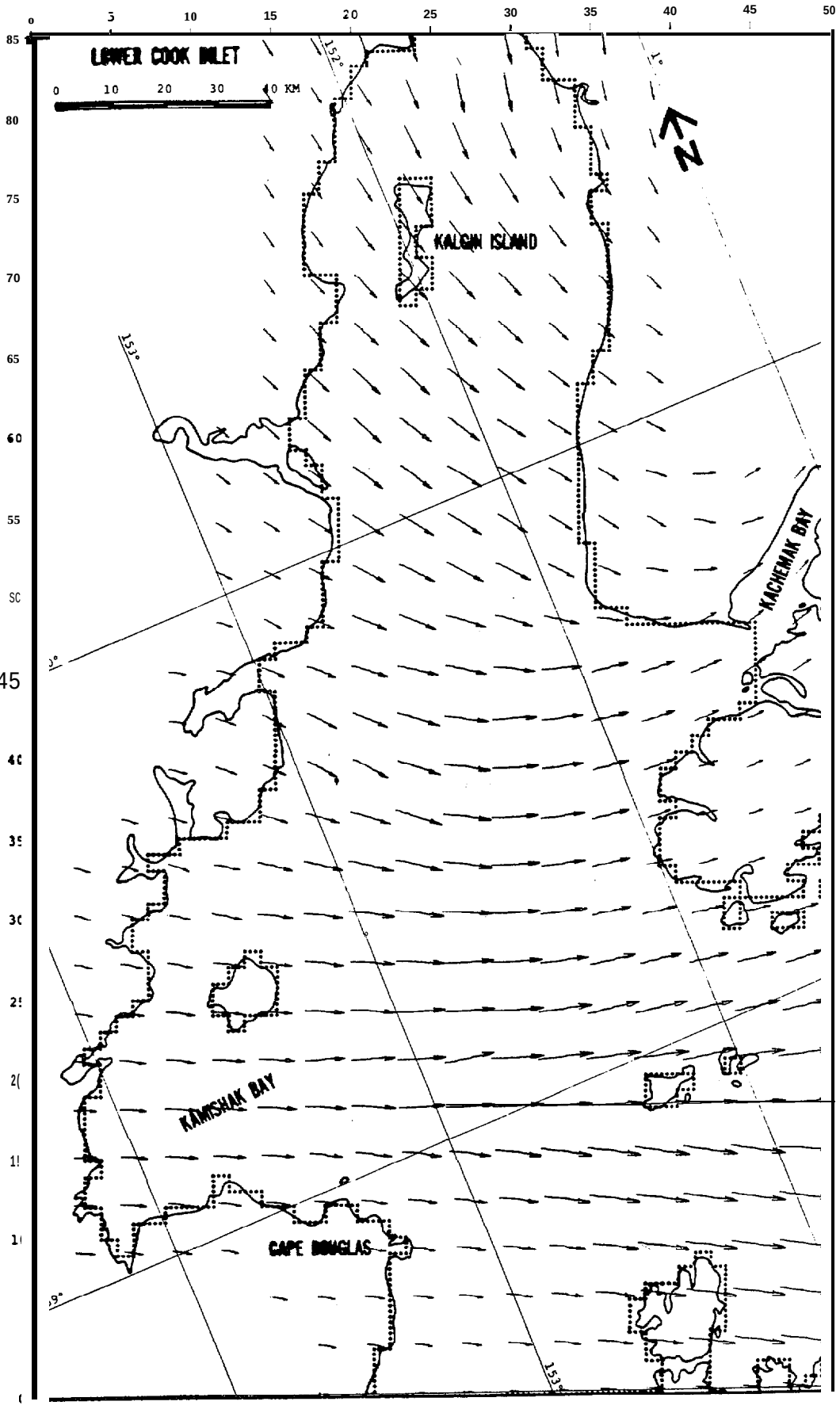

FIGURE 7: WIND PATTERN 8

TABLE 1

DIRECTION, SPEED, AND FREQUENCY OF EIGHT WIND PATTERNS

Pattern	Direction[a]	Speed[b] (knots)	Frequency (percent) Jan	Apr	Jul	Oct	Annual
1	N	16-26	12	14	4	8	10
2	N	32-52	4	5	1	3	3
3	SE	10-25	15	12	26	10	17
4	SE	20-50	5	4	9	3	6
5	Sw	11-16	0	2	7	3	3
6	Sw	22-32	0	1	2	1	1
7	E	12-22	22	12	5	12	13
8	Nw	11-27	7	17	12	24	15
	Total Frequency		67	65	67	65	66

[a] Lower Cook Inlet--vicinity of Barren Islands

[b] Annual mean speed range

surface circulation component, and a tidally induced surface current component. The net circulation component was assumed to remain constant in time, while the tidal current component was phased with the tide and with location within Lower Cook Inlet.

The following sections provide details on the derivation and input of the net surface circulation and tidal current components.

NET SURFACE CIRUCLATION

The net surface ciruclation pattern developed for the 1976 study was primarily based on previously published information contained in Burbank (1974) and Alaska Department of Fish and Game (ADF&G) (1975). In the 1976 study, the magnitude of the net circulation was estimated from the ADF&G work in Kachemak Bay and from the differences in average maximum flood and ebb tide currents measured by NOAA in Lower Cook Inlet. Adjustments to the data were made based on judgment and subjective interpretations.

Although it is generally agreed that surface circulation within Lower Cook Inlet is still not well defined, improvements to the 1976 circulation pattern have been obtained by utilization of data recently made available from the data sources described below:

PMEL Current Measurements - Mean currents at a 20-meter depth (below MLLW) at five locations in Lower Cook Inlet (see Figure 8). The duration of measurements ranged from 156 to 185 days during the months from May to October 1977.

NOS Current Measurements - Mean currents at a 6.7-meter depth (below MLLW) at 21 locations in Lower Cook Inlet (see Figure 8). The duration of measurements ranged from 5 to 60 days during the months from May to August 1973.

In addition, use was made of Meunch et al. (1977) and Burbank (1977) to delineate current patterns between the above current stations.

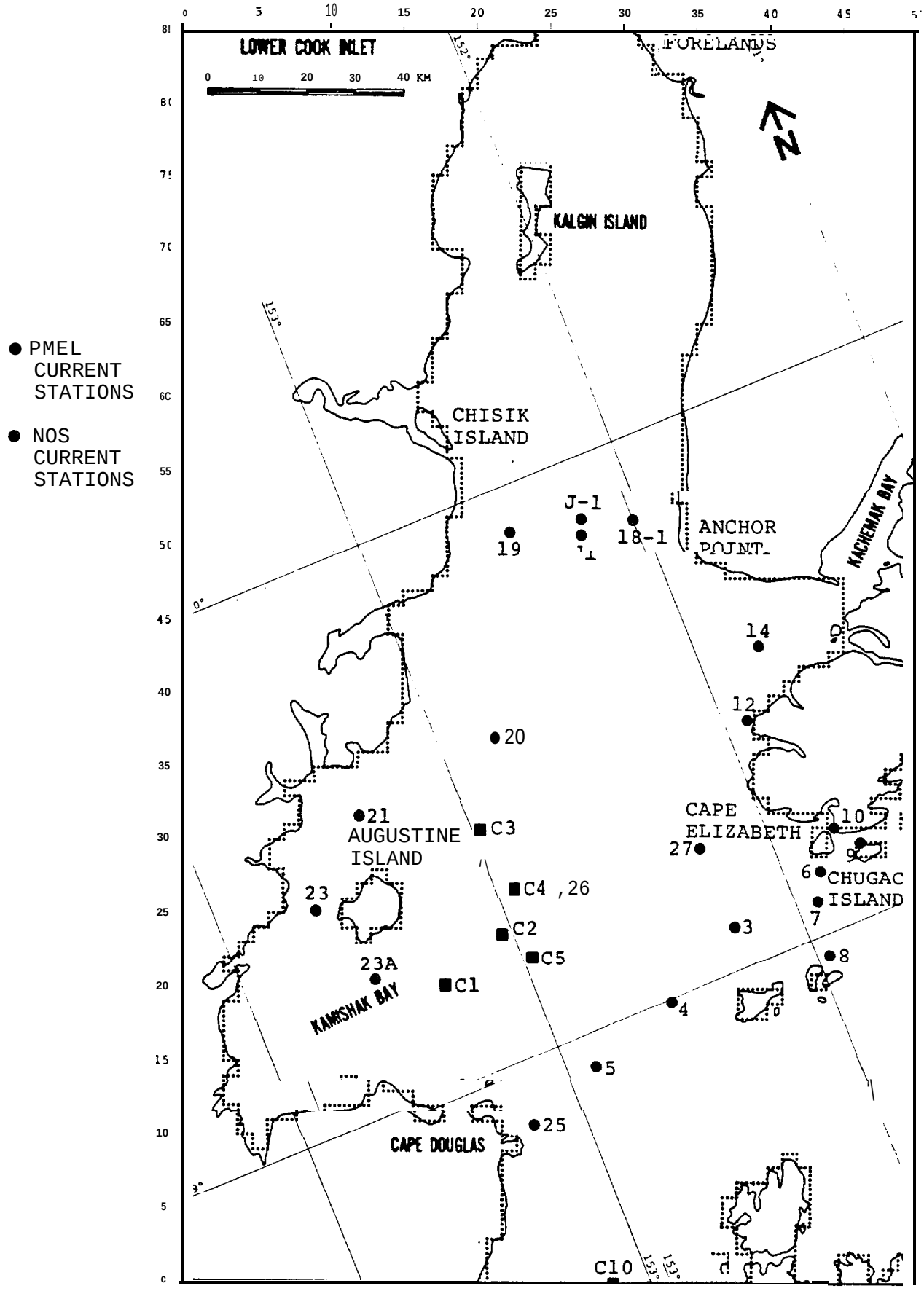

● PMEL CURRENT STATIONS

● NOS CURRENT STATIONS

FIGURE 8: CURRENT METER STATION LOCATION

It should be pointed out that the circulation pattern derived from the use of these data is actually representative of average circulation conditions occurring during the summer months. Both the PMEL and NOS data were taken within the 6-month period from May to October. Therefore, the seasonal variations that would occur during the winter months are not included in the current measurement data. It can be hypothesized that during the summer months, surface circulation would be stronger and assume a different pattern than during winter months, due to the high runoff from snowmelt. Changes in seasonal circulation patterns, however, are not known nor easily estimated from presently available data.

Summary forms of the current data obtained from PMEL included data listings, current vector plots, and current histograms. The data represent 35-hour low pass, filtered mean currents. A summary of the data for those stations and depths used in this effort is presented in Table 2. Figure 8 shows the location of the current stations in relation to Lower Cook Inlet. It can be seen from Table 2 that the NOS current measurements were taken at a depth of 6.7 meters below MLLW and thus are not truly representative of surface current conditions. However, measurements taken at this depth will not respond to significant portions of the wind drift component that would be highly reflected in surface current measurements. This is important in that the wind drift surface current is handled separately in the model. The PMEL current measurements shown in Table 2 were taken at a depth of 20 meters. These are less representative of surface currents than the NOS measurements, but presently provide the best available data for estimating the net surface circulation in the complex central portion of Lower Cook Inlet between Augustine Island and Cape Elizabeth,

Figure 8 shows that the available current measurements cover that portion of Lower Cook Inlet from a line between Cape Douglas and Chugach Island northward to a line between Anchor Point and Chisik Island. Farther northward to the area of the Forelands, current measurement data were not available. NOS has taken extensive curent measurements in that area from May through September 1974, however, summaries of the data were not

TABLE 2

PMEL AND NOS NET CURRENT DATA

Station	Net Speed (cm/see) ii	Net Direction (° North) θ	Standard Deviation (cm/sec) $\sigma_{\parallel}(1)$	(cm/sec) $\sigma_{\perp}(2)$	Station Depth (m) z	Measurement Duration (days)	Installation Date (m/ally)
PMEL							
cl	15.92	201	10.07	4.71	20.0	156.3	5/10/77
C2	8.02	229	10.62	4.41	20.0	125.0	6/10/77
C3	8.17	238	6.08	3.40	20.0	155.0	6/10/77
C4	3.25	278	8.70	6.56	20.0	155.3	6/10/77
C5	20.70	251	14.49	8.75	20.0	155.3	6/10/77
C10	27.77	230	21.47	10.49	20.0	155.0	5/10/77
NOS							
1	3.08	268	4.03	5.41	6.7	59.6	6/16/73
J-1	3.68	295	4.50	4.15	6.7	24.8	5/8/73
3	23.16	291	10.28	11.00	6.7	27.0	6/23/73
4	2.12	118	11.39	9.63	6.7	25.5	7/21/73
5	4.43	231	12.97	11.06	6.7	23.0	7/10/73
6	12.66	282	8.71	7.88	6.7	26.8	7/21/73
7	4.17	232	7.49	4.34	6.7	11.3	8/22/73
8	12.62	147	10.73	7.91	6.7	10.3	8/10/73
9	14.01	276	14.52	9.49	6.7	12.0	6/22/73
10	14.13	74	2.95	3.74	6.7	10.0	7/2/73
12	4.97	331	2.82	17.47	6.7	11.5	8/27/73
14	5.74	190	1.55	2.06	6.7	12.0	6/5/73
18-1	9.46	39	3.28	1.29	6.7	20.3	5/22/73
19	13.20	66	3.06	2.13	6.7	26.0	5/21/73
20	4.94	30	1.77	2.90	6.7	5.8	5/18/73
21	4.33	217	2.42	4.05	6.7	6.3	8/6/73
22	8.37	210	8.36	3.61	6.7	12.5	8/23/73
23	6.90	264	1.16	1.19	6.7	4.5	7/27/73
25	62.80	166	16.96	4.88	6.7	10.3	7/25/73
26	1.91	243	20.97	15.31	6.7	13.5	8/23/73
27	2.21	355	7.18	7.51	6.7	27.0	6/18/73

(1) $\sigma_{\parallel}$: Standard deviation in direction of net current.

(2) $\sigma_{\perp}$: Standard deviation perpendicular to direction of net current.

available for this study. Therefore, the net surface circulation in this portion of Lower Cook Inlet was estimated without the benefit of current meter measurements; the net surface circulation input data for this region is, at best, a rough estimate.

Using the above data sources the net surface circulation pattern in Lower Cook Inlet was updated from that presented in the 1976 study utilizing the following approach:

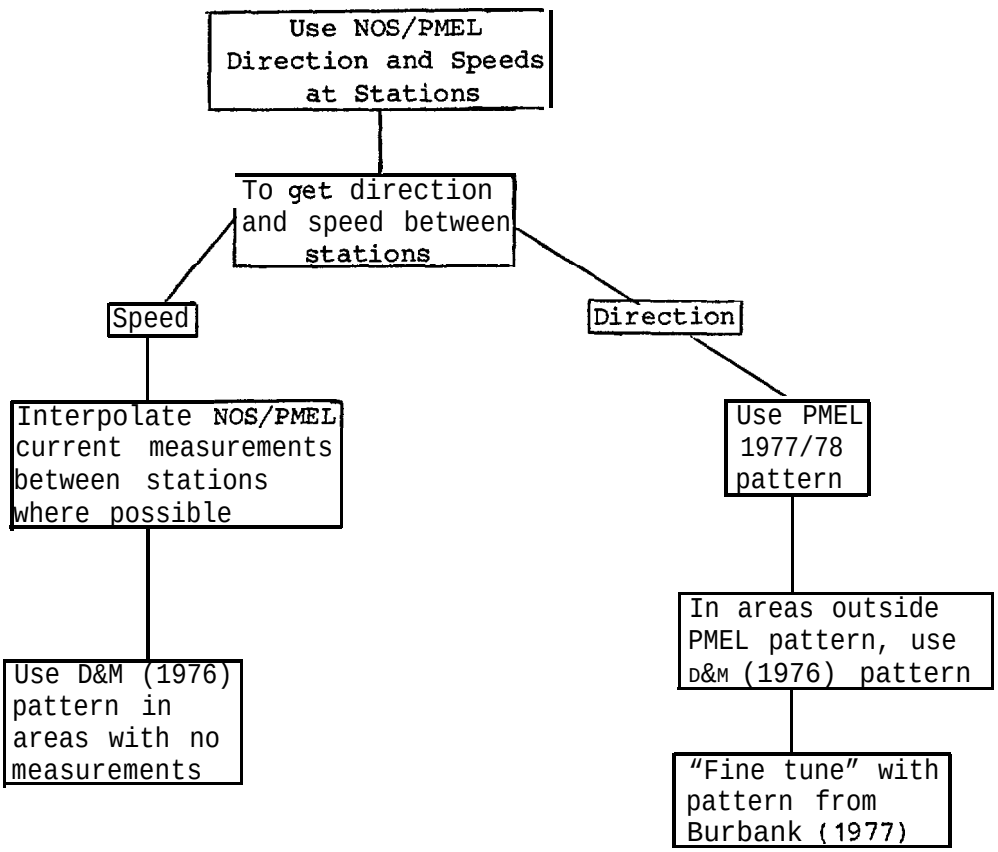

Departures from the above approach were made in order to ignore the vortex currents presented by Burbank (1977), and to discount the results of Station 20 (NOS data) due to the short duration (6 days) of measurement (Pearson and Muench, 1978). Stations 19 and 20 indicate northerly flow along the western portion of Lower Cook Inlet. Due to lack of data, there

is no general agreement as to the net surface circulation above Station 19. However, a northerly surface current is possible due to the southerly extending shoal below Kalgin Island that may effectively separate flow.

Figure 9 shows the updated net current pattern that was developed using the above approach and the previously defined sources of data. To establish some measure of reliability in the interpretation and interpolation of the data, two independent investigators developed net circulation patterns and their results compared. Close agreement was obtained among the major features of the circulation patterns. Minor differences were resolved through further interpretation of the data.

This pattern was reviewed by PMEL on October 18, 1978 and based on their comments, minor revisions were made to current speeds at selected locations. Once agreement was attained regarding the pattern shown in Figure 9, the model grid was overlaid and the net current speed and direction were read off or interpolated at every other grid point. A vector plot of the interpolated net current input data is shown in Figure 10 and the input data file is presented in Appendix D.

TIDAL CURRENTS

The tidal currents developed for the 1976 study were based on preliminary results of the 1973 NOS current measurements for the southerly portion of Lower Cook Inlet and personal communication with Mr. Muirhead of the Oceanographic Division of the National Ocean Survey for selected peak values of the 1974 NOS current measurements for the northerly portion of Lower Cook Inlet. At that time, harmonic analyses of the tidal current measurements were not available. The change of phase of tidal currents throughout Lower Cook Inlet was not considered in the 1976 study.

In updating the tidal current data from the 1976 study, several areas of improvement were obtained. First, harmonic analyses were available for not only the 1973 NOS current data but also for current measurement data taken by PMEL in 1977. (Neither harmonic analyses nor summary results were

NOTE :

- DIRECTION OF CURRENT GIVEN BY ARROWS
- SPEED OF CURRENT GIVEN IN (KM/HR) NEXT TO ARROW

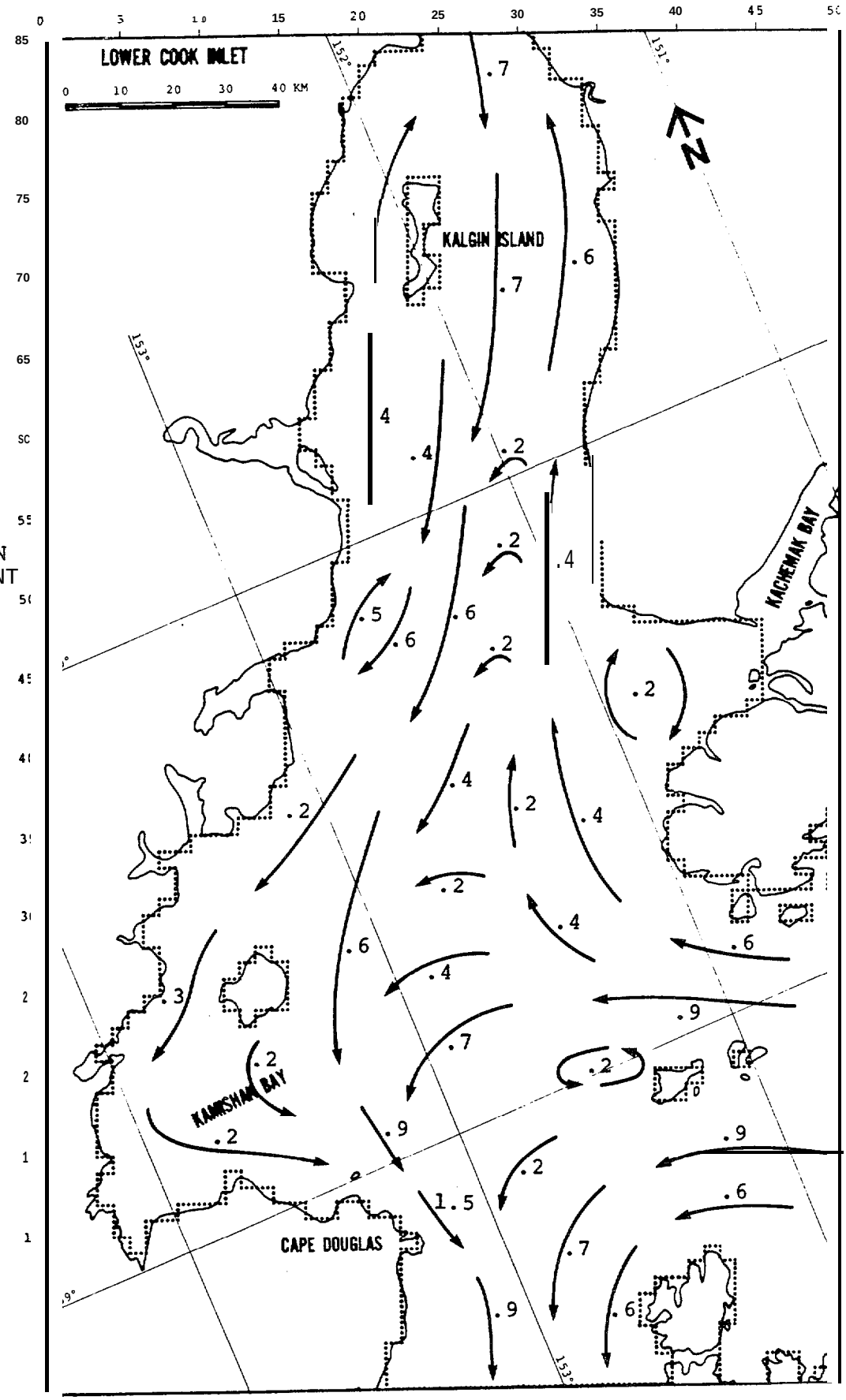

478

FIGURE 9: NET CURRENT PATTERN

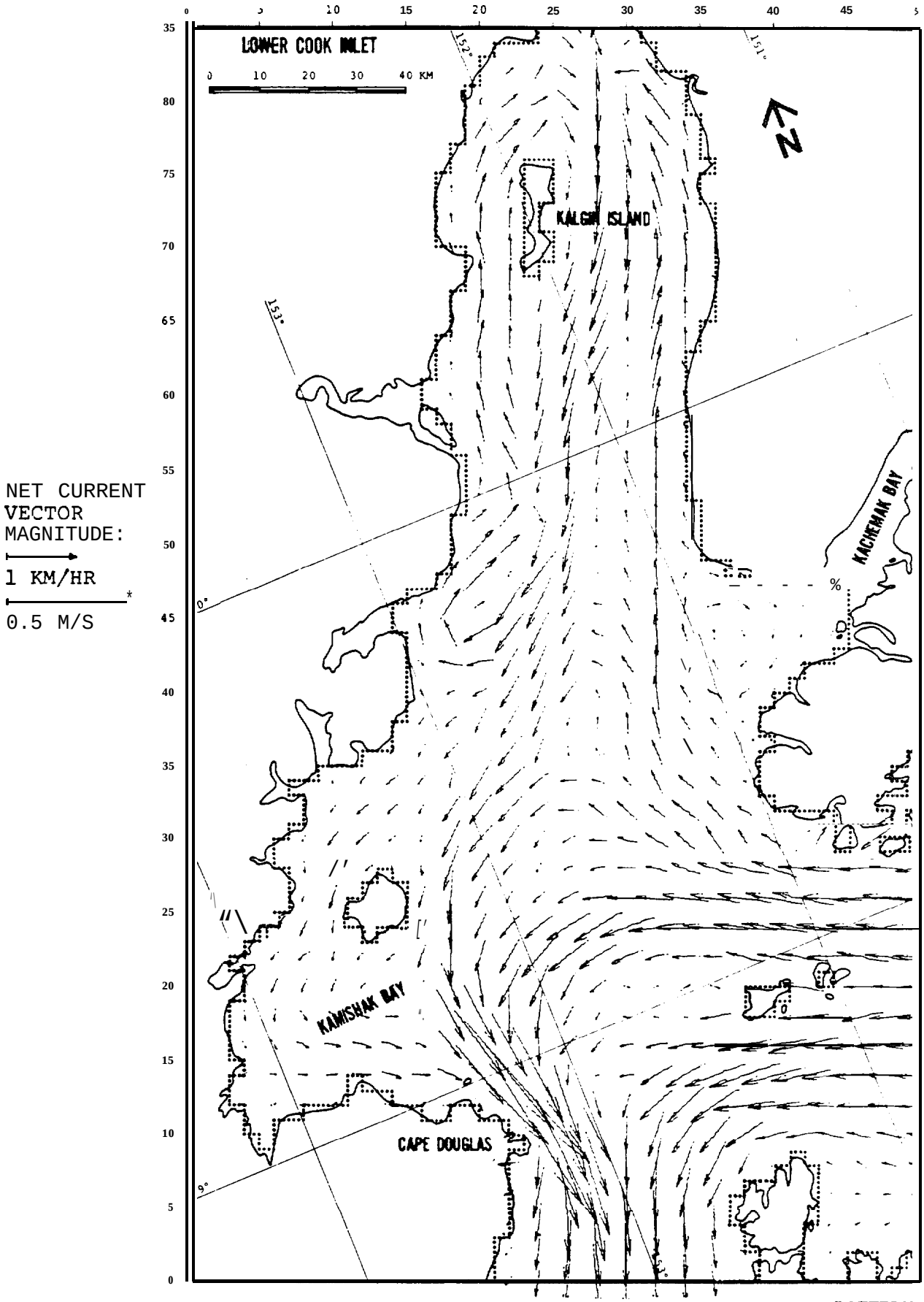

FIGURE 10: DIGITIZED NET CURRENT **PATTERN**

available for the 1974 NOS data (Muirhead, 1978)). Secondly, because harmonic analyses were available it was possible to compare measured results with results predicted from a hydrodynamic model of Cook Inlet (Mungall, 1978). If the comparisons were favorable, more confidence could be placed on the results of the hydrodynamic model, which, because of its ability to provide more detailed information on tidal currents, could be used to assess the spatial distribution of tidal currents in Lower Cook Inlet. Thirdly, the phasing of tidal currents within Lower Cook Inlet could be easily estimated from the hydrodynamic model and measurements, thus permitting a more realistic treatment of tidal currents.

The tidal current data were provided by PMEL in three basic formats. These were plots of the M2 tidal current ellipses, computer printouts of the east and north tidal current components of the M2 constituent with corresponding phase relationships, and listing of the tidal current harmonic components for the 01, K1, N2, M2, and S2 constituents. The above data were made available for the stations and depths presented in Table 3. Also included in Table 3 are the summarized data that were utilized in this analysis.

A review of the data revealed that tidal currents exhibit a large range of characteristics within Lower Cook Inlet. Rotary-type tidal currents (M2 constituent) were found to exist at PMEL Stations Cl, C4, C5, Clo, and NOS Stations 3 and 27. NOS Stations 1, 4, 6, and 19 exhibited more of a reversing type of current (M2 constituent) than a rotary-type current.

The direction of major axis and magnitude of the current speed varied widely throughout Lower Cook Inlet. The largest magnitudes occur in the eastern portion of the inlet, presumably due to the larger tidal ranges caused by the Coriolis affect within Cook Inlet. The lowest magnitudes occur in the southern an west-central areas of Lower Cook Inlet. No harmonic analyses of tidal current data were obtained for Lower Cook Inlet north of Anchor Point. Harmonic analysis of the current measurements taken in northern Lower Cook Inlet during 1974 will reportedly be available late in 1979 or early in 1980 (Muirhead, 1978).

TABLE 3

PMEL AND NOS TIDAL CURRENT DATA

Station	Constituent	East H (cm/s)	East G°	North H (cm/s)	North G°	Major Axis θ	Major Axis H (cm/s)	Major Axis G°	Minor Axis H (cm/s)	Rotation
	01	2.7	296	3.6	203	354	3.6	199	2.6	C
PMEL	K1	4.4	352	5.9	259	354	5.9	255	4.4	C
cl	N2	4.6	55	4.7	298	317	5.6	269	3.4	C
	M2	29.4	57	30.4	300	317	36.1	271	22.1	C
	S2	11.5	93	11.9	336	317	14.1	307	8.6	C
	01	2.1	254	5.2	1s3	9	5.3	186	2.0	C
PMEL	K1	3.5	310	8.6	239	9	8.7	242	3.2	C
C4	N2	3.0	36	7.3	298	356	7.3	296	3.0	C
	M2	19.4	3s	46.8	300	356	46.9	298	19.2	C
	S2	7.6	74	18.4	336	356	18. 4	334	7.5	c
	01	2.2	349	3.6	180	329	4.2	177	0.4	C
PEML	K1	3.6	45	6.0	236	329	7.0	233	0.6	C
C5	N2	2.8	97	4.4	309	329	5.0	301	1.3	C
	M2	17.9	99	28.1	311	329	32.3	303	8.2	C
	S2	7.0	136	11.0	353	329	12.6	339	3.2	C
	01	1.9	40	1.9	213	315	2.7	216	0.2	CC
	K1	3.1	96	3.1	269	315	4.4	272	0.3	CC
PMEL	N2	1.1	59	1.7	1	26	1.8	14	0.9	C
Clo	M2	7.2	61	10.7	3	26	11.6	16	5.6	C
	S2	2.8	97	4.1	39	26	4.5	52	2.2	C
	01	1.4	45	13.0	202					
NOS	K1	0.3	5	21.2	221					
1	N2	3.2	15	25.9	283					
	M2	18.1	94	123.1	323					
	S2	4.0	123	40.0	347					
	01	3.9	14	3.1	149					
Nos	K1	9.4	36	6.5	22s					
3	N2	16.2	S4	6.8	321					
	M2	54.0	98	29.8	305					
	S2	23.8	140	10.6	316					
	01	4.4	34	1.0	157					
NOS	K1	5.3	38	2.2	163					
4	N2	3.1	23	6.4	229					
	M2	22.9	101	7.5	281					
	S2	11.7	132	3.5	354					
	01	6.1	351	7.5	214					
NOS	K1	15.0	9	12.5	196					
6	N2	14.2	59	15.1	227					
	M2	75.1	88	65.3	263					
	S2	31.3	115	29.0	2s4					
	01	4.2	150	5.6	171					
NOS	K1	5.5	169	11.9	206					
19	N2	6.6	254	18.6	265					
	M2	38.8	295	97.3	304					
	S2	11.5	319	32.0	330					

H = current speed

G° = tidal current' constituent epoch (relative to Greenwich, Meridian)

θ = direction of major axis (clockwise from north)

C = clockwise rotation

CC = counterclockwise rotation

The tidal current input data for the 1976 study was an estimate of average tidal current conditions based on preliminary tabulations of current measurements. In order to update the 1976 data with those made available for the present study, some measure of comparison was necessary. It was agreed that the basis for the tidal current input data for the present study remain the same as for the 1976 study; that is, tidal current input data should represent average tidal conditions. Therefore, a simplified approach was taken to provide a comparison between the harmonic tidal current constituents and average tidal conditions. January 5, 1978 was selected for which tidal predictions indicated a mean tidal range would occur in Lower Cook Inlet, using Seldovia, Alaska as the reference station. Using the results of the harmonic analyses, (five major tidal constituents: 01, Kl, M2, N2, s2), tidal currents were predicted at three stations for this particular mean tidal range, based on the methods presented in Schureman, 1958. It was hypothesized that since the M2 constituent was the dominant constituent, perhaps it alone might be used to provide an estimate of average tidal current conditions within Lower Cook Inlet. Therefore, the M2 tidal current constituent was calculated separately for this particular mean tidal range. Summary results of these calculations are presented in Table 4.

Comparison of the results indicated that the magnitude of the peak M2 tidal current constituent would provide a reasonable approximation to average peak tidal currents in Lower Cook Inlet. For those stations examined, the magnitude of the peak M2 tidal current constituent fluctuates between being slightly larger and slightly smaller than the peak predicted tidal current. This would, over a series of tidal cycles, tend to cancel out and provide a reasonable approximation to average tidal current effects.

The oil spill model has the capability to accept rotary-type tidal current input. Some discussion in the early stage of the present study was centered around the possibility of utilizing rotary tidal currents. However, from the standpoint of available data distribution in the southern and west-central portions of Lower Cook Inlet and the lack of data in the northern section, it was decided that accurate specification of rotary

TABLE 4

COMPARISON OF PREDICTED TIDAL CURRENT WITH M2 CONSTITUENT

Station	Predicted Peak Current Along Major Axis (cm/see) Ebb	Flood	Predicted Peak M2 Component Along Major Axis (cm/see) Ebb	Flood
NOS-1	**130**	**133**	**125**	**122**
PMEL C-1	**31**	**28**	**37**	**37**
PMEL C-4	*45*	*54*	*48*	*47*

[1]Predictions were made for January 5, 1978, when tidal predictions indicated a mean tidal range at Seldovia, Alaska. Predictions for tidal currents included the O1, Kl, M2, N2, and S2 constituents.

[2]The major and minor axes refer to the axes of the tidal current ellipse used to represent tidal current characteristics in harmonic form, see Shureman, 1958. The orientation of the major axis of the ellipse is usually identical with the maximum flood-maximum ebb direction, the exception being at geographical bends where the difference in flood and ebb directions is not equal to 180", the direction of the major axis of a constituent, say the M2 component, does not necessarily equal the direction of the major axis of the tidal current ellipse.

currents was beyond the credibility of the data base. Although greater refinement could be obtained by inputting the actual elliptical nature of the tidal currents observed at many of the stations, this refinement was not justified compared to the rather uncertain accuracy of other input parameters, such as the net current pattern and the assumption of constant wind patterns.

Thus, the peak M2 tidal current components for ebb and flood conditions were selected as the tidal current input to the oil spill trajectory model. The M2 current component was derived from a two-dimensional hydrodynamic model by Mungall; description of the model, its application, and results are well documented (for example, see Matthews and Mungall, 1972; Mungall and Matthews, 1973; Mungall, 1973). This numerical model, which includes Coriolis and frictional terms, has been applied to Cook Inlet for the prediction of tides and currents and the results have been shown to be in good agreement with the few available observations. Because the model is two-dimensional the predicted currents are depth-averaged. However, it has been shown that the predicted currents are in close agreement with observed surface currents. Further, it has been concluded that the relatively shallow waters of Cook Inlet respond as a whole to the tidal motion showing little variability with depth (Mathews and Mungall, 1972). Thus, it was felt that the use of Mungall's model to provide a tidal current distribution in Lower Cook Inlet would result in a more reliable set of tidal current input data than subjective interpolation from available tidal current measurements.

The model-generated tidal currents represented the M2 tidal current component for a mean tidal range in Cook Inlet. Thus, they provide a reasonably direct comparison with the results of the harmonic analyses from the PMEL and NOS current measurements, with the exception that the model predicted currents were depth-averaged while the PMEL and NOS current measurements were taken at 20.0 and 6.7 meter depths, respectively. Table 5 presents a comparison of PMEL and NOS M2 tidal current component characteristics with the predictions provided by Mungall's model at the closest output grid point to the measurement station. Based on this comparison it

TABLE 5

COMPARISON OF MEASURED AND PREDICTED M2 TIDAL CURRENT COMPONENTS

	Measured			Predicted			Difference		
	Major Axis		Minor Axis	Major Axis		Minor Axis	Major Axis		Minor Axis
Station	Speed (cm/see)	Direction (ON)	Speed (cm/see)	Speed (cm/see)	Direction (ON)	Speed (cm/see)	Speed (%)	Direction (°)	Speed (%)
NOS-1	125	354	13	99	19	4	21	25	69
NOS-19	105	21	5	100	12	7	5	9	-40
NOS-27	95	340	15	85	11	22	11	31	-47
PMEL C-1	36	317	22	38	351	13	-6	34	41
PMEL C-4	47	356	19	43	8	13	9	12	32
PMEL C-5	32	329	8	37	10	10	-16	41	-25

[1]Predicted from Mungall's hydrodynamic model of Cook Inlet based on mean tidal range (Mungall, 1978)

2The major and minor axes refer to the axes of the tidal currentellipse used to represent tidal current characteristics in harmonic form, see Schureman, 1958. The orientation of the major axis of the ellipse is usually identical with the maximum flood-maximum ebb direction, the exception being at geographical bends where the difference in flood and ebb directions is not equal to 180°. The direction of the major axis of a constituent, say the M2 component, does not necessarily equal the direction of the major axis of the tidal current ellipse.

was decided that the model predicted currents would be used to provide interpolation between the currents determined by NOS and PMEL measurements. In view of the absence of measurements in the northern portion of Lower Cook Inlet, the hydrodynamically predicted M2 current magnitudes and directions were used as input for this area. These were adjusted slightly based on the tidal current patterns developed in the 1976 study. The directions for ebb and flood currents for the southern portion of Lower Cook Inlet were based on the NOS and PMEL measurements and interpolated with the directions from the 1976 study.

As previously mentioned, the tidal current input data for the 1976 study did not account for phasing of tidal currents as a function of location within Lower Cook Inlet. Although the addition of tidal current phase relationships would not significantly alter the results of the oil spill trajectory model, it was felt that this improvement could rapidly be developed and implemented, resulting in a more realistic treatment of this oceanographic input parameter. Tidal current phase relationships were obtained from the publication of tidal current predictions (NOAA, 1978), the harmonic analyses of PMEL and NOS current measurements and results of Mungall's tidal model of Cook Inlet. The tidal current cophase lines derived from the results of Mungall's model were in general agreement with the trend of the tidal current phase relations that could be inferred from the measured and published tidal current sources. Figure 11 presents the approximate tidal current phase distribution within Lower Cook Inlet derived from the above sources. The phase relationships shown are representative of peak tidal currents occurring during a mean tidal range. A single phase is given in degrees and represents an average of the peak ebb and flood current phases. A zero phase was arbitrarily selected for the southern portion of Lower Cook Inlet on a line between Cape Douglas and Cape Elizabeth (see Figure 11). The lag of the peak ebb or flood currents within Lower Cook Inlet were then referenced to this arbitrary zero phase line.

PHASE GIVEN IN DEGREES RELATIVE TO TIDAL CURRENTS AT ENTRANCE TO COOK INLET

360°=12.4 HRS.

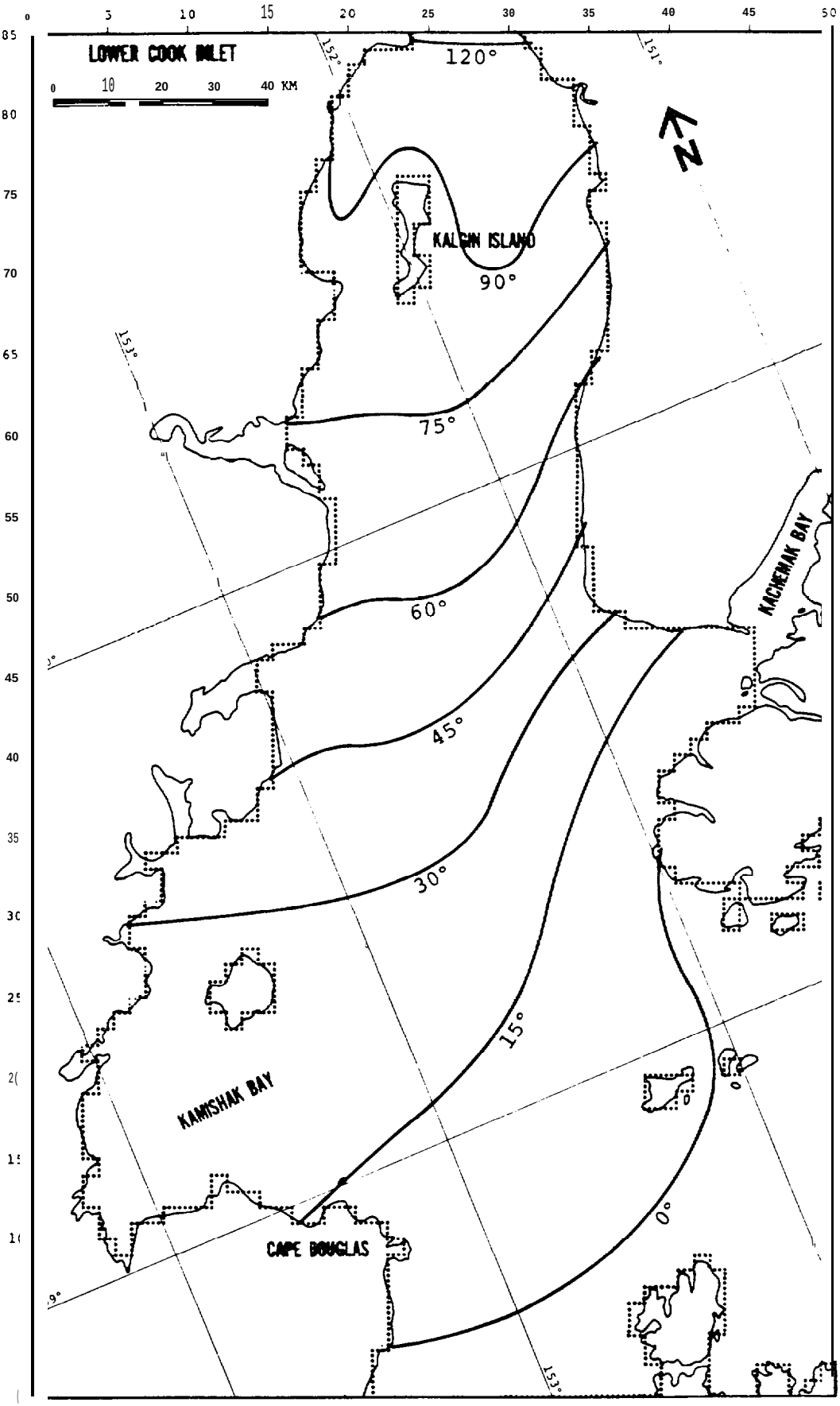

FIGURE 11: TIDAL CURRENT PHASE DISTRIBUTION

Using the results of PMEL and NOS harmonic analyses of tidal currents and the results of Mungall Es model, distributions of peak ebb and flood M2 tidal current magnitudes and directions were developed for Lower Cook Inlet. Figures 12 to 15 show vector plots of tidal current input data with the current phase relationships included for various phases of the tidal cycle. Selected input data files are presented in Appendix D for tidal phases equal to O, 90, 180, and 270 degrees.

D. MISCELLANEOUS DATA

Several other quantities must be input to the model in order to completely define the simulation parameters. Those that are of importance to the study are primarily control parameters that affect the numerical algorithms within the program and are described below.

- Time step - 0.5 hour
  This is the time step used in Equation (1) (see Appendix A) to compute slick centroid movement. It was chosen so that the maximum centroid displacement in any one time step would not exceed one cell width.

- Stop time = 150 hours = 6.21 days
  The stop time defines the period over which centroid movement is simulated. It was chosen to cover 12 complete tidal cycles or just over 6 days. The period of the predominant tidal cycle in Cook Inlet is 12.42 hours.

- Initial tidal phase
  The ultimate disposition of the oil slick depends on the point in time within the tidal cycle at which the spill occurs. Four points along the tidal cycle, at the O phase line, previously defined, were selected for simulation: maximum flood, and ebb, and the two slack tides midway between the extreme.

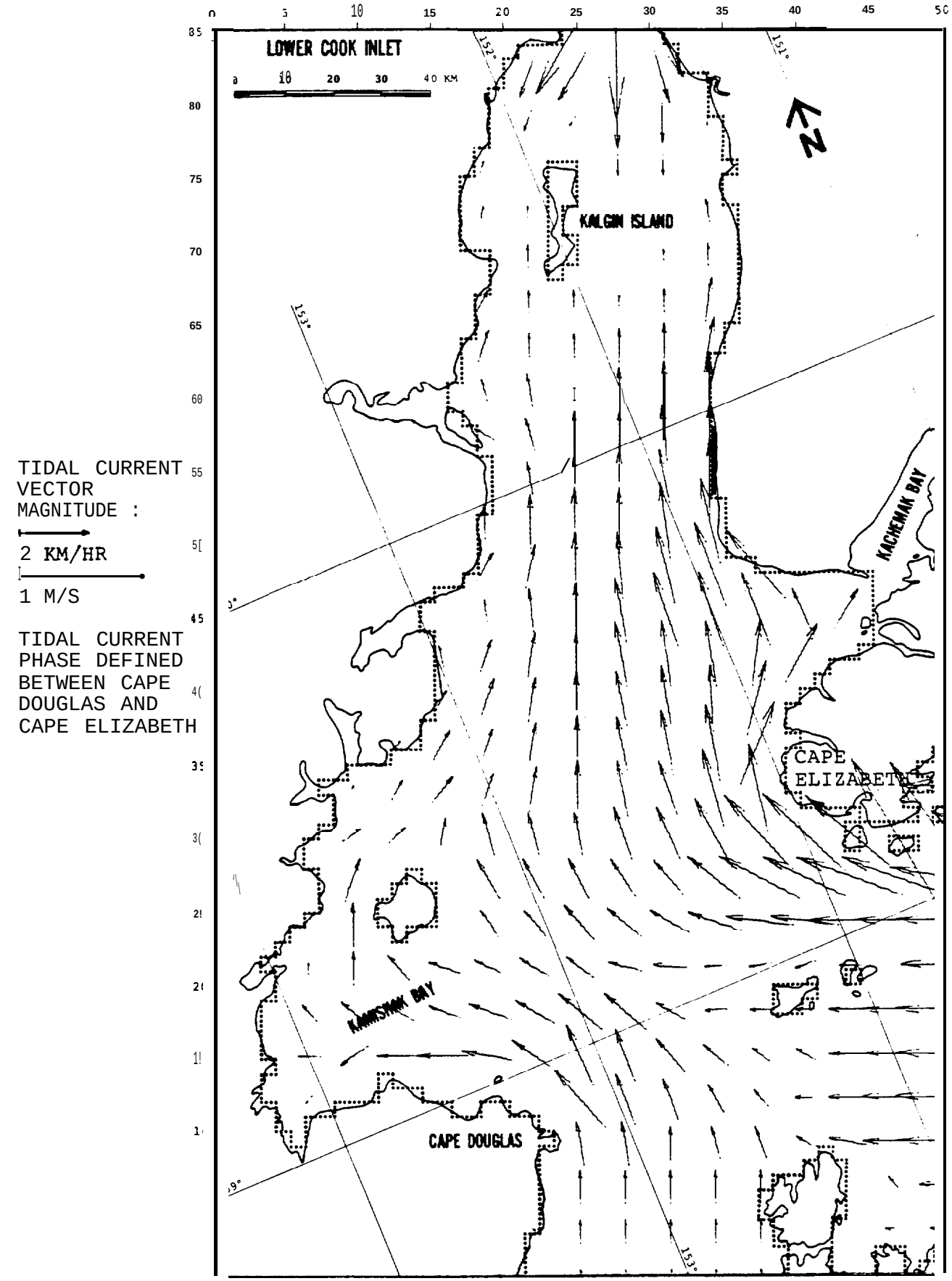

FIGURE 12: TIDAL CURRENT PATTERN AT T=0HRS. [PHASE OF 0 DEG]

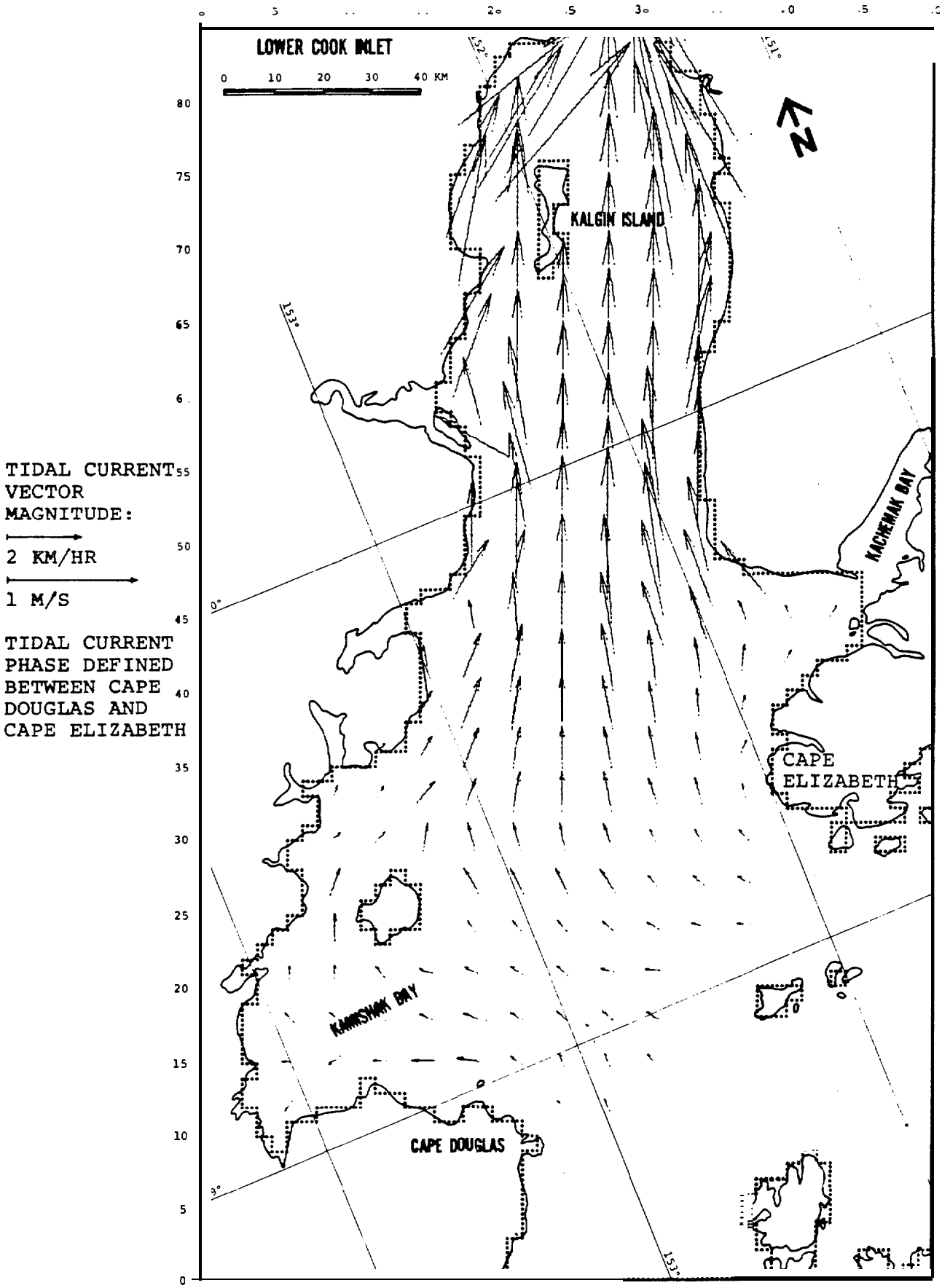

FIGURE 13: TIDAL CURRENT PATTERN AT T=3.11 HRS. (PHASE OF 90 DEG

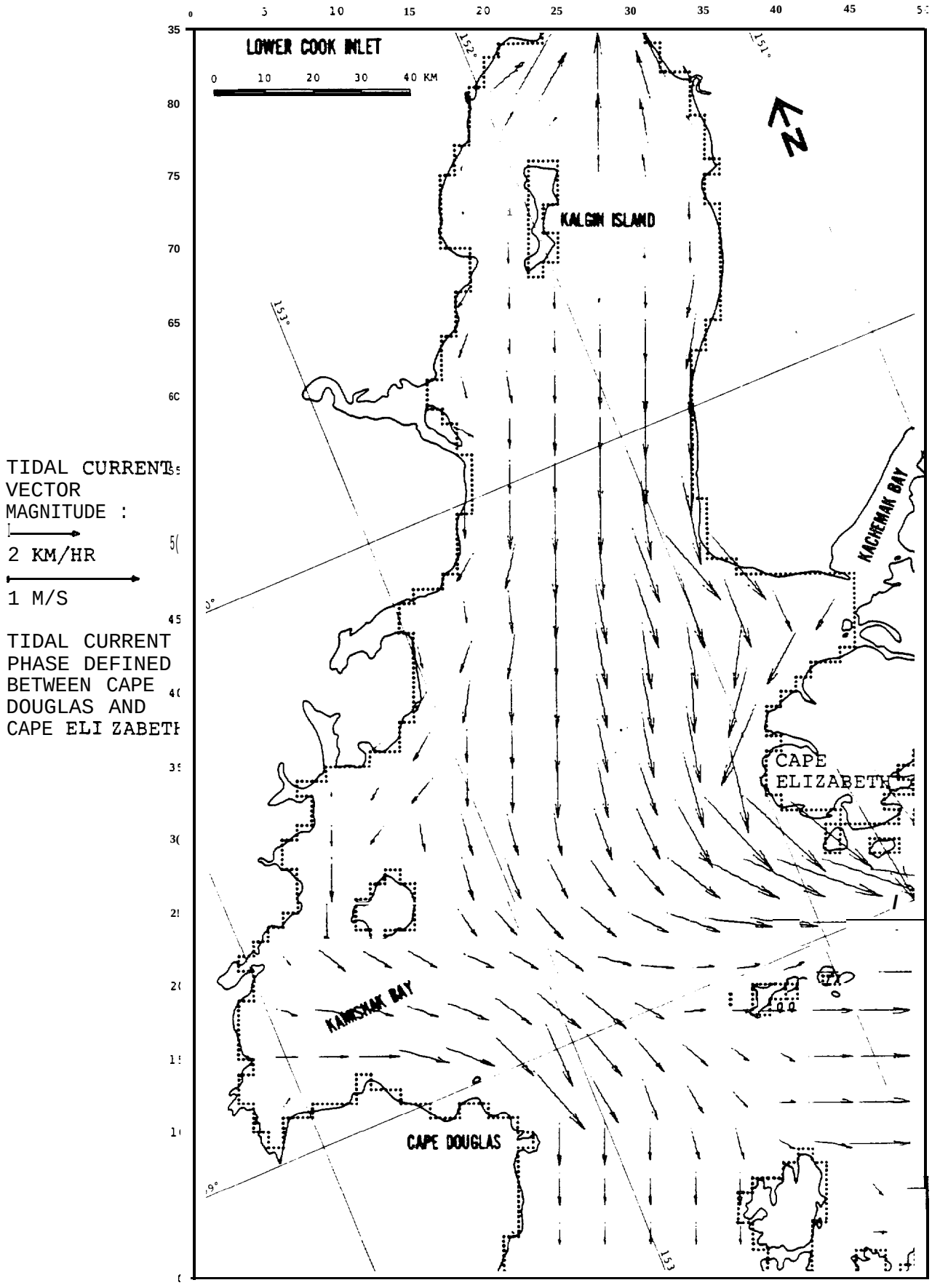

FIGURE 14: TIDAL CURRENT PATTERN AT T=6.21 HRS. [PHASE OF 180 DEG]

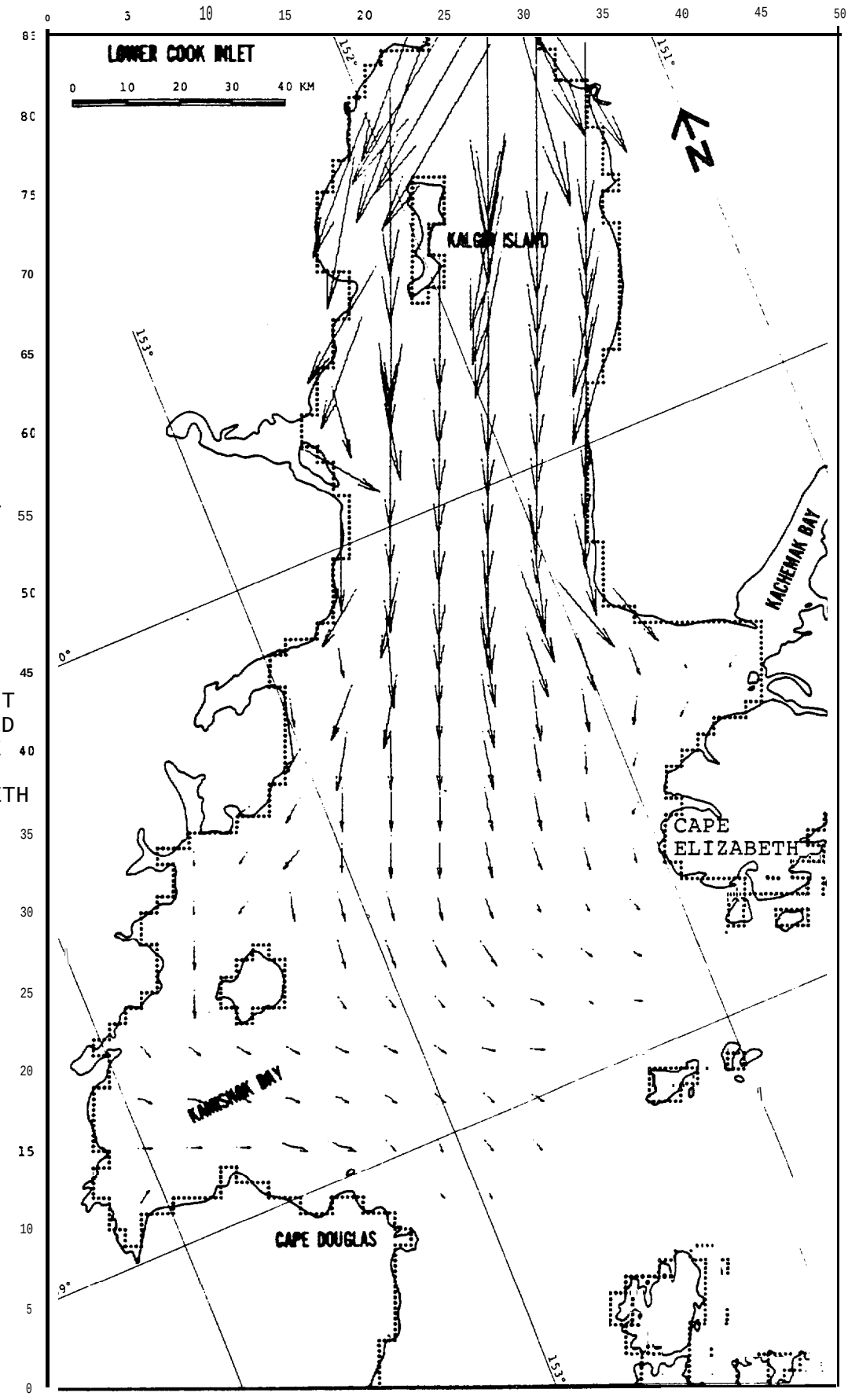

TIDAL CURRENT VECTOR MAGNITUDE :

2 KM/HR

1 M/S

TIDAL CURRENT PHASE DEFINED BETWEEN CAPE DOUGLAS AND CAPE ELIZABETH

FIGURE 15: TIDAL CURRENT PATTERN AT T=9.32 HRS. (PHASE OF 270 DEG)

IV. SIMULATION RESULTS

A. BASE CASES

Using the methodology described in Section II and the hypothetical oil spill scenarios described in the previous section, a total of 288 trajectories simulations were run. These trajectories are denoted base case trajectories and are displayed in Appendix B. In reviewing the simulated trajectories for various starting phases of the tide at a given site, it was observed that they did not deviate significantly from each other. Therefore, the base case trajectories presented in Appendix B are shown for all sites and wind conditions for only one tidal phase (phase of 0 degrees). The trajectories are separated and presented in the order of the eight wind patterns simulated for each site, which shows the dominance of the wind drift current component over the net and tidal current components. The numbers printed along the trajectories represent the cumulative elapsed time in hours from the start time of the trajectory simulation.

Potential Boundary Contact Zones

When a trajectory terminates at a boundary cell, the termination cell and the elapsed time are known. These two items of information were summarized for each site and combined for all sites to give potential boundary contact zones. Graphical results for each site are presented in Appendix B, Figures B-73 to B-81. The termination cell for each trajectory has been identified for each postulated spill site by one or more numbers adjacent to the cell. The number represents the wind pattern(s) used to produce a trajectory termination at that cell. The dots over each number indicate the number of times that cell was contacted for each set of four trajectories for each wind pattern. The four trajectories correspond to the four different release phases of the tide. For example, in Figure B-73, the cipher $\dot{8}$ near Kachemak Bay indicates that shoreline cell was impacted by two of the four trajectories run for wind field Number 8.

Also provided for each contact cell are ranges of times to impact. These ranges are given as occurring within 1, 3, or 6 days and are distinguished by corresponding symbols defined in the figures. Table 6 presents a listing of the base case boundary contact cells and the termination times for all sites and simulated conditions. This table allows comparison of actual termination times rather than the previously described ranges of termination times. Figure 16 allows a graphical interpretation of the combination of the potential boundary contact zones for all nine sites. For the eight wind patterns and oceanographic conditions selected for use in this study, Figure 16 shows the potential distribution of centroid trajectory contact zones.

Figure 16 shows a wide distribution of potential contact zones within Lower Cook Inlet. It is interesting to note that the eastern shoreline of Lower Cook Inlet north of Anchor Point is free of potential contact zones. Due to the locations of the hypothetical oil spill sites, all south of Anchor Point, the meteorologic and oceanographic input data fields do not provide a driving force that would create impact on this area of the shoreline. The wind patterns, with the exception of wind pattern No. 8, are either directed parallel to, or away from this area. Wind pattern No. 8 could create an impact if a spill site was located somewhat above Anchor Point. The net and tidal currents in this area (the eastern shoreline north of Anchor Point) are essentially parallel to shore and could not easily force a trajectory to impact the shoreline. Likewise, the shorelines of Kamishak Bay are relatively free of potential contact zones. This appears to be the result of the absence of spill sites, with the exception of Site 7, in the central portion of Lower Cook Inlet below Augustine Island. The net current pattern would drive a trajectory out of Kamishak Bay and the tidal currents, being very weak in this area, could not significantly affect net transport of the centroid. However, wind pattern No. 7 could drive a trajectory directly into Kamishak Bay if the spill site were located in the central portion of Lower Cook Inlet reasonably close to and slightly south of Augustine Island.

TABLE 6

BASE CASE
BOUNDARY CONTACT CELLS

	SITE 1			SITE 2		
	Cell Location[1] X	Y	Time to Impact[2] (hrs)	Cell Location[1] X	Y	Time to Impact[2] (hrs)
Wind 1						
Tidal Phase 1	39	20	86	39	7	88
Tidal Phase 2	39	20	78	39	7	83
Tidal Phase 3	39	19	87	39	7	88
Tidal Phase 4	39	19	95	39	7	91
Wind 2						
Tidal Phase 1	40	20	39	42	9	43
Tidal Phase 2	40	20	36	42	9	41
Tidal Phase 3	40	20	38	42	9	43
Tidal Phase 4	40	20	41	42	9	45
Wind 3						
Tidal Phase 1	27	86	126	17	63	94
Tidal Phase 2	26	86	125	18	58	75
Tidal Phase 3	26	86	122	18	65	95
Tidal Phase 4	26	86	118	18	65	91
Wind 4						
Tidal Phase 1	24	69	38	18	65	49
Tidal Phase 2	25	70	37	18	66	52
Tidal Phase 3	25	70	35	18	65	50
Tidal Phase 4	25	70	32	18	66	48
Wind 5						
Tidal Phase 1	24	69	150	27	56	151
Tidal Phase 2	25	71	118	27	57	151
Tidal Phase 3	25	63	151	27	54	151
Tidal Phase 4	26	61	151	27	54	151
Wind 5						
Tidal Phase 1	25	70	75	25	70	127
Tidal Phase 2	25	75	87	25	70	132
Tidal Phase 3	25	70	73	25	70	127
Tidal Phase 4	25	70	78	25	70	120
Wind 7						
Tidal Phase 1	15	41	49	14	37	40
Tidal Phase 2	15	40	53	9	35	60
Tidal Phase 3	15	41	50	12	36	49
Tidal Phase 4	14	46	53	14	37	38
Wind 8						
Tidal Phase 1	45	49	50	46	45	67
Tidal Phase 2	46	47	47	46	44	72
Tidal Phase 3	45	49	47	46	45	70
Tidal Phase 4	36	50	17	46	46	64

[1] Contact cell defined by X and Y location corresponding to the long and short grid axes, as shown on Figures 16 and 17.

[2] 151-hour truncation employed on time to contact (≤ 150 hours contact was made: 151 hours no contact).

TABLE 6

BASE CASE
BOUNDARY CONTACT CELLS

	SITE 3			SITE 4		
	Cell Location[1]		Time to Impact[2]	Cell Location[1]		Time to Impact[2]
	X	Y	(hrs)	X	Y	(hrs)
Wind 1						
Tidal Phase 1	39	1	94	41	8	70
Tidal Phase 2	39	1	91	41	8	63
Tidal Phase 3	39	1	94	39	19	40
Tidal Phase 4	39	1	96	41	8	73
Wind 2						
Tidal Phase 1	39	7	43	39	20	18
Tidal Phase 2	39	7	42	39	20	16
Tidal Phase 3	39	7	41	39	20	17
Tidal Phase 4	39	7	44	39	20	20
Wind 3						
Tidal Phase 1	15	39	37	25	83	151
Tidal Phase 2	14	38	43	26	84	151
Tidal Phase 3	15	39	37	24	79	151
Tidal Phase 4	15	39	38	23	79	151
Wind 4						
Tidal Phase 1	15	40	20	24	85	76
Tidal Phase 2	15	39	18	25	86	76
Tidal Phase 3	15	39	17	23	85	81
Tidal Phase 4	15	42	24	23	85	78
Wind 5						
Tidal Phase 1	25	56	151	36	50	51
Tidal Phase 2	22	47	1s1	36	50	61
Tidal Phase 3	24	50	151	36	50	57
Tidal Phase 4	26	54	151	36	50	52
Wind 6						
Tidal Phase 1	26	85	151	36	50	39
Tidal Phase 2	25	70	151	38	49	45
Tidal Phase 3	24	69	133	36	50	43
Tidal Phase 4	26	86	141	36	50	39
Wind 7						
Tidal Phase 1	8	32	38	6	30	86
Tidal Phase 2	6	30	48	7	28	81
Tidal Phase 3	7	31	42	6	29	86
Tidal Phase 4	8	33	37	6	30	86
Wind 8						
Tidal Phase 1	41	33	83	41	37	30
Tidal Phase 2	41	33	88	40	35	28
Tidal Phase 3	41	33	85	40	36	28
Tidal Phase 4	40	34	75	40	38	25

[1] Contact cell defined by X and Y location corresponding to the long and short grid axes as shown on Figures 16 and 17.

[2] 151-hour truncation employed on time to contact (≤ 150 hours contact was made; 151 hours no contact).

TABLE 6

BASE CASE
BOUNDARY CONTACT CELLS

	SITE 5			SITE 6		
	Cell Location[1] X	Y	Time to Imps.ct[2] (hrs)	Cell Location[1] X	Y	Time to Impact[2] (hrs)
Wind 1						
Tidal Phase 1	40	7	57	38	6	76
Tidal Phase 2	41	8	52	38	6	73
Tidal Phase 3	39	19	27	38	6	75
Tidal Phase 4	40	7	59	38	6	78
Wind 2						
Tidal Phase 1	39	20	12	41	8	39
Tidal Phase 2	39	20	10	41	8	38
Tidal Phase 3	39	19	12	41	8	38
Tidal Phase 4	39	19	14	41	8	40
Wind 3						
Tidal Phase 1	19	56	100	17	48	68
Tidal Phase 2	18	65	130	17	48	73
Tidal Phase 3	17	62	126	17	48	69
Tidal Phase 4	19	53	88	17	48	65
Wind 4						
Tidal Phase 1	19	68	65	17	48	32
Tidal Phase 2	22	85	87	19	53	38
Tidal Phase 3	23	85	83	18	49	32
Tidal Phase 4	21	84	88	18	52	34
Wind 5						
Tidal Phase 1	36	50	75	25	52	151
Tidal Phase 2	36	50	76	25	51	151
Tidal Phase 3	36	51	74	25	48	151
Tidal Phase 4	35	54	79	26	50	151
Wind 6						
Tidal Phase 1	36	50	52	25	69	151
Tidal Phase 2	39	49	59	25	69	151
Tidal Phase 3	39	49	55	25	68	151
Tidal Phase 4	36	50	51	25	70	150
Wind 7						
Tidal Phase 1	15	27	44	6	30	67
Tidal Phase 2	15	27	46	6	29	68
Tidal Phase 3	15	27	45	6	29	67
Tidal Phase 4	14	28	47	7	31	61
Wind 8						
Tidal Phase 1	43	33	51	40	38	46
Tidal Phase 2	44	31	54	41	37	53
Tidal Phase 3	45	32	53	40	38	48
Tidal Phase 4	41	33	38	40	39	45

[1] Contact cell defined by X and Y location corresponding to the long and short grid axes, as shown on Figures 16 and 17.

[2] 151-hour truncation employed on time to contact (≤ 150 hours contact was made; 151 hours no contact).

TABLE 6

BASE CASE
BOUNDARY CONTACT CELLS

	SITE 7			SITE 8		
	Cell Location[1] X	Y	Time to Impact[2] (hrs)	Cell Location[1] X	Y	Time to Impact[2] (hrs)
Wind 1						
Tidal Phase 1	38	6	42	38	1	40
Tidal Phase 2	39	7	42	38	1	37
Tidal Phase 3	38	6	41	38	1	39
Tidal Phase 4	38	6	43	38	1	43
Wind 2						
Tidal Phase 1	41	8	22	38	5	19
Tidal Phase 2	41	8	21	39	3	20
Tidal Phase 3	40	7	22	38	5	18
Tidal Phase 4	40	7	22	38	6	20
Wind 3						
Tidal Phase 1	15	39	98	15	25	67
Tidal Phase 2	15	43	120	14	25	76
Tidal Phase 3	15	40	101	14	25	80
Tidal Phase 4	14	37	90	14	25	79
Wind 4						
Tidal Phase 1	17	48	52	14	37	50
Tidal Phase 2	17	48	50	14	37	56
Tidal Phase 3	17	48	50	14	37	55
Tidal Phase 4	18	49	53	14	37	51
Wind 5						
Tidal Phase 1	26	53	151	27	49	151
Tidal Phase 2	27	58	151	28	51	151
Tidal Phase 3	26	50	151	27	45	151
Tidal Phase 4	26	48	151	25	38	151
Wind 6						
Tidal Phase 1	25	70	140	27	65	151
Tidal Phase 2	25	70	135	37	50	94
Tidal Phase 3	25	70	145	27	60	151
Tidal Phase 4	25	67	151	27	62	151
Wind 7						
Tidal Phase 1	3	18	98	22	8	38
Tidal Phase 2	3	17	103	22	8	43
Tidal Phase 3	3	17	102	22	9	38
Tidal Phase 4	3	18	97	22	8	38
Wind 8						
Tidal Phase 1	51	27	97	41	8	46
Tidal Phase 2	51	27	94	39	7	41
Tidal Phase 3	51	27	102	41	8	46
Tidal Phase 4	51	27	99	42	9	50

[1]Contact cell defined by X and Y location corresponding to the long and short grid axes, as shown on Figures 16 and 17.

[2]151-hour truncation employed on time to contact (≤ 150 hours contact was made; 151 hours no contact).

TABLE 6

BASE CASE
BOUNDARY CONTACT CELLS

SITE 8A

	Cell Location[1] X	Cell Location[1] Y	Time to Impact[2] (hrs)
Wind 1			
Tidal Phase 1	38	6	27
Tidal Phase 2	38	6	24
Tidal Phase 3	38	6	26
Tidal Phase 4	38	5	29
Wind 2			
Tidal Phase 1	39	7	12
Tidal Phase 2	39	7	13
Tidal Phase 3	39	7	13
Tidal Phase 4	39	7	13
Wind 3			
Tidal Phase 1	14	37	111
Tidal Phase 2	14	37	110
Tidal Phase 3	14	37	111
Tidal Phase 4	14	37	107
Wind 4			
Tidal Phase 1	17	48	60
Tidal Phase 2	17	48	62
Tidal Phase 3	16	48	64
Tidal Phase 4	16	48	63
Wind 5			
Tidal Phase 1	36	50	125
Tidal Phase 2	36	51	128
Tidal Phase 3	35	54	135
Tidal Phase 4	36	53	139
Wind 6			
Tidal Phase 1	39	49	89
Tidal Phase 2	38	49	89
Tidal Phase 3	39	49	91
Tidal Phase 4	39	49	87
Wind 7			
Tidal Phase 1	22	8	52
Tidal Phase 2	22	8	52
Tidal Phase 3	22	9	49
Tidal Phase 4	22	8	50
Wind B			
Tidal Phase 1	51	9	59
Tidal Phase 1	51	9	56
Tidal Phase 3	51	9	63
Tidal Phase 4	51	10	62

[1] Contact cell defined by X and Y location corresponding to the long and short grid axes, as shown on Figures 16-and 17.

[2] 151-hour truncation employed on time to contact (≤ 150 hours contact was made; 151 hours no contact).

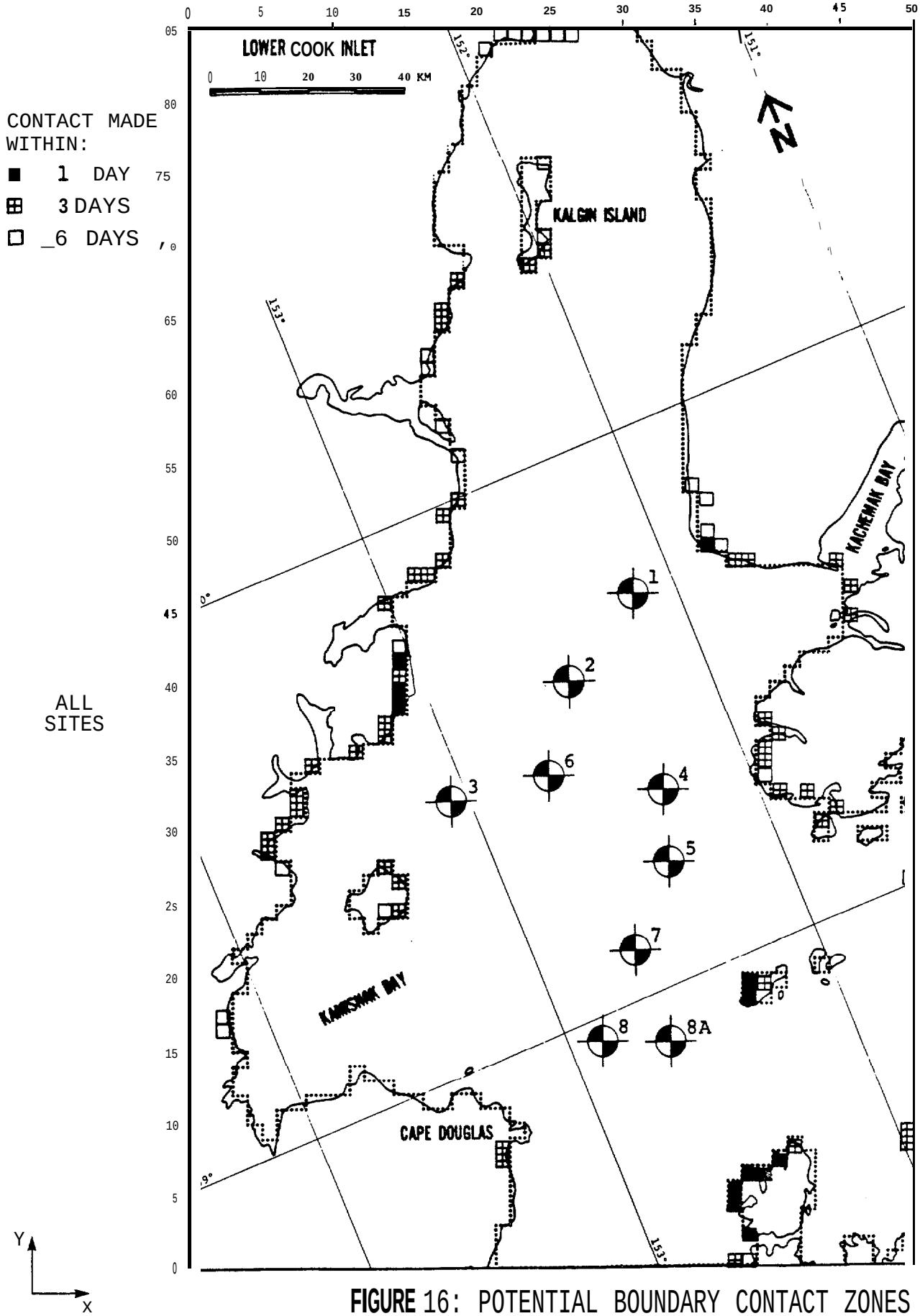

FIGURE 16: POTENTIAL BOUNDARY CONTACT ZONES

Given the specified meteorologic and oceanographic driving fields, the potential contact zones shown on Figure 16 are as expected for the distribution of the hypothetical spill sites investigated in this study. For example, consider Site 1. Under the influence of wind patterns Nos. 1 and 2, which have a predominant southerly direction in this area, the trajectories for both patterns impact Ushagat Island slightly to the west of south from spill Site 1 as shown in Figures B-1 and B-10. This indicates the dominance of the wind drift current component compared with the net and tidal current components. The net current moves the trajectories to the west as the trajectories pass south of Cape Elizabeth, which is consistent with the change in the net current direction from northerly to westerly. The effect of the tidal currents on the base case trajectories evidently does not significantly alter the impact zones.

Wind pattern No. 3 is primarily northerly and the trajectories from Site 1 show that again the wind drift current component dominates the net and tidal current components throughout this region. These trajectories come close to contacting Kalgin Island and pass just to the west of the island. The trajectories progress northeasterly as the wind drift and net current vectors parallel each other along the island. An eastward component of the net current north of Kalgin Island shifts the trajectory further to the northeast, moving it to the boundary of the Forelands as shown in Figure B-19.

Wind pattern No. 4 is similar to 3, except the magnitude of the wind is greater. The larger wind drift current component moves the trajectory from Site 1 through this region faster, which does not allow the net current component to affect the trajectory for as long a period of time as in wind pattern No. 3. The net current has a westerly component in this region, but because the trajectory moves more rapidly with wind pattern No. 4, the effect of the westerly component is diminished. The trajectory does not traverse the west shoreline of Kalgin Island as was the c_ase with wind pattern No.3, but terminates on the southern shoreline of the island as shown in Figure B-28.

Wind patterns Nos. 5 and 6 consist primarily of winds moving directly up the northern portion of Lower Cook Inlet. The vectoral combination of the wind drift and net curent components result in a northerly drift. The movement of the trajectories confirm this; impacts occurred along Kalgin Island and two trajectories were terminated just south of the island after 150 hours as shown in Figures B-37 and B-46.

Wind pattern No. 7 is directed to the northwest in the region of spill site No. 1. The vectoral combination of the wind drift and net current components provide a resultant westerly movement of the trajectory. The contact cells from wind pattern No. 7 are all located almost directly west of spill site No. 1 as shown in Figure B-55.

Wind pattern No. 8 has an easterly direction in the vicinity of spill site No. 1. The net current magnitude in this region is relatively small and does not significantly influence the trajectory movement. Thus, the trajectories move toward the east and are shown to contact the northern shoreline of Kachemak Bay *as* shown in Figure B-64. The effect of the tide can be seen to influence to some extent where the contact will occur along the shoreline.

Similar reasoning can be applied to the other spill sites to show that the resulting trajectory movements shown in Figures B-1 through B-72 are as expected given the specified environmental forcing fields. Careful examination of these figures will show the relative importance or dominance of the specified environmental forcing fields. Summarily, it can be stated that the wind drift current component provides the primary driving force for centroid movement. In certain areas, such as offshore Cape Douglas, the net current significantly influences trajectories. Although the tidal current, with few exceptions, does not significantly alter the net trajectory it should be noted that the specified wind patterns and to a degree the net current pattern are all rather uniform. The tidal currents or other environmental forcing fields could become more important if transient and nonuniform conditions were specified. For example, if a wind field was rotated and the wind speed varied with time, then the tidal current phase at time of release might become an important factor in trajectory movement.

Annual Percent Probability of Exposure

As was done in the 1976 study, an assessment was made of the annual percent probability of shoreline exposure. The exposure probabilities were based entirely on the annual percent frequencies assigned to each of the wind patterns as discussed in Section III. The annual probabilities of exposure were determined for a spill occurring at each site in the following manner:

1. For each boundary cell contacted, the wind pattern or patterns associated with that contact cell were identified.

2. The cumulative annual frequency of the wind pattern or patterns associated with that contact cell were computed. The annual frequency of a wind pattern was counted only once in determining a cumulative frequency, even if that wind pattern was identified as producing more than one contact for that cell.

3. The cumulative annual percent frequencies of the wind patterns associated with a contact cell were assumed to represent the annual probability of exposure for that cell.

Although the above assessment is a first-order approximation, it provides a means of evaluating or comparing the expected exposure level for the specified spill sites and environmental driving forces. Further refinement in assessing exposure probabilities is not justified given the limitations inherent in determining the contact cell locations.

Graphical representation of the annual percent probability of exposure given that a spill occurs at each site is presented in Appendix B, Figures B-82 through B-90. For each cell contacted, the range of probability of exposure calculated for that cell has been coded according to the legend given on the figures. No attempt has been made to smooth or-add exposure probabilities between contact cells. However, it should be noted that the probability of exposure is not a discrete function, but in reality a continuous one.

A summary of the annual probability of exposure for all nine sites is presented in Figure 17. This figure represents the annual probability of exposure given that a single spill is equally probable from any of the nine potential spill sites. The probabilities were calculated by dividing the cumulative probabilities for each cell (the summation of probabilities for all sites) by the number of sites.

The relative exposure levels along the boundary cells thus provides within the limitations of the model and specified input data, an estimate of those portions of Lower Cook Inlet which are most likely to experience impact by the centroid of a hypothetical oil spill from the nine sites under consideration.

It should be noted that the annual probabilities expressed in this assessment are based on the assumption that, on the average, one spill would occur annually from any of the hypothetical spill sites. Therefore, since specific oil spill statistics were not used in this study, the exposure probabilities should be interpreted only from a comparative viewpoint. In addition, an assessment of shoreline exposure should include both the likelihood of exposure, and the time to exposure. Less likely exposure sites with shorter times to impact could be more significant due to greater volumes of oil likely to exist at the surfce upon impact, dosage and toxicity considerations, and shorter response time available for spill containment, diversion, and cleanup operations.

The overall strategy in simulating the base *case* trajectories shown in Figures B-1 through B-72 was deterministic in that all quantities were uniquely specified. However, both systematic and random fluctuations may affect the base case shoreline impact distribution. The purpose of the following perturbation analyses is to determine the sensitivity of the shoreline distribution of contact cells and times to impact to perturbations in the base cases.

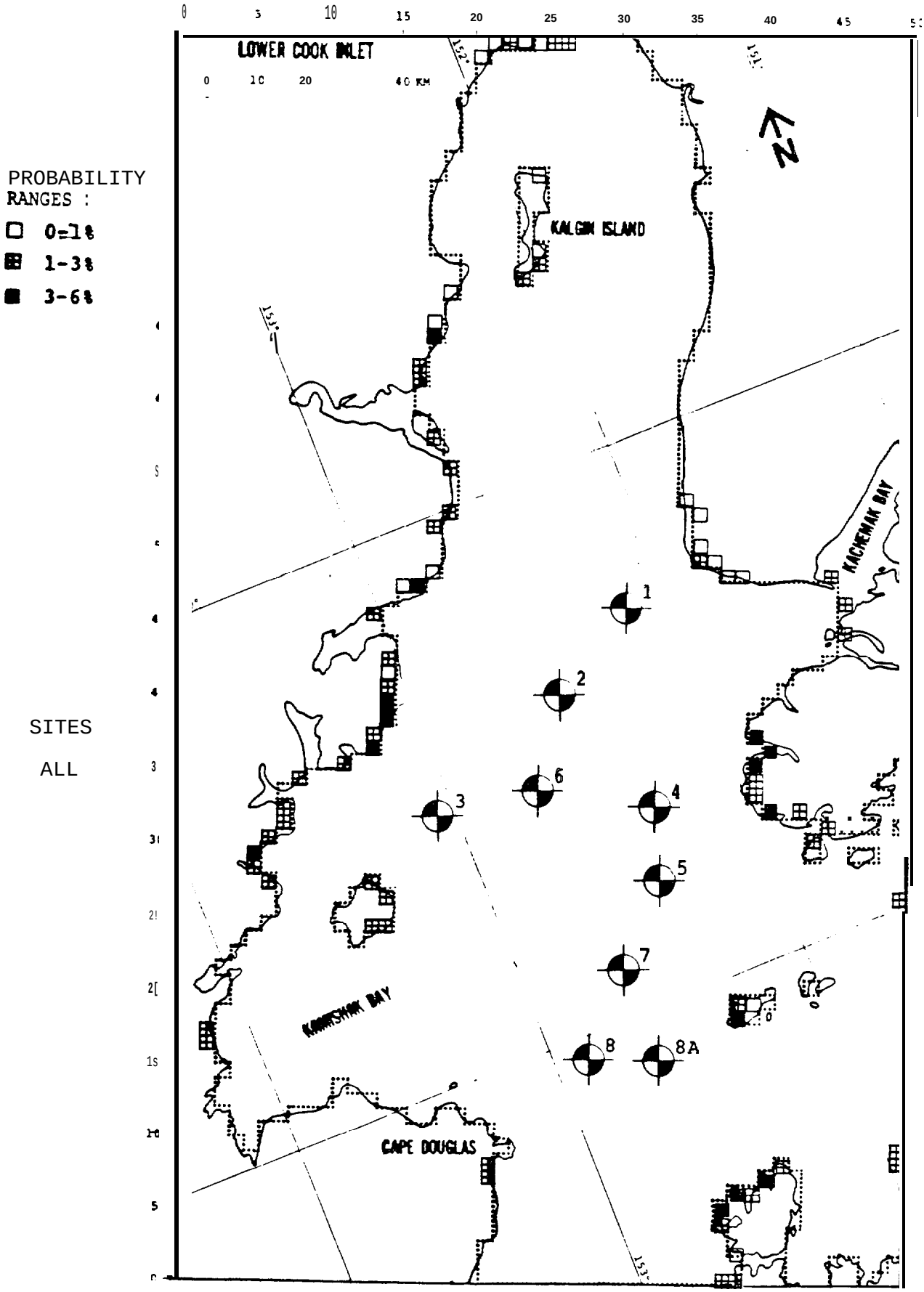

FIGURE 17: ANNUAL PERCENT PROBABILITY OF EXPOSURE

B. SYSTEMATIC PERTURBATION ANALYSIS

Sites 1, 3, and 7 were chosen to investigate the sensitivity of the results to variations on the wind and net current patterns because they yielded a fairly wide distribution of shoreline impact points for the base cases. A systematic perturbation was defined to be one where the wind and current exhibit the same directional distribution as in the base cases while the speed can be weaker (speeds less) or stronger (speeds greater).

For Sites 1 and 7, a set of four runs were made: 1) winds weaker by 25%, 2) winds stronger by 25%, 3) net current weaker by 25%, and 4) net current stronger by 25%. In each case, an initial tidal current phase of zero degrees was used. (As discussed for the base case trajectories, the starting phase of the tidal current was not found to significantly alter the resulting trajectories.)

Trajectories for the systematic perturbation analyses for Sites 1 and 7 are presented in Appendix C, Figures c-1 to C-64. The figures are arranged by wind patterns; that is, Figures C-1 to C-8 present the perturbation trajectories for wind pattern No. 1. Figures C-1 to C-4 present the perturbation trajectories for spill site No. 1 including trajectories for the systematic perturbation of the net current ($\pm$25%) and the wind drift current ($\pm$25%). Figures C-5 to C-8 present the trajectories for Site 7 with the same perturbation conditions specified above. This arrangement allows comparisons between trajectories from the same site and a particular wind pattern to be easily made.

Table 7 presents a summary listing of the termination cells and times to impact of the systematic perturbation analysis. Since only three sites were analyzed for the systematic perturbation analysis, development of potential contact zones was not made since comparison with the base case potential contact zones would be incomplete and possibly misleading. In order to provide some means of comparing the effect that the systematic perturbation has on the trajectory termination cells and times, Table 8 was developed. This table presents the variation in contact cell termination by means of the distance, (in kms), between the base case termination cell

TABLE 7

SYSTEMATIC PERTURBATION BOUNDARY CONTACT CELLS

Site 1

	Net +25%			Net -25%		
	Cell Location		Time to	Cell Location		Time to
Wind Pattern	X	Y	Impact * (hrs)	X	Y	Impact * (hrs)
1	39	20	80	39	20	69
2	41	20	36	51	4	56
3	24	69	106	24	69	85
4	24	69	36	24	69	36
5	36	50	21	37	50	23
6	35	57	27	36	53	23
7	14	38	62	15	39	66
8	46	48	42	46	48	42

	Wind +25%			Wind -25%		
	Cell Location		Time to	Cell Location		Time to
Wind Pattern	X	Y	Impact* (hrs)	x	Y	Impact * (hrs)
1	40	20	59	39	20	105
2	51	6	44	40	20	48
3	24	69	70	24	69	147
4	25	70	30	25	70	51
5	36	51	20	36	50	25
6	35	54	16	36	50	21
7	15	39	47	12	36	105
8	46	48	34	46	47	105

* 151-hour truncation employed on timeto contact (≤150hours contact was made; 151 hours no contact).

TABLE 7

SYSTEMATIC PERTURBATION BOUNDARY CONTACT CELLS

Site 7

Net +25%

Wind Pattern	Cell Location X	Y	Time to Impact* (hrs)
1	38	5	43
2	40	7	21
3	13	37	100
4	17	48	55
5	27	52	151
6	26	67	151
7	12	14	73
8	48	24	151

Net -25%

Cell Location X	Y	Time to Impact * (hrs)
39	7	40
41	8	20
18	49	120
18	49	52
36	51	49
36	50	74
4	20	88
51	23	69

Wind +25%

Wind Pattern	Cell Location X	Y	Time to Impact* (hrs)
1	39	7	33
2	41	8	17
3	17	48	98
4	18	49	42
5	28	63	151
6	36	50	61
7	3	19	73
8	51	24	58

Wind -25%

Cell Location X	Y	Time to Impact * (hrs)
39	3	61
39	7	29
13	37	141
18	51	79
26	41	151
28	61	151
14	13	91
48	23	151

* 151-hour truncation employed on time to contact ($\leq$150 hours contact was made; 151 hours no contact).

TABLE 8

VARIABILITY BETWEEN BASE CASE AND

SYSTEMATIC PERTURBATION TRAJECTORIES

Site 1

Wind Pattern (Tidal Current Starting Phase = 0 Degrees)	Perturbation Cases: Net +25% ΔX (km)	Net +25% ΔT (hrs)	Net -25% ΔX (km)	Net -25% AT (hrs)	Wind +25% AX (km)	Wind +25% ΔT (hrs)	Wind -25% Ax (km)	Wind -25% AT (hrs)
1	0.0	6	0.0	17	3.0	27	0.0	-19
2	3.0	3	58.2	-17	53.4	-5	0.0	-9
3	51.8	20	51.8	41	51.8	56	51.8	-21
4	0.0	2	0.0	2	4.2	8	4.2	-13
5	67.4	129	69.1	127	64.9	130	67.4	125
6	49.2	48	60.7	52	56.6	59	68.5	54
7	-9.5	-13	6.0	-17	6.0	2	17.5	-56
8	4.2	8	4.2	8	4.2	16	6.7	-55

Site 7

Wind Pattern (Tidal Current Starting Phase = 0 Degrees)	Perturbation Cases: Net +25% ΔX (k	Net +25% AT (hrs)	Net -25% Ax (km)	Net -25% ΔT (hrs)	Wind +25% Ax (km)	Wind +25% AT (hrs)	Wind -25% Ax (km)	Wind -25% ΔT (hrs)
1	3.0	-1	4.2	2	4.2	9	9.5	-19
2	4.2	1	0.0	2	0.0	5	6.7	-7
3	8.5	-2	31.3	-22	27.7	0	8.5	-43
4	0.0	-3	4.2	0	4.2	10	9.5	-27
5	4.2	0	30.6	102	30.6	0	36.0	0
6	9.5	-11	68.5	66	68.5	79	28.5	-11
7	29.5	25	6.7	10	3.0	25	36.2	7
8	12.7	-54	12.0	28	9.0	40	15.0	-54

ΔX = radial distance from base case termination cell to perturbation termination cell

AT = difference in termination times between base case and perturbation case ($T_{base} - T_{perturbation}$). Positive ΔT indicates perturbation trajectory terminated sooner than base case trajectory.

developed. This table presents the variation in contact cell termination by means of the distance (in kms), between the base case termination cell and the systematic perturbation case termination cell. Table 8 *also* provides the time difference between base case times to impact and systematic perturbation case times to impact. A positive time indicates that the perturbation trajectory terminated sooner, a negative time indicates the perturbation trajectory took longer to terminate. This information provides direct comparison of the expected variability of the results of the oil spill simulation when subjected to the specified systematic perturbation of the input data.

For Site 1, wind pattern No. 1, Table 8 shows that all perturbation trajectories terminated close to or at the base case termination cell (see Figures C-1 through C-4). The times to impact are shown to be sooner than the base case for the perturbation cases net ±25 percent and wind +25 percent, and later for wind -25 percent. In light of the wind and net current patterns, the only unexpected result is the shorter termination time for the perturbation case, net +25 percent. Comparison between the base case trajectory and the net +25 percent trajectory shows that the later trajectory is moved closer to Port Graham and into. a weaker net current field, even after being increased 25 percent. This allows the wind to move the trajectory further south in the same period of time resulting in an earlier contact time compared to the base case.

As shown in Table 8 the distances and termination times for perturbation cases net +25 percent and wind -25 percent for Site 1 are similar for both wind patterns Nos. 1 and 2 (see Figures C-1, C-4, C-9, and C-12). However, large variations exist for perturbation cases net -25 percent and wind +25 percent for site 1 wind patterns Nos. 1 and 2, (see Figures C-2, c-3, C-10, and C-71). The perturbation trajectories shown in Figures C-10 and C-11 do not impact Ushagat Island as the trajectories shown in Figures C-2 and C-3 do, but traversed slightly to the east between Ushagat and W. Amatuli Islands, and terminated on the grid boundary. This provides the large variations in these two similar sets of perturbation cases. The stronger winds associated with the perturbation case wind +25 percent for

wind patterns No'. 2 drive the trajectory through the northwesterly flowing net current field in Kennedy Entrance faster, thus reducing the westerly component imparted to the base case trajectory by the net current. The increased wind velocity also reduces the westerly component of the resulting vectoral addition of the various current components, also aiding the more easterly perturbation trajectory.

The perturbation case for Site 1 wind pattern No. 2 net -25 percent generates the same effect. Reducing the net current in Kennedy Entrance reduces the westerly drift in that area, however, the time element is not as important. The trajectory passes through the Barren Islands slightly sooner than it took the base case to impact Ushagat Island. This is mainly attributed to the reduced northerly component of net current above Cape Elizabeth.

For Site 1 wind pattern No. 3 (see Figures C-17 through C-20), the results of all the perturbation cases show a difference in distance of 51.8 km from the base case trajectory termination cell. The base case trajectories narrowly passed Kalgin Island and terminated at the grid boundary between The Forelands. All perturbation trajectories for Site 1 wind pattern No. 3 terminated at the southern tip of Kalgin Island. The times to impact show the relative influence of the current field being systematically increased or decreased. The relative times to impact are also consistent with logical expectations given the relative magnitudes of the wind drift and net current component fields through this region of Lower Cook Inlet.

The trajectories for Site 1 wind pattern No. 4 show little variation in distance between termination cells compared with the base case trajectory termination cell (see Figures C-25 through C-28). All trajectories terminate along the southern portion of Kalgin Island. Since wind pattern No. 4 is the same as wind pattern No. 3, except for greater wind speeds, it becomes apparent that the wind drift current component dominates the trajectory for this site. The times to impact also show that the wind field dominates as perturbation cases wind +25 percent produce the only significant variation.

wind patterns No. 2 drive the trajectory through the northwesterly flowing net current field in Kennedy Entrance faster, thus reducing the westerly component imparted to the base case trajectory by the net current. The increased wind velocity also reduces the westerly component of the resulting vectoral addition of the various current components, also aiding the more easterly perturbation trajectory.

The perturbation case for Site 1 wind pattern No. 2 net -25 percent generates the same effect. Reducing the net current in Kennedy Entrance reduces the westerly drift in that area, however, the time element is not as important. The trajectory passes through the Barren Islands slightly sooner than it took the base case to impact Ushagat Island. This is mainly attributed to the reduced northerly component of net current above Cape Elizabeth.

For Site 1 wind pattern No. 3 (see Figures c-17 through C-20), the results of all the perturbation cases show a difference in distance of 51.8 km from the base case trajectory termination cell. The base case trajectories narrowly passed Kalgin Island and terminated at the grid boundary between The Forelands. All perturbation trajectories for Site 1 wind pattern No. 3 terminated at the southern tip of Kalgin Island. The times to impact show the relative influence of the current field being systematically increased or decreased. The relative times to impact are also consistent with logical expectations given the relative magnitudes of the wind drift and net current component fields through this region of Lower Cook Inlet.

The trajectories for Site 1 wind pattern No. 4 show little variation in distance between termination cells compared with the base case trajectory termination cell (see Figures C-25 through C-28). All trajectories terminate along the southern portion of Kalgin Island. Since wind pattern No. 4 is the same as wind pattern No. 3, except for greater wind speeds, it becomes apparent that the wind drift current component dominates the trajectory for this site. The times to impact also show that the wind field dominates as perturbation cases wind $\pm$25 percent produce the only significant variation.

Table 8 shows large variations between all perturbation cases for Site 1 wind pattern No. 5 and the base case termination cell and time to impact (see Figures C-33 through C-36). The base case trajectory slowly moves northward and impacts the southern tip of Kalgin Island (wind patterns Nos. 5 and 6 are similar in direction to Nos. 3 and 4 in the upper portion of Lower Cook Inlet). However, all perturbation trajectories for Site 1 wind pattern No. 5 move easterly and terminate along the shoreline in the vicinity of Anchor Point.

Since wind pattern No. 6 is similar to wind pattern No. 5, the results of the systematic perturbation analysis for Site 1 are also similar (see Figures C-41 through c-44). The base case trajectory for Site 1 under the influence of wind pattern No. 6 moved northward and terminated on Kalgin Island. As for wind pattern No. 5, the perturbation trajectories for wind pattern No. 6 moved eastward and terminated along the shoreline in the vicinity of Anchor Point.

The base case trajectories for Site 1 wind pattern No. 7 all move basically westward, making contact between Chinitna and Iniskin Bays (see Figures C-49 through C-52). Wind pattern No. 7 is predominantly westward in this section of the inlet. The net current changes from northeasterly to northwesterly to southwesterly as one moves from east to west across the inlet from spill site No. 1. The strongest net currents are the northeasterly and southwesterly flows. The perturbation cases for Site 1 wind pattern No. 7 show relatively small variations in termination cell distances. This indicates the dominance of the wind for these trajectories. The perturbation case net +25 percent terminates further south than the base case as expected due to the increased southwesterly flow near the western shoreline. The time to contact is increased over the base case as the trajectory moves further from Site 1.

The perturbation case net -25 percent for Site 1 wind pattern No. 7 allows the stronger tidal currents along the eastern side of Lower Cook Inlet to have a greater effect on the trajectory as it moves more southerly than the base case trajectory during its initial movement away from spill

site No. 1. This results in the perturbation trajectory terminating slightly south of the base case trajectory. Due to the reduced westerly component from the net current, the time to contact is increased.

The perturbation cases wind ±25 percent for Site 1 wind pattern No. 7 also show termination cells and times to contact as expected (see Figures C-51 and C-52). The wind +25 percent perturbation case takes less time to contact and is slightly south of the base case, not being affected by the northerly component of net current in the southern edge of the net current eddy off of Chinitna Bay. The wind -25 percent trajectory takes longer to impact and makes contact south of the base case trajectory termination cell as the stronger tidal currents on the eastern side of the inlet have a longer period of time to affect the trajectory movement. The southwesterly flowing net current along the western portion of the inlet drives the trajectory further south.

The perturbation cases for Site 1 wind pattern No. 8 (see Figures C-57 through C-60), show relatively little variation in contact cell compared with the base case trajectory. The winds near spill site No. 1 from wind pattern No. 8 are easterly and because the net currents are small in magnitude, the winds dominate trajectory movement. This is readily apparent from the variation of the perturbation cases net ±25 percent, which are identical. As expected, the perturbation case wind +25 percent arrives sooner and wind -25 percent arrives later.

Similar reasoning can be applied to the systematic perturbation trajectories run for site 7 to provide insight to the variations in contact cell distances and termination times presented in Table 8. As can be seen from the values listed in the table and the trajectories shown in Figures C-1 through C-64, significant variation can exist from selected sites and wind patterns.

It should be emphasized that the systematic perturbations 'were applied to rather spatially uniform current fields with only one simplified time-dependent current component (tidal current). In reality, the current fields

would experience a wide range of spatially and temporally varying perturbations. However, the results of the systematic perturbation analysis show that trajectory variations do exist and can be quite large. Perturbation trajectories should be examined closely in order to understand the variation in termination cell distances and time differences presented in Table 8.

A special systematic perturbation analysis was conducted for postulated spill site Number 3. This site is the most westerly of all the postulated spill sites. Questions arose during the study regarding the impact that might occur along the shoreline of Kamishak Bay and Augustine Island due to a reduced wind field magnitude imposed on the trajectories originating from Site 3. A limited systematic perturbation analysis was performed for Site 3 using all eight wind patterns reduced in magnitude by 25 percent. An initial tidal current phase of zero degrees was selected for each run. The eight trajectories are presented in Appendix C, Figures C-65 through c-72.

Trajectories from Site 3 for wind patterns 1 and 2 would have the potential to impact Augustine Island if the wind vector magnitudes were reduced so that the wind drift current component was nearly equal to the net current component. As seen in Figures C-65 and C-66, the wind drift current component still dominates even after being reduced 25 percent and the trajectories move southerly and southeasterly away from Kamishak Bay.

If wind patterns Nos. 3 and 4 were reduced in magnitude so that the wind drift current component were equal to or less than the net current component, the resulting trajectories could be driven in a westerly or southwesterly direction. This would result in potential contact being made along the northern shoreline of Kamishak Bay or on Augustine Island. As shown on Figures c-67 and C-68, the 25 percent reduction in the wind magnitude did not result in contact being made along Kamishak Bay or Augustine Island. The winds still dominate the trajectory movements driving them into the shoreline between Iniskin and Chinitna Bays.

Due to the vectoral combinations of the wind drift and net current components, wind patterns Nos. 5 and 6 would need to be severely reduced in

magnitude to result in trajectory movement from Site 3 into Kamishak Bay. Figures C-69 and C-70 show that this situation was not created, even for a 25-percent reduction in the wind field magnitudes. The trajectory for wind pattern No. 5 moves slowly toward the southeast until it encounters the weaker net currents in the central portion of Lower Cook Inlet. The trajectory then moves toward the northeast until it exceeds the simulation time limit and terminates in the middle of the inlet. The trajectory driven by wind Pattern 6 shows a similar fate, with the influence of the wind field being more dominant and driving the trajectory further up the middle of the inlet.

Wind Pattern 7 is directed toward the northwest near Site 3, and the base case trajectory is shown on Figure B-57 to move almost due west making contact just north of Ursus Cove. If the winds were reduced, the net current might drive the trajectory further south into Kamishak Bay. As shown on Figure C-71, with the wind field reduced 25 percent in magnitude, the trajectory does move further south than the base case and takes nearly twice as long to make contact. However, with the 25-percent reduction in wind field magnitude, the trajectory terminates only 10 km from the base case trajectory and does not move into the southern portion of Kamishak Bay.

Wind Pattern 8 would need to be reduced to nearly zero magnitude before a trajectory from Site 3 would have even a remote chance of moving into and making contact along the shoreline of Kamishak Bay. However., for continuity this wind pattern was reduced in magnitude by 25 percent and a trajectory simulated. The base case trajectory for Site 3 wind Pattern 8 made contact near Cape Elizabeth. The reduction in the wind speed allows the trajectory, shown in Figure c-72, to be driven further south due to the increased influence of the net current component. As the trajectory approaches Kennedy Entrance the net current and wind drift current components become nearly equal in magnitude and opposite in direction. This results in the centroid of the trajectory oscillating with the tidal currents in a northwest and southeast direction until it exceeds the simulation time limit and terminates.

C. RANDOM PERTURBATION ANALYSIS

A random perturbation analysis was performed in recognition that the environmental forcing fields are not smooth and deterministic, but are affected by naturally occurring turbulent phenomena. As in the systematic error analysis, the purpose of the random perturbation analysis is to measure the sensitivity of the final shoreline distribution of impact points to these fluctuations.

To carry out this approach, the probability distribution functions for the wind and current fields are needed. The only data for which measurements of standard deviations were readily available were for net currents. These data were only available at a few stations, where the standard deviation was given parallel and perpendicular to. the mean net current vector. The measured net current standard deviations were used to estimate a simplified distribution of the standard deviation for the entire net current field as shown in Figure 18.

The deviations are largest in the Kennedy Entrance area where the net current field exhibited considerable variability. While the net currents in Kamishak Bay are generally weak, they also appear to be relatively stable and consequently show small standard deviations in both components. Similarly, the net current field in the middle portion of Lower Cook Inlet west of Kachemak Bay is relatively well defined compared to the southern portion of the Inlet. The standard deviations are larger than in Kamishak Bay since the current field itself is stronger. The standard deviations of net currents in the vicinity of Kalgin Island are not defined since current meter data are not presently available. Hence, no random perturbation cases were run in this area.

At each time step, the net current was perturbed by adding vectors parallel and perpendicular to the mean net current. The magnitudes of these additional vectors were randomly drawn from a normal distribution with a mean of zero and the standard deviation as defined in Figure 18.

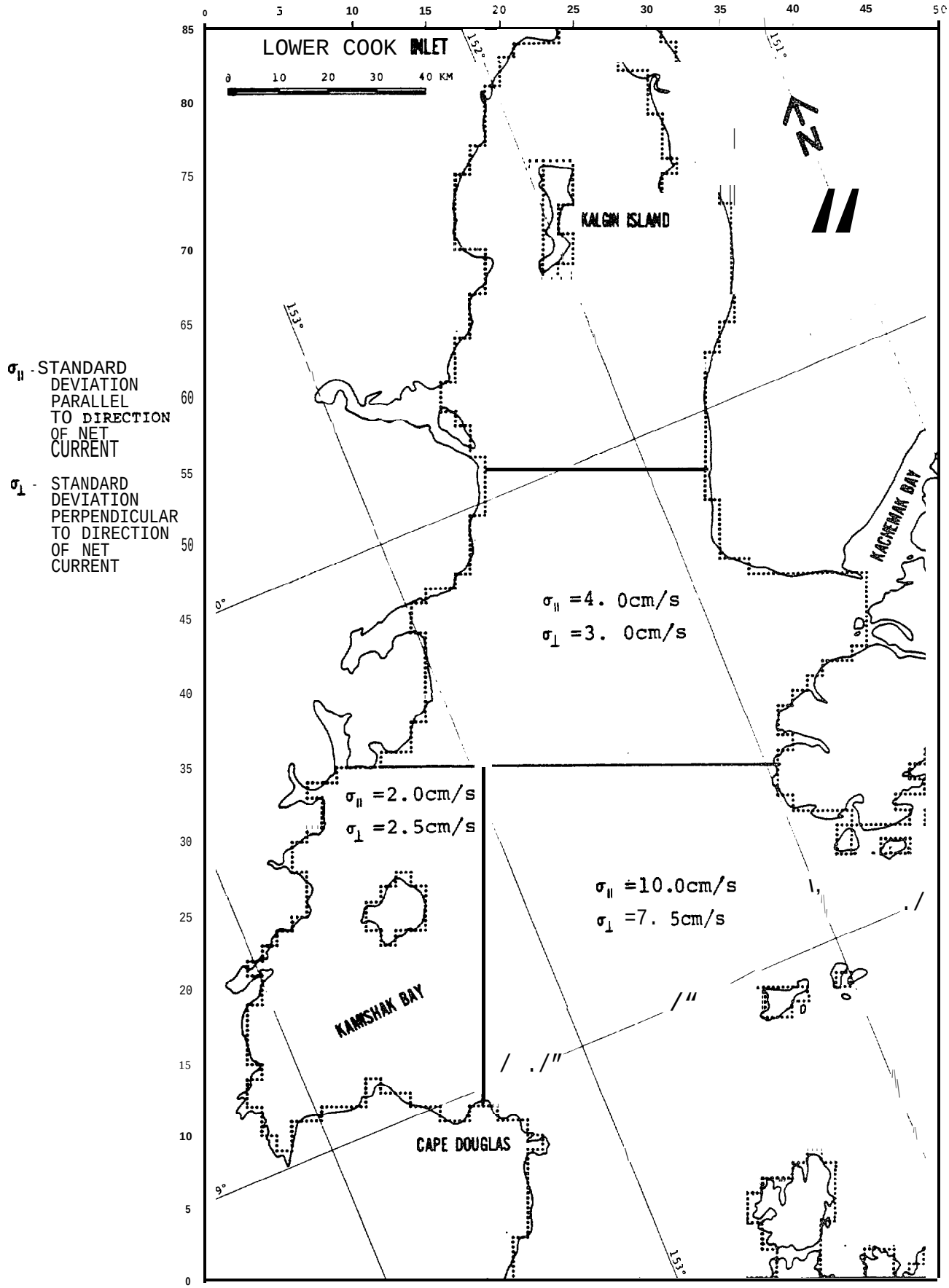

FIGURE 18: NET CURRENT STANDARD DEVIATION DISTRIBUTION

A series of 18 trajectories were run for each selected base case where the net current field was subjected to a random distortion throughout the entire period of simulation. These trajectories are shown in Appendix C, Figures C-73 through C-78, (note that, for purposes of clarity, only nine trajectories are plotted in each figure). By chosing 18 trajectories, it can asserted that 90 percent of the trajectory population lies within the extremes of the observed shoreline distribution at the 75-percent confidence level.

The results of this perturbation analysis must be interpreted with some care. The computed distribution of shoreline impact points is not representative of any annual distribution. Rather, the distribution of shoreline impact points is what might possibly be expected, given that the base case simulation conditions are prevailing and assuming that the standard deviation derived from the current meter records are uncorrelated with space and time. Specifically, the net current standard deviations must be assumed to be uncorrelated with the wind and current fields. The trajectory deviations from the base cases, then, are due only to purely random phenomena acting to modify the bse case environmental fields.

Adopting this point of view, an important conclusion can be drawn based on the relatively narrow range of shoreline impact points. This range--approximately three grid cells or 10 km--is less than what is believed to be attributed to unknowns in the base case data itself. For example, the range of impact points observed in the systematic perturbation analysis is much greater than that computed here.

Since the random deviations imposed on the net current field are selected from a Gaussian distribution, it is possible to derive approximate results that indicate the functional dependence of these results on step size. Consider an idealized case where:

1) $U_{,t} \cong 0$

2) the base case net current field is uniform in space and constant in time.

The resultant distribution on a line perpendicular to the net current field would be normal with a standard deviation given by

$$\sigma_s = \sqrt{n} \cdot \sigma_1 \cdot \Delta t \qquad (2)$$

where σ_s = standard deviation of the impact point distribution

n = number of steps required to reach the trajectory end point

Δt = time step

σ_1 = standard deviation of the random component of the net current distribution

The trajectories shown in Figures C-73 and C-74, remain in the region where σ_1 is a constant 7.5 cm/s (270 m/hr). Ignoring divergencies in the wind and current driving fields, and noting that the base case trajectory contacted the shoreline after 84 time steps, a value for σ_s of 1.2 km is obtained. Thus, it would be expected that two-thirds of the random perturbation cases would impact within approximately 2.5 km of the shoreline. This is less than one grid cell. Clearly, except for long trajectories or those moving through areas of high variability, the deviations in the base case trajectories introduced by random perturbations in the net current field are small.

The effect of the time step, At, on the shoreline distribution can be determined by rewriting Equation (2). Since, in the idealized case, there is no velocity perturbation parallel to the constant, uniform base case net current field, the number of time steps in the simulation is given by

$$n = \frac{T}{\Delta t}$$

where T = period of simultation, a constant. Using this result, Equation (2) can be written as

$$\sigma_s = \sqrt{T \cdot \Delta t} \quad .0,$$

Thus, the standard deviation of the distribution of shoreline impact points is proportional to the root of the time step.

Information on the persistence of the net current field from the field observations was not available during this study so At was chosen to be equal to the time step size used in the base case simulations, one-half hour. If, in fact, the persistence is greater than this value, the dispersion of shoreline impact points would be underestimated by the value of 1.2 km calculated for us. If the persistence is, say, an order of magnitude larger than assumed here, then the value of σ_s would only be approximately 4 km, or just over one cell width. In order to have a major impact on the results presented, the net current persistence would have to be on the order of 100 hours. However, if this is true, then the basic assumptions inherent in this random perturbation analysis are not likely to be valid and an entirely different approach to the analysis of random fluctuations in the net current field would have to be taken.

Figures C-77 and C-78 illustrate the importance of the base case driving fields relative to their random deviations. The clear bifurcation of the 18 trajectories can be understood by noting the divergence of the tidal current field in the lower portion of Kamishak Bay as illustrated in Figure 12. The resulting direction each trajectory takes is determined by which of the divergent current vectors is first encountered due to the random fluctuations. The bifurcation results in larger trajectory deviations than introduced by random fluctuations alone.

This explanation suggests that the shoreline distributions shown in Figures c-77 and C-78 might be basically different if starting tidal phases other than zero degrees were selected for initiating the trajectory from Site 7. For example, the tidal current pattern for an assumed phase of 180 degrees, (see Figure 14), does not show the divergence that caused the observed bifurcation in Figures C-77 and C-78.

v. RECOMMENDATIONS

'The results and conclusions arising from this project are summarized *in the* Executive Summary. Consequently, the following discussion focuses on recommendations for future work directed toward developing a more accurate, comprehensive understand ng of the fate and behavior of oil spills, particularly in Lower Cook Inlet.

One primary area of concern is the nature, extent, and quality of the wind and current data used to develop the basic spill centroid driving forces. As indicated in the Executive Summary, winds dominate the oil spill movement simulated in this study. However, the meteorological data base has not been developed to the level of detail believed required for reliable oil spill simulation analyses. For example, using constant wind fields over a period of up to 150 hours does not accurately represent the expected wind persistence in the Lower Cook Inlet region.

An improved method is needed to simulate more representative wind fields that approximate the time histories and persistence of winds over Lower Cook Inlet. It is suggested that the. same basic typology of wind patterns developed by Putnins (1966 and 1967) be used in conjunction with a first-order transition matrix, which would link the wind patterns in simulating a meteorological event. Such a matrix would give, for any wind pattern, the probability of transition to any other wind pattern.

In place of the deterministic base cases developed here, an ensemble of simulations from each site could be run to directly develop the equivalent of Figure ES-2, the annual percent probability of shoreline exposure. While the results of such an approach are difficult to predict, a much broader distribution of impact points would be generally expected due to the variability of wind patterns imposed. For example, realistic sequences of events could lead to impacts in, say, the Cape Douglas area that do not occur under the present approach (see Figure C-77).

An example trajectory generated by the implementation of a simplified version of such a scheme is shown in Figure 19. While this trajectory is based on a hypothetical sequence of events, it does illustrate that explicit inclusion of the time dependency of the winds can potentially lead to trajectories and impact points not attainable under the approach used in this study . This trajectory was generated in the following manner:

1) Net and tidal currents were unchanged from the base case simulations.

2) Wind fields were the same as the base case with the exception that they were (arbitrarily) assumed to persist for only 30 hours.

3) Wind field transition probabilities were taken to be 1/7. That is, given any wind field, the probability of transition to any other was equally likely.

4) Using random numbers, several sets of wind field sequences were generated until a "reasonable" one was available. Typically, the reasonable criteria was used to eliminate transition sequences such as 7-8-7.

5) The selected sequence of Patterns 6-5-7-7-2 was input to the oil spill model and the trajectory calculated.

The nature of the resultant trajectory makes evident the clear need to include the time-dependency to the meteorological data in future efforts.

It is proposed that a fundamentally different scheme might be considered which would link a meso-scale wind model directly to the oil spill model to provide direct input representation of wind fields. One noteworthy advantage of this approach would be its ability to more accurately represent local wind field disturbances than are presently available in the use of Putnins wind types. In addition, this methodology would permit the modeling of realistic meteorologic events such as the passage of a front across Cook Inlet.

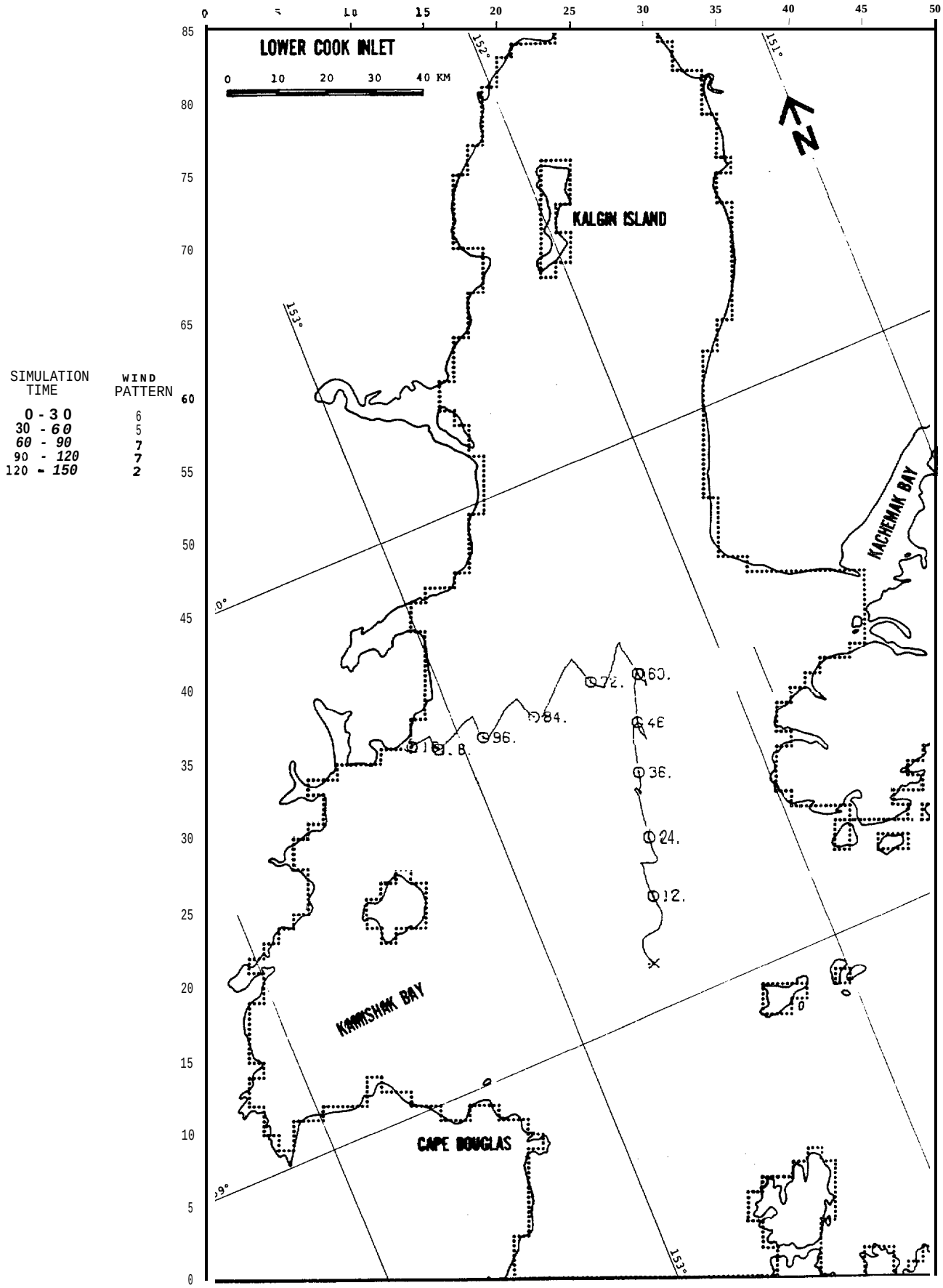

FIGURE 19: TIME DEPENDENT WINDFIELD TRAJECTORY

The use of such a meso-scale wind field model, while expensive to run repeatedly is a step toward the development of an operational real-time oil spill model. A bank of results could be developed for commonly observed meteorologic events and the results filed for quick recall or the model could be run when a spill occurred given the specified prevailing wind conditions.

Additional efforts to improve the net and tidal current information must also focus on more objective techniques to develop the requisite vector fields. However, the principal difficulty here is not the existence, but rather the availability of field data. As a result of several ongoing programs, a wealth of water column hydrodynamic data has been collected but largely remains unprocessed. The minimal hydrodynamic modeling work done on this project suggests that an expanded hydrodynamic modeling effort using the field data on hand, would likely be successful.

Completion of these proposed activities would increase the confidence placed in the results of future oil spill modeling efforts. Other areas of investigation will need to be addressed in the long-term. Several field observers have noted the important role that density fronts can play in retarding the movement and spread of an oil slick. Lower Cook Inlet in the heavy runoff season will likely exhibit such fronts. One potential means to deal with this facet of Cook Inlet hydrodynamics is through the use of satellite data.

In addition, the presence of ice in Cook Inlet can have a very significant effect on the distribution of spilled oil. For example, oil trapped in or beneath ice may be transported well beyond the region otherwise contaminated or may be held without significant decay for extended periods, possibly as long as several years. Oil spills entrained by ice is an area of research that has yielded little information to date for use by modelers.

The oil spill model used in this study is based on a relatively simple, well accepted methodology to predict spill centroid movement.

While sophisticated transport models are available, evaluations of the environmental data base weaknesses indicate that more sophisticated approaches are presently inappropriate.

As the quality and extent of the environmental data increase, more sophisticated numerical modeling efforts should initially focus on applying a two-dimensional surface transport model. Unfortunately, the strong shear exhibited by both the net and tidal currents (more realistic wind fields are also likely to exhibit more shear than the ones used in this study) may preclude the use of the Fay-Holt model (Fay, 1969 and Holt, 1972) for spreading in calm water as used by several previous investigators (Isakson, 1975; Premach and Brown, 1973; and Wang, 1974). A two-dimensional model that could realistically treat shearing forces would contribute to the state-of-the-art.

It is difficult to assess the importance and viability of applying three-dimensional hydrodynamic models. Presently, existing limitations on knowledge of the physical processes, as discussed in Section II, hamper progress toward a 3-D model of oil dispersion. In addition, obtaining carefully controlled verification data, particularly from field experiments, has proven difficult. As a result, limited model verification data are available.

Evaporation can be easily modeled, while wave-slick interaction, although recognized to be important in sinking, is very poorly understood. A prudent approach for future development would be to pursue two-dimensional modeling, accounting for forces known to play a dominant role in oil movement. The approach selected, however, should be easily extendable to three dimensional modeling when appropriate.

BIBLIOGRAPHY

Alaska Department of Fish & Game, 1975. Miscellaneous data obtained from radar drogue study .

Burbank, D.C., 1974. Suspended sediment transport and deposition in Alaskan coastal waters, University of Alaska, Masters Thesis, 222p.

Burbank, D.C., 1977. Circulation studies in Kachemak Bay and Lower Cook Inlet, Alaska. Department of Fish & Game, Anchorage, Alaska (unpublished manual).

Dames & Moore, 1976, Report, oil spill trajectory analysis, Lower Cook Inlet, Alaska, for National Oceanic and Atmospheric Administration, Job Number 6769-003-20.

Fallah, M.H., and R.M. Stark, 1976. Literature Review: Movement of Spilled Oil at Sea, Marine Technology Society Journal, Vol. 10, No. 1, January.

Fay, J.A., 1969. The Spread of Oil Slicks on a Calm Sea, Fluid Mechanics Laboratory, Publication No. 69-6, Department of Mechanical Engineering, Massachusetts Institute of Technology, August.

Hoult, D.P., 1972. Oil Spreading on the Sea, in Annual Review of Fluid Mechanics, Vol. 4, pp. 341-368.

Isakson, J.S. , et al., 1975. Comparison of Ecological Impacts of Postulated Oil Spills at Selected Alaskan Locations, Mathematical Sciences Northwest, National Technical Information Service, Springfield, Virginia (Accession No. AD-A017-600), June.

Matthews, J.B., and J.C.Mungall, 1972, A Numerical tidal model and its application to Cook Inlet, Alaska, Journal of Marine Research, Volume 30, Number 1, January 15, pp 27-38.

Meunch, R.D., Mofjeld, H.O., Charnell, R.L., 1977. Oceanographic conditions in Lower Cook Inlet; spring and summer 1973. Contribution No. 351 from the NOAA ERL, Pacific Marine Environmental Laboratory.

Muirhead, C., 1978. Personal communication regarding availability of analyzed net and tidal current summaries from 1974 summer data measurement program in Cook Inlet, National Ocean Survey, National Oceanic and Atmospheric Administration, Rockville, Maryland, November.

Mungall, J.C.H., and J.B. Matthews, 1973. Numerical tidal models with unequal grid spacings, technical report R73-2, Institute of Marine Science, University of Alaska, Fairbanks, Alaska, January, 213 p.

Mungall, J.C.H., 1973. Cook Inlet tidal stream atlas, technical report R73-6, Institute of Marine Science, University of Alaska, Fairbanks, Alaska.

Mungall, J.C.H., 1978. Personal communication regarding interpretation of output data from runs of a hydrodynamic model of Cook Inlet. Runs made on Dames & Moore computer facilities and output maintained in job file, Los Angeles, California.

National Oceanic and Atmospheric' Administration, 1978. Tidal Current Tables, Pacific Coast of North America and Asia, 1978. National Ocean Survey, annual publication.

Oceanographic Institute of Washington, 1977. Modeling Methods for Predicting Oil Spill Movement, submitted to Oceanographic Commission of Washington, Seattle, Washington. March.

Pearson, C., and R.D. Muench, 1978. Personal communication regarding development of a net circulation pattern for Lower Cook Inlet, Pacific Marine Environmental Laboratory, National Oceanic and Atmospheric Administration, Seattle, Washington.

Premack, J., and G.A. Brown, 1973. Prediction of Oil Slick Motions in Narragansett Bay, Proceedings Joint Conference on Prevention and Control of Oil Spills, Washington, D.C., 13-15 March 1973, pp. 531-540.

Putnins, Paul, 1966. Studies on the Meteorology of Alaska: First Interim Report (The sequences of basic weather patterns over Alaska), U.S. Department of Commerce, ESSA, EDS, Silver Spring, MD 10910, 107 p.

Putnins, Paul, 1969. Studies on the Meteorology of Alaska: Final Report (Weather situations in Alaska during the occurrences of specific basic weather patterns), U.S. Department of Commerce, ESSA, Research Laboratories, Boulder, CO 80302, 267 p.

Schureman, Paul, 1958, Manual of Harmonic Analysis and Prediction of Tides, Coast and Geodetic Survey, U.S. Department of Commerce, Washington, D.C.

Wang, S., 1974. A Numerical Model for Simulation of Oil Spreading and Transport and its Application for Predicting Oil Slick Movement in Bays, Tetra Tech., Inc., Report No. TT-P-345-74-1, February.

APPENDIX A

OIL SPILL MODEL DOCUMENTATION

A-1 OVERVIEW

This appendix is intended to expand on the discussion contained in Section II describing the oil spill model used in the study. Particular emphasis is placed on the numerical algorithms in the model and the schemes used to implement them. Also included are several verification cases that illustrate the correct operation of the model.

A-2 TRAJECTORY ALGORITHM

One key aspect of the model operation is the input and interpolation of the wind and current fields. Data defining the spatial and temporal variation of the wind and current fields are prescribed at the intersection of the grid lines. Since the number of intersection points can become large (there are over 45,000 for the grid used in this study, see Figure 1), the model has been designed to accept input only at every nth intersection point where "n" is any integer up to the maximum dimension of the grid. Selection of this quantity is based on the variability of the wind and current fields and the level of detail of the input data. For this study, the net current field were input at every second grid point and the tidal current and wind fields at every third grid point.

The temporal variation of each of these fields is defined by specifying the entire spatial distribution at one or more times. If only *one* distribution is given for a field, that field is taken to be constant throughout the period of simulation. This was, in fact, the case for both the net current and wind fields. The temporal variation of the tidal current field was defined by specifying tidally driven currents at 12 points in the tidal cycle.

Once this data is input, certain initialization and "housekeeping" functions are performed and the actual computations begin. The program interpolates the wind and currents to the location of the spill centroid. The interpolation scheme used is a three-way linear interpolation on the two spatial dimensions and on time. Each of the vectors, wind, tidal

current and net current is interpolated independently. For each vector the program interpolates speed and direction separately using the following expressions :

$$S(x_0,y_0,t) = \frac{t_2-t}{t_2-t_1}\cdot\left[\frac{y_2-y_0}{y_2-y_1}\cdot\left(\frac{x_2-x_0}{x_2-x_1}\cdot S(x_1,y_1,t_1)+\frac{x_0-x_1}{x_2-x_1}\cdot S(x_2,y_2,t_1)\right)\right.$$

$$\left.+\frac{y_0-y_1}{y_2-y_1}\cdot\left(\frac{x_2-x_0}{x_2-x_1}\cdot S(x_1,y_2,t_1)+\frac{x_0-x_1}{x_2-x_1}\cdot S(x_2,y_2,t_1)\right)\right]$$

$$+\frac{t-t_1}{t_2-t_1}\cdot\left[\frac{y_2-y_0}{y_2-y_1}\cdot\left(\frac{x_2-x_0}{x_2-x_1}\cdot S(x_1,y_1,t_2)+\frac{x_0-x_1}{x_2-x_1}\cdot S(x_2,y_1,t_2)\right)\right.$$

$$\left.+\frac{y_0-y_1}{y_2-y_1}\cdot\left(\frac{x_2-x_0}{x_2-x_1}\cdot S(x_1,y_2,t_2)+\frac{x_0-x_1}{x_2-x_1}\cdot S(x_2,y_2,t_2)\right)\right]$$

where $S(x,y,t)$ = component of speed at a point (x,y) at time t

x_0,y_0 = location of spill centroid at time to

t_1,t_2 = times where input data are given where $t_1 \leq t \leq t_2$

and where x_1,y_1,x_2,y_2 are grid coordinates surrounding the spill centroid as shown in the following diagram.

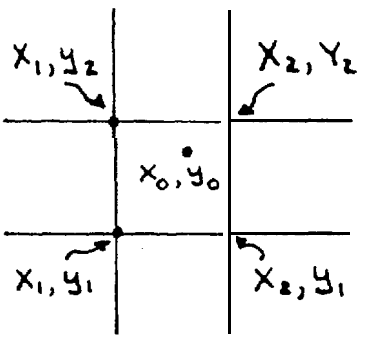

The total drift vector is then computed using Equation (1) of Section II and the movement of the oil slick centroid is then determined by that drift vector.

For example, suppose that the centroid is at a location (x_o,y_o) at time t. The drift vector (u_o,v_o) computed at that point then determines the new location (x_n,y_n) at time $t + \Delta t$ by

$$x_n(t+\Delta t) = x_o(t) + u_o\Delta t,$$

$$y_n(t+\Delta t) = ye(t) + v_o\Delta t.$$

The trajectory is terminated when either the simulation time exceeds an upper limit or the trajectory intersects a land or water boundary cell.

The program produces a printed output which summarizes the input parameters and the location of the spill at the termination point of the trajectory. Apart from the printed results, a plot of the trajectories is also produced. Up to 13 different trajectories can be displayed on one plot with each marked by a different symbol at selected times along the trajectory.

A-3 MODEL INPUT

The operational structure of the model input and output is illustrated below.

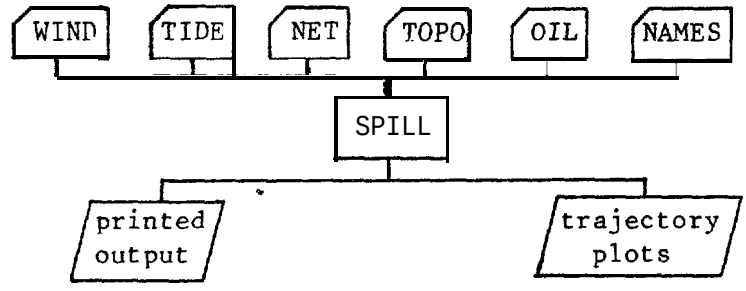

where denotes input data
denotes program
denotes output.

A brief description of each entity follows:

Entity	Description
WIND	Data file describing the spatial and temporal behavior of the wind field
TIDE	Data files describing the spatial and temporal behavior of the tidal current field
NET	Data files describing the spatial and temporal behavior of the net current field
OIL	Data file containing information on the oil itself (i.e., spill location, density, etc.), and the spill area (i.e., grid size, direction of magnetic north, etc.)
TOPO	Data file containing gridded information on location of land, water, and boundary cells
NAMES	Data file containing control names for data files
SPILL	Program that combines movement and spreading algorithms to produce map of oil distribution
RESULTS	Final output file containing listing of input data and the location of the spill at specified time steps. This file may be sent directly to the printer.
PLOTS	Trajectory plot.

A detailed listing of the data in each of these files is given below:

OIL

Variable	Units	Description
RUN	--	80-character alphanumeric description of the case this data file represents
SOP	--	Spreading option: = 1 - spreading = 2 - trajectory
DOP	--	Display option: (valid for SOP = 2 only) = 0 - display trajectory termination only = 1 - display trajectory at every PSTEP = 2 - display trajectory at every time step (DT)

PS TEP	--	Printing frequency given as an integer multiple of the time step (DT).
RH20*	gm/cc	density of seawater
ROIL*	gin/cc	density of oil
SIG*	dynes/cm	net surface tension spreading coefficient
NU*	cm^2/se	kinematic viscosity of seawater
YSPILL	kilometers	Y - coordinate of spill location
XSPILL	kilometers	x - coordinate of spill location
CW	--	wind coupling coefficient
C1*	--	inertial spreading coefficient
C2*	--	viscous spreading coefficient
C3*	--	surface tension spreading coefficient
ADE FL	degrees	angle between wind vector and resultant oil velocity vector
MAXDOSE*	gin/meter	maximum shoreline dosage
MINTHIK*	meters	minimum oil film thickness
IMAX	--	number of horizontal cells
JMAX	--	number of vertical cells
DS	kilometers	grid size

*These parameters were not used in this study, but are utilized in applications of the **Dames & Moore oil spill model** involving spreading as well as transport.

AGRI D	degrees	angle from x-axis to magnetic north, measured positive clockwise
DT	hours	time step
ST	hours	simulated period
DCYCLE*	hours	simulation period for force calculation
CUTOFF*	- -	first numerical constant for spreading calculation
RSALG*	--	second numerical constant for spreading calculation
CT(1)	hours	calculation start time in wind cycle
CT(2)	hours	calculation start time in tidal current cycle
CT(3)	hours	calculation start time in net current cycle
MFAC(1)	- -	number of cells at which wind data are input
MFAC(2)	- -	number of cells at which tidal current data are input
MFAC(3)	- -	number of cells at which net current data are input
EVAPP*	percent	maximum percent evaporation loss
EVAPT*	hours	maximum period of evaporation
XAXI S	inches	length of x-axis on plot
YAXIS	inches	length of y-axis on plot
Q*	kiloliters	volume of spill

Both wind and current data are input in the same format. For any given parameter, the total set of data can be schematically represented as follows:

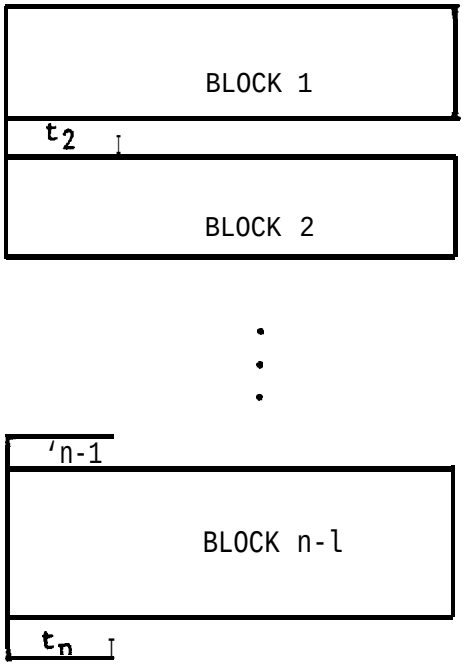

Block 1 data describe the spatial dependence of the wind or current fields at time t = 0. Block 2 describes the fields at t2, and so on. The last time, t_n, denotes the cycle time of that wind or current field. For times greater than t_n, the input file is rewound and reused with each time value increased by tn.

Within each block, the wind or current fields are input at every nth grid intersection. They are specified in the order (speed, direction) with FORMAT (16F5.0). The direction is relative to magnetic north (positive clockwise) and speed is in meters per second.

INPUT DATA FILES: TOPO

The topographic data file uses the following convention:

Cell	Value
"valid" water	4
"invalid" water	3
land	2
water boundary	1

Here "valid" and "invalid" denote water areas where oil may and may not be allowed by the model. These areas must be separated by a line of cells having a value of 1, the water boundary cell value.

Each cell within the grid is assigned, one value. For input convenience, each row may be specified by values in cells that are different from the adjacent cell in that row. The program will fill in the grid with the proper values.

The input is formatted so that the first five columns for each row is an identifier. Columns 6 to 80 correspond on a one-to-one basis with cells in a row. If there are more than 75 cells in a row, the same scheme is continued on the next record in columns 6 to 80.

INPUT DATA FILE: NAMES

Several sets of data may be processed in one run of the oil spill model. Input data file NAMES is the main control file for the spill model, directing it to the correct data files.

Each input line represents one case. The file names are input as follows :

COLUMNS	FILE
1 - 7	Name of the "OIL" data file
11 - 17	Name of the "TOPO" data file
21 - 27	Name of the "WIND" data file
31 - 37	Name of the "TIDE" data file
41 - 47	Name of the "NET" data file

The last card of this file must have the letter "END" in Column 1-3.

Examples of these input data files are included in the next section.

A-4 VERIFICATION

A series of test runs have been made where the trajectory can be analytically described from the solution of a set of differential equations. In addition, three test cases were run where the wind and net current fields were isolated to give a more qualitative the verification of the model.

The four analytic verification cases are all based on one set of driving forces that are simplified analogies of the actual environmental forcing fields used for this study. A constant wind, a spatially varying net current field and *a* temporally varying tidal current field defined on a 13 x 13 grid were run singly or in combination to test the model. The necessary data files used to run the verification cases are shown in Table A-1.

The OIL data file shown is best understood by reading it left to right, line by line, in correspondence with the list of input parameters given above (also, see Table A-2 for a restatement of the input data by the program itself).

TABLE A-1

VERIFICATION DATA FILES

OIL data file

2.	0.	20.	7.769	7.769			
1.	.85	9.5	00012	1000.	14.	50	8.
0.03	1.14	1.45	2.3	0.0	0.0	0.0	30.
13	13.	1.5	270.	0.1	8.	0.3	
0.0	0.0	O*O	13.	13.	13.0	0.0	0.1

TOPO data file

13	2	2
12	23314	42
11	2314	42
10	214	41
9	24	42
8	24	42
7	24	42
6	24	42
5	24	42
4	24	42
3	24	42
2	24	42
1	1	1

WIND data file

6.	180.	6.0	180.
6.	180.	6.0	180.
30.			

NET data file

0.0	270.	0.6	270.
0.0	270.	0.6	270.
30.			

TIDE data file

.4	0.	.4	0.
.4	0.	.4	0.
2.0			
.4	90.	.4	90.
.4	90.	.4	90.
4.0			
.4	180.	.4	180.
.4	180.	.4	180.
6.0			
.4	270.	.4	270.
*4	270.	.4	270.
8.0			

TABLE A-2

SAMPLE OF PROGRAM OUTPUT

D A M E S A N D M O O R E O I L S P I L L M O D E L

RUN IDENTIFICATION: VERIFICATION TEST TRAJECTORY MODE.

SPREADING OPTION 2
PRINT FREQUENCY 5
DENSITY OF OIL .850 (GM/CC)
KINEMATIC VISCOSITY .012 (CM**2/SEC)
WIND COUPLING COEFFICIENT .0300
VISCOUS SPREADING COEFFICIENT 1.45
WIND/OIL DEFLECTION ANGLE 0.0 (DEG)
MINIMUM FILM THICKNESS 0. (M)
NUMBER OF VERTICAL CELLS 13
MAG. NORTH-HORIZONTAL AXIS ANGLE 270.0 (DEG)
STOP TIME 30.0 (HRS)
SPREADING ALGORITHM 0
PRIMARY CURRENT START TIME 0.0000 (HRS)
WIND GRID MULTIPLE 13
RESIDUAL CURRENT GRID MULTIPLE 13
Y-COORDINATE OF SPILL LOCATION 5.00000E+00 (KM)
MAXIMUM PERIOD OF EVAPORATION .1 (HRS)
DATA CYCLE PERIOD 8.0000 (HRS)
Y-AXIS LENGTH 7.77 (INCHES)

DISPLAY OPTION O
DENSITY OF SEAWATER 1.000 (GM/CC)
SPREADING COEFFICIENT 9.500 (DYNES/CM)
SPILL VOLUME 1000.00 (KLS)
INERTIAL SPREADING COEFFICIENT 1.14
SURFACE TENSION SPREADING COEFFICIENT 2.30
MAXIMUM SHORE DOSEAGE 0.00 (GM/M)
NUMBER OF HORIZONTAL CELLS 1 3
GRID SIZE 1.50 (KM)
TIME STEP • &ofl(l (HRS)
CLJ1OFF .30
WIND START TIME 0.0000 (HRS)
RESIDUAL CURRENT START TIME 0.0000 (HRS)
PRIMARY CURRENT GRID MULTIPLE 13
X-COORDINATE OF SPILL LOCATION 1.40000E+01 (K
MAXIMUM EVAPORATIVE LOSS 0. PERCENT
DRIFT COMPUTATION END TIME 8.0000 (HRS)
X-AXIS LENGTH 7.77 (INCHES)

FIELD LENGTH REQUIRED IS 053502B

TRAJECTORY	1 TERMINATED AT CELL	10	13	AT TIME	20.400 HOURS.
TRAJECTORY	2 TERMINATED AT CELL	10	13	AT TIME	17.600 HOURS.
TRAJECTORY	3 TERMINATED AT CELL	2	10	AT TIME	13.600 HOURS.
TRAJECTORY	4 TERMINATED AT CELL	2	10	AT TIME	14.980 HOURS.

The TOPO data for this 13 x 13 grid was given a file name of TOPO. The first five columns are numbered 1 to 13 to correspond to the row numbers. Notice how the various areas are coded to represent land, water, and boundary cells.

The WIND file is very compact since a constant wind is easily specified. This file represents a wind with speed of 6 m/s and a direction of 180°. Since the grid is 13 x 13 and, by reference to the OIL data, input is specified at every 13th grid points, only four values are required to fill the entire grid.

The NET CURRENT file illustrates data varying in space. This data represents a current that gradually changes its speed along the X axis. At X = 0 the current is 0.0 m/s, at X = 13 cells, the current is 0.6 m/s. This current is at constant direction of 270 degrees (current toward west) .

The TIDE CURRENT file illustrates data changing with time. This is a tide of constant speed of 0.4 m/s that periodically changes its direction in a circular manner from 0 degrees at t=0 to 360 degrees at t=8 hours.

The four verification cases run using these input data files are listed below:

CASE I. Constant Drift

This case shows the spill movement as a result of a constant wind. The analytic solution is:

$$\bar{V} = C_w \cdot V_w \hat{j} \cdot 0.648 \hat{j}$$
$$y(t) = 0.648 \cdot t + y_0$$
$$x(t) = x_0$$

where C_w = wind coupling coefficient = 0.03
V_w = wind speed = 6 m/s
x_0, y_0 = centroid starting position
$x(t), y(t)$ = centroid position as a function of time

CASE 11. Time-Dependent Drift

This case tests input data varying with time and shows the location of the spill centroid *as* a result of the wind and tide. The analytic solution is:

$$\bar{v} = c_w \cdot v_w \hat{j} + v_t \cdot \cos\left(\frac{\pi}{4} \cdot t\right)\hat{j} + v_t \cdot \sin\left(\frac{\pi}{4} \cdot t\right)\hat{i}$$

$$= 0.648\,\hat{j} + 1.44 \cdot \cos\left(\frac{\pi}{4} \cdot t\right)\hat{j} + 1.44 \cdot \sin\left(\frac{\pi}{4} \cdot t\right)\hat{i}$$

$$y(t) = 0.648 \cdot t + 1.44 \cdot \frac{4}{\pi} \cdot \sin\left(\frac{\pi}{4} \cdot t\right) + y_0$$

$$x(t) = -1.44 \cdot \frac{4}{\pi} \cdot \cos\left(\frac{\pi}{4} \cdot t\right) + x_0 + 1.44 \cdot \frac{4}{\pi}$$

where the same parameters as Case I are in use.

CASE III. Space-Dependent Drift

This case tests input data varying over space and shows the location of the spill centroid as a result of the wind and net current. The analytic solution is:

$$\bar{v} = c_w \cdot v_w \hat{j} - v_n \cdot x \hat{i}$$

$$= 0.648\,\hat{j} - \frac{216}{1950} \cdot x \hat{i}$$

$$x = x_0 \cdot e^{\frac{-216}{1950} t}$$

$$y = 0.648 \cdot t + y_0$$

CASE IV. Compound Drift

This case illustrates both time and spatially-dependent driving fields and is a combination of Cases II and III. The analytic solution is:

$$\bar{V} = C_w \cdot V_w \hat{j} + V_t \cdot \cos\left(\frac{\pi}{4} \cdot t\right) \hat{j} + V_t \cdot \sin\left(\frac{\pi}{4} \cdot t\right) \hat{i} - V_n \cdot x \hat{i}$$

$$= 0.648 \hat{j} + 1.44 \cdot \cos\left(\frac{\pi}{4} \cdot t\right) \hat{j} + 1.44 \cdot \sin\left(\frac{\pi}{4} \cdot t\right) \hat{i} - \frac{216}{1950} \cdot x \hat{i}$$

$$y(t) = 0.648 \cdot t + 1.44 \cdot \frac{4}{\pi} \cdot \sin\left(\frac{\pi}{4} \cdot t\right) + y_0$$

$$x(t) = 0.2s3s \cdot \sin\left(\frac{\pi}{4} \cdot t\right) - 1.7977 \cdot \cos\left(\frac{\pi}{4} \cdot t\right) + 15.7977 \cdot e^{-\frac{216}{1950} \cdot t}$$

These four cases were run using the oil spill program with a time step of 0.1 and 0.4 hours. The printer output, plots of the analytic solution, and plots of the verification runs are shown in Table A-2 and Figures A-1 to A-3. The differences between the analytic and computed solutions are due to a finite time step and are summarized below.

Displacement (km) of Spill at t = 10 hrs

		Computed Solutions		Relative Difference	
Trajectory	Analytic Solution	Δt = 0.1 hr	Δt = 0.4 hr	Δt = 0.1 hr	Δt = 0.4 hr
1	6.48	6.48	6.48	0.0%	0.0%
2	8.51	8.57	8.72	0.7%	2.4%
3	11.40	11.42	11.49	0.17%	0.78%
4	11.91	12.03	12.38	1.00%	3.9%

These results provide confidence that the program correctly implements the basic movement algorithm and that a 0.4-hour time step was adequate for use in the remainder of the production runs.

The remaining verification runs were made after the input data for the actual current and wind data was ready for analysis. These runs, which consisted of using the net current and selected wind fields in isolation, serve to partially verify these data sets and to verify operation of the model under more complex conditions than the analtyic verification cases. The results are shown in Figures A-4 through A-9. Hand calculations indicate that these trajectories are consistent with "eyeball''i nterpolation of the input data.

REVISIONS
BY _____ DATE _____

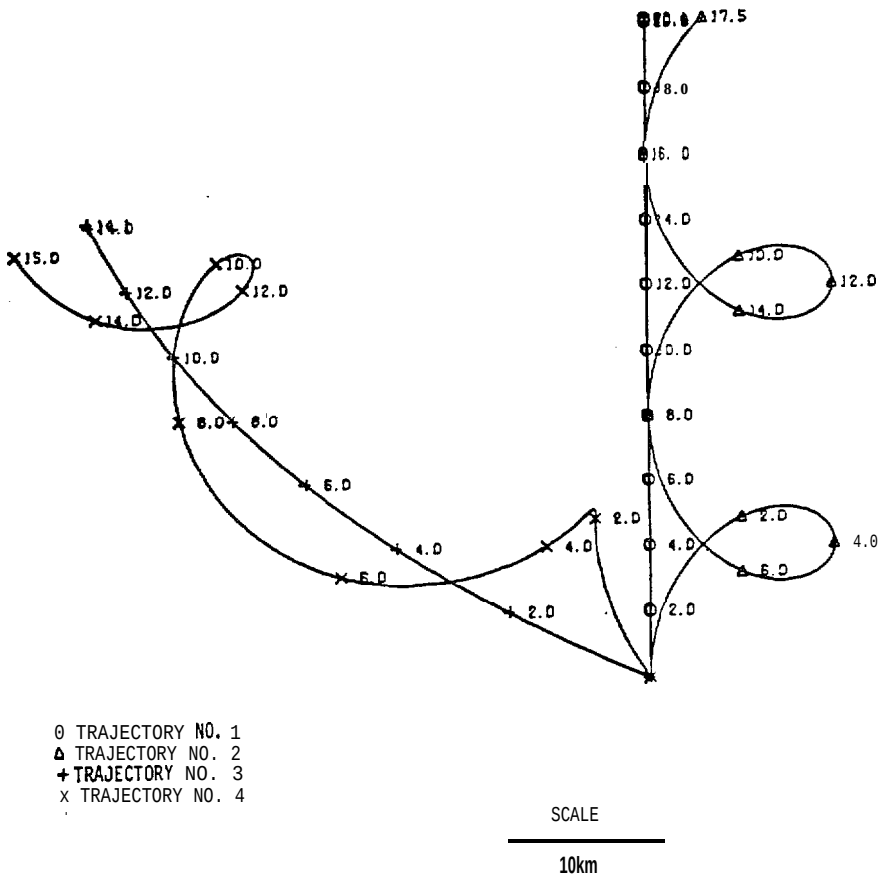

FIGURE A-1: ANALYTIC SOLUTION-VERIFICATION RUNS

DAMES & MOORE

BY _____ DATE _____
CHECKED BY _____

946.7 (REV. 6-61)

REVISIONS BY DATE

BY DATE

CHECKED BY FILE

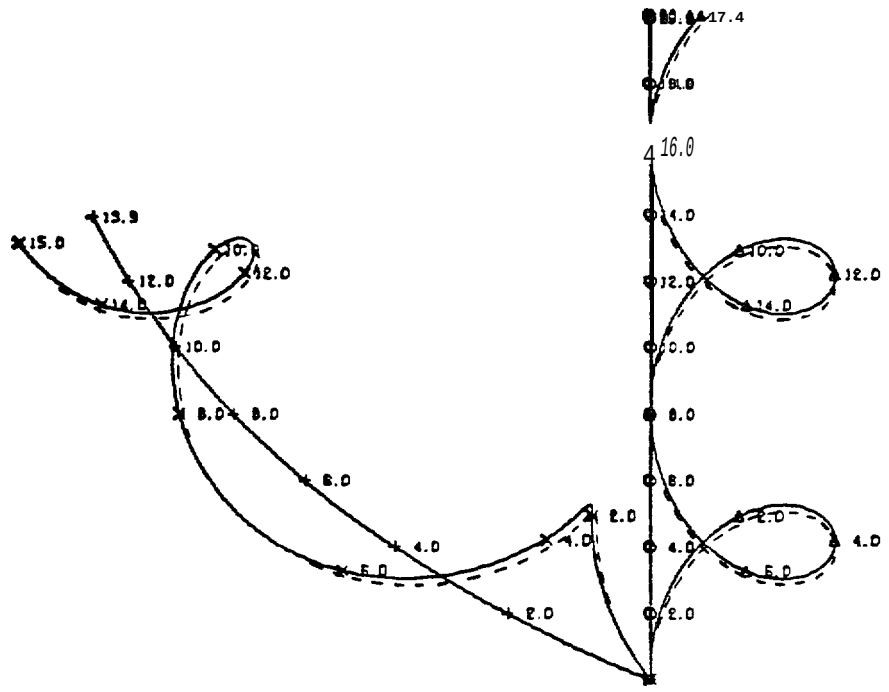

----- **ANALYTIC** TRAJECTORY

— COMPUTED TRAJECTORY

o TRAJECTORY NO. 1
Δ TRAJECTORY NO. 2
\+ TRAJECTORY NO. 3
X TRAJECTORY NO. 4

SCALE

10km

FIGURE A-2: COMPUTED SOLUTION-VERIFICATION RUNS, ΔT=0.1 HRS

DAMES & MOORE

946.7 (REV. 6-61)

REVISIONS BY DATE

FILE

BY DATE

CHECKED BY

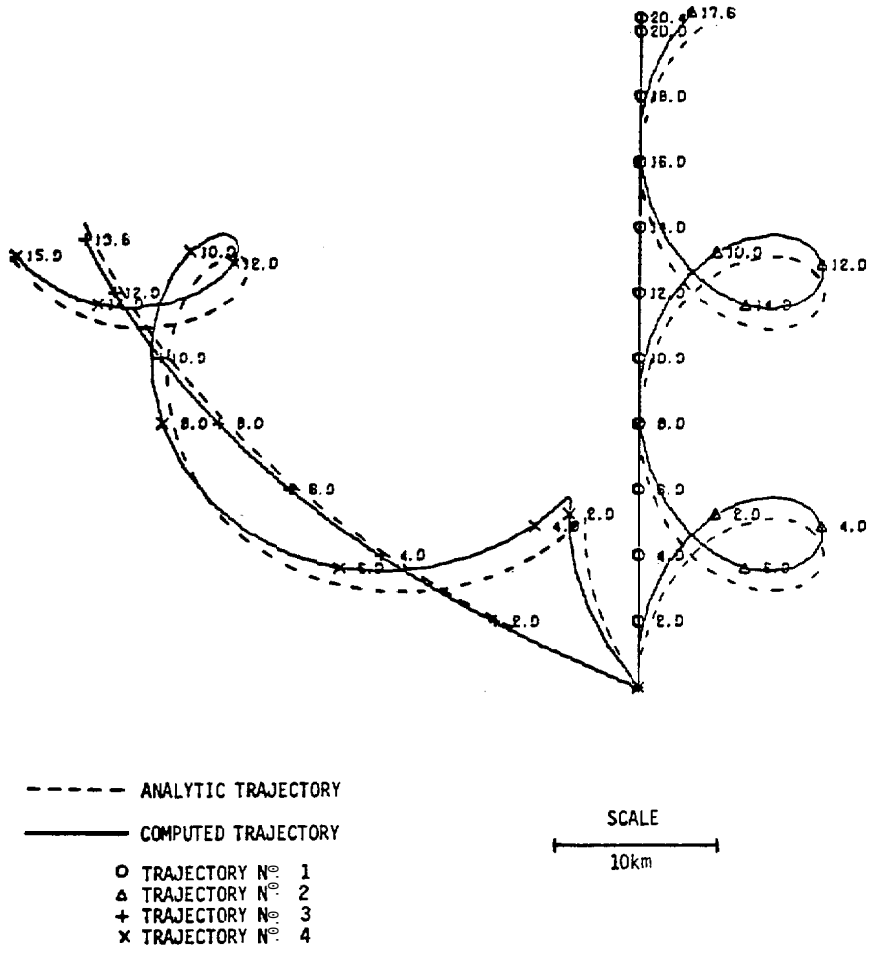

FIGURE A-3: COMPUTED SOLUTION-VERIFICATION ≥UNS. ΔT=0.4 HRS

DAMES & MOORE

946.7 (REV. 6-61)

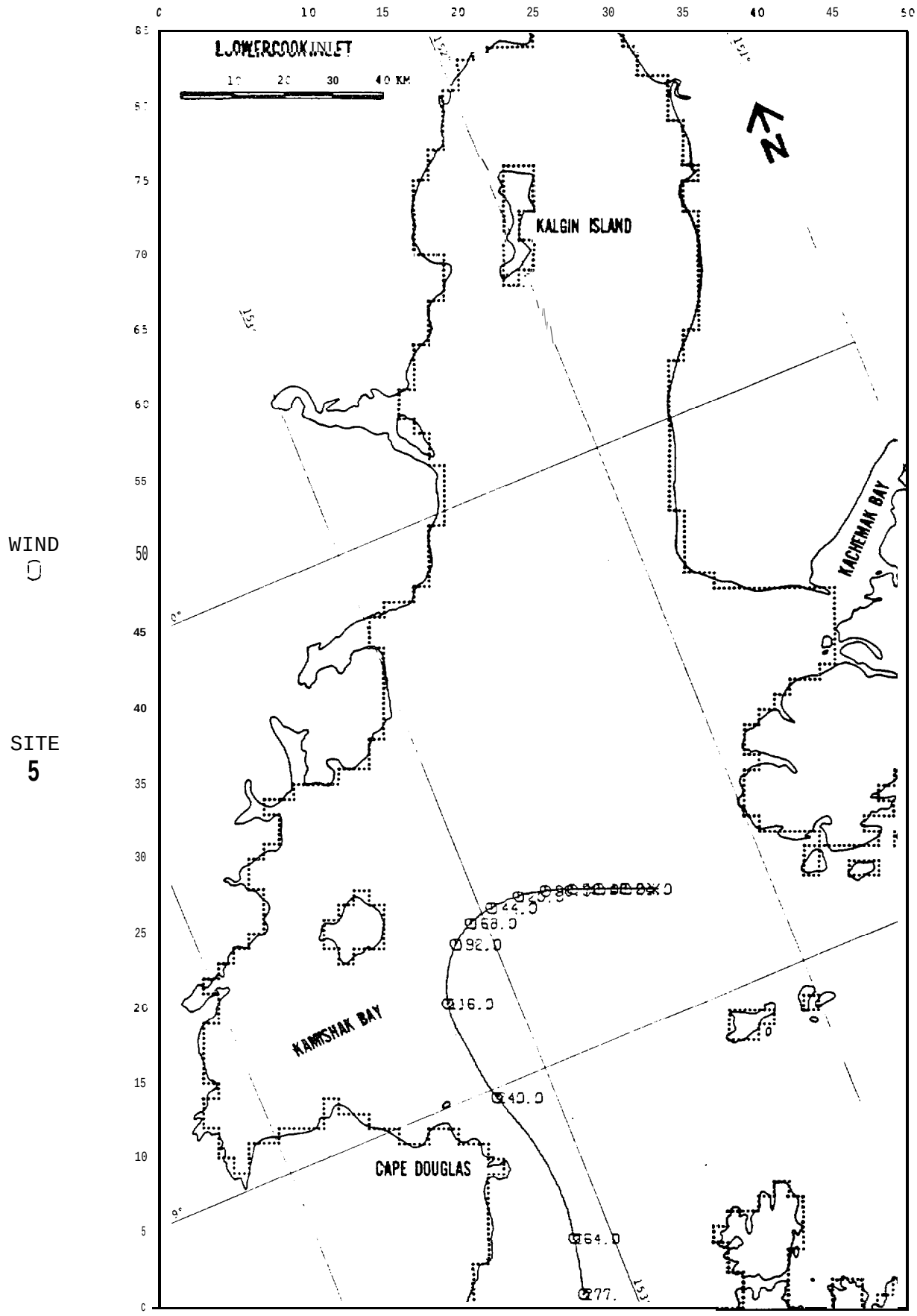

FIGURE A-4: VERIFICATION: NET CURRENT ONLY

WIND
1

SITE
5

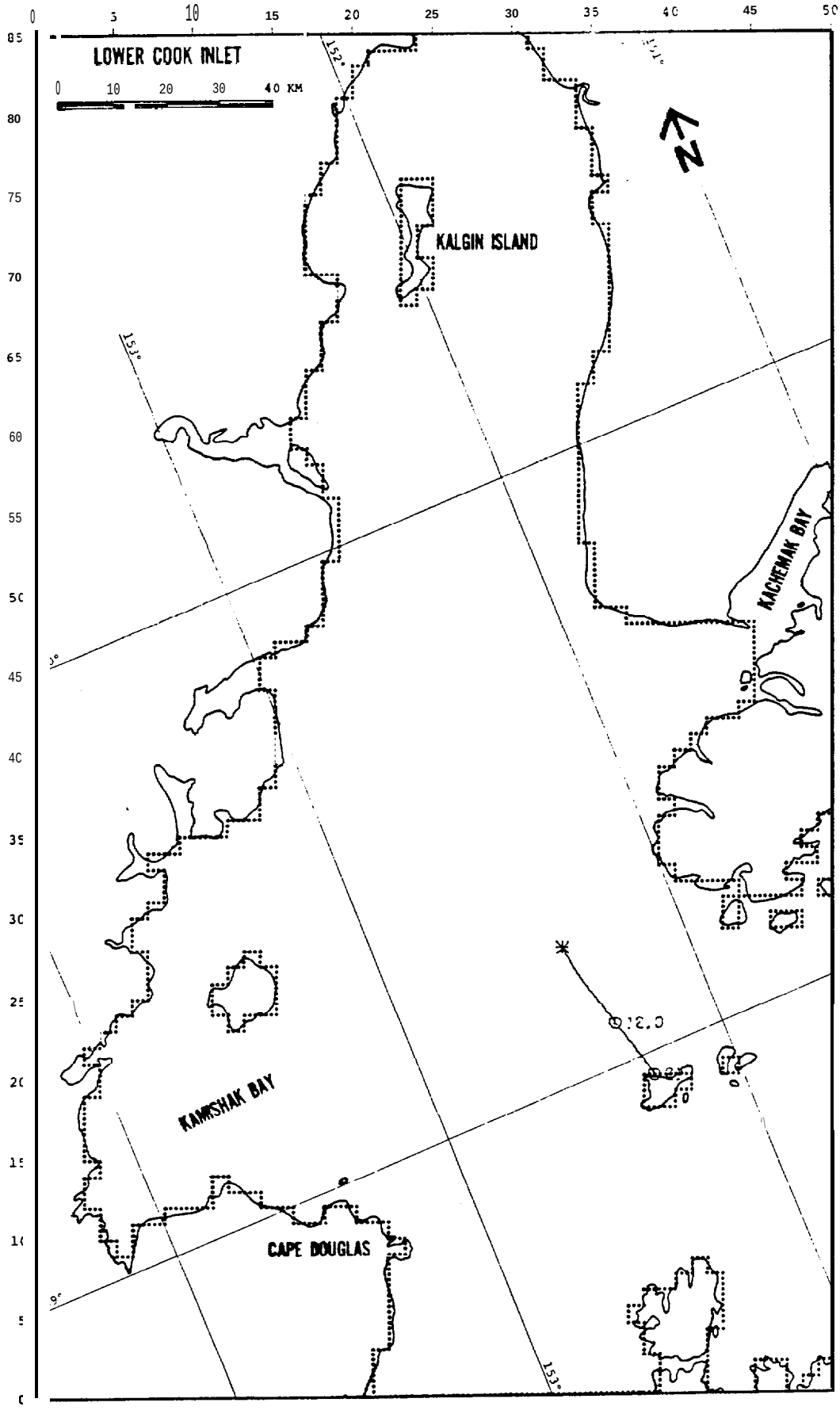

FIGURE A-5: VERIFICATION: WIND 0NL%

WIND
3

SITE
5

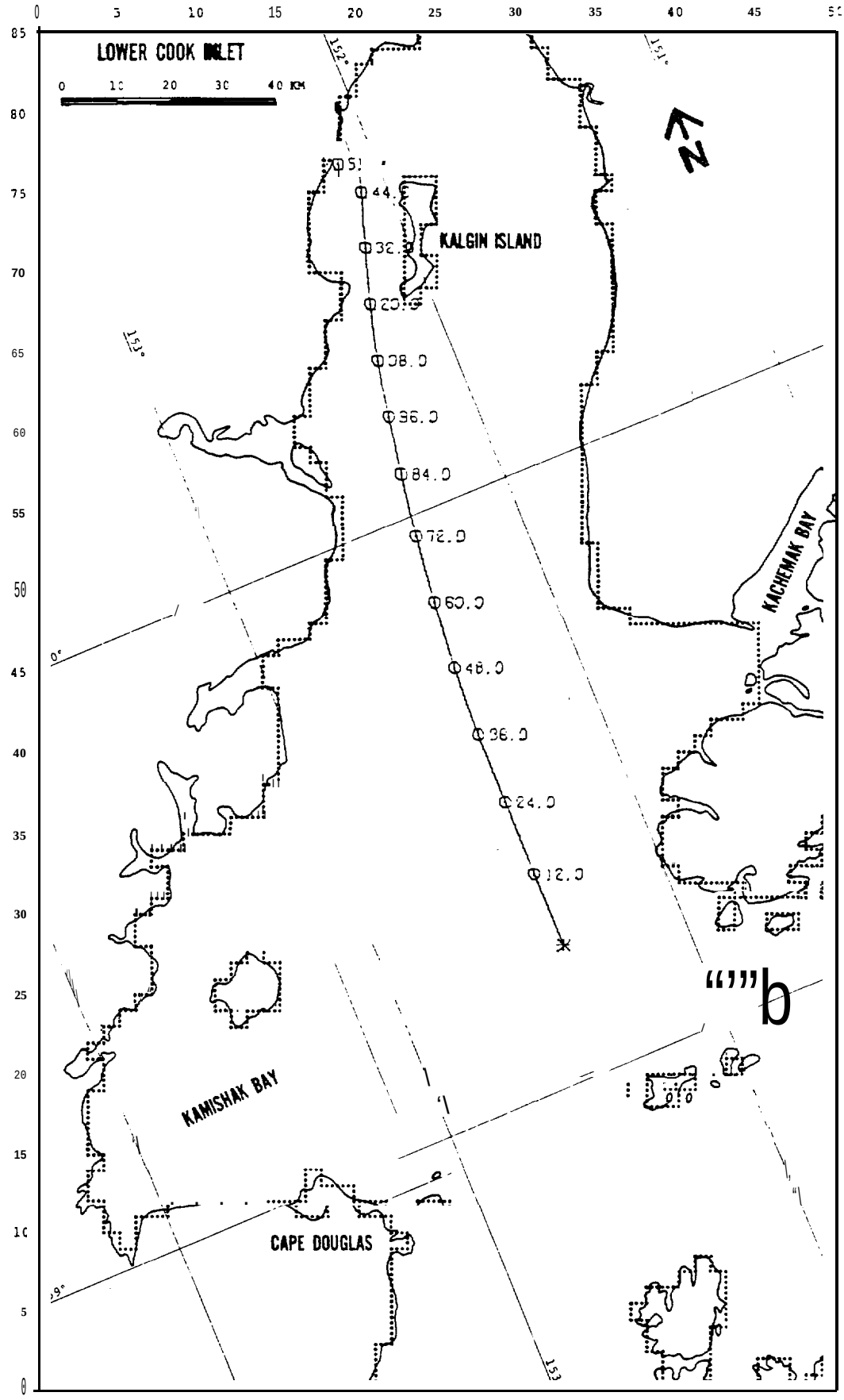

FIGURE A-6: VERIFICATION: WIND ONLY

WIND
5

SITE
5

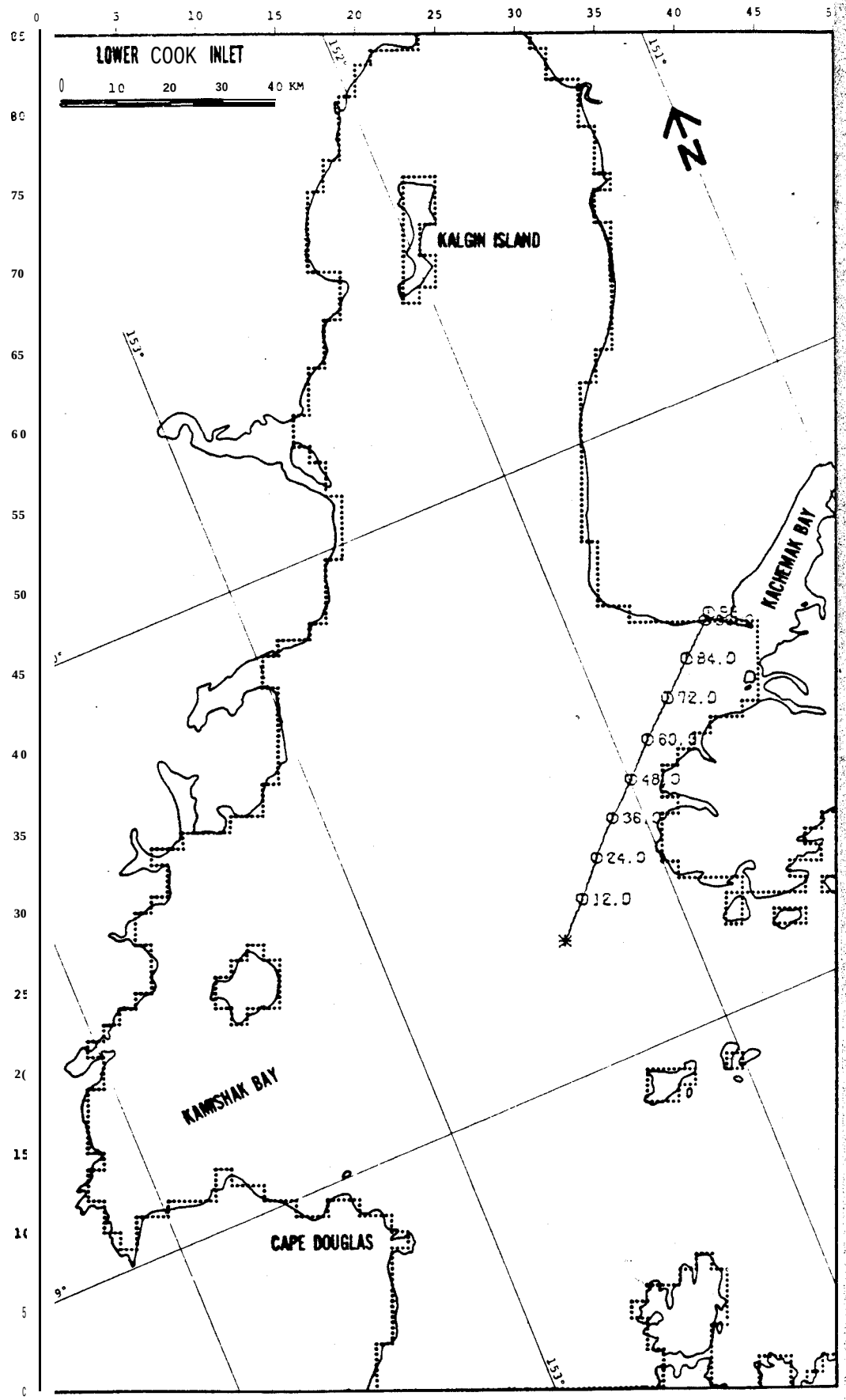

FIGURE A-7: VERIFICATION: WIND ONLY

PROGRAM LISTING

OIL SPILL PROGRAM LISTING

PROGRAM SPILL

```
*DECK SPILL
      PROGRAM SPILL (INPUT,OUTPUT,TAPE1,TAPE2,TAPE3,TAPE4,TAPE7,TAPE9,
     .              TAPE5=INPUT,TAPE6=OUTPUT)
      COMMON X(1)
C*********************************************************************
c     TAPE1 - WIND DATA (INPUT)                                      *
c     TAPE2 - TIDE DATA (INPUT)                                      .
c     TAPE3 - NET CURRENT DATA   (INPUT)                             .
c     TAPE4 - GEOGRAPHIC DATA  (CELL DEFINITION) (INPUT)             .
c     TAPE5 - CONTROL INFORMATION (INPUT)                            .
c     TAPE6 - HESSAGE FILE (OUTPUT)                                  .
c     TAPE7 OIL DATA FILE   (INPuT}                                  .
c     TAPE9 - PLOT FILE (OUTPUT)                                     .
C*********************************************************************
      CALL PREP
      END
```

SUBROUTINE CELLIO

```
*DECK CELLIO
      SUBROUTINE CELLIO(CELL,IMAX,JMAX)
C*********************************************************************
c     THIS SUBROUTINE READS THE CELLS DEFINITION.                    .
c     CONVENTION USED:                                               .
C     1 - WATER BOUNDARY                                             .
C   2  -  LAND                                                       .
C     3 - INVALID WATER                                              .
c     4 - VALID WATER                                                .
c     BLANK  CELL IS OF THE SAME TYPE AS THE CELL TO ITS LEFT        *
C*********************************************************************
      INTEGER CELL (IMAX,JMAX),FIRST
      IER=0
      DO 5 JJ=1,JMAX
      J=JMAX-JJ+1
      N=O
      READ(4,1009) ID,(CELL (I,J),I=1,IMAX)
      DO 5 I=1,IMAX
C**   CHEKING VALIDITY OF CELL TYPE.
      IF(CELL(I,J).GE.0.AND.CELL(I,J).LE.4) GO TO 1
      IER=1
      WRITE(6,1004) ID,I,J,CELL(I,J)
    1 N=N+1
      IF(CELL(I,J).EQ.0) GO To 5
      IF(N.EQ.1) GO TO 4
      IF(FIRST.NE.CELL(I,J)) GO TO 2
      N=I-N
      00 3 K=N,I
    3 CELL(K,J)=FIRST
      GO TO 4
    2 WRITE(6S1OO5) ID,I,J,FIRST,CELL(I,J)
      IER=1
    4 FIRST=CELL(I,J)
      N=0
    5 CONTINUE
      DO 8I=1,IMAX
      DO 8J=1,JMAX
    8 CELL(I,J)=CELL(I,J)-4
      RETURN
 1004 FORMAT(3X,*CELL VALUF OUT OF RANGE.ID=  ●OA5S*I= ● 913**J= ● 9139
     .        *CELL(I,J)= *,I1)
 1005 FORMAT(3X,*ERROR IN cE LL DATA AT LINE ID ● QA5s* Row *,I4,* COL ● S
     .        I4,* LABEL *,I2,* TO ● ,12)
 1009 FORMAT(A5,75I1,/,(5X,75I1))
      END
```

SUBROUTINE PREP

```
      *DECK PREP
            SUBROUTINE PREP
      C*************************************************************************
      c     SUBROUTINE PREP READS AND PRINTS THE PROBLEM PARAMETERS          *
      c     AND CONVERS THIS PARAMETERS TO THE UNITS USED BY THE PROGRAM.    *
      C*************************************************************************
            COMMON X(1)
            INTEGER PSTEP,SOP,DOP,RUN(8),BLANK,CELLS,PROB,SALG,PLNO,WIND, TIDE
            REAL NU,MAXDOSE,MINTHK
            COMMON /DATA/ PSTEP,DT,ST,DS,CELLS,BLANK ,AGRID,ADEFL,CW,DOP,
           .              XSPILL,YSPILL,MFAC(3),CT(3)
            COMMON /CPLOT/ XAXIS,YAXIS,XPLFAC,YPLFAC,PLNO
            DATA BLANK /10H          /, IEND /3HEND/,PLNO /0/
      C**   PROB  - FILE OF PROBLEM Parameters.
      C**   CELLS - FILE CONTAINS CELLS DEFINITION.
      C**   WIND  - FILE OF WIND DATA.
      C**   TIDE  - FILE OF TIDIAL CURRENT.
      C**   NET   - FILE OF NET CURRENT DATA.
            CALL PLOTS(-5.0,-200.0,9)
            CALL PLOT(0.,3.,-3)
          1 READ(5,1001)PROB,CELLS,WIND,TIDE,NET
      C**   PLNO - TRAJECTORY NUMBER.
            PLNO=PLNO+1
            IF(PROB.EQ.IEND)9,8
          9 CALL PLOT(0.0,0.0,999)
            STOP
          8 IF(PROB.EQ.BLANK) GO TO 3
            REWIND 7
            CALL DFUR(3HGET,7,PROB,0,ISTA)
            IF(ISTA.EQ.0) GO TO 2
            URITE[6S 1OO2)PROB,ISTA
            STOP 7
      C**   READING PROBLEM PARAMETERS.
          2 READ(7s1OO1) RUN
            I?EAD(7$1OO3) RSOP,RDOP,RPSTEP,XAXIS,YAXIS
            READ(7,1003) RH20,ROIL,SIG,NU,Q,XSPILL,YSPILL,PERIOD
            READ(7*1OO3) CW,C1,C2,C3,ADEFL,MAXDOSE,MINTHK,ST
            READ(791Oos) RIMAX,RJMAX,DS,AGRID,DT,DCYCLE,CUTOFF,RSALG
            READ(7,1003) CT(1),CT(2),CT(3),RMFACW,RMFACP,RMFACR,EVAPP,EVAPT
            PLNO=1
            DECOLIE (1OS91OOWIND) IWIND
            DECOOE( 1OSY1O9PROMI ISPILL
      910   FORMAT(4X,A1)
            PSTEP=RPSTEP
            SOP=RSOP
            DOP=RDOP
            IMAX=RIMAX
            JMAX=RJMAX
            SALG=RSALG
            MFAC(1)=RMFACW
            MFAC(2)=RMFACP
            MFAC(3)=RMFACR
      C**   PRINTING PROBLEM PARAMETERS.
            WRITE(6,1006) ISPILL,IWIND,SOP,DOP,PSTEP,RH20,ROIL ,SIG,NU,Q,CW
           .,C1,C2,C3
            WRITE(6,1007) ADEFL,MAXDOSE,MINTHK, IMAX,JMAX ,DS,AGRID,DT,ST,
           .              CUTOFF,SALG,CT(1),CT(2),CT(3),MFAC(1),MFAC(2)
            WRITE(6,1005) MFAC(3),XSPILL,YSPILL ,EVAPP,EVAPT,DCYCLE,PERIOD,
           .              XAXIS,YAXIS
            IMAXP1=IMAX+1
            JMAXP1=JMAX+1
            IJ=IMAX*JMAX
            IJP1=IMAXP1*JMAXP1
      C**   GRID SIZE IN METERS.
            DS=DS*1000.
```

```
C**   COORDINATES OF SPILL LOCATIONS IN METERS.
      XSPILL=XSPILL*1000.
      YSPILL=YSPILL*1000.
C**   PLOTTING SCALE-FACTOR.
      XPLFAC=XAXIS/FLOAT(IMAX)/DS
      YPLFAC=YAXIS/FLOAT(JMAX)/DS
    3 IF (CELLS.EQ.BLANK) GO TO  4
C**   GETTING CELLS DEFINITION FILE.
      REWIND 4
      CALL DFUR(3HGET,4,CELLS,0,ISTA)
      IF(ISTA.EQ.0) GO TO 4
      WRITE(6,1002) CELLS,ISTA
      STOP 3
C**   GETTING WIND DATA FILE.
    4 REWIND 1
      IF(WIND.EQ.BLANK) GO TO  5
      CALL DFUR(3HGET,1,WIND,0,ISTA)
      IF(ISTA.EQ.0) 60 TO 5
      WRITE(6,1002)WIND,ISTA
      STOP 1
C**   GETTING TIDEDATAFILE
    5 REWIND 2
      IF(TIDE.EQ.BLANK)GO TO 6
      CALL DFUR(3HGET,2,TIDE,0,ISTA)
      IF(ISTA.EQ.0) GO TO 6
      WRITE(691002) TIOEVIS1 A
      STOP 2
C**   GETTINGNET CURRENT OATA FILE.
    6 REWIND 3
      IF(NET.EQ.BLANK) GO TO 7
      CALL DFUR(3HGET,3,NET,0,ISTA)
      IF(ISTA.EQ.0) GO TO 7
      WRITE(6s 1OU2)NETSISTA
      STOP 3
    7 N1=5
      N2=N1+6*IJP1
      N3=N2+6*IJP1
      N4=N3+IJ
      N9=LOCF(X(1))+N4
      IF (PROB.NE.BLANK) WR1TE(6S1OO8) N9
C** FOR NOAA JOB 1978
      CT(2)=FLOAT(PLNO-1)*PERIOD/1O*
C**   INITIALIZE TRAJECTORY PLOT.
       CALL PLINIT
     .      (PLNO,XAXIS,YAXIS,XPLFAC,YPLFAC,XSPILL,YSPILL,PROH,WIND)
      CALL SLICK(IMAX,JMAX,IMAXP1,JMAXP1,X(N1),X(N2),X(N3))
      GO TO 1
 1001 FORMAT(8A10)
 1002   FORMAT(1H1,3X,*UNABLE TO GET FILE *,A7,*ISTA=*,I2)
 1003 FORMAT(8F10.0)
 1005 FORMAT(T10,*NET CURRENT GRID MULTIPLE *,I3,
     .       T65,*X-COORDINATE OF SPILL LOCATION *,1PE12.5,*(KM)*,/,
     .       TIOt*Y-COORDINATE OF SPILL LOCATION*,1PE12.5,*(KM)*,
     .       T65,*MAXIMUM EVAPORATIVE LOSS*,0PF3.0,* PERCENT *,/,
     .       TIO**MAXIMUM PERIOD OF EVAPORATION *,F4.1,*(HRS)*,
     .       T65,*DRIFT COMPUTATION END TIME *,F8.4,6H(HRS),/,
     .       TIOT*OATA CYCLE PERIOD*,F8.4,6H(HRS),
     .       T65,*X-AXIS LENGTH *,F7.2,9H (INCHES),/,
     .       T10,*Y-AXIS LENGTH*,F7.2,9H (INCHES))
 1006*FOHMAT (1H1ST3OS*D A M E S   A N D   H O O R E   O I L   S P I L L*,
     .       *  M O D E L*,///,
     .       T20,*RUN IDENTIFICATION: *,8A10
     .     //T10,*SPREADING OPTION *I2,
     .       T65,*DISPLAY OPTION *,I2,/,
     .       T10,*PRINT FREQuENCY ● *13s
     .       T65,*DENSITYOF SEAWATER ● *F6,3#8H (GM/CC),/,
     .       TIO**DENSITY OF OIL *,F6.3,8H(GM/CC),
     .       T65,*SPREADING COEFFICIENT *,F6.3,*(DYNES/CM)*,/,
     .       TIOS*KINEMATIC VISCOSITY ● sF6.3s12H (CM**2/SEC),
     .       T65,*SPILL VOLUME ● *FB.2** (KLS)*,/,
```

```
     .       TIO**WIND COUPLING COEFFICIENT *,F6.4,
     .       T65,*INERTIAL SPREADING COEFFICIENT ● sF5.2*/s
     .       TIOS*VISCOUS SPREADING COEFFICIENT *,F5.2,
     .       T65,*SURFACE TENSION SPREADING COEFFICIENT *,F5.2)
140  1007 FORMAT(T10,*WIND/OIL DEFLECTION ANGLE ● *F5.1,6H (DEG),
     .       T65,*MAXIMUM SHORE DOSAGE*,F6.2,*(GM/M)*,/,
     .       TIO**MINIMUM FILM THICKNESS *,1PE12.5,*(M)*,
     .       T65,*NUMBER OF HORIZONTAL CELLS ● 9149/9
     .       T10,*NUMBER OF VERTICAL CELLS ● *140
145  .       T65,*GRID SIZE *,0PF6.2,* (KM)*,/,
     .       TIO$*MAG. NORTH-HORIZONTAL AXIS ANGLE *,F6.1,6H(DEG),
     .       T65,*TIME sT EP *,F8.4,6H(HRS),/,
     .       TIOS*STOP TIME *,F8.1,6H(HRS),
     .       T65,*CUTOFF ● sF5.2s/s
150  .       T10,*SPREADING ALGORITHM *,I2,
     .       T65,*WIND START TIME ● oF8.4s6H (HRS),/,
     .       T10,*TIDE CURRENT START TIME ● $F8.4S6H (HRS),
     .       T65,*NET CURRENT START TIME *,F8.4,6H(HRS),/,
     .       T10,*WINDGRID MULTIPLE *,I3,
155  .       T65,*TIDE CURRENT GRID MuLTIPLE ● ,13)
     1008 FORMAT(//8X,*FIELD LENGTH REQUIRED IS *,06*8*//)
          END
```

SUBROUTINE SLICK

```
1         *DECK SLICK
          SUBROUTINE SLICK(IMAX,JMAX,IMAXP1,JMAXP1,SPD,DIR,CELL)
          C*****************************************************************
          c     THIS sUBROUTINE COMPUTE THE TRAJECTORY OF THE SPILL.       *
5         c     UNITS OF CALCULATION ARE IN M,K,S                          .
          C     BESIDES:                                                   *
          c               SPEED = METERS/HR                                *
          c               T,DT  = HRS.                                     *
          C*****************************************************************
10        INTEGER STEP,PSTEP,BLANK,CELLS,DOP,CELL,PLNO
          DIMENSION CELL(IMAX,JMAX),
          .          SPD(IMAXP1,JMAXP1,6),DIR(IMAXP1,JMAXP1,6)
          COMMON /DATA/ PSTEP,DT,ST,DS,CELLS,BLANK,AGRID,ADEFL,CW,DOP,
          .             XSPILL,YSPILL,MFAC(3),CT(3)
15        COMMON /CPLOT/ XAXIS,YAXIS,XPLFAC,YPLFAC,PLNO
          DIMENSION PERIOD(3),CYCLE(3),SPEED(3),DIRCT(3),TDRIFT(3,2)
          DATA PI /180./,TWOPI /360./
          C**   READ CELLS DEFINITION.
          IF(CELLS.NE.BLANK) CALL CELLIO(CELL,IMAX,JMAX)
20        C***  INITIALIZATION.
          T=O,
          XMAX=DS*FLOAT(IMAX)
          YMAX=DS*FLOAT(JMAX)
          XOLD=XSPILL
25        YOLD=YSPILL
          IOLD=INT(XSPILL/DS)+1
          JOLD=INT(YSPILL/DS)+1
          NSTEPS=ST/DT+1
          DO 5 K=1,3
30        K2=K+3
          TDRIFT(K,2)=-CT(K)
          TDRIFT(K,1)=9999.9
          CYCLE(K)=1.
          PERIOD(K)=0.
35        NJUMP=MFAC(K)
          C**   READING DRIFT INFORMATION
          DO 5 JJ=1,JMAXP1,NJUMP
          J=JMAXP1-JJ+1
          READ(Ks51O) (SPD(I,J,K2),DIR(I,J,K2),I=1,IMAXP1,NJUMP)
40     5 CONTINUE
          C-------- -------- --------------- -------- -------- ------ . . . . . -----
          C     START MAIN CALCULATION LOOP
          c---------------  --------  ----------------------  ------------
          DO 2STEP=1,NSTEPS
45        C*** CHECK WHETHER TO READ NEW DRIFT VALUES.
```

```
      DO 40 K=1,3
   10 IF (T.GE.TDRIFT(K,1).AND.T.LE.TDRIFT (K,2)) GOTO 40
C**   REPLACEMENT.
      K2=K+3
   50 NJUMP=MFAC(K)
      TDRIFT(K,1)=TDRIFT(K,2)
      DO 15 J=1,JMAXP1,NJUMP
      DO 15I=1,IMAXP1,NJUMP
      SPD(I,J,K)=SPD(I,J,K2)
   55 15 DIR(I,J,K)=DIR(I,J,K2)
C**   READING SPEED ANO DIRECTION AT NEW TIME LEVEL.
      READ(K,510) TIM
   20 DO 25 JJ=1,JMAXP1,NJUMP
      J=JMAXP1-JJ+1
   60 READ(K*51O) (SPD(I,J,K2),DIR(I,J,K2),I=1,IMAXP1,NJUMP)
      IF (EOF(K)) 30,25
   30 REWIND K
      CYCLE(K)=CYCLE(K)+1.
      PERIOD(K)=TIM
   65 TIM=0.
      GOTO 20
   25 CONTINUE
      TDRIFT(K,2)=(CYCLE(K)-1.)*PERIOD(K)-CT(K)+TIM
      GOTO 10
   70 40 CONTINUE
C**   INTERPOLATING SPEED ANDDIREECTION TO THE CURRENT LOCATION
      DO 45 K=1,3
      K2=K+3
C**   WEIGHTING FACTORS.
   75 TFM=(TDRIFT(K,2)-T)/(TDRIFT(K,2)-TDRIFT(K,1))
      TFP=1.-TFM
      NJUMP=MFAC(K)
      I1=((IOLD-1)/NJUMP)*NJUMP+1
      I2=I1+NJUMP
   80 J1=((JOLD-1)/NJUMP)*NJUMP+1
      J2=J1+NJUMP
      XFM=((I2-1)*DS-XOLD)/DS/NJUMP
      XFP=1.-XFM
      YFM=((J2-1)*DS-YOLD)/DS/NJUMP
   65 YFP=1.-YFM
C**   SPEED INTERPOLATION.
      SPEED(K)=TFM*(YFM*(XFM*SPD(I1,J1,K)+XFP*SPD(I2,J1,K))+
     .           YFP*(XFM*SPD(I1,J2,K)+XFP*SPD(I2,J2,K)))+
     .         TFP*(YFM*(XFM*SPD(I1,J1,K2)+XFP*SPD(I2,J1,K2))*
   90 .           YFP*(XFM*SPD(I1,J2,K2)+XFP*SPD(I2,J2,K2)))
C**   DIRECTIN INTERPOLATION.
      DUM1=DIR(I2,J1,K)
      DUM2=DIR(I1,J1,K)
      IF((DUM2-DUM1).GT.PI)DUM1=DUM1+TWOPI
   95 IF((DUM1-DUM2).GT.PI)DUM2=DUM2+TWOPI
      AYM=XFM*DUM2+XFP*DUM1
      IF(AYM.GT.TWOPI)AYM=AYM-TWOPI
      DUM1=DIR(I2,J2,K)
      DUM2=DIR(I1,J2,K)
  100 IF((DUM2-DUM1).GT.PI)DUM1=DUM1+TWOPI
      IF((DUM1-DUM2)● GT.P1)OuM2=DUM2+TMOPI
      AYP=XFM*DUM2+XFP*DUM1
      IF(AYP.GT.1WOPI)AYP=AYP-TWOPI
      IF((AYM-AYP).GT.PI)AYP=AYP+TWOPI
  105 IF ((AYP-AYM).GT.PI)AYM=AYM+TWOPI
      ATM=YFM*AYM+YFP*AYP
      IF(ATM.GT.TWOPI)ATM=ATM-TWOPI
      DUM1=DIR(I2,J1,K2)
      DUM2=DIR(I1,J1,K2)
  110 IF((DUM2-DUM1).GT.PI)DUM1=DUM1+TWOPI
      IF((DUM1-DUM2).GT.PI)DUM2=DUM2+TWOPI
      AYM=XFM*DUM2+XFP*DUM1
      IF(AYM.GT.1WOPI)AYM=AYM-TWOPI
      DUM1=DIR(I2,J2,K2)
```

```
      DUM2=DIR(I1,J2,K2)
      IF((DUM2-DUM1).GT.PI)DUM1=DUM1+TWOPI
      IF((DUM1-DUM2).GT.PI)DUM2=DUM2+TWOPI
      AYP=XFM*DUM2+XFP*DUM1
      IF(AYP.GT.TWOPI)AYP=AYP-TWOPI
      IF((AYM-AYP).GT.PI)AYP=AYP+TWOPI
      IF((AYP-AYM).GT.PI)AYM=AYM+TWOPI
      ATP=YFM*AYM+YFP*AYP
      IF(ATP.GT.TWOPI)ATP=ATP-TWOPI
      IF((ATM-ATP).GT.PI)ATP=ATP+TWOPI
      IF((ATP-ATM).GT.PI)ATM=ATM+TWOPI
C**   TRANSFORMINGDIRECTION TO TRIGONOMETRIC COORDINATE SYSTEM.
      DIRCT(K)=TWOPI-TFM*ATM-TFP*ATP-AGRID
C     IF (K.EQ.1) DIRCT(1)= DIRCT(1)-ADEFL+PI
C**   DEGREES TO RADIANSO
      DIRCT(K)=DIRCT(K)*3.14159265/PI
   45 CONTINUE
C**   TRANSFORMING SPEEDTOM/HR.
      SPEED(1) =SPEED(1)*1854.
      SPEED(2)=SPEED(2)*3600.
      SPEED(3)=SPEED(3)*1000.
C**   RANDOMIZE NET CURRENT
      CALL RANDOM(SPEED(3),DIR(3),IOLD,JOLD,V2,D2)
C**   CALCULATE COMPONENTS OFTHEDRIFT VECTOR.
      UT=CW*SPEED(1)*COS(DIRCT(1))+V2*COS(D2)+
     .     SPEED(2)*COS(DIRCT(2))+SPEED(3)*COS(DIRCT(3))
      VT=CW*SPEED(1)*SIN(DIRCT(1))+V2*SIN(D2)+
     .     SPEED(2)*SIN(DIRCT(2))+SPEED(3)*SIN(DIRCT(3))
C**   CALCULATE NEW LOCATION OF THE SPILL.
C**   XNEW,YNEWNEW COORDINATES OF SPILL LOCATION.
      XNEW=XOLD+DT*UT
      YNEW=YOLD+DT*VT
      XNEW=AMIN1(XMAX,AMAX1(XNEW,0.0))
      YNEW=AMIN1(YMAX,AMAX1(YNEW,0.0))
C**   INEW,JNEW  NEW CELL OF SPILL LOCATION,
      INEW=INT(XNEW/DS)+1
      JNEW=INT(YNEW/DS)+1
C**   CHECK IF SPILL ADVANCED MORE THAN oNE CELL.
      IF((IABS(IOLD-INEW)+IABS(JOLD-JNEW)).LE.1) GO TO 60
      XINC=(XNEW-XOLD)/20.
      YINC=(YNEW-YOLD)/20.
      TINC=DT/20.
      XNEW=XOLD
      YNEW=YOLD
      T=T-DT
      DO 50 N=1,20
      XNEW=XNEW+XINC
      YNEW=YNEW+YINC
      T=T+TINC
      INEW=INT(XNEW/DS)+1
      JNEW=INT(YNEW/DS)+1
C**   CHECK IF SPILL REACHED WATER BOUNDARY.
      IF (CELL(INEW,JNEW).LT.0) GOTO 60
   50 CONTINUE
   60 CONTINUE
C**   PREPARATION FORNEXT TIME STEP.
      T=T+DT
      IOLD=INEW
      JOLD=JNEW
      XOLD=XNEW
      YOLD=YNEW
C***  XPC,YPC LOCATION OF SPILL ON THE PLOT.
      XPC=XNEW*XPLFAC
      YPC=YNEW*YPLFAC
C**   CHECK IF SPILL REACHED WATER BOUNDARY.
      IF (CELL(INEW,JNEW).LT.0)GOTO 70
      IF (DOP.EQ.2) WRITE(6,1003) T,XNEW,YNEW, INEW,JNEW
C***  PLOTTING A LINE IN TRAJECTORY MODE.
C     IF (PLND.NE.1) GOTO 2
      CALL PLOT(XPC,YPC,2)
      IF (MOD(STEP,PSTEP).NE.0) GOTO 7
```

```
      IF (DOP.EQ.1) WRITL(6*1003) T,XNEW,YNEW,INEW,JNEW
      CALL SYMBOL(XPC,YPC,0.082,PLNO,0.0,-1)
      CALL NUMBER(XPC,YPC-0.041,0.082,T,0.0,4HF4.0)
      CALL PLOT(XPC,YPC,3)
    2 CONTINUE
      WRITE (6Q1OO1)
   70 WRITE(6,1002) PLNO,INEW,JNEW,T
C***  TERMINATING THE LINE IN TRAJECTORY MODE.
C     IF (PLNO.NE.1) RETURN
      XPC=AMIN1(XPC,XAXIS)
      YPC=AMIN1(YPC,YAXIS)
      XPC=AMAX1(XPC,0.0)
      YPC=AMAX1(YPC,0.0)
      CALL PLOT(XPC,YPC,2)
      CALL SYMBOL(XPC,YPC,0.082,PLNO,0.0,-1)
      CALL NUMBER(XPC,YPC-0.041,0.082,T,0.0,4HF4.0)
      RETURN
  510 FORMAT(16F5.0)
 1001 FORMAT(3X,*STOP TIME REACHED*)
 1002 FORMAT(3X,*TRAJECTORY*,I3,*TERMINATED AT CELL *,2I5,*  AT TIME .
     .     ,F5.0,* HOURS. *)
 1003 FORMAT(3X,*T =*,F8.3,* X =*,F8.2,* Y =*,F8.2,*  AT CELL*,2I5)
      END
```

SUBROUTINE PLINIT

```
*DECK PLINIT
      SUBROUTINE PLINIT
     .          (N,XAXIS,YAXIS,XPLFAC,YPLFAC,XSPILL,YSPILL,PROB,WIND)
C*************************************************************************
c     PLOT INITIALIZATION ROUTINE.                                       *
c     PARAMETERS:                                                        *
c     N       - TRAJECTORY NUMBER.                                       *
c     XAXIS   - X-AXIS LENGTH IN INCHES.                                 *
c     YAXIS   - Y-AXIS LENGTH IN INCHES.                                 *
C     XPLFAC - SCALING FACTOR IN THE x DIRECTION (INCH ON PLOT/METER ).  *
c     YPLFAC -  SCALING FACTOR IN THE Y DIRECTION.                       *
c     XSPILL = x COORDINATE OF SPILL LOCATION.                           *
c     YSPILL - Y COORDINATE OF SPILL LOCATION.                           *
C*************************************************************************
      INTEGER PROB,WIND
      DATA SPACE/4.0/
      IF (N.GT.1) GOTO 1
C***  ADVANCING PEN FOR NEW FRAME.
      CALL PLOT(XAXIS+SPACE,0.,-3)
C***  DRAW A BOX
c     CALL PLOT(XAXIS,0.0,2)
c     CALL PLOT(XAXIS,YAXIS,2)
c     CALL PLOT(0.0,YAXIS,2)
c     CALL PLOT(0.0,0.0,2)
C***  MARKERS FOR OVERLAY.
      CALL SYMBOL(-1.0,0.,0.15,3,0.0,-1)
      CALL SYMBOL(-1.0,YAXIS-1.,0.15,3,0.0,-1)
C***  PRINT RUN IDENTIFICATION.
      DECODE (10,910,WIND) IWIND
      DECODE (10,910,PROB) ISPILL
      CALL SYMBOL(-1.,5.5,0.15,IWIND,0.0,1)
      CALL SYMBOL(-1.,4.0,0.15,ISPILL,0.0,1)
C***DRAW A SYMBOL AT THE SPILL POINT.
    1 XPC=XSPILL*XPLFAC
      YPC=YSPILL*YPLFAC
      IF(N.EQ.1) CALL SYMBOL(XPC,YPC,0.082,11,0.0,-1)
      CALL PLOT(XPC,YPC,3)
      RETURN
  910 FORMAT(4X,A1)
      END
```

SUBROUTINE RANDOM

```
1                   SUBROUTINE RANDOM(SPD,DIR,I,J,V2,D2)
                    V2=0.
                    D2=DIR+1.5707963
                    IF (J.GT.55) RETURN
5                   IF (J.LT.35) GOTO 3
                    V1=GAUSS(4.)
                    V2=GAUSS(3.)
                    GOTO 5
                3   IF (I.GT.19) GOTO 4
10                  V1=GAUSS(2.)
                    V2=GAUSS(2.5)
                    GOTO 5
                4   V1=GAUSS(10.)
                    V2=GAUSS(7.5)
15              5   SPD=SPD+V1
                    RETURN
                    END
```

FUNCTION GAUSS

```
1                   FUNCTION GAUSS(S)
                    A=0.
                    DO 10 I=1,12
               10   A=A+RANF(N)
5                   GAUSS=(A-6.)*S+36.
                    RETURN
                    END
```

APPENDIX B

BASE CASE TRAJECTORIES AND RESULTS

WIND
1

SITE
1

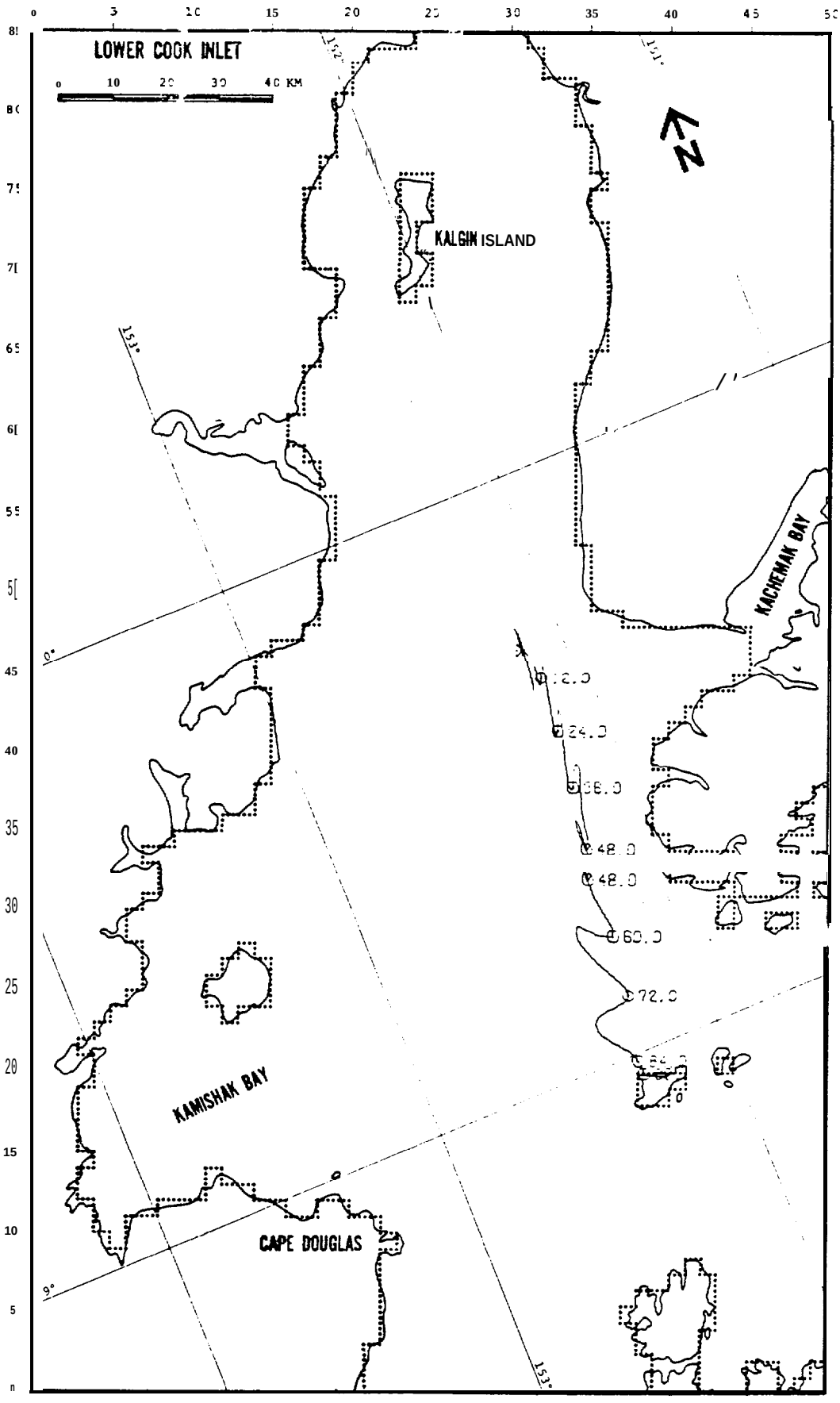

FIGURE B-1: BASE CASE

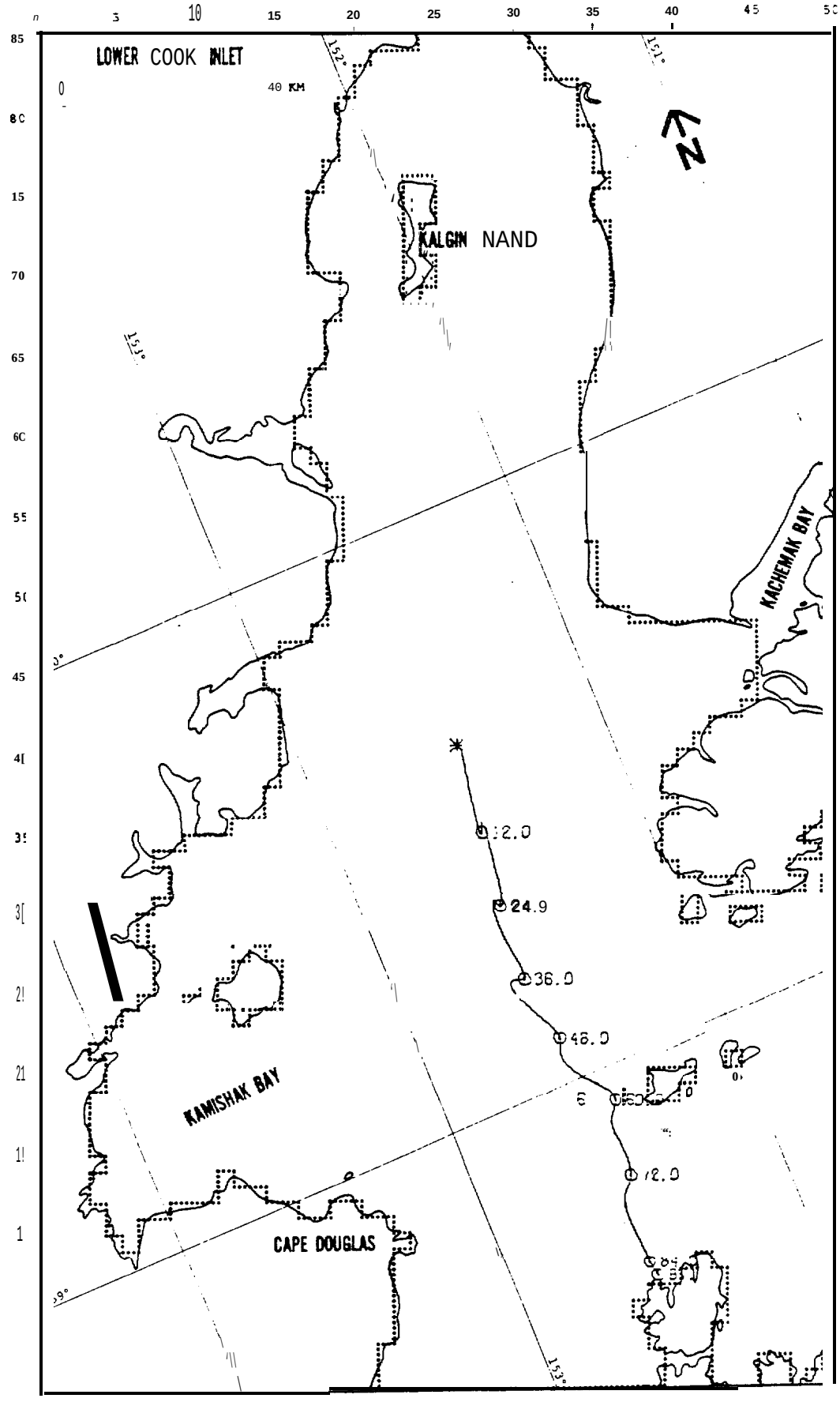

WIND
1

SITE
2

FIGURE B-2: BASE CASE

WIND
1

SITE
3

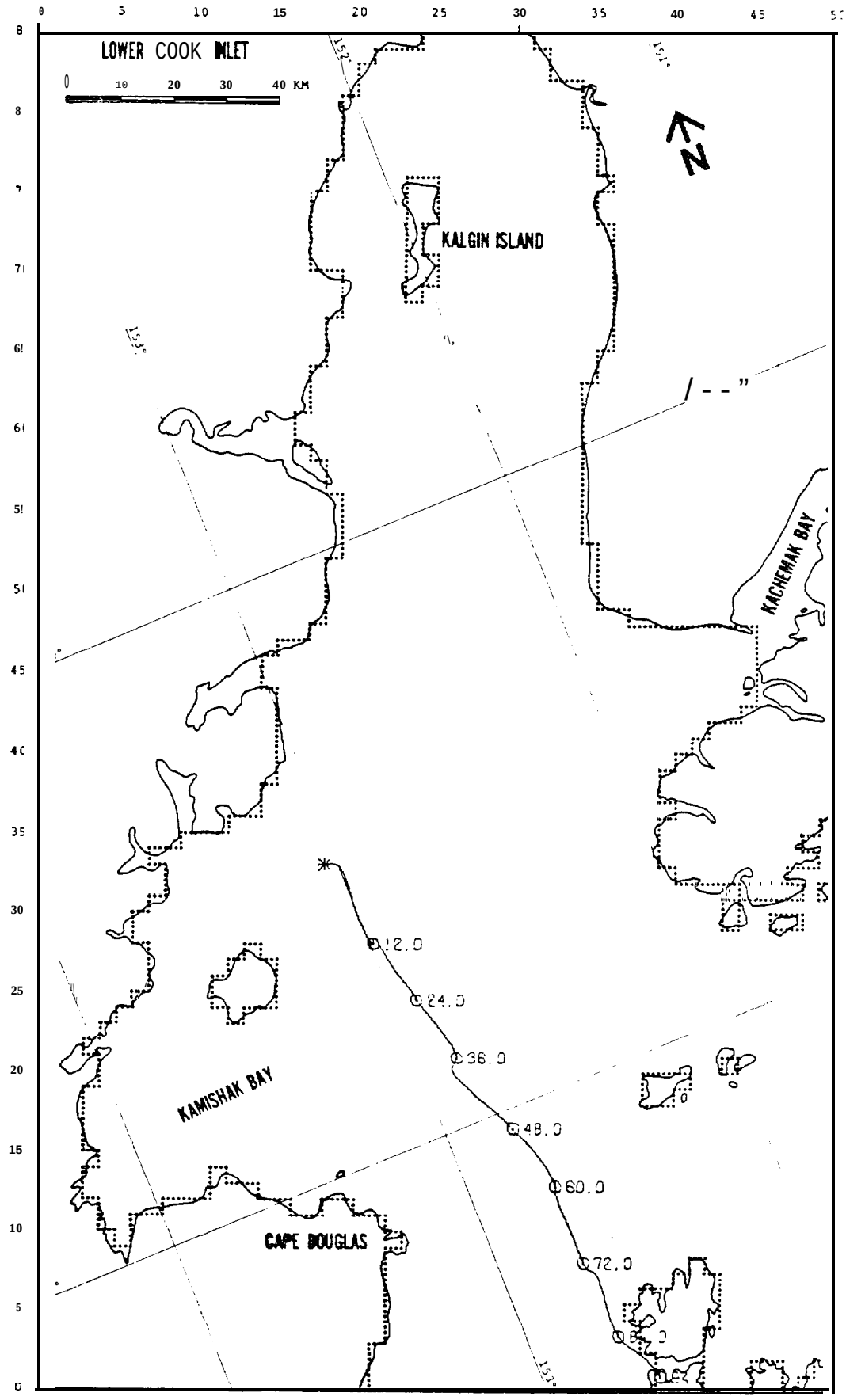

FIGURE B-3: BASE CASE

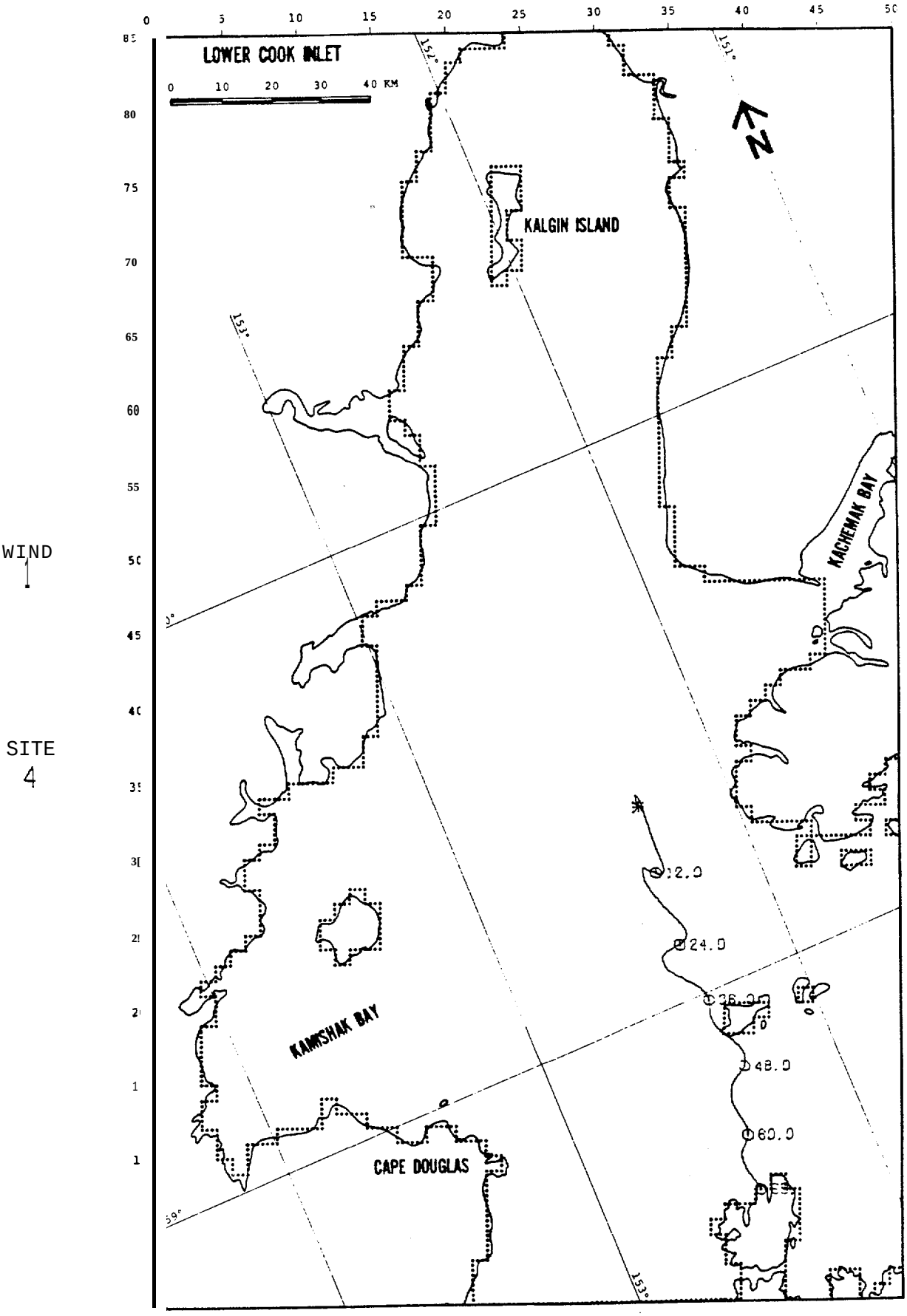

WIND

SITE 4

FIGURE B-4: BASE CASE

WIND
1

SITE
5

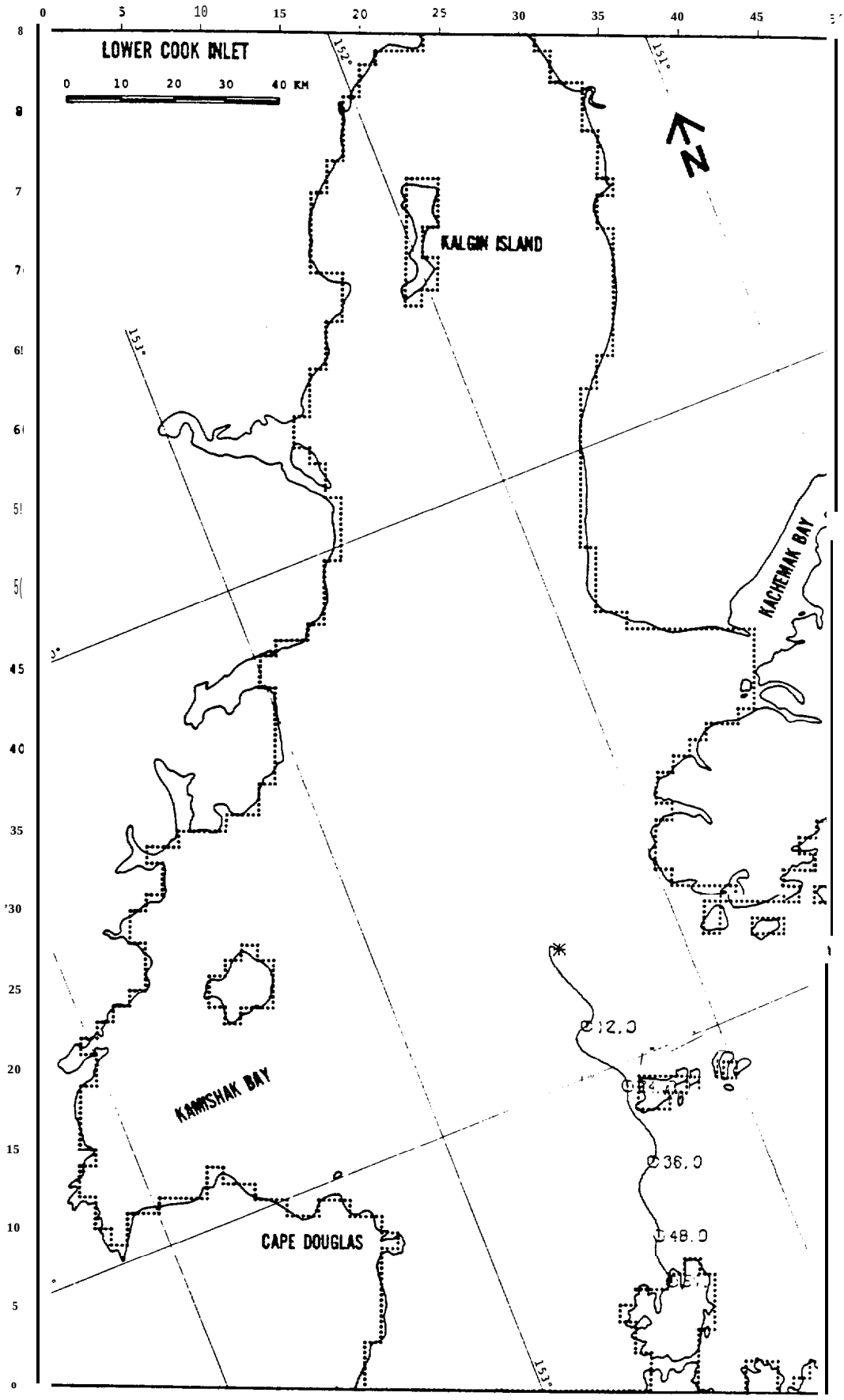

FIGURE B-5: BASE CASE

WIND
1

SITE
6

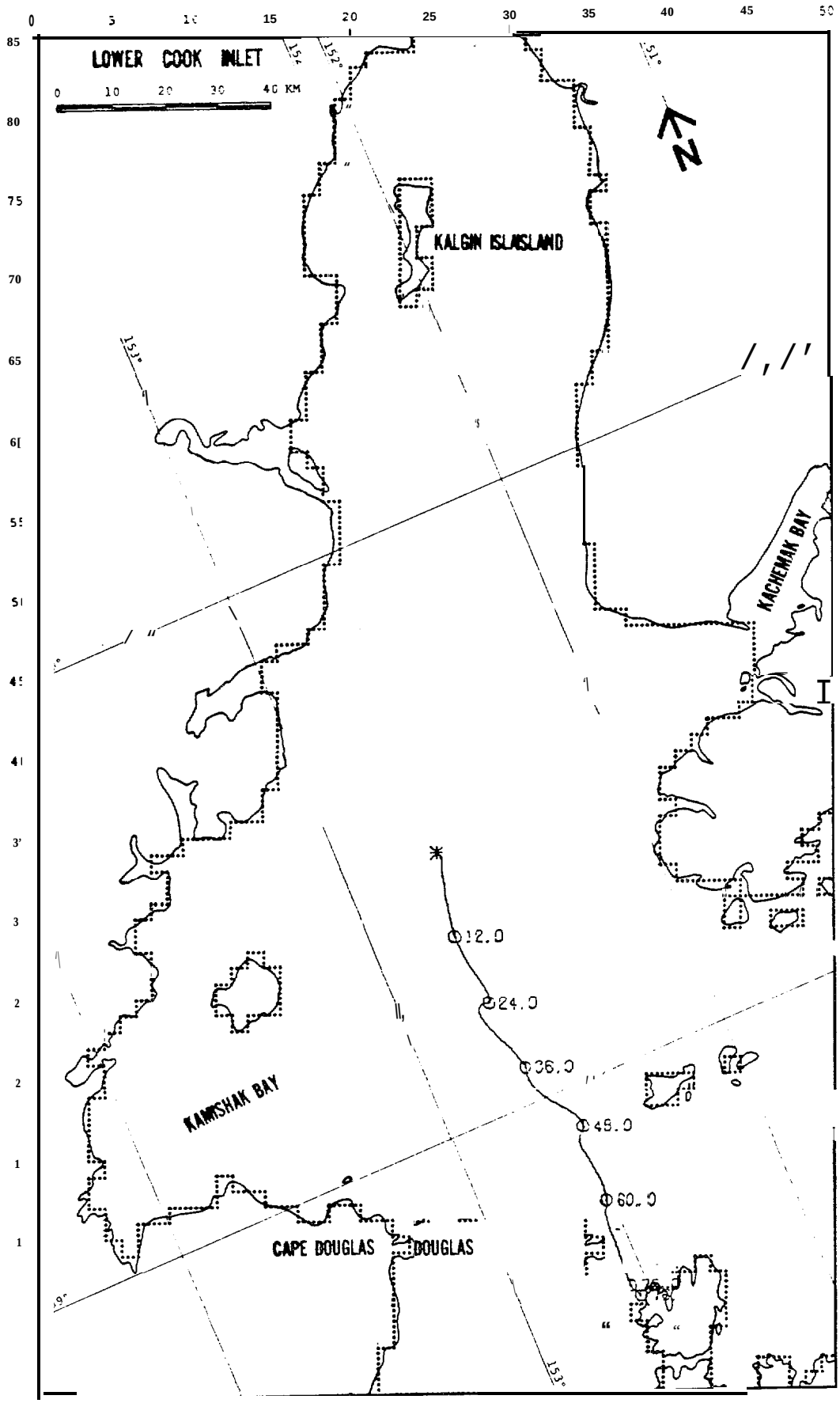

FIGURE B-6: BASE CASE

WIND

SITE

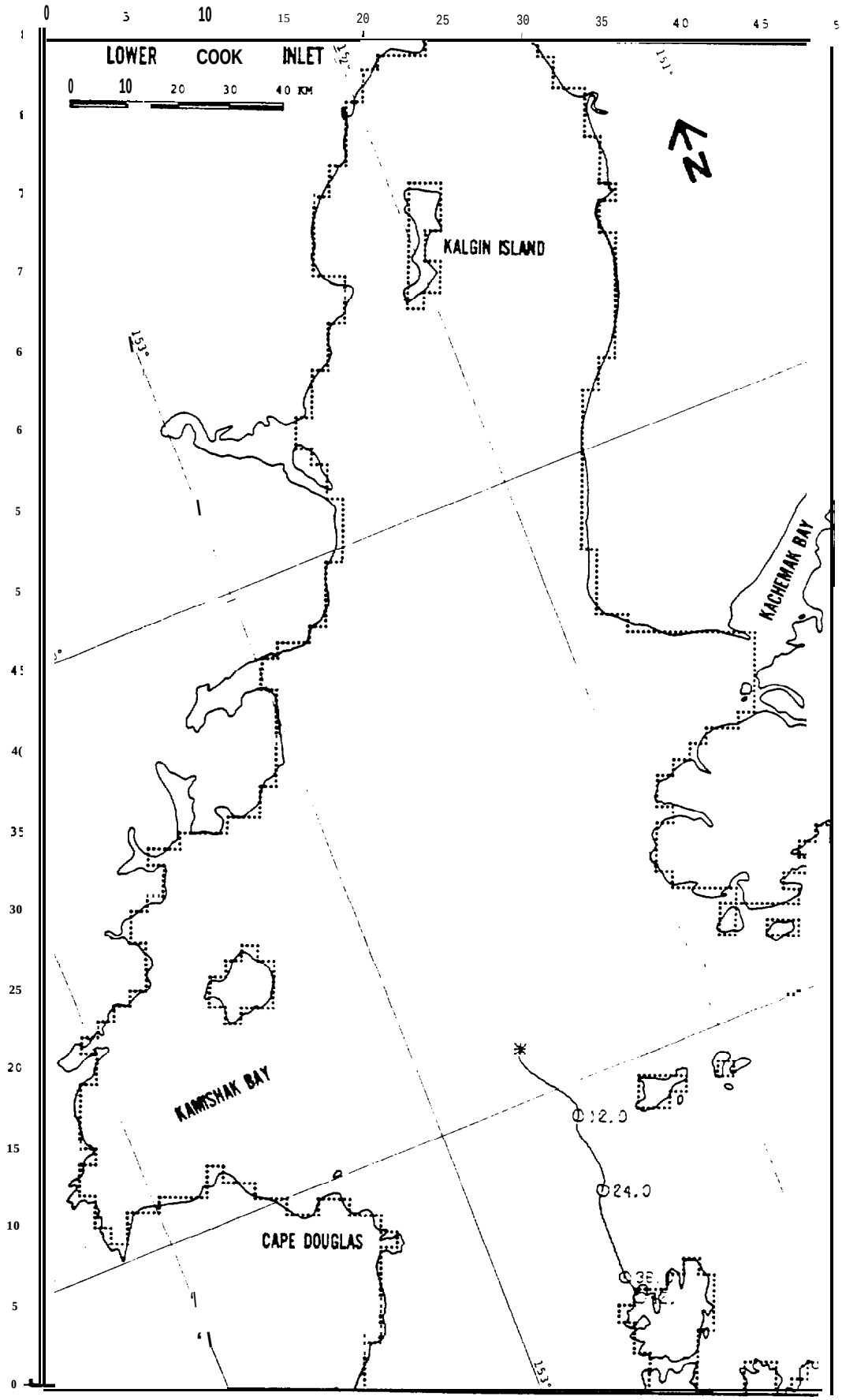

FIGURE B-7: BASE CASE

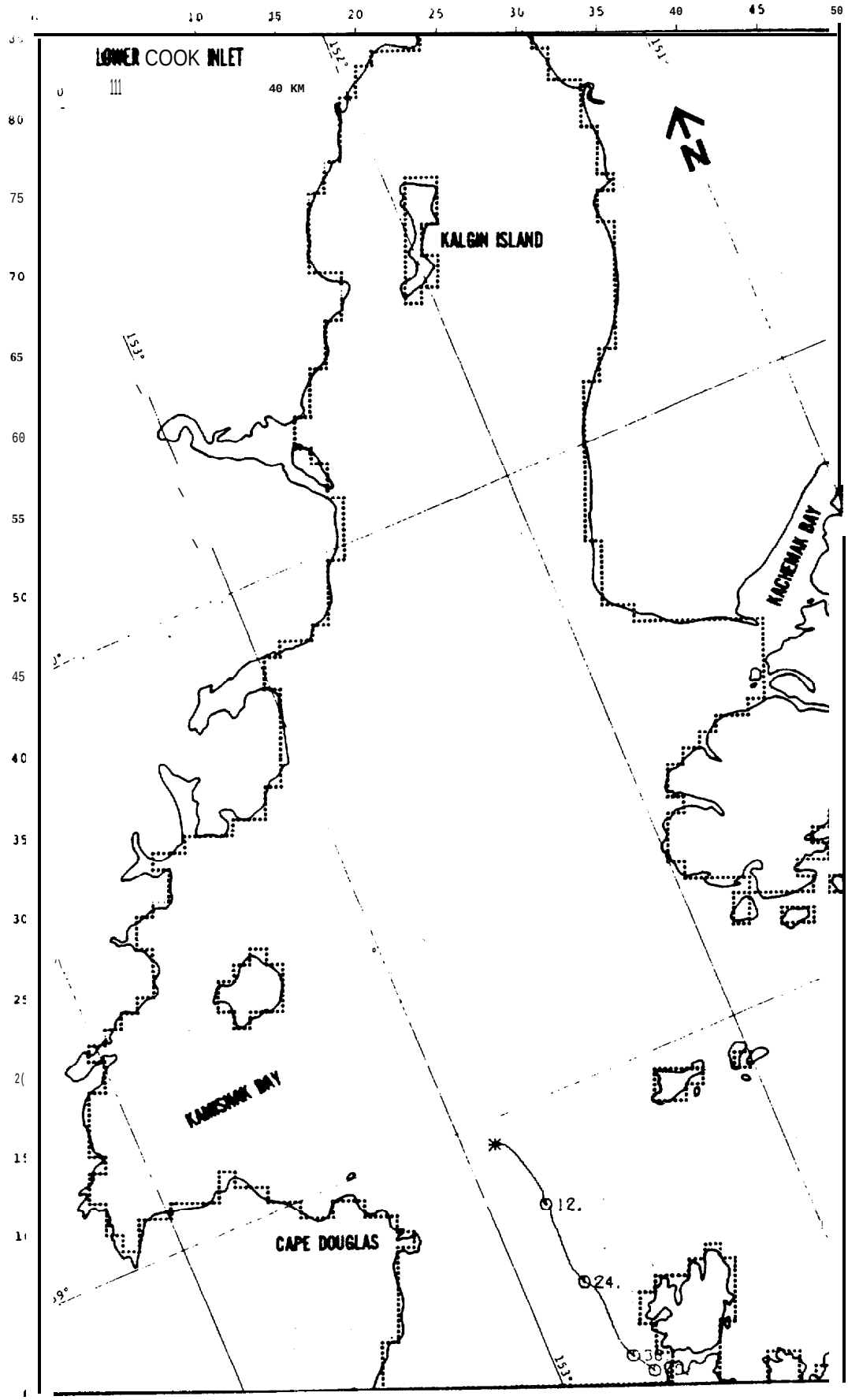

FIGURE B-8: BASE CASE

WIND
1

SITE
8A

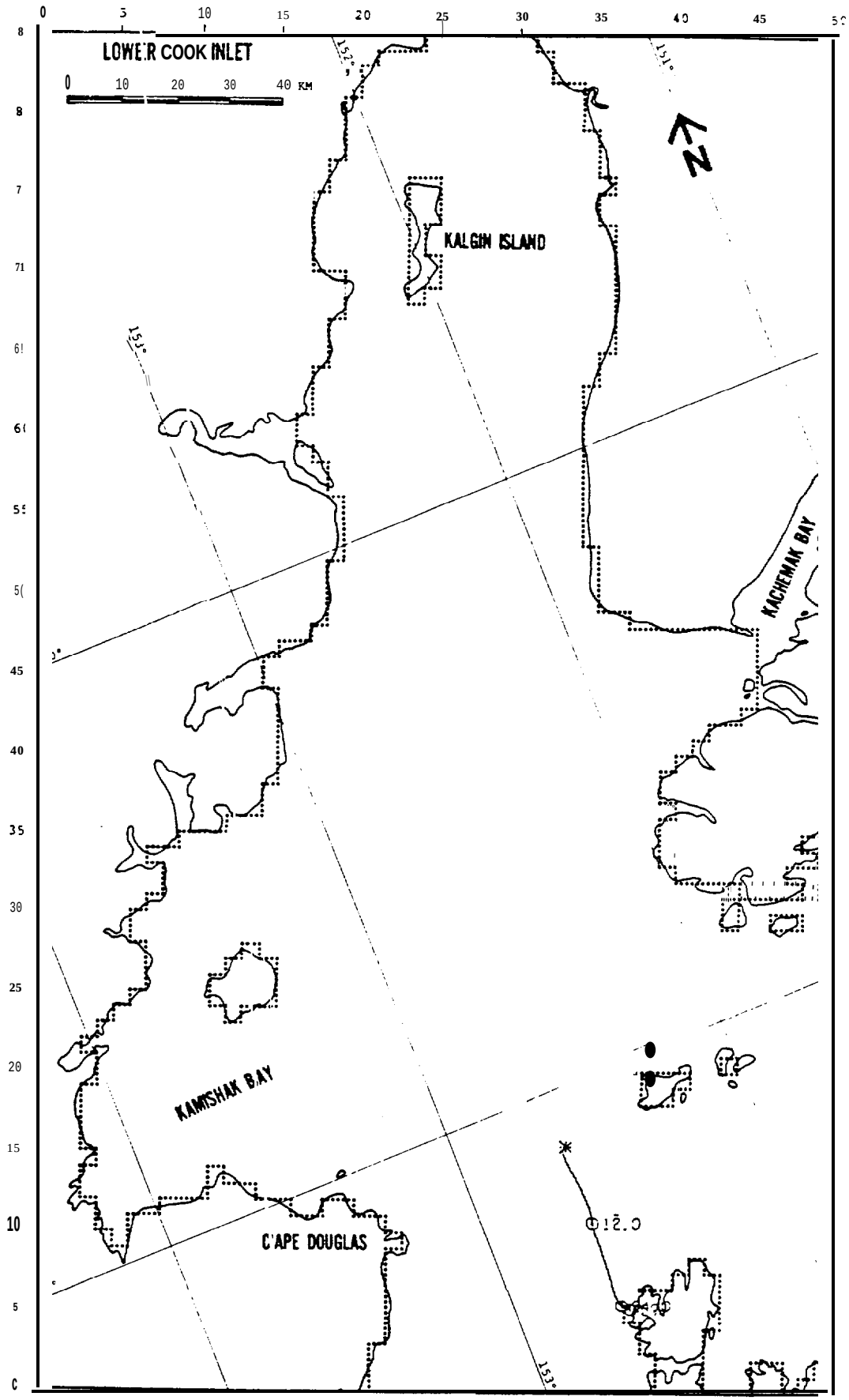

FIGURE B-9: BASE CASE

WIND
2

SITE
1

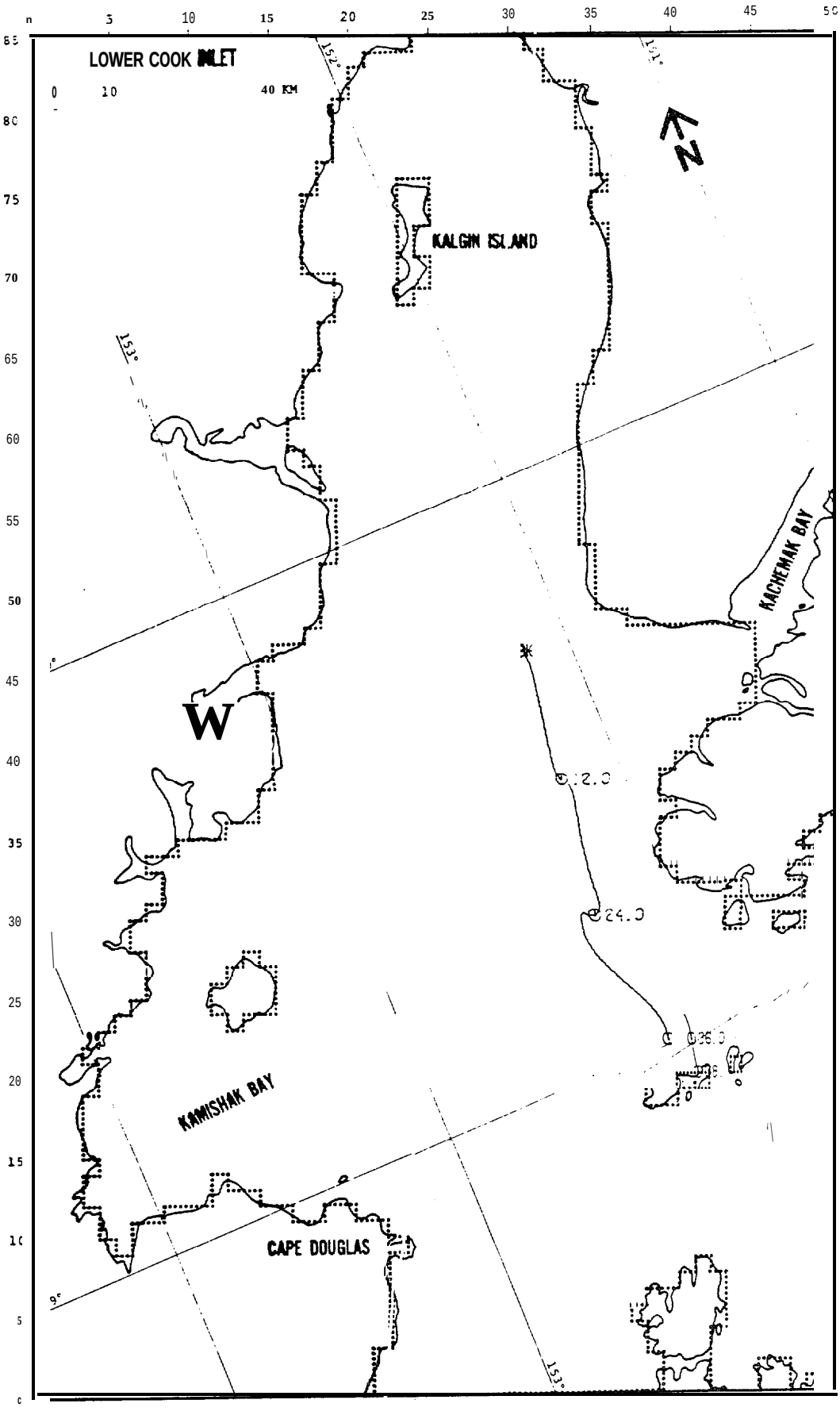

570

FIGURE B-10: BASE CASE

WIND
2

SITE
2

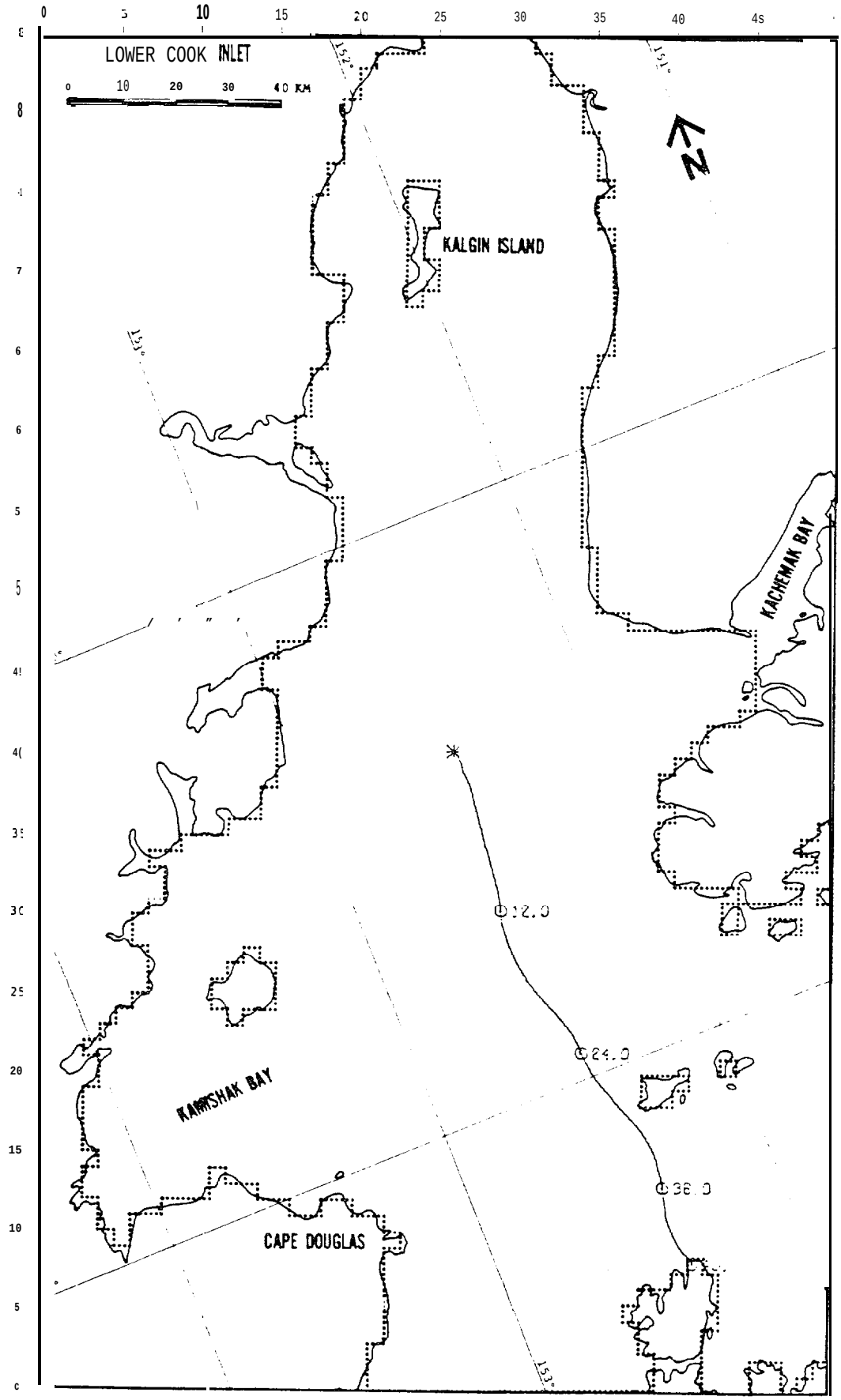

FIGURE B-11: BASE CASE

WIND
2

SITE
3

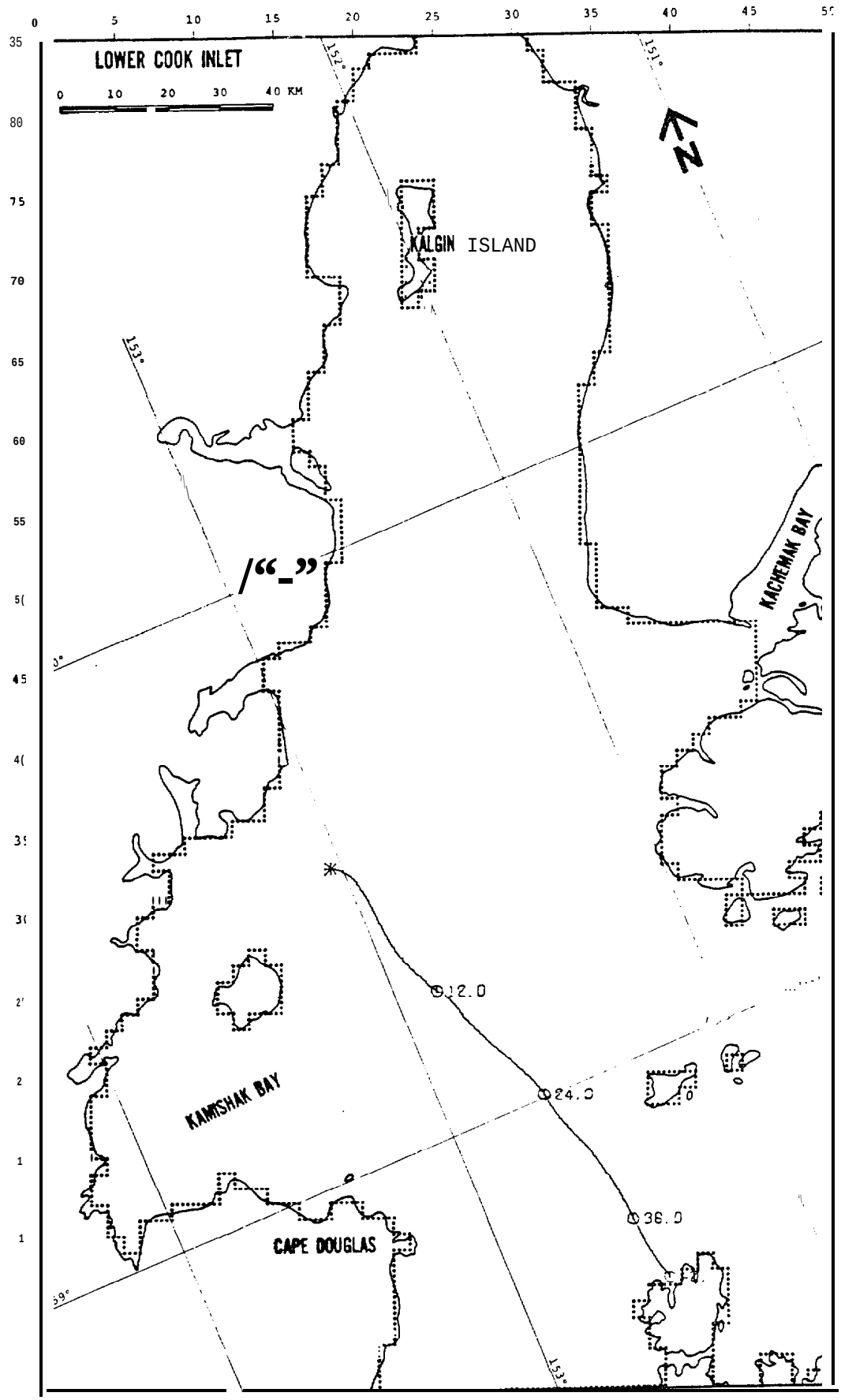

FIGURE B-12: BASE CASE

WIND
2

SITE
4

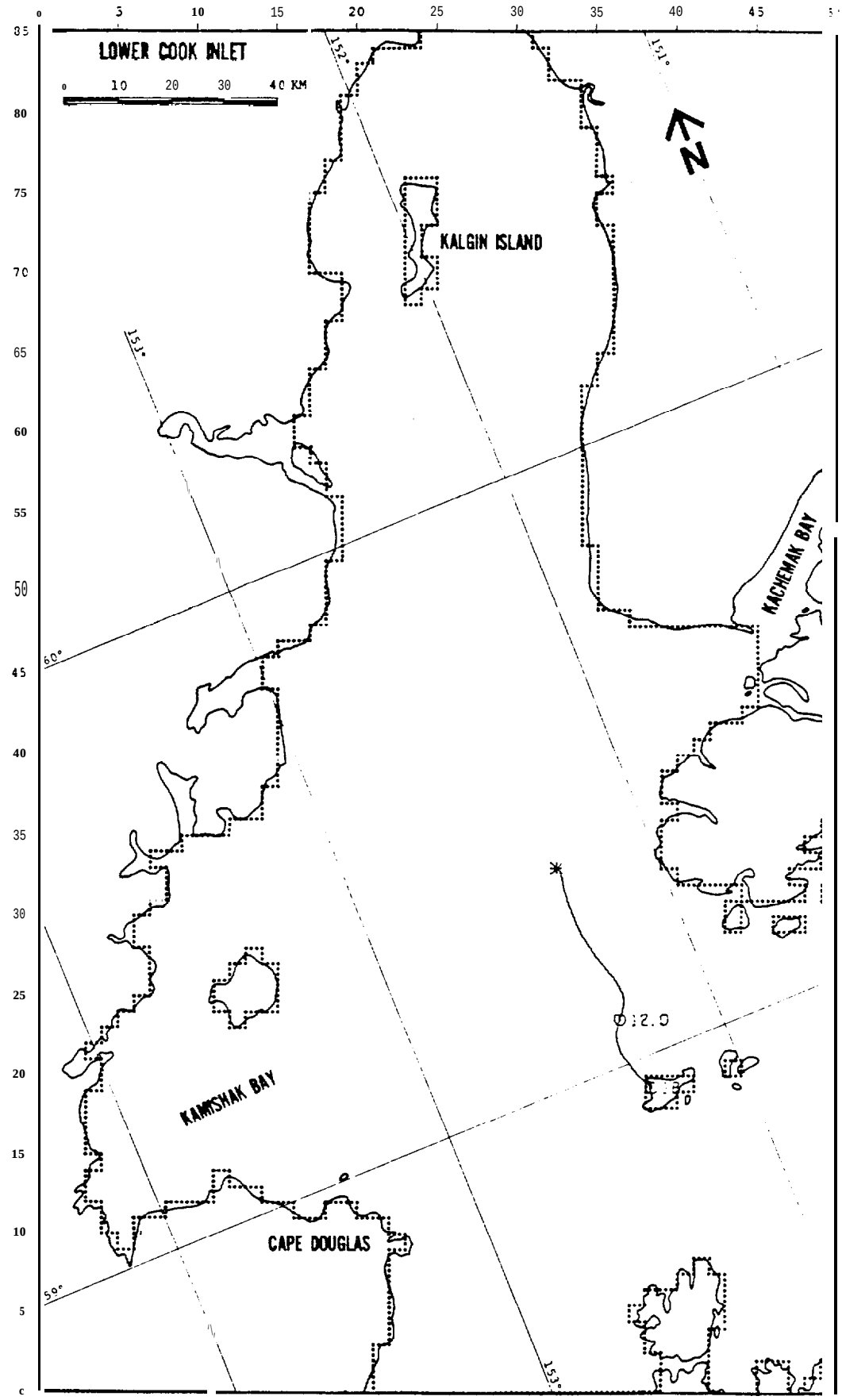

FIGURE B-13: BASE CASE

WIND
2

SITE
5

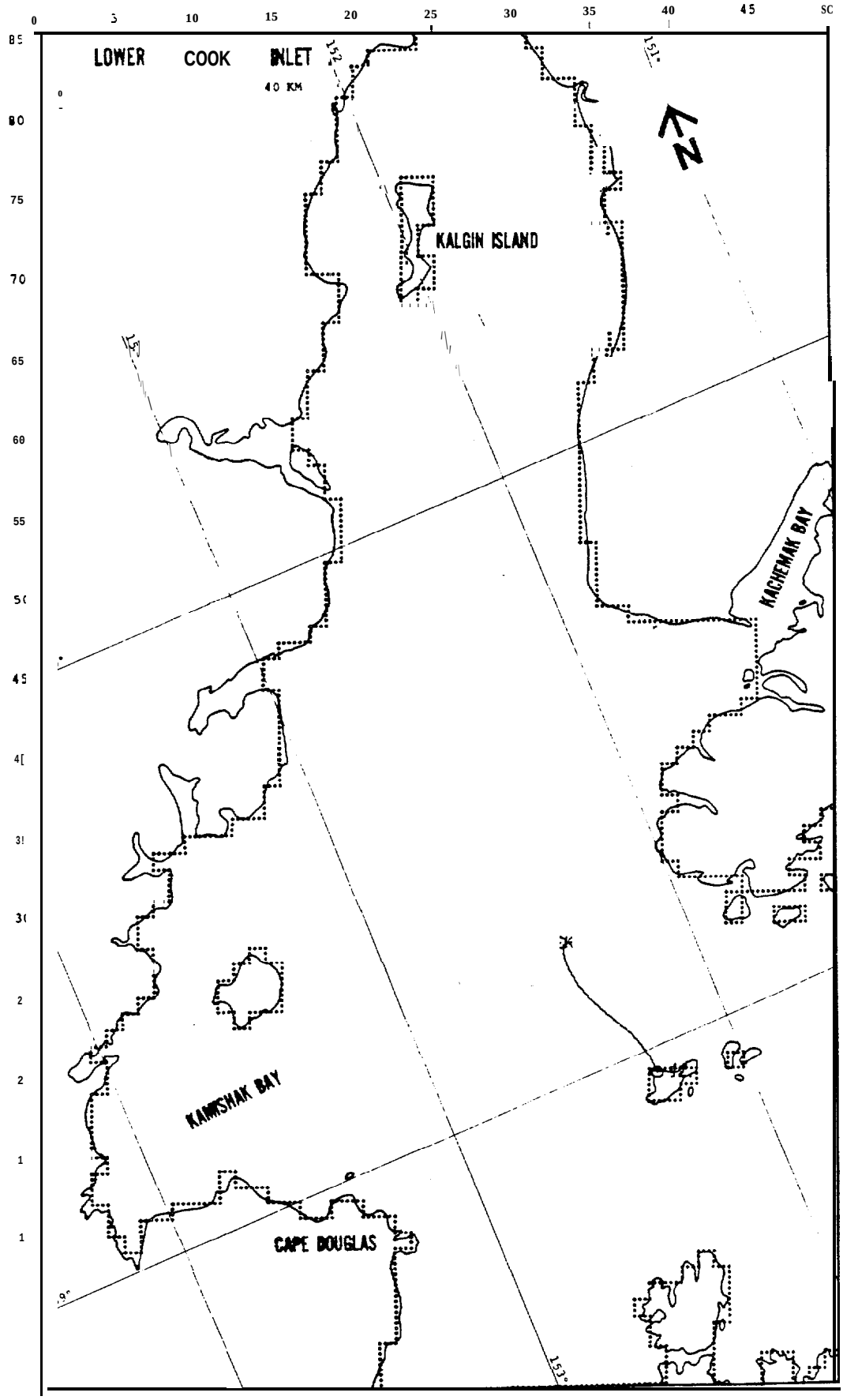

FIGURE B-14: BASECASE

WIND
2

SITE
6

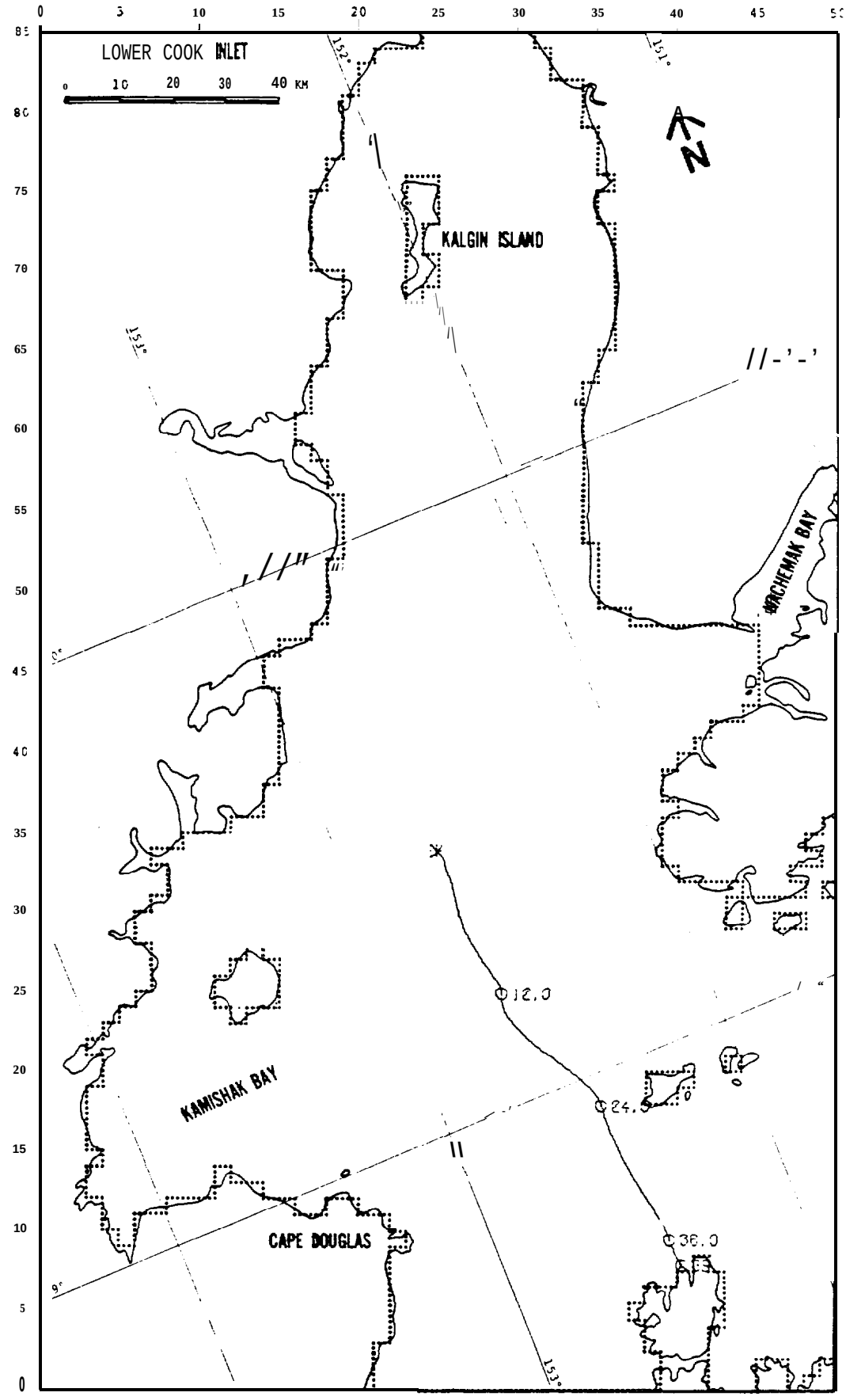

FIGURE B-15: BASE CASE

WIND
2

SITE
7

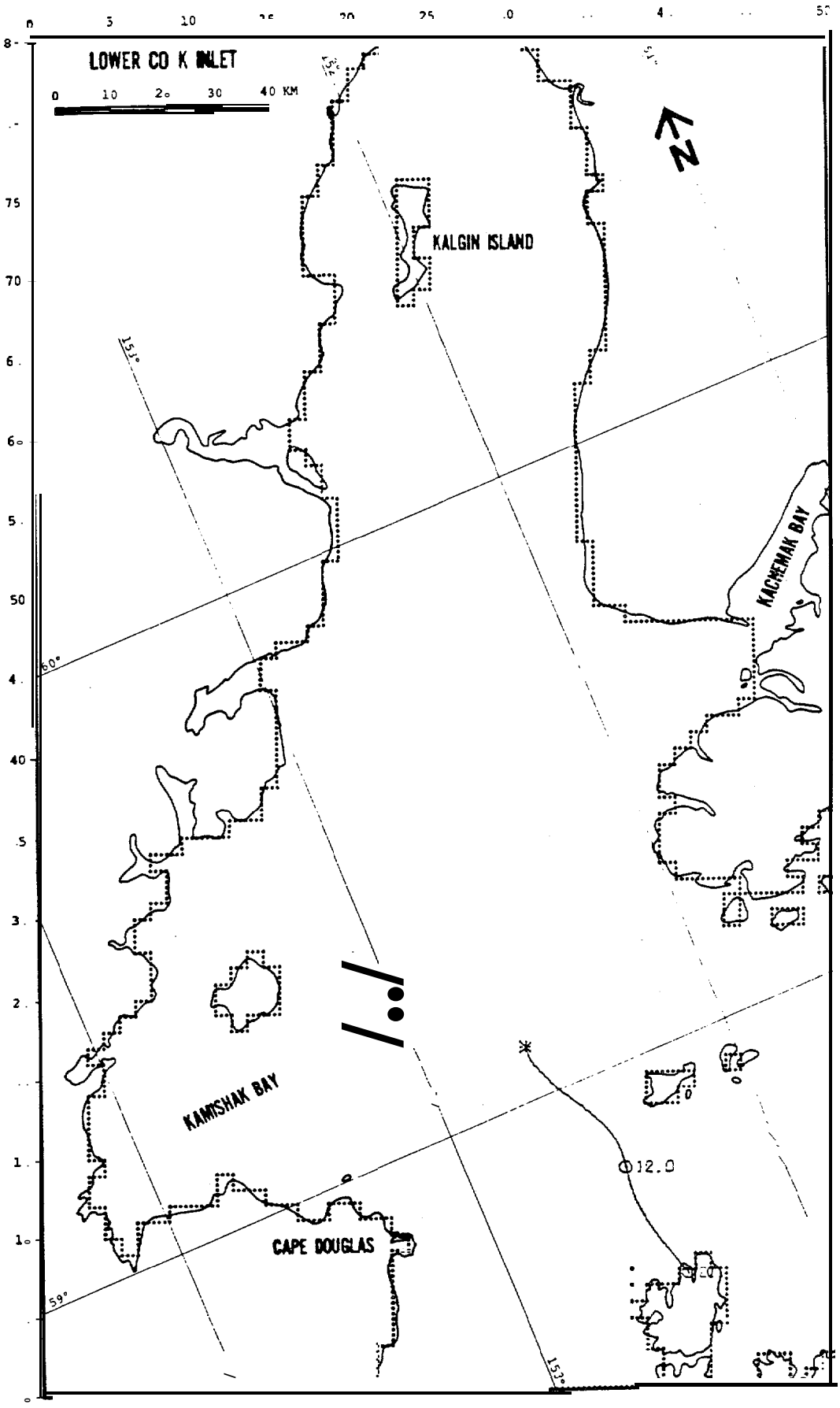

FIGURE -16: BASE CASE

WIND
2

SITE
8

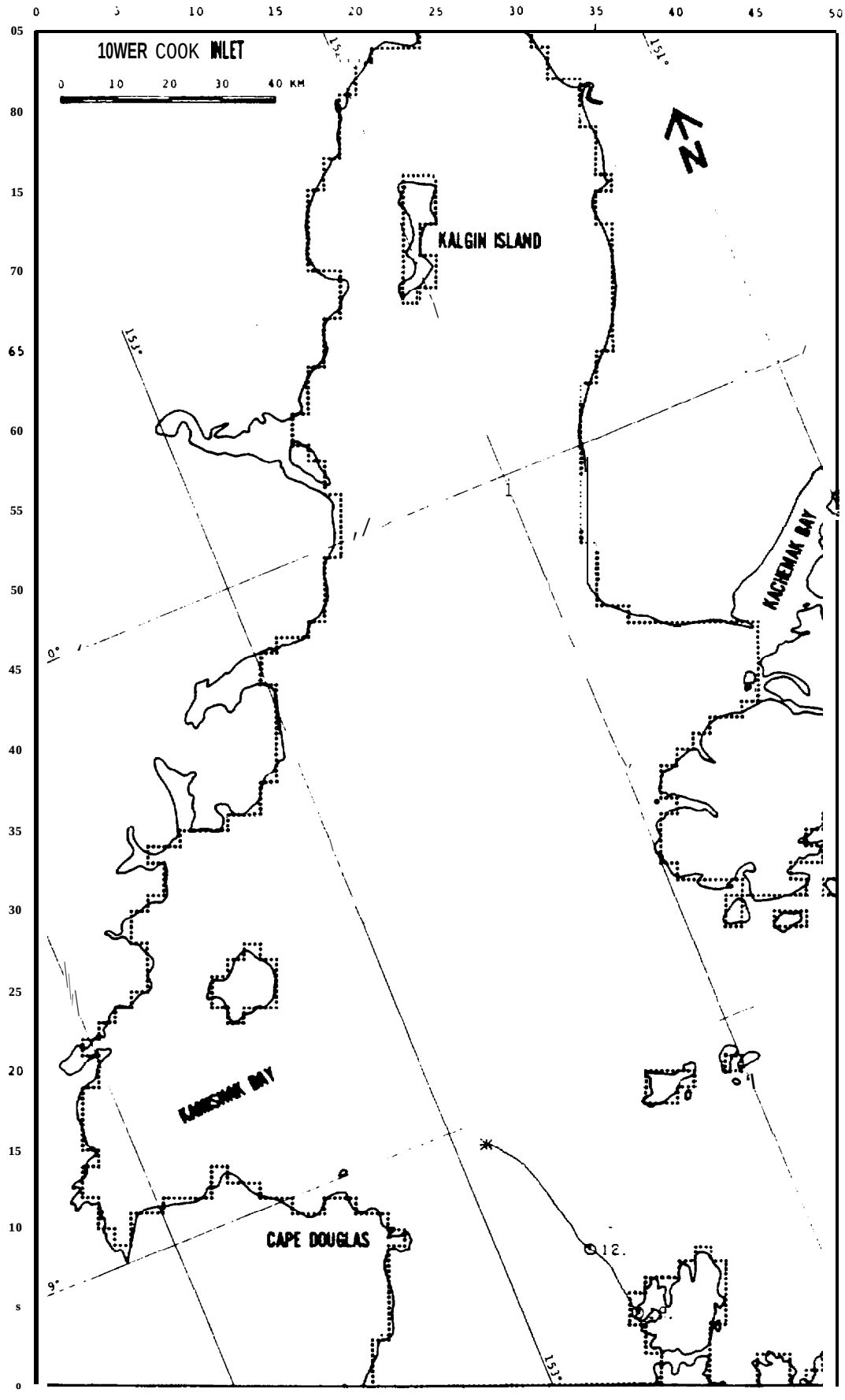

FIGURE B-17: BASE CASE

WIND
2

SITE
8A

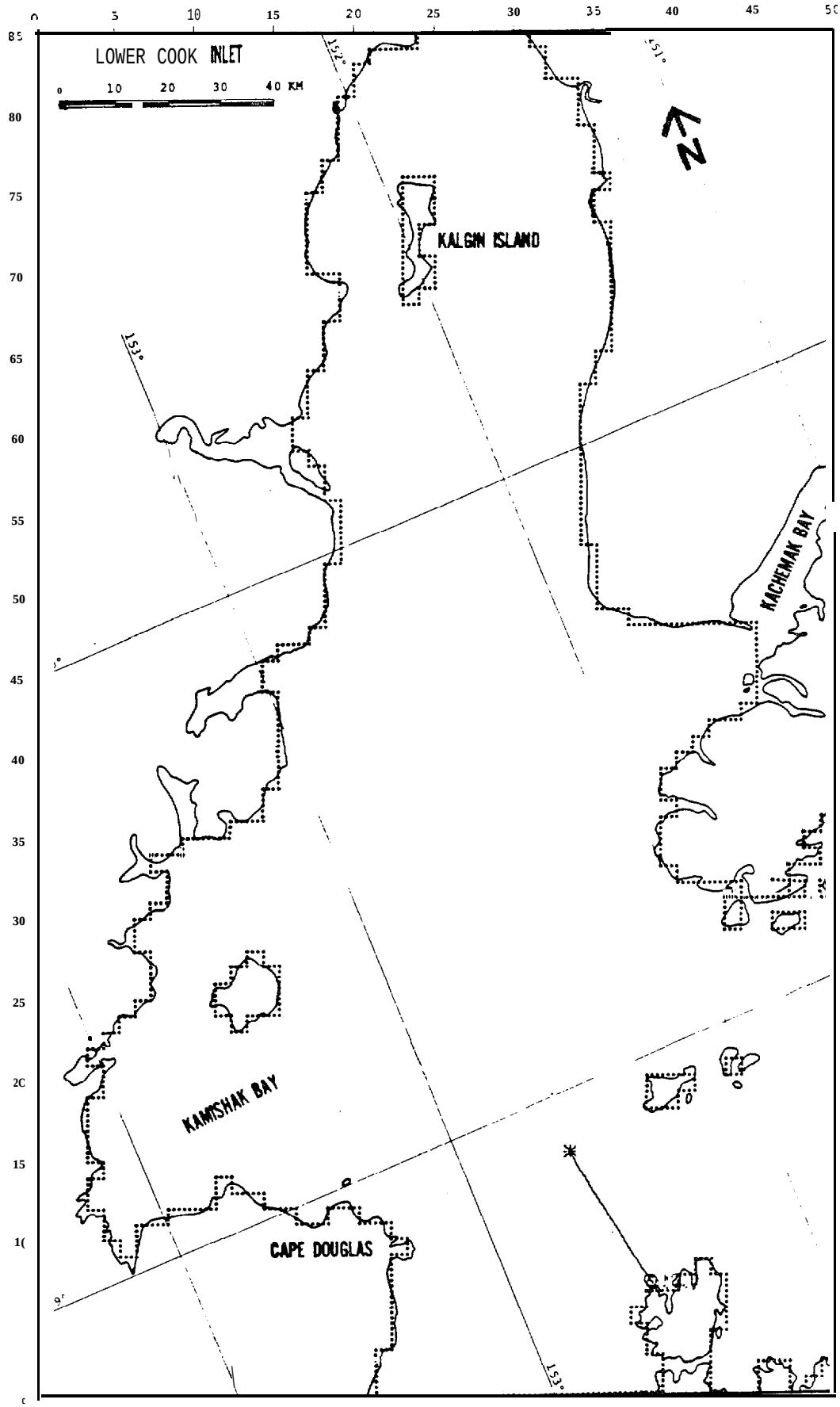

FIGURE B-18: BASE CASE

WIND
3

SITE

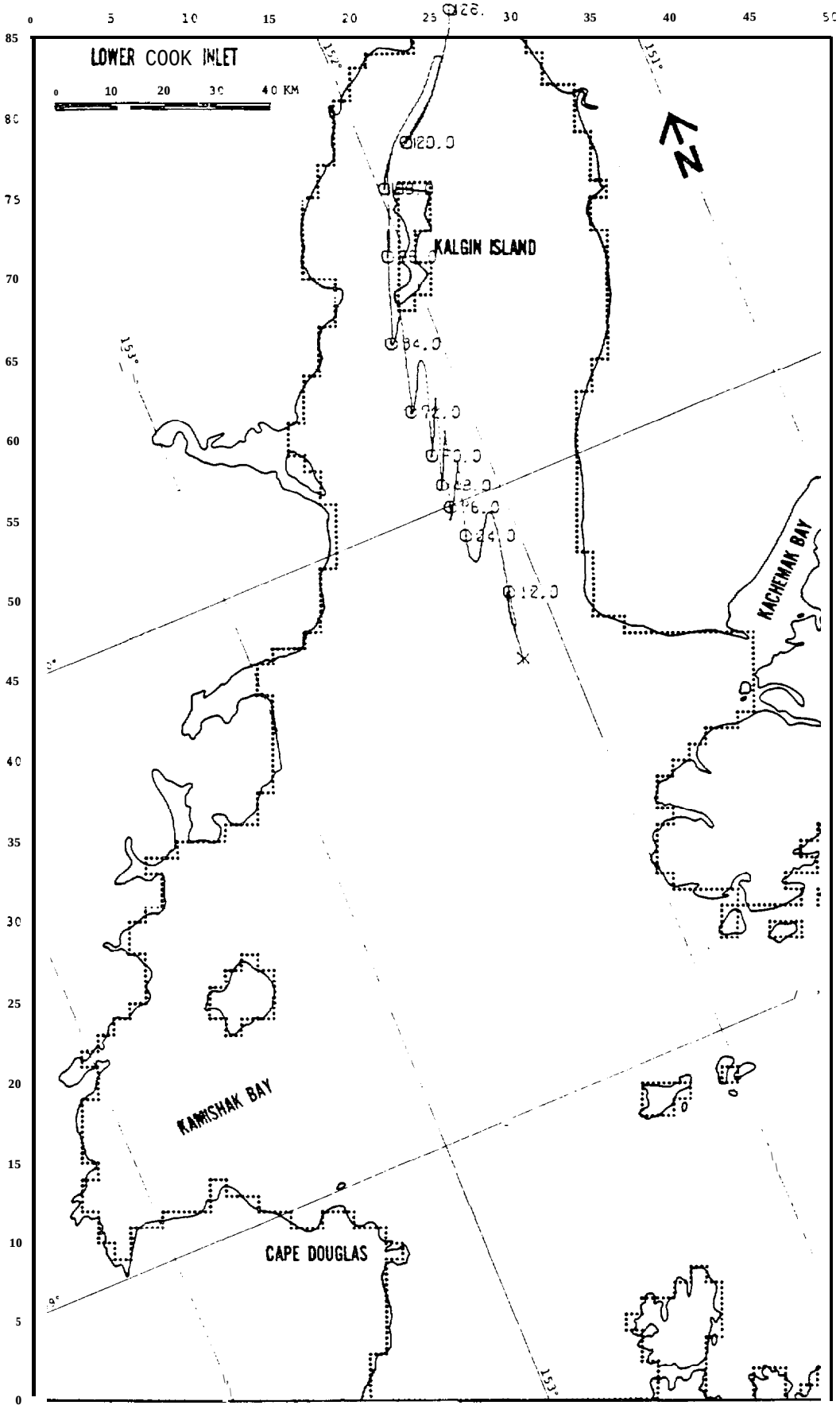

FIGURE B-19: BASE CASE

WIND
3

SITE
2

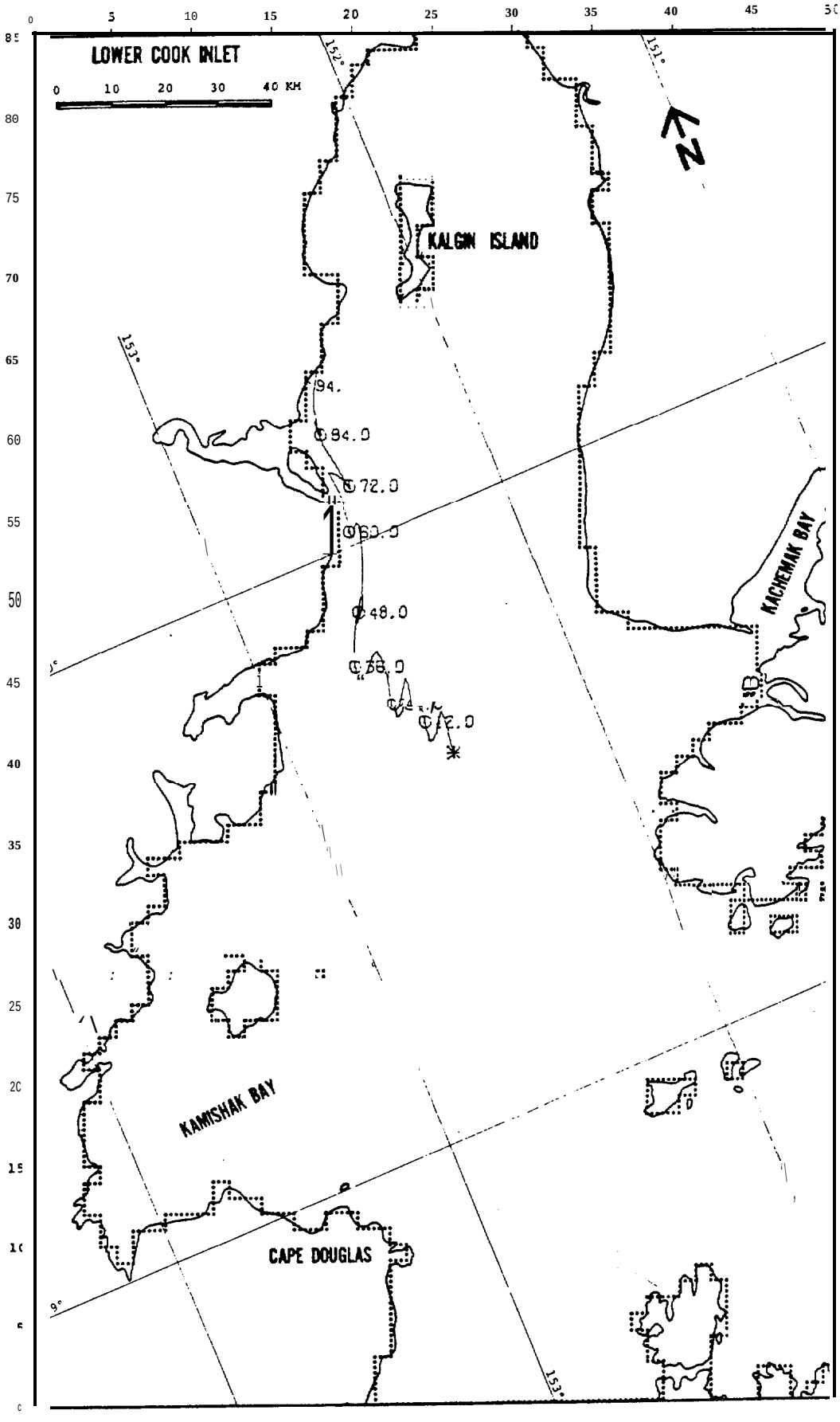

FIGURE B-20: BASE CASE

WIND
3

SITE
3

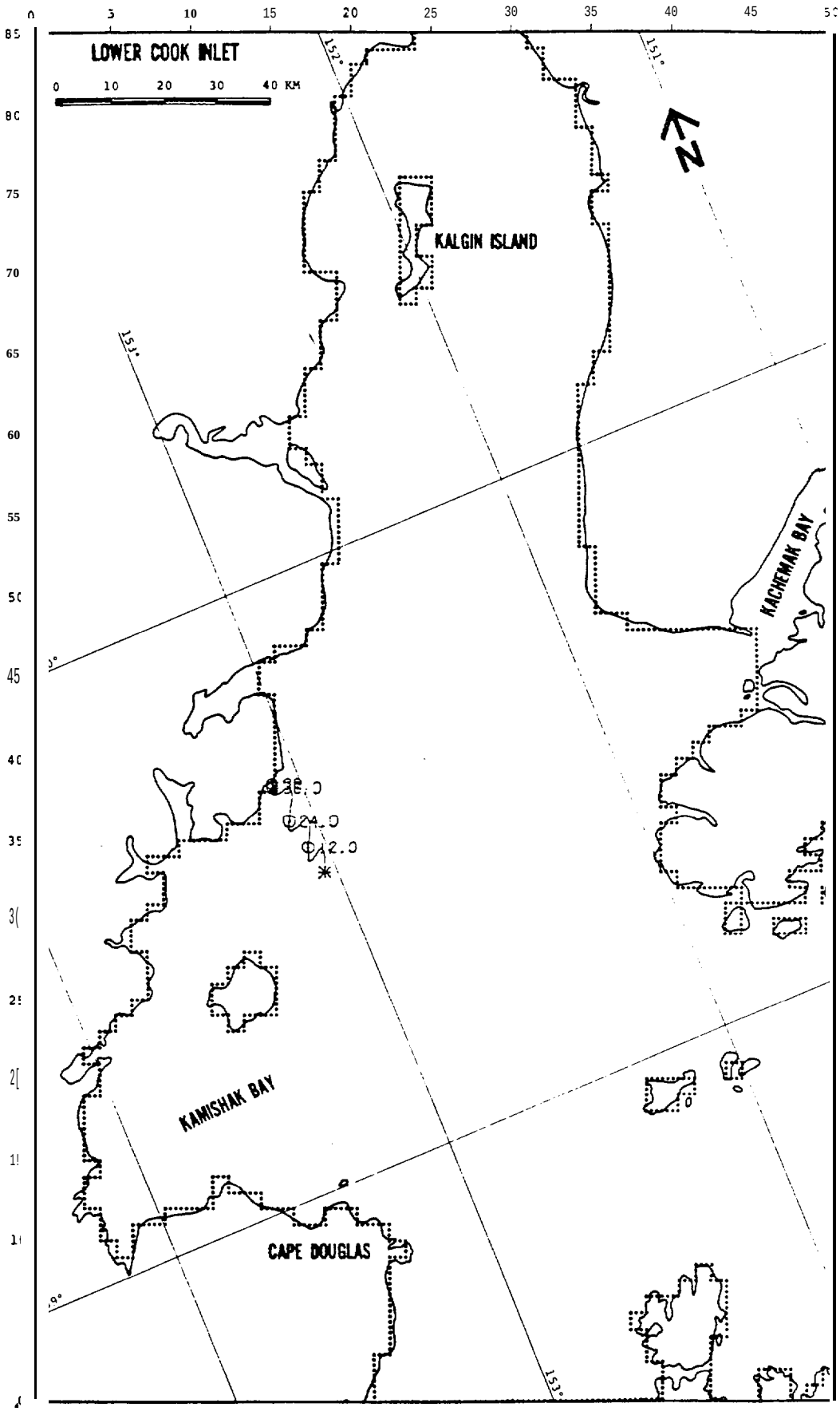

FIGURE B-21: BASE CASE

WIND
3

SITE
4

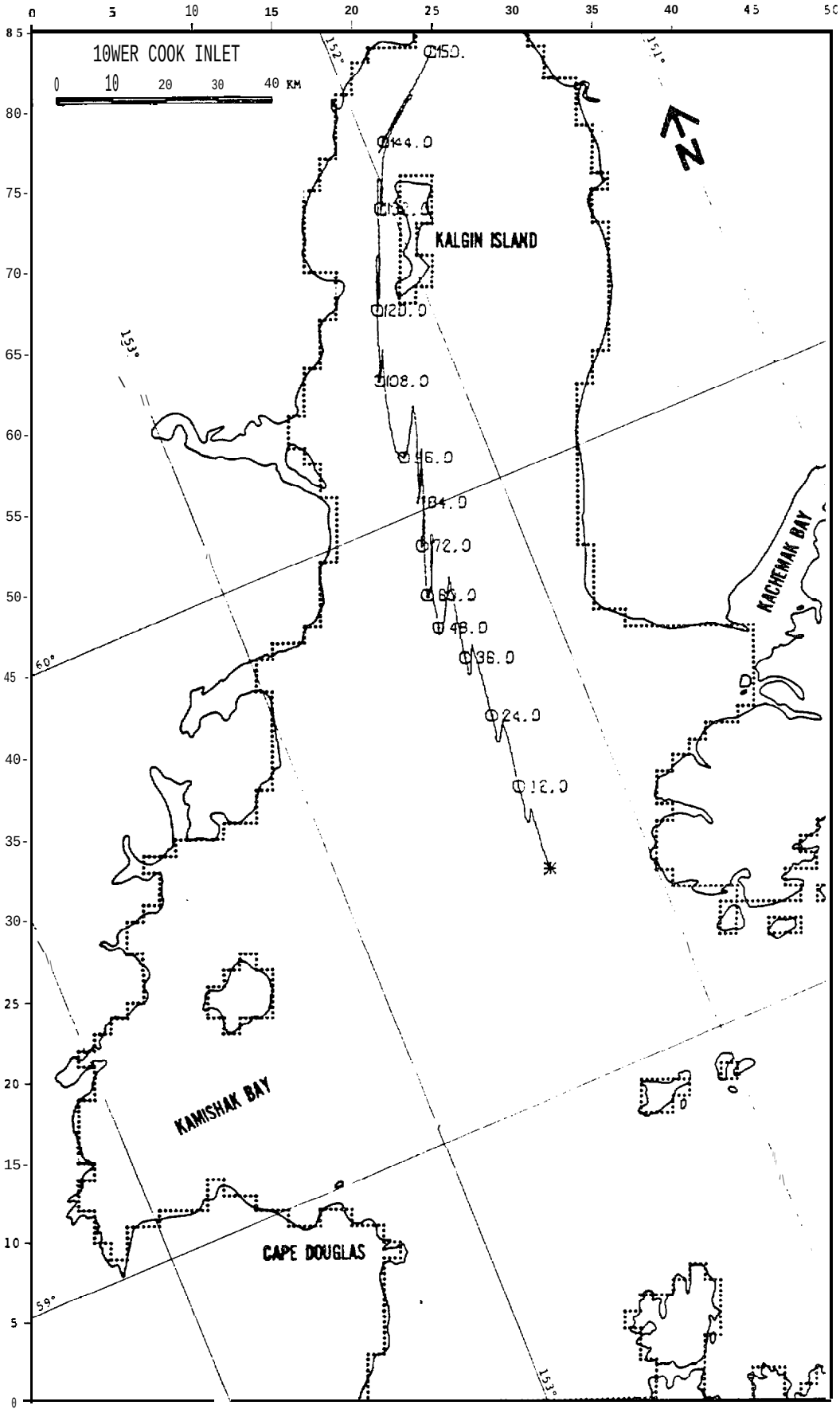

FIGURE B-22: BASE CASE

WIND
3

SITE
5

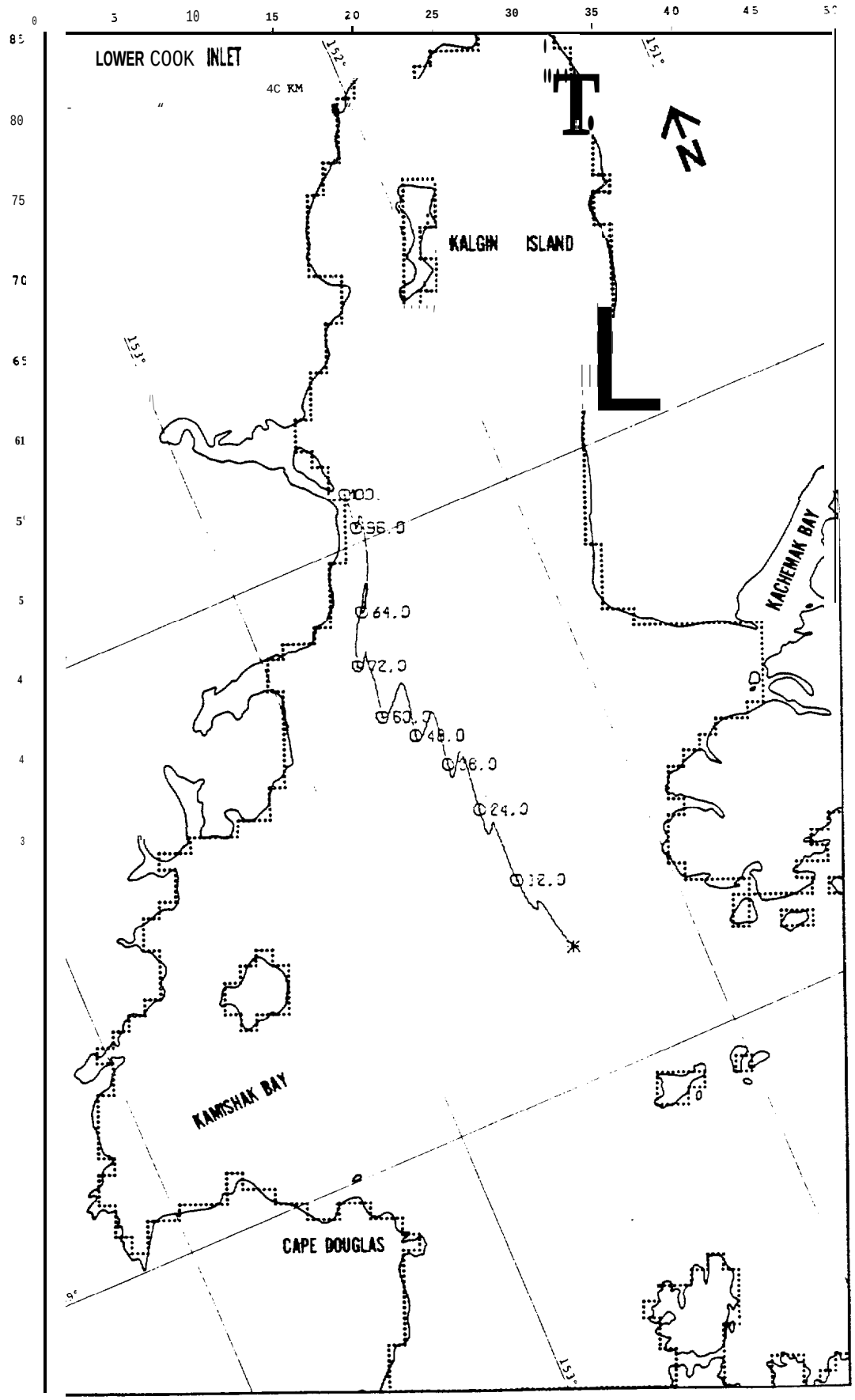

FIGURE B-23: BASE CASE

WIND
3

SITE
6

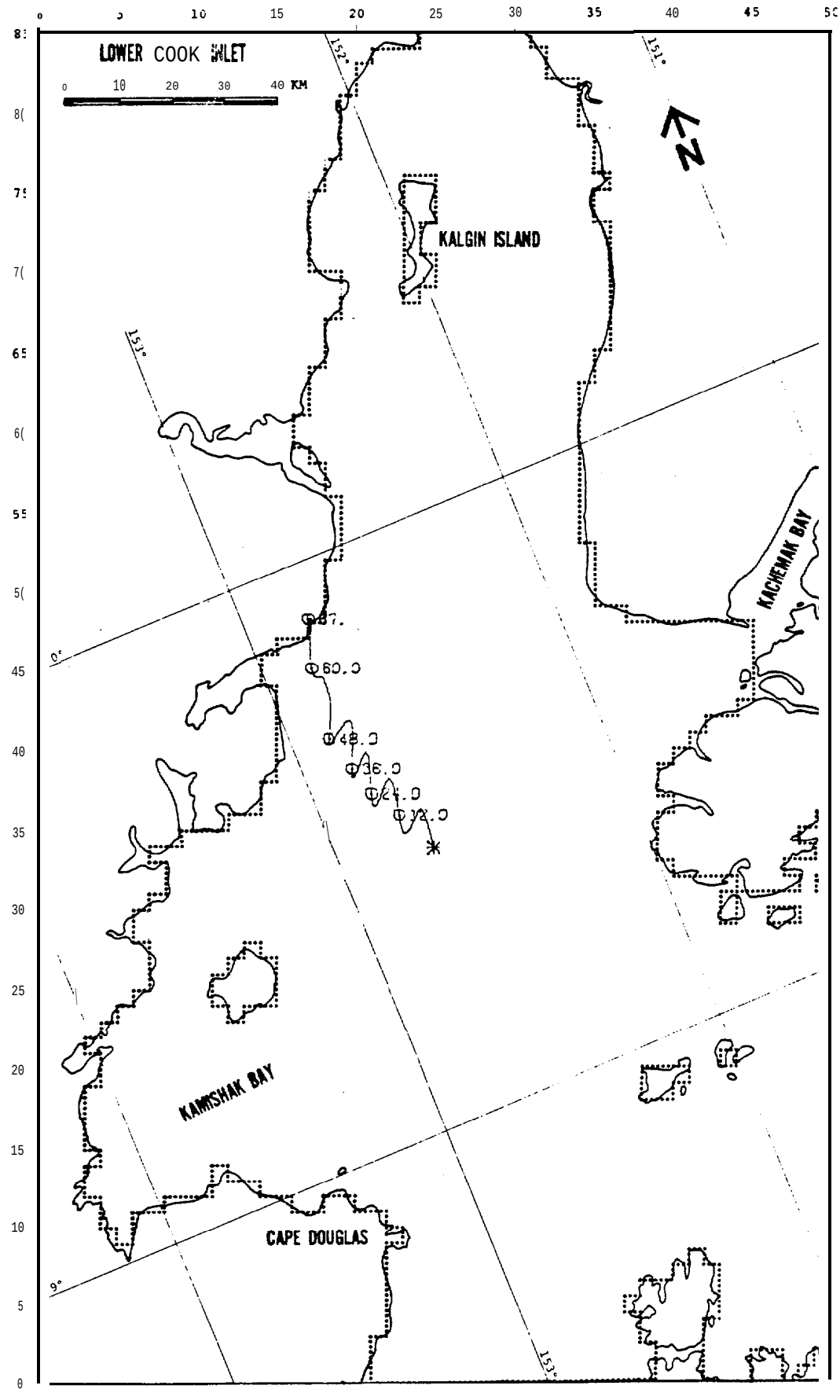

FIGURE B-24: BASE CASE

WIND
3

SITE
7

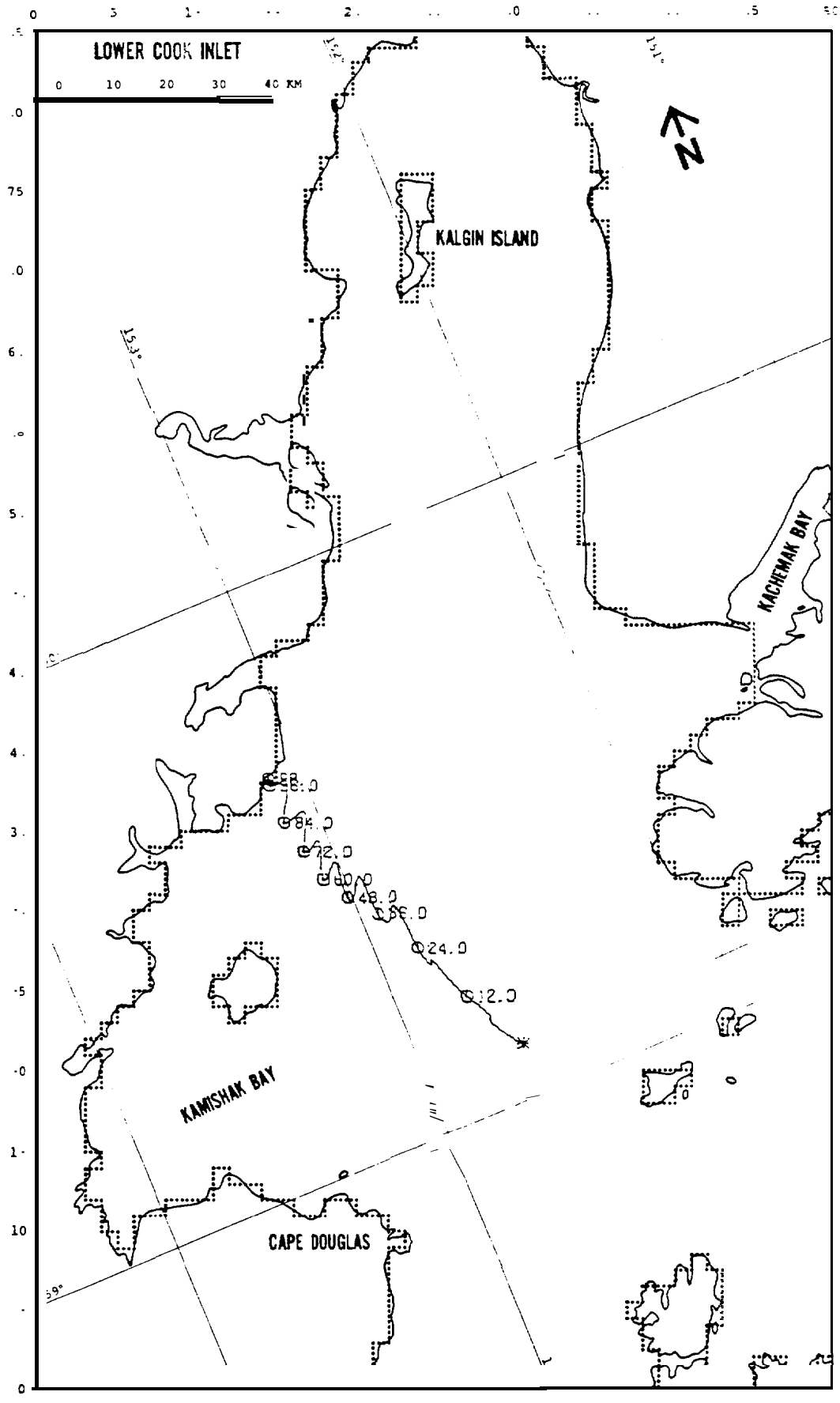

FIGURE B-25: BASE CASE

WIND
3

SITE
8

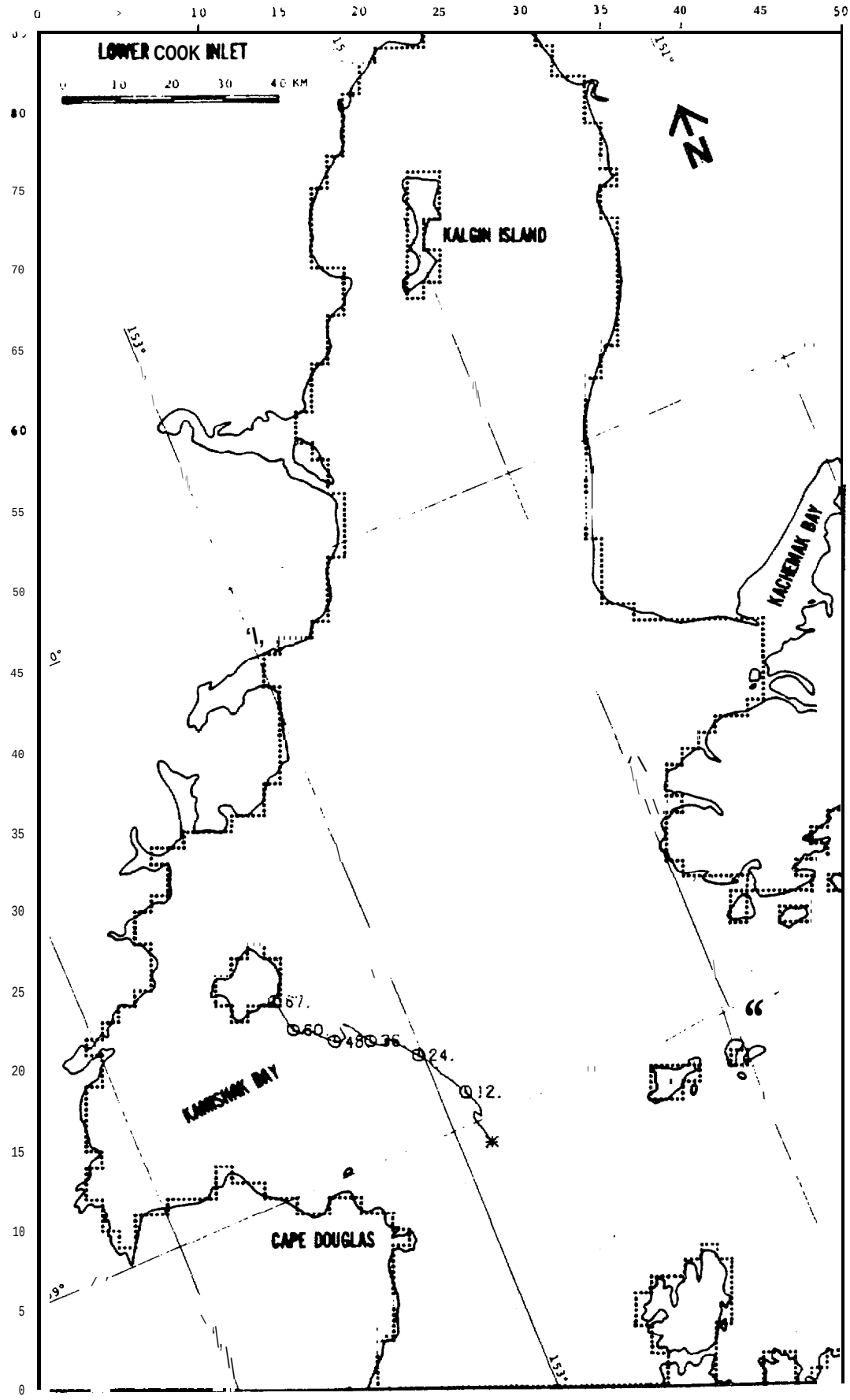

FIGURE B-26: BASE CASE

WIND
3

SITE
8A

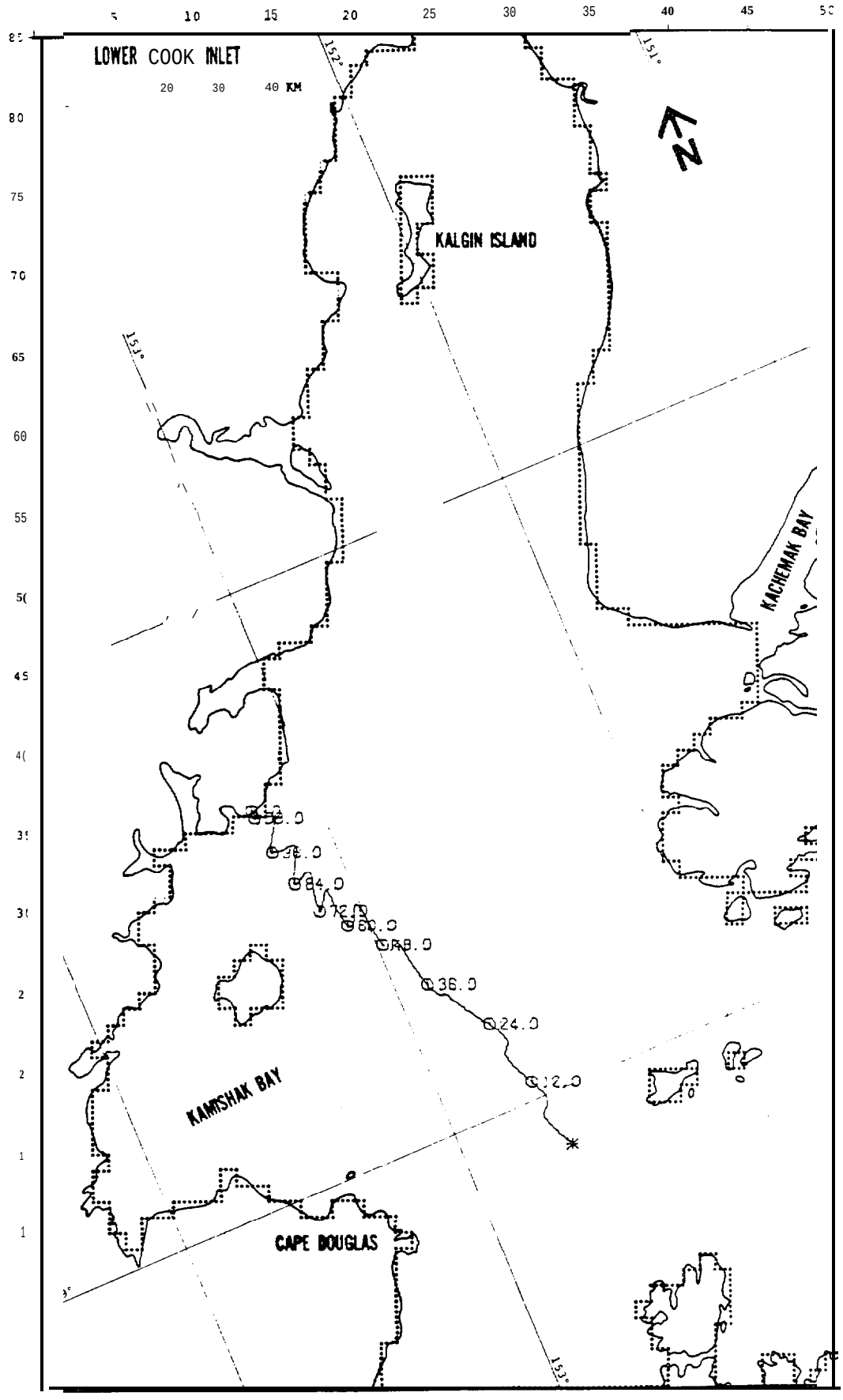

FIGURE B-27: BASE CASE

WIND
4

SITE
1

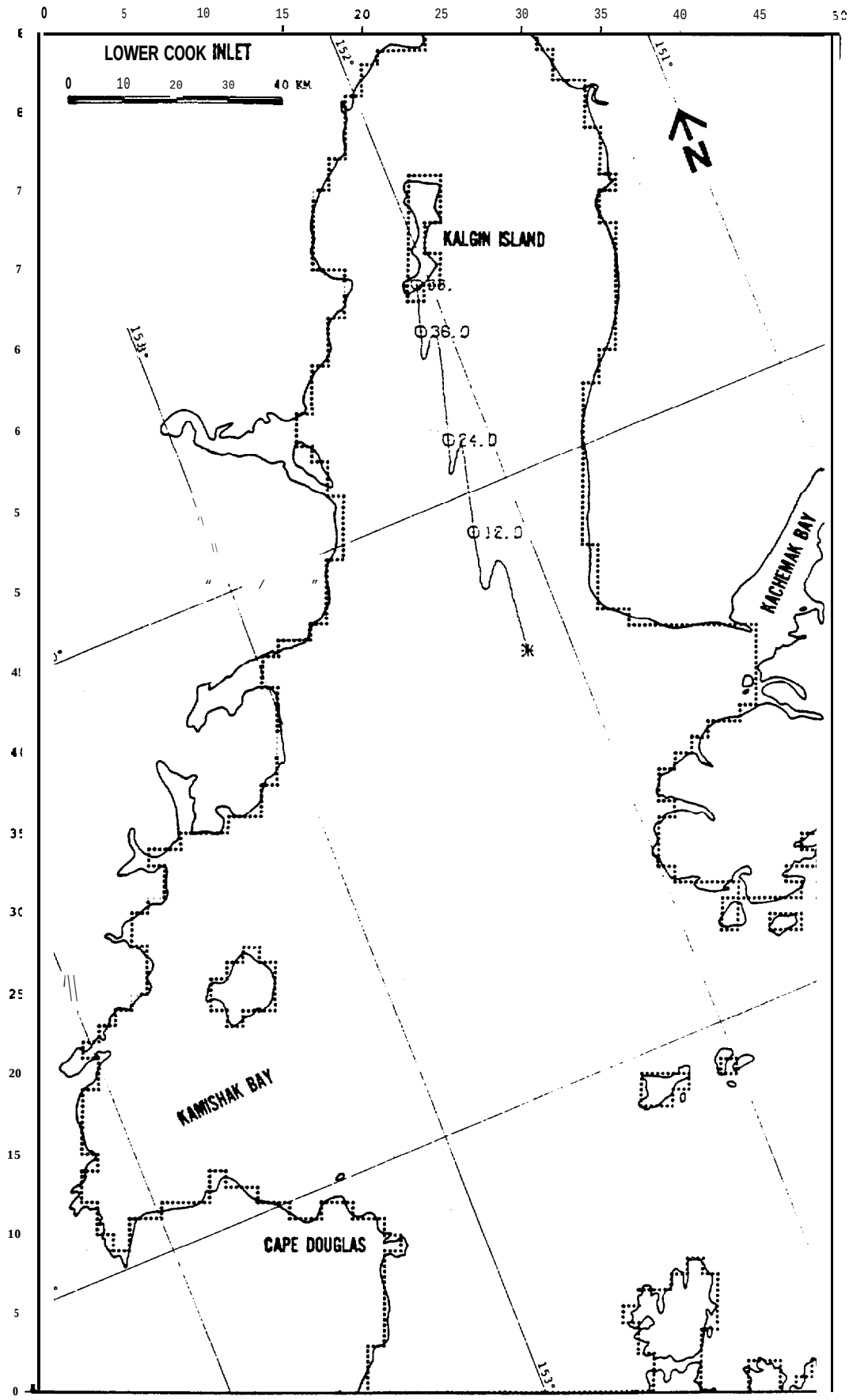

FIGURE B-28: BASE CASE

WIND
∠

SITE
2

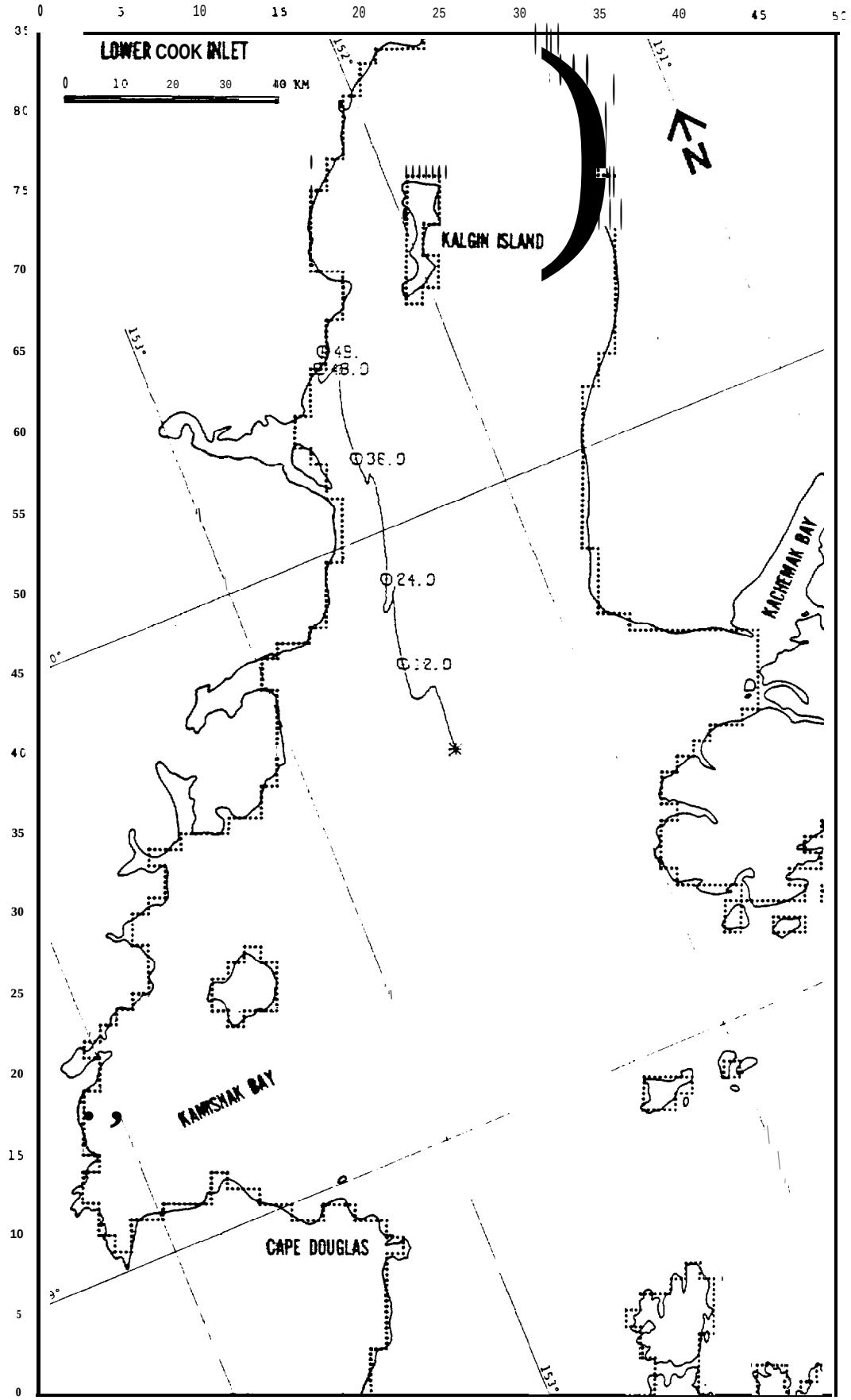

FIGURE B-29: BASE CASE

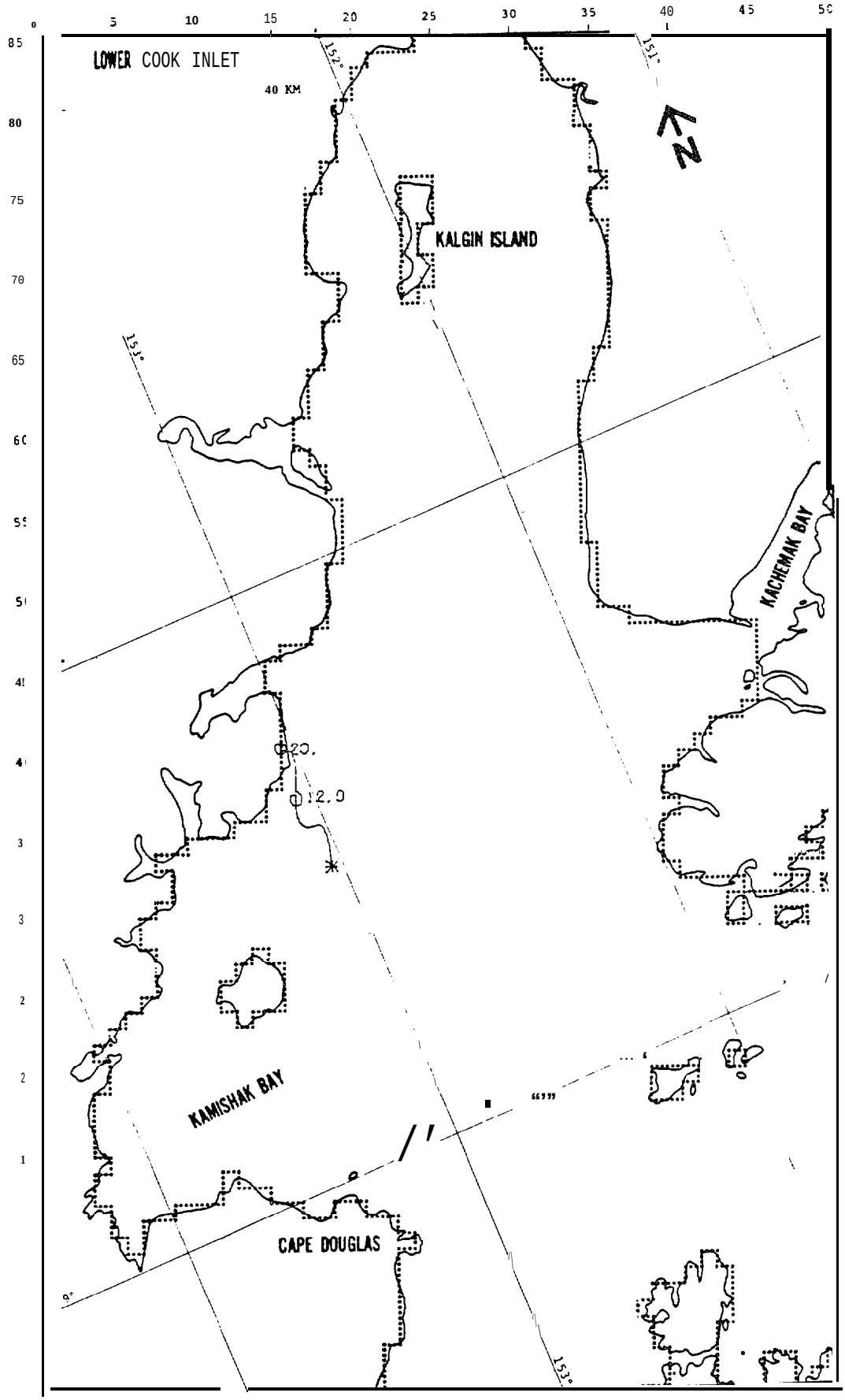

FIGURE B-30: BASE CASE

WIND
4

SITE
4

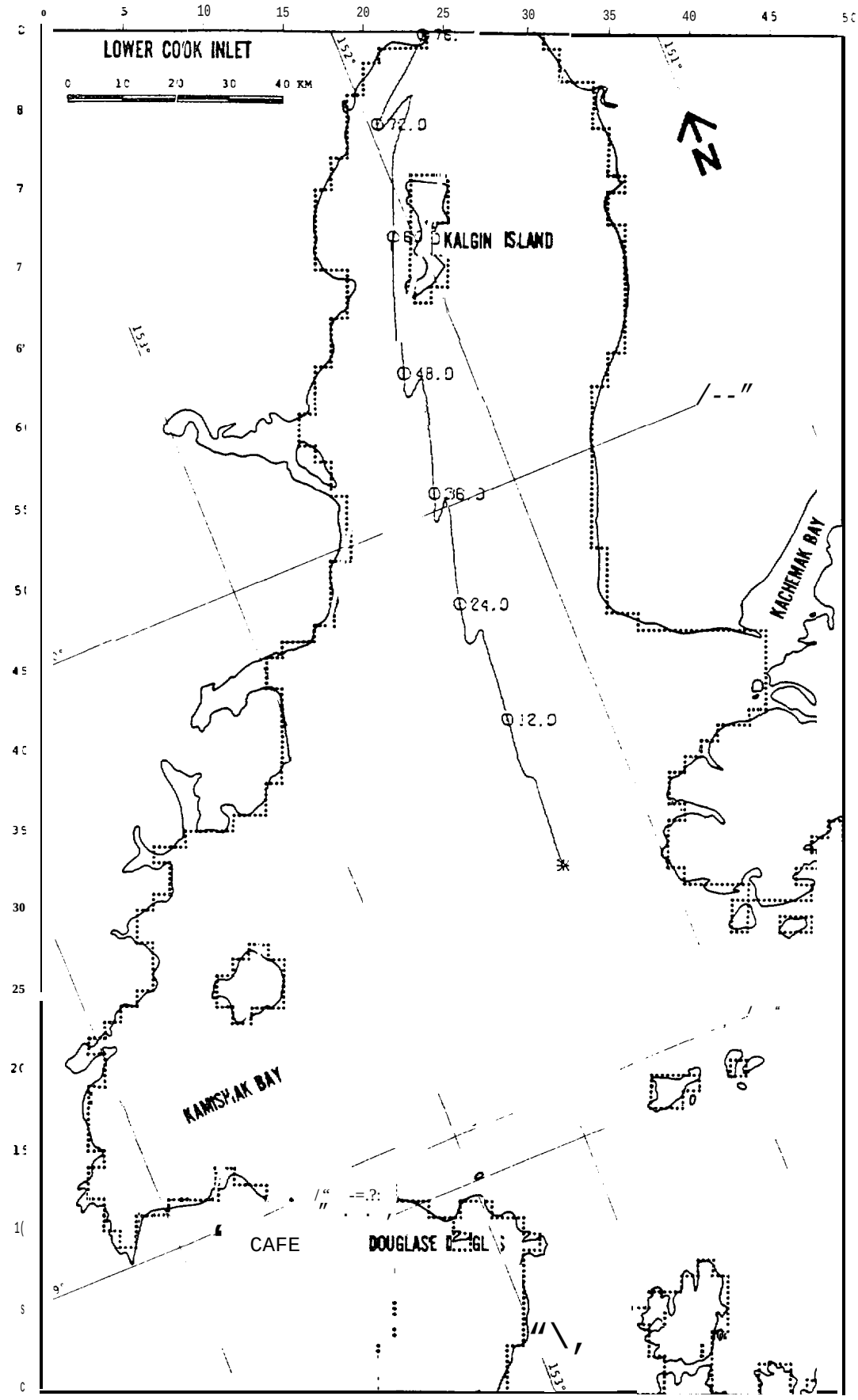

FIGURE B-31: BASE CASE

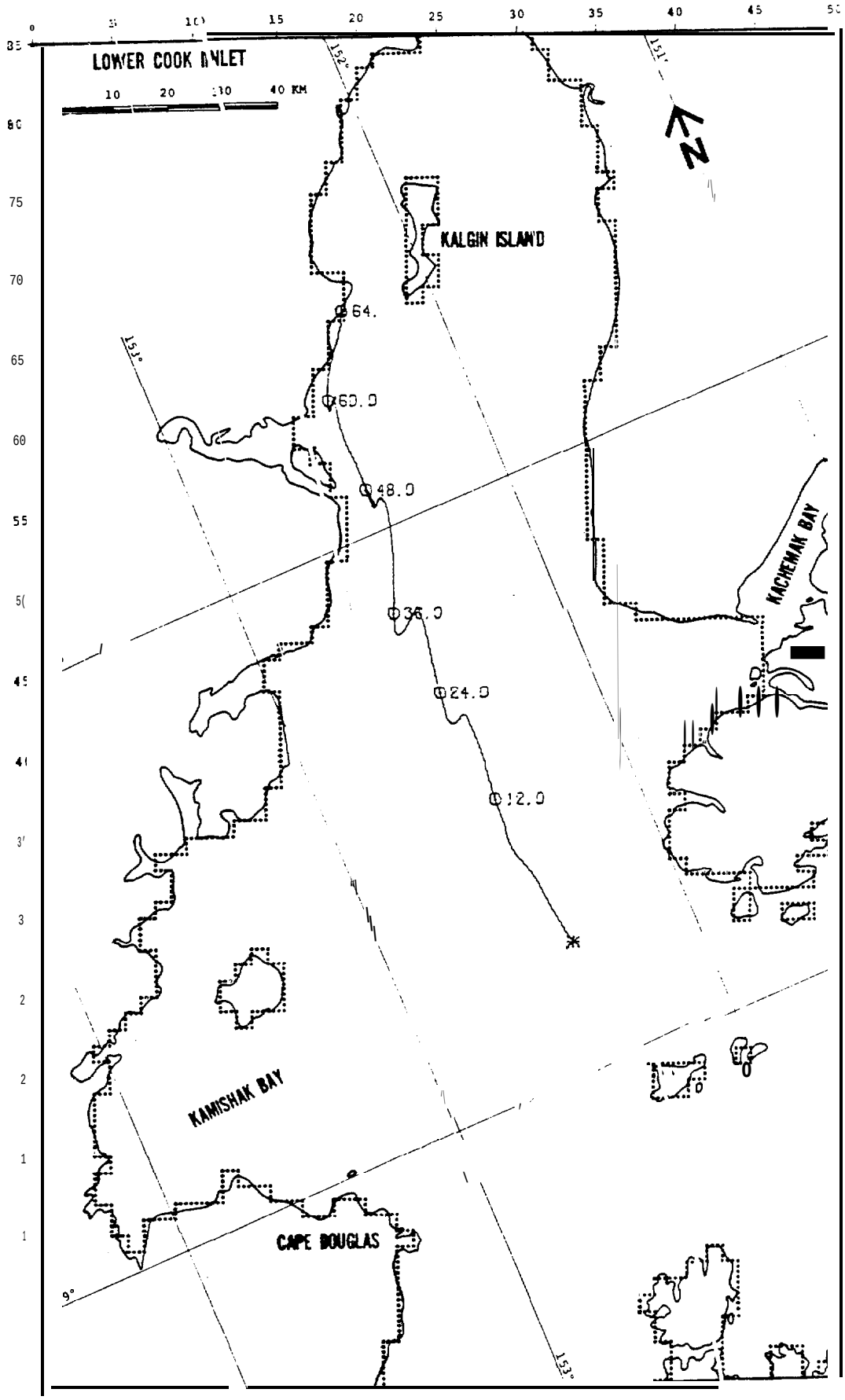

WIND
4

SITE
5

592, 4

FIGURE B-32: BASE CASE

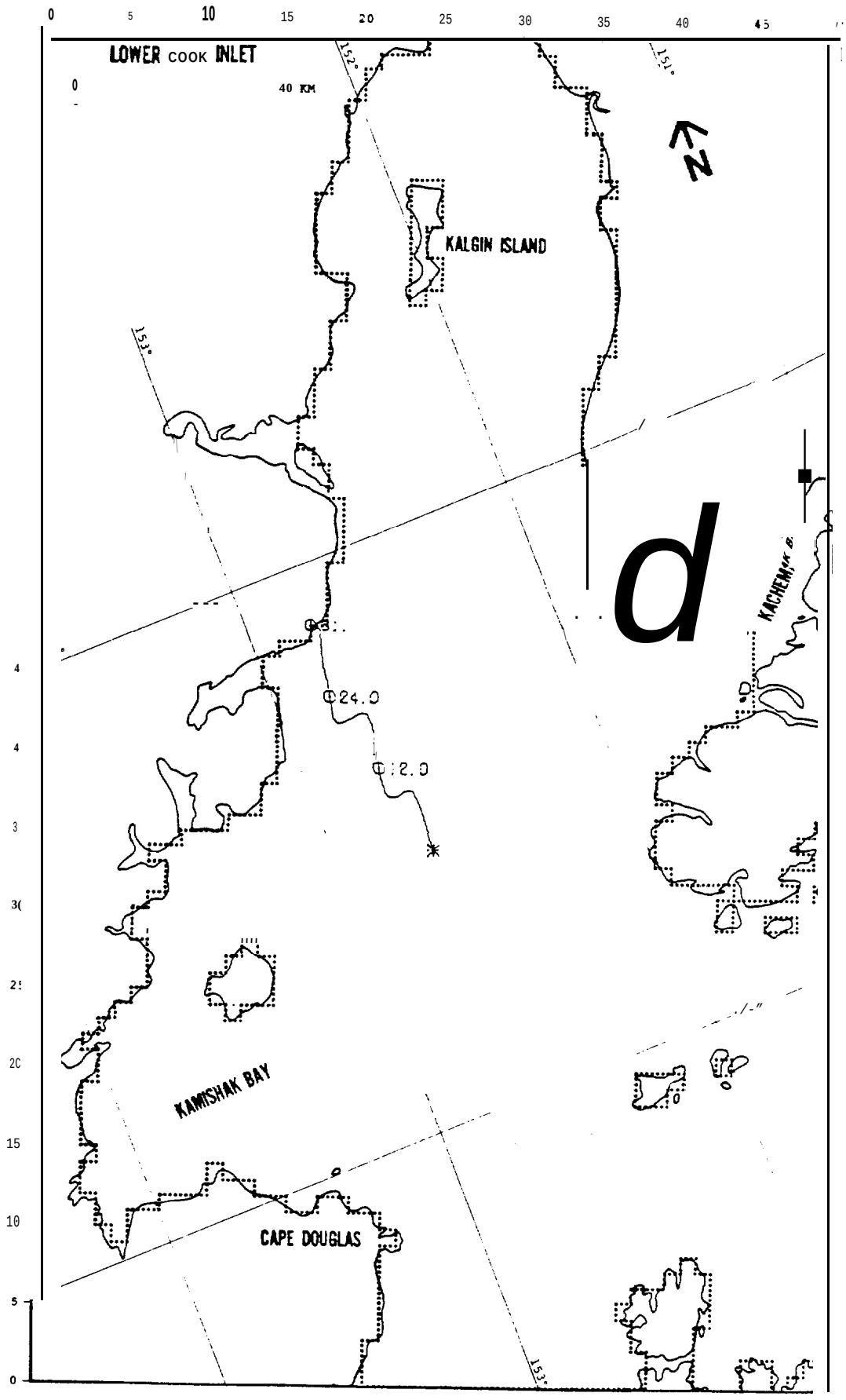

WIND
4

SITE
6

FIGURE B-33: BASE CASE

WIND
4

SITE
7

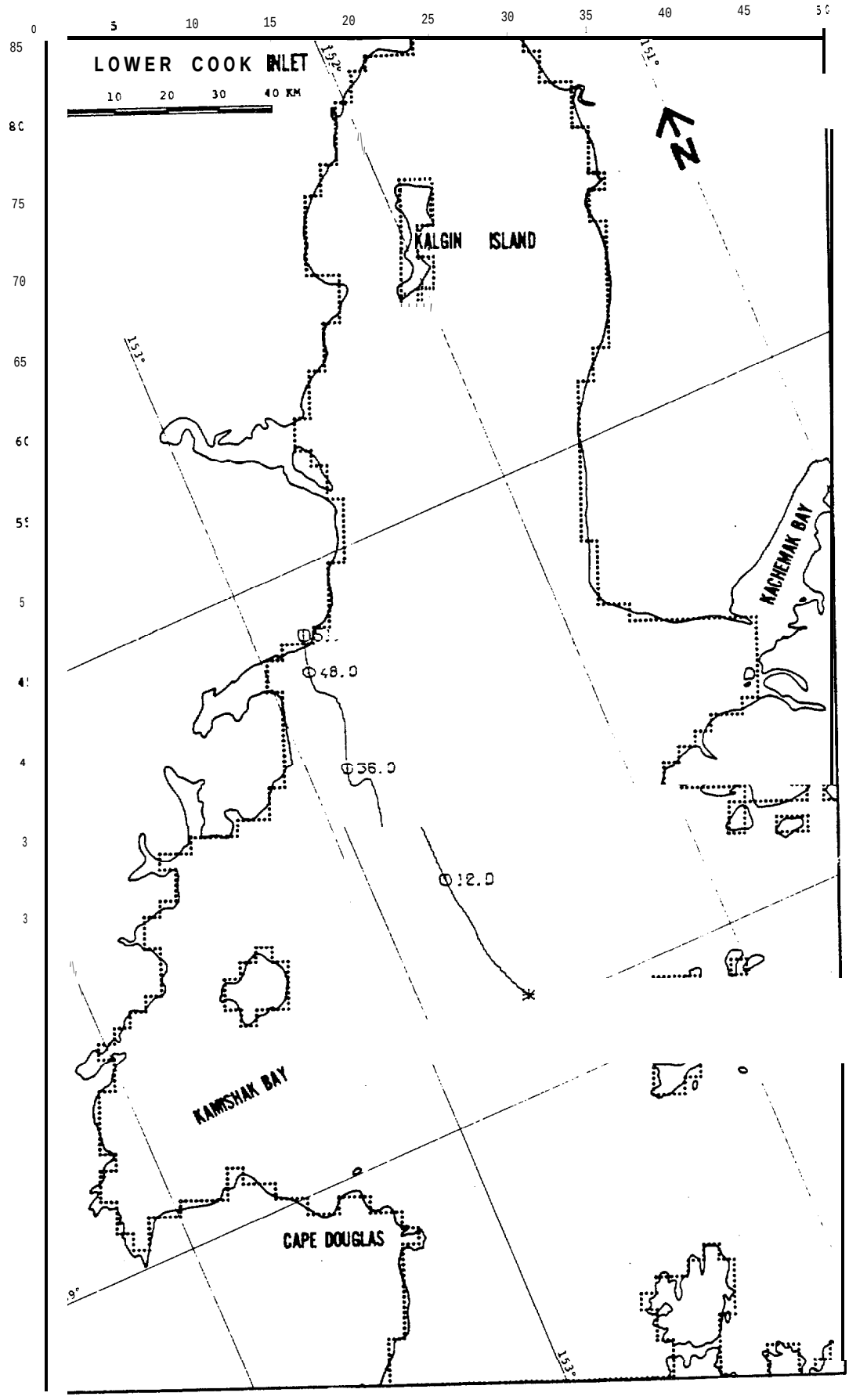

FIGURE B-34: BASE CASE

WIND
4

SITE
8

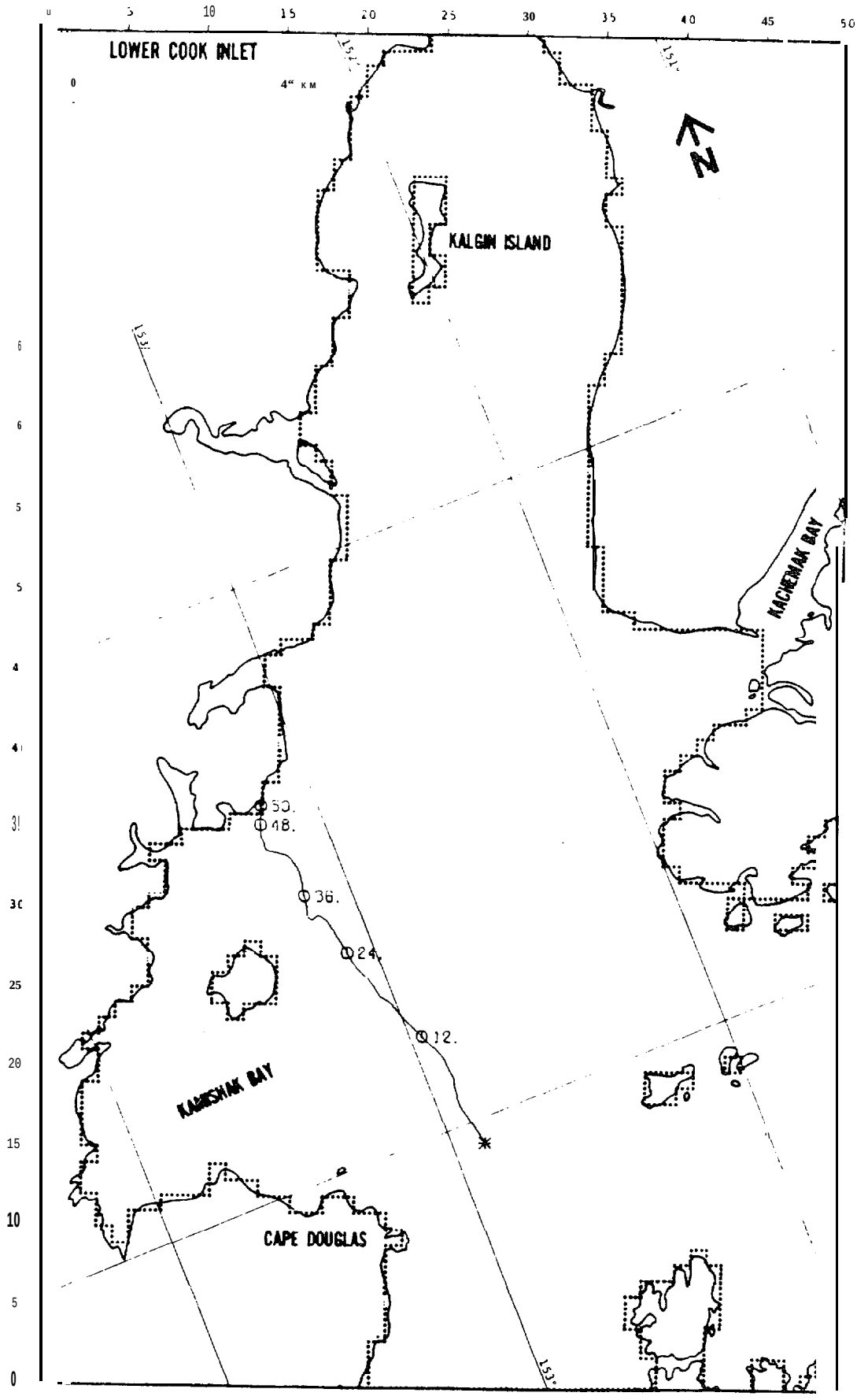

FIGURE B-35: BASE CASE

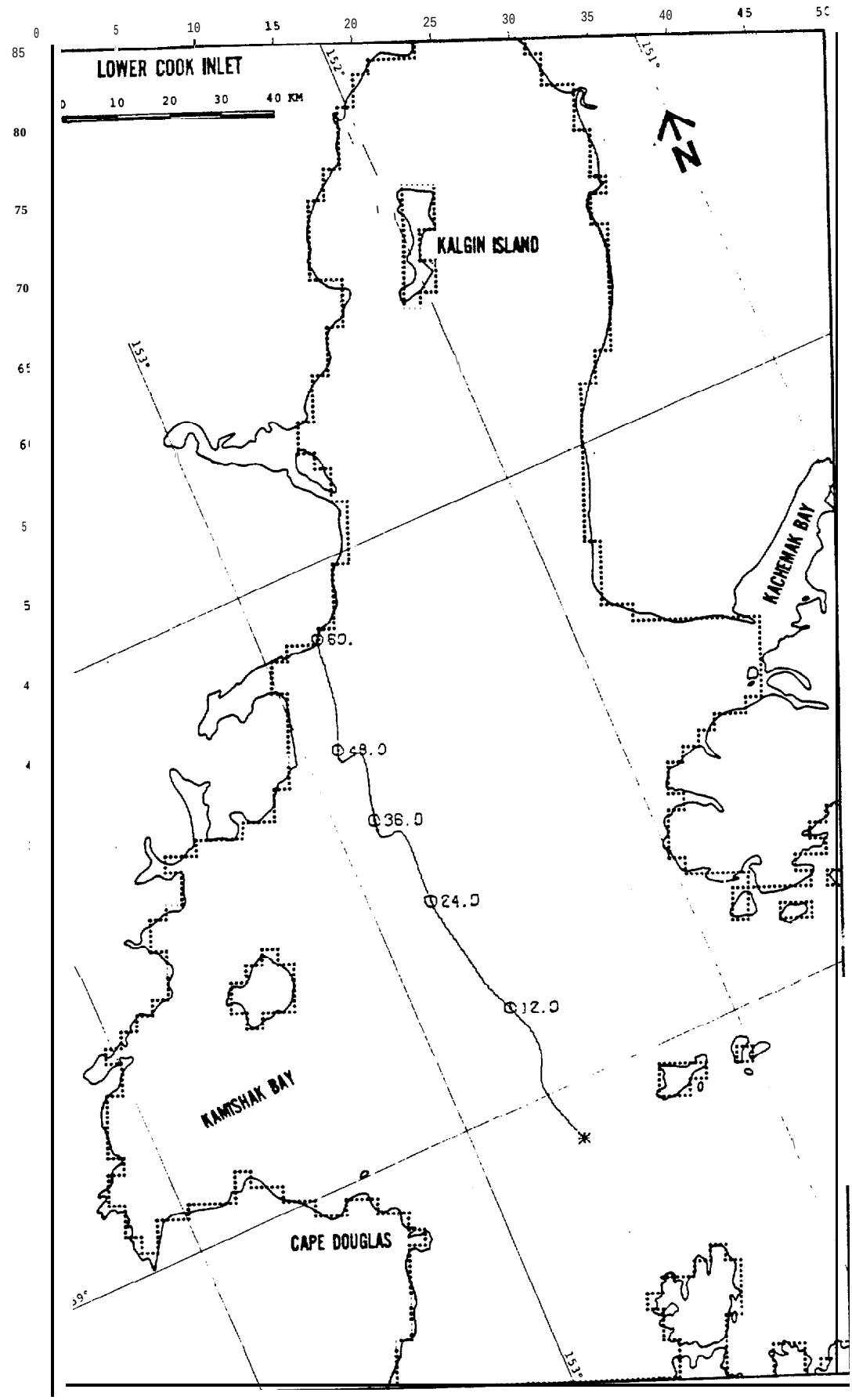

WIND
4

SITE
8 A

FIGURE B-36: BASE CASE

WIND
5

SITE
1

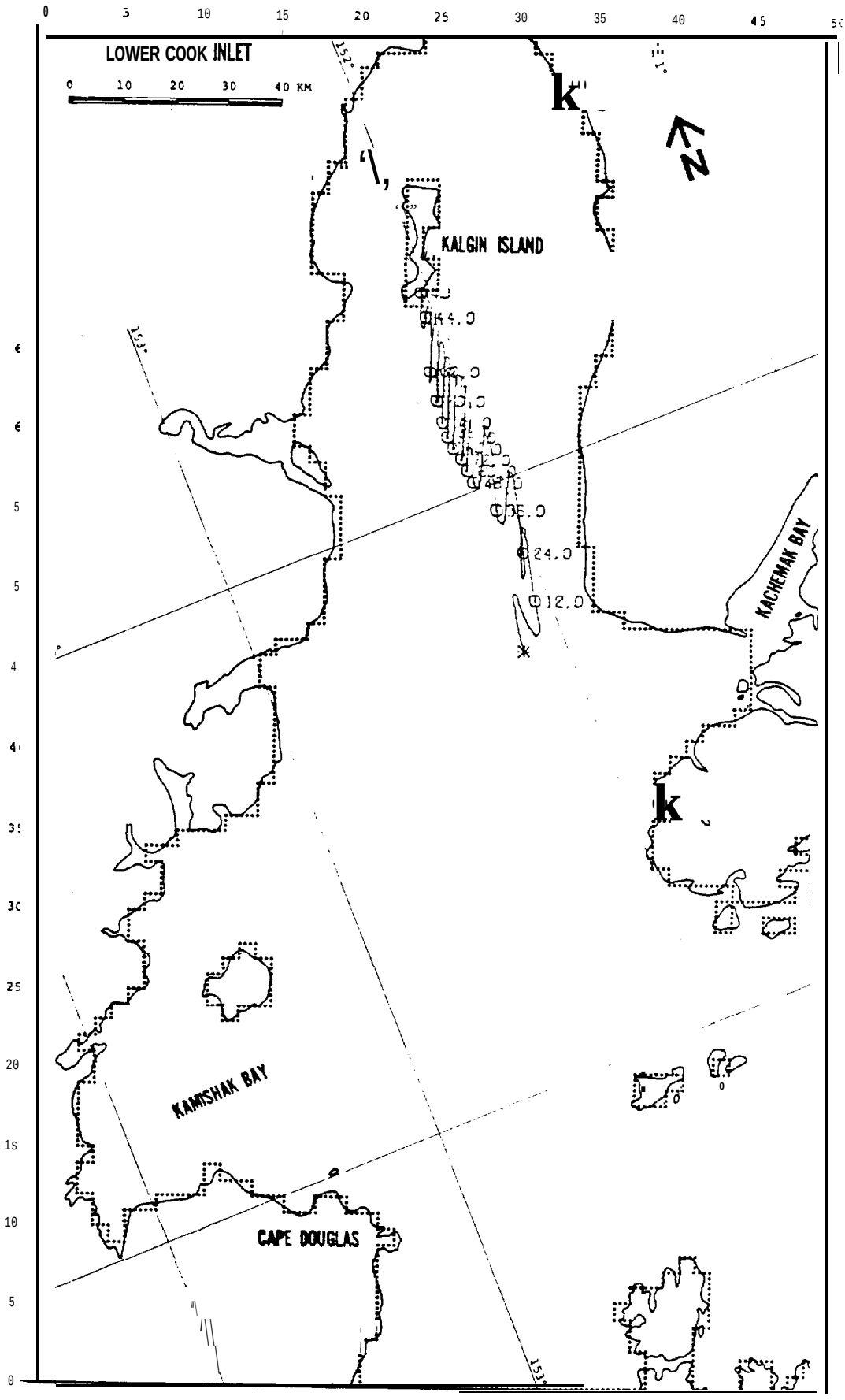

FIGURE B-37: BASE CASE

WIND
5

SITE
2

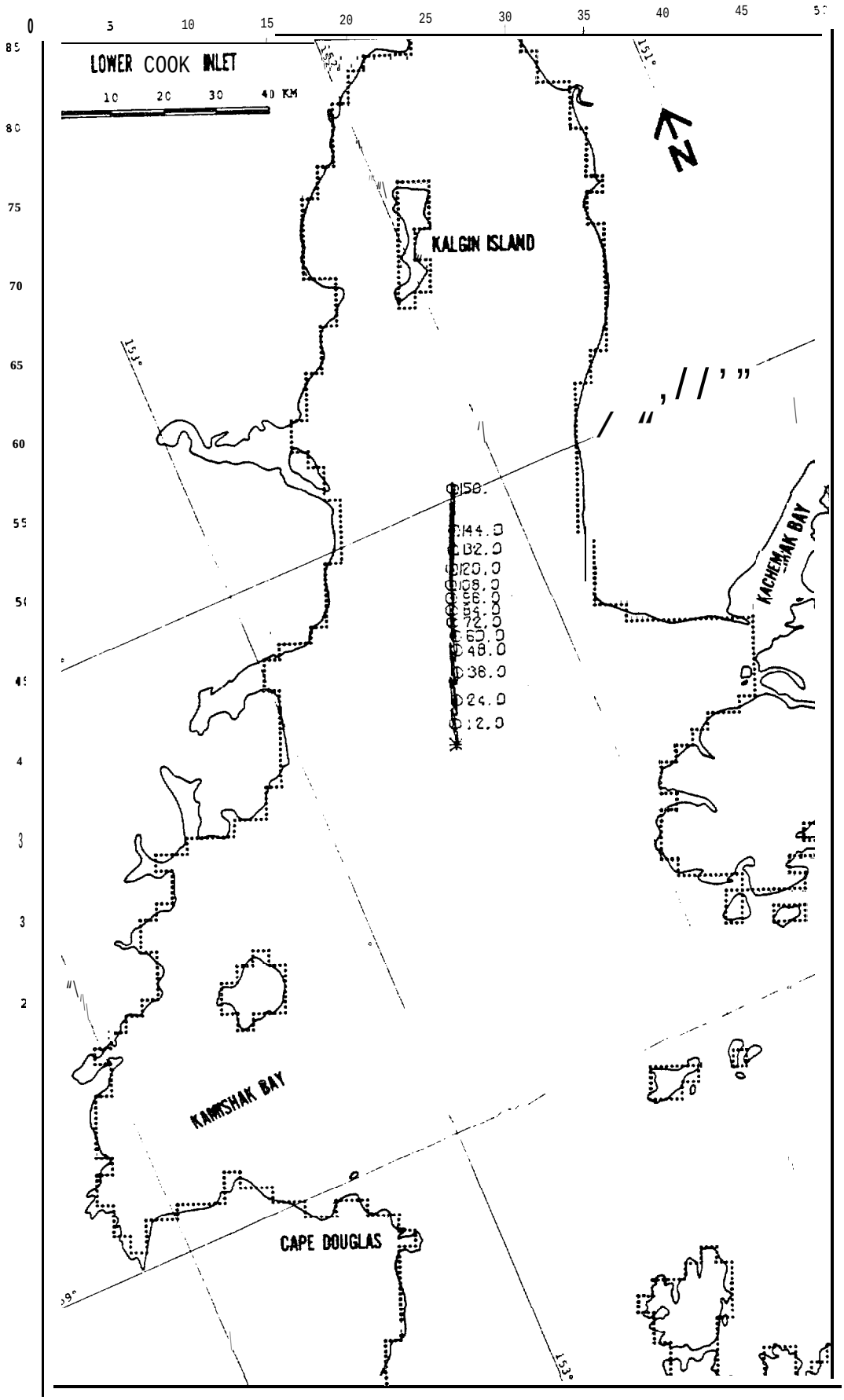

FIGURE B-38: BASE CASE

WIND
5

SITE
3

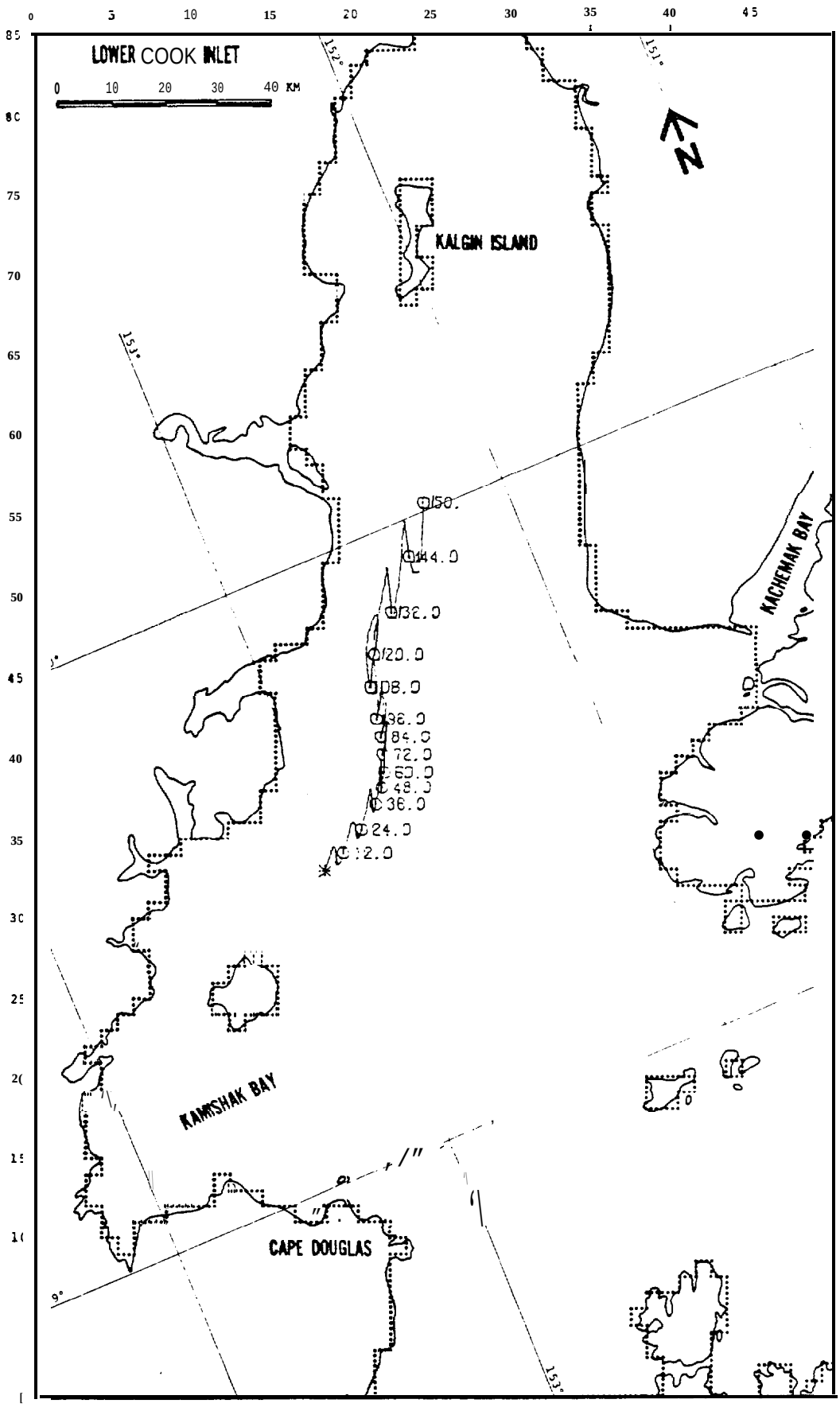

FIGURE B-39: BASE CASE

WIND
5

SITE
4

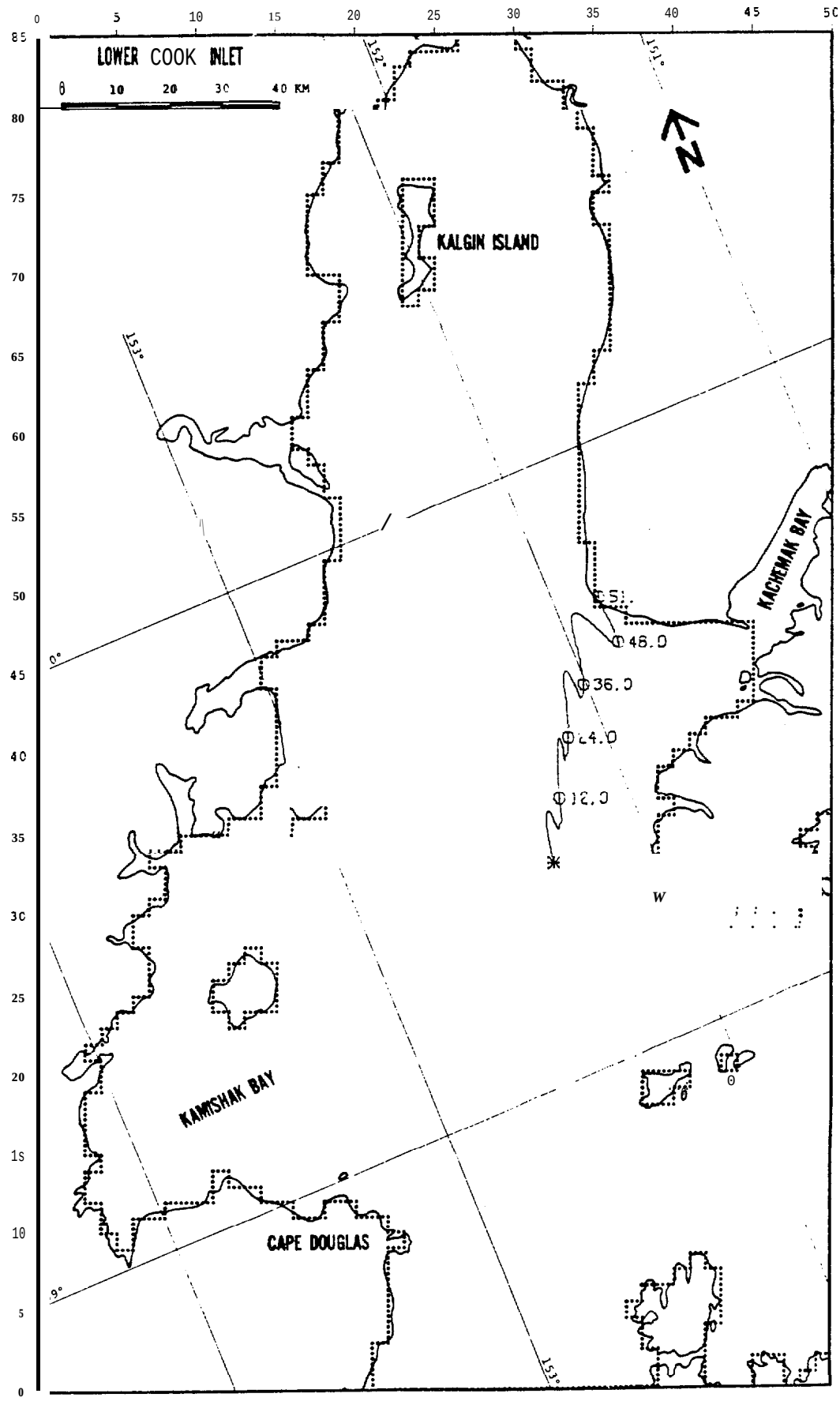

FIGURE B-40: BASE CASE

WIND
5

SITE
5

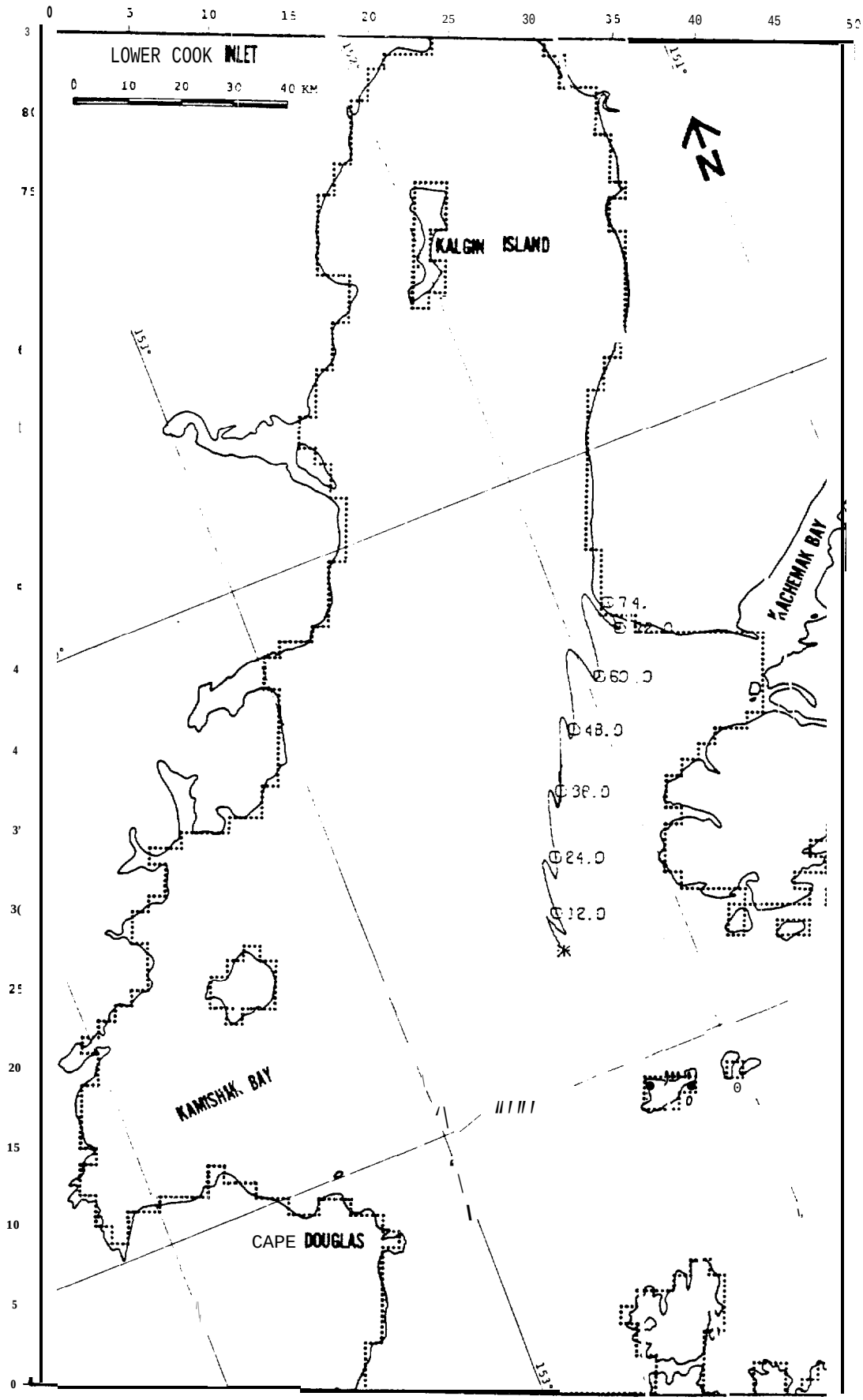

601

FIGURE B-41: BASE CASE

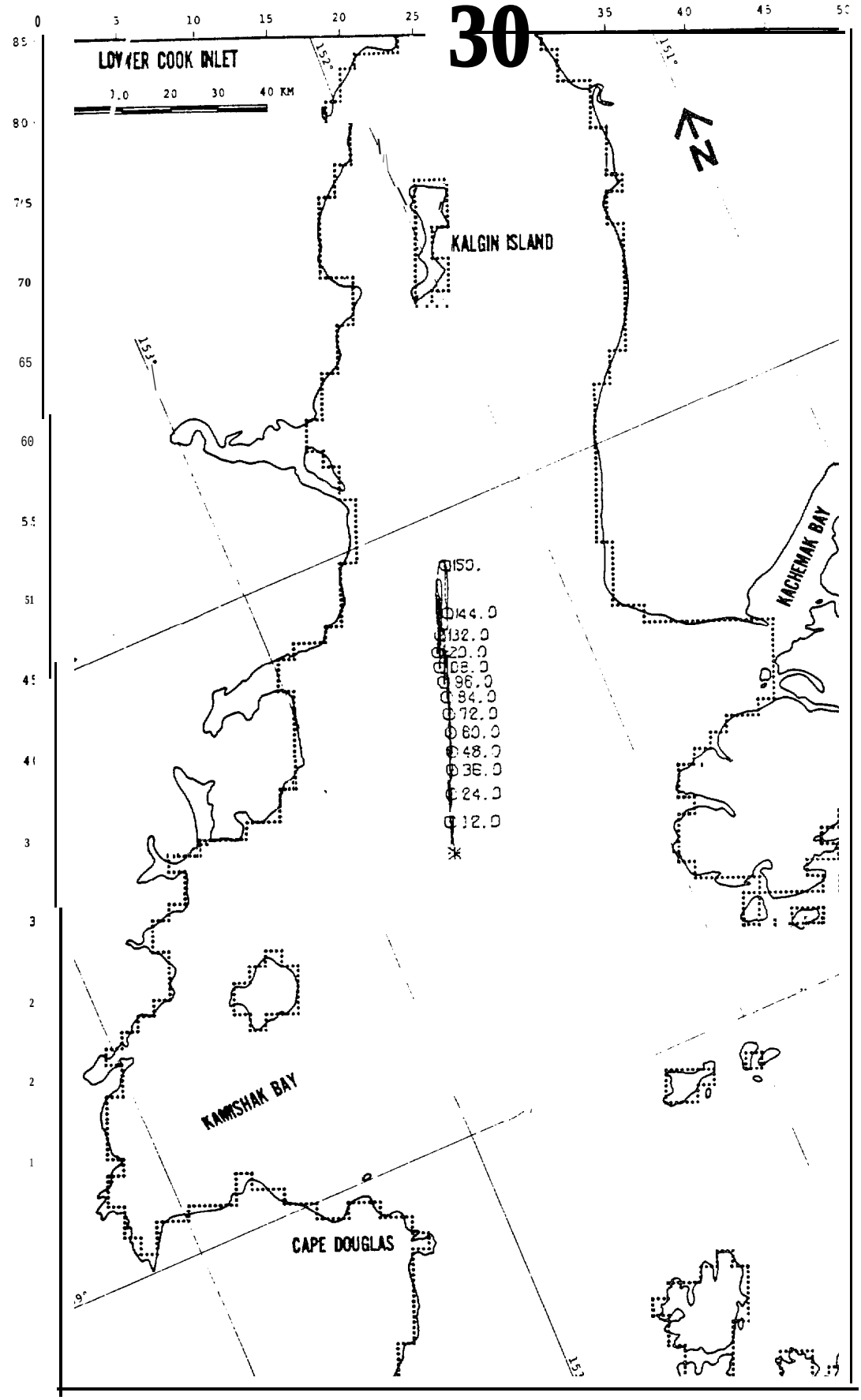

FIGURE B-42: BASE CASE

WIND
5

SITE
7

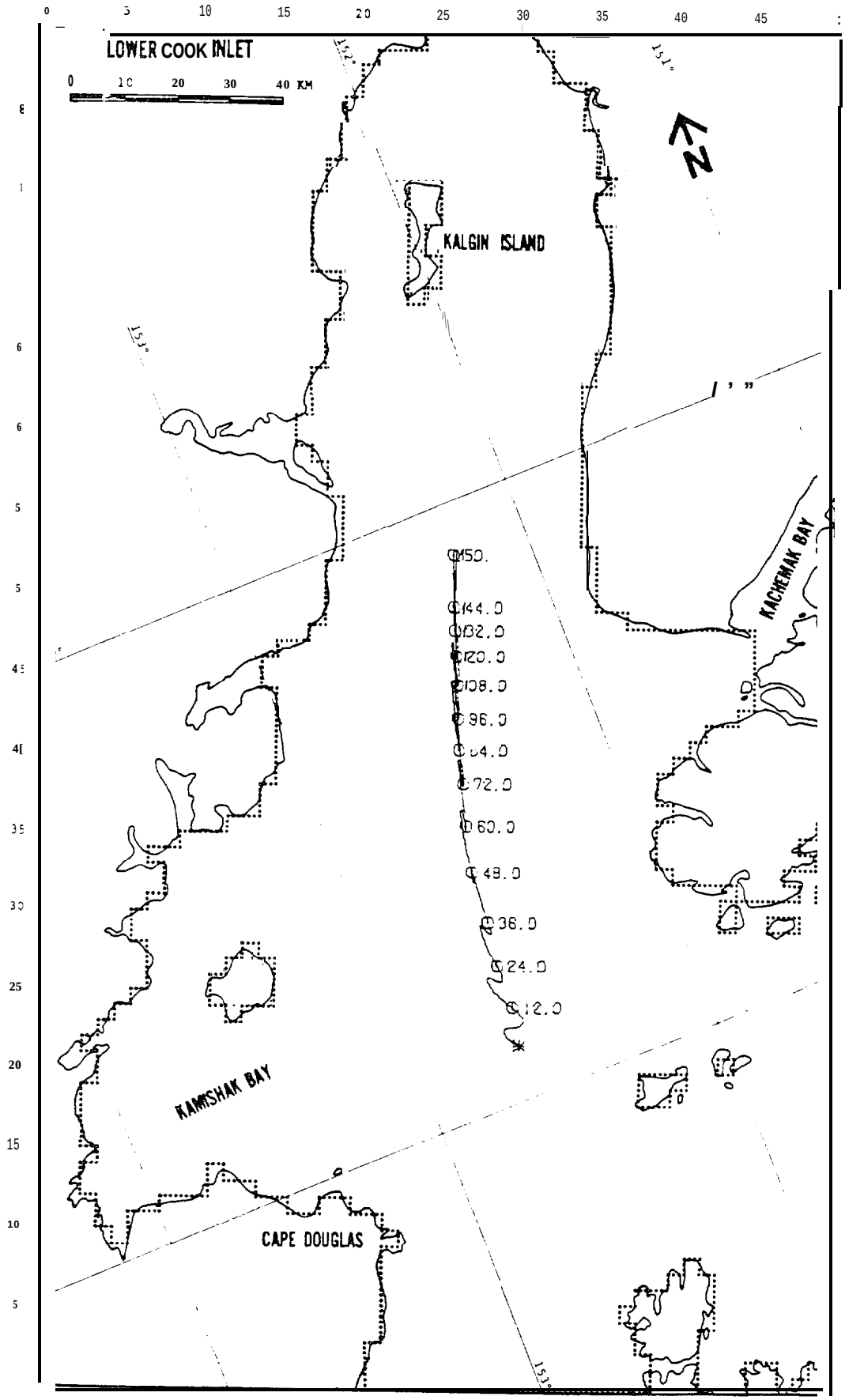

FIGURE B-43: BASE CASE

WIND
5

SITE
8

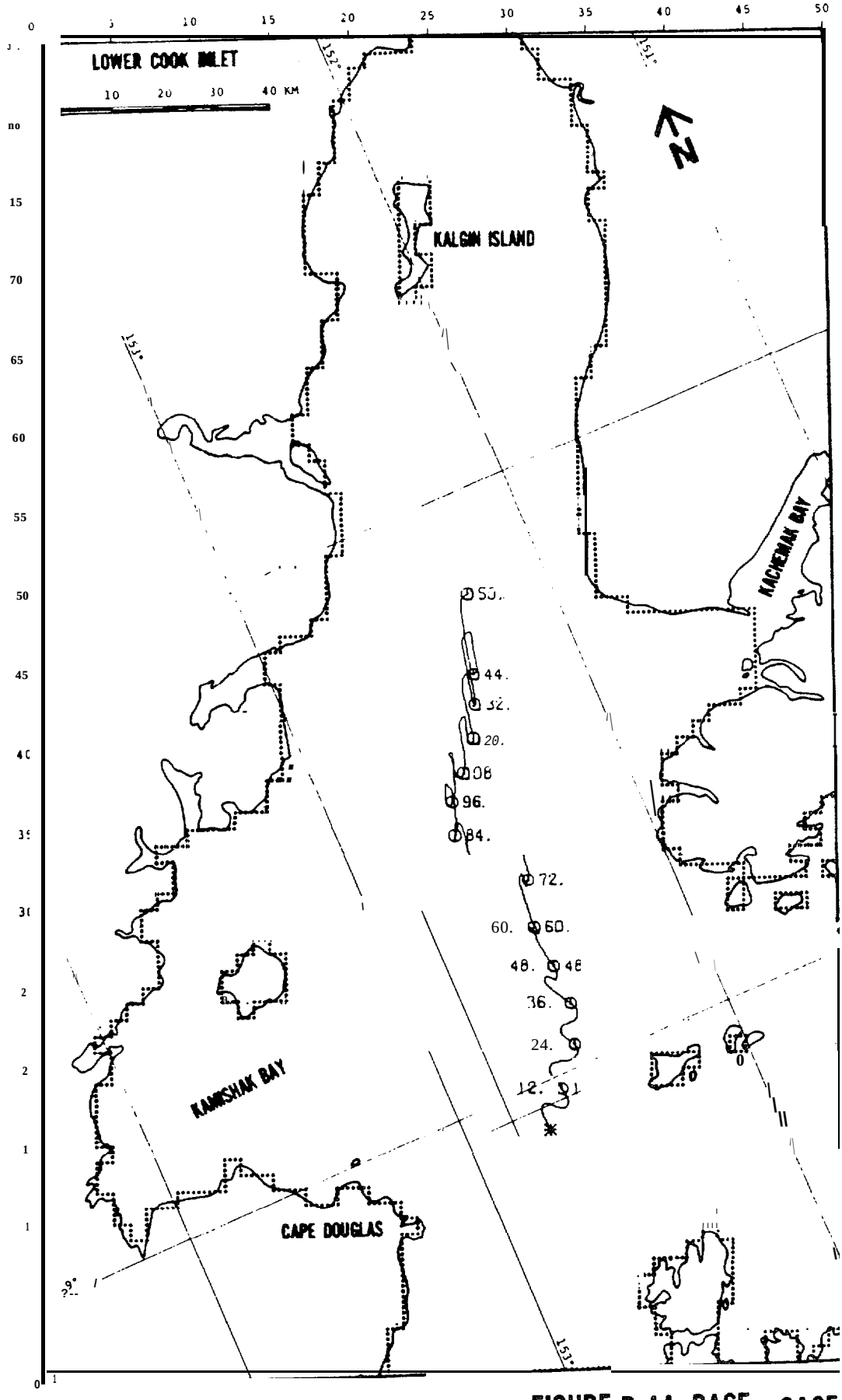

FIGURE B-44: BASE CASE

WIND
5

SITE
8A

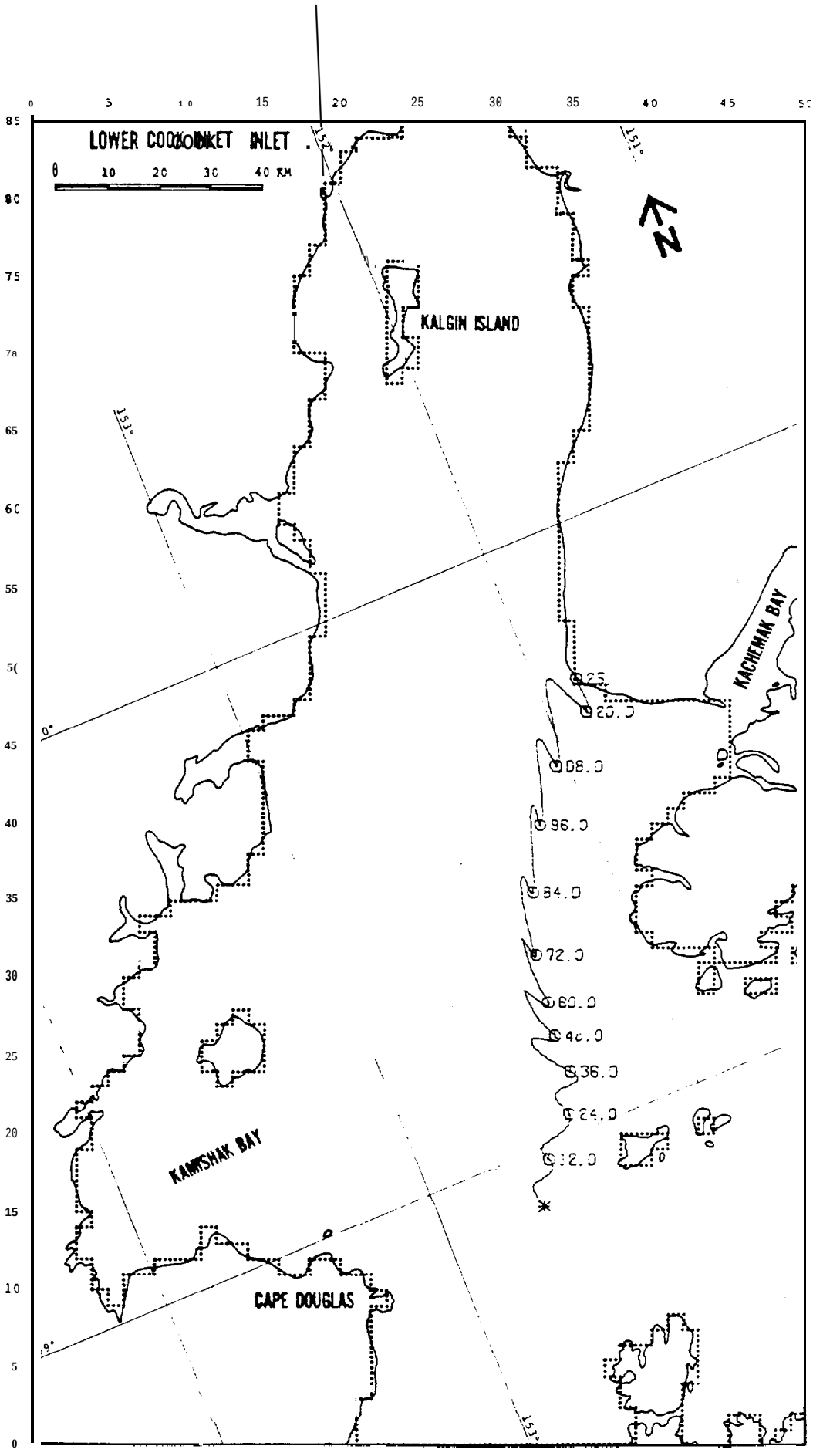

FIGURE B-45: BASE CASE

WIND
6

SITE
1

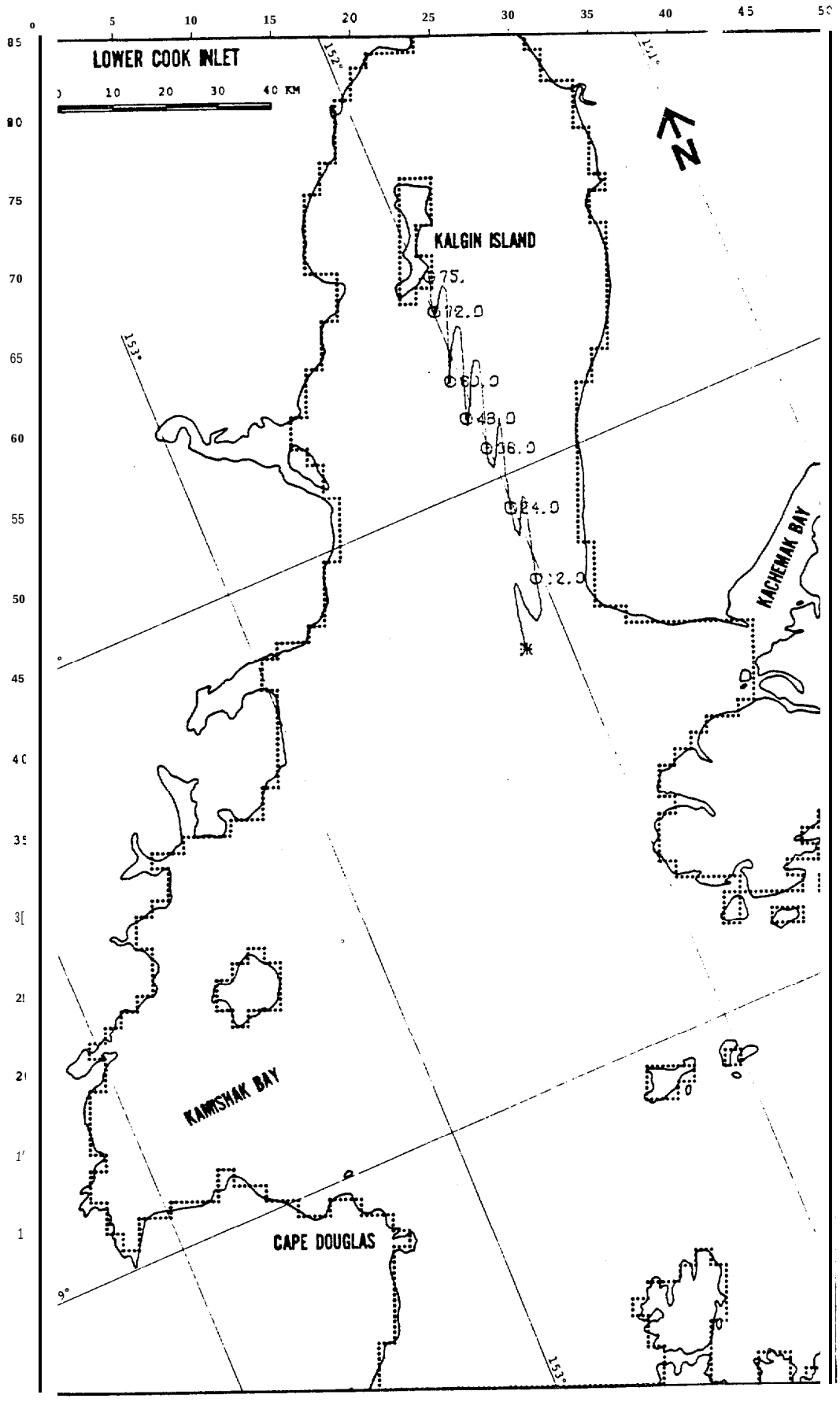

FIGURE B-46: BASE CASE

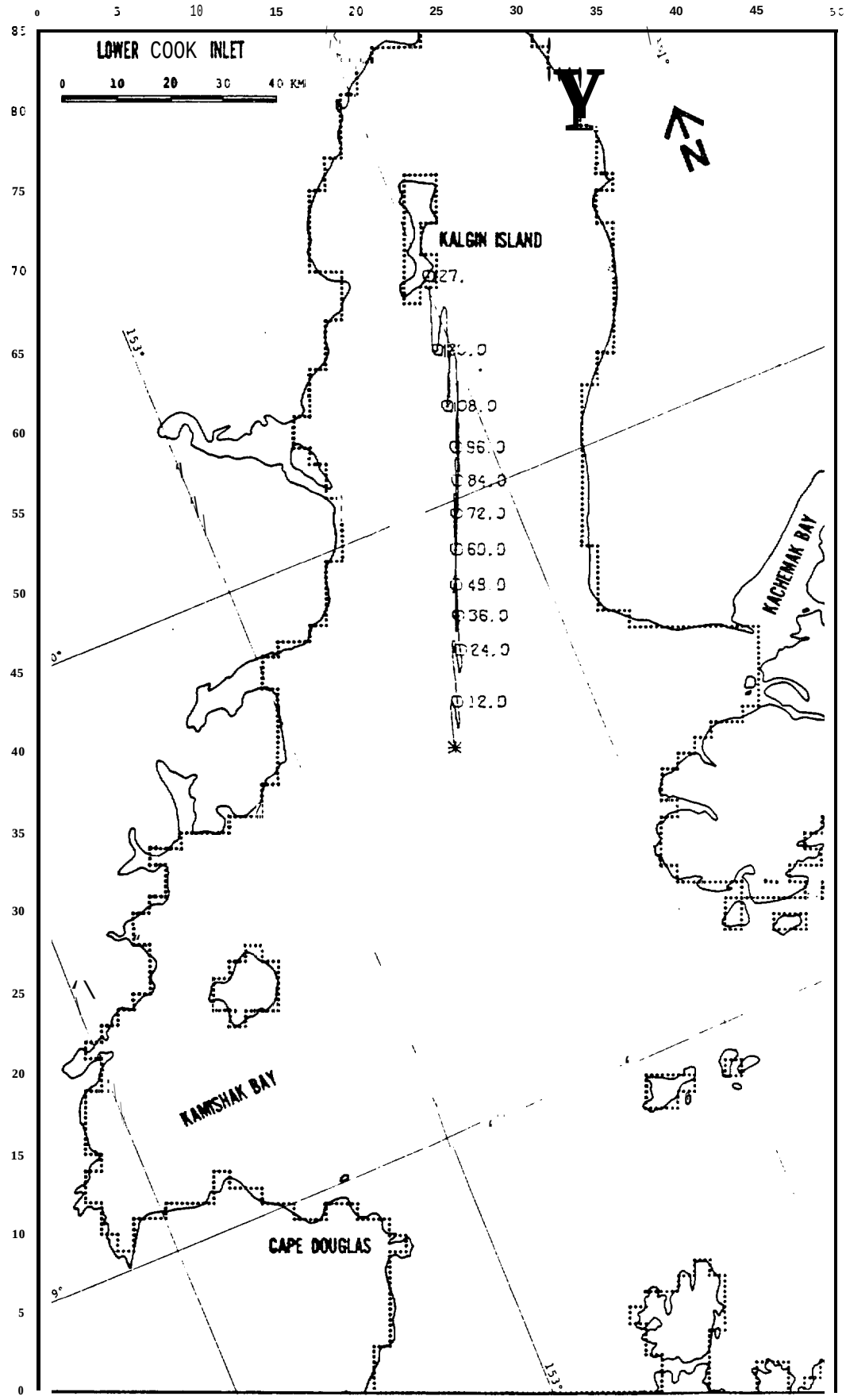

FIGURE B-47: BASE CASE

WIND
6

SITE
3

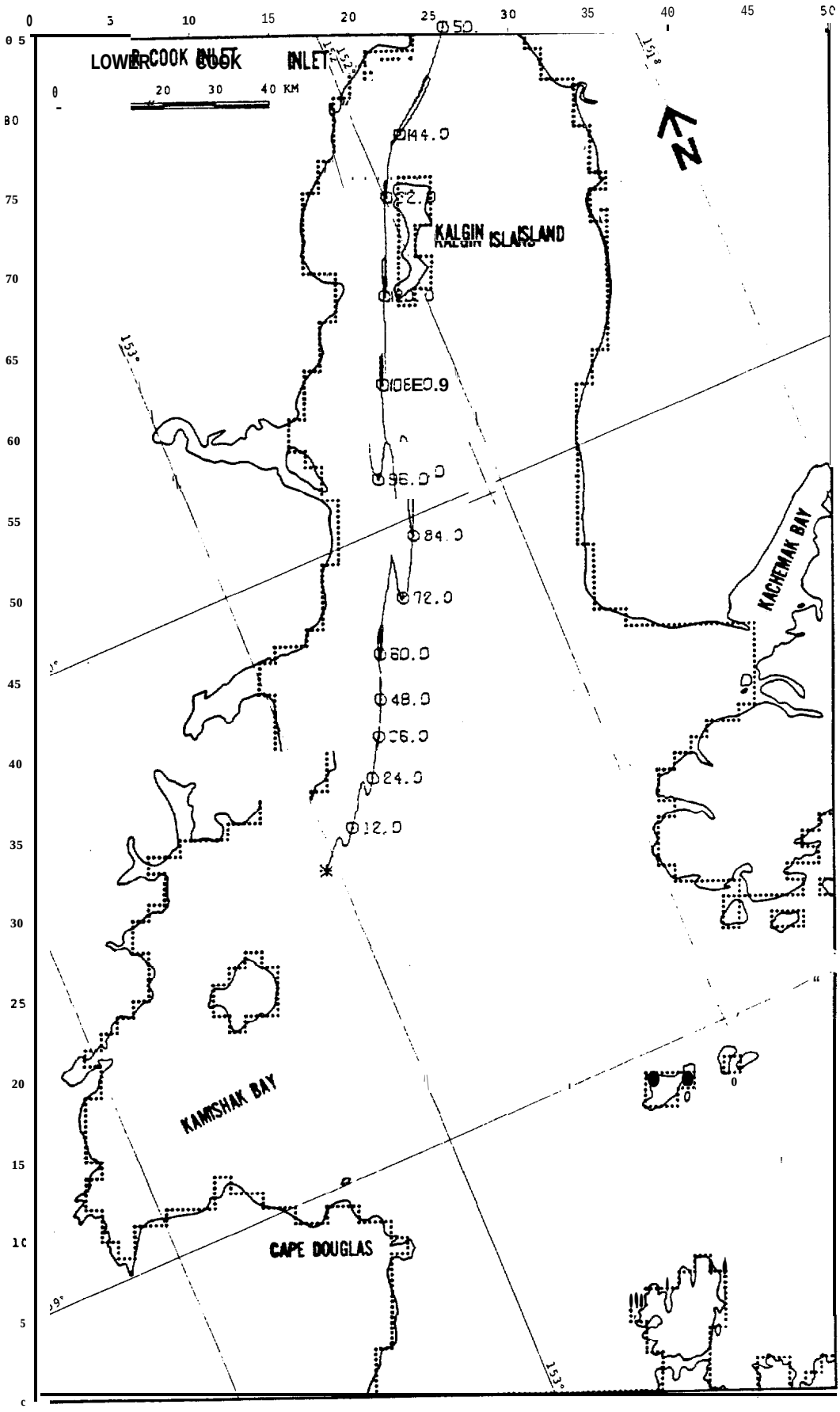

608

FIGURE B-48: BASE CASE

WIND
6

SITE
4

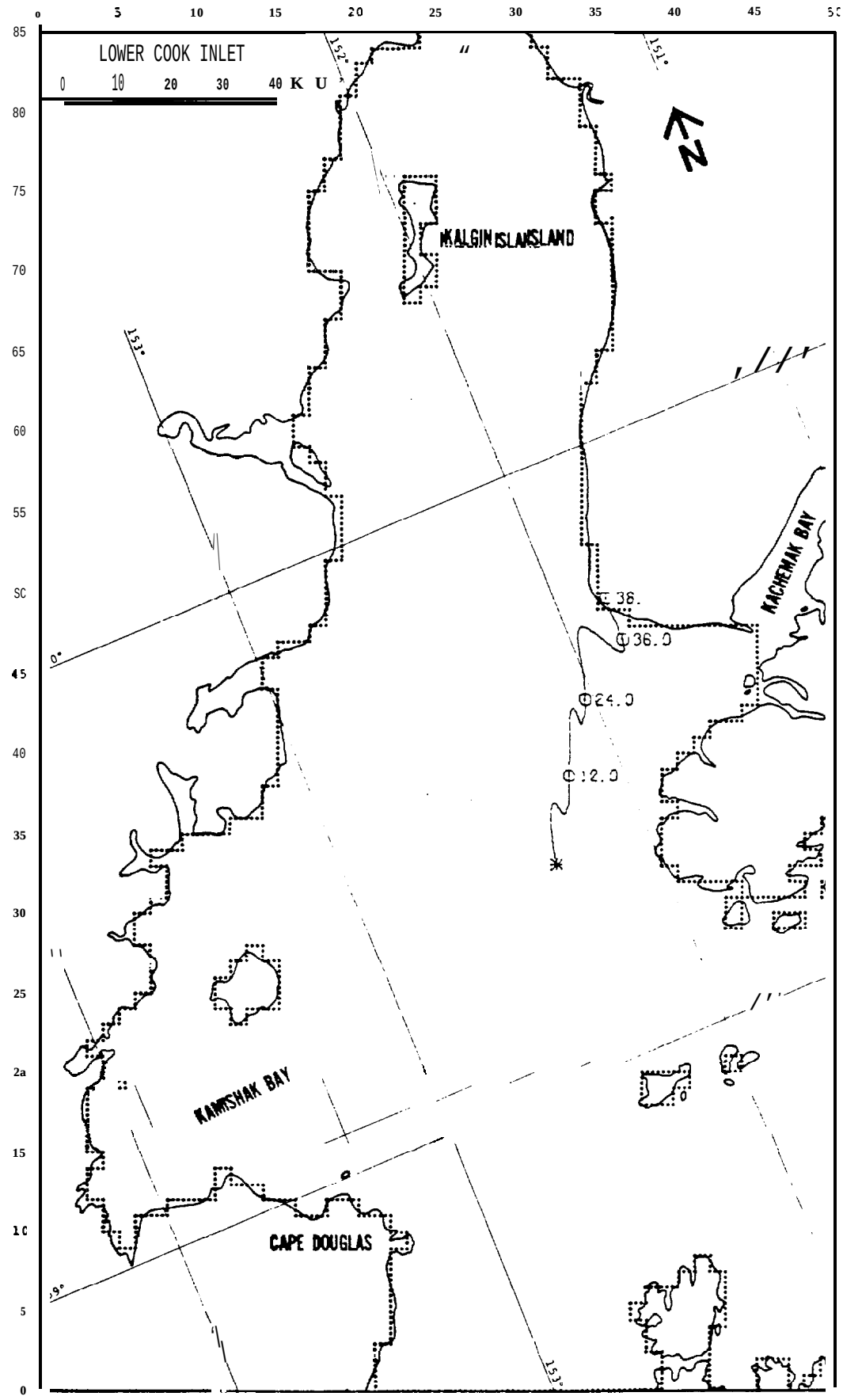

FIGURE B-49: BASE CASE

WIND
6

SITE
5

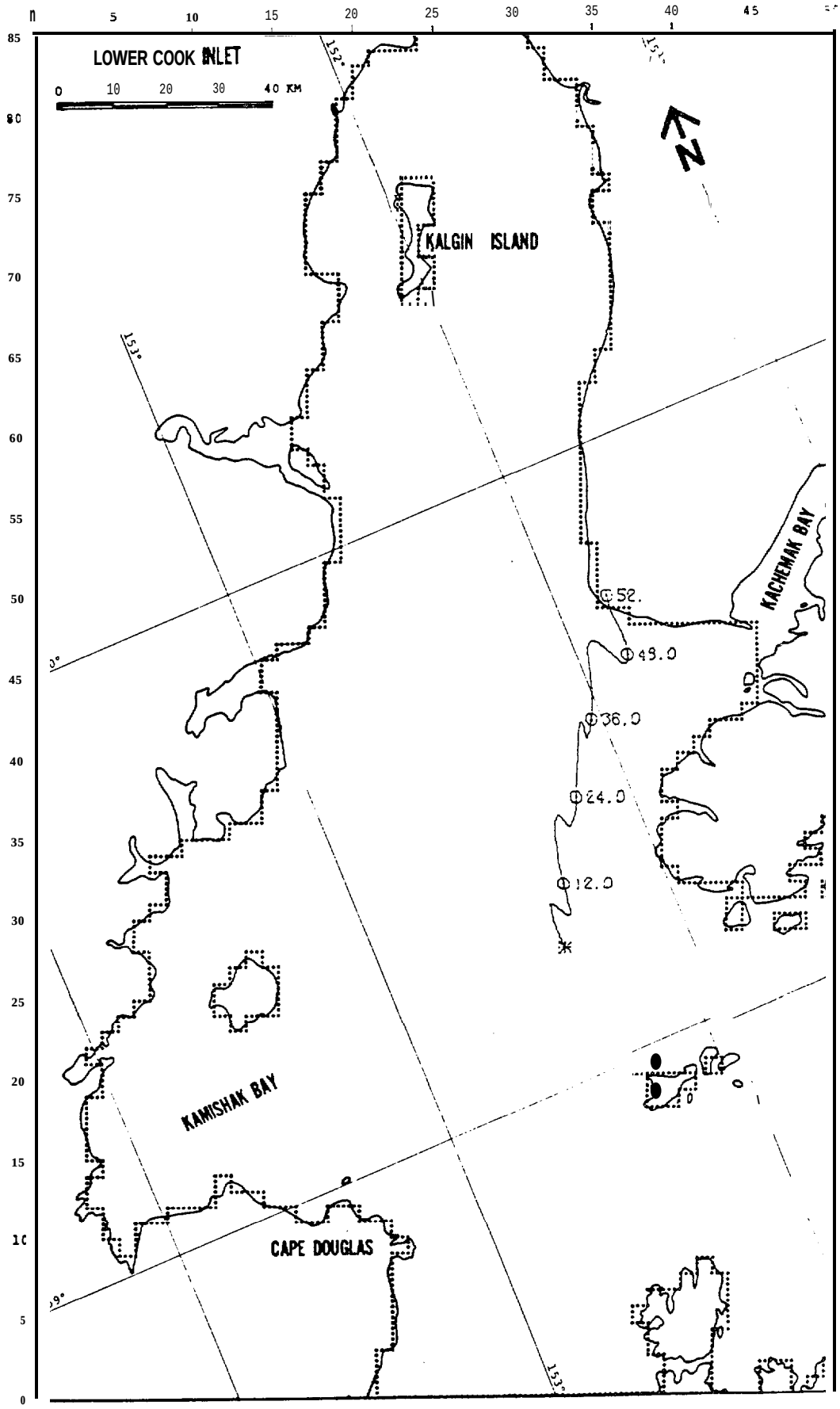

FIGURE B-50: BASE CASE ,

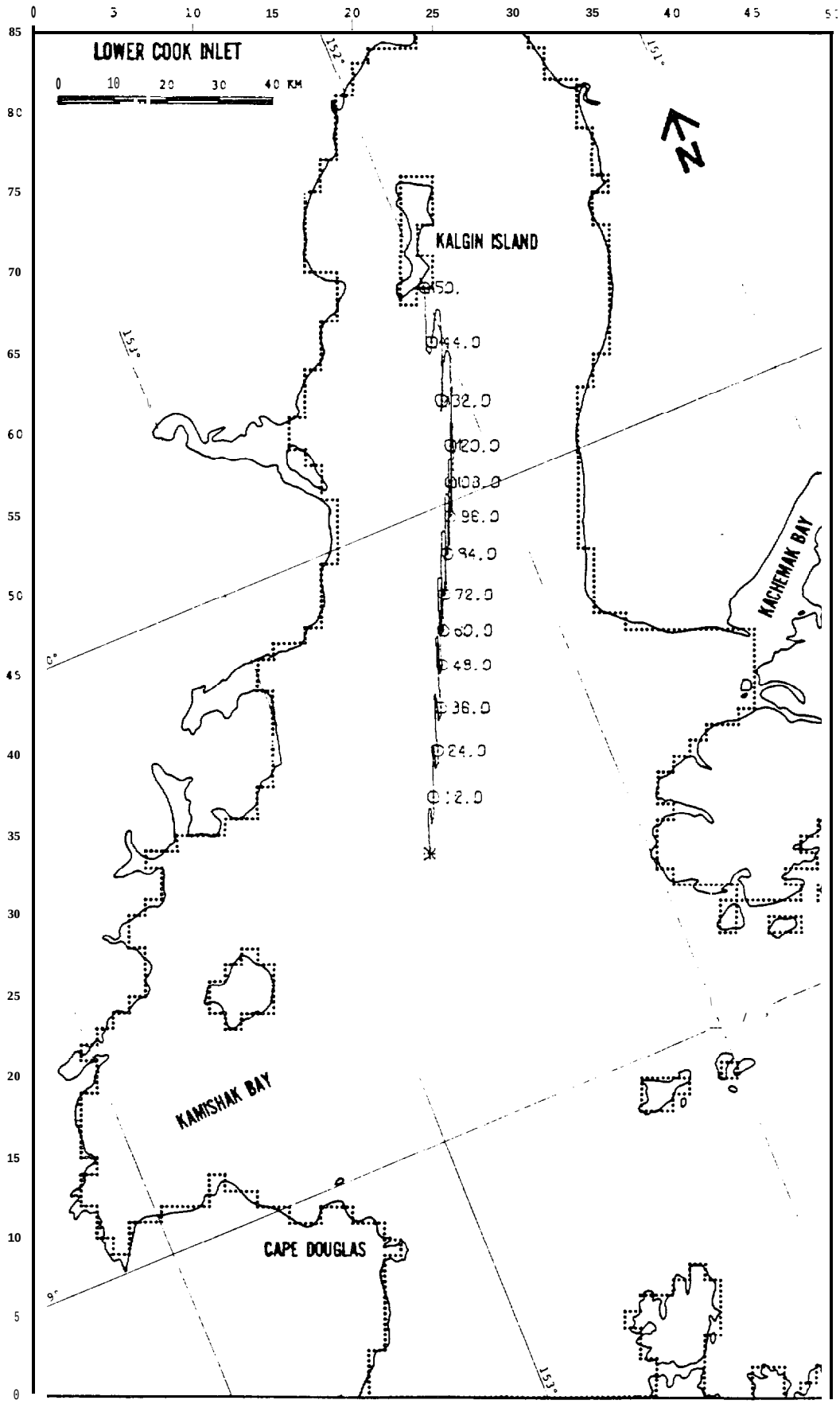

WIND
6

SITE
6

FIGURE B-51: BASE CASE

WIND
6

SITE
7

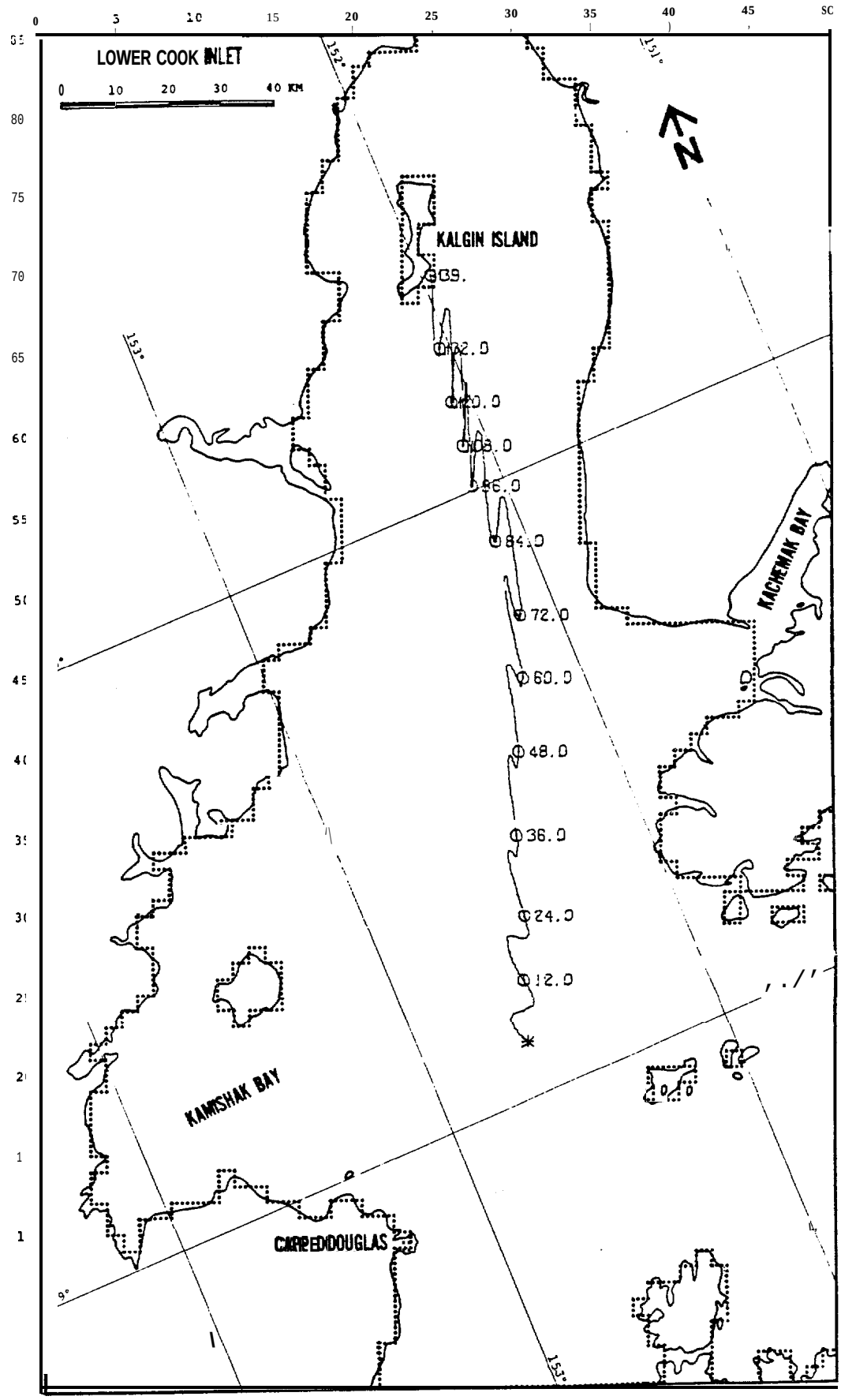

FIGURE B-52: BASE CASE

WIND
6

SITE
8

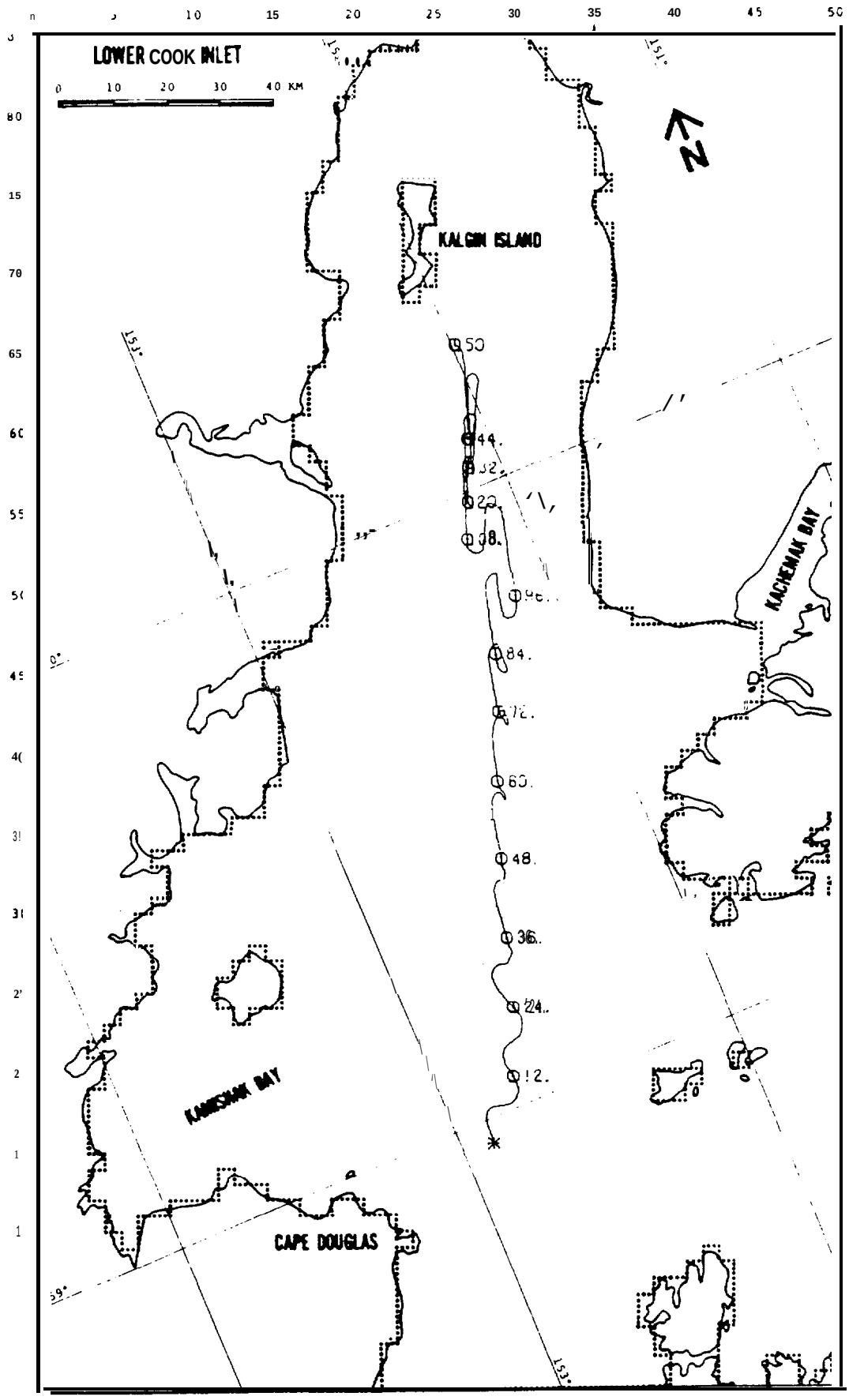

FIGURE B-53: BASE CASE

WIND
6

SITE
8A

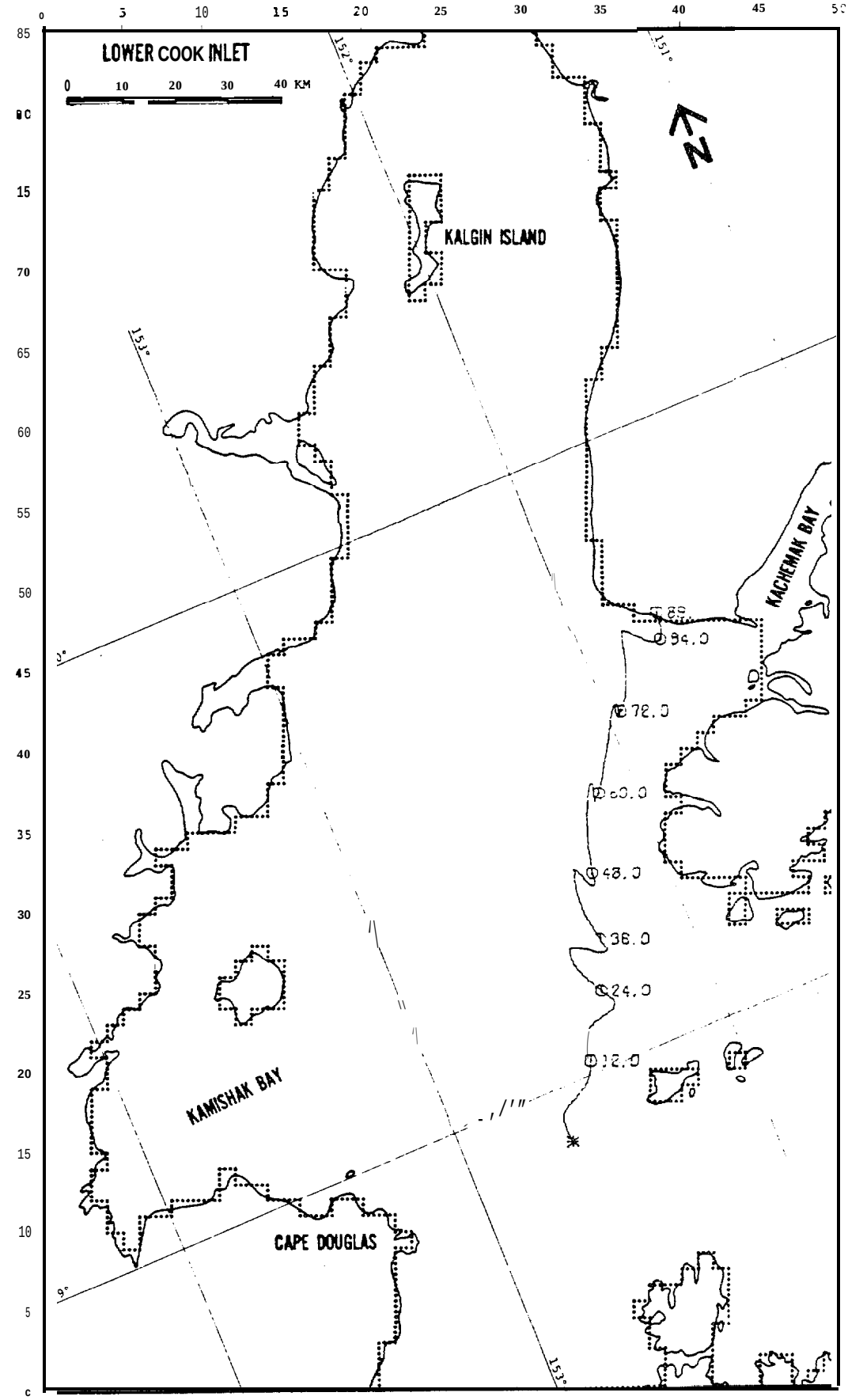

FIGURE B-54: BASE CASE

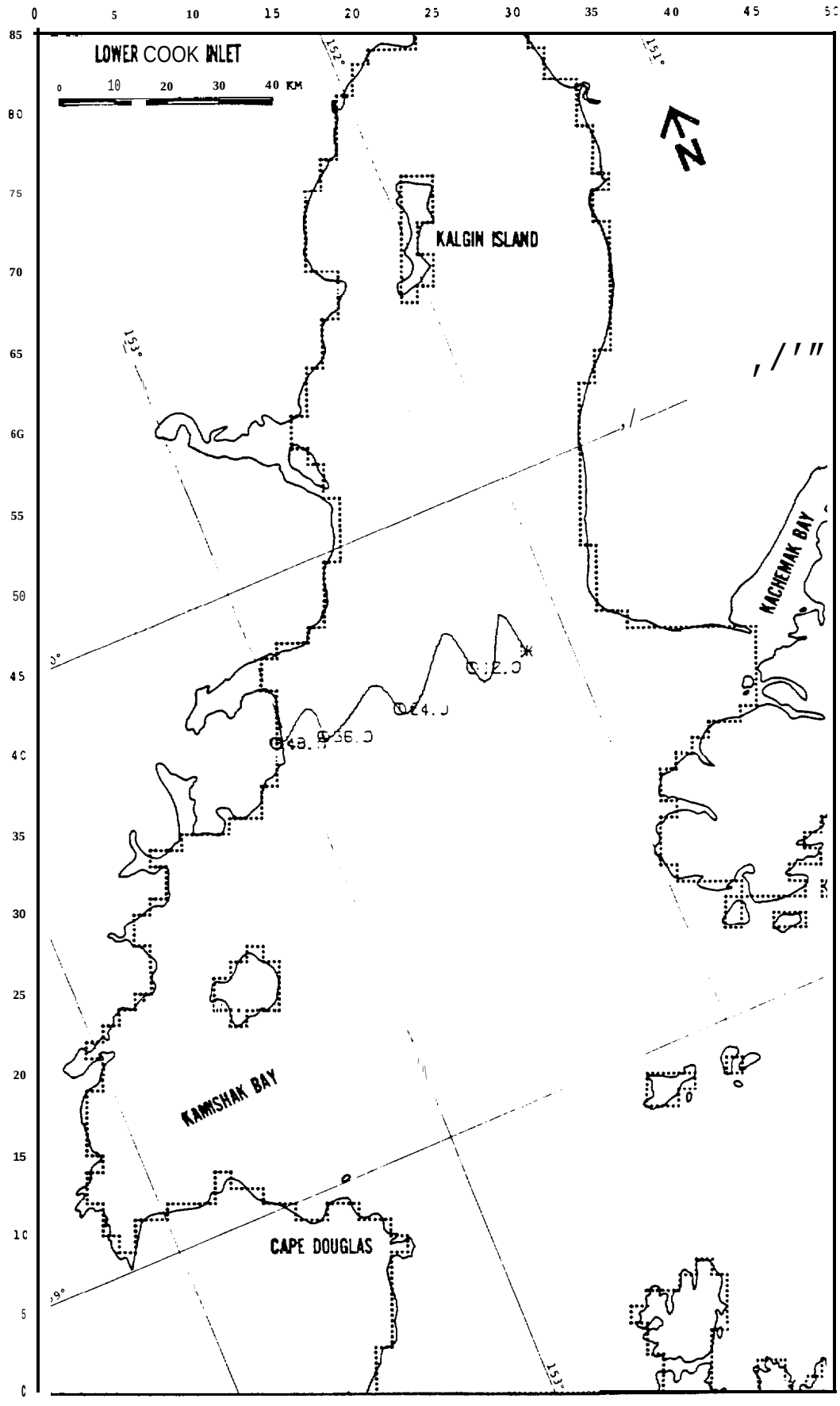

FIGURE B-55: BASE CASE

WIND
7

SITE
2

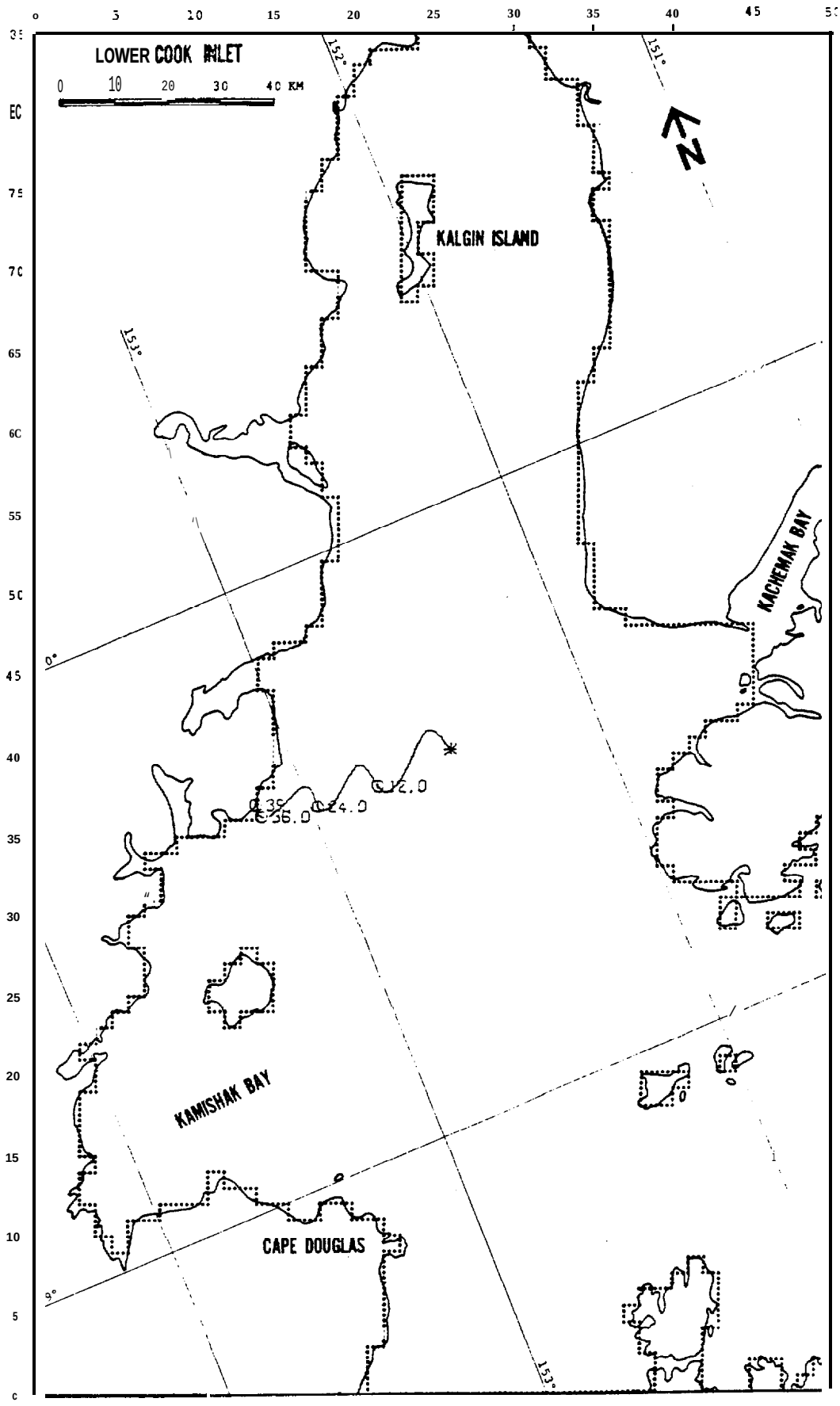

FIGURE B-56: BASE CASE

WIND
7

SITE
3

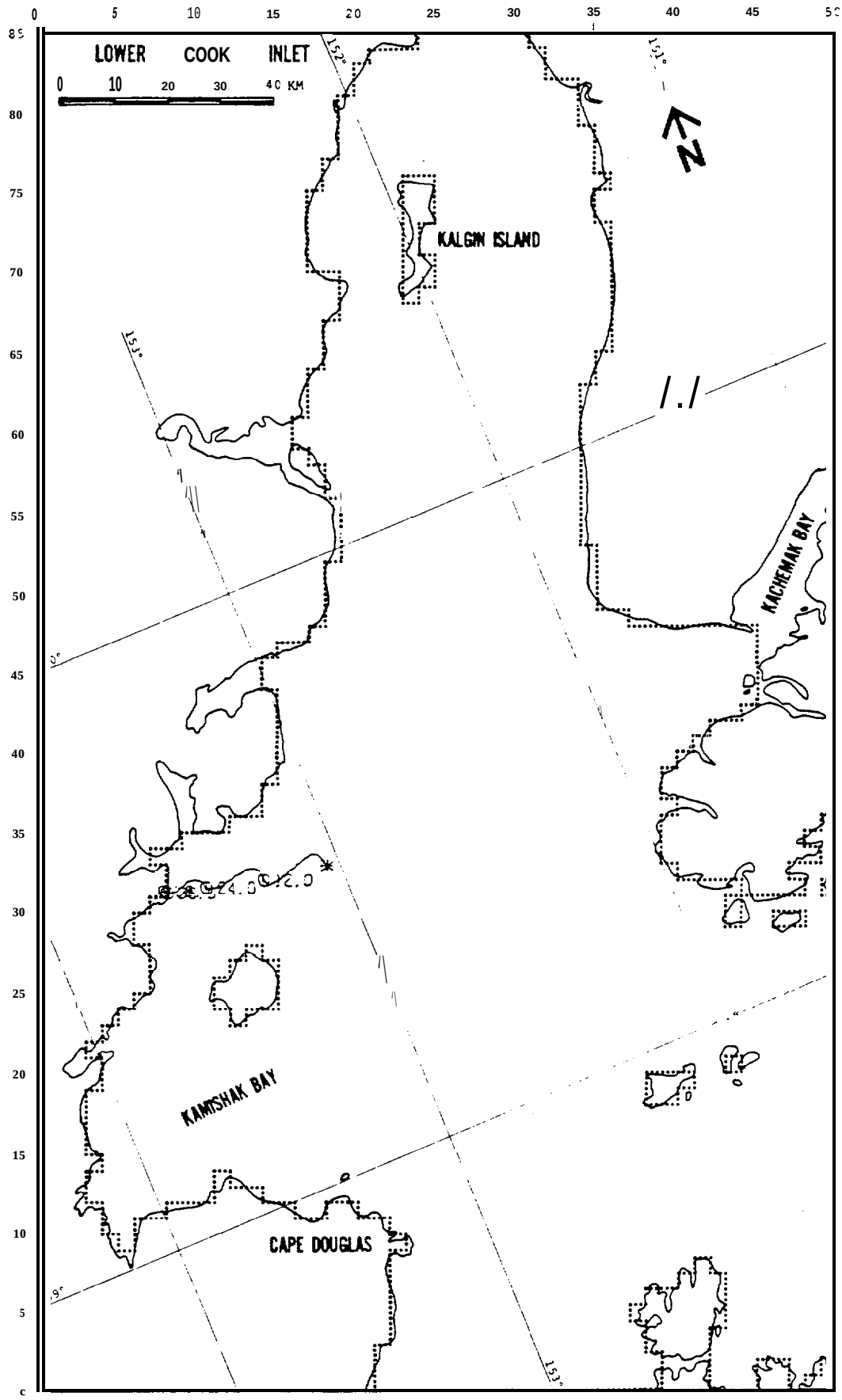

FIGURE B-57: BASE CASE

WIND
7

SITE
4

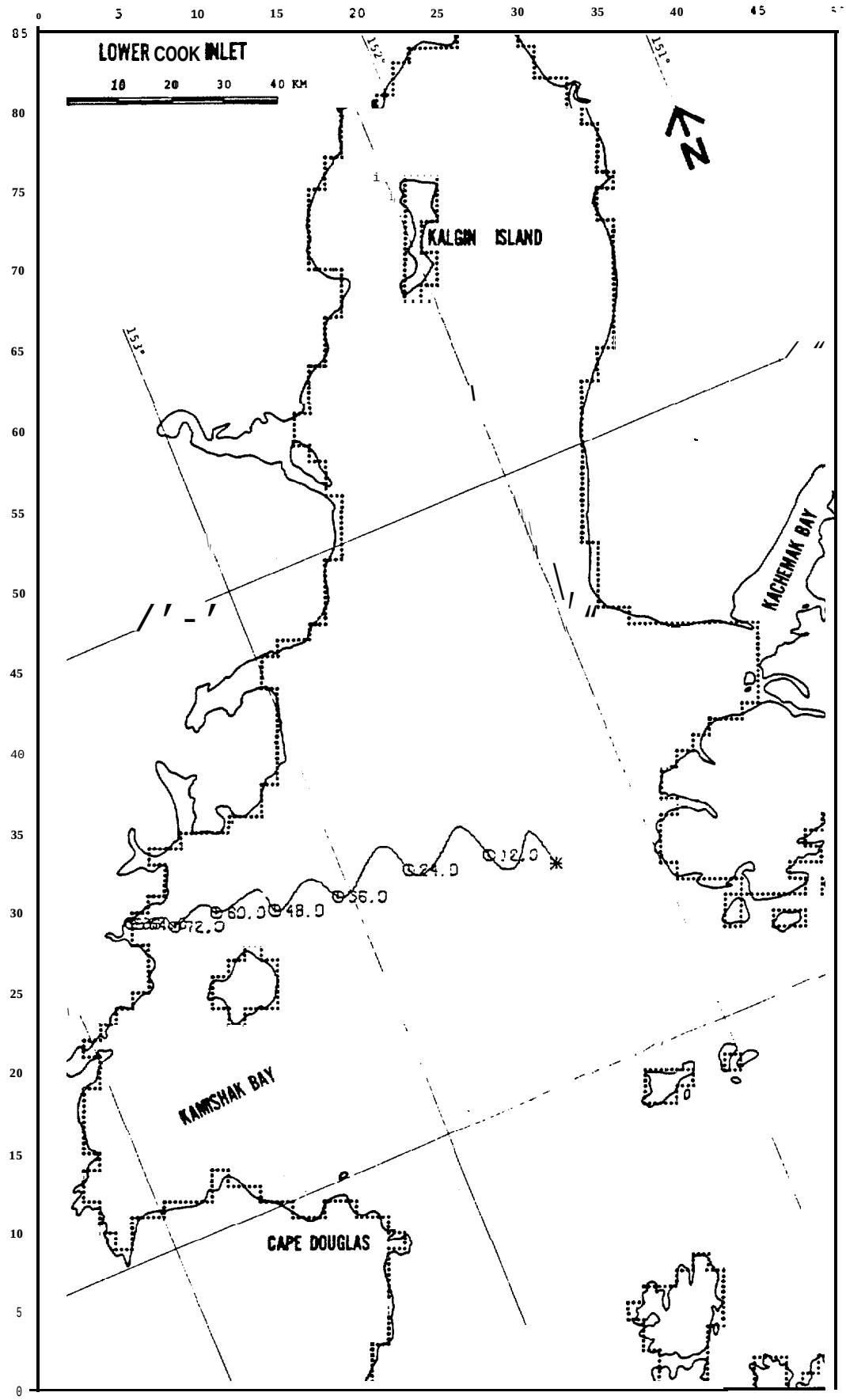

FIGURE B-58: BASE CASE

WIND
7

SITE
5

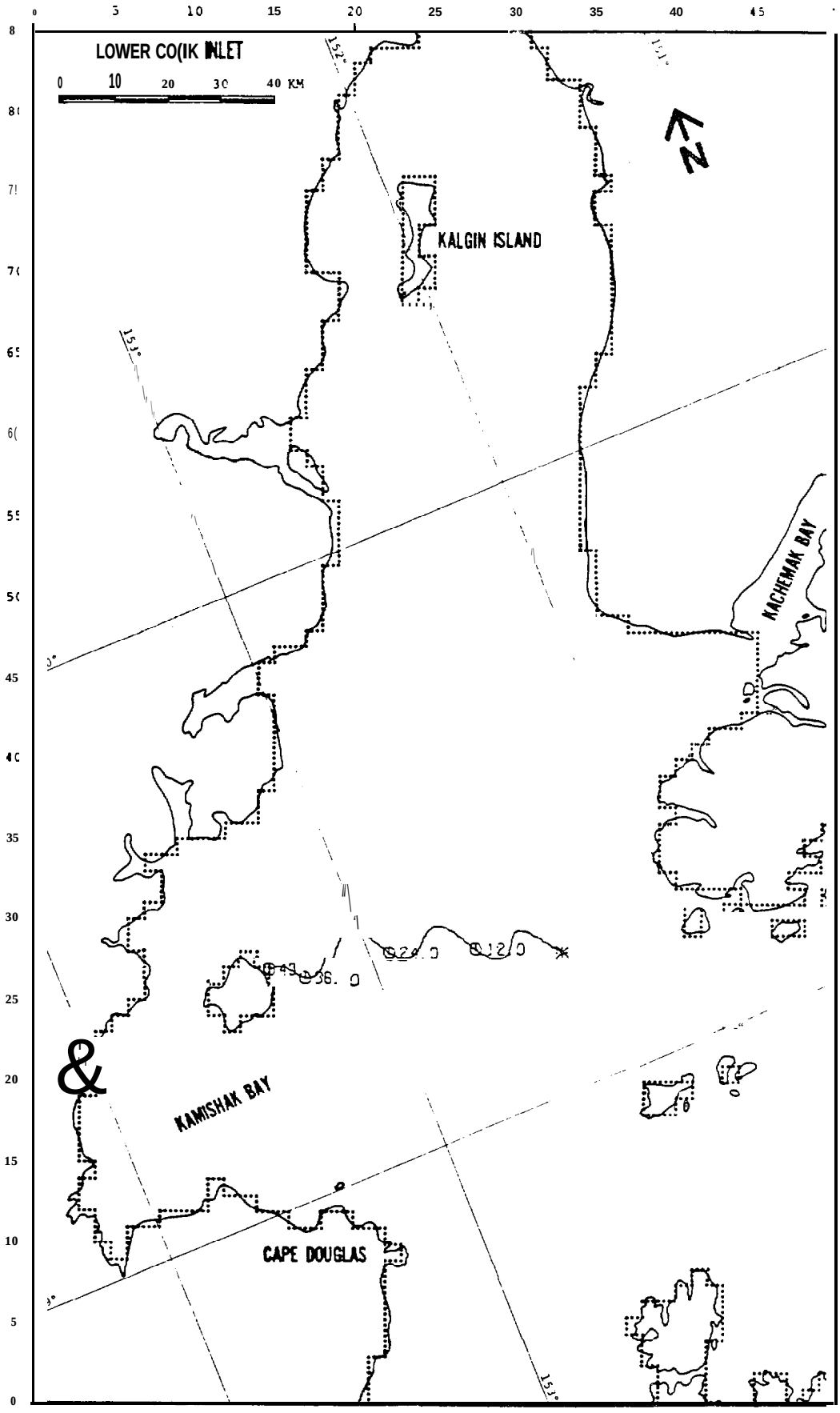

FIGURE B-59: BASE CASE

WIND
7

SITE
6

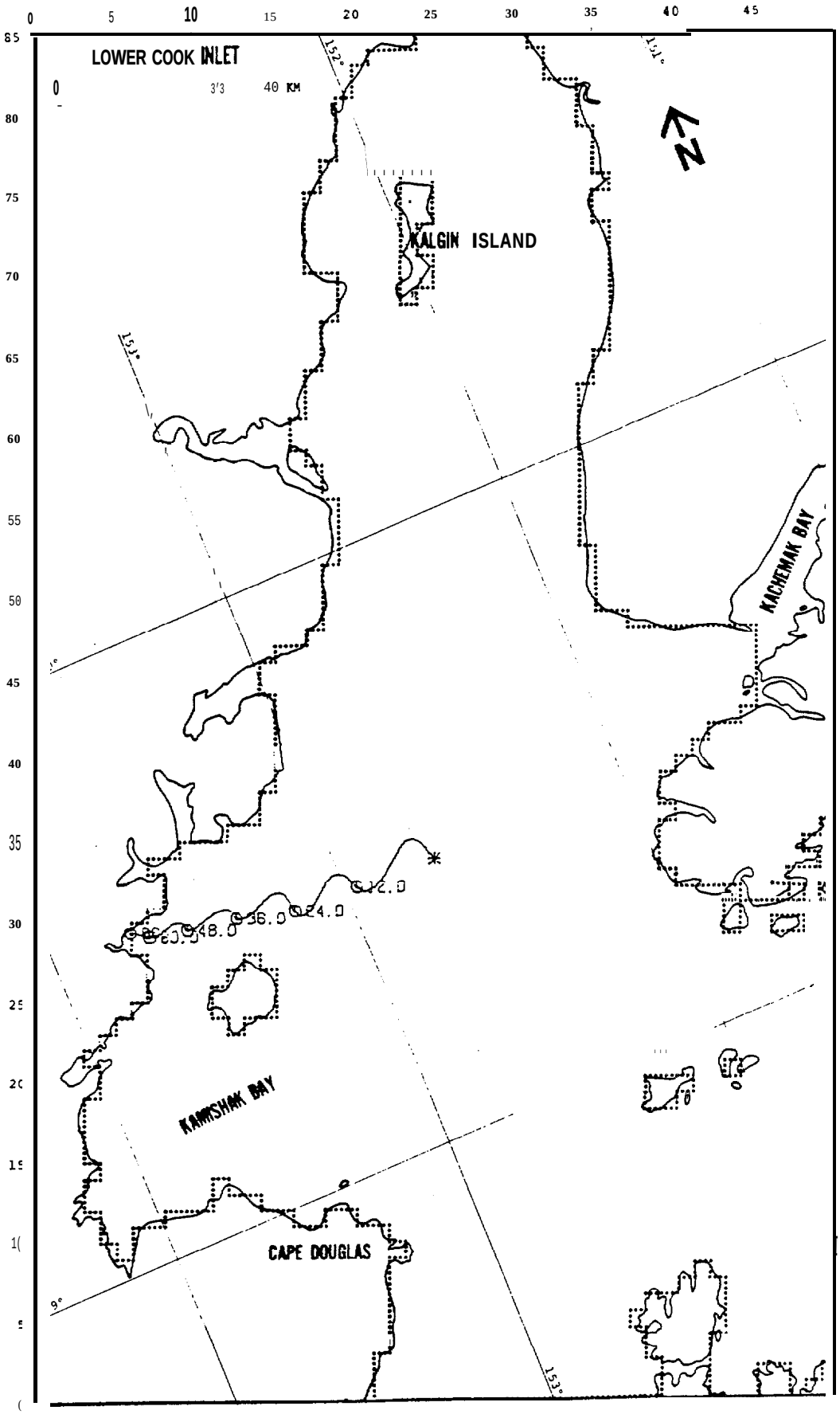

FIGURE B-60: BASE CASE

WIND
7

SITE
7

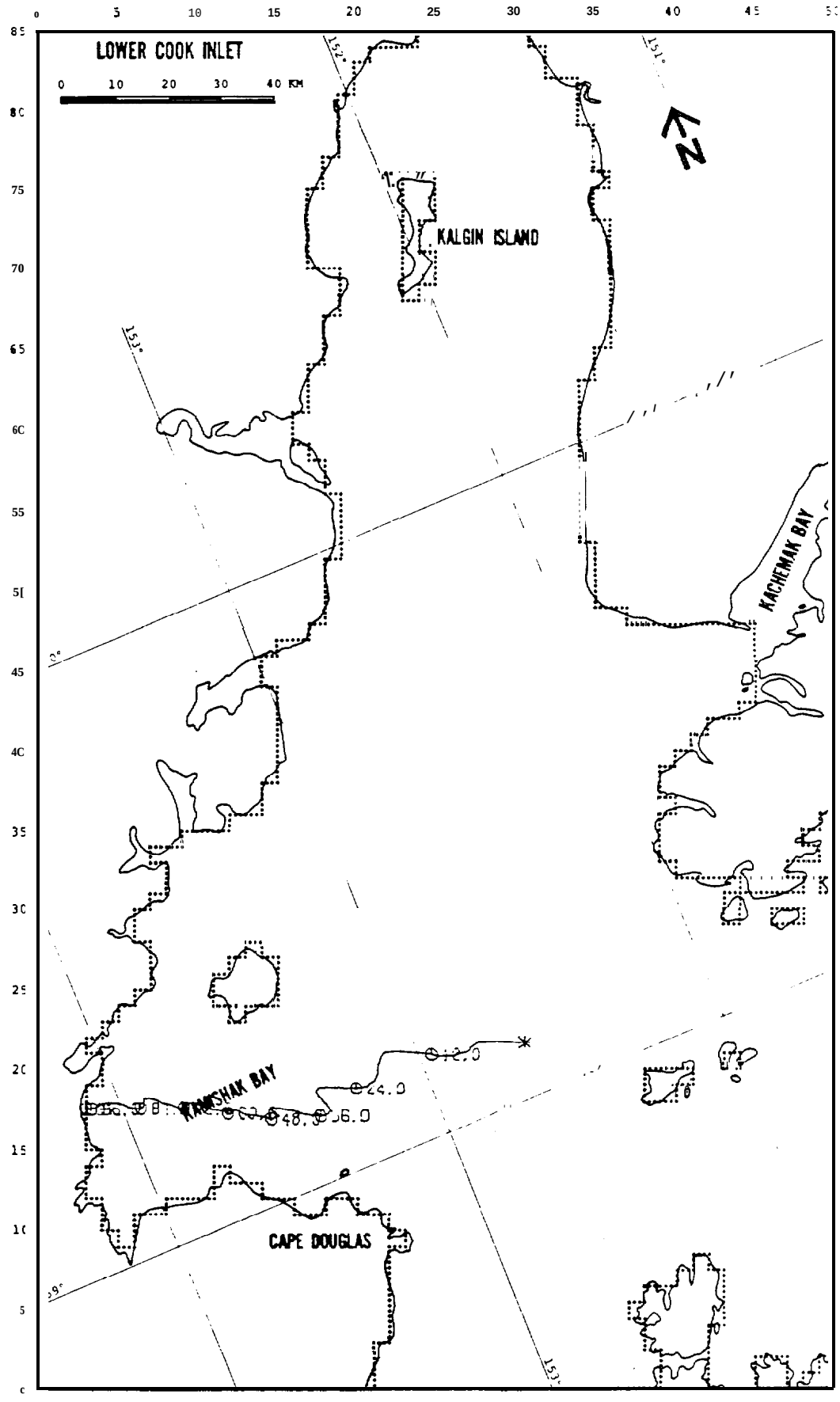

FIGURE B-61: BASE CASE

WIND
7

SITE
8

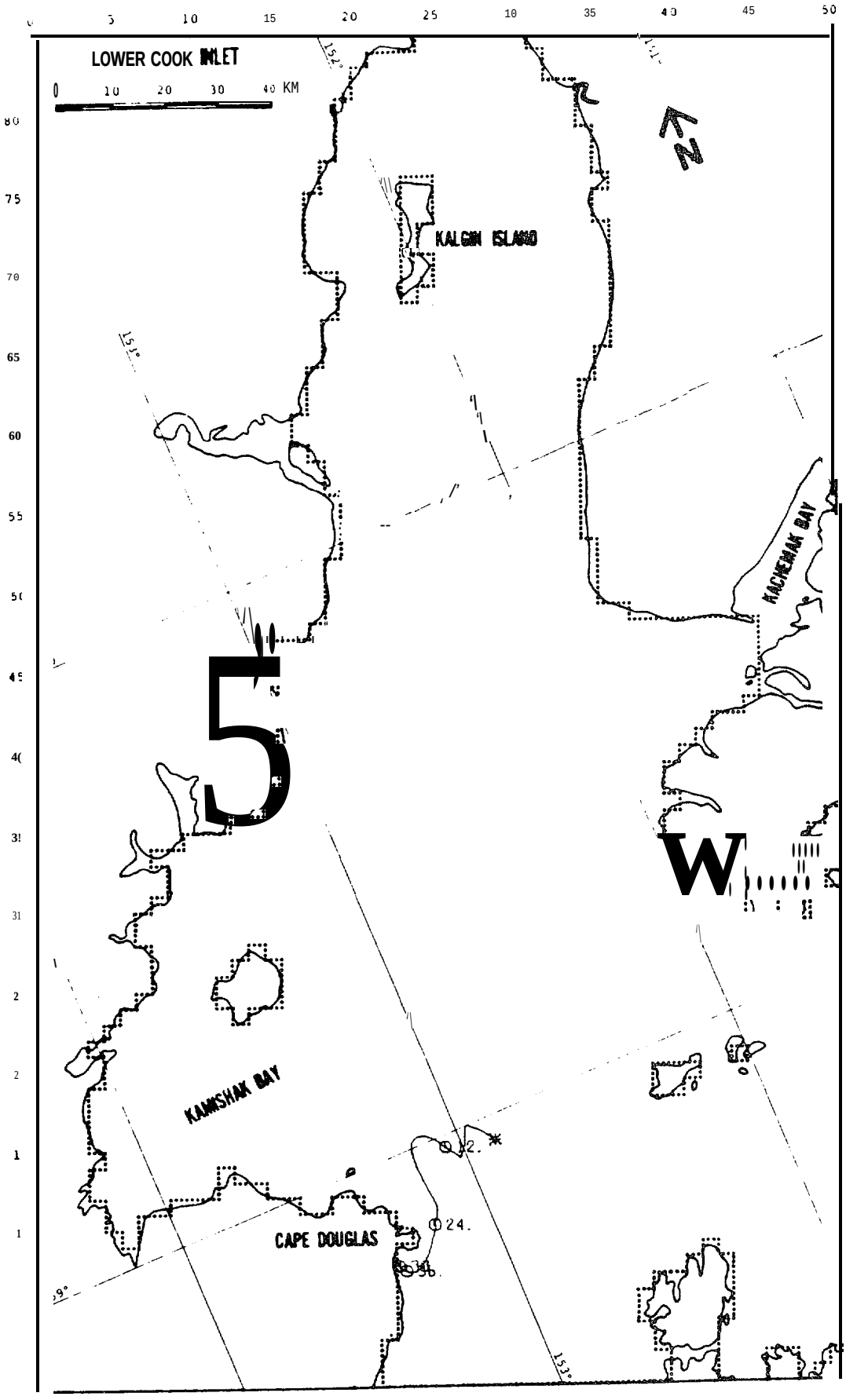

FIGURE B-62: BASE CASE

WIND
7

SITE
8A

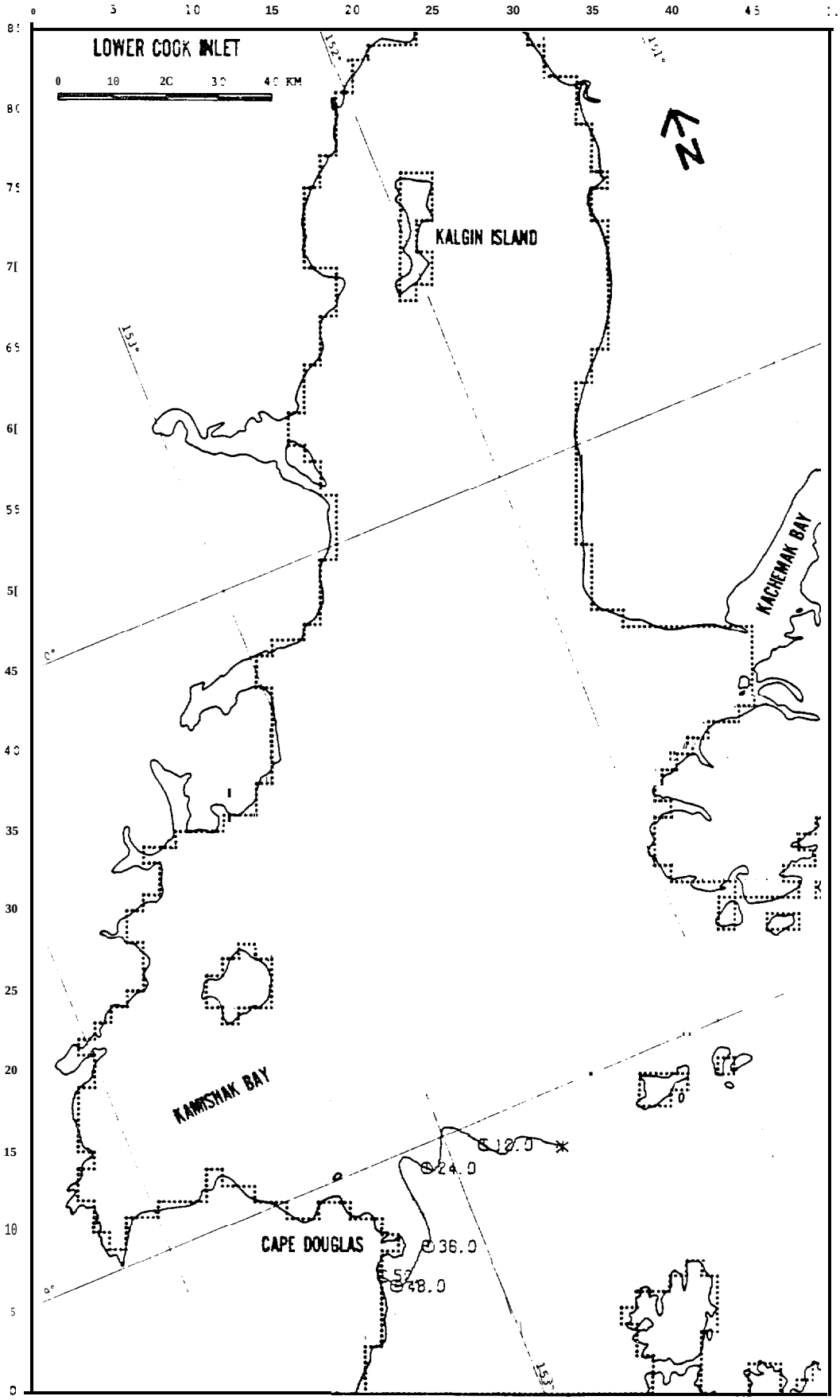

FIGURE B-63: BASE CASE

WIND
8

SITE
1

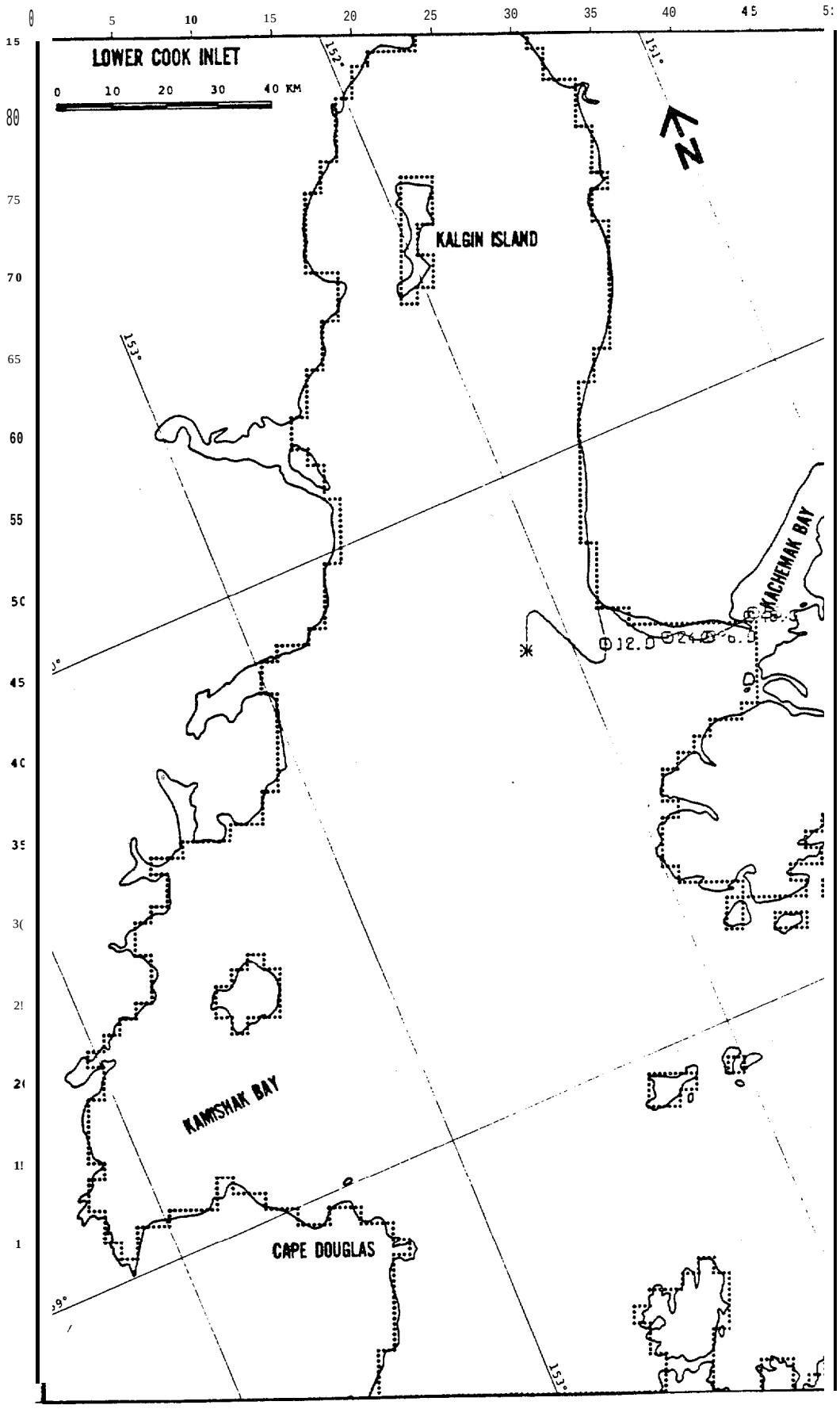

FIGURE B-64: BASE CASE

WIND
8

SITE
2

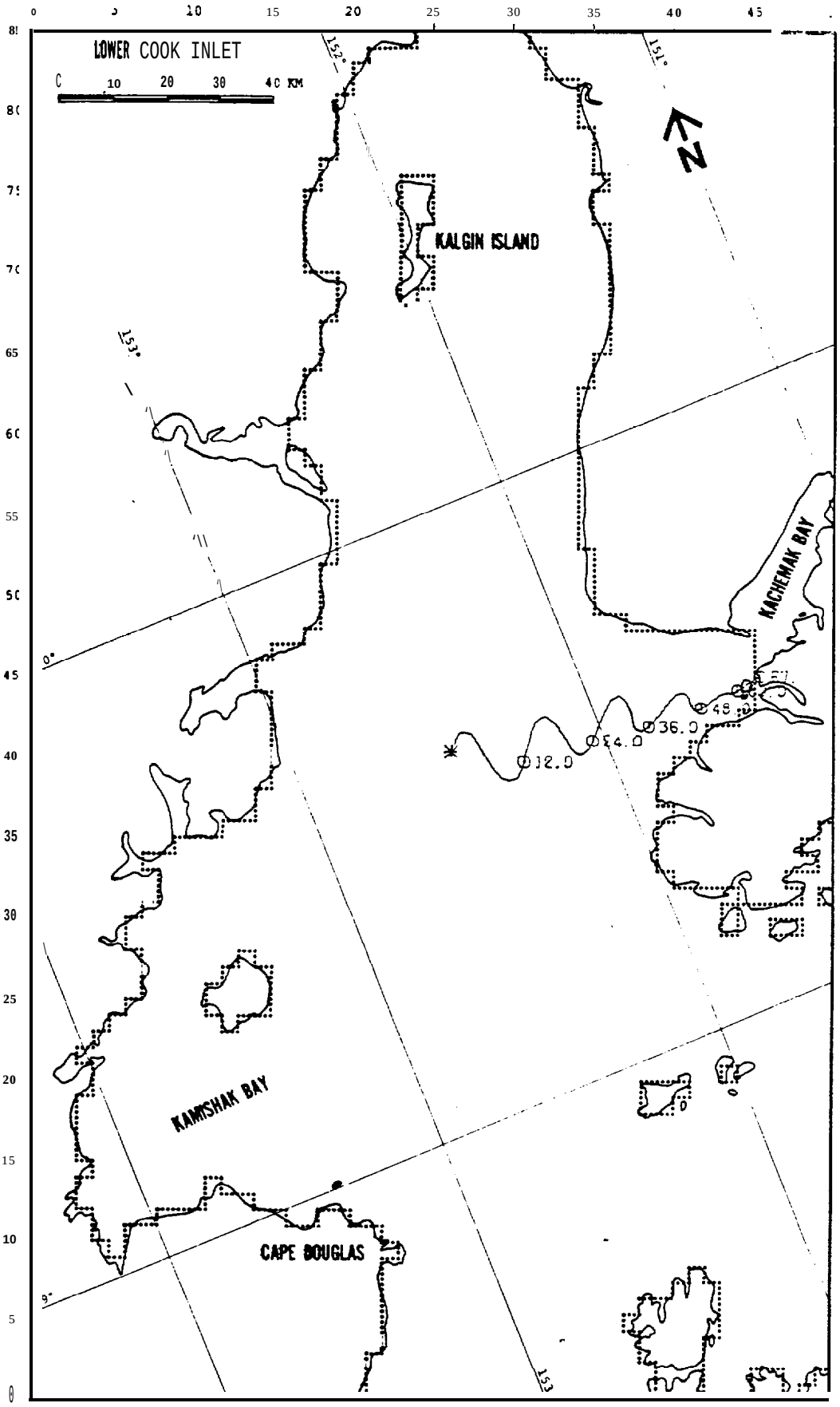

FIGURE B-65: BASE CASE

WIND
8

SITE
3

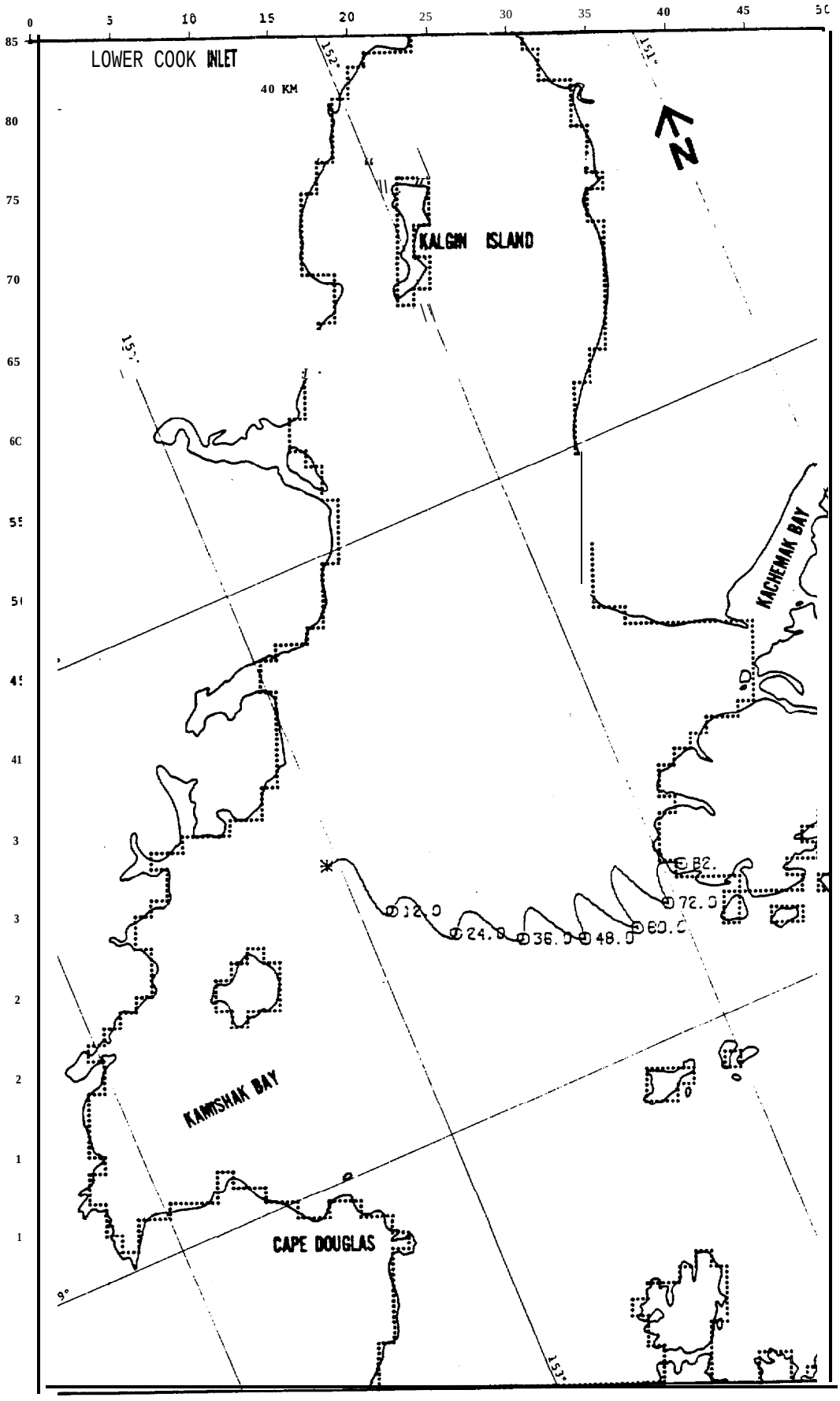

FIGURE B-66: BASE CASE

WIND
8

SITE
4

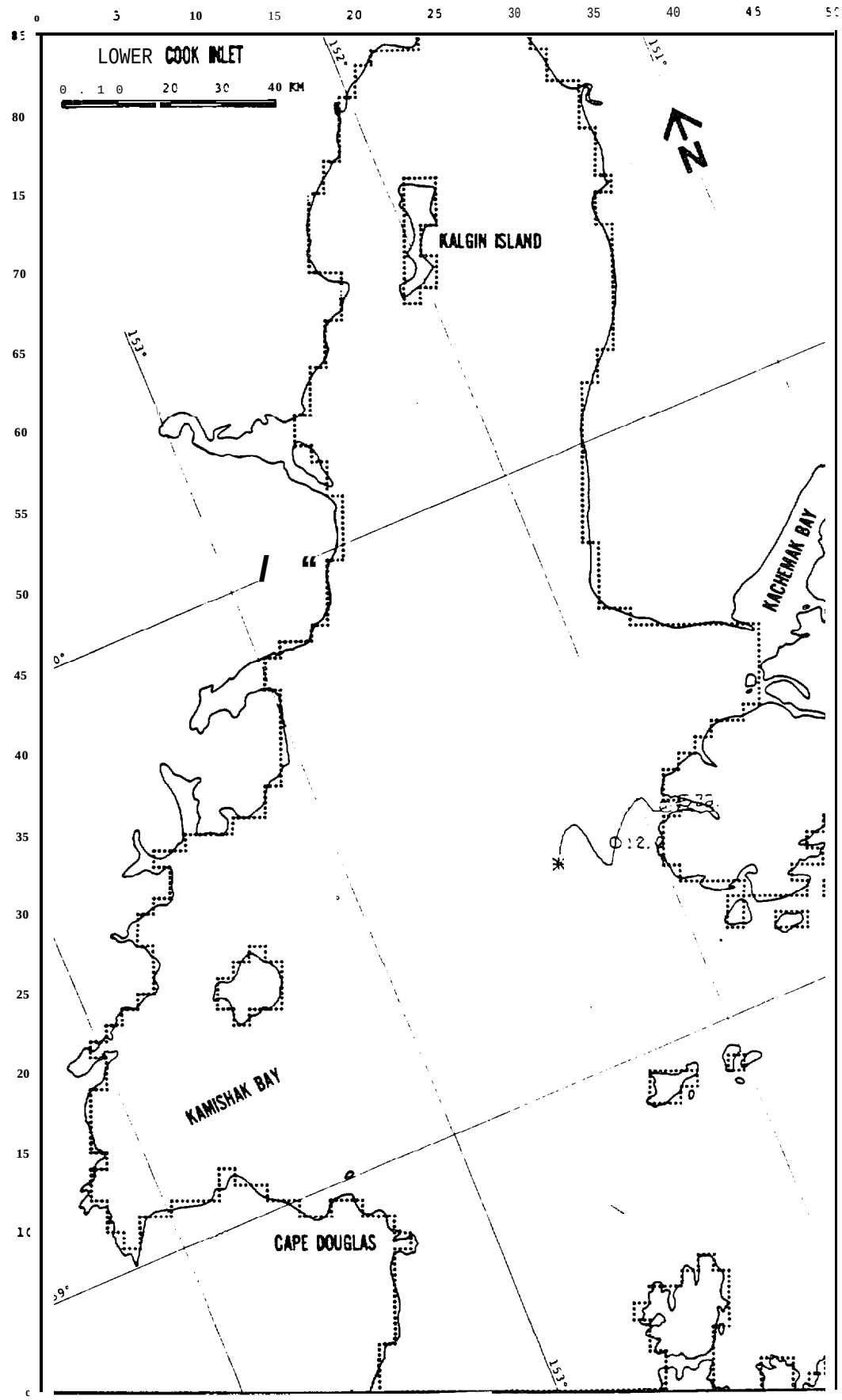

FIGURE B-67: BASE CASE

WIND
8

SITE
5

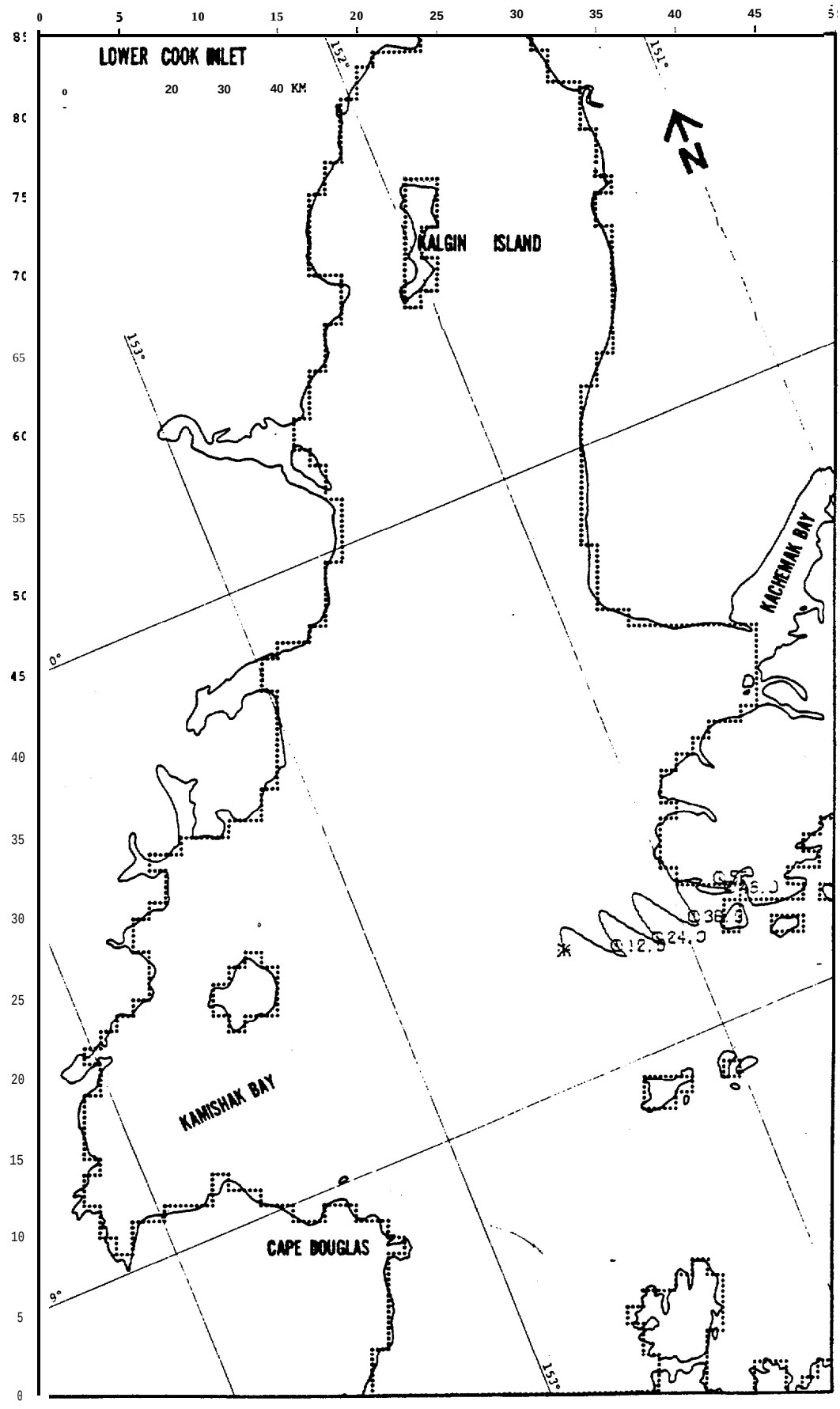

FIGURE B-68: BASE CASE

WIND
8

SITE
6

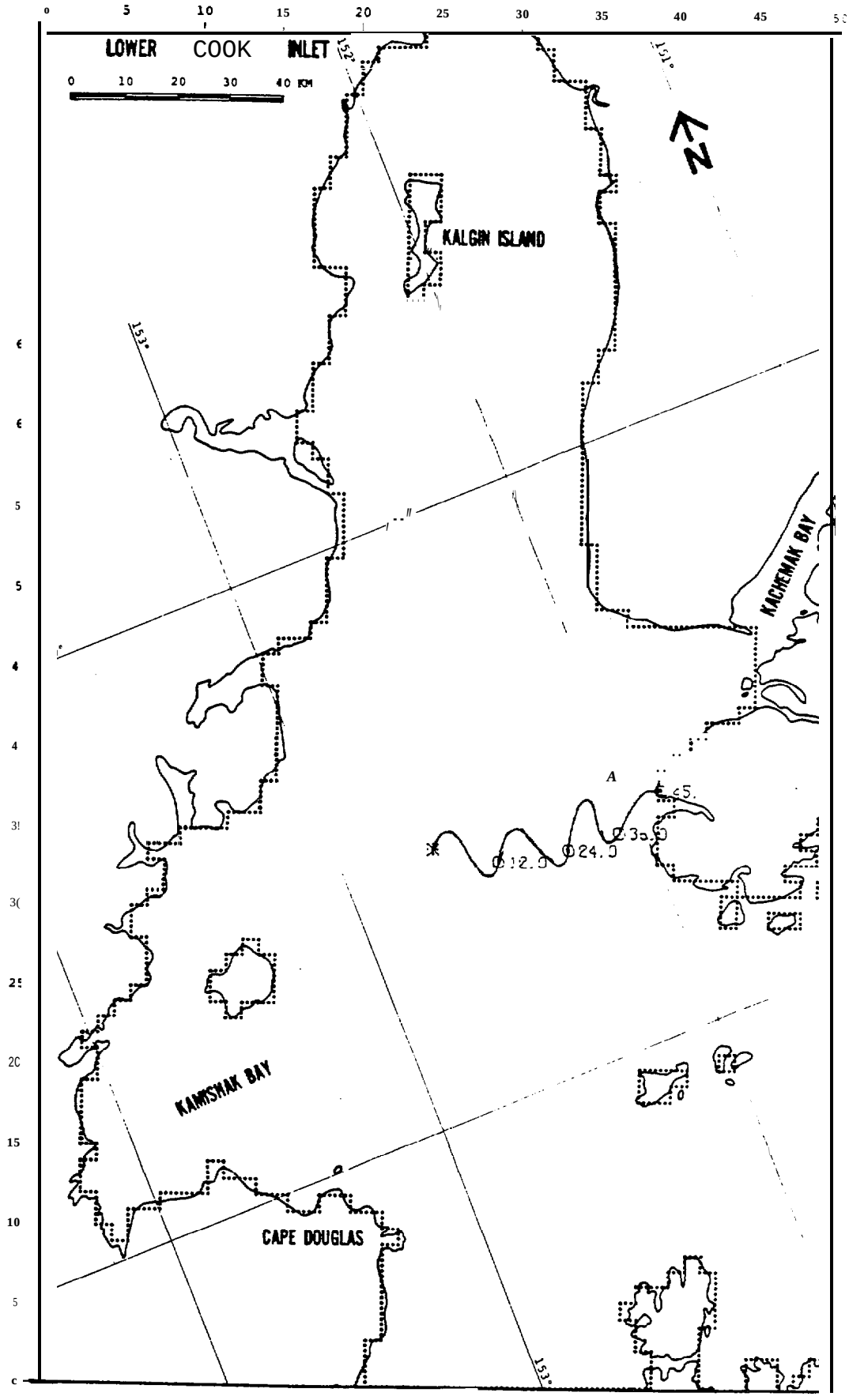

FIGURE B-69: BASE CASE

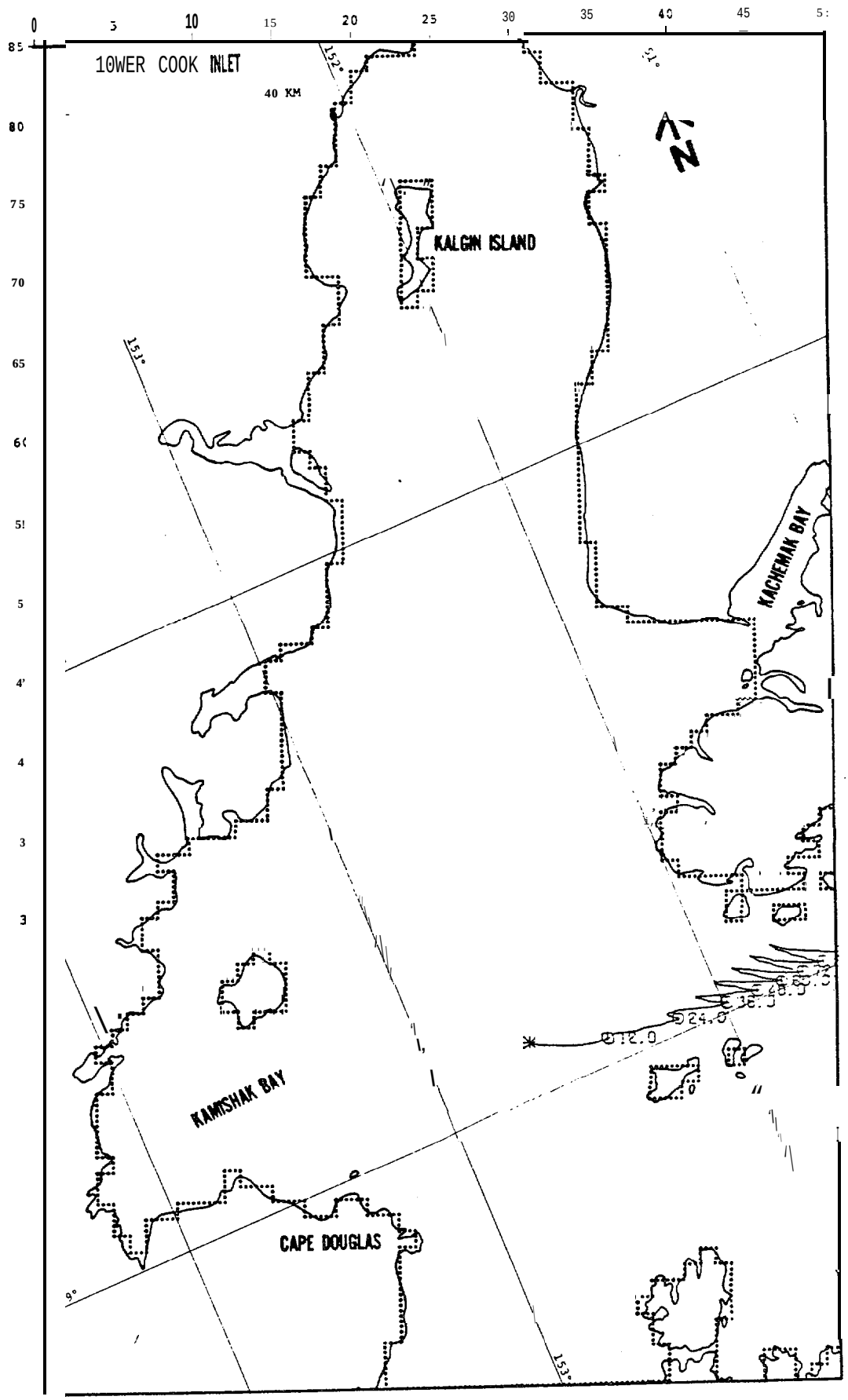

WIND
8

SITE
7

FIGURE B-70: BASE CASE

WIND
8

SITE
8

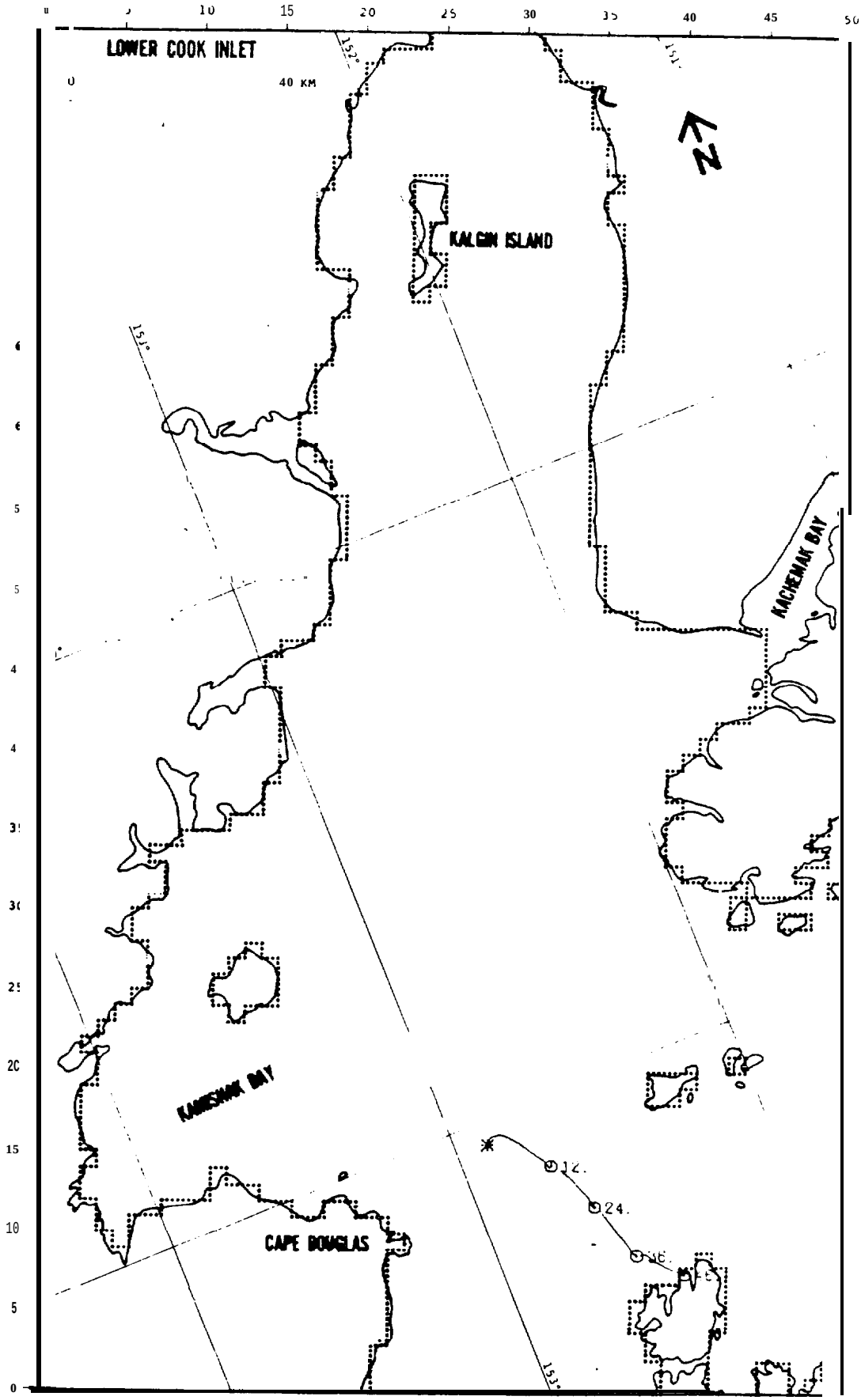

FIGURE B-71: BASE CASE

WIND
8

SITE
8A

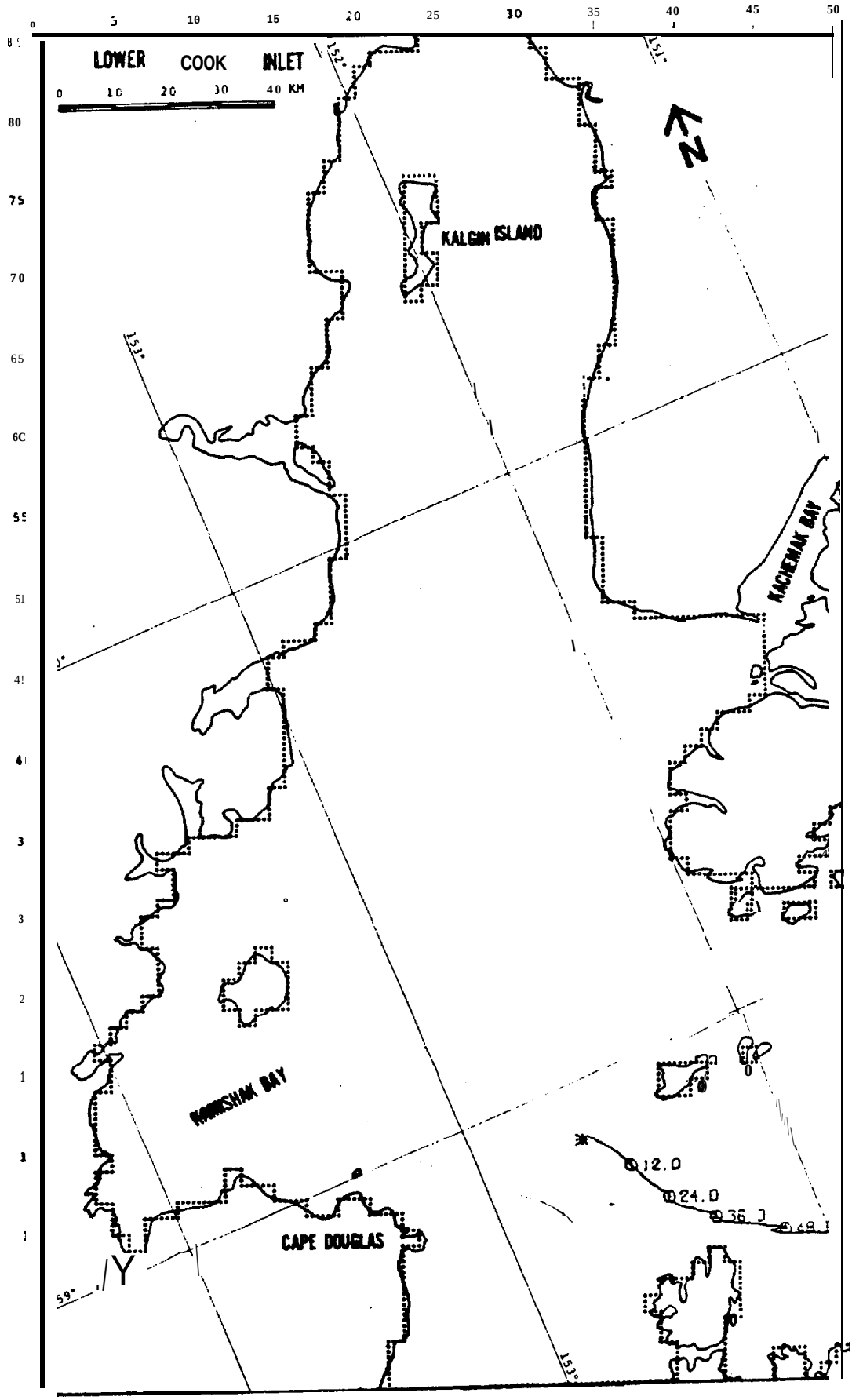

FIGURE B-72: BASE CASE

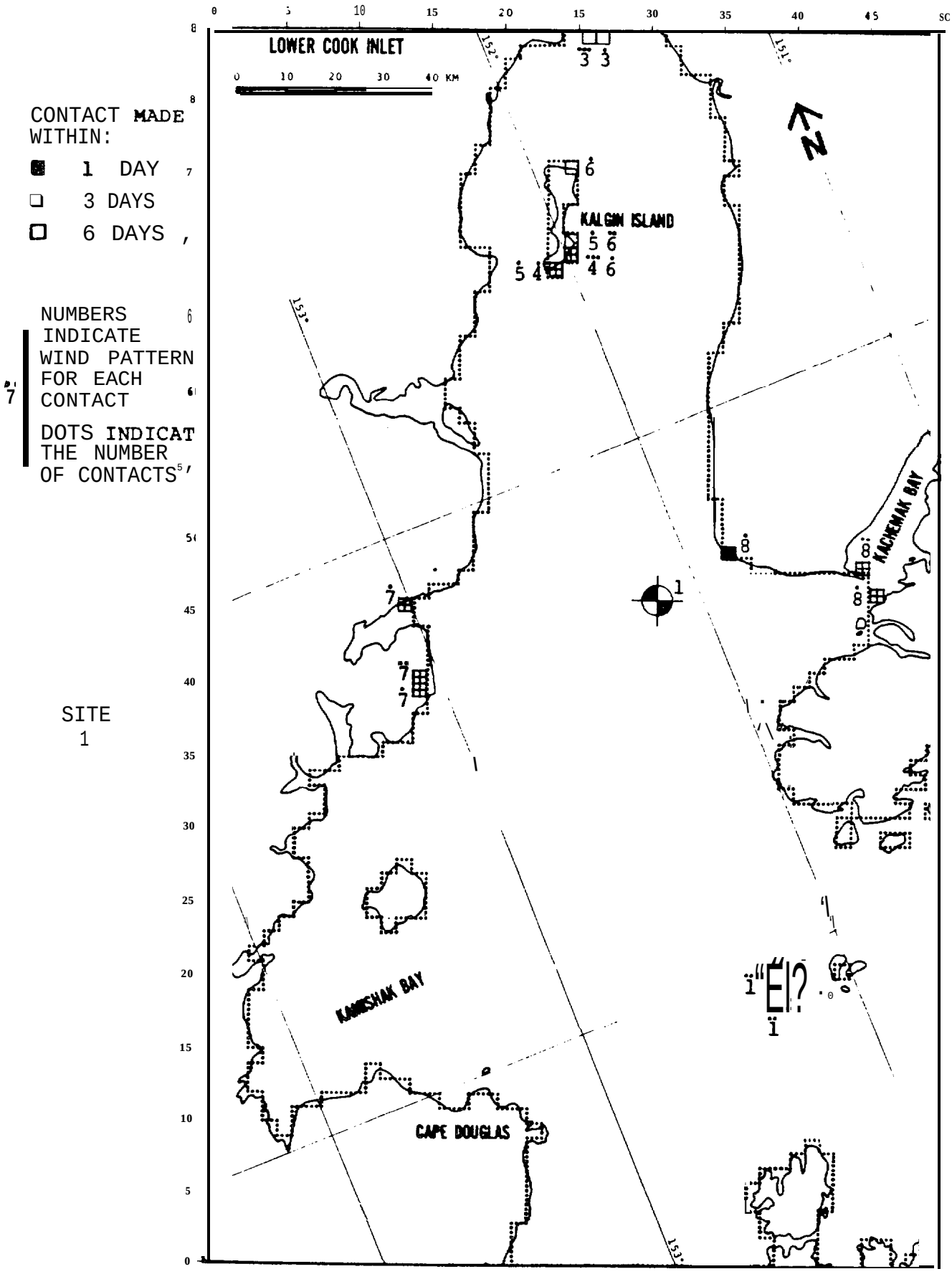

FIGURE B-73: POTENTIAL BOUNDARY CONTACT ZONES

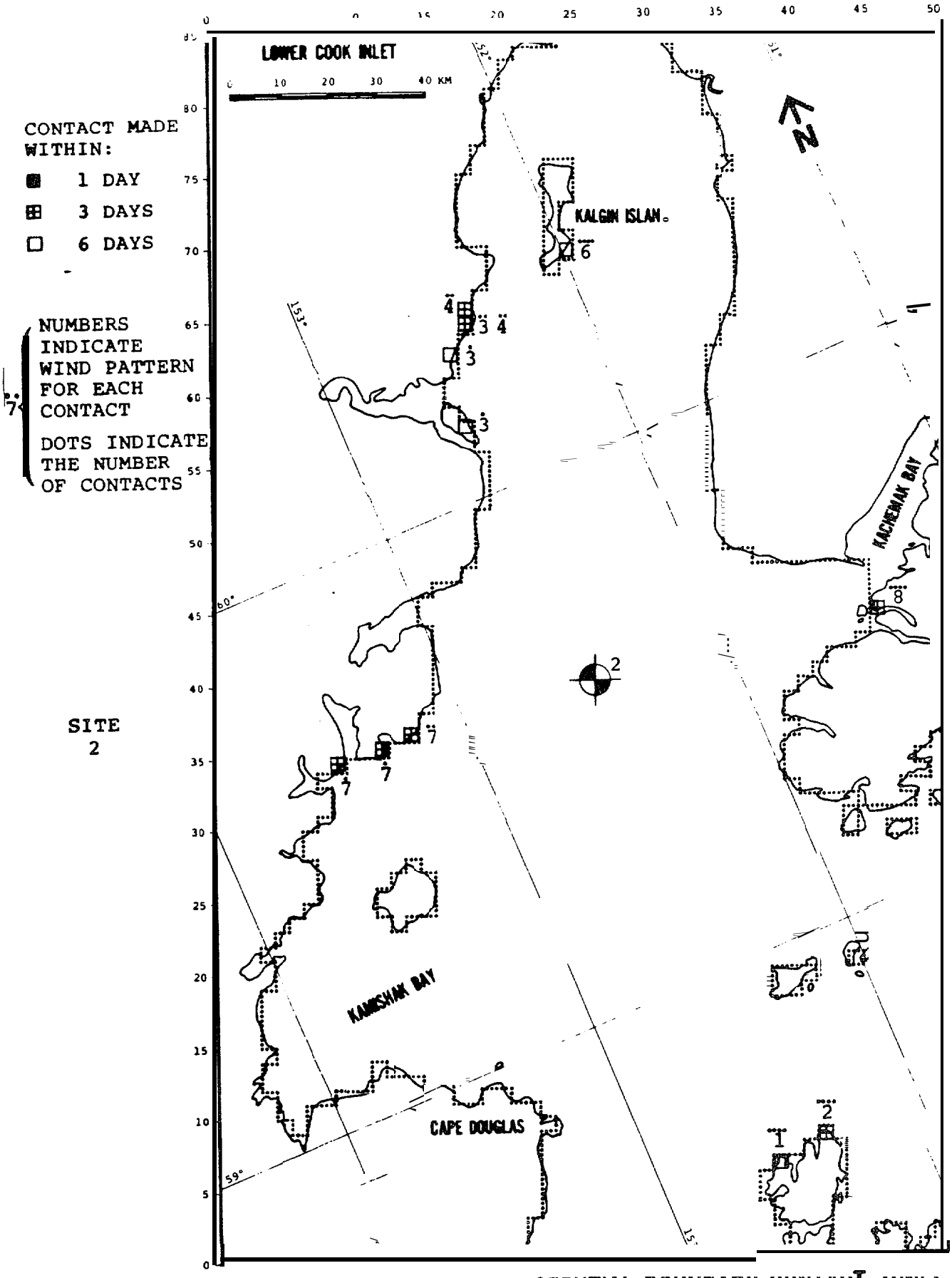

FIGURE 74: POTENTIAL BOUNDARY CONTACT ZONES

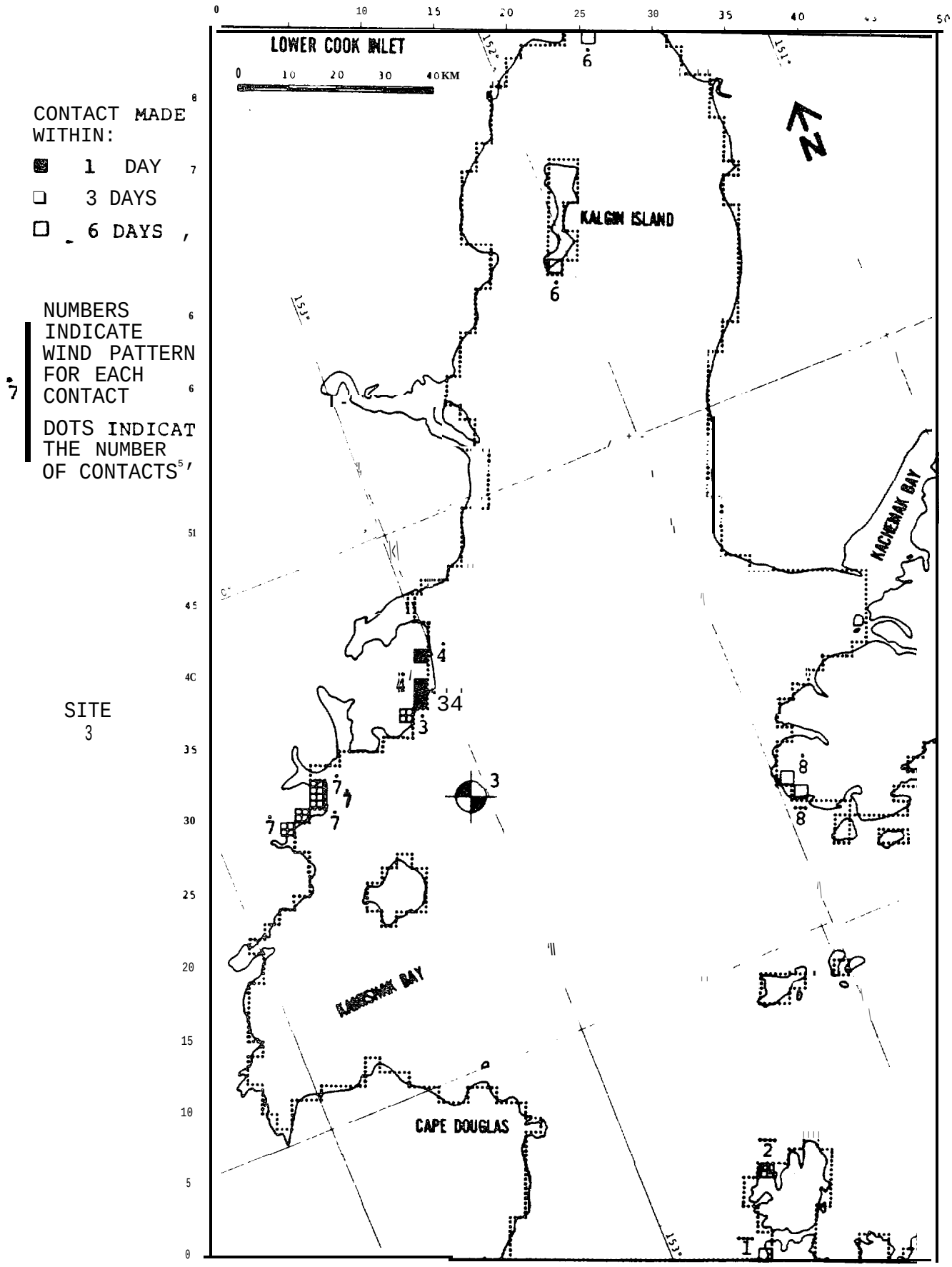

FIGURE B-75: POTENTIAL BOUNDARY CONTACT ZONES

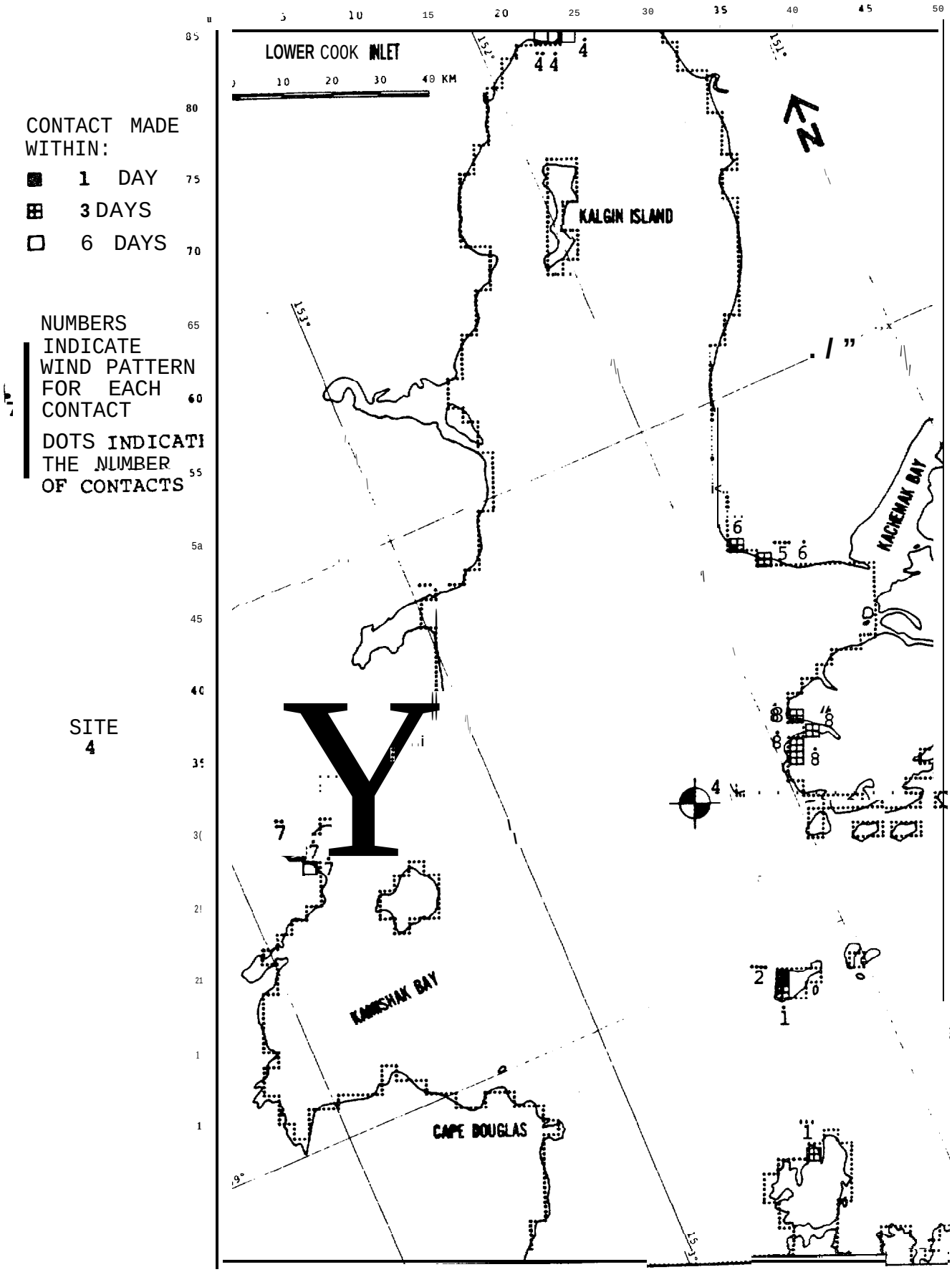

FIGURE B-76: POTENTIAL BOUNDARY CONTACT ZONES

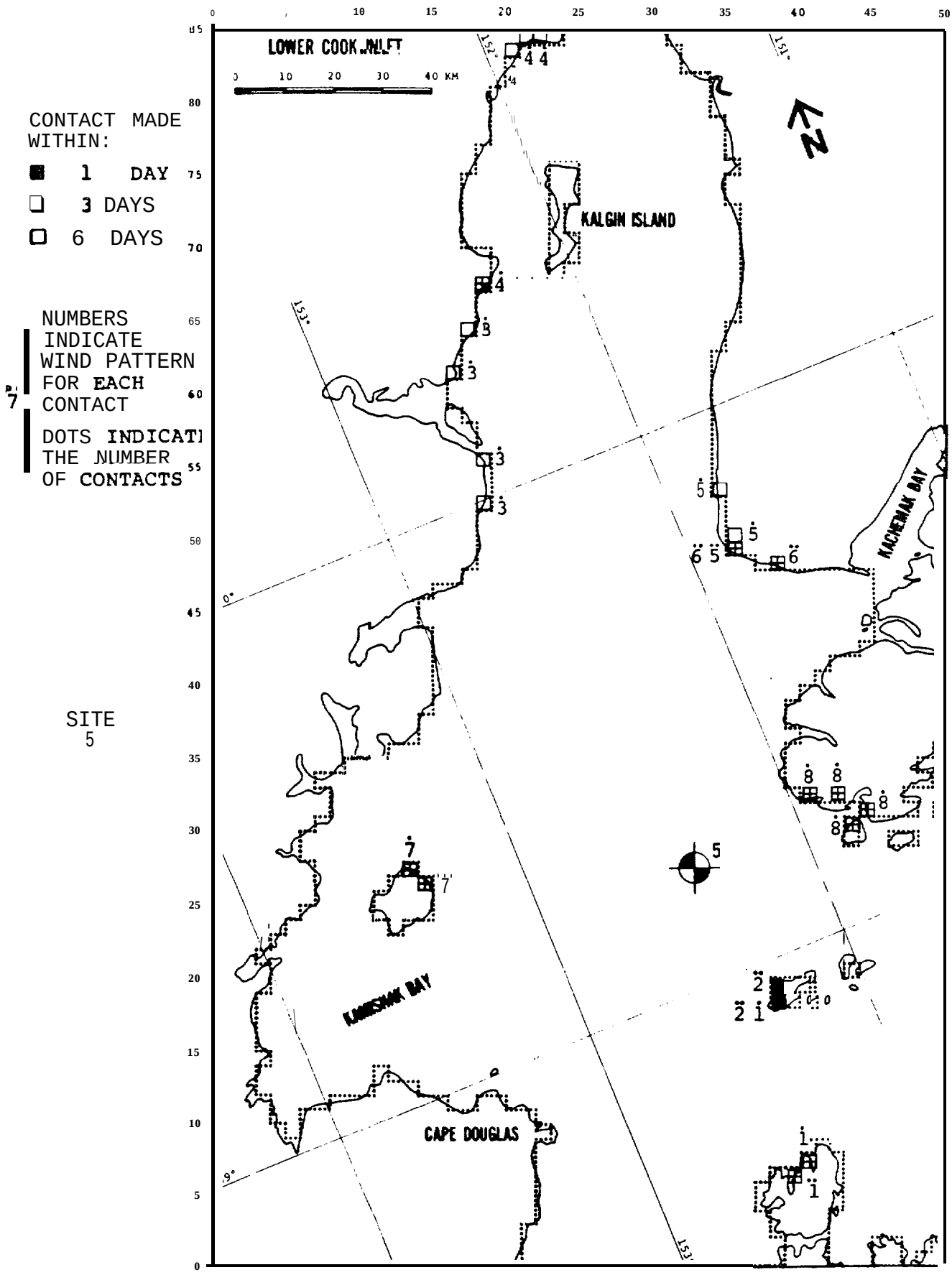

FIGURE B-77: POTENTIAL BOUNDARY CONTACT ZONES

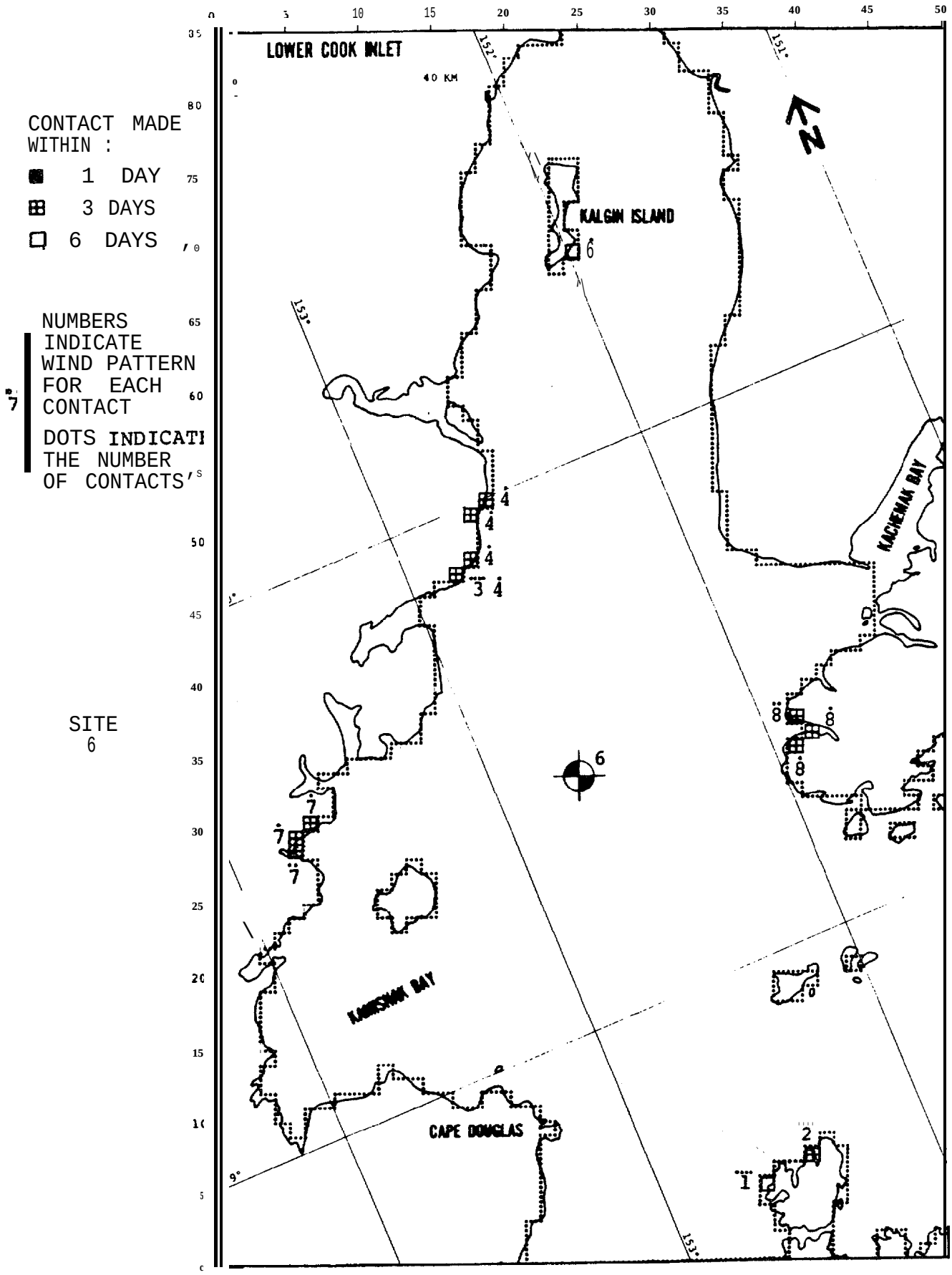

FIGURE B-78: POTENTIAL BOUNDARY CONTACT ZONES

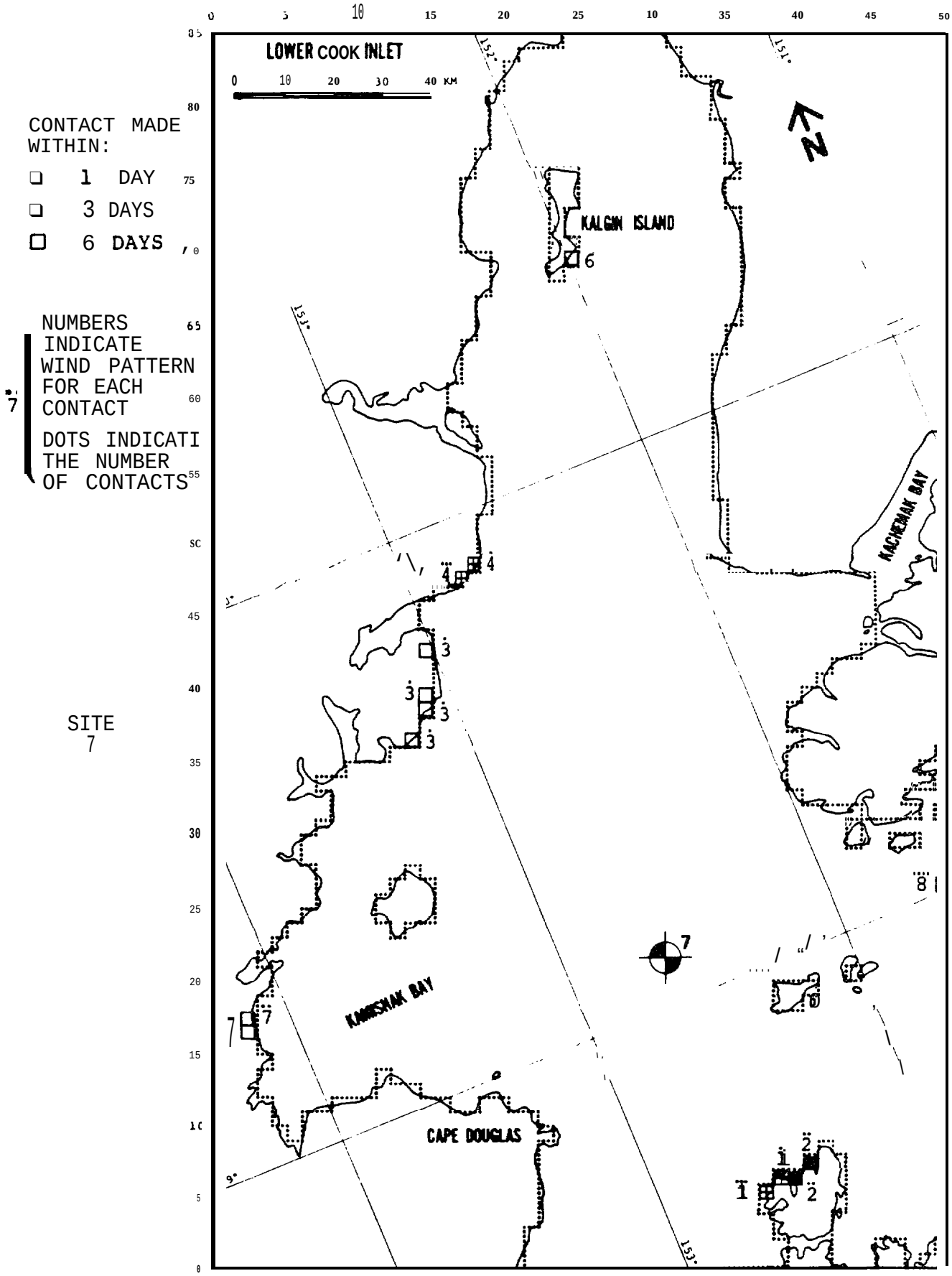

FIGURE B-79: POTENTIAL BOUNDARY CONTACT ZONES

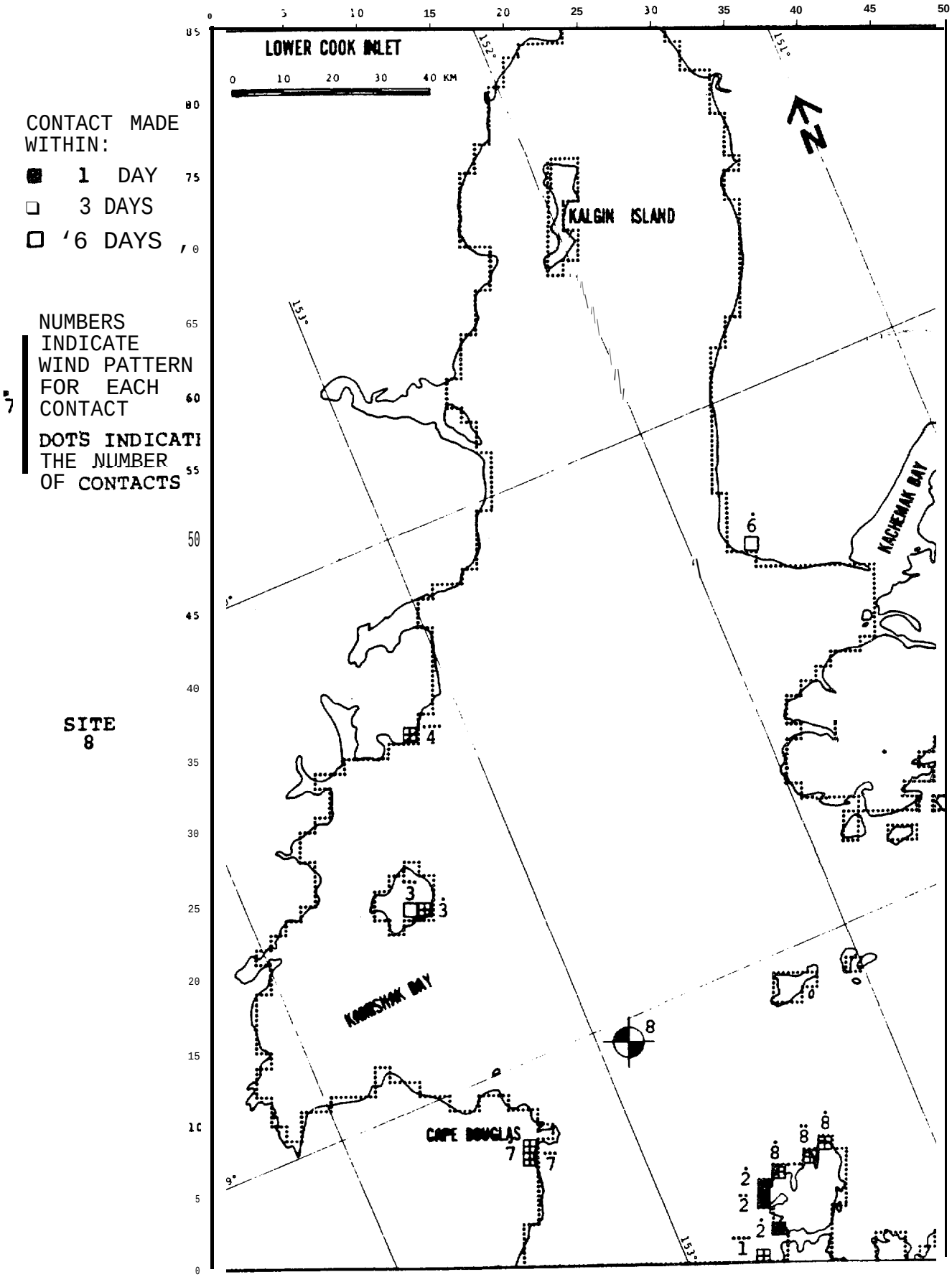

FIGURE B-80: POTENTIAL BOUNDARY CONTACT ZONES

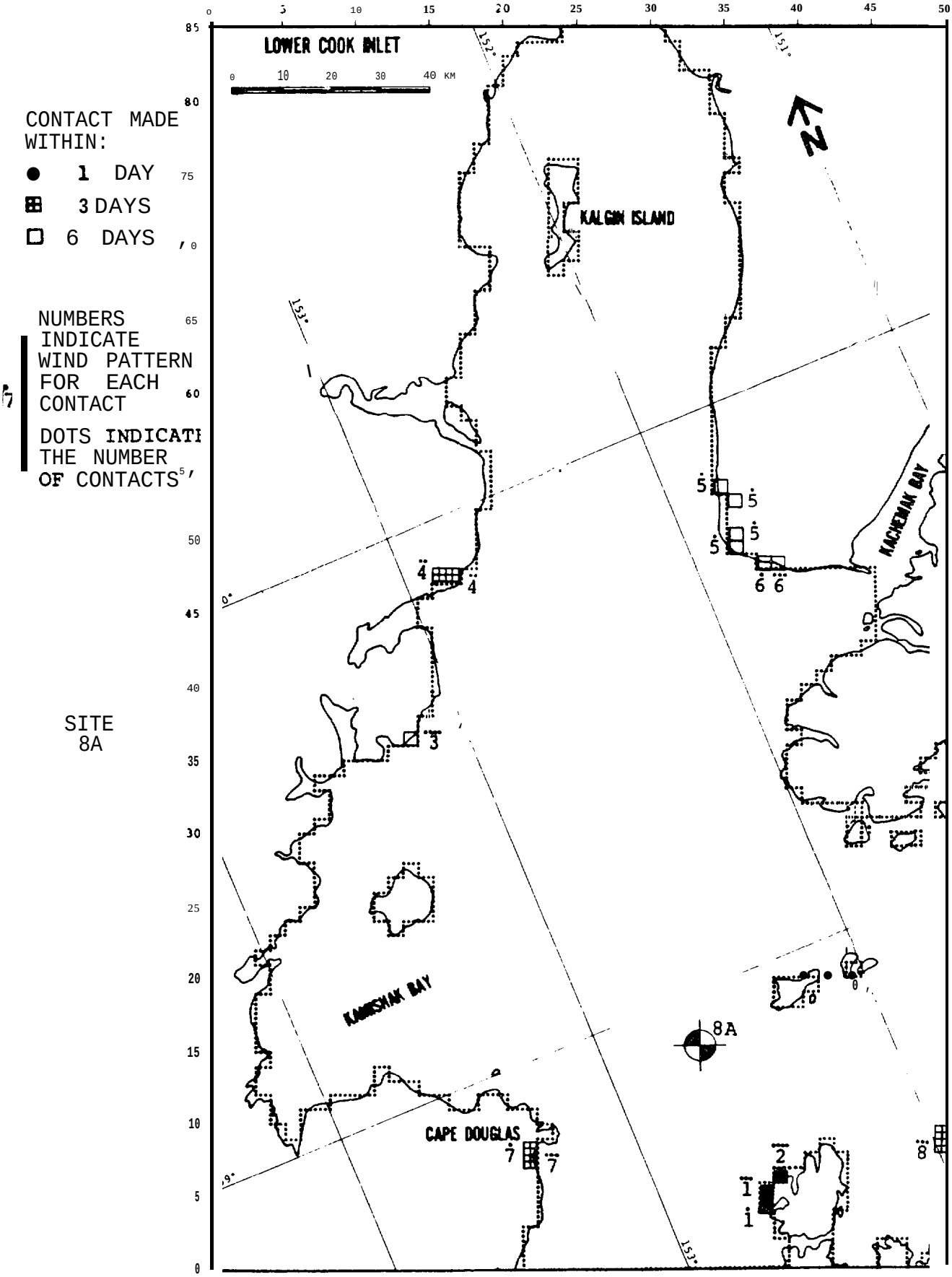

FIGURE B-81: POTENTIAL BOUNDARY CONTACT ZONES

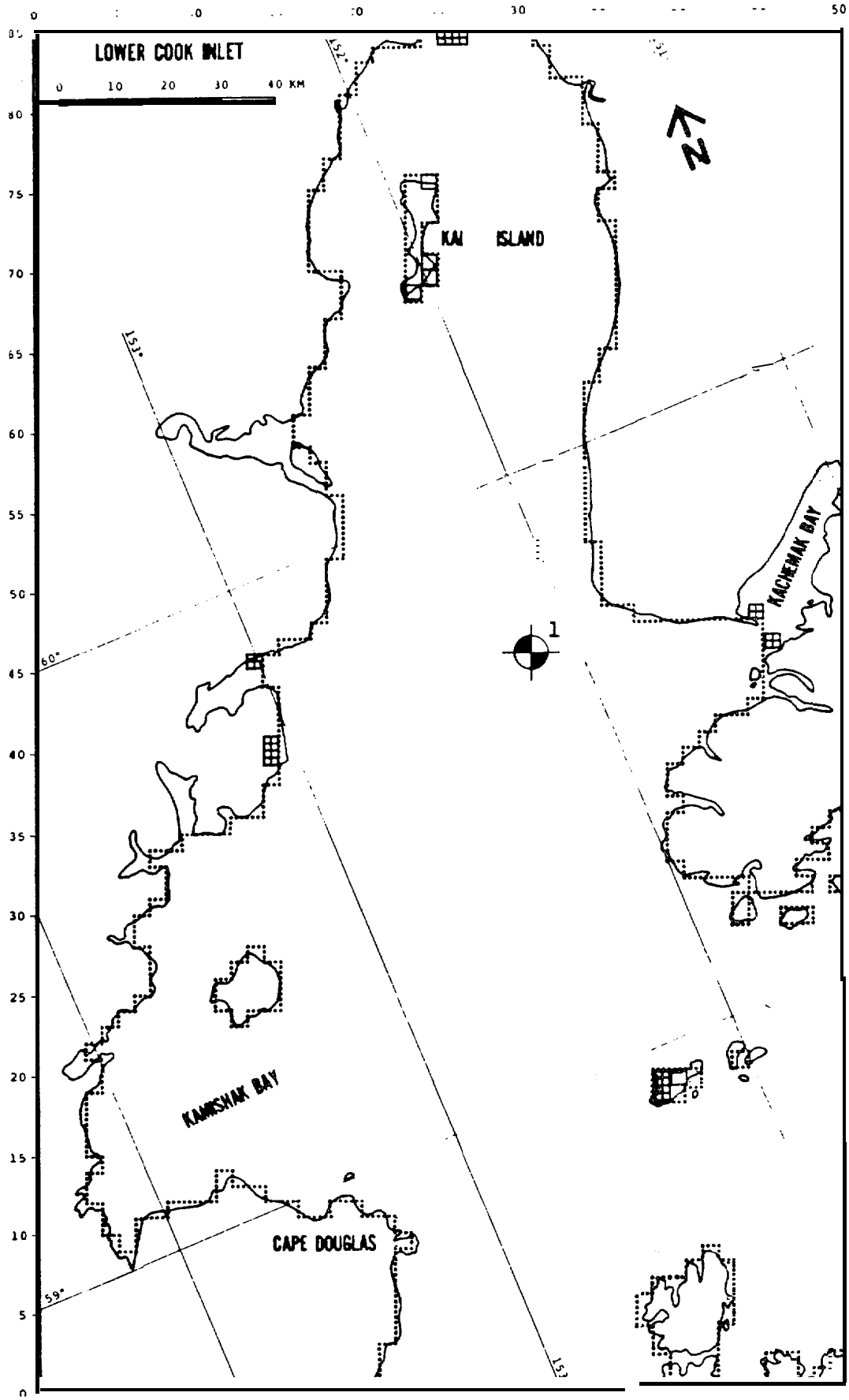

FIGURE B-82: ANNUAL PERCENT PROBABILITY OF EXPOSURE

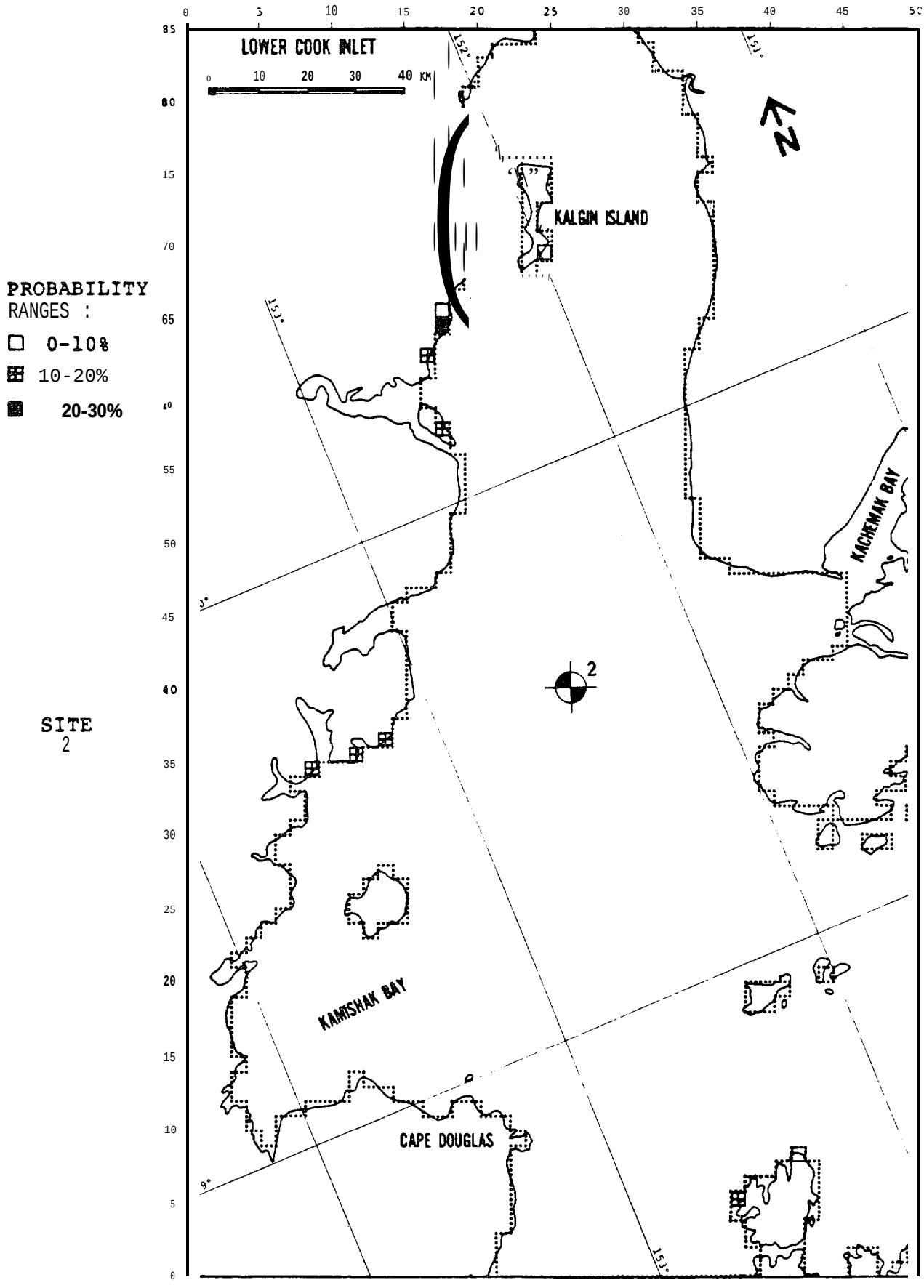

FIGURE B-83: ANNUAL PERCENT PROBABILITY OF EXPOSURE

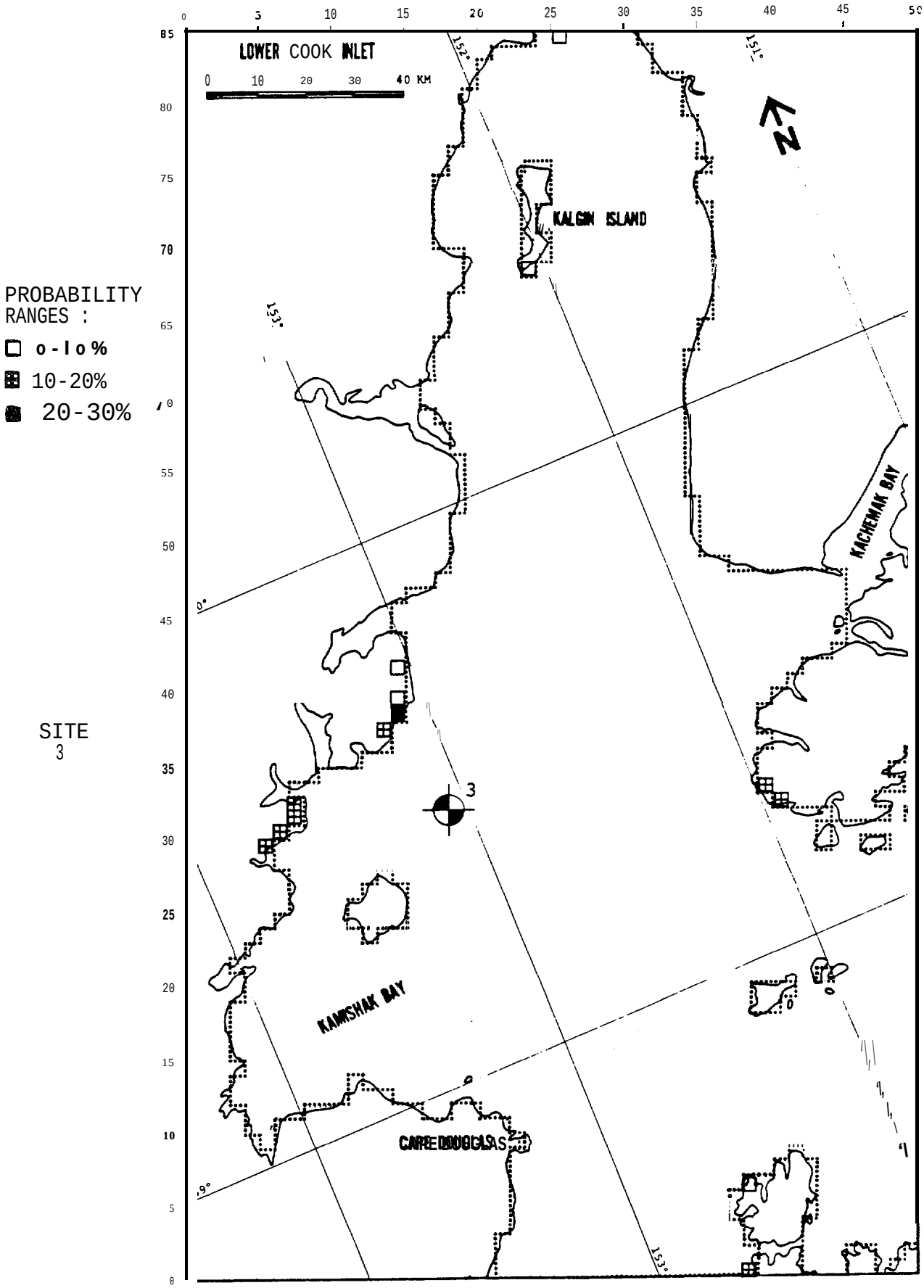

FIGURE B-84: ANNUAL PERCENT PROBABILITY OF EXPOSURE

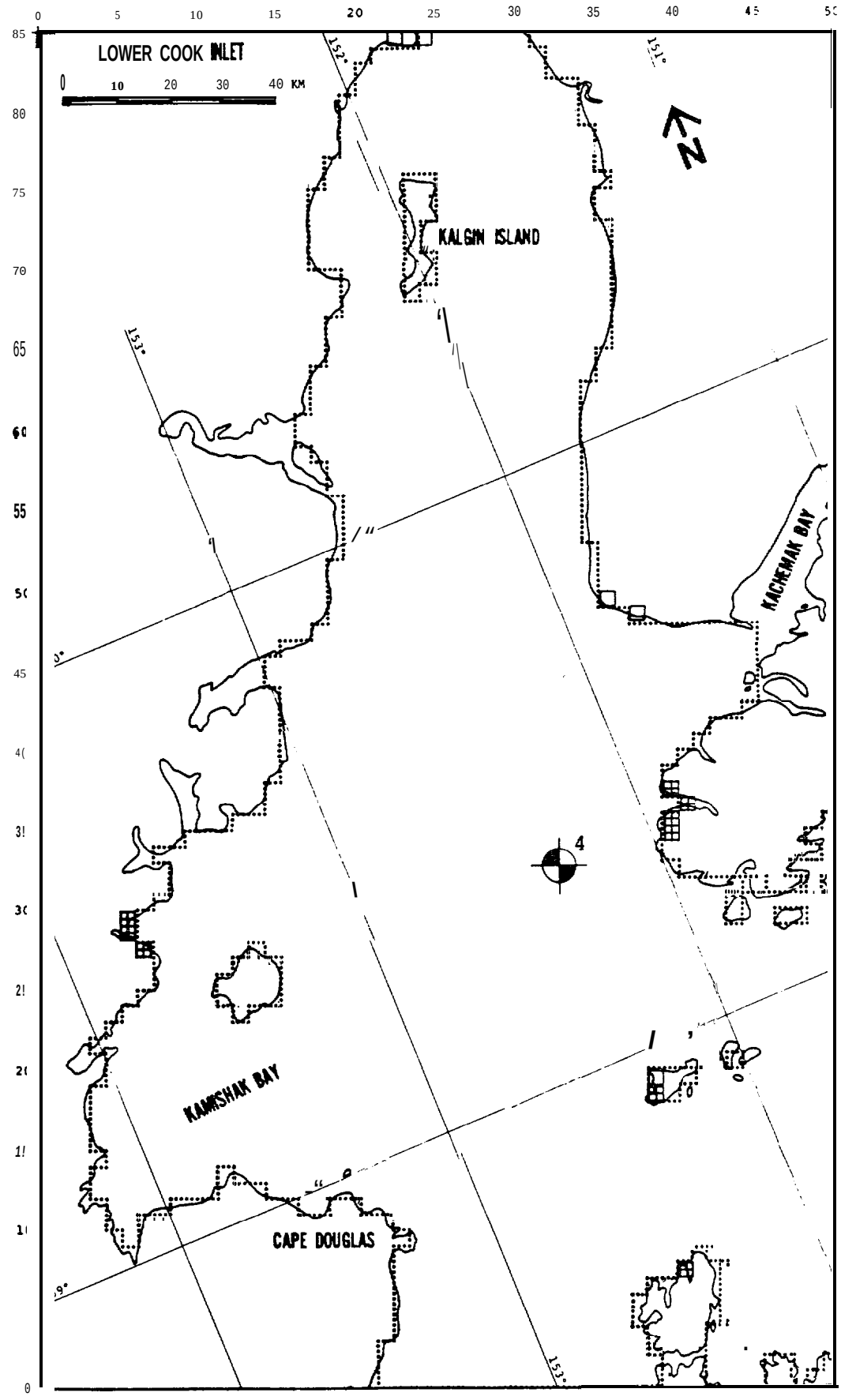

FIGURE B-85: ANNUAL PERCENT PROBABILITY OF EXPOSURE

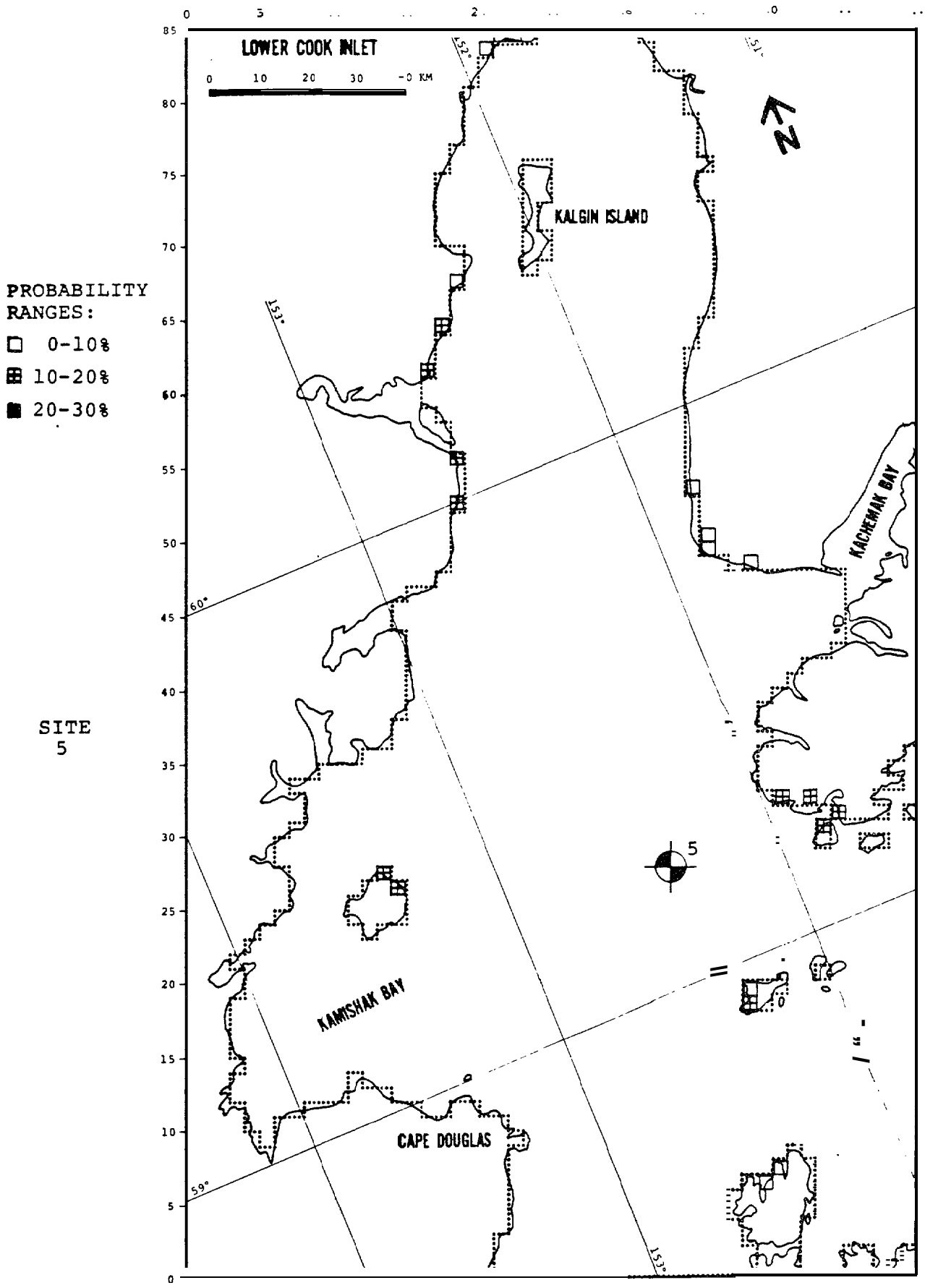

FIGURE B-86: ANNUAL PERCENT PROBABILITY OF EXPOSURE

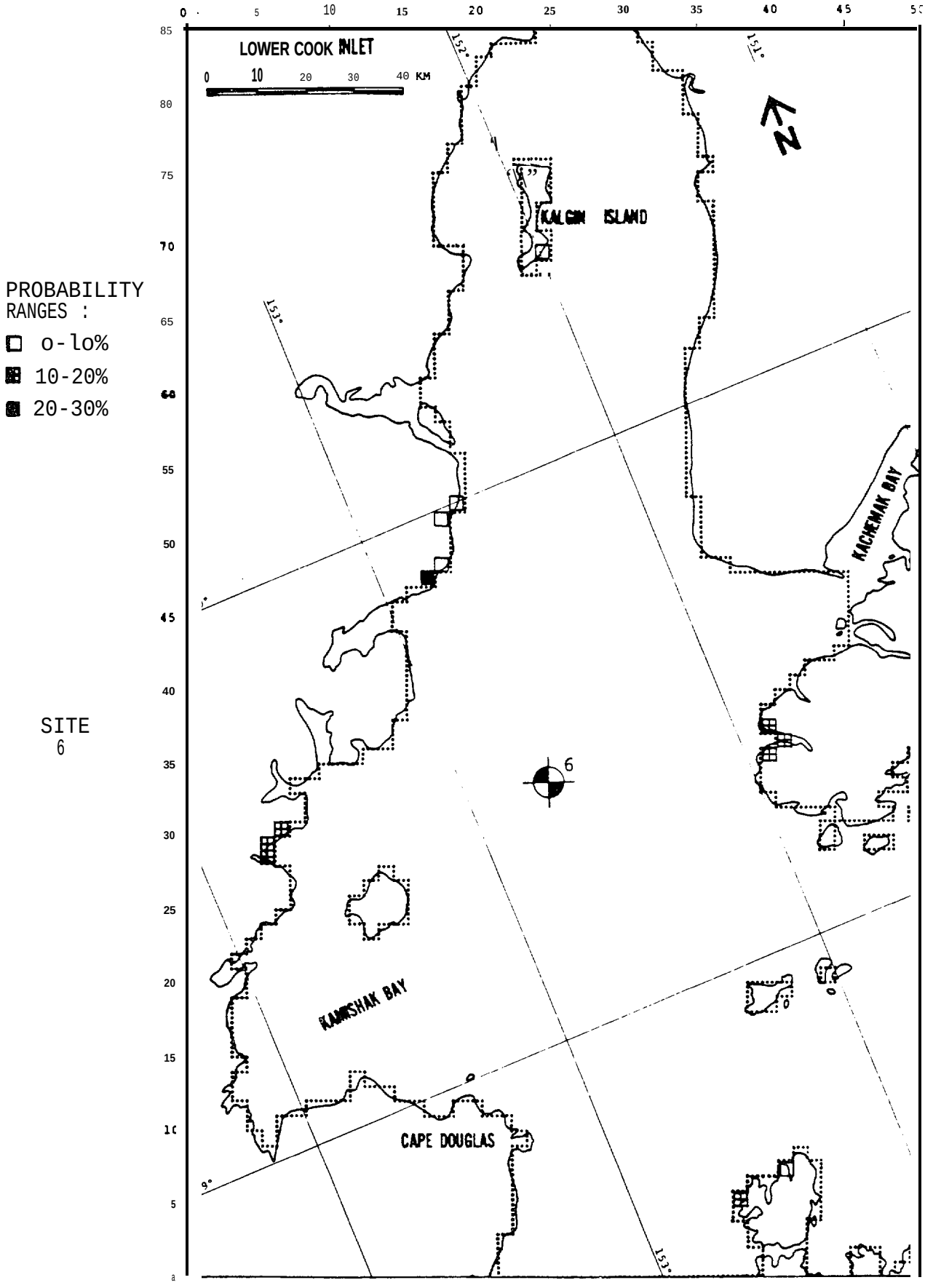

FIGURE B-87: ANNUAL PERCENT PROBABILITY OF EXPOSURE

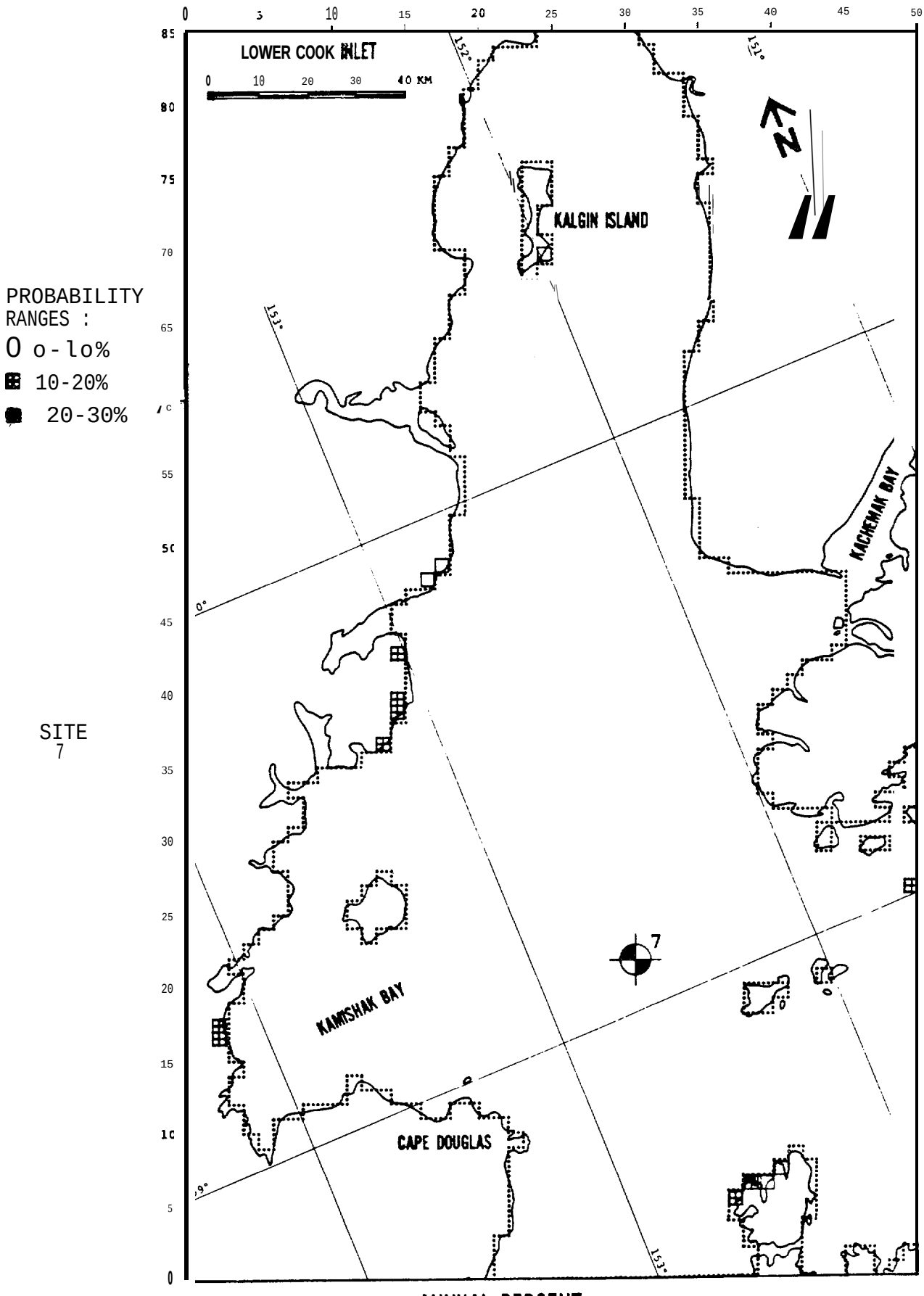

FIGURE B-88: ANNUAL PERCENT PROBABILITY OF EXPOSURE

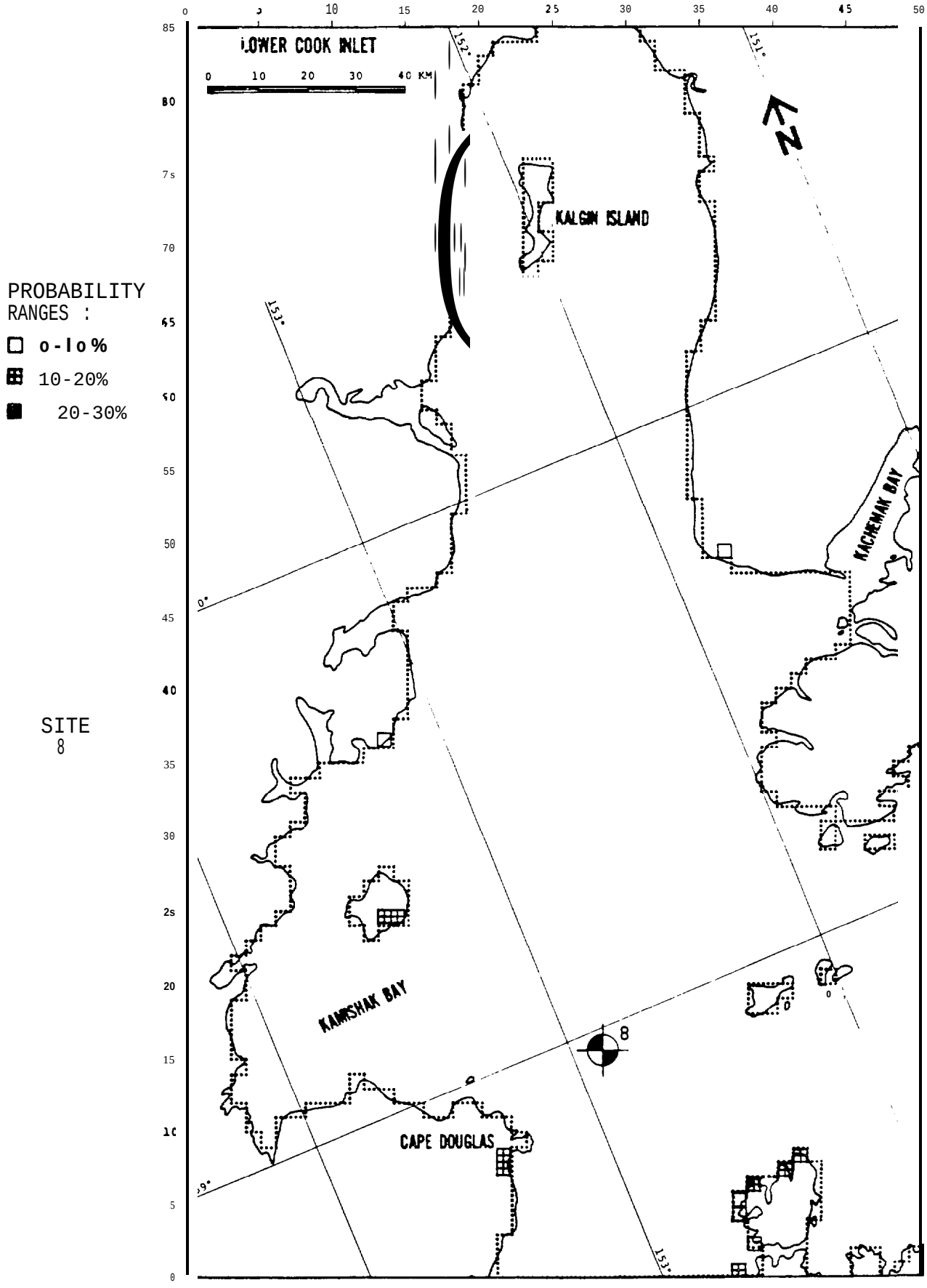

FIGURE B-89: ANNUAL PERCENT PROBABILITY OF EXPOSURE

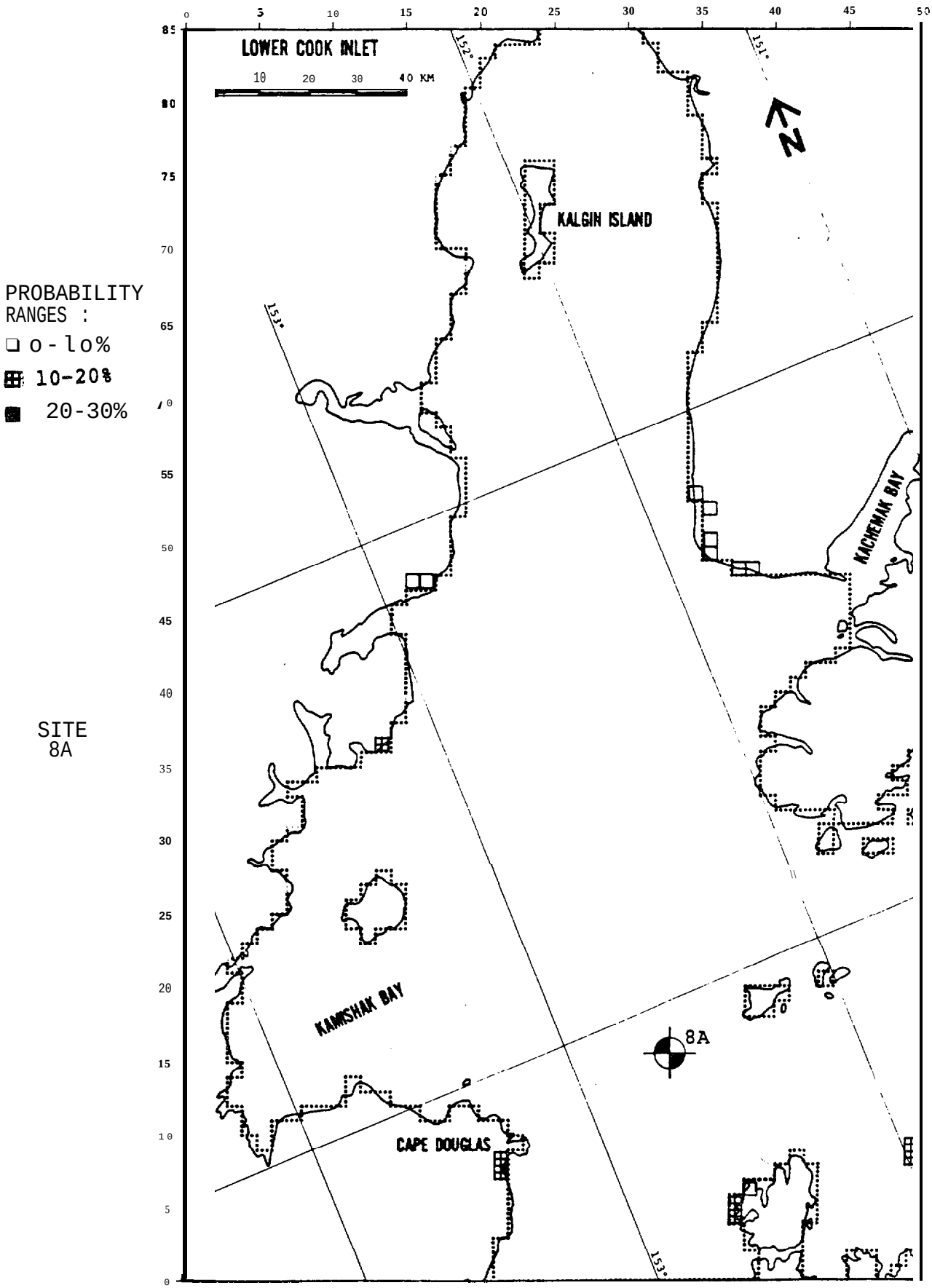

FIGURE B-90: ANNUAL PERCENT PROBABILITY OF EXPOSURE

APPENDIX C

PERTURBATION CASE TRAJECTORIES

WIND
1

SITE
1

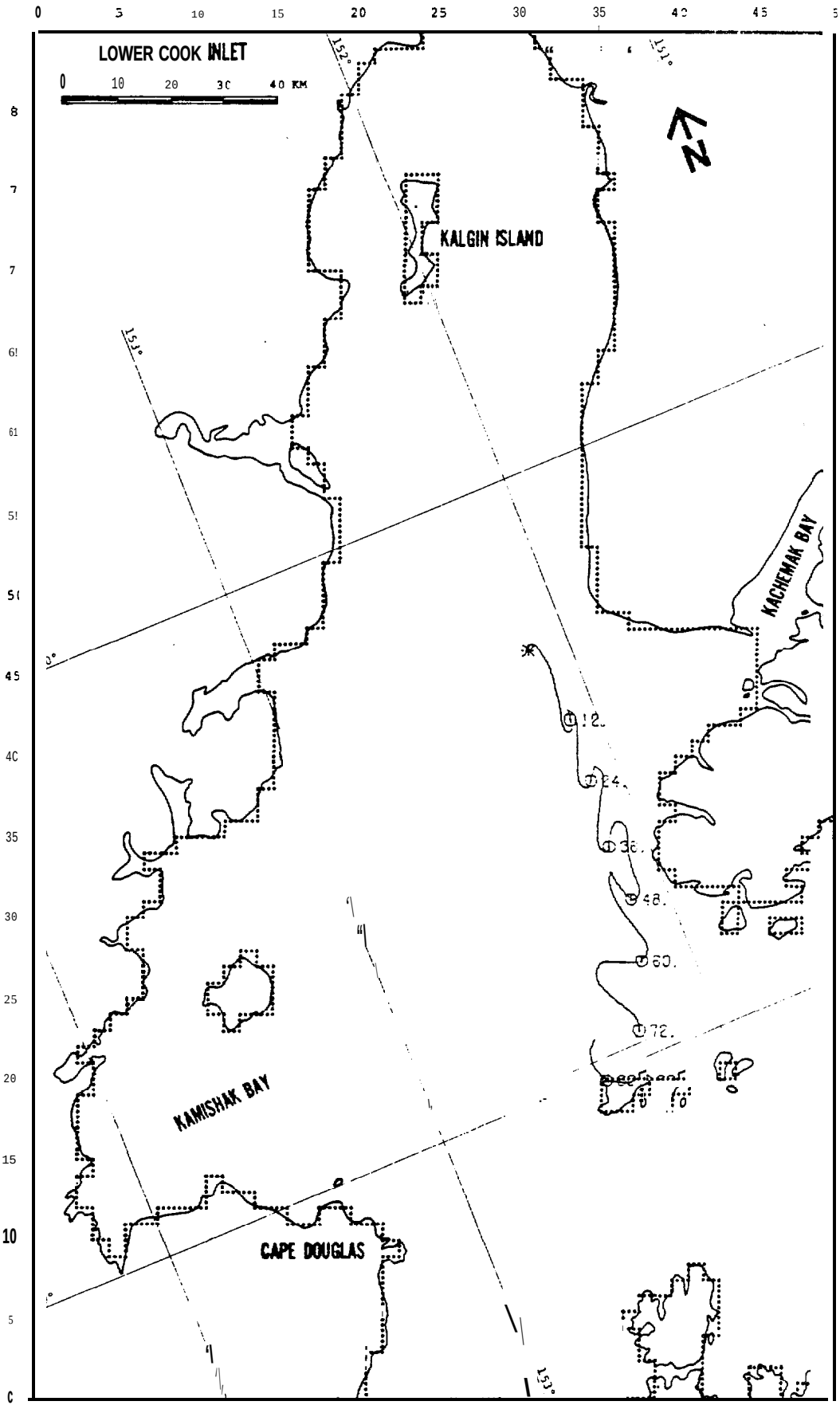

FIGURE C-1: PERTURBATION CASE: NET +25%

WIND
1

SITE
1

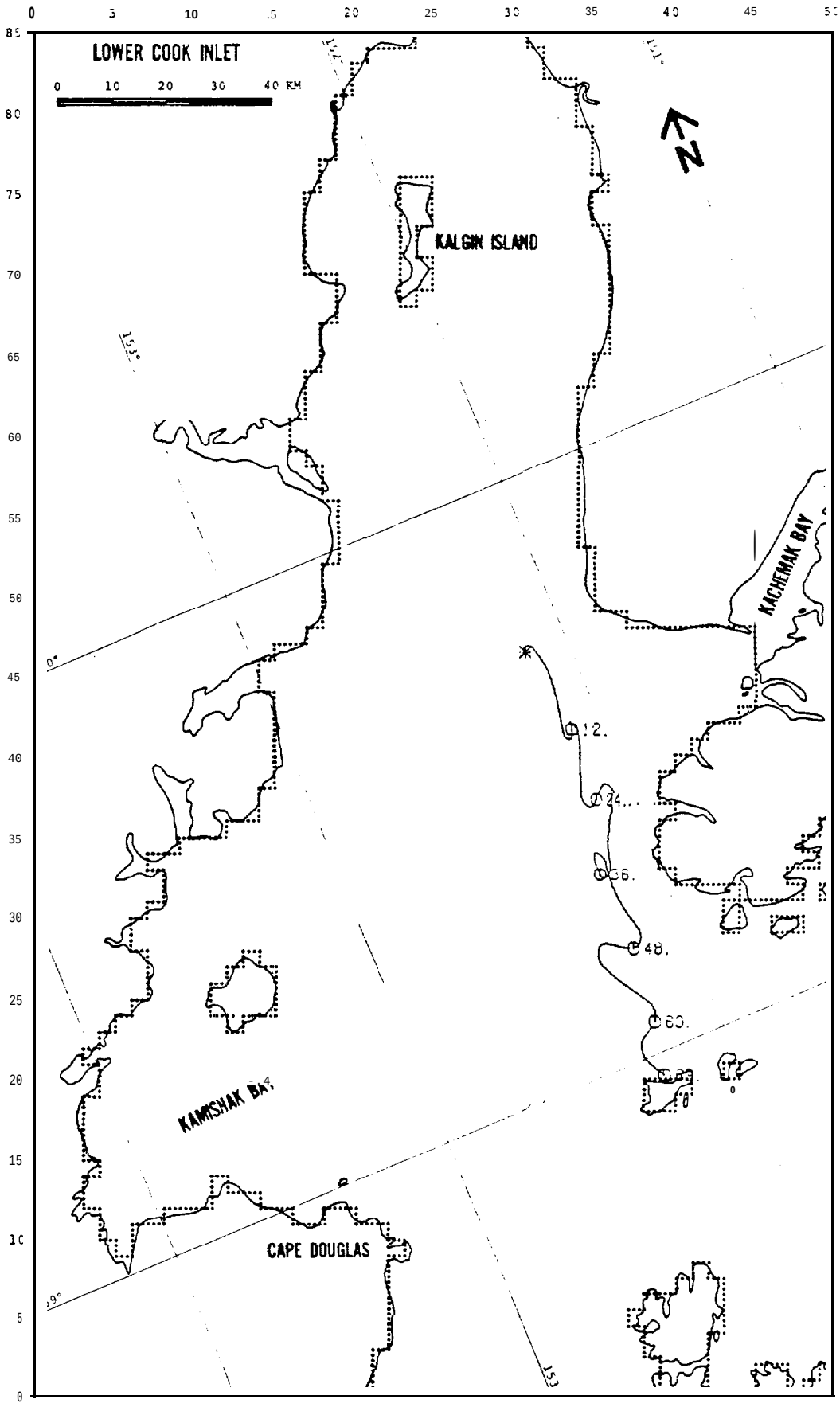

FIGURE C-2: PERTURBATION CASE: NET -25%

WIND
1

SITE
1

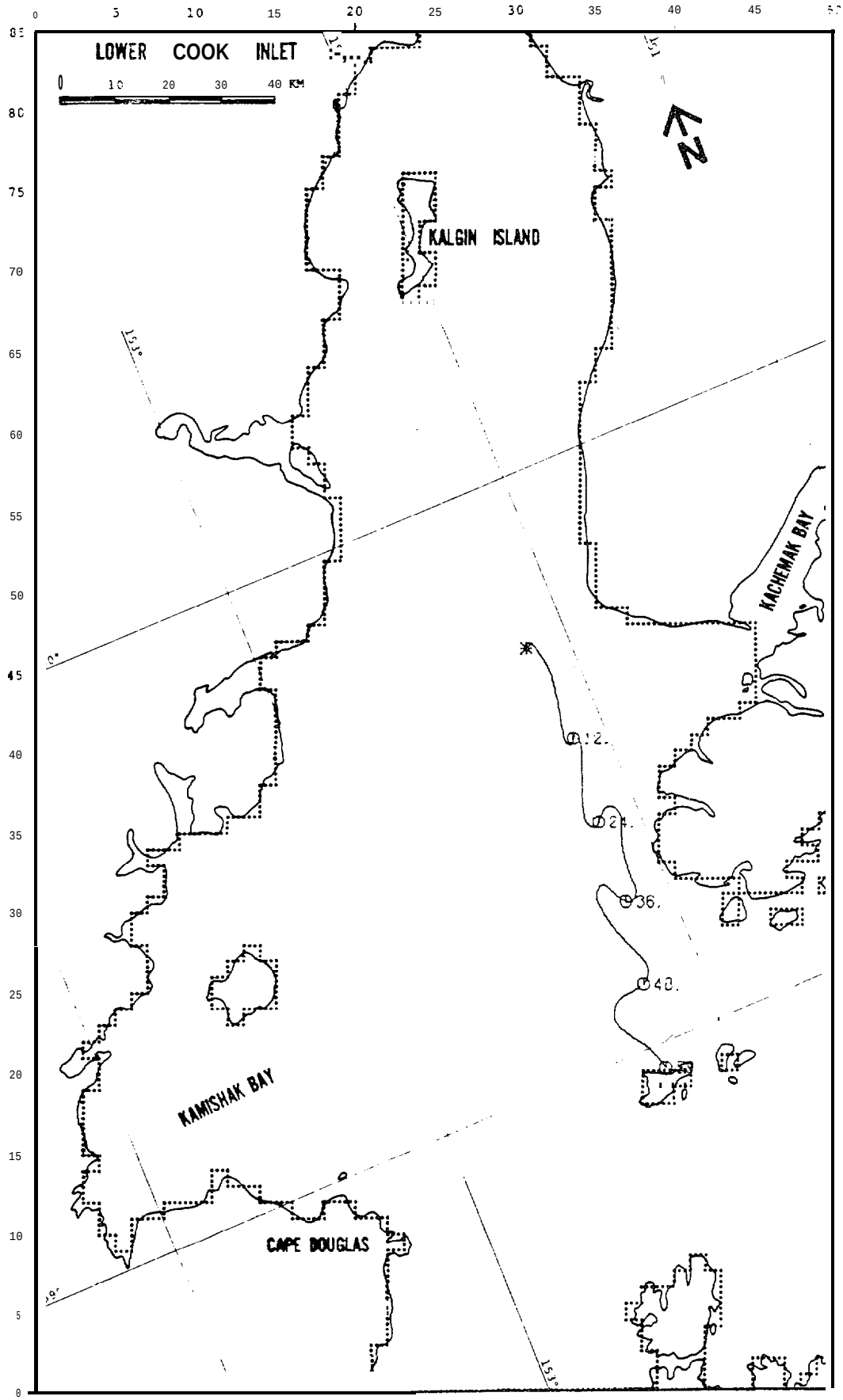

FIGURE C-3: 'PERTURBATION CASE: WIND +25%

WIND
1

SITE
1

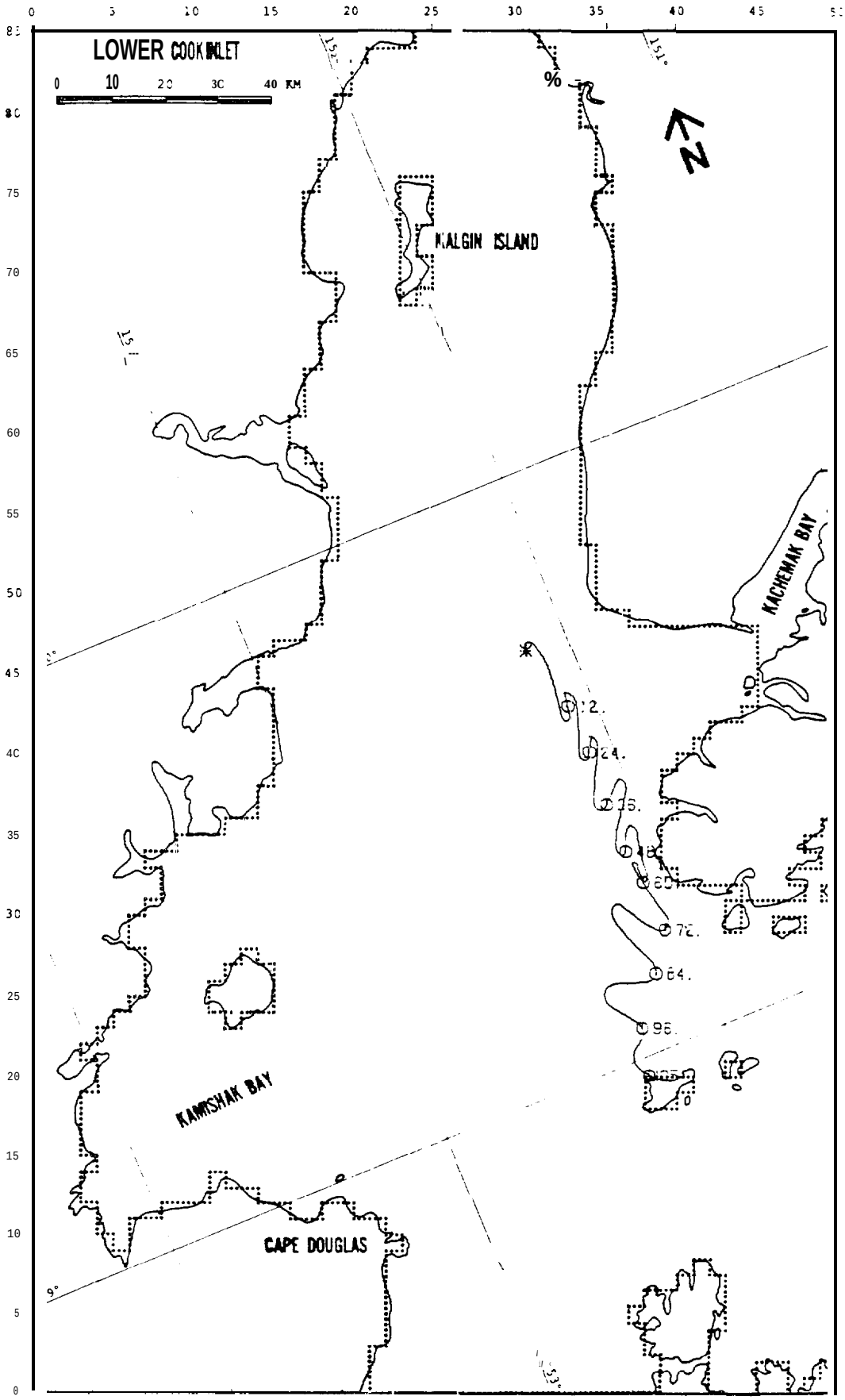

FIGURE C-4: PERTURBATION CASE: WIND -25%

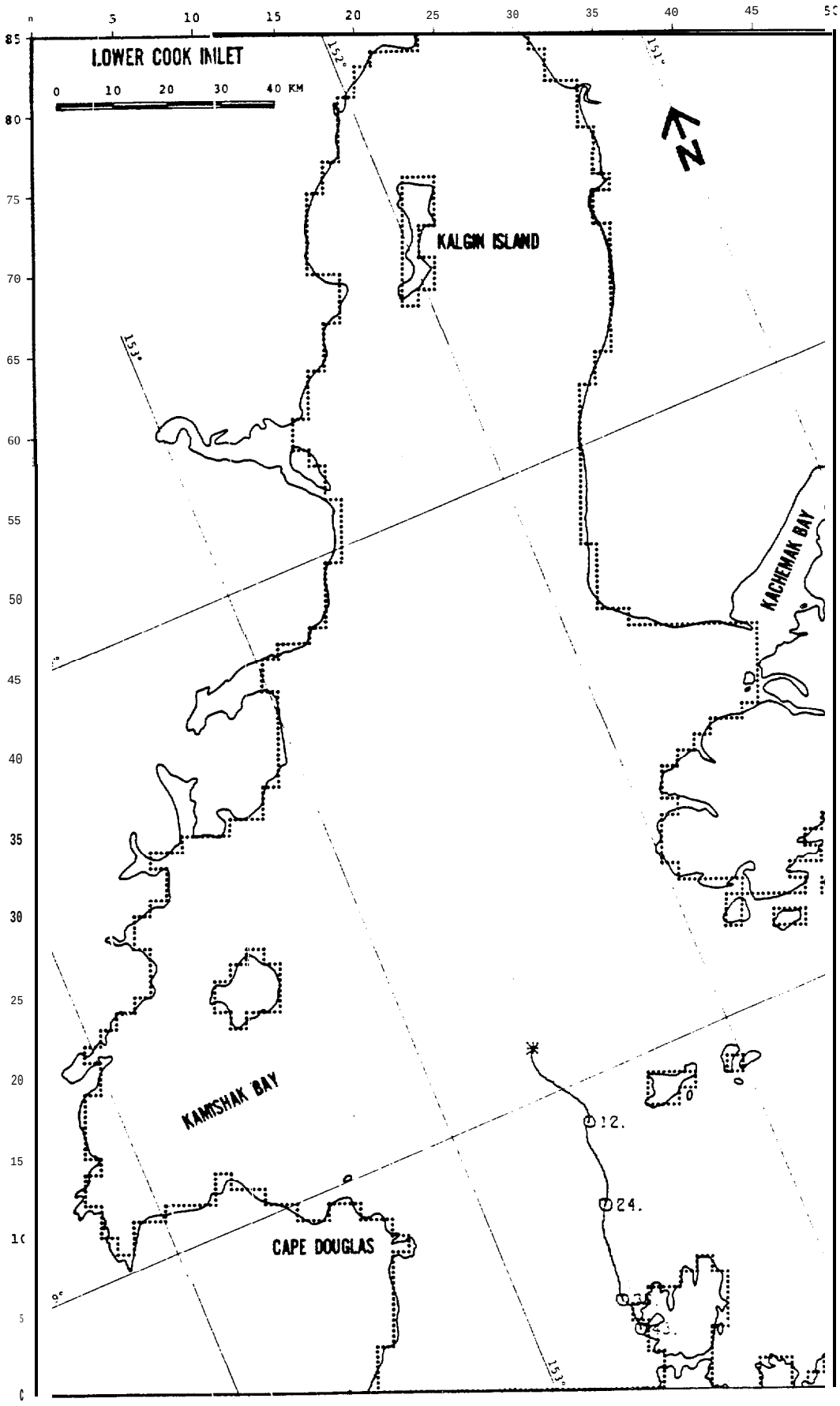

WIND
1

SITE
7

FIGURE C-5: PERTURBATION CASE: NET +25%

WIND
1

SITE
7

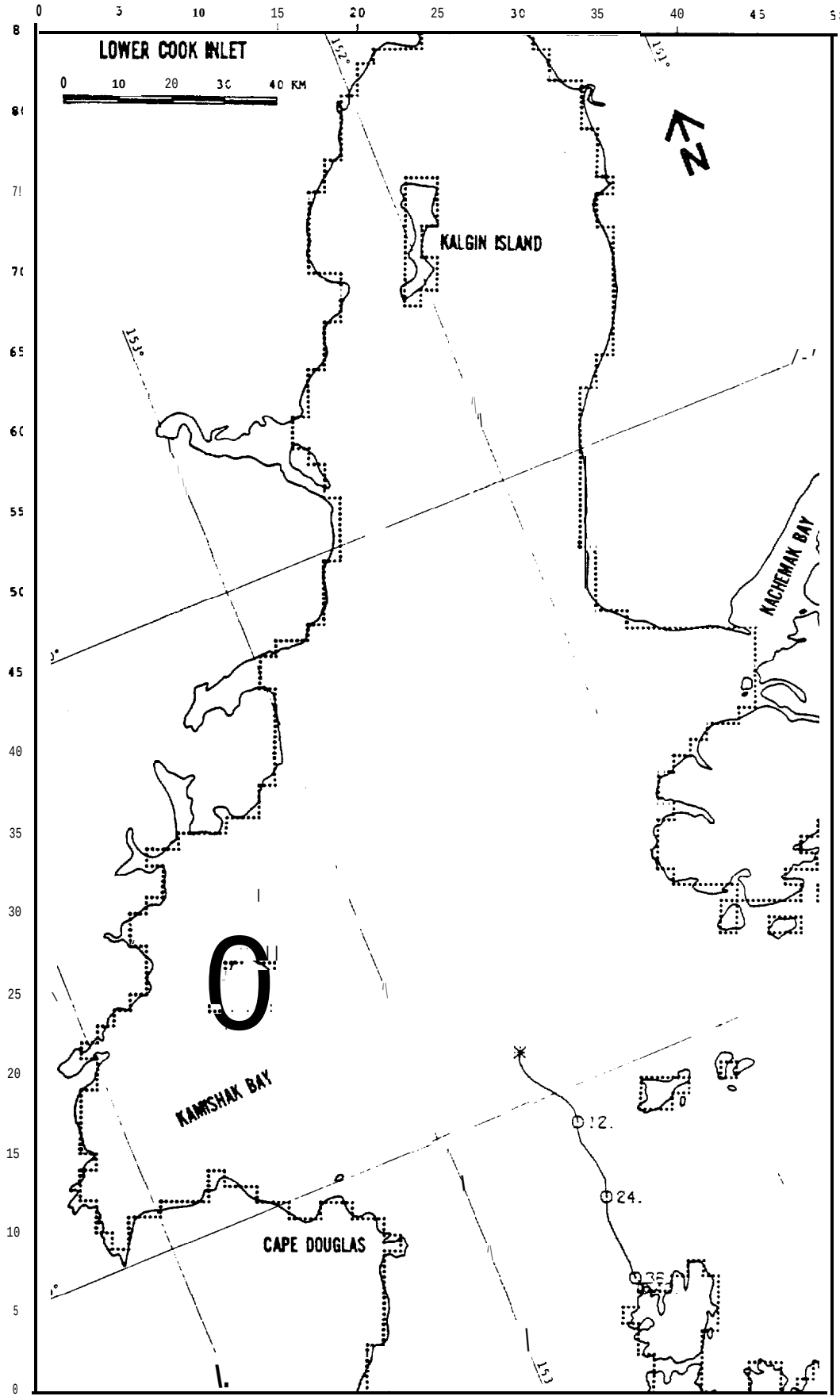

FIGURE C-6: PERTURBATION CASE: **NET -25%**

WIND
1

SITE
7

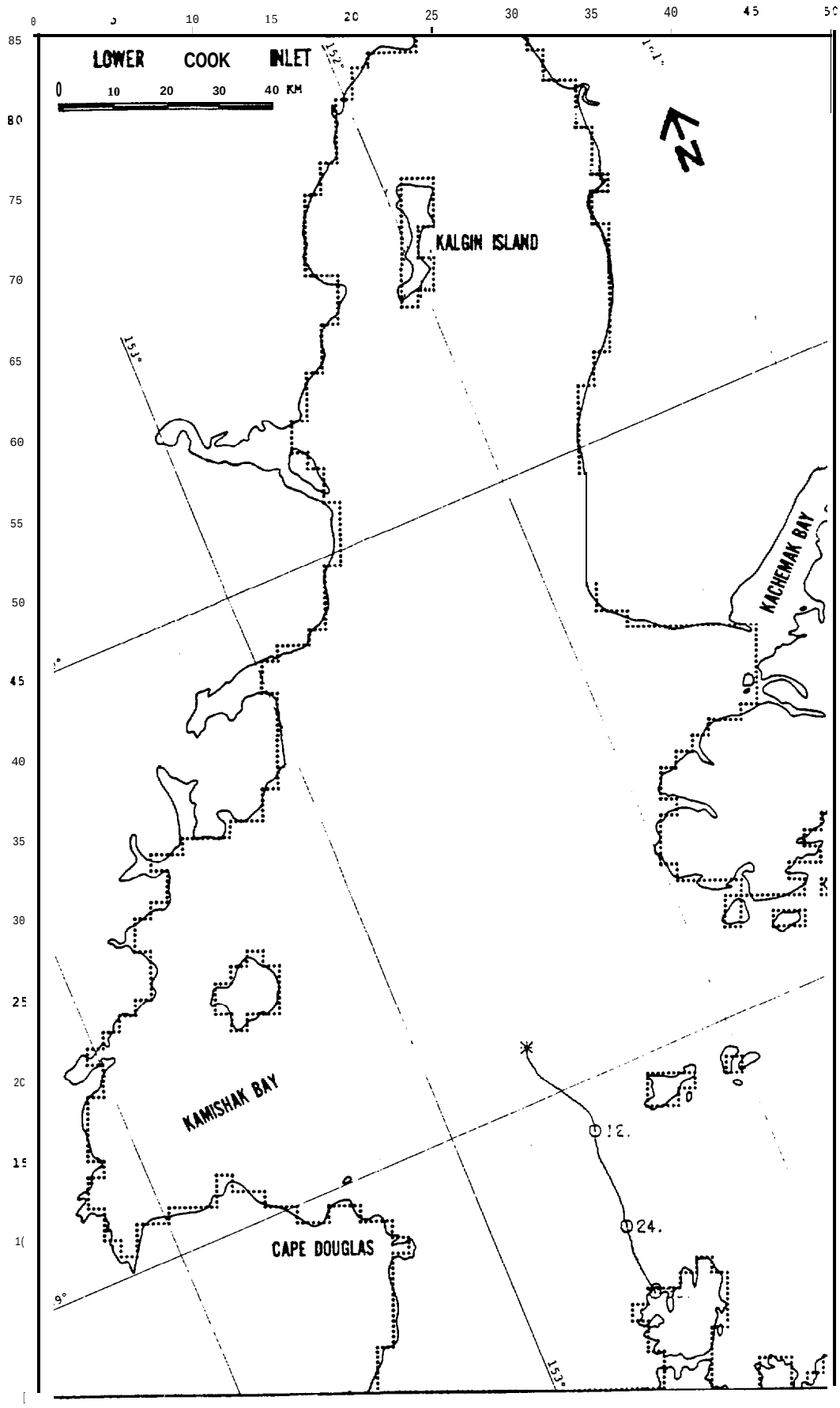

FIGURE C-7: PERTURBATION CASE: WIND +25%

WIND

1

SITE

7

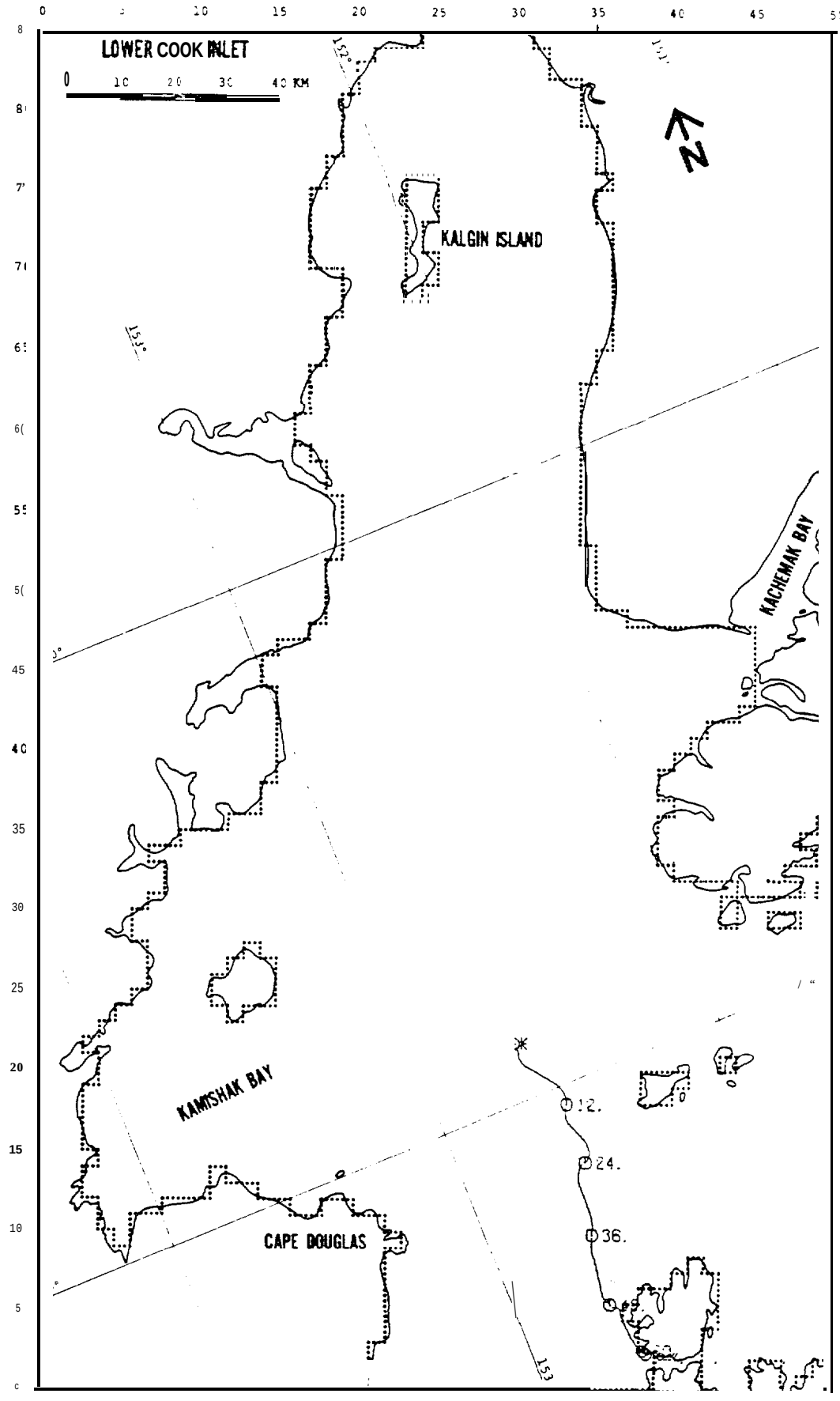

FIGURE C-8: PERTURBATION CASE: WIND -25%

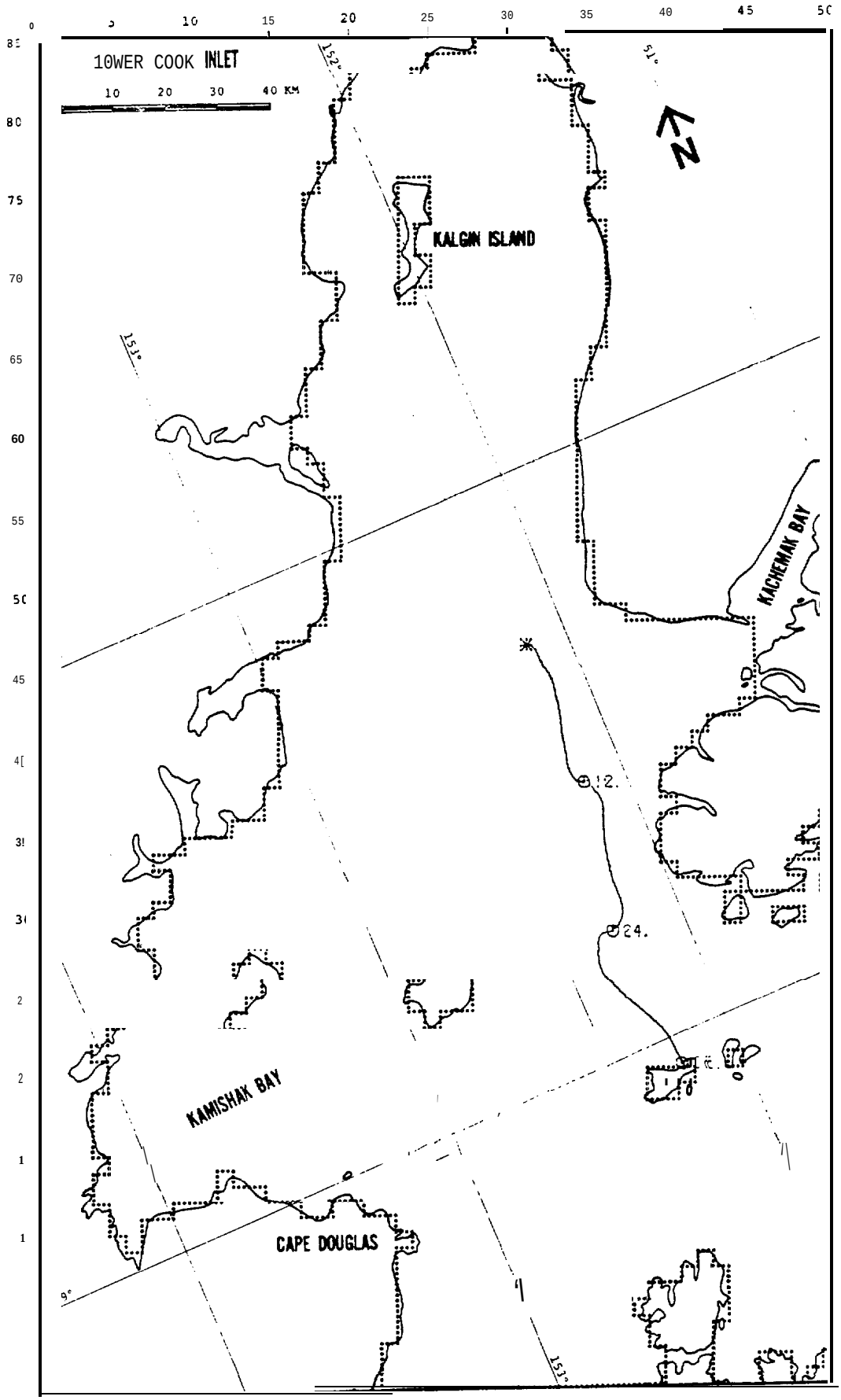

WIND
2

SITE
1

FIGURE C-9: PERTURBATION CASE: NET +25%

WIND
2

SITE
1

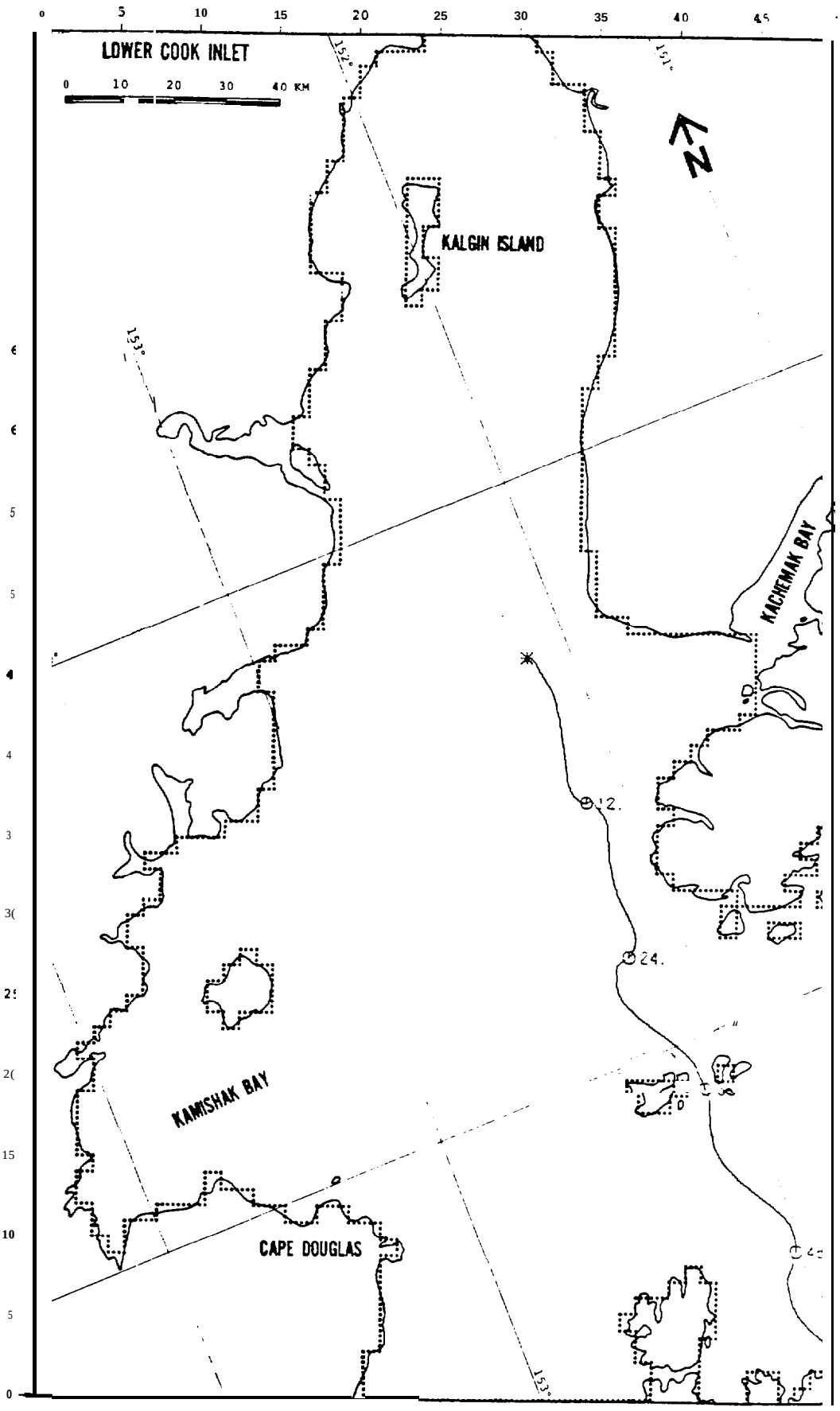

FIGURE C-10: PERTURBATION CASE: NET -25%

WIND
2

SITE
1

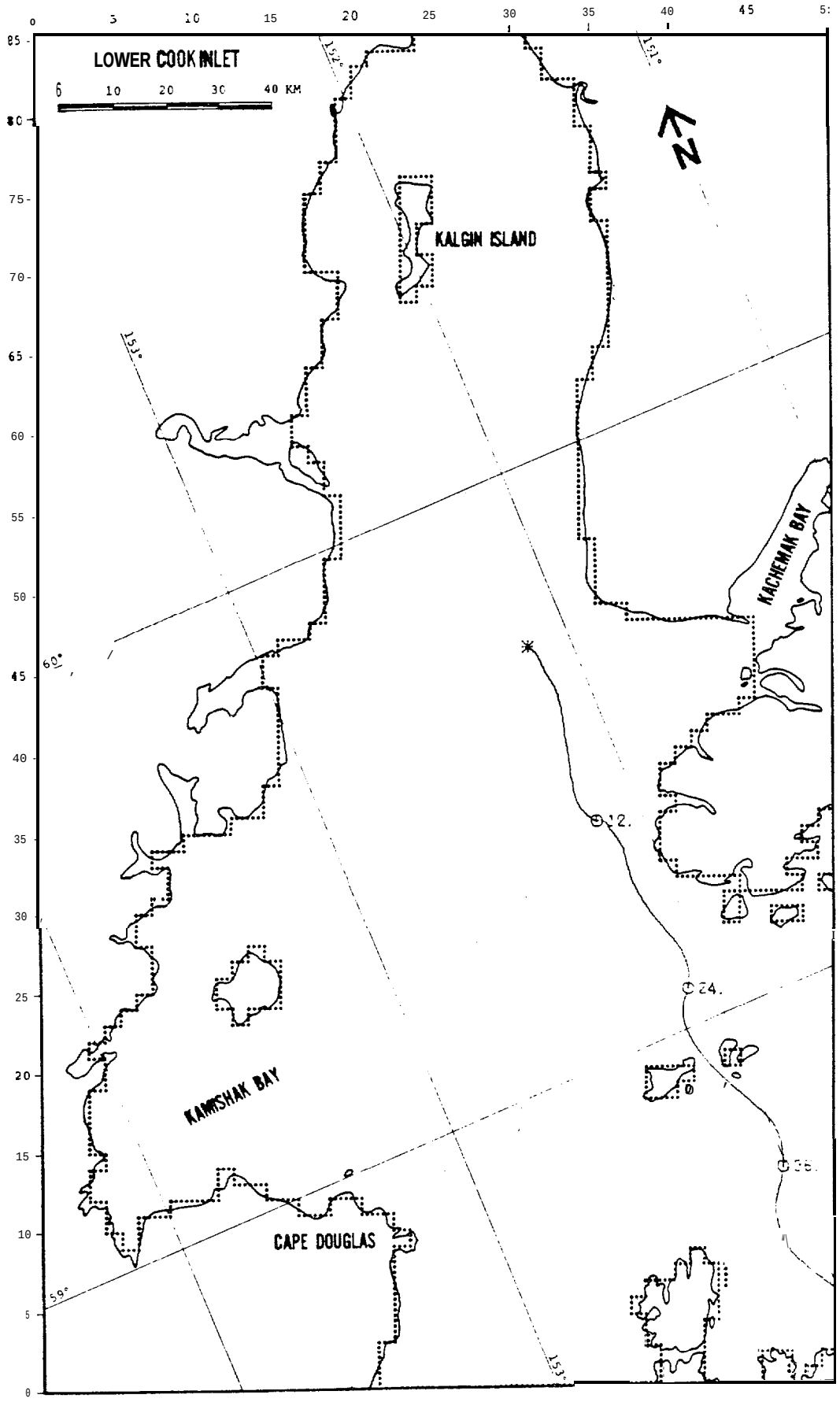

FIGURE C-11: PERTURBATION CASE: WIND +25%

WIND
2

SITE
1

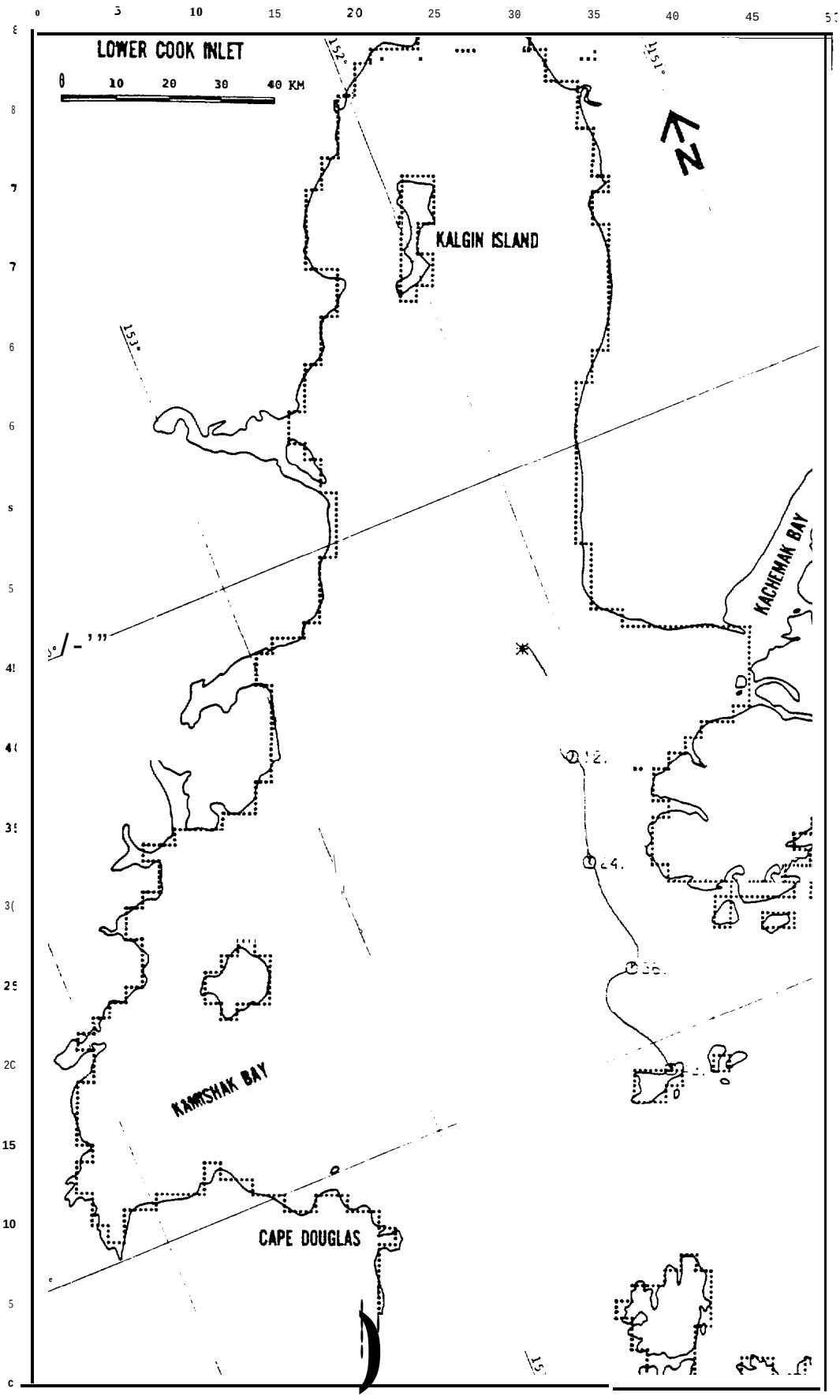

FIGURE C-12: PERTURBATION CASE: WIND -25%

WIND
2

SITE
7

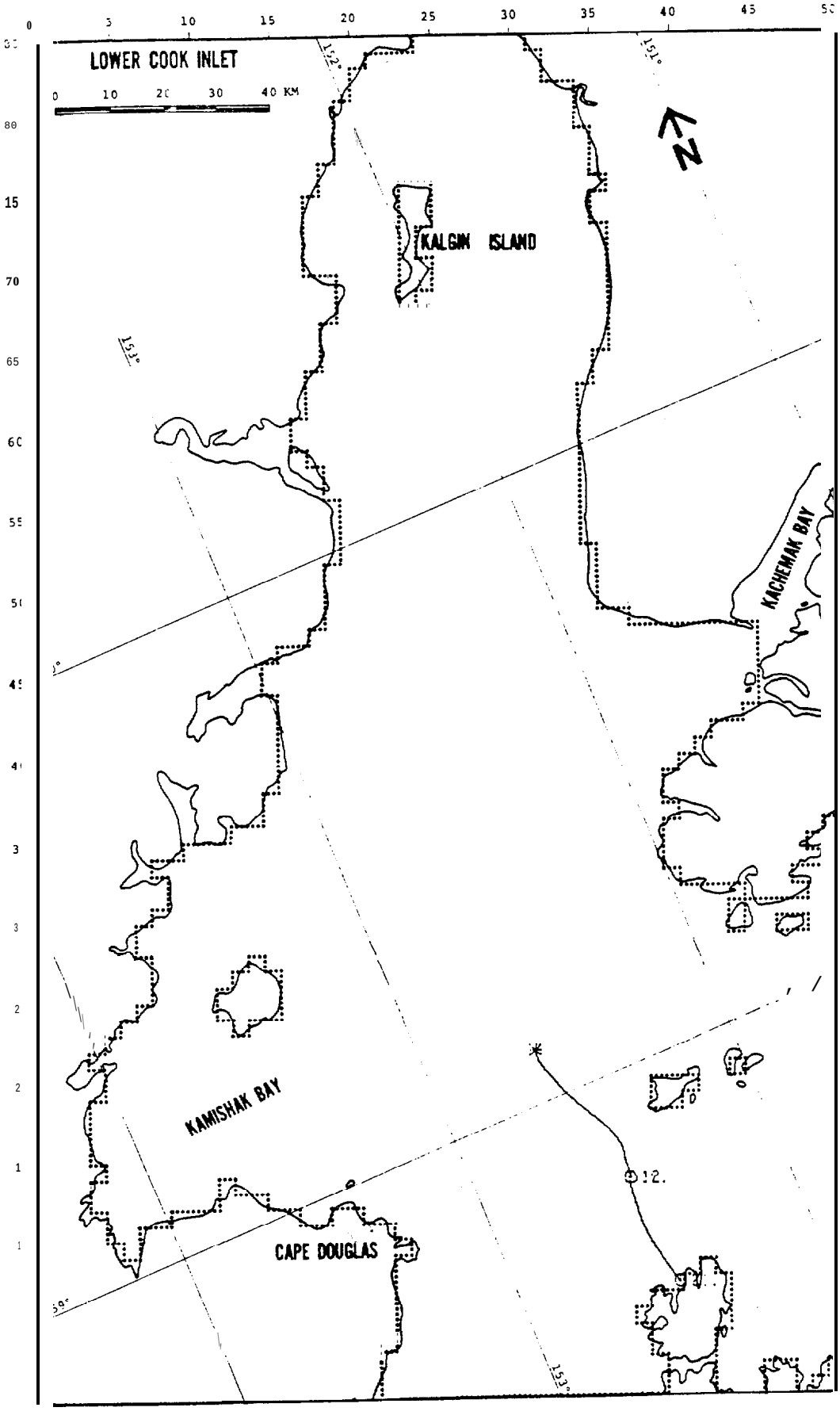

FIGURE C-13: PERTURBATION CASE: NET +25%

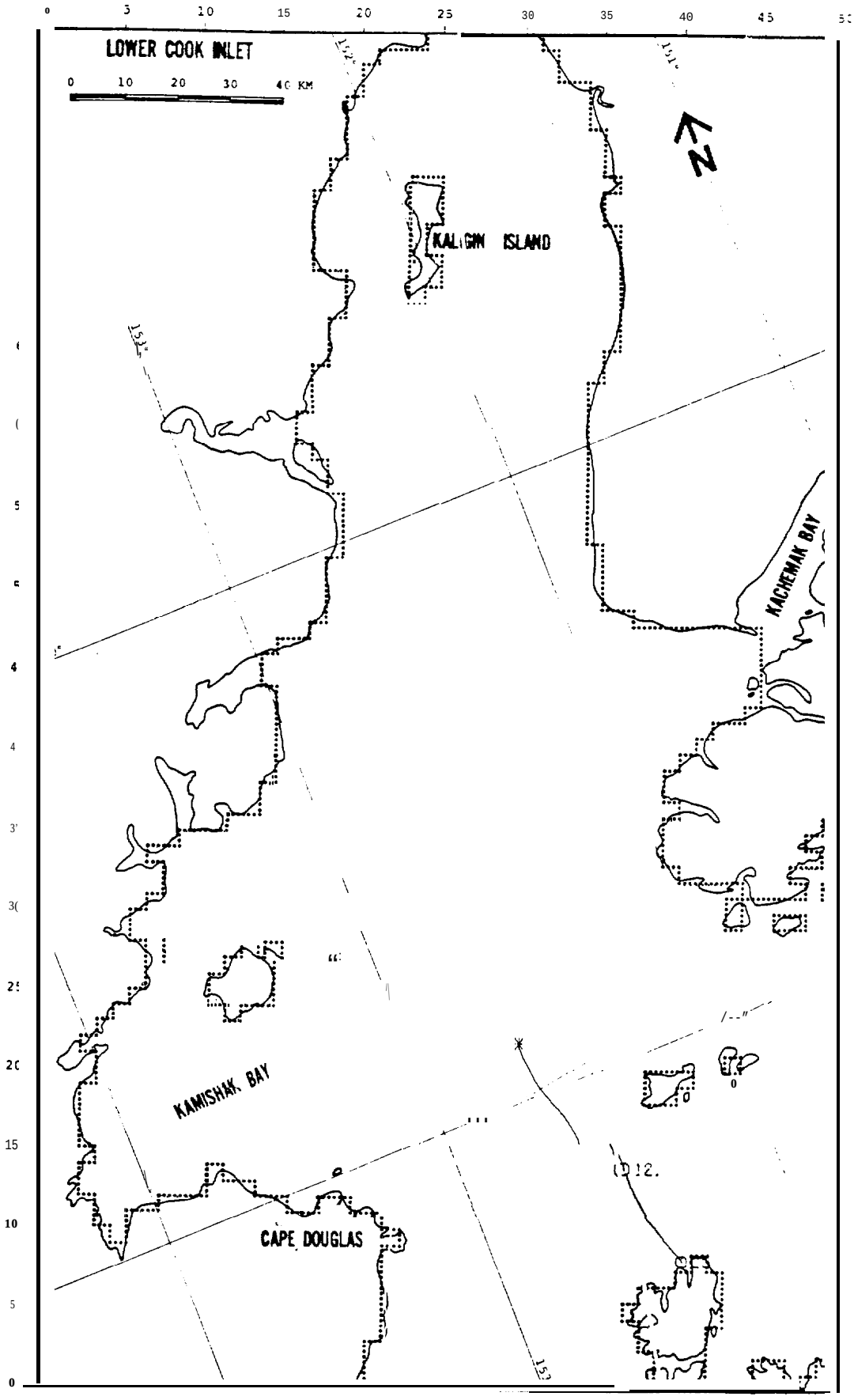

FIGURE C-14: PERTURBATION CASE: NET -25%

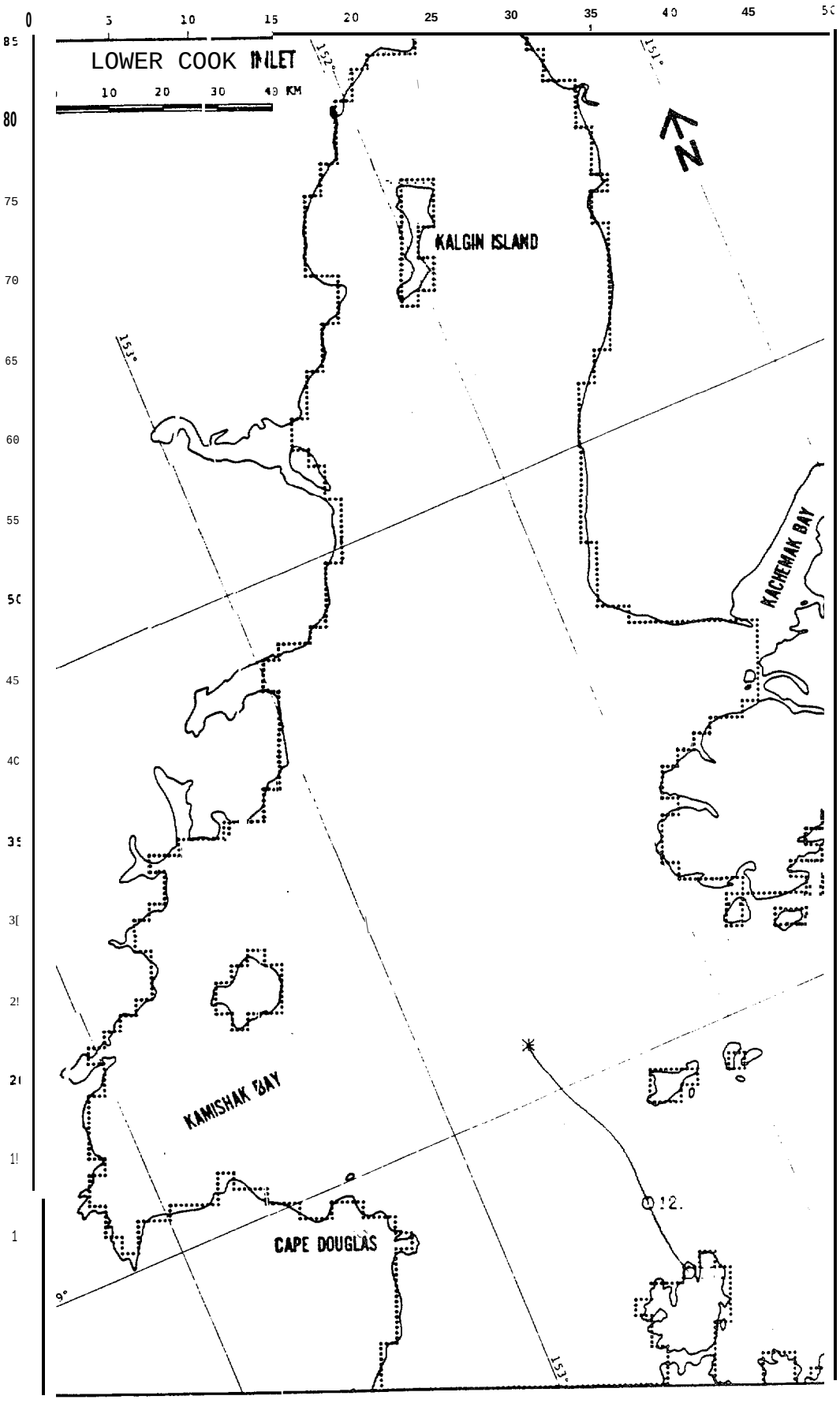

WIND
2

SITE
7

FIGURE C-15: PERTURBATION CASE: WIND +25%

WIND
2

SITE
7

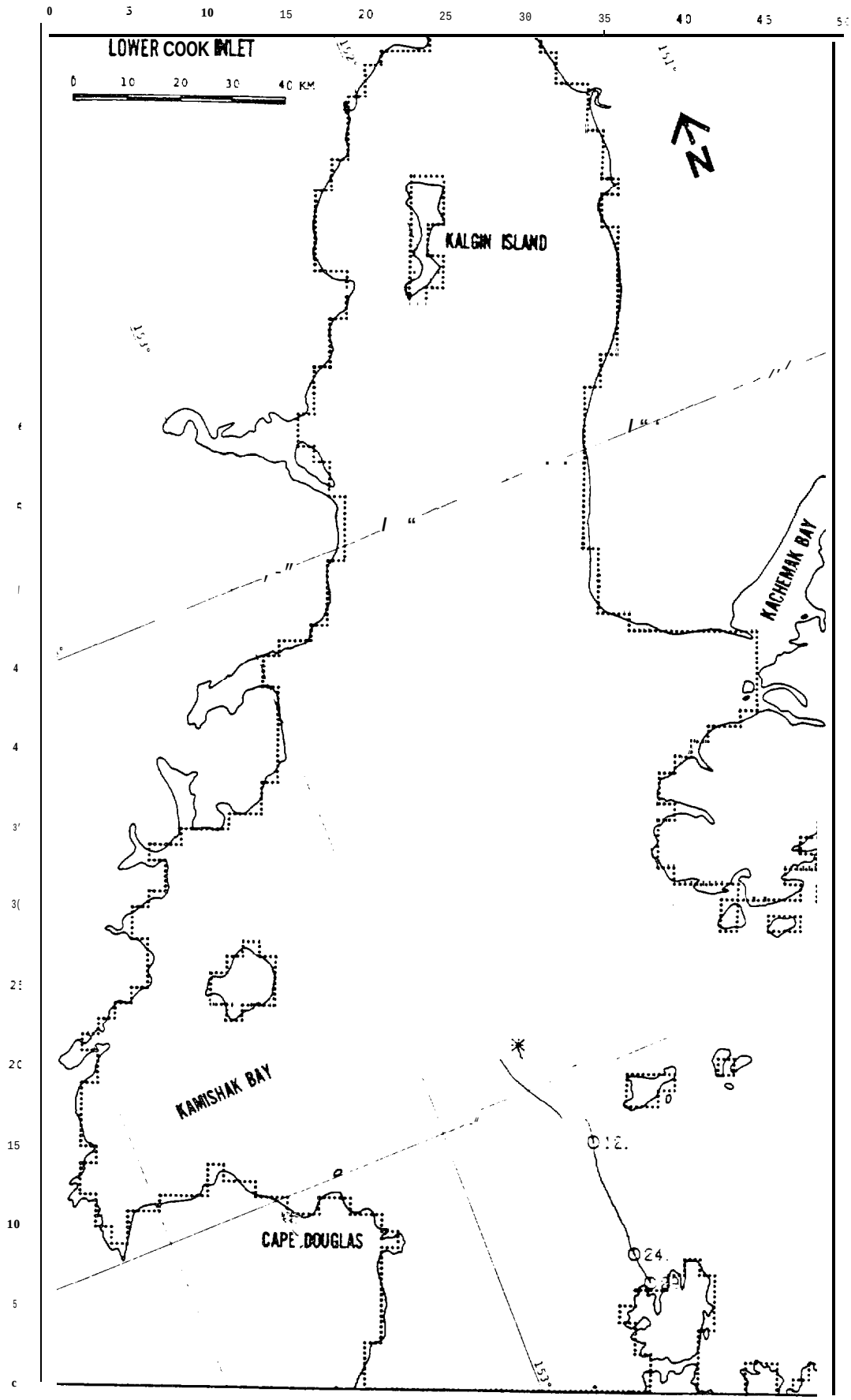

FIGURE C-16: PERTURBATION **CASE:** WIND -25%

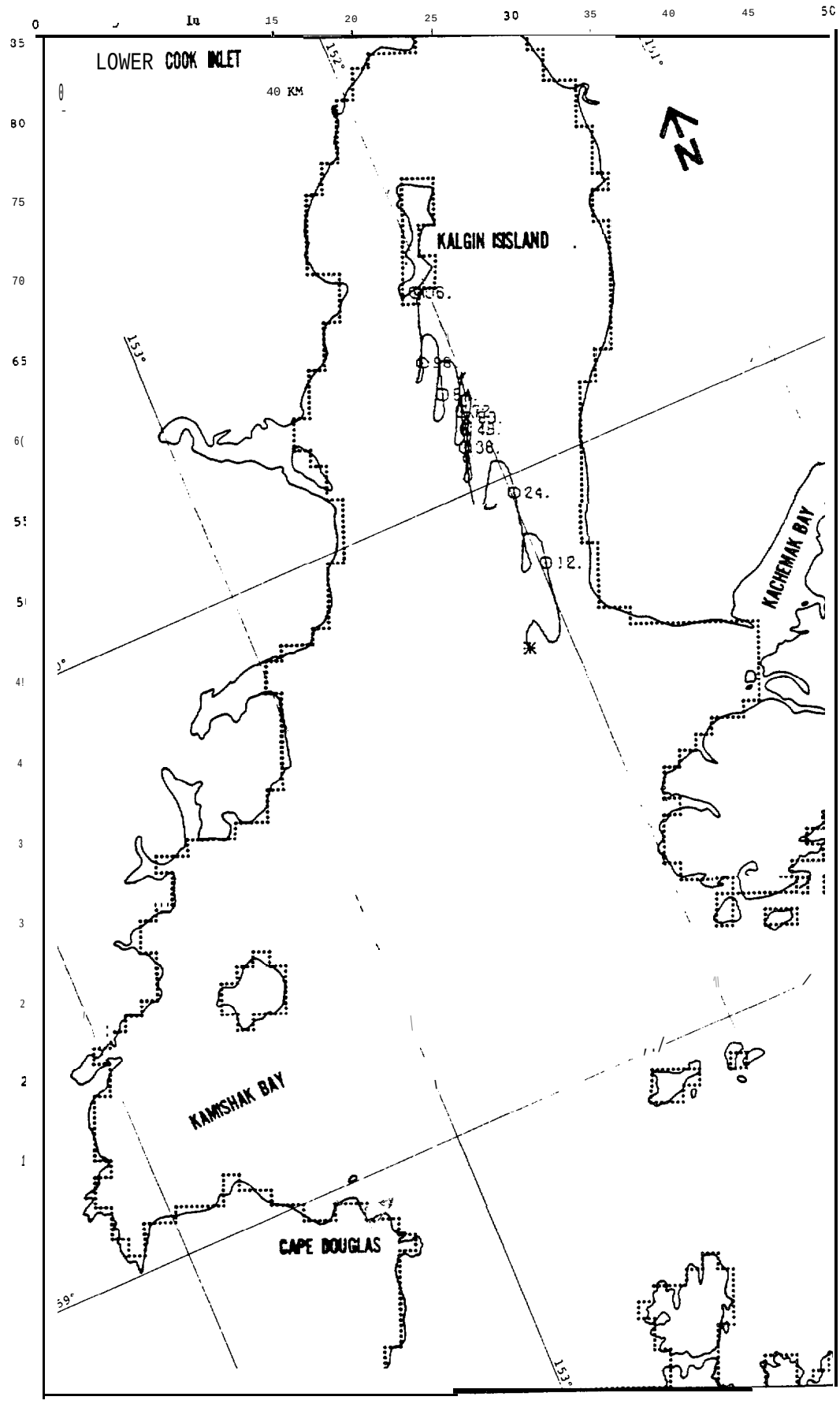

WIND
3

SITE
1

FIGURE C-17: PERTURBATION CASE: NET +25%

WIND
3

SITE
1

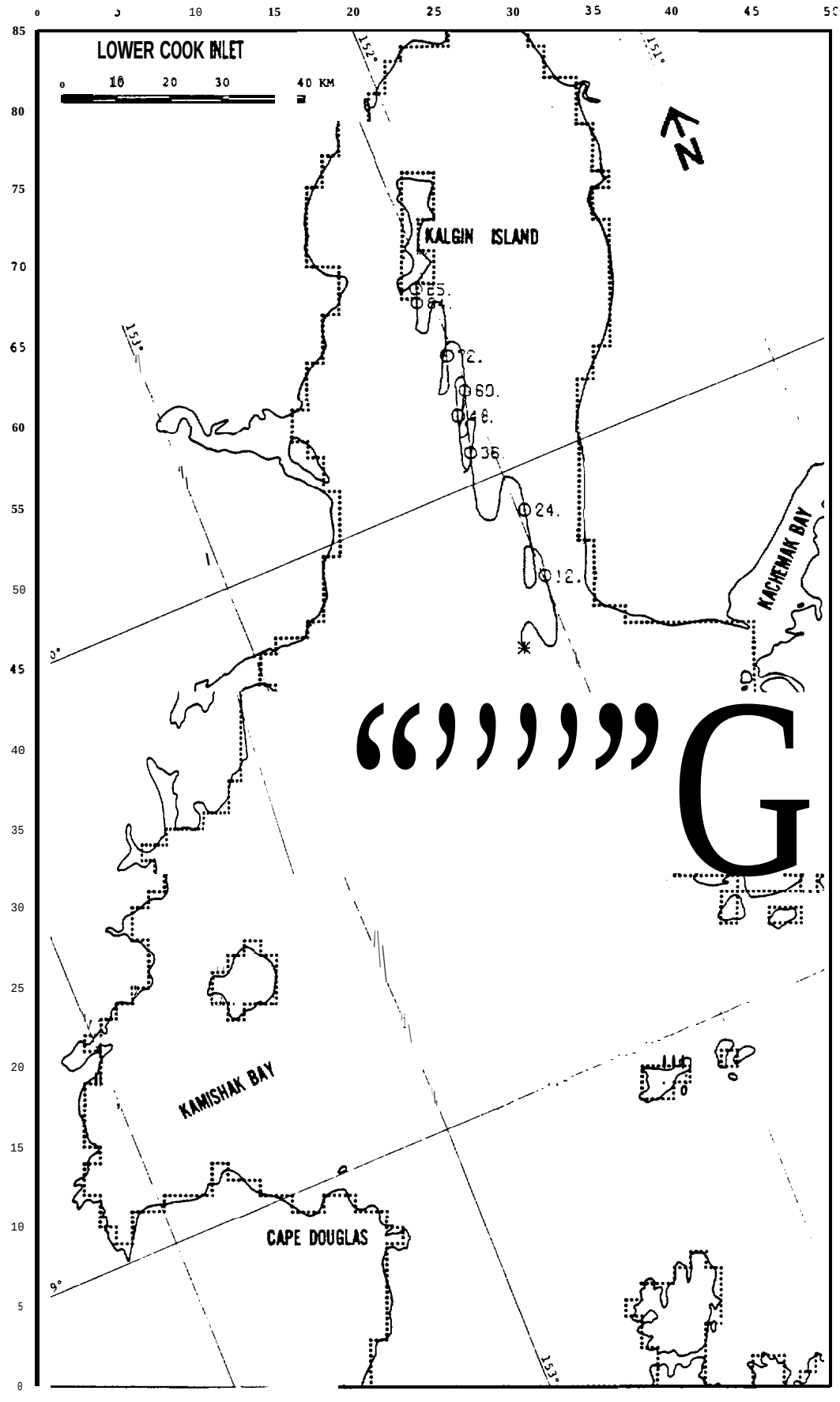

FIGURE C-18: PERTURBATION CASE: NET -25%

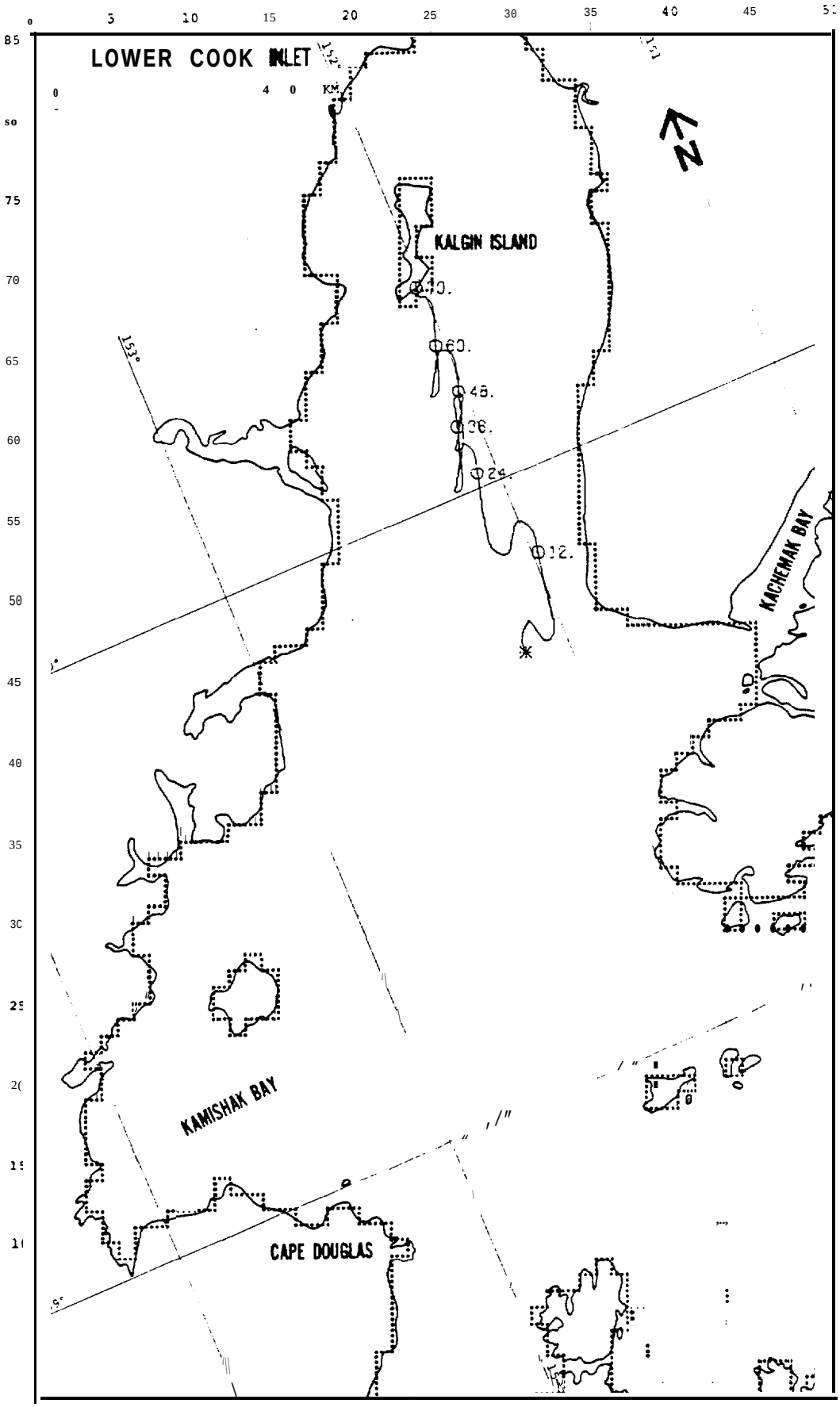

WIND
3

SITE
1

FIGURE C-19: PERTURBATION CASE: WIND +25%

WIND
3

SITE
1

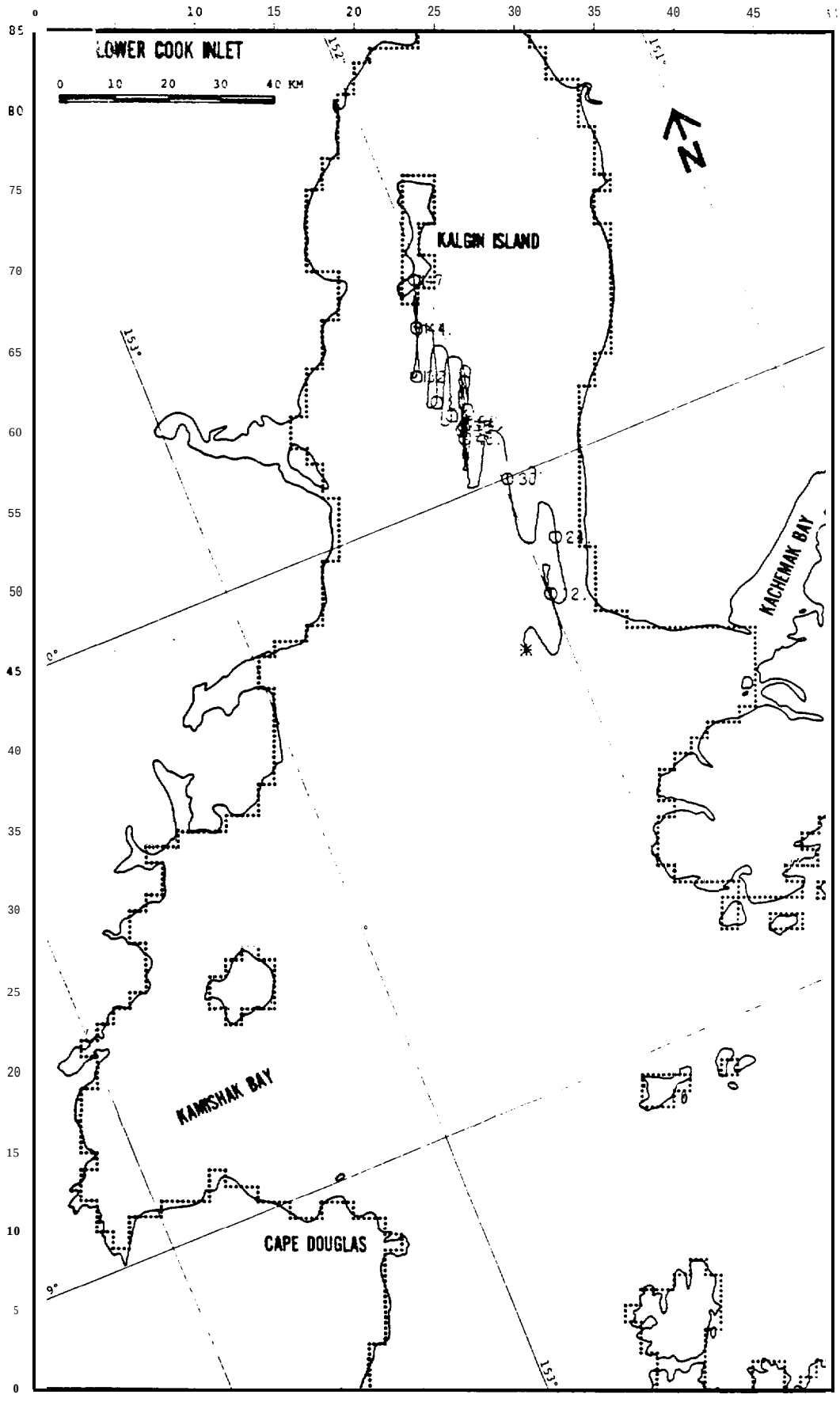

FIGURE C-20: PERTURBATION CASE: WIND -25%

WIND
3

SITE
7

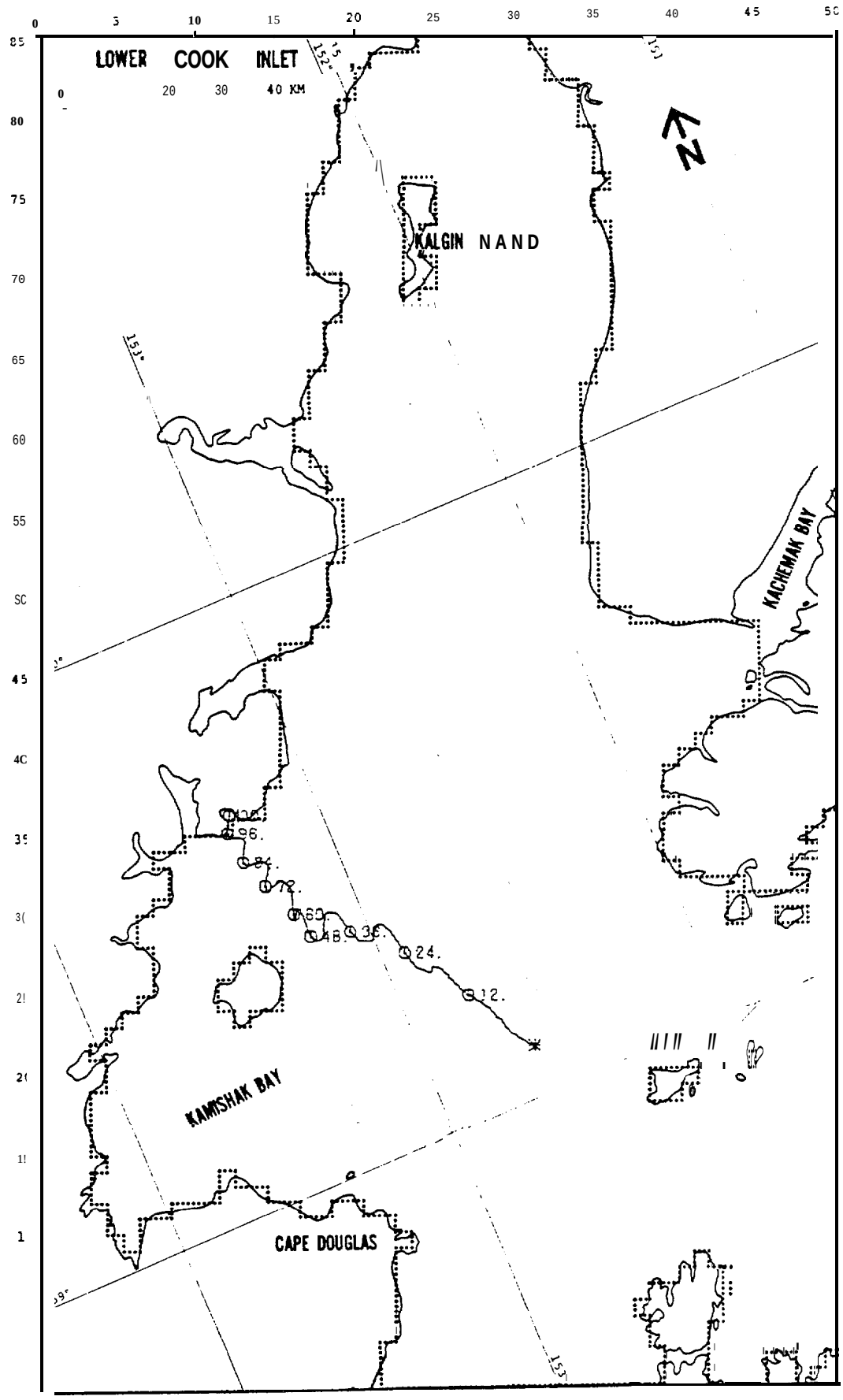

FIGURE C-21: PERTURBATION CASE: NET +25%

WIND
3

SITE
7

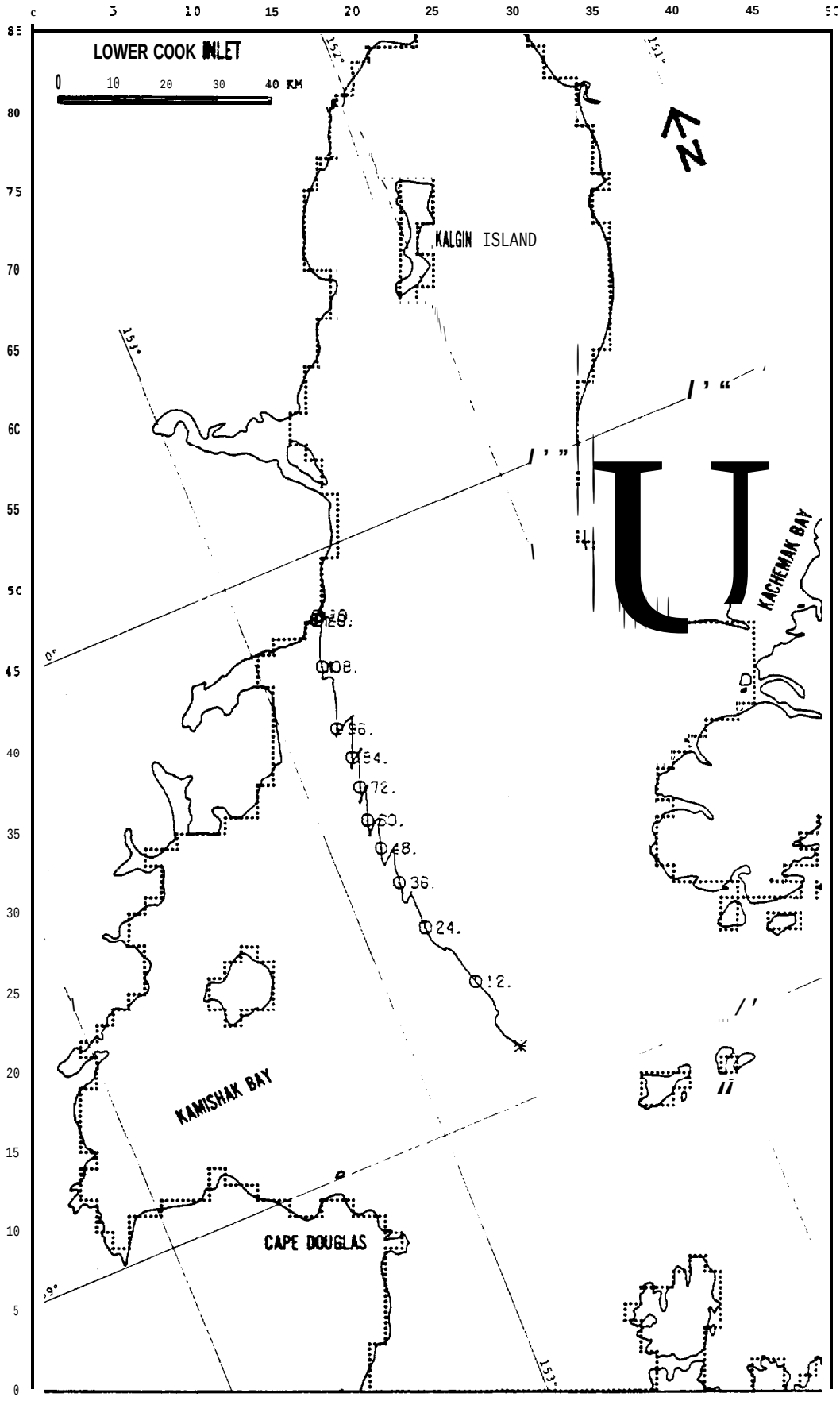

FIGURE C-22: PERTURBATION CASE: NET ● 25Yo

WIND
3

SITE
7

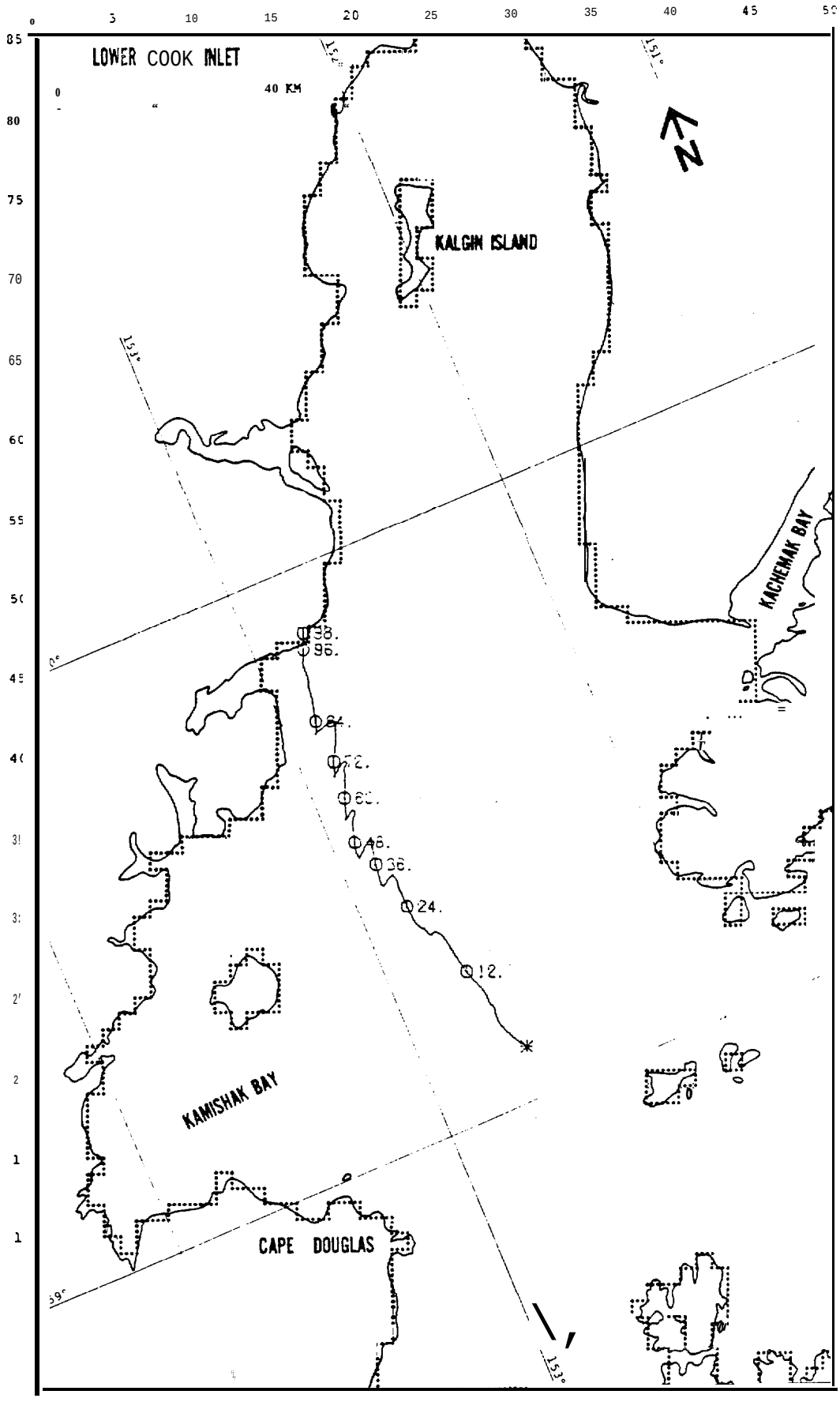

FIGURE C-23: PERTURBATION CASE: WIND +25%

WIND
3

SITE
7

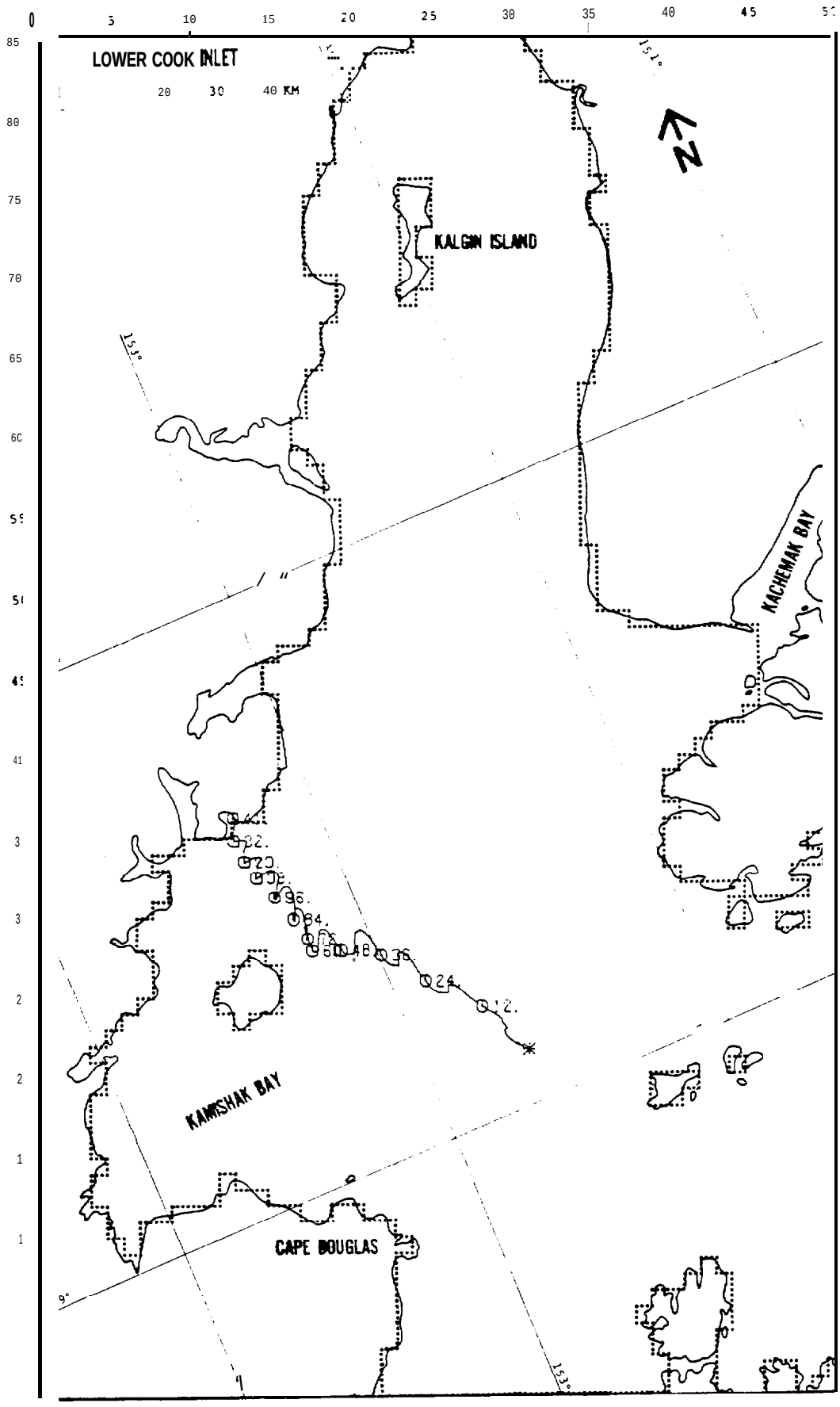

FIGURE C-24: PERTURBATION CASE: WIND -25%

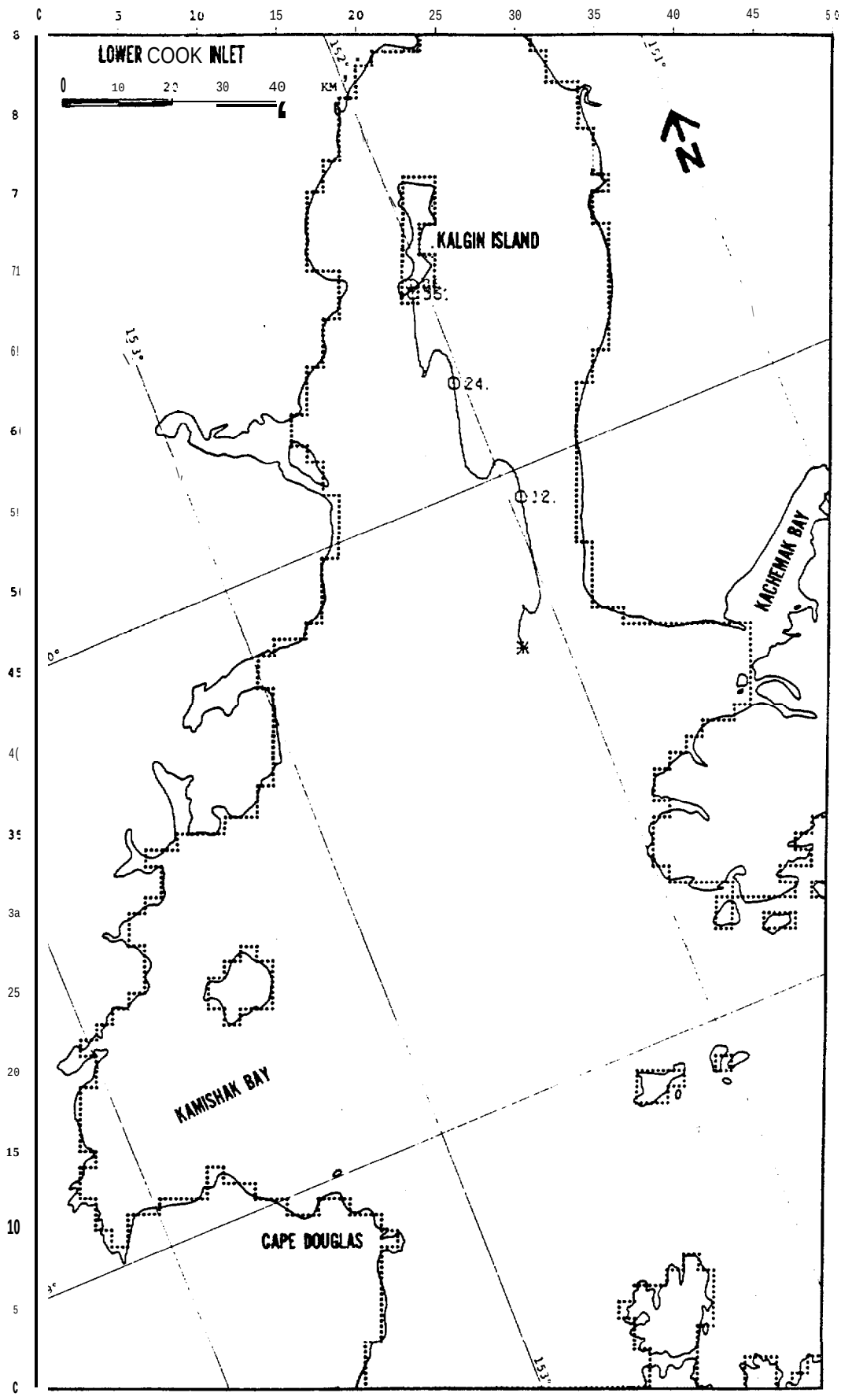

WIND
4

SITE
1

FIGURE C-25: PERTURBATION CASE: **NET +25%**

WIND
4

SITE
1

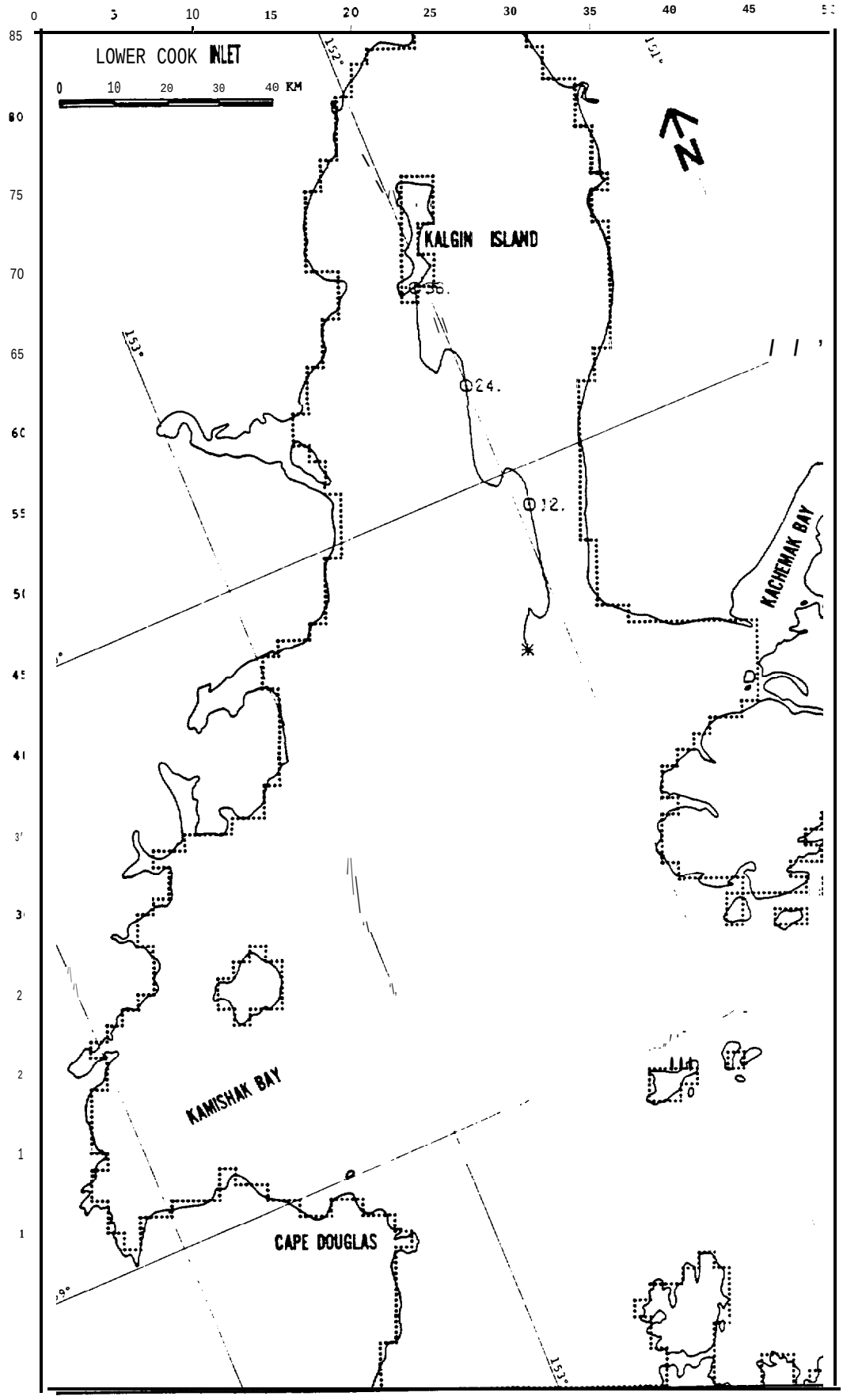

FIGURE C-26: PERTURBATION CASE: NET -25%

WIND
4

SITE
1

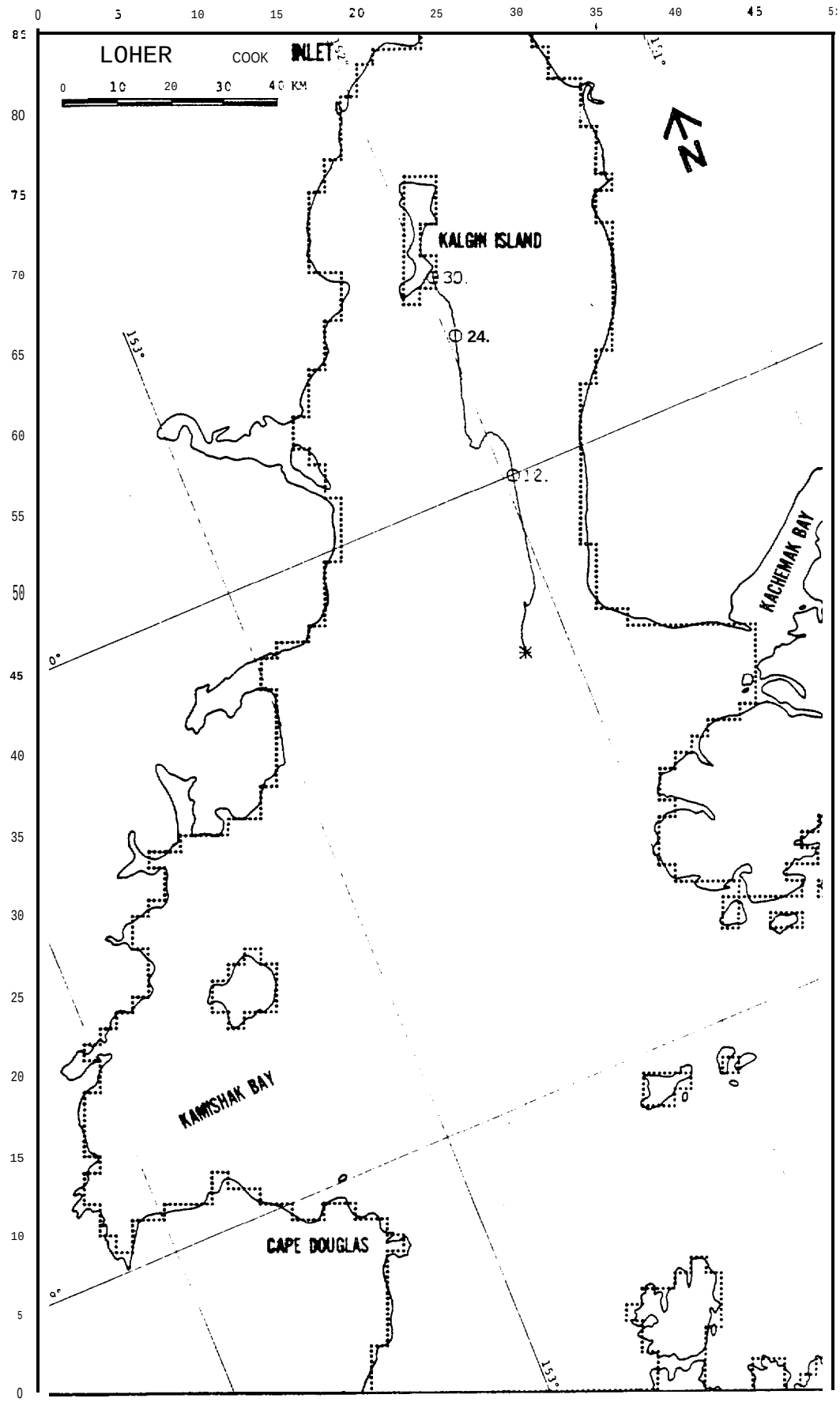

FIGURE C-27: PERTURBATION CASE: WIND +25%

WIND
A

SITE
1

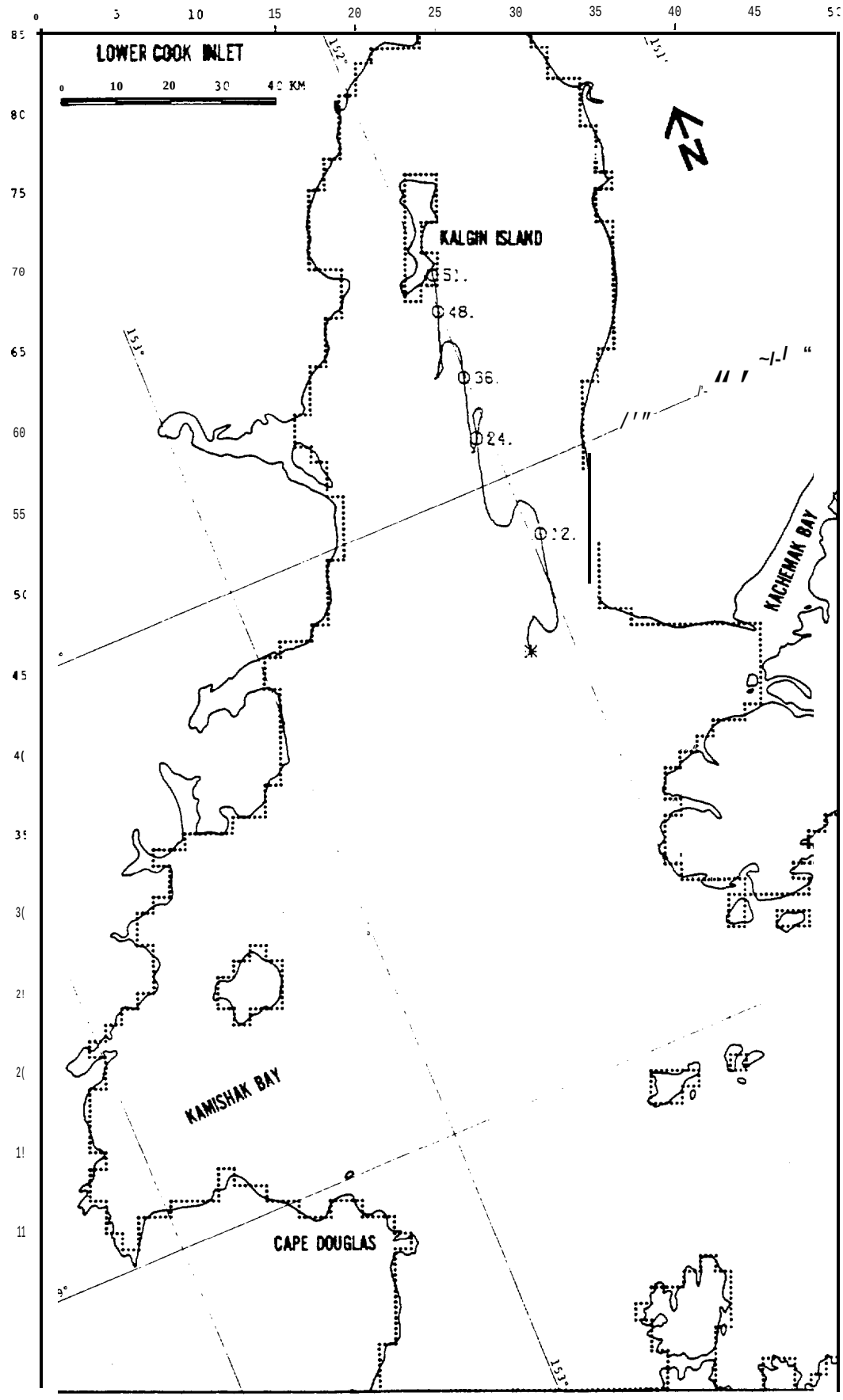

FIGURE C-28: PERTURBATION CASE: WIND -25%

WIND
A

SITE
7

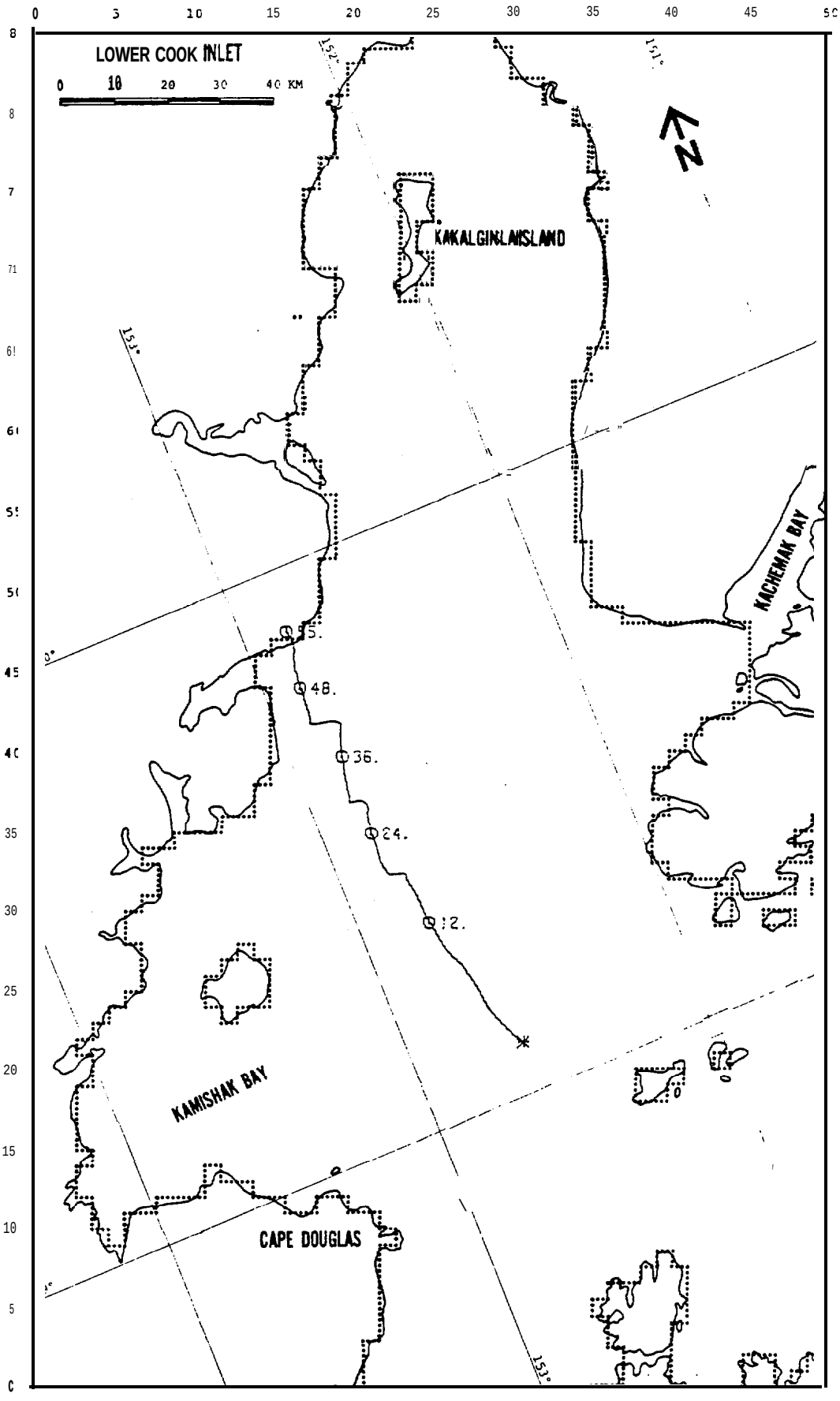

FIGURE C-29: PERTURBATION CASE: NET +25%

WIND
4

SITE
7

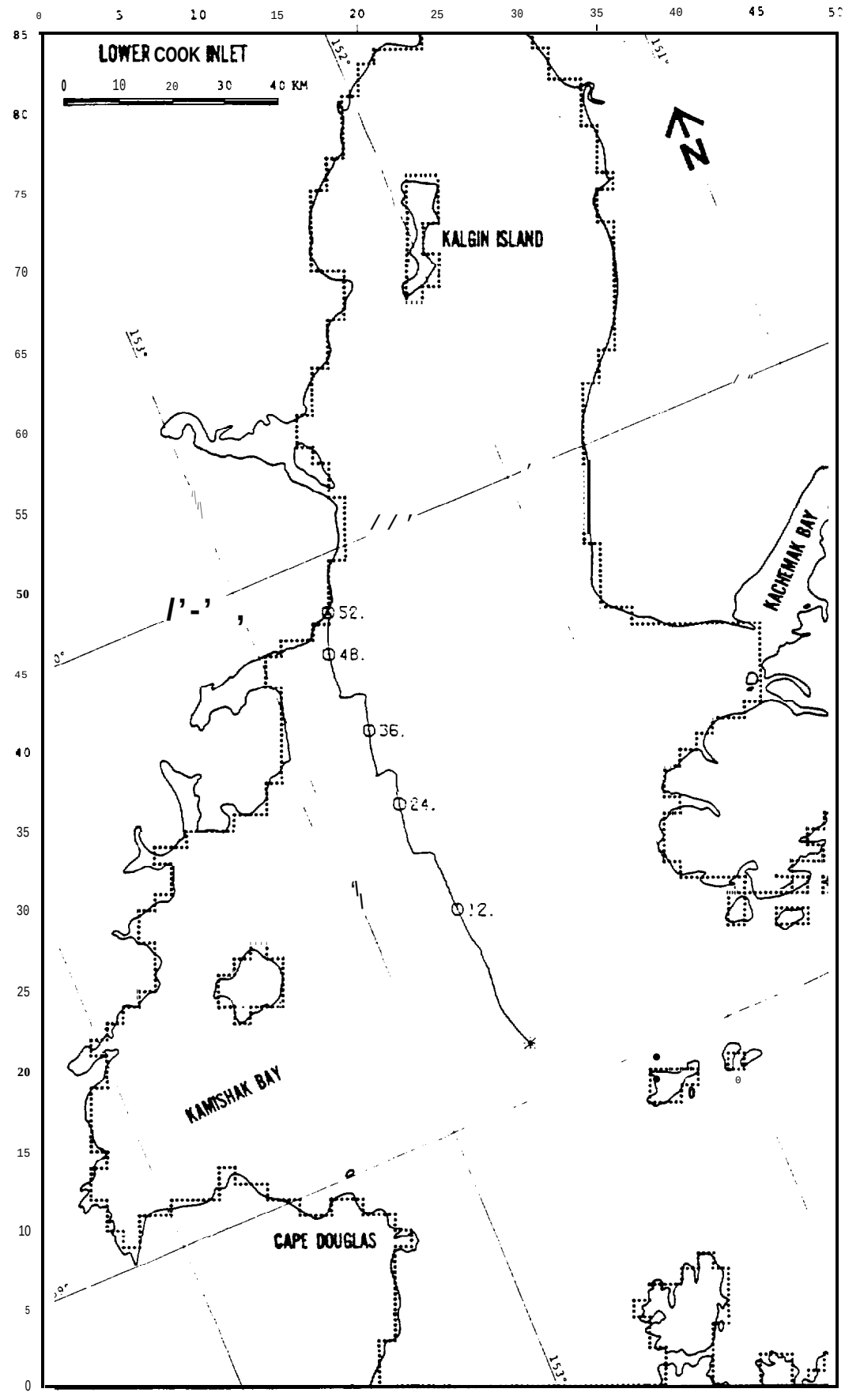

FIGURE C-30: PERTURBATION CASE: NET -25%

WIND
A

SITE
7

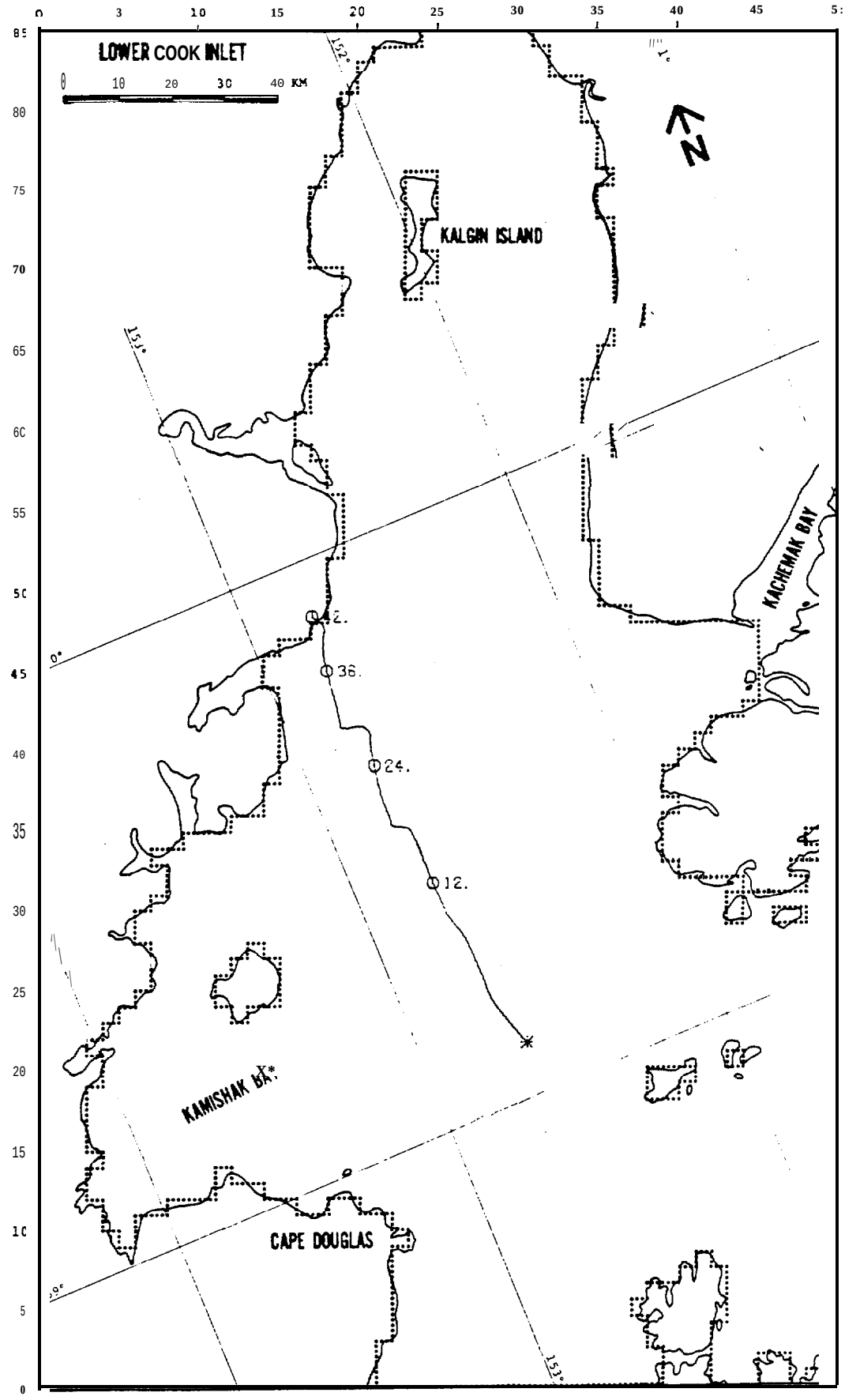

FIGURE C-31: PERTURBATION CASE: WIND +25%

WIND
A

SITE
7

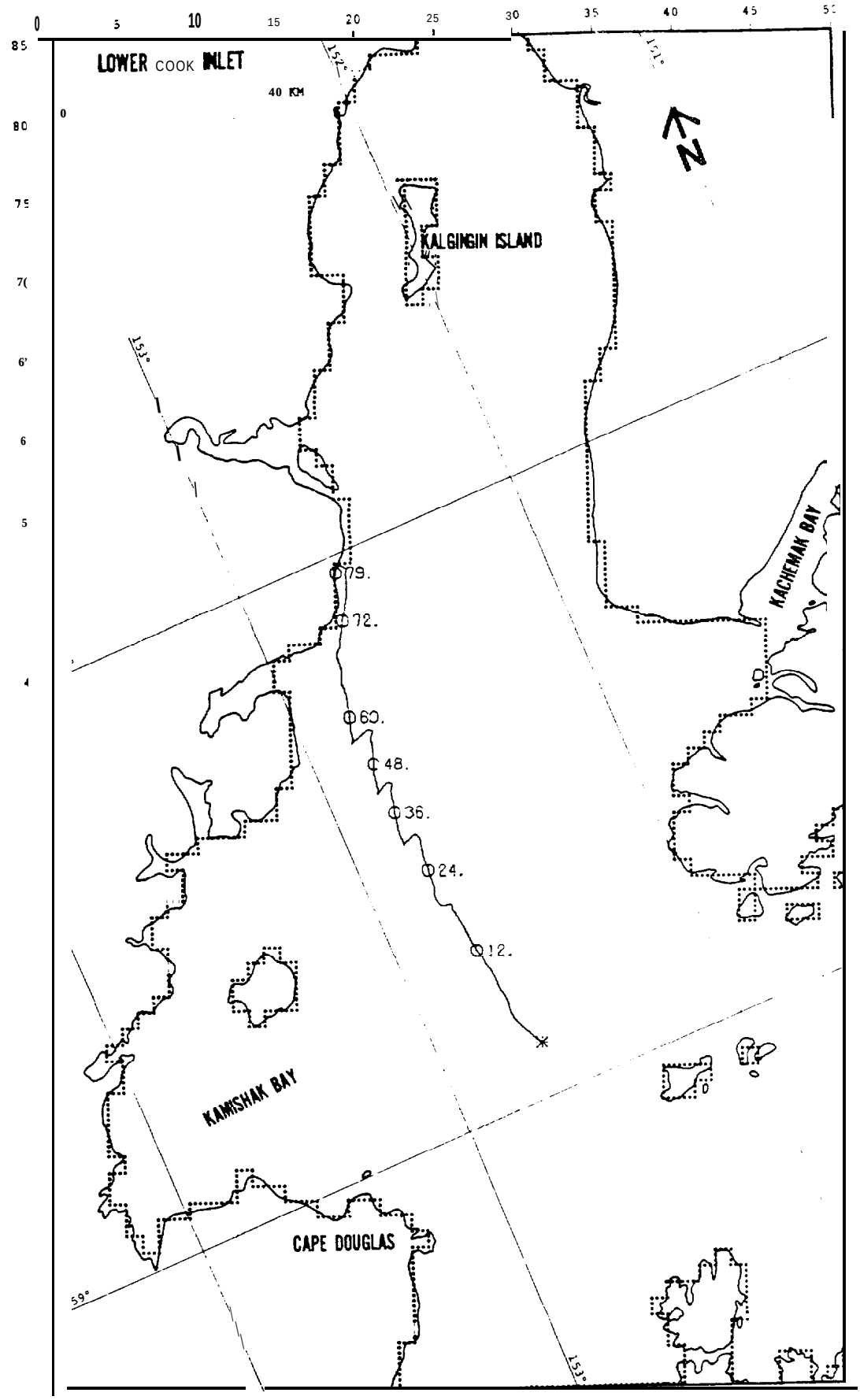

FIGURE C-32: PERTURBATION CASE: WIND-25%

WIND
5

SITE
1

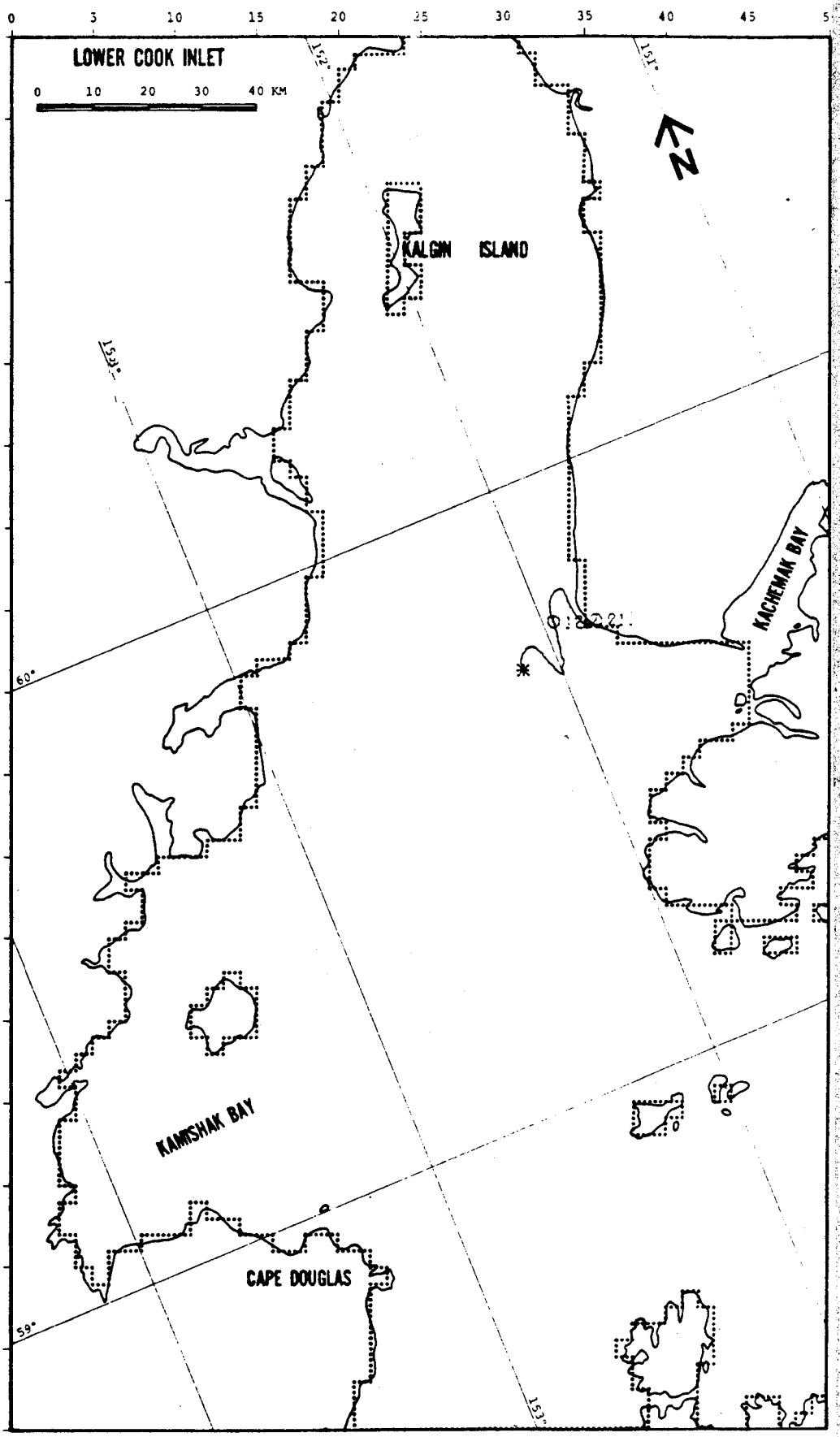

FIGURE C-33: PERTURBATION CASE: NET +25%

WIND
5

SITE
1

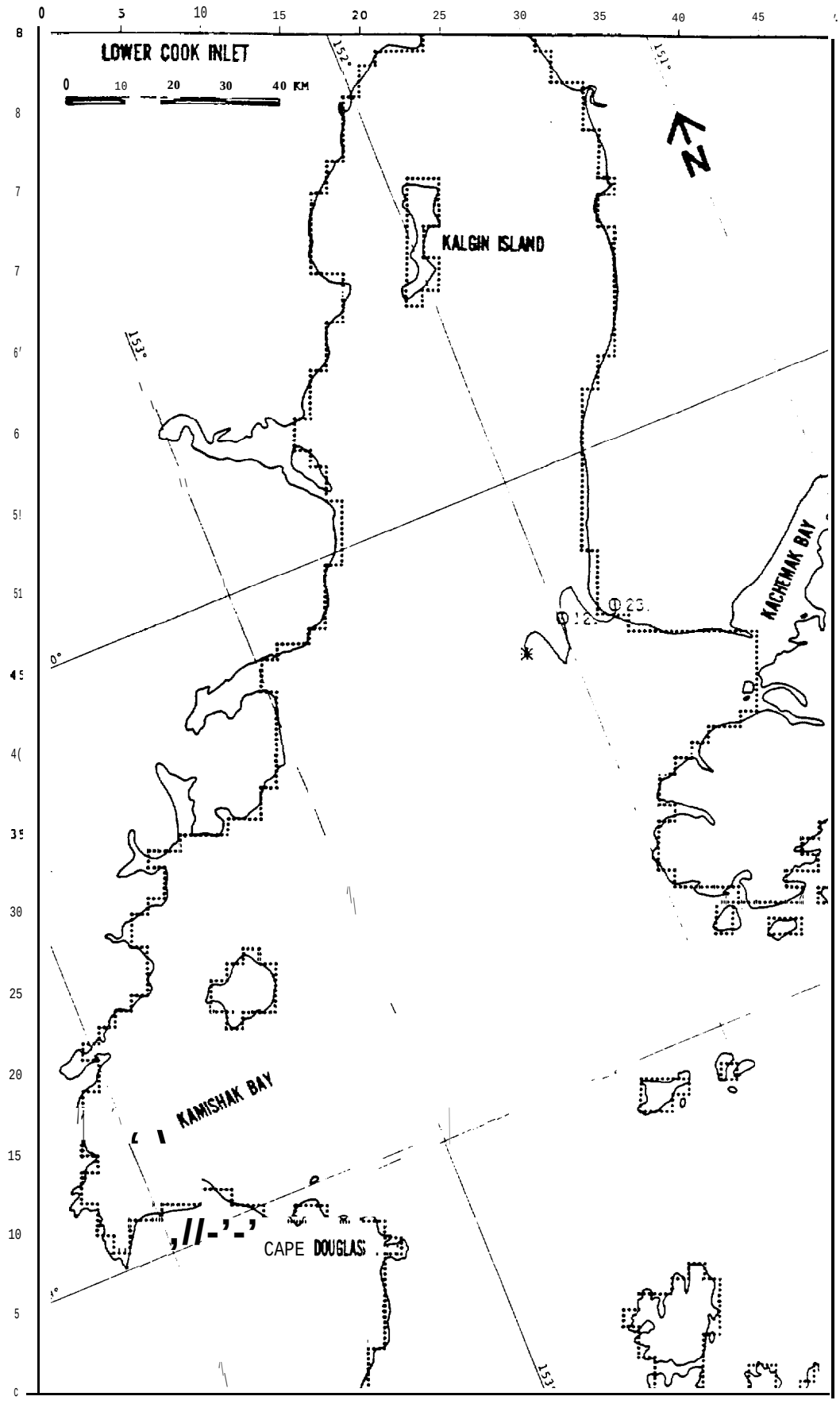

FIGURE C-34: PERTURBATION CASE: NET -25%

WIND
5

SITE
1

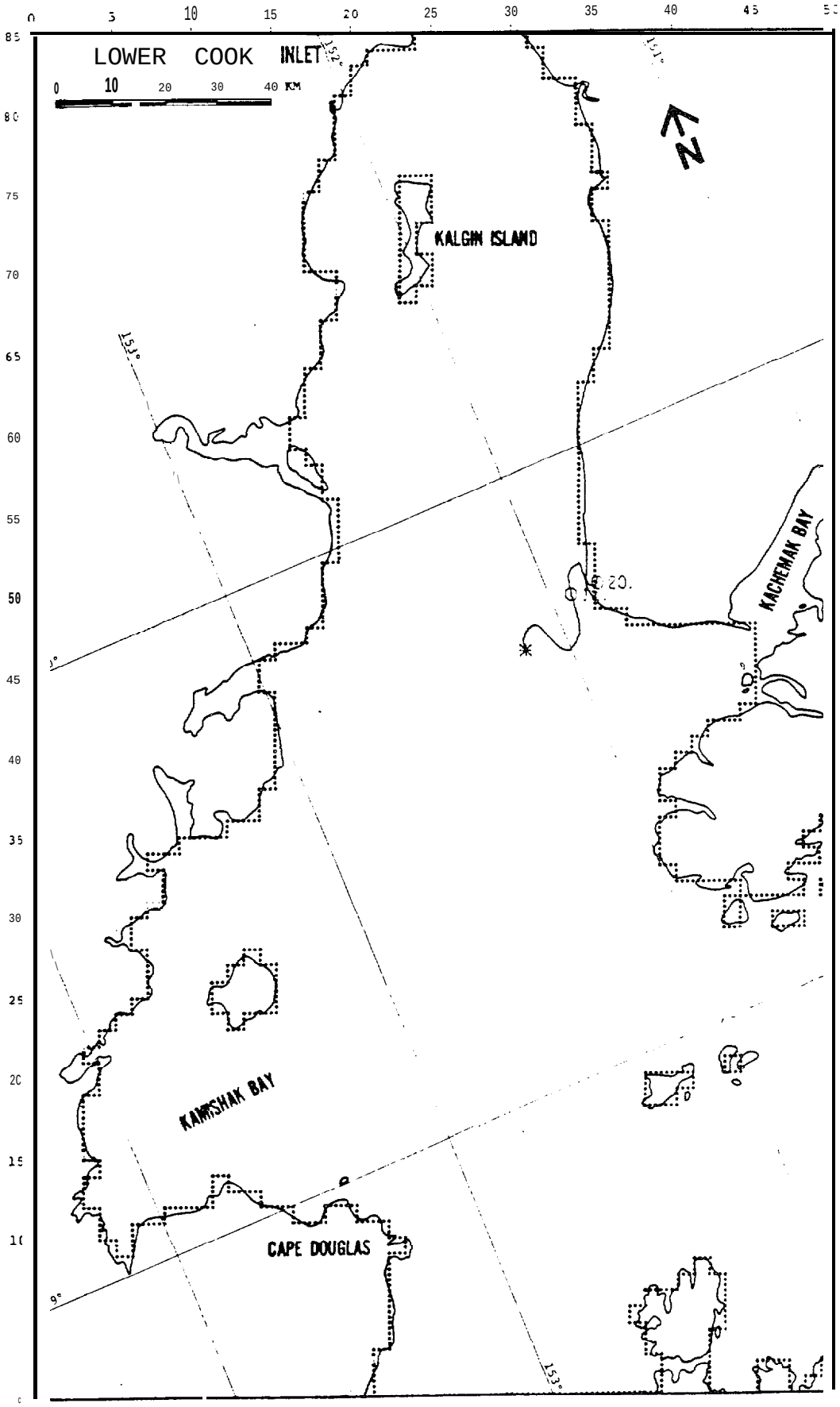

FIGURE C-35: PERTURBATION CASE: WIND +25%

WIND
5

SITE
1

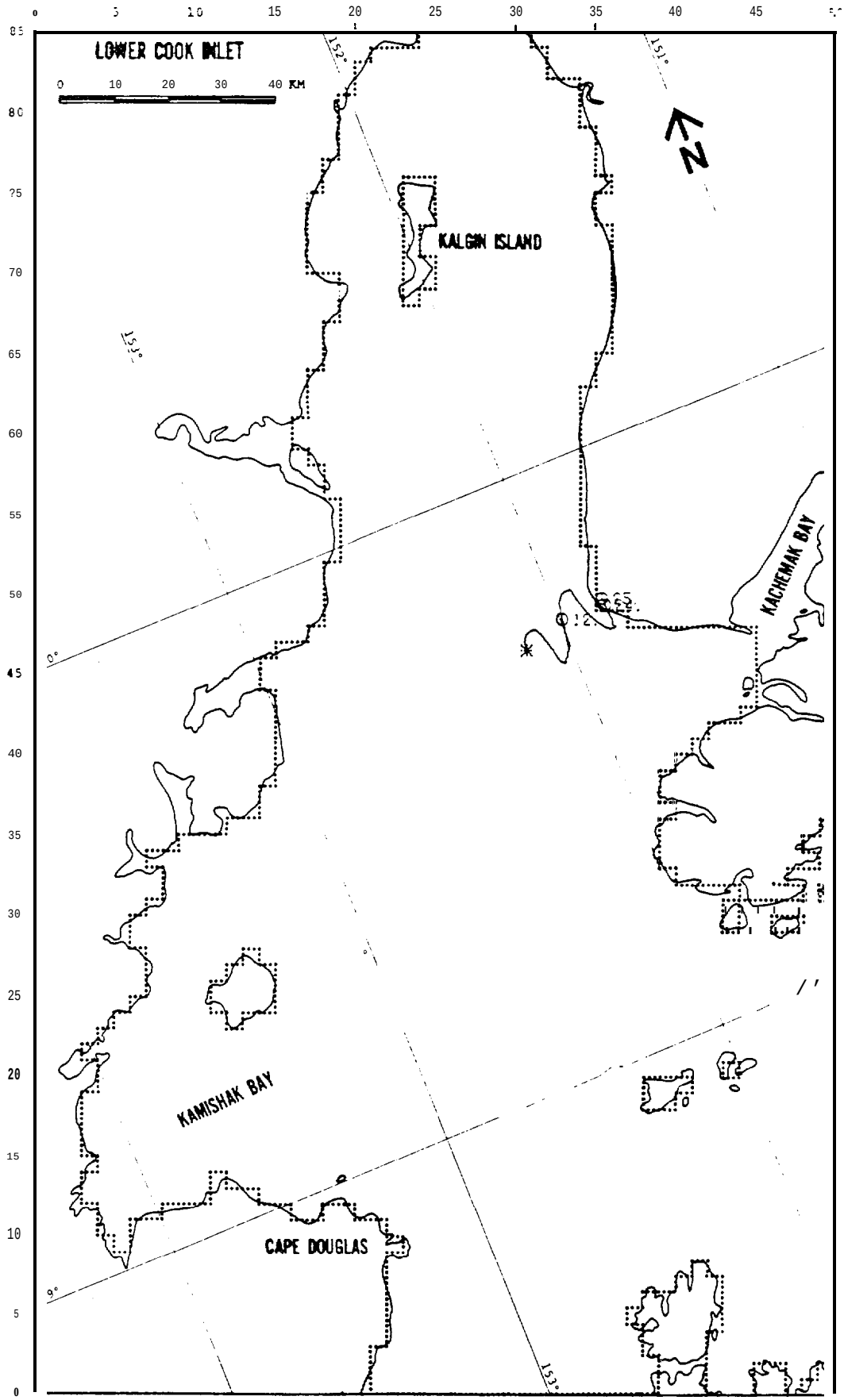

FIGURE C-36: PERTURBATION "CASE: WIND -25%

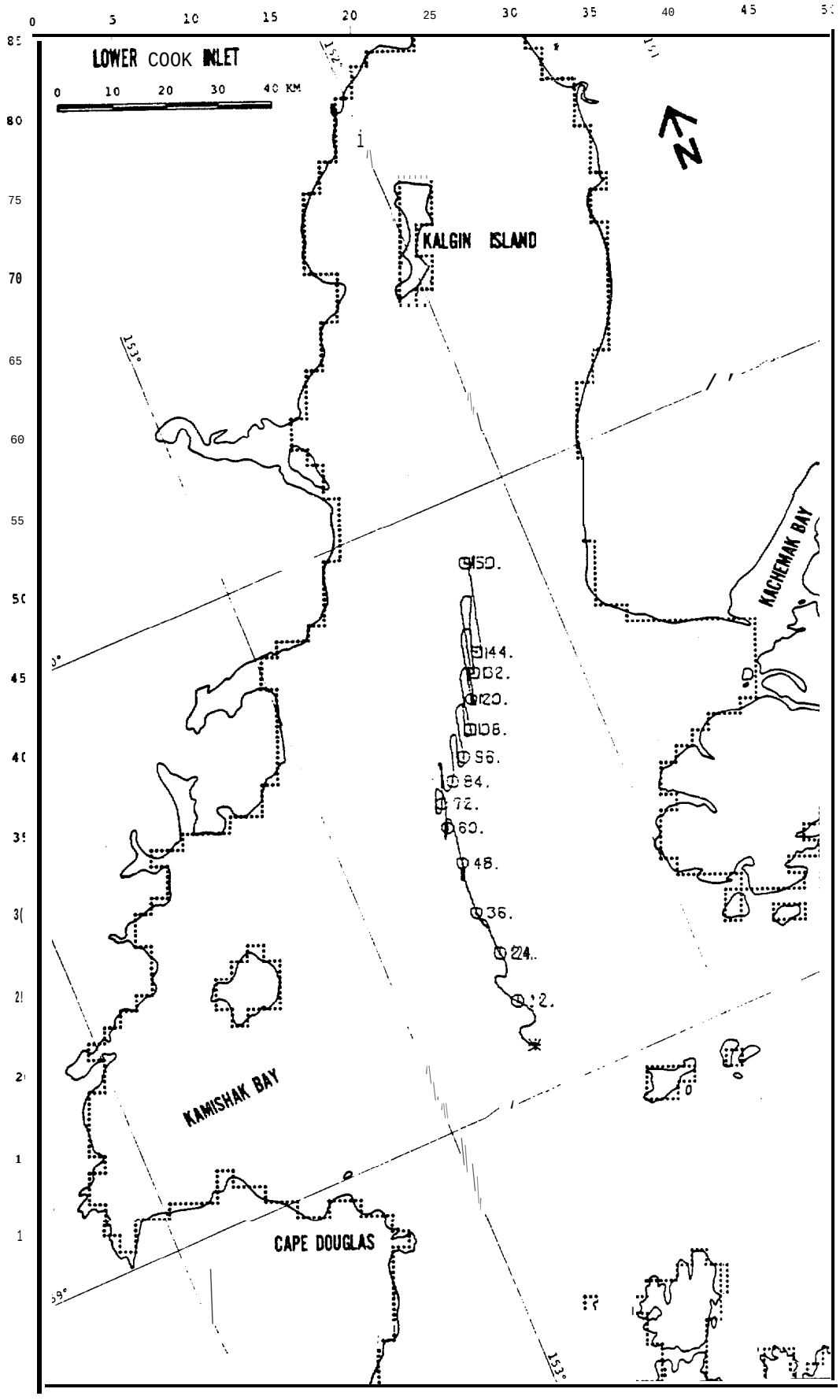

WIND 5

SITE 7

FIGURE C-37 PERTURBATION CASE: NET +25%

WIND
5

SITE
7

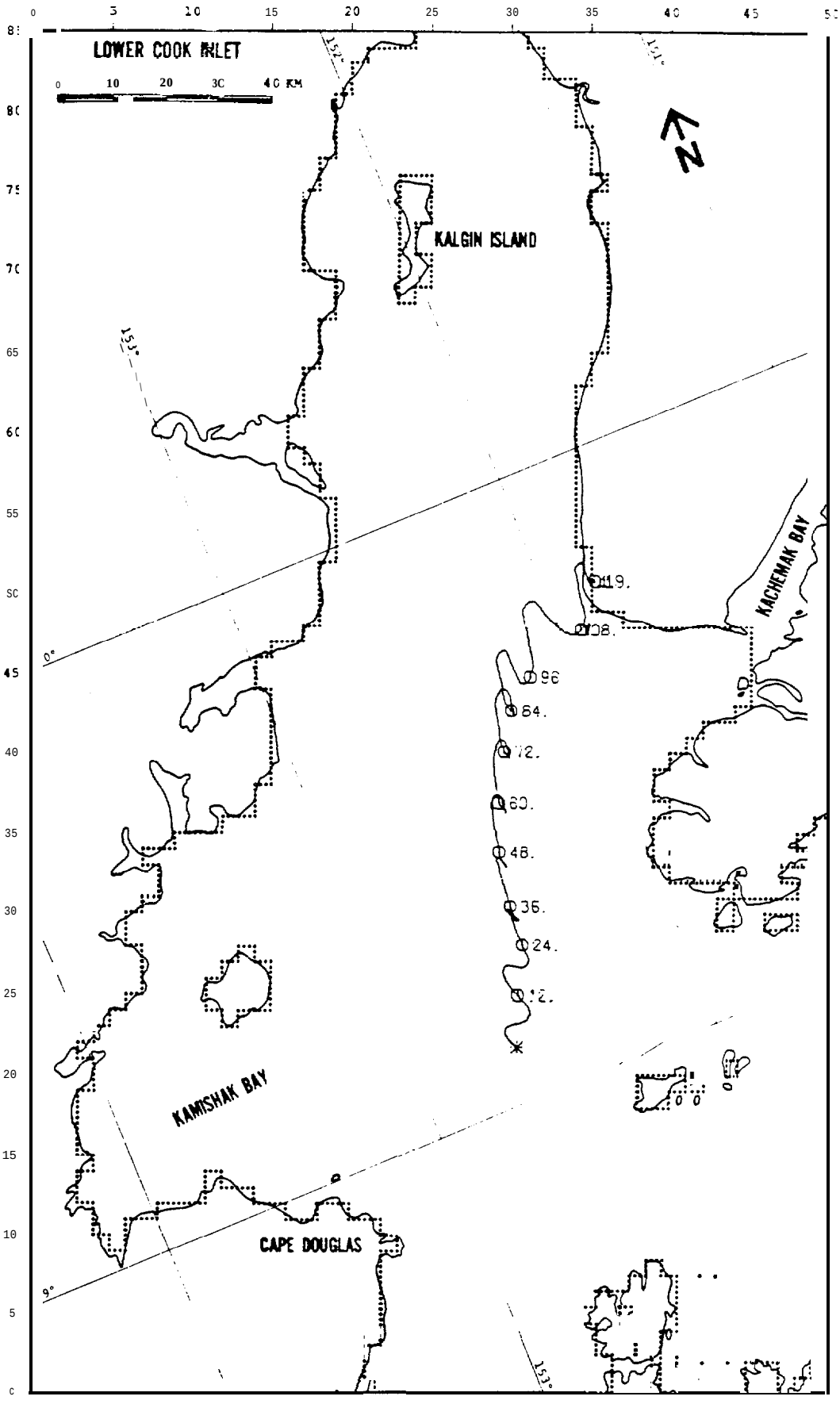

FIGURE C-38: PERTURBATION CASE: NET -25%

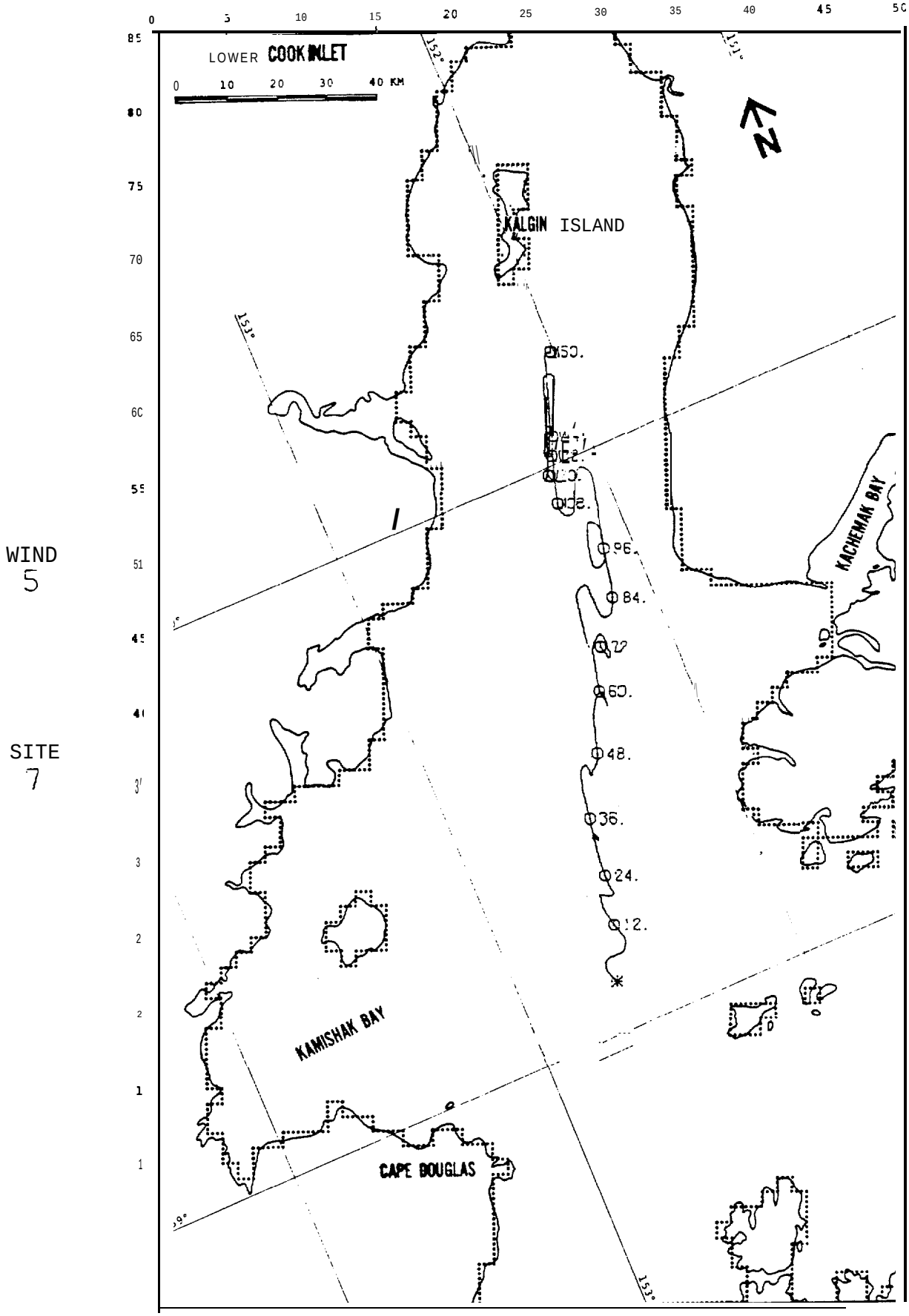

WIND
5

SITE
7

FIGURE C-39: PERTURBATION CASE: WIND +25%

WIND
5

SITE
7

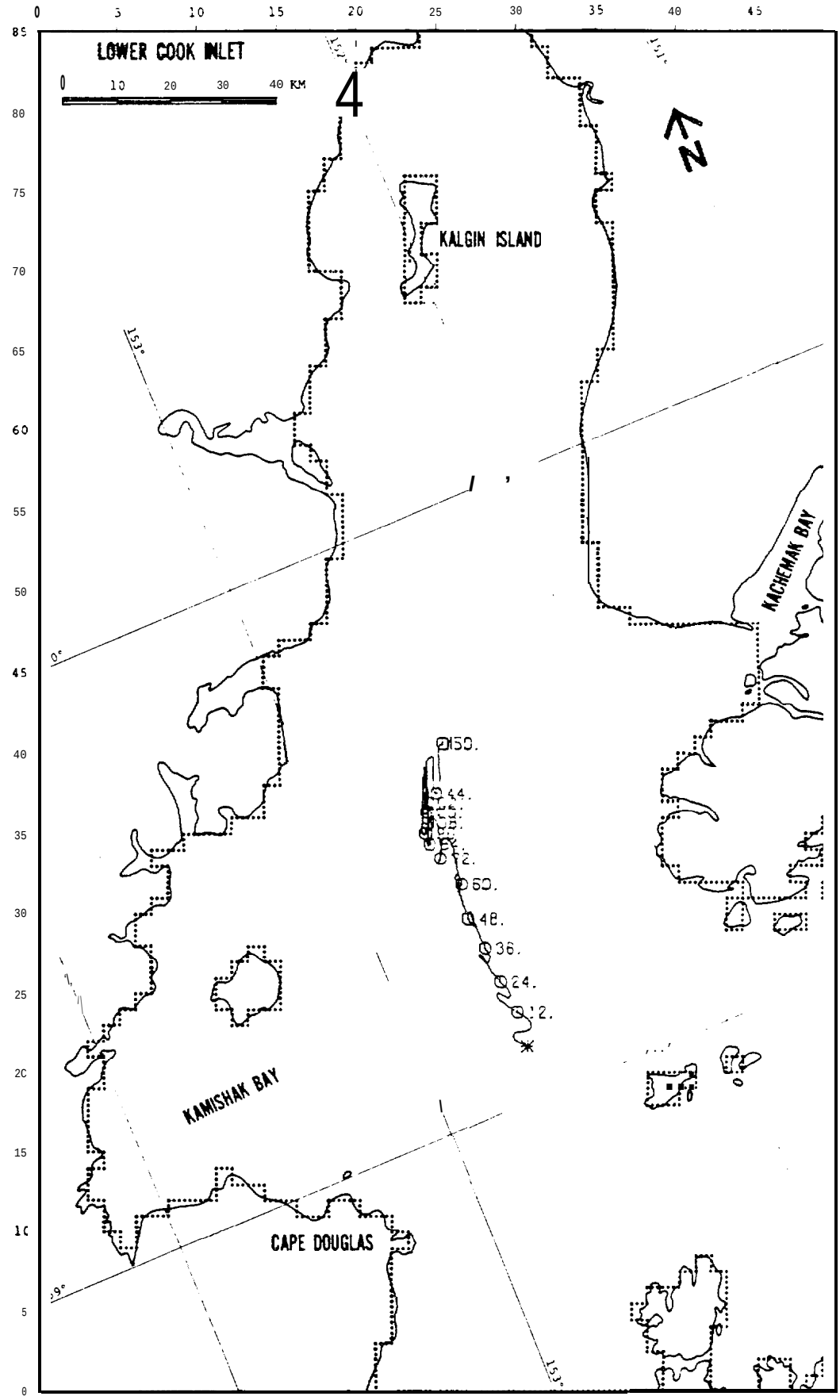

FIGURE C-40: PERTURBATION CASE: WIND -25%

WIND
6

SITE
1

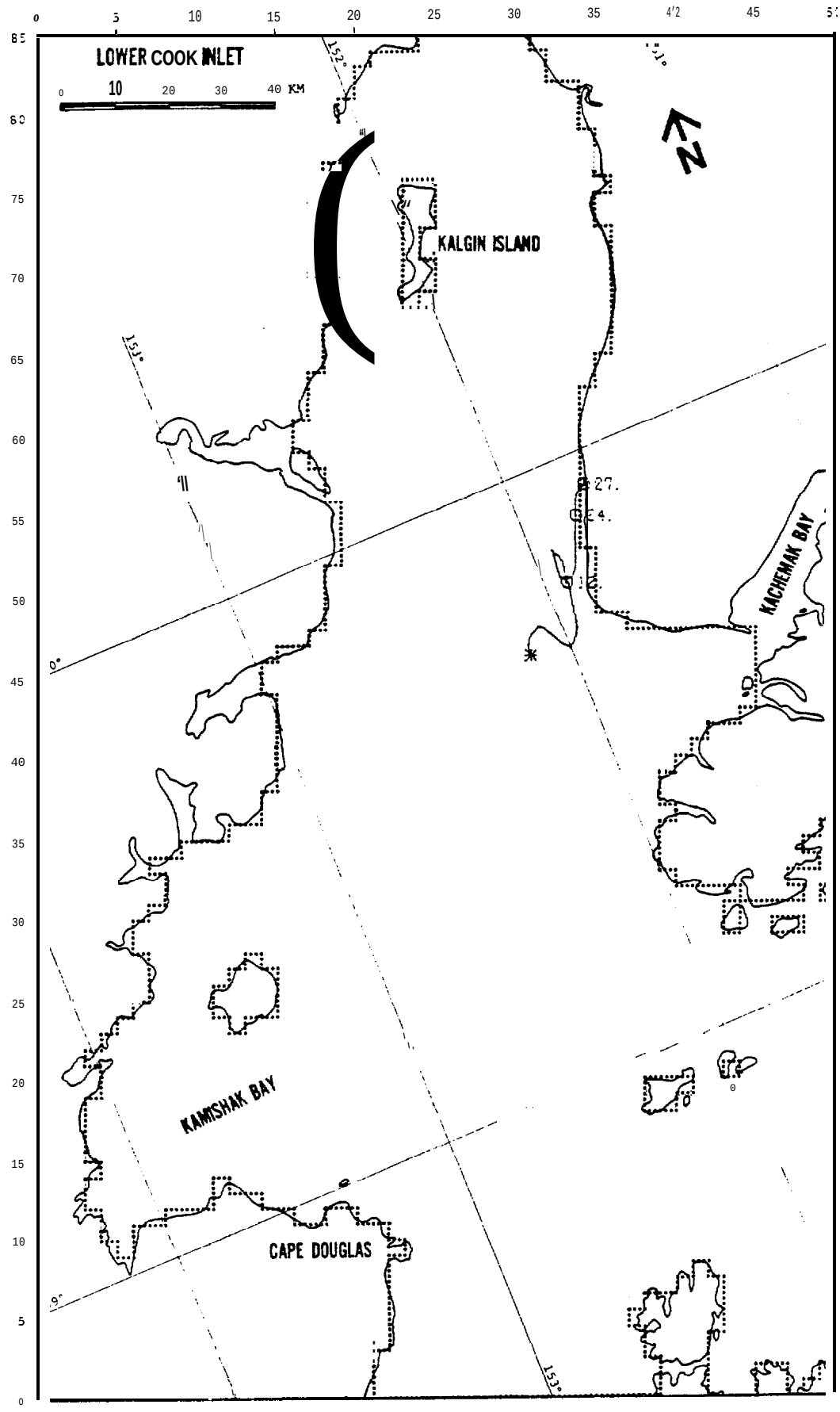

FIGURE C-41: PERTURBATION CASE: NET +25%

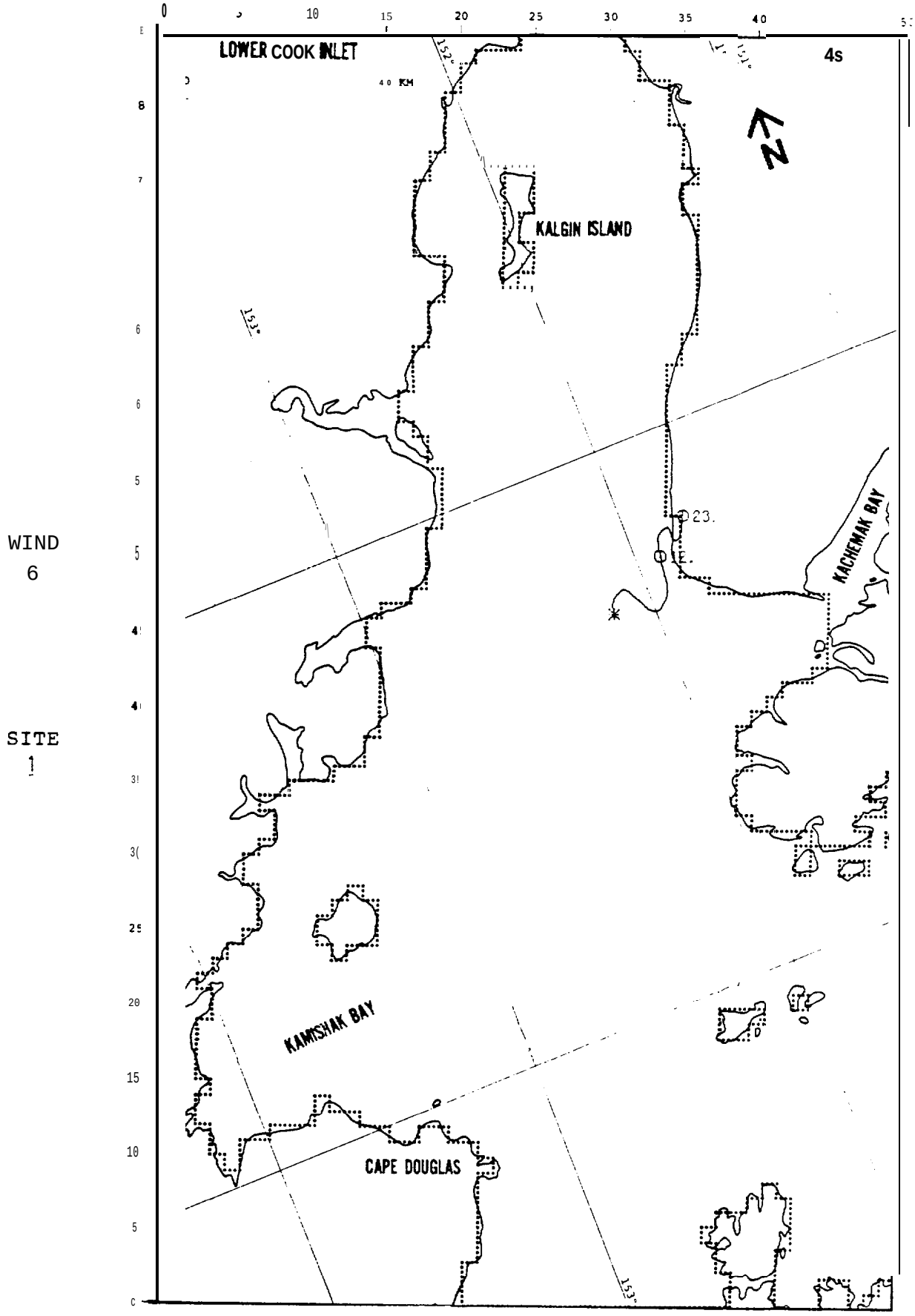

FIGURE C-42: PERTURBATION CASE: NET -25%

WIND
6

SITE
1

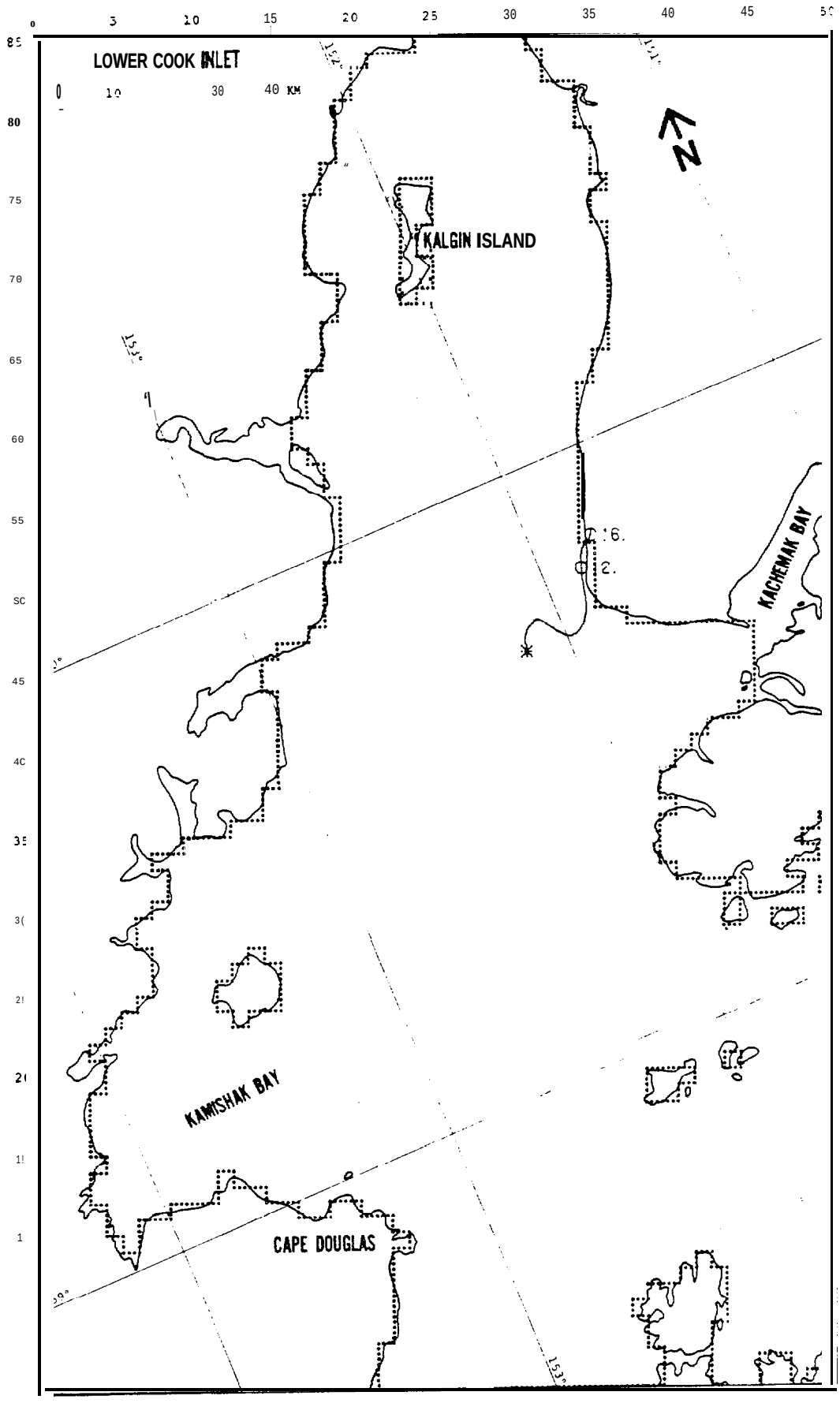

FIGURE C-43: PERTURBATION CASE: WIND +25%

WIND
6

SITE
1

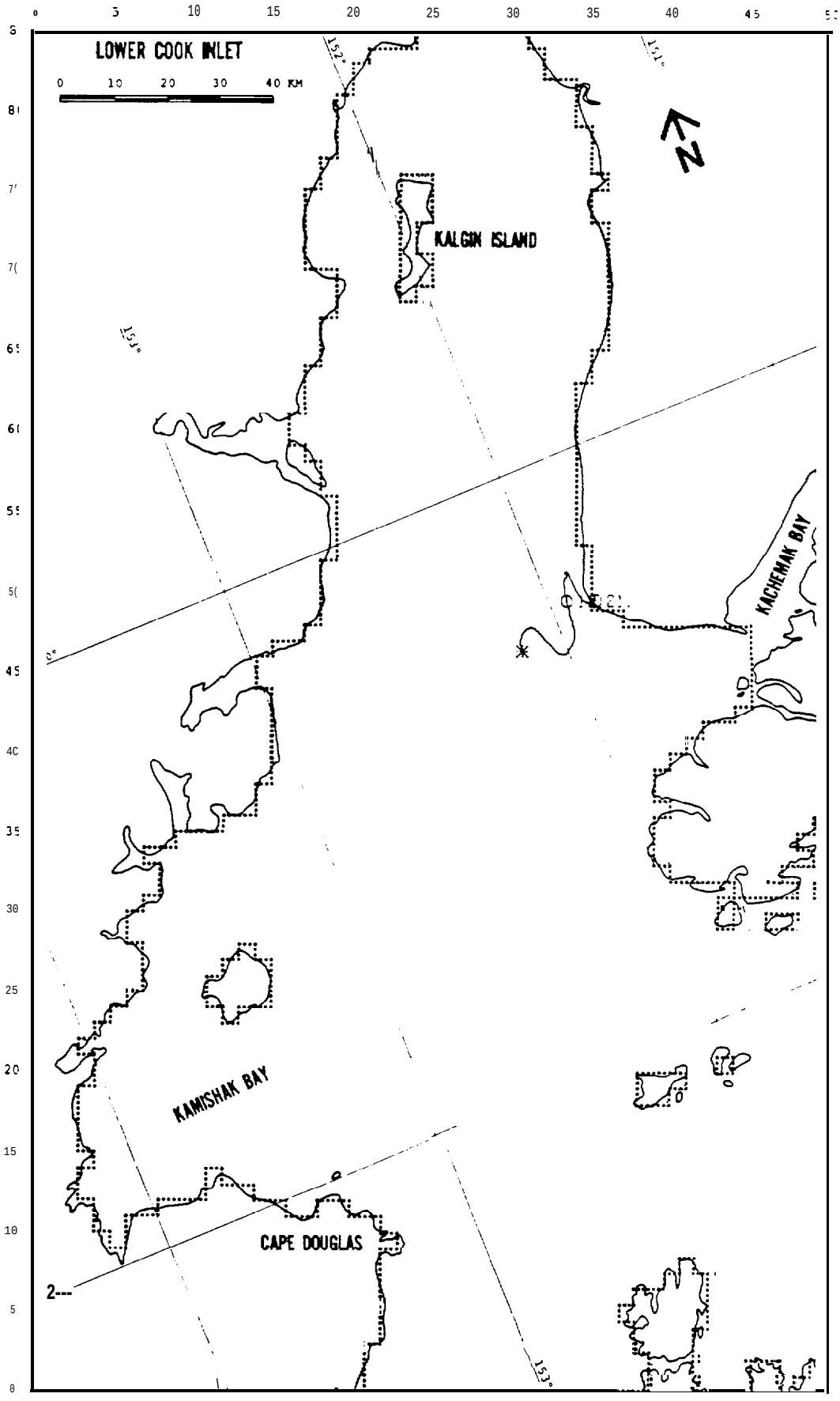

FIGURE C-44: PERTURBATION **CASE:** WIND -25%

WIND
6

SITE
7

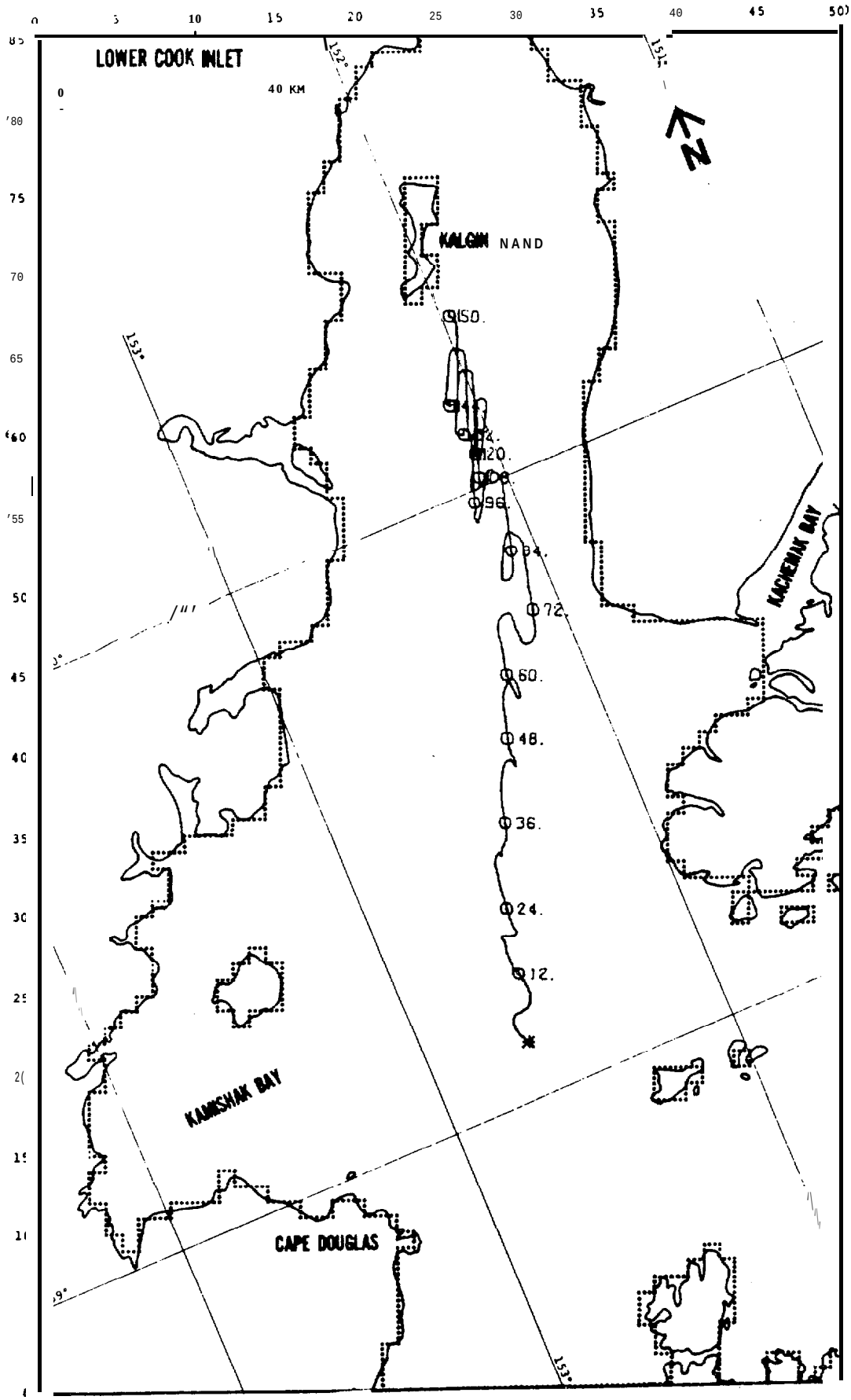

FIGURE C-45: PERTURBATION CASE: NET +25%

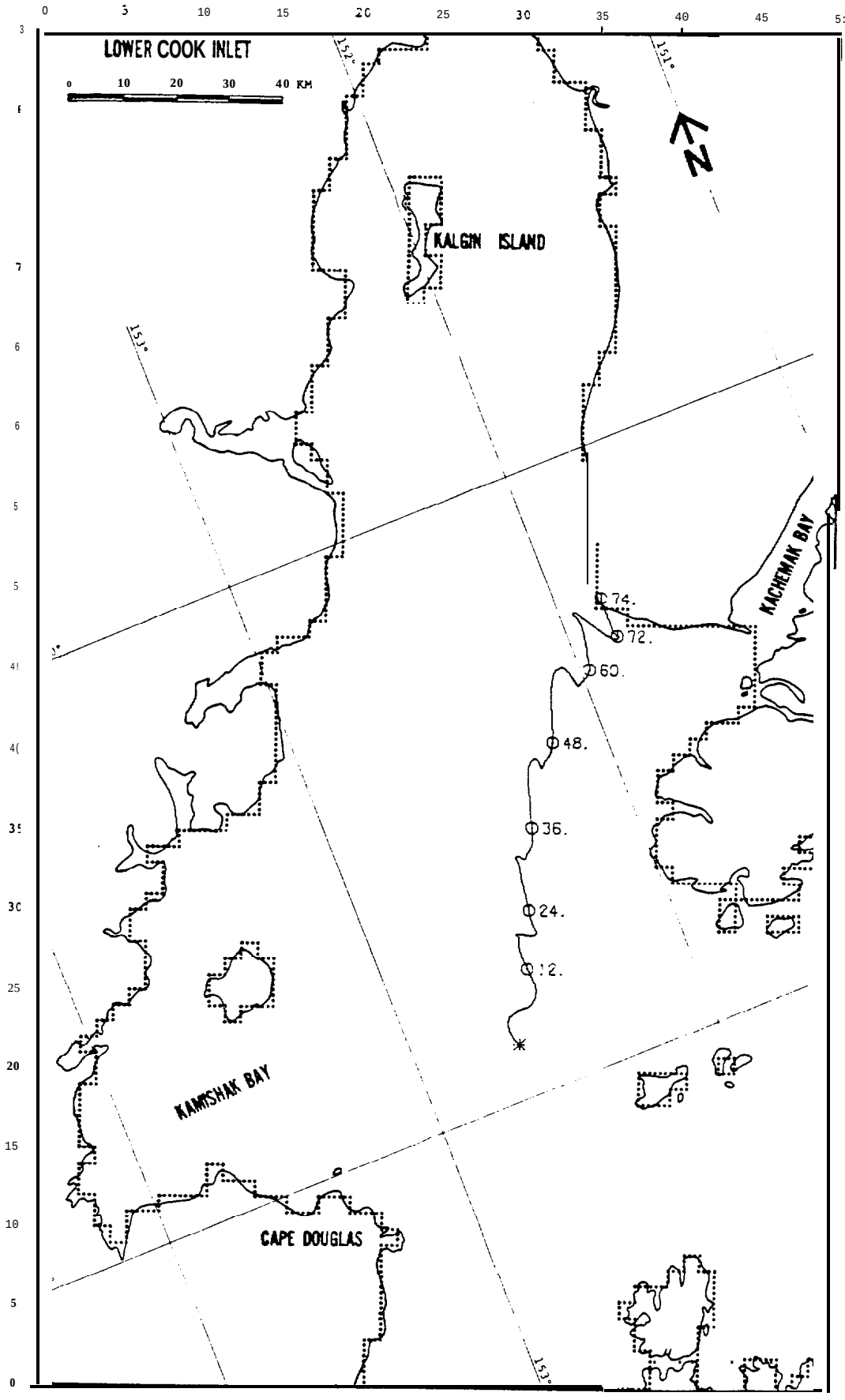

WIND
6

SITE
"7

FIGURE C-46: PERTURBATION CASE: NET -25%

WIND
6

SITE
7

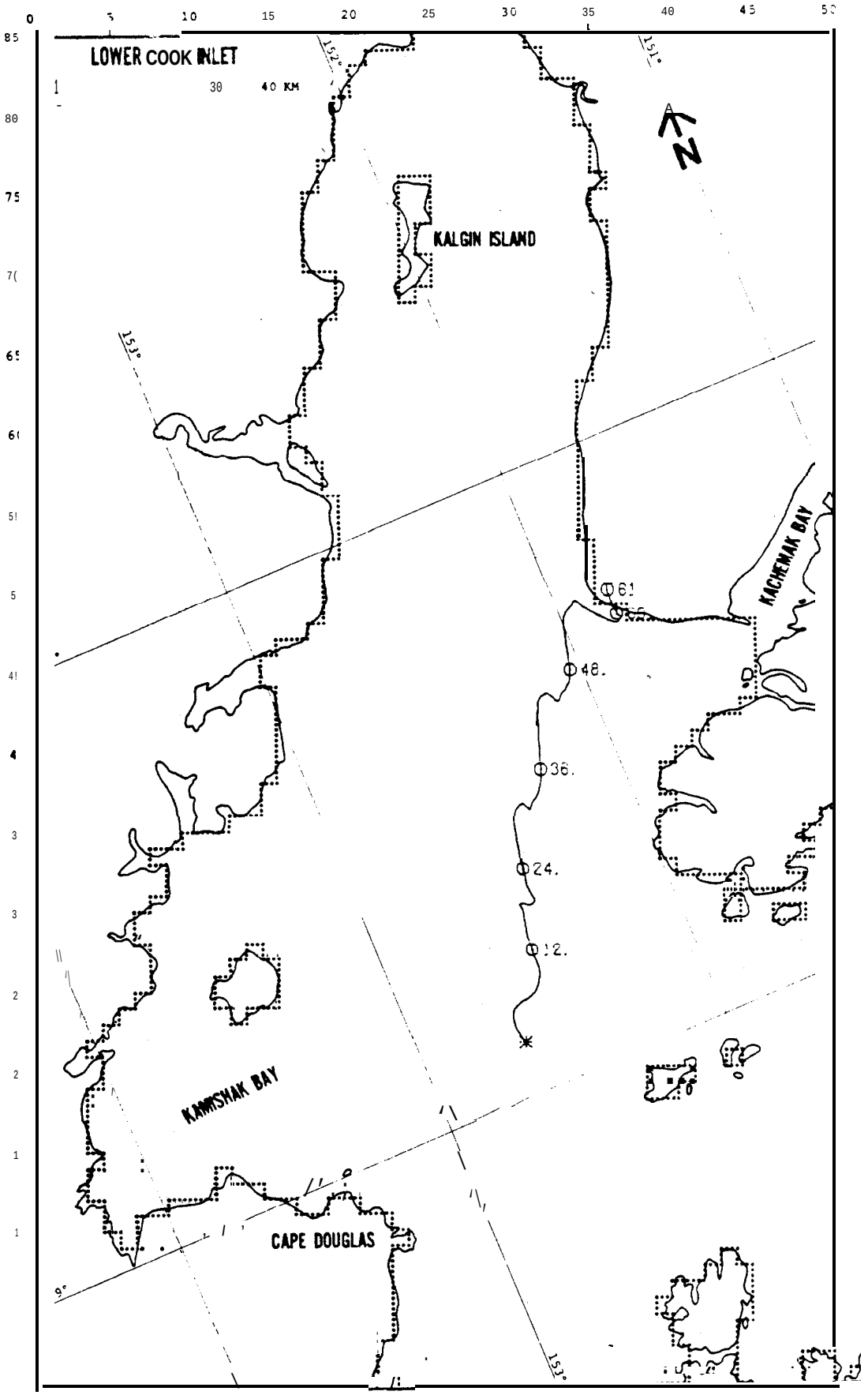

FIGURE C-47: PERTURBATION CASE: WIND +25%

WIND
6

SITE
7

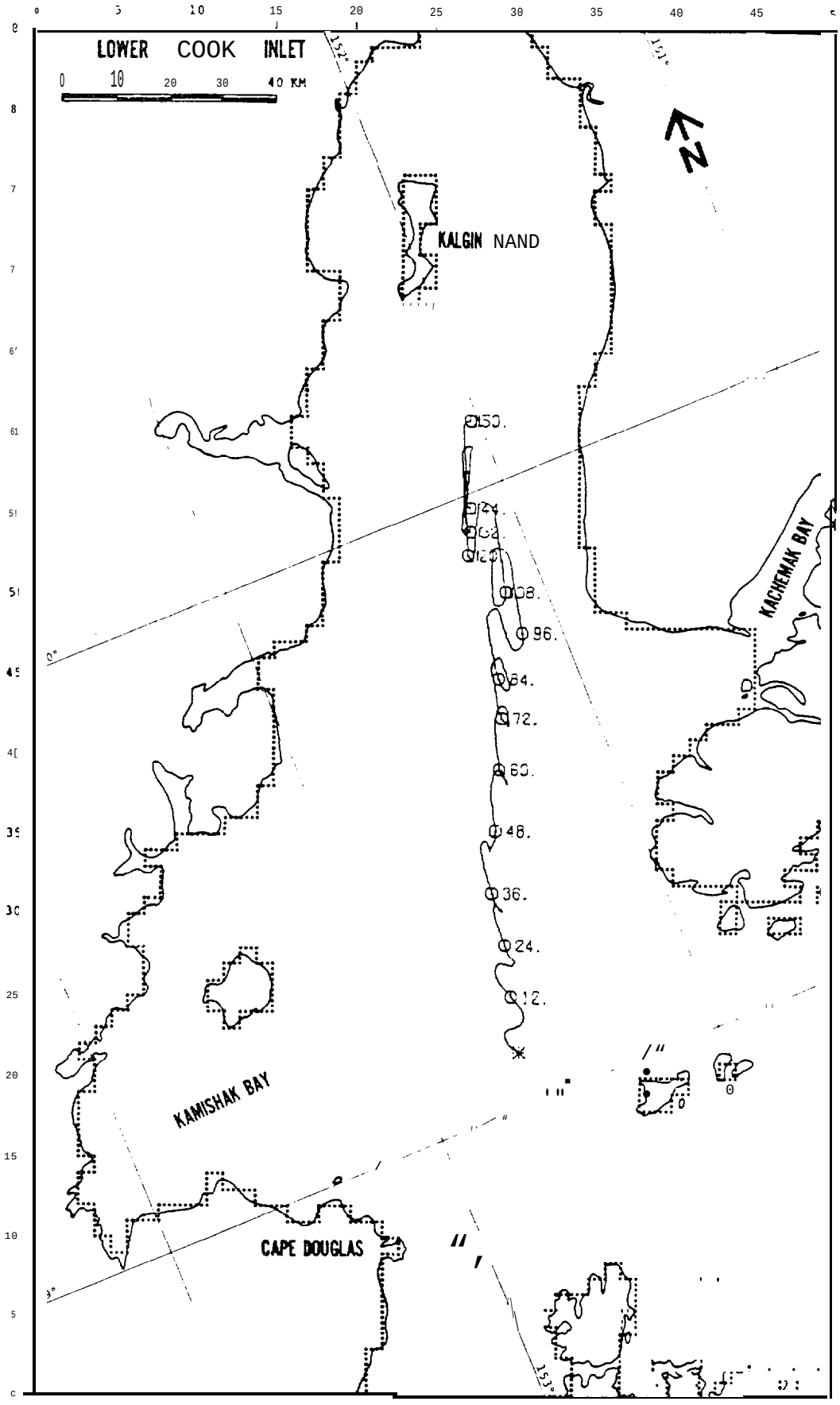

FIGURE C-48: PERTURBATION CASE: WIND -25%

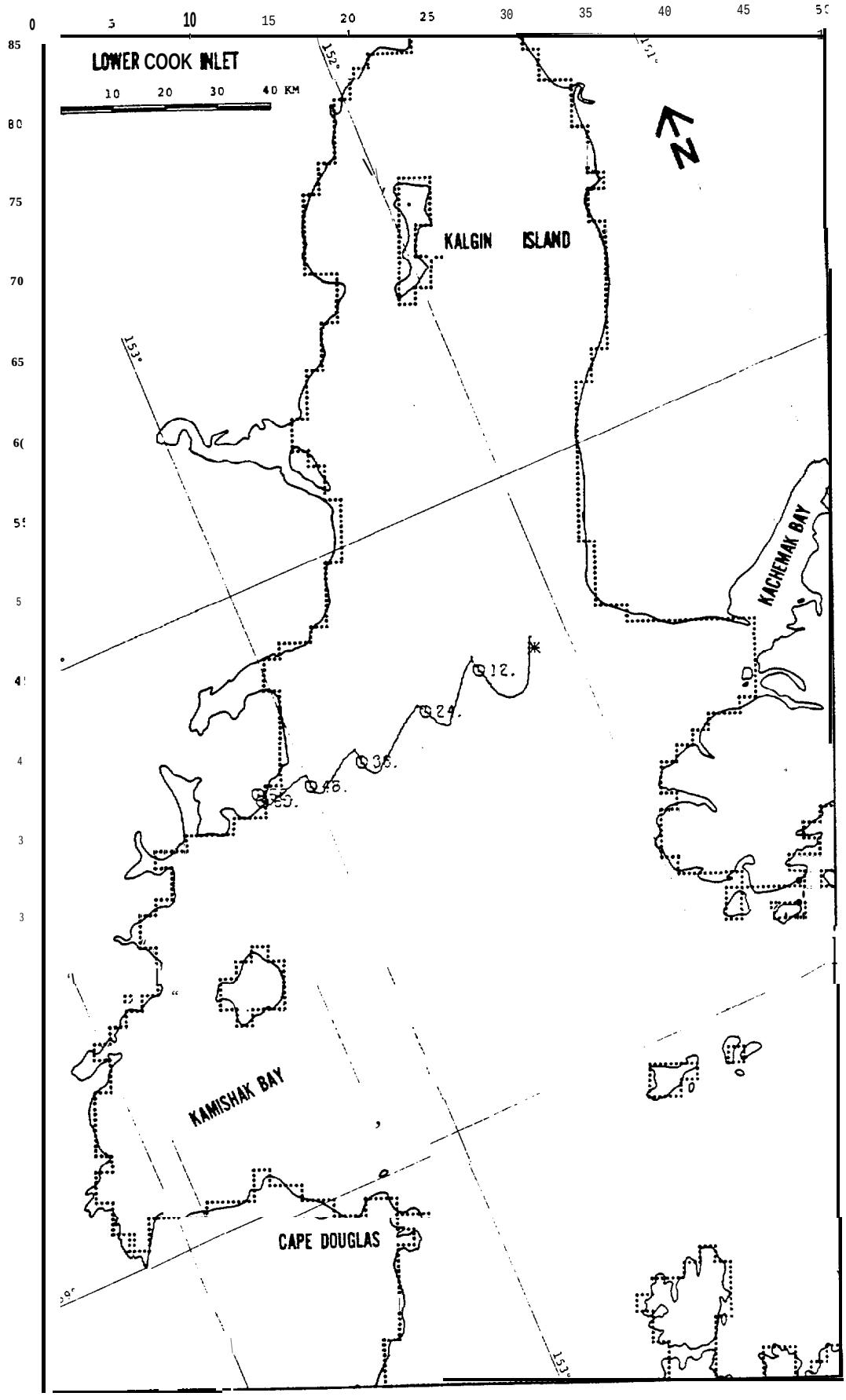

WIND
7

SITE
1

FIGURE C-49: PERTURBATION CASE: NET +25%

WIND
7

SITE
1

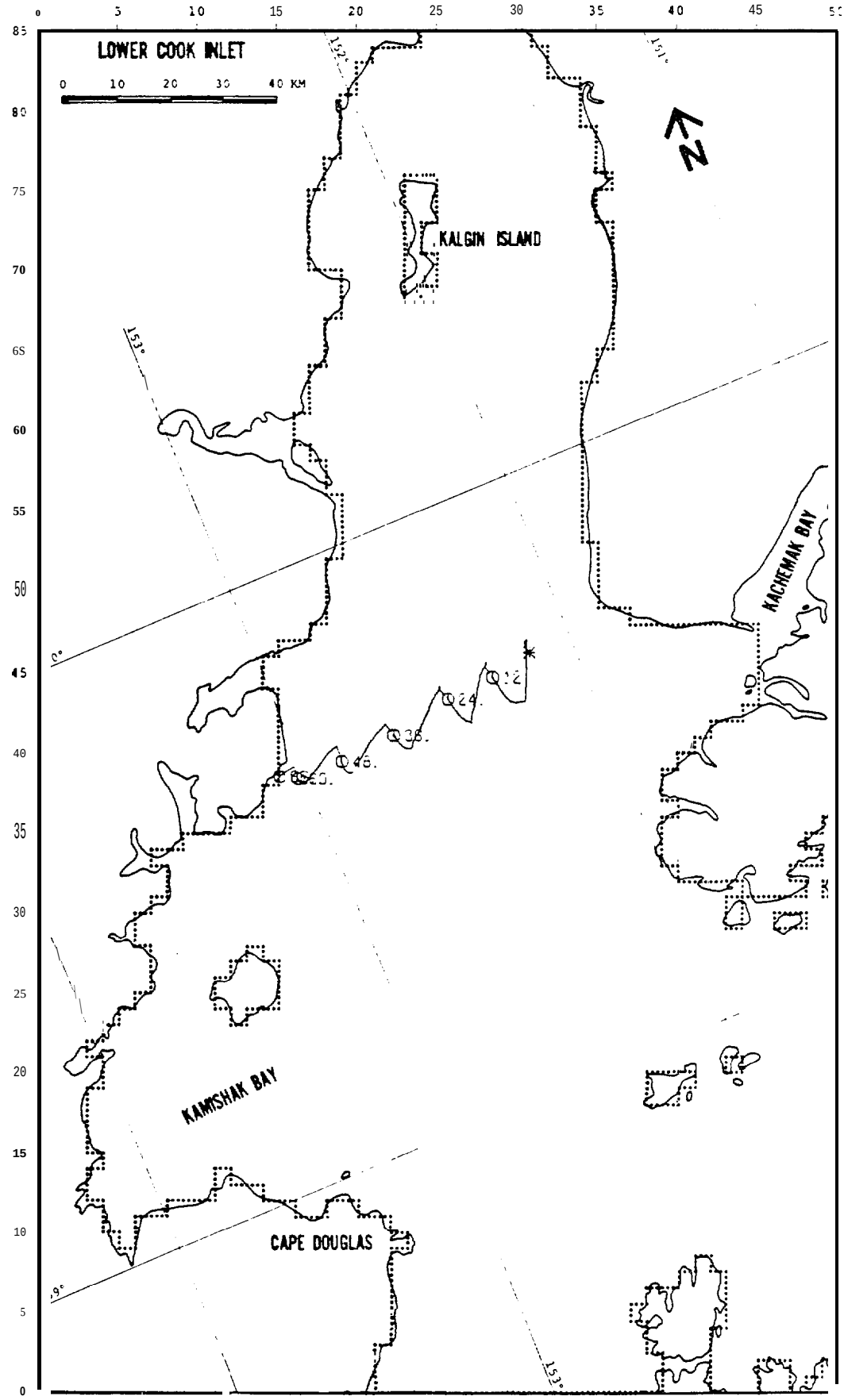

FIGURE C-50: PERTURBATION CASE: NET -25%

WIND
"7

SITE
1

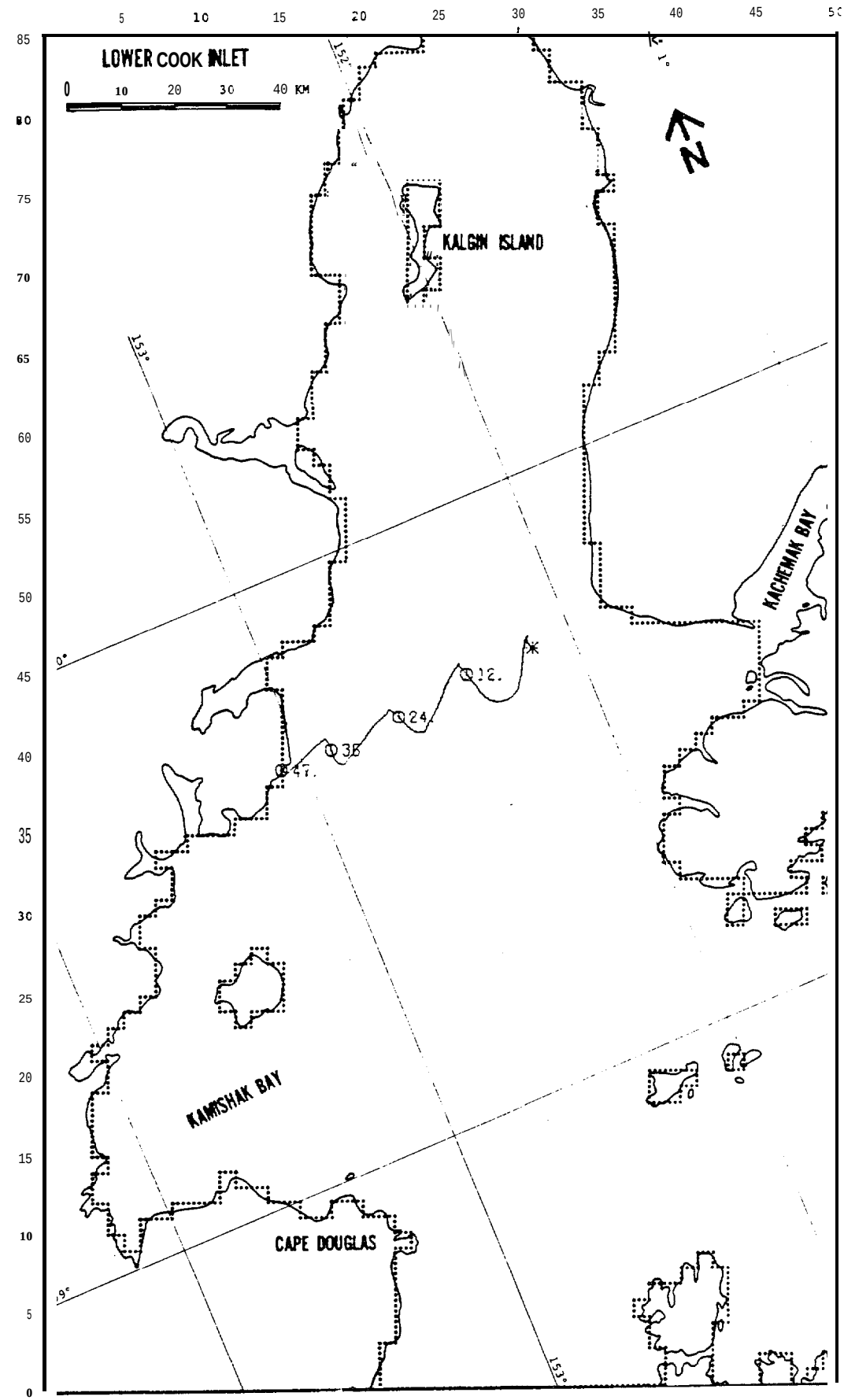

FIGURE C-51: PERTURBATION CASE: WIND +25%

WIND
7

SITE
1

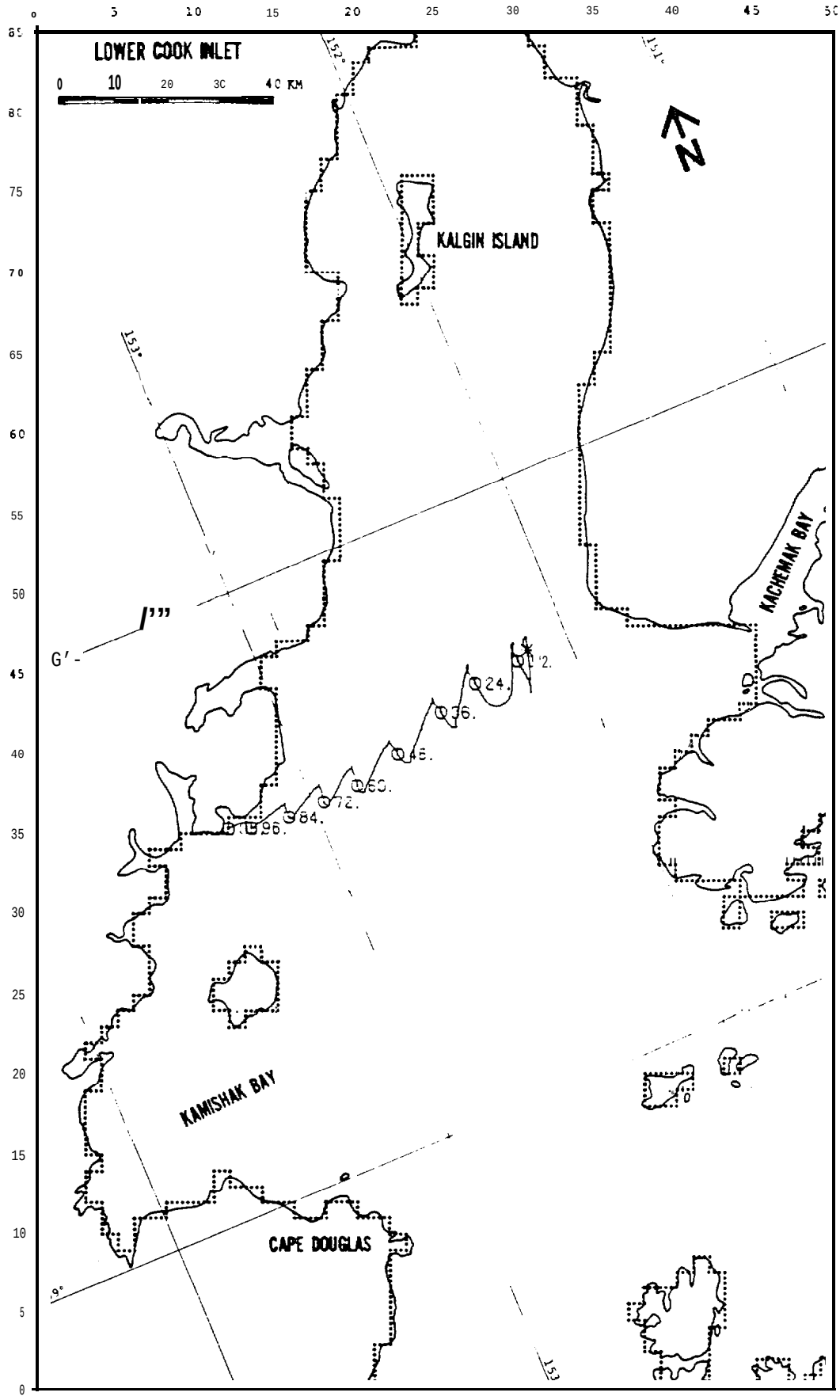

FIGURE C-52: PERTURBATION CASE: WIND -25%

WIND
7

SITE
7

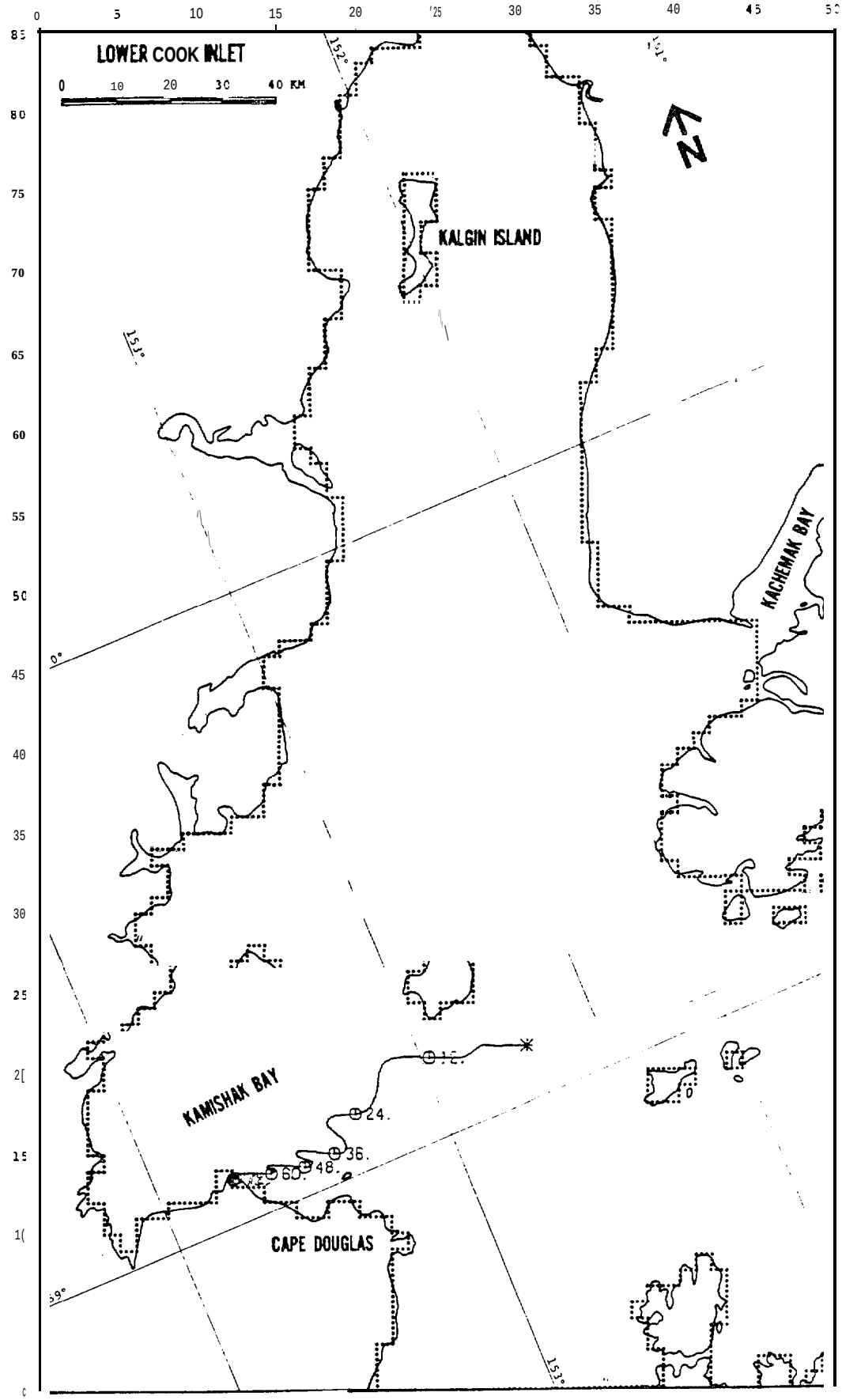

FIGURE C-53: PERTURBATION CASE: NET +25%

WIND
7

SITE
7

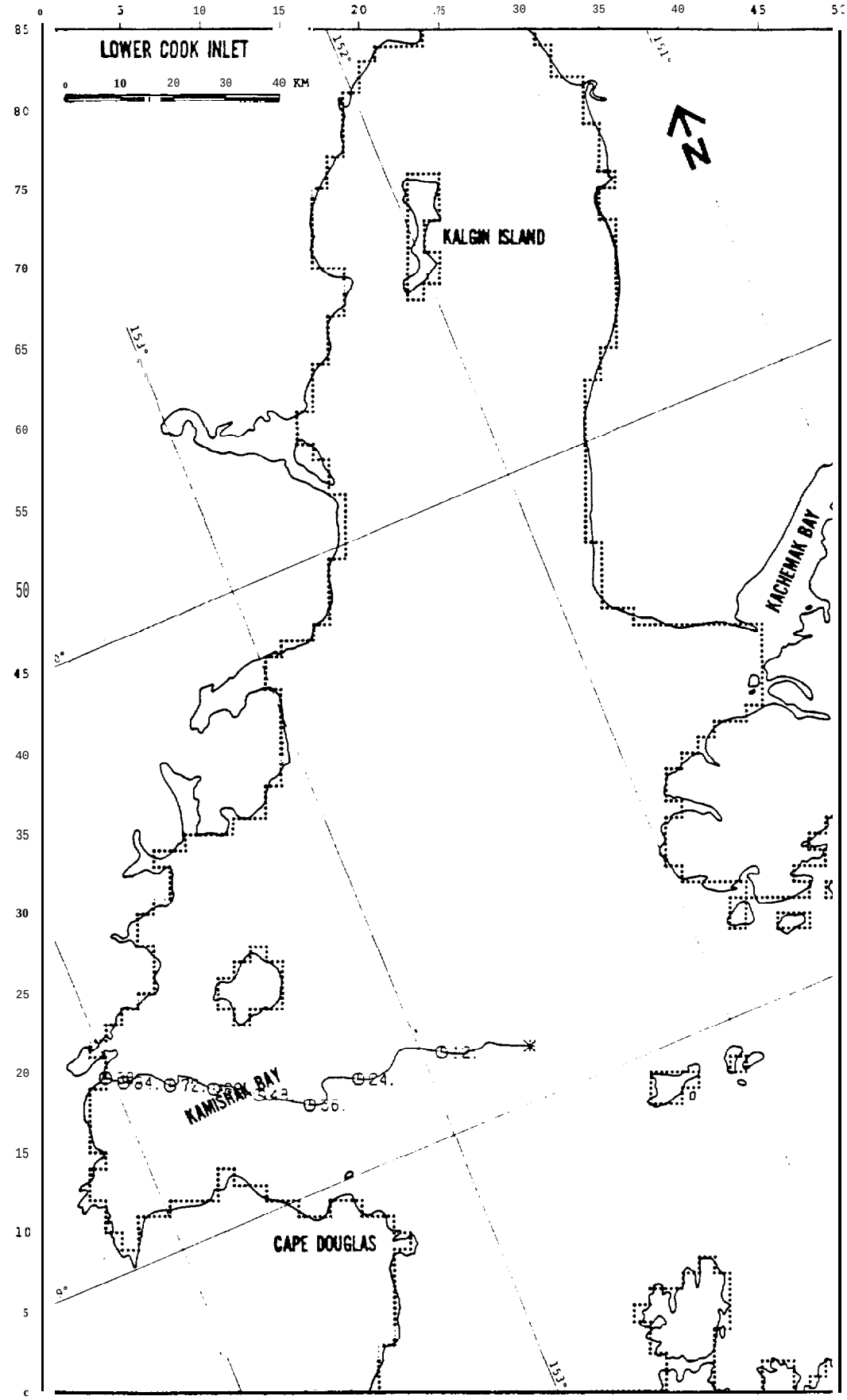

FIGURE C-54: PERTURBATION CASE: NET -25%

WIND
"7

SITE
7

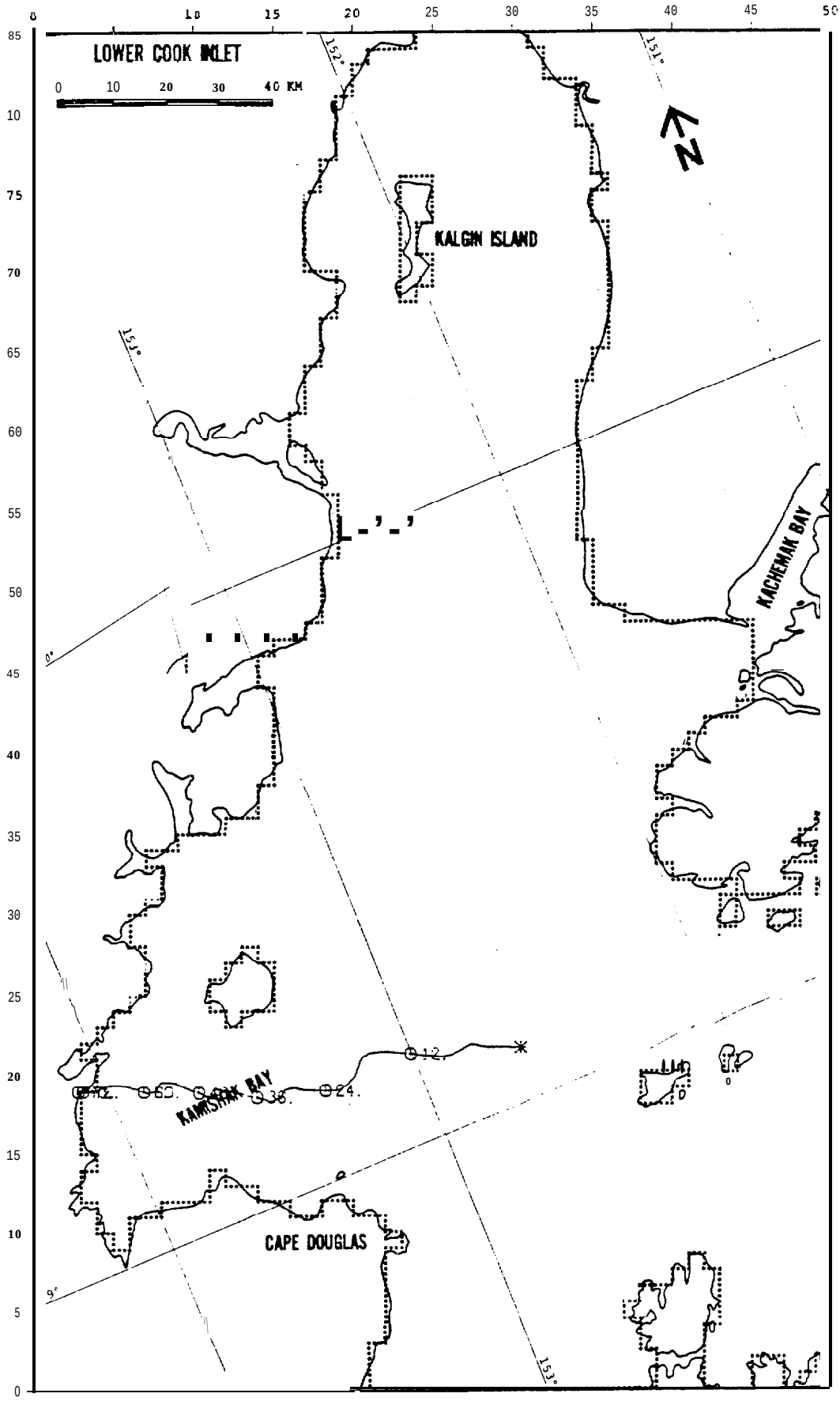

FIGURE C-55: PERTURBATION CASE: WIND +25%

WIND
7

SITE
7

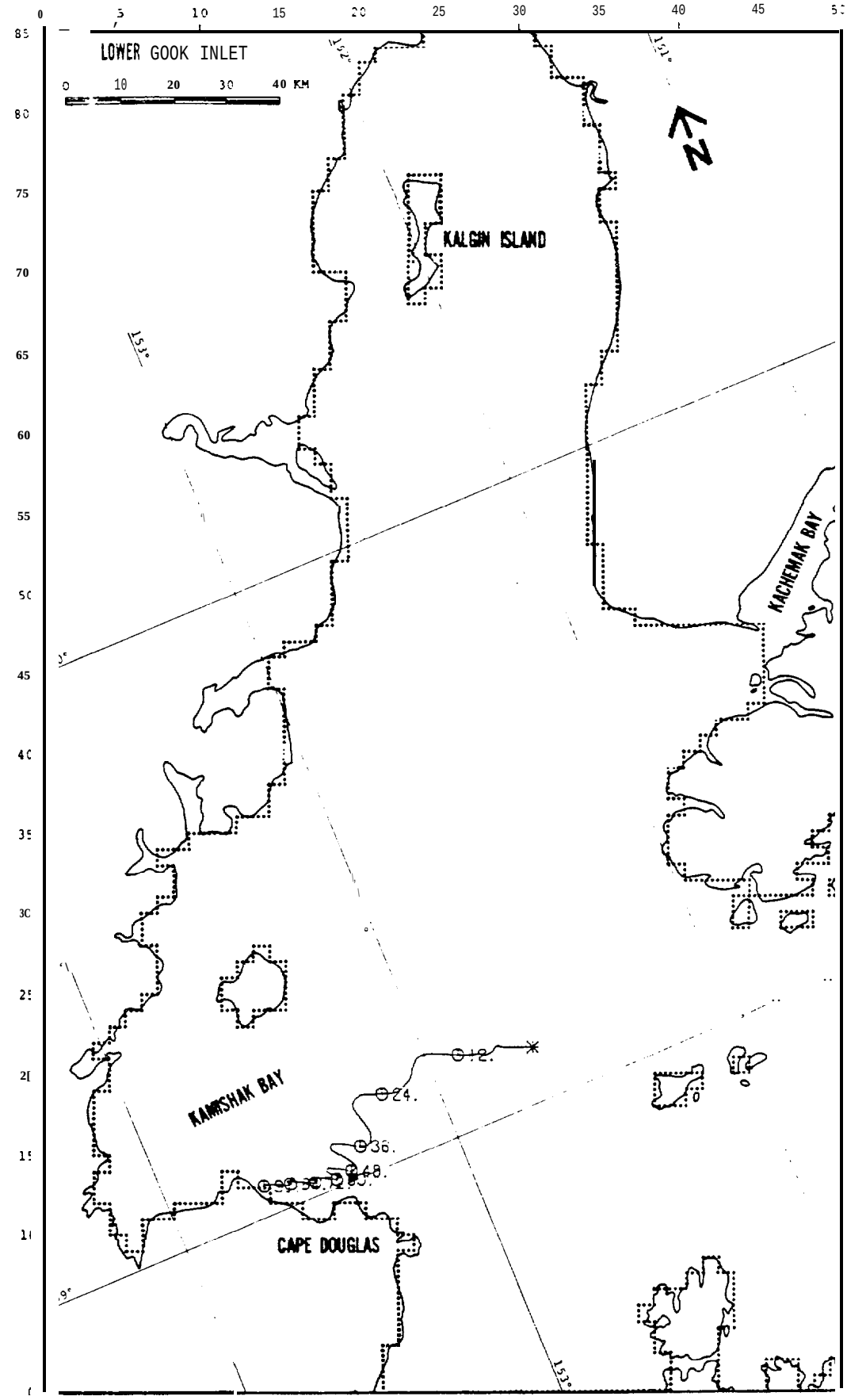

FIGURE C-56: PERTURBATION CASE: WIND -25%

WIND
8

SITE
1

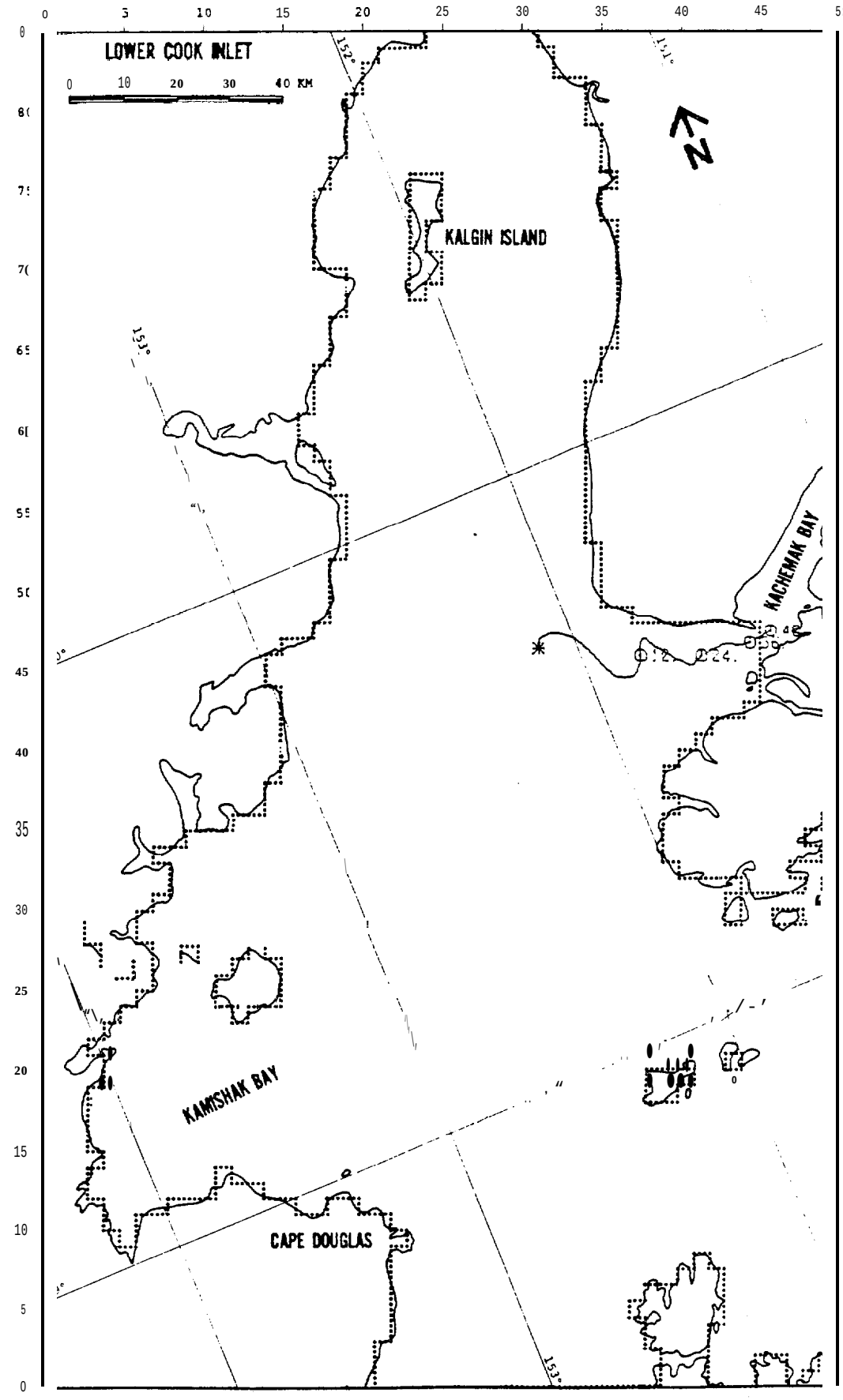

FIGURE C-57: PERTURBATION CASE: NET +25%

WIND
8

SITE
1

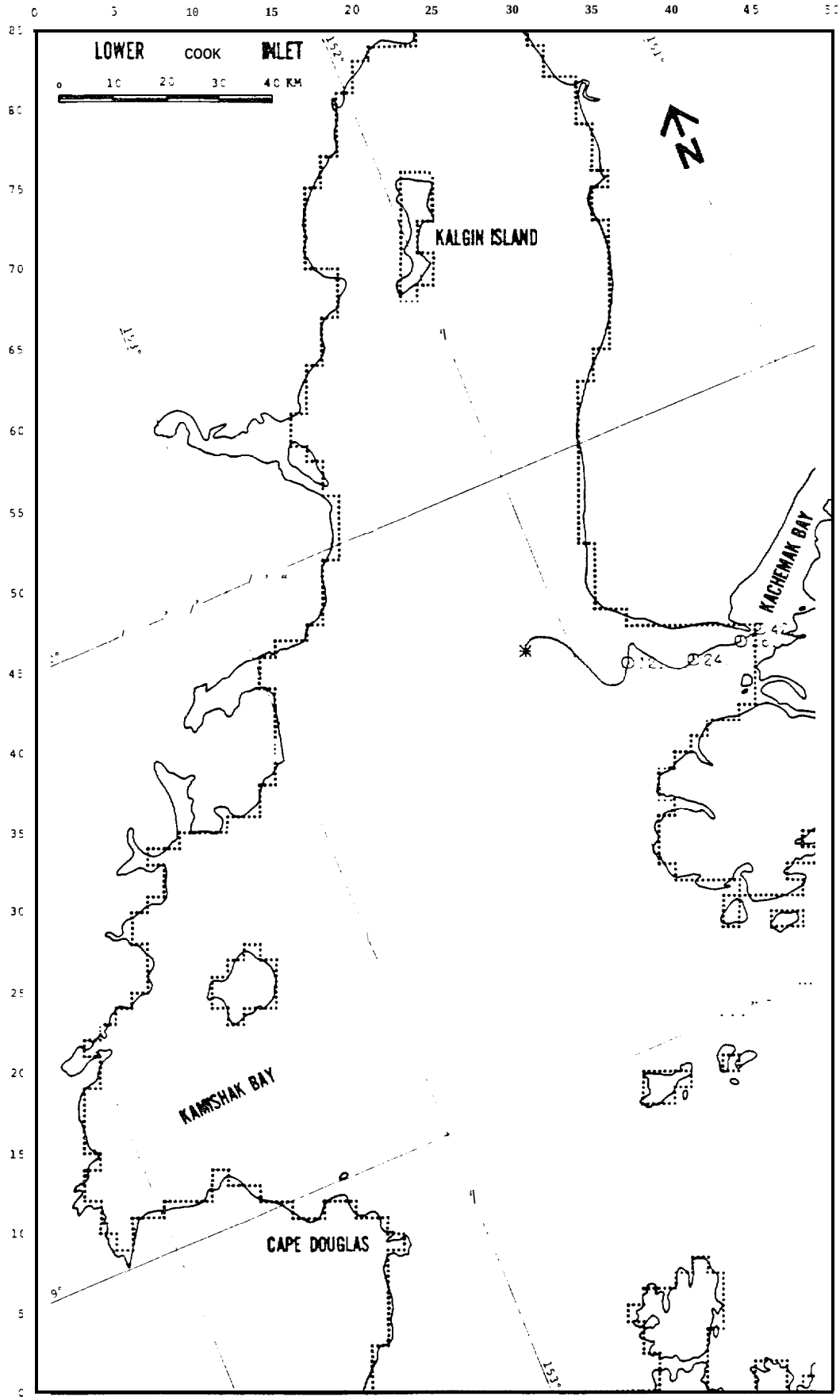

FIGURE C-58: PERTURBATION CASE: NET -25%

WIND
8

SITE
1

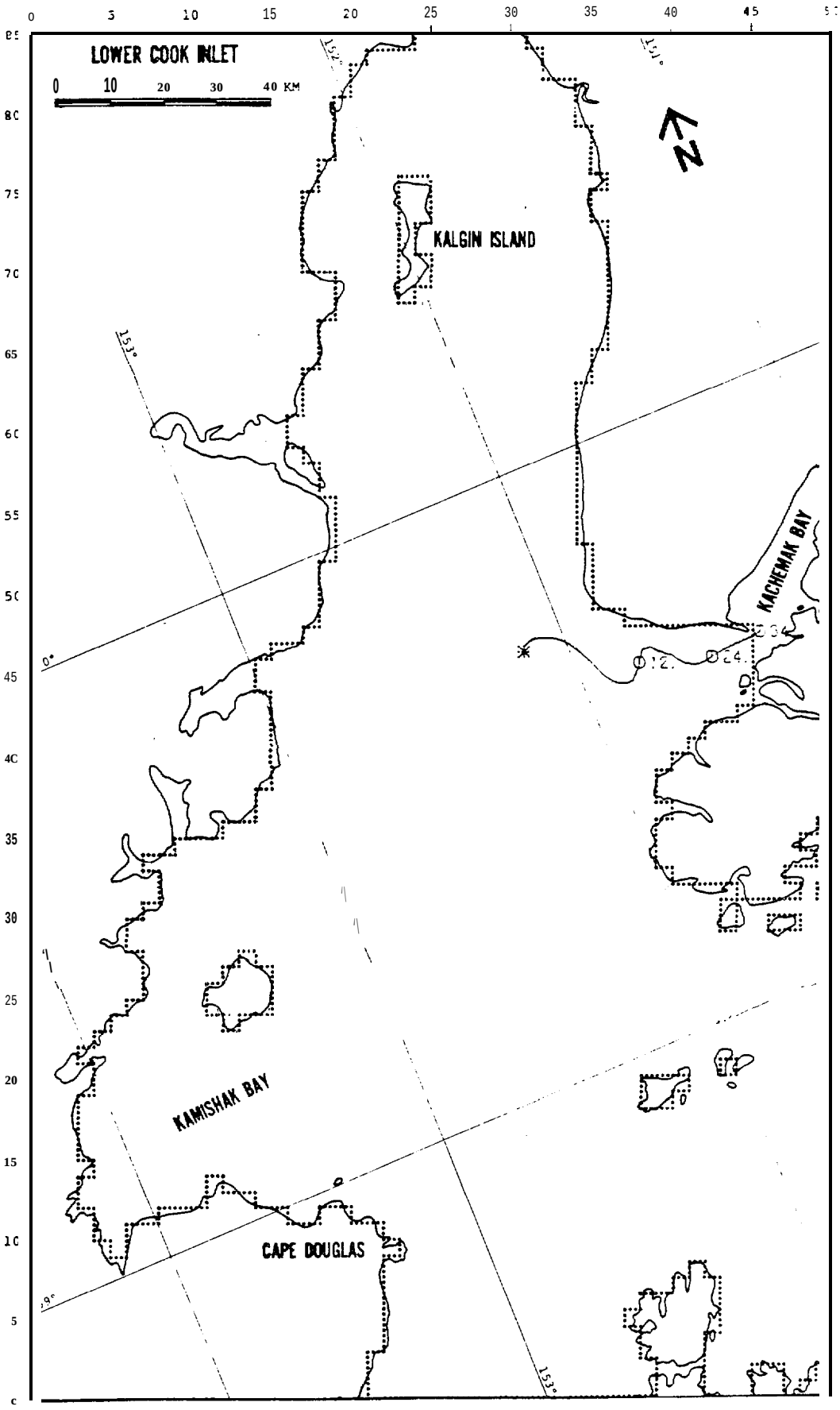

FIGURE C-59: PERTURBATION CASE: WIND +25%

WIND
8

SITE
1

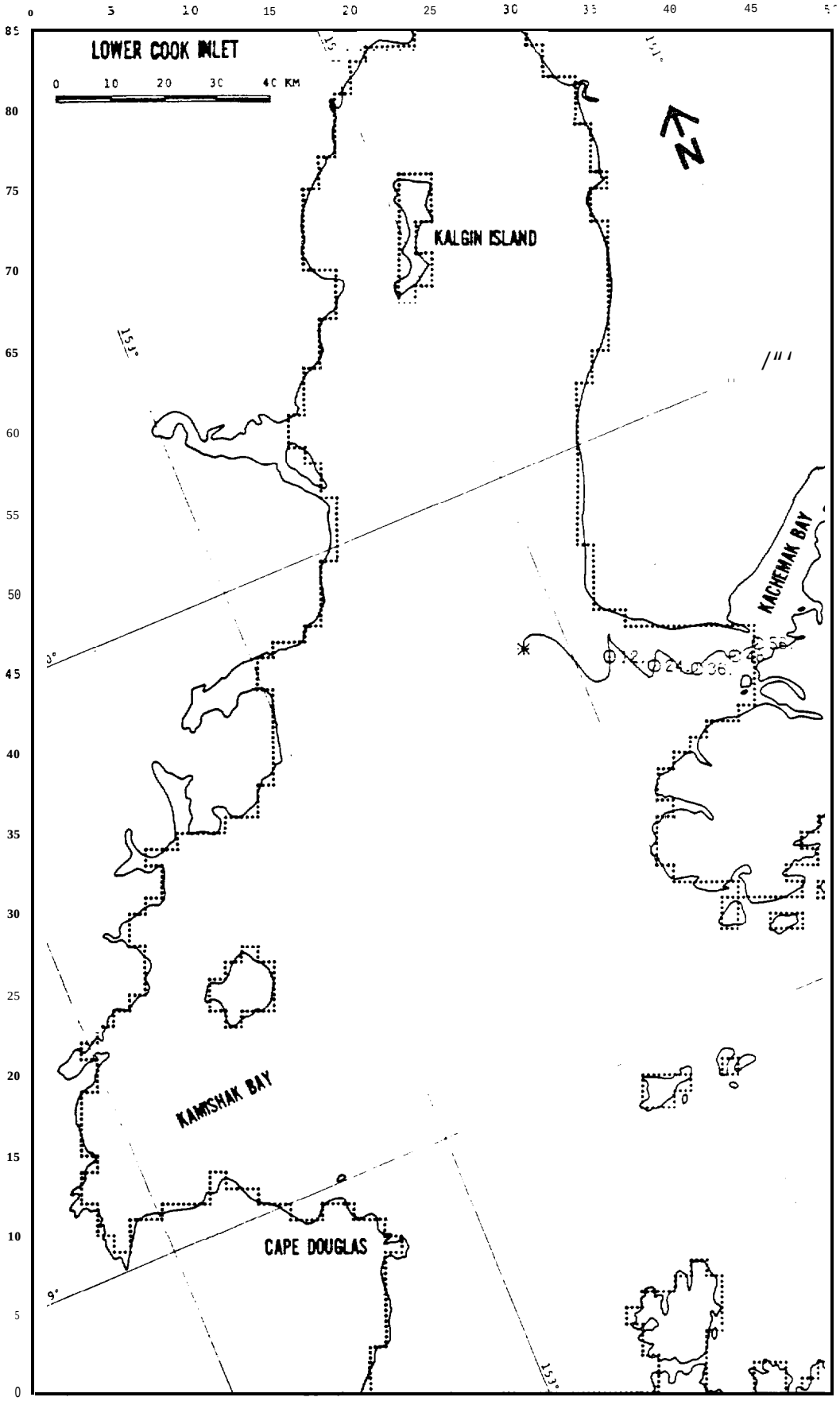

FIGURE C-60: PERTURBATION CASE: WIND -25%

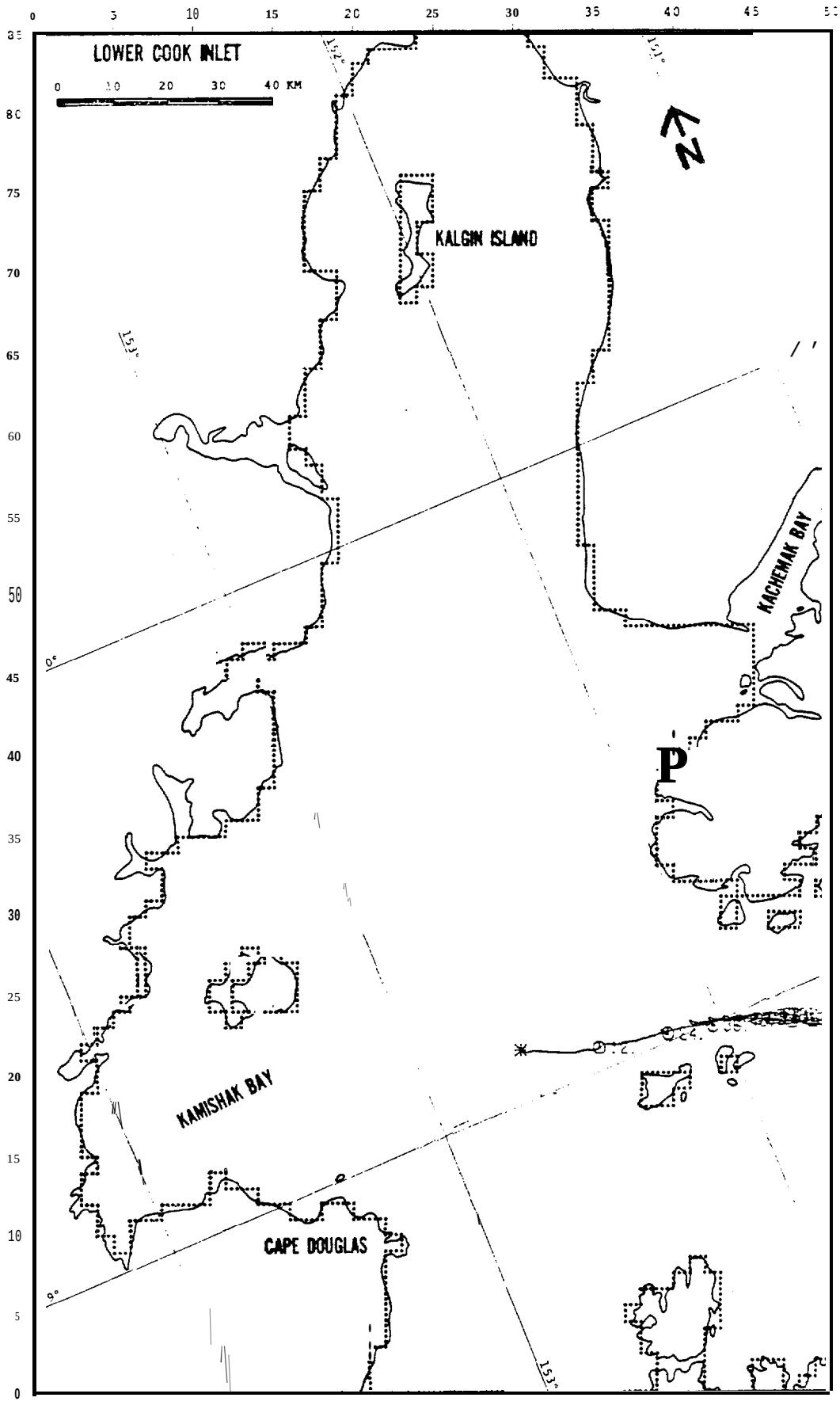

FIGURE C-61: PERTURBATION CASE: NET +25%

WIND
8

SITE
7

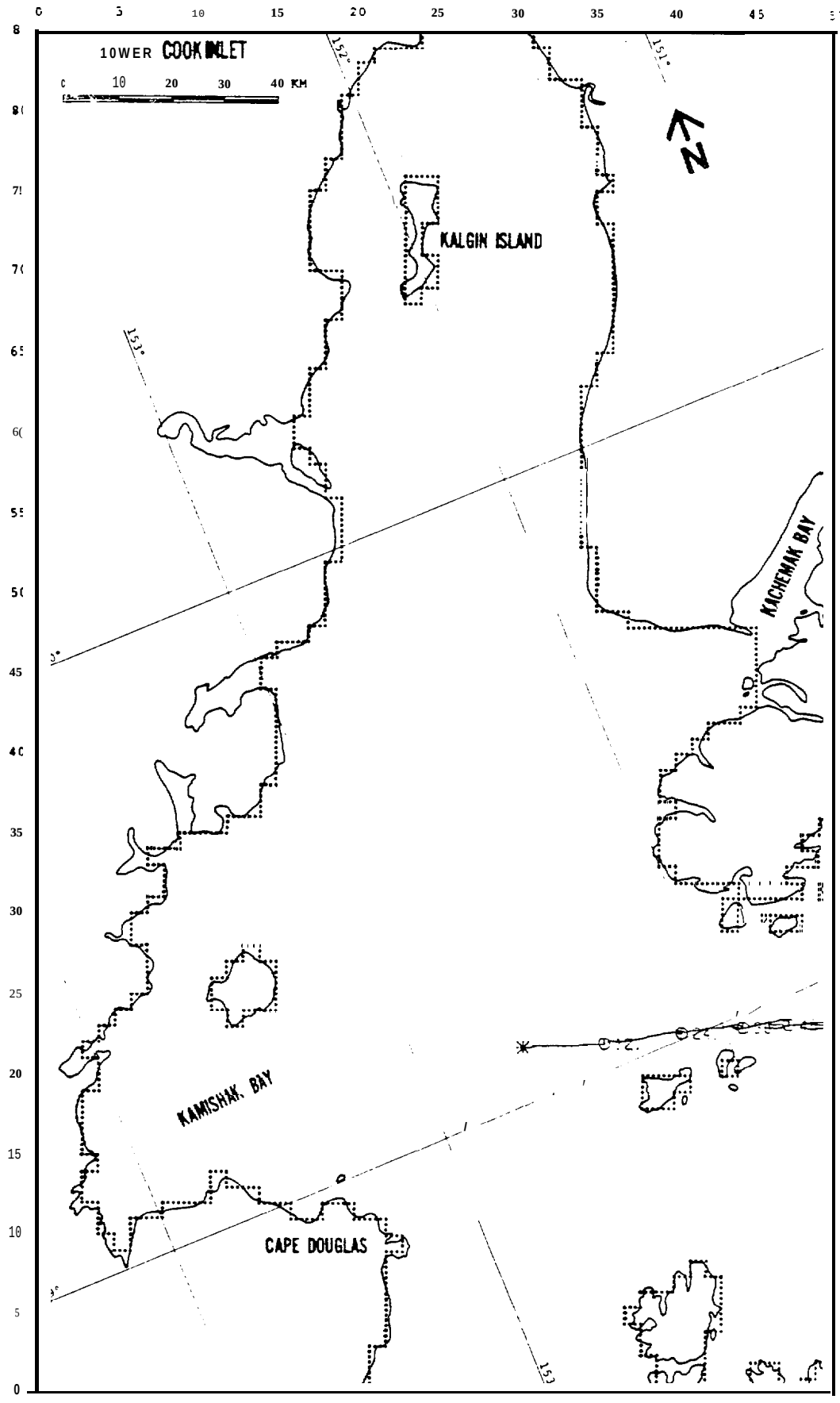

FIGURE C-62: PERTURBATION CASE: NET -25%

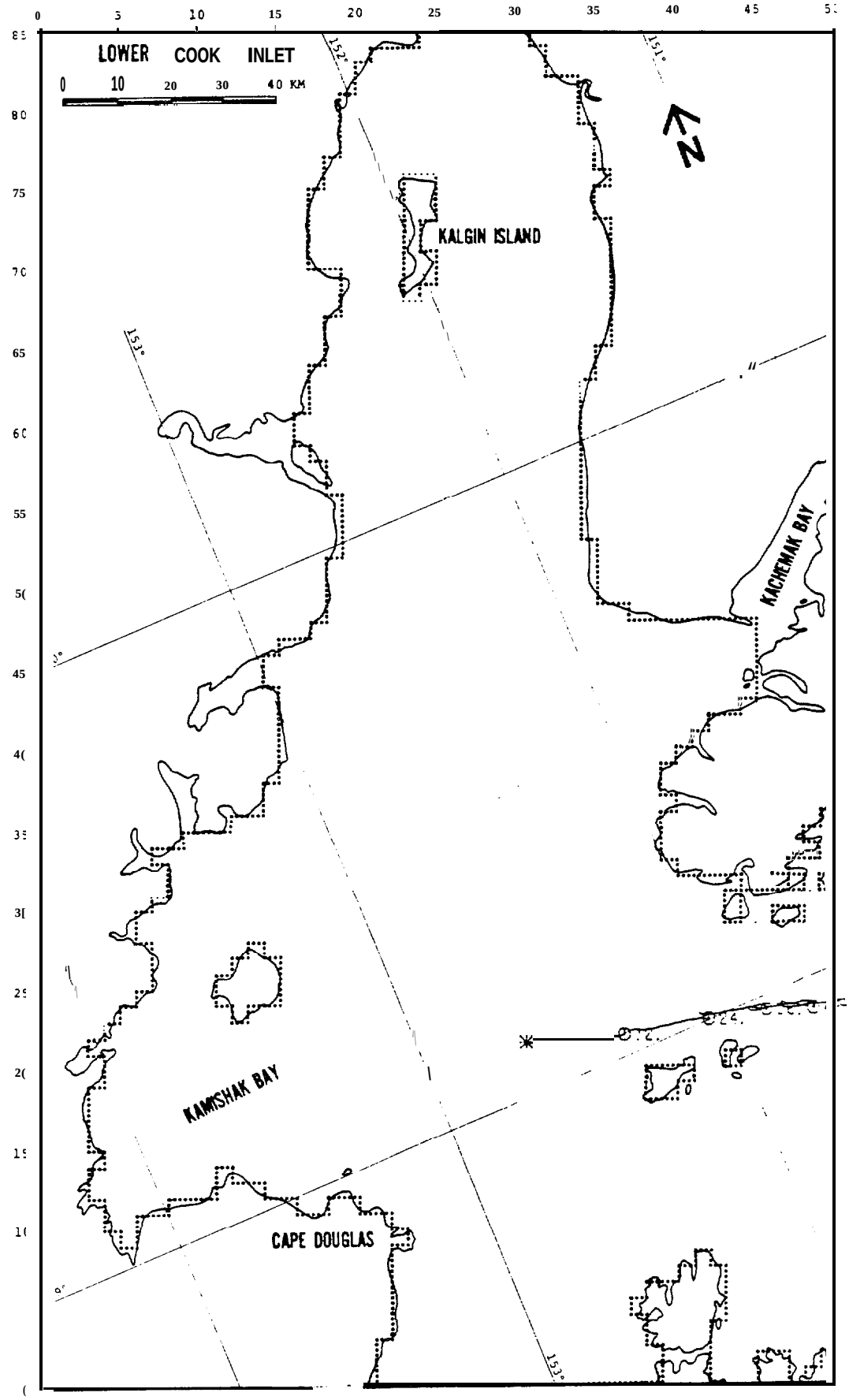

WIND
8

SITE
7

FIGURE C-63: PERTURBATION CASE: WIND +25%

WIND
8

SITE
7

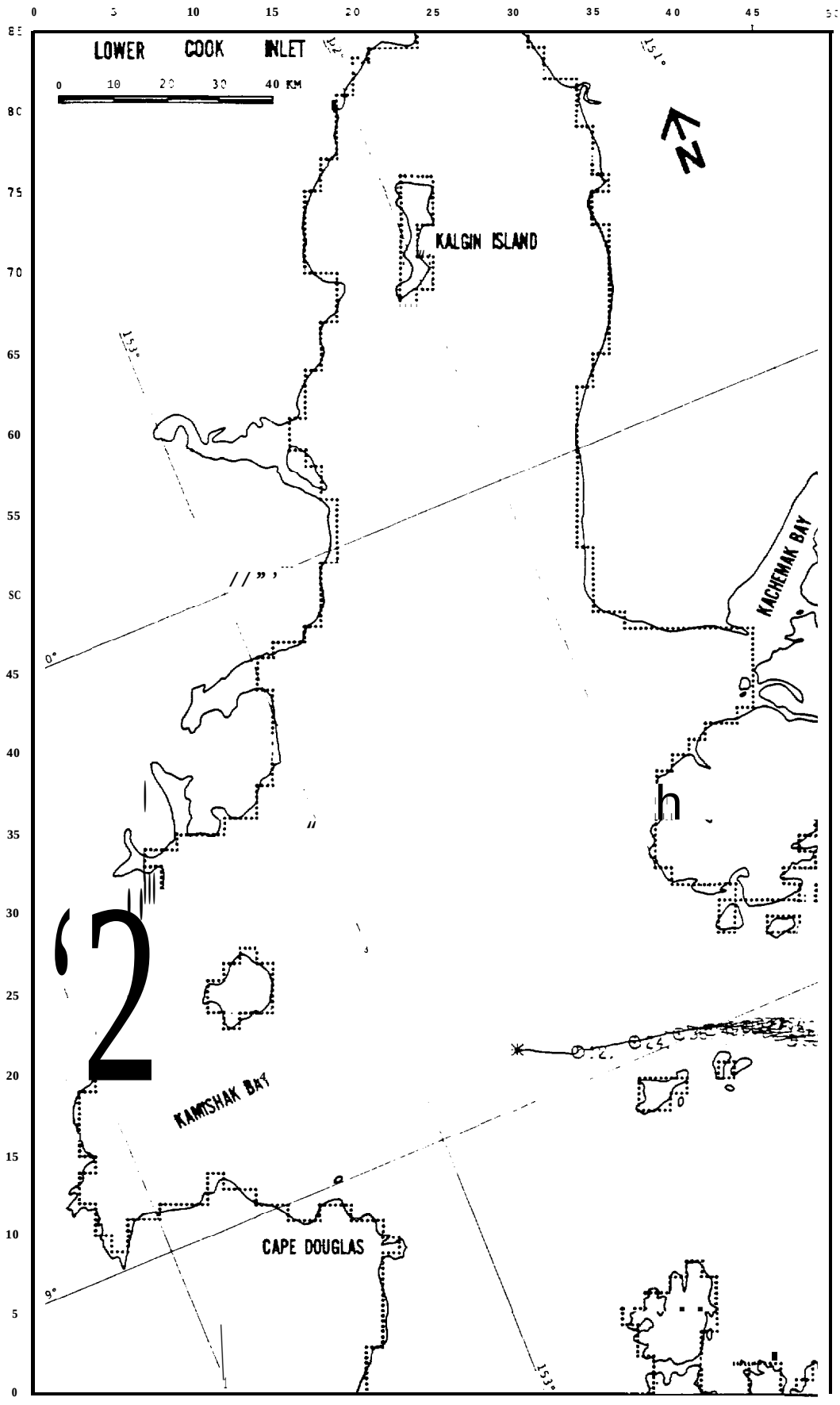

FIGURE C-64: PERTURBATION CASE: WIND-25%

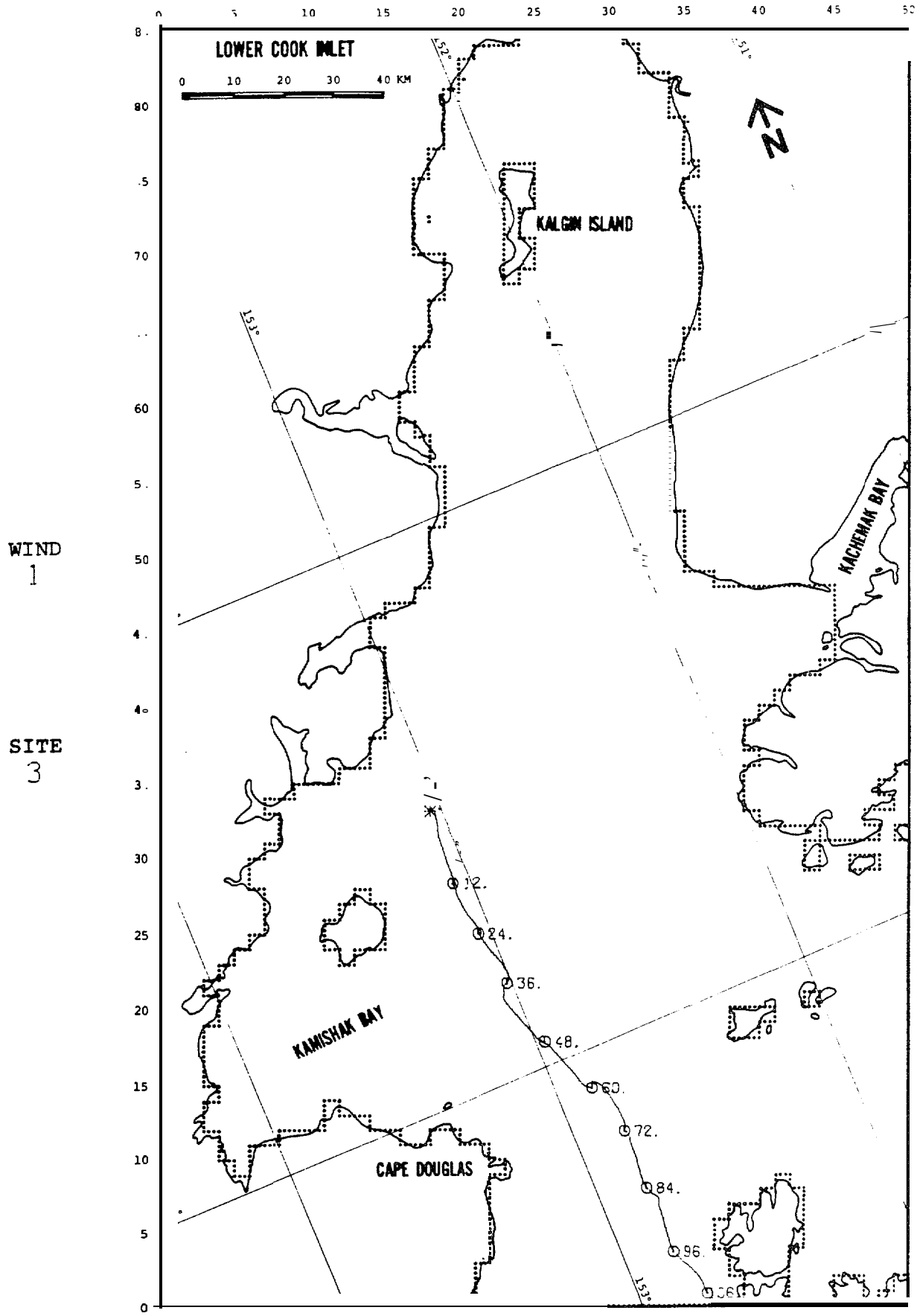

WIND
1

SITE
3

FIGURE C-65: PERTURBATION CASE: WIND -25%

WIND
2

SITE
3

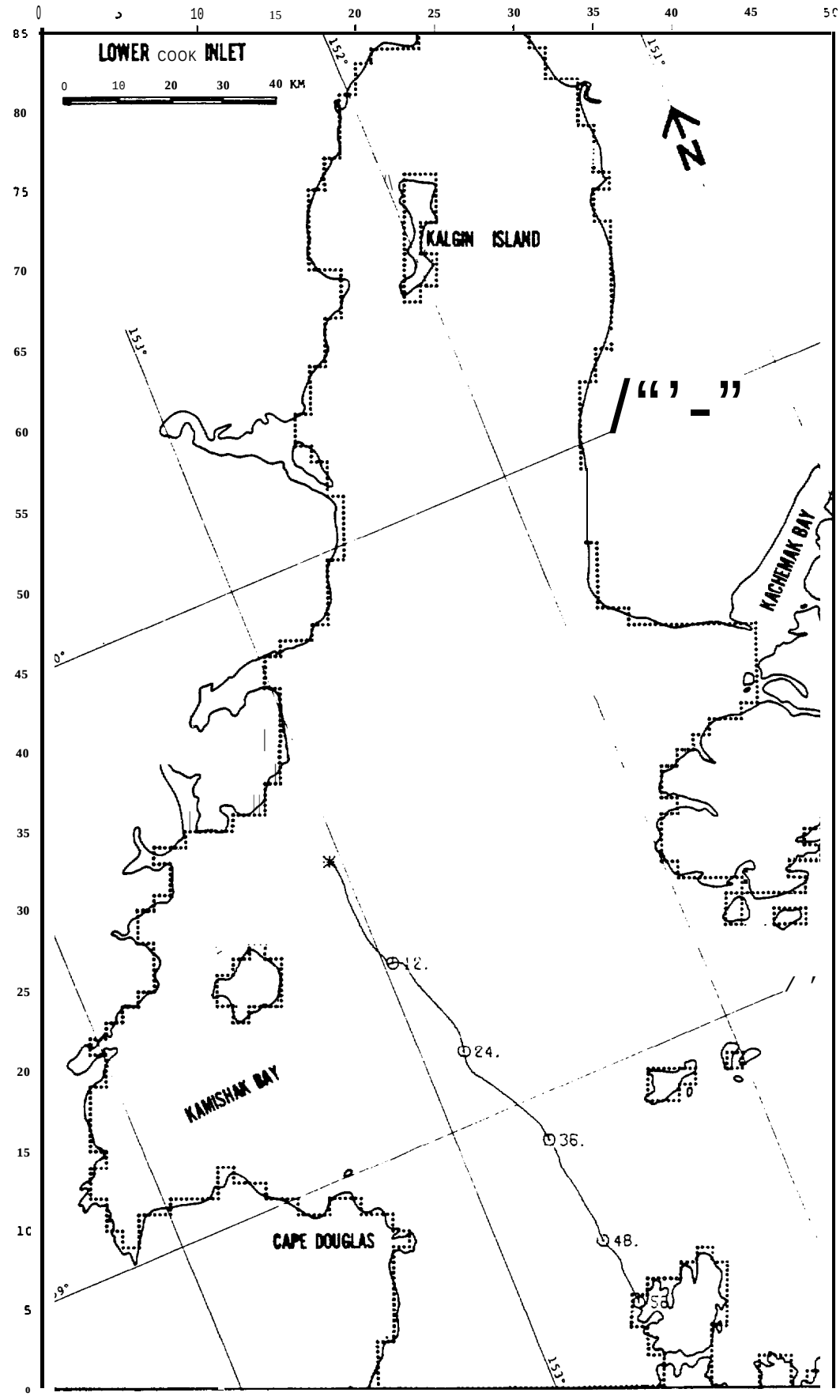

FIGURE C-66: PERTURBATION CASE: WIND -25%

WIND
3

SITE
3

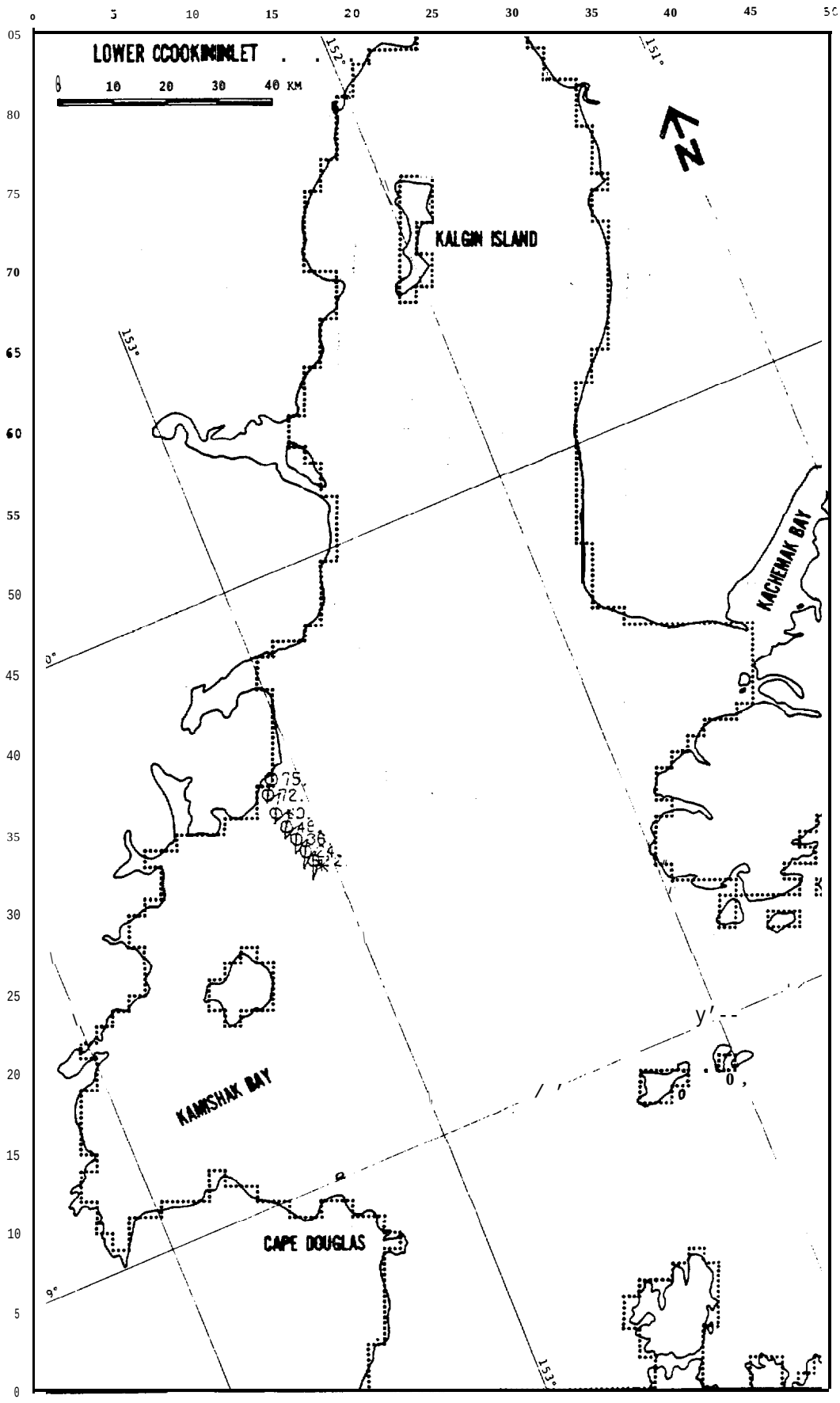

FIGURE C-67: ' PERTURBATION CASE: WIND -25%

WIND
4

SITE
3

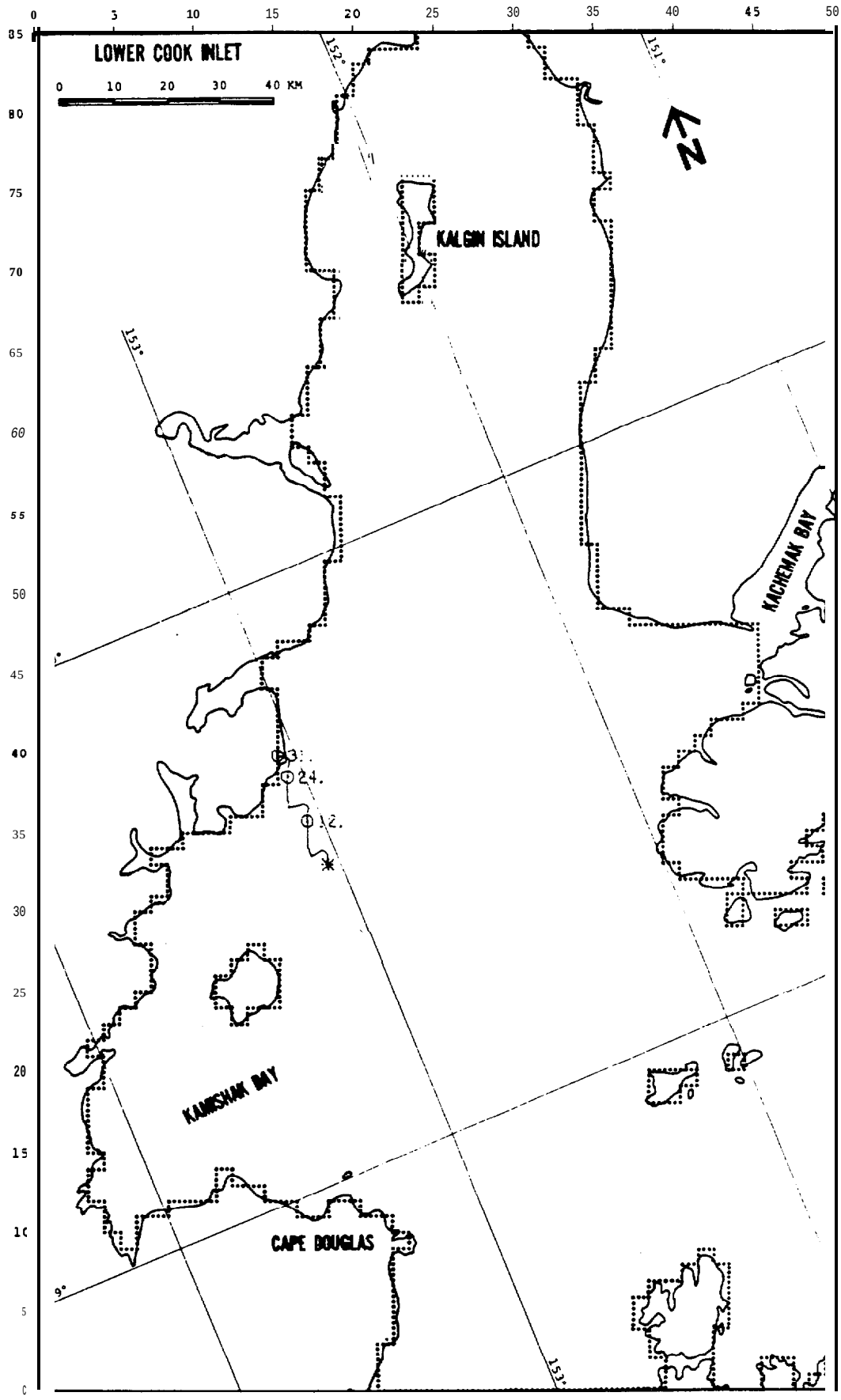

FIGURE C-68: PERTURBATION CASE: WIND -25% “

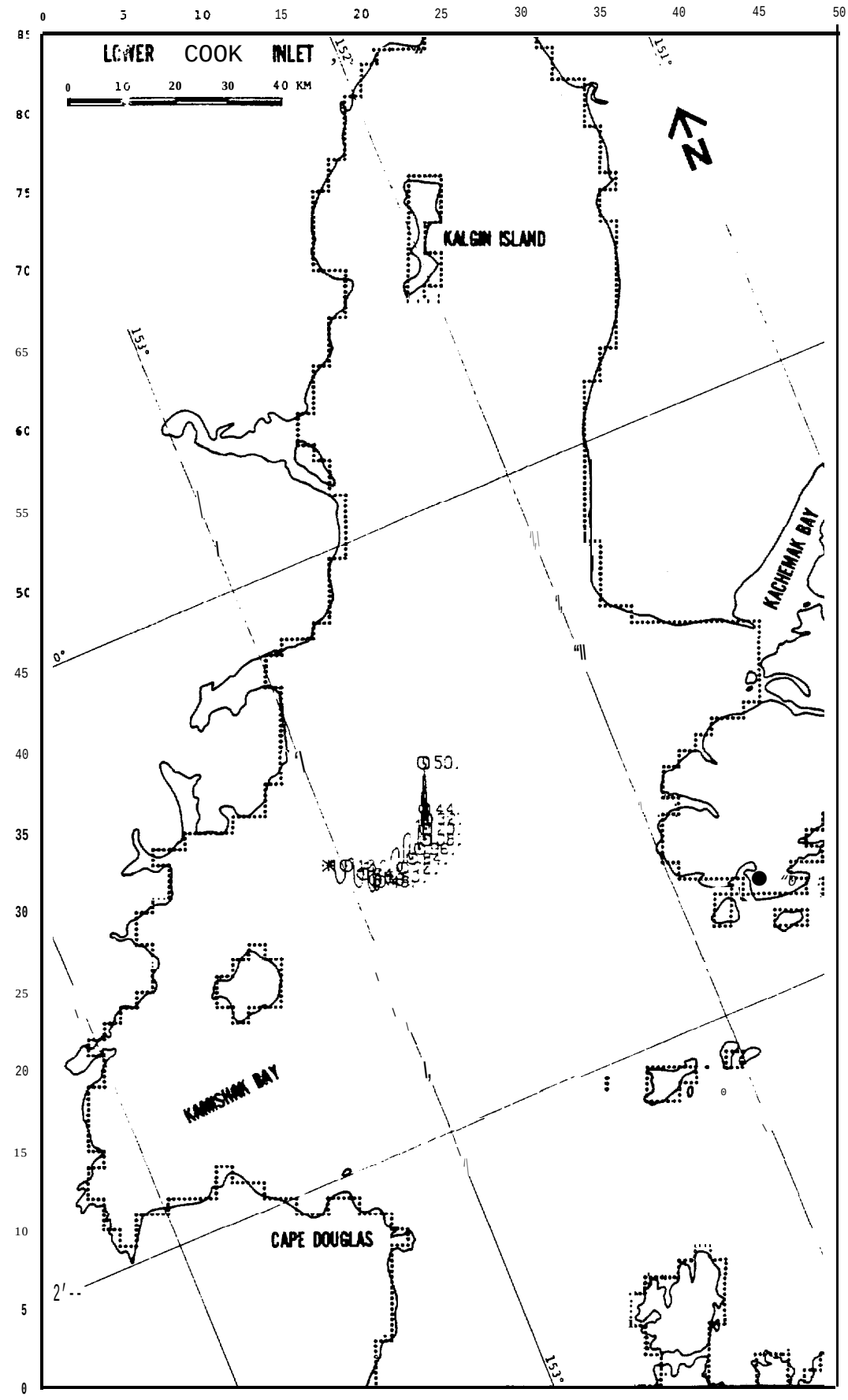

FIGURE C-69: PERTURBATION CASE: WIND -25%"

WIND
6

SITE
3

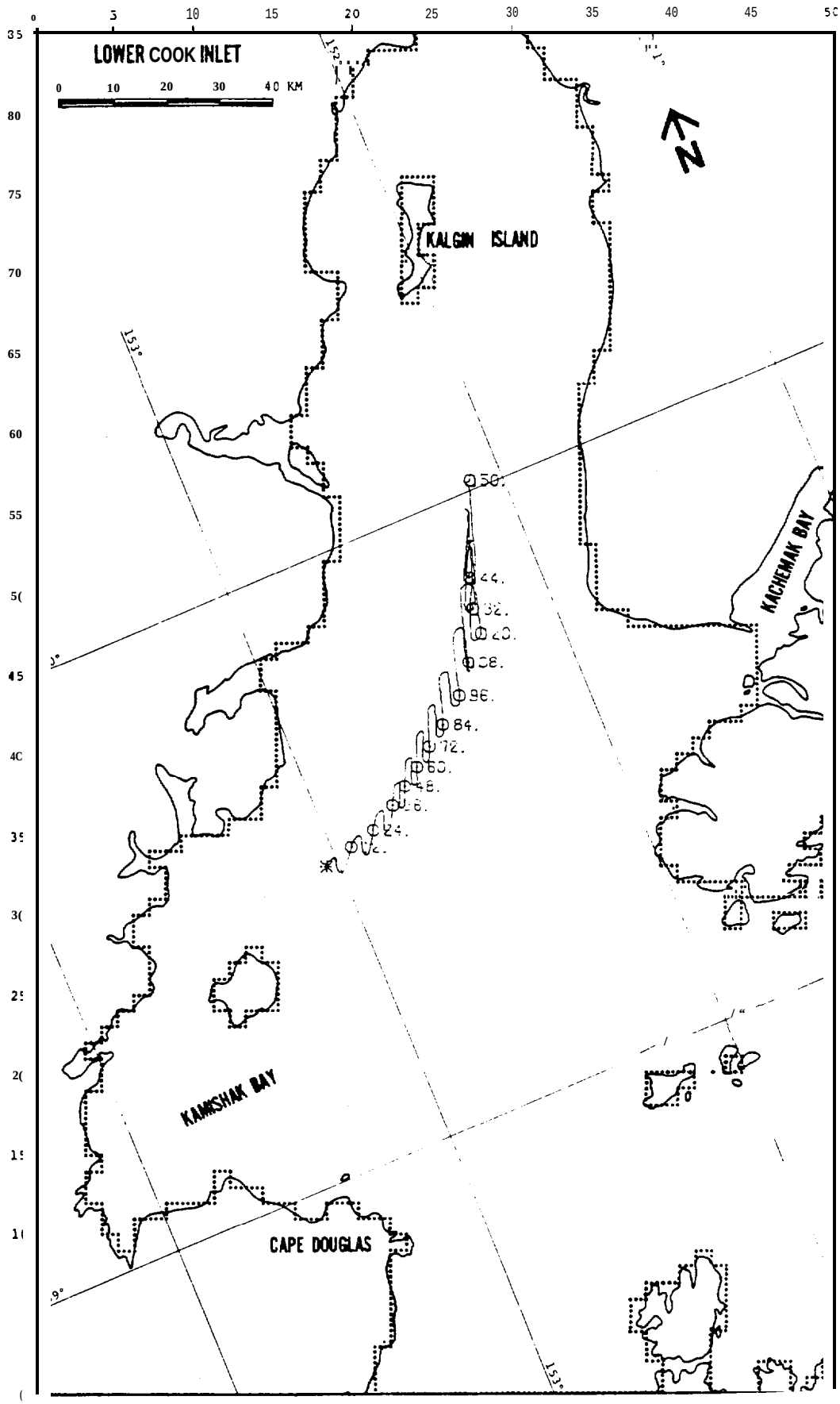

FIGURE C-70: PERTURBATION CASE: WIND -25%

WIND
"7

SITE
3

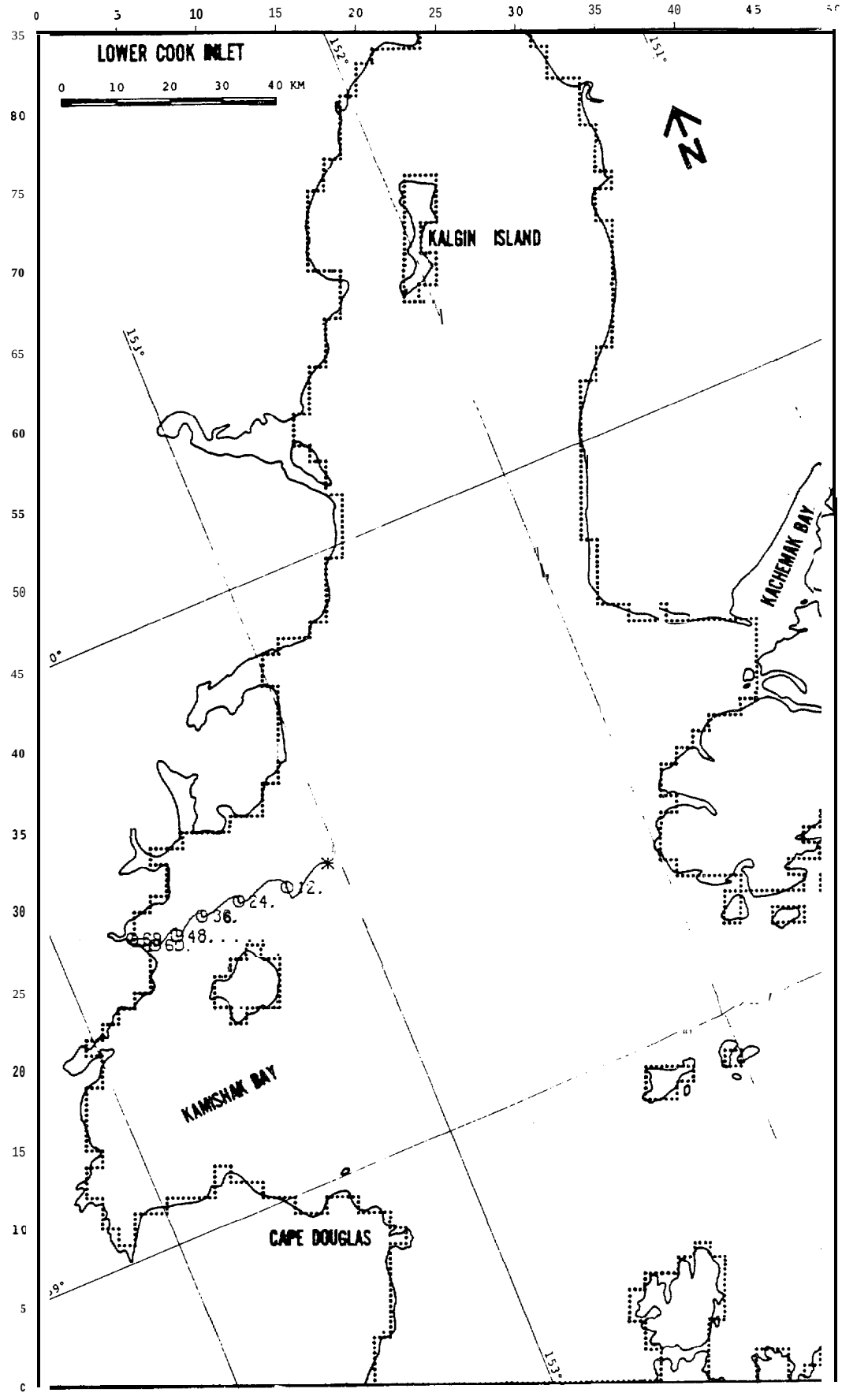

FIGURE C-71: PERTURBATION CASE: WIND -25%

WIND
8

SITE
3

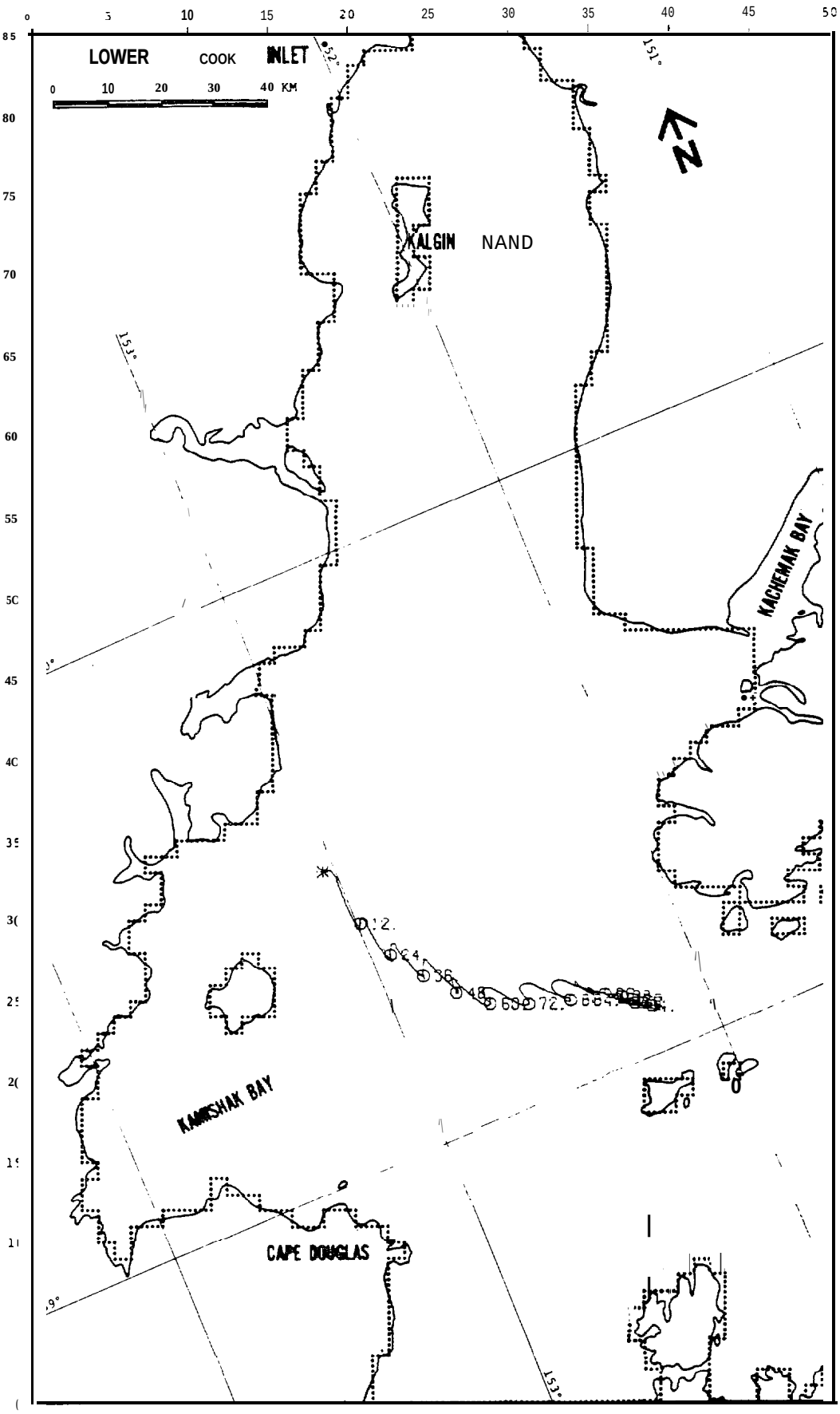

FIGURE C-72: PERTURBATION CASE: WIND -25%

WIND
1

SITE
7

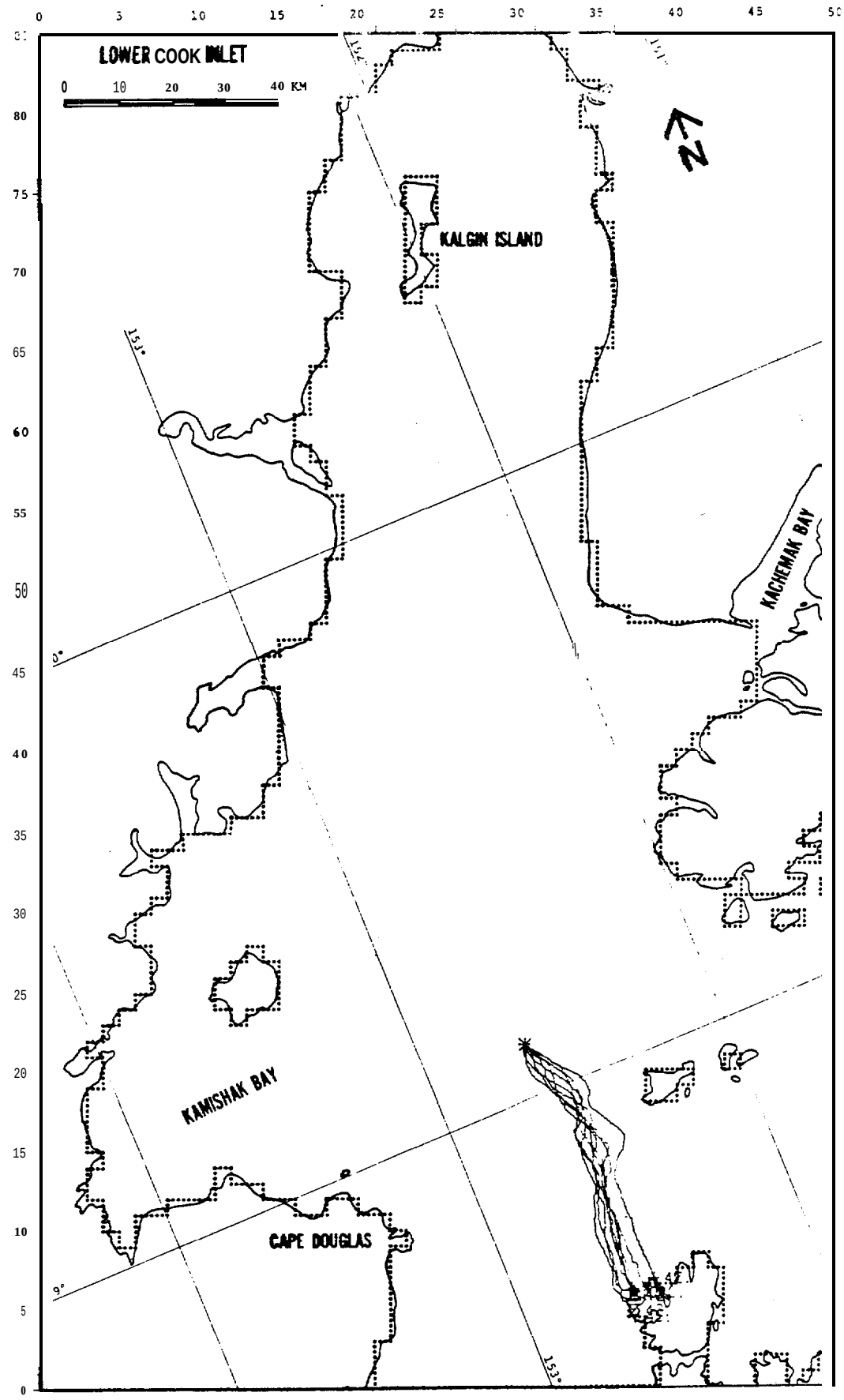

FIGURE C-73: RANDOM PERTURBATION ANALYSIS CASE

WIND
1

SITE
7

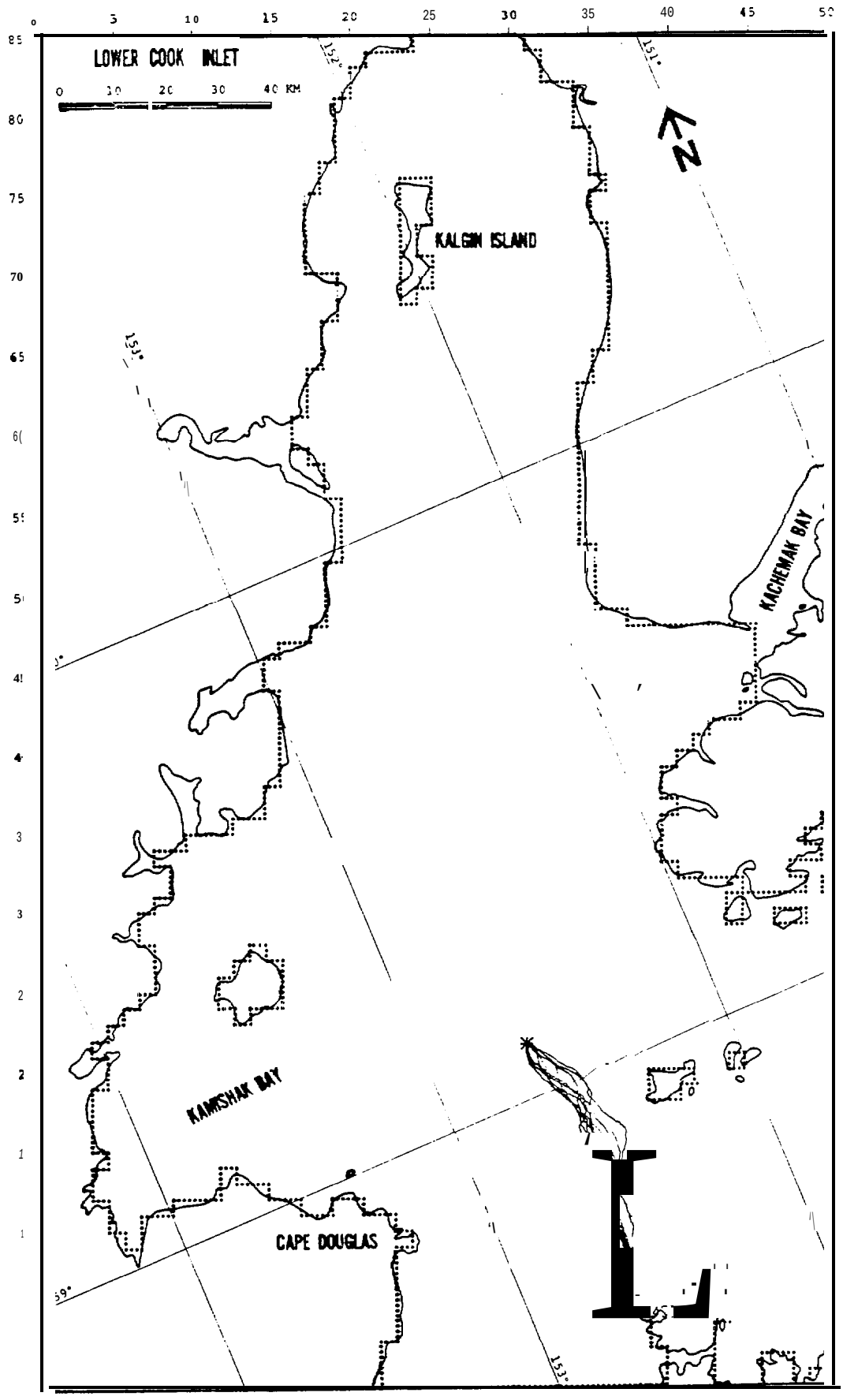

FIGURE C-74: RANDOM PERTURBATION ANALYSIS CASE

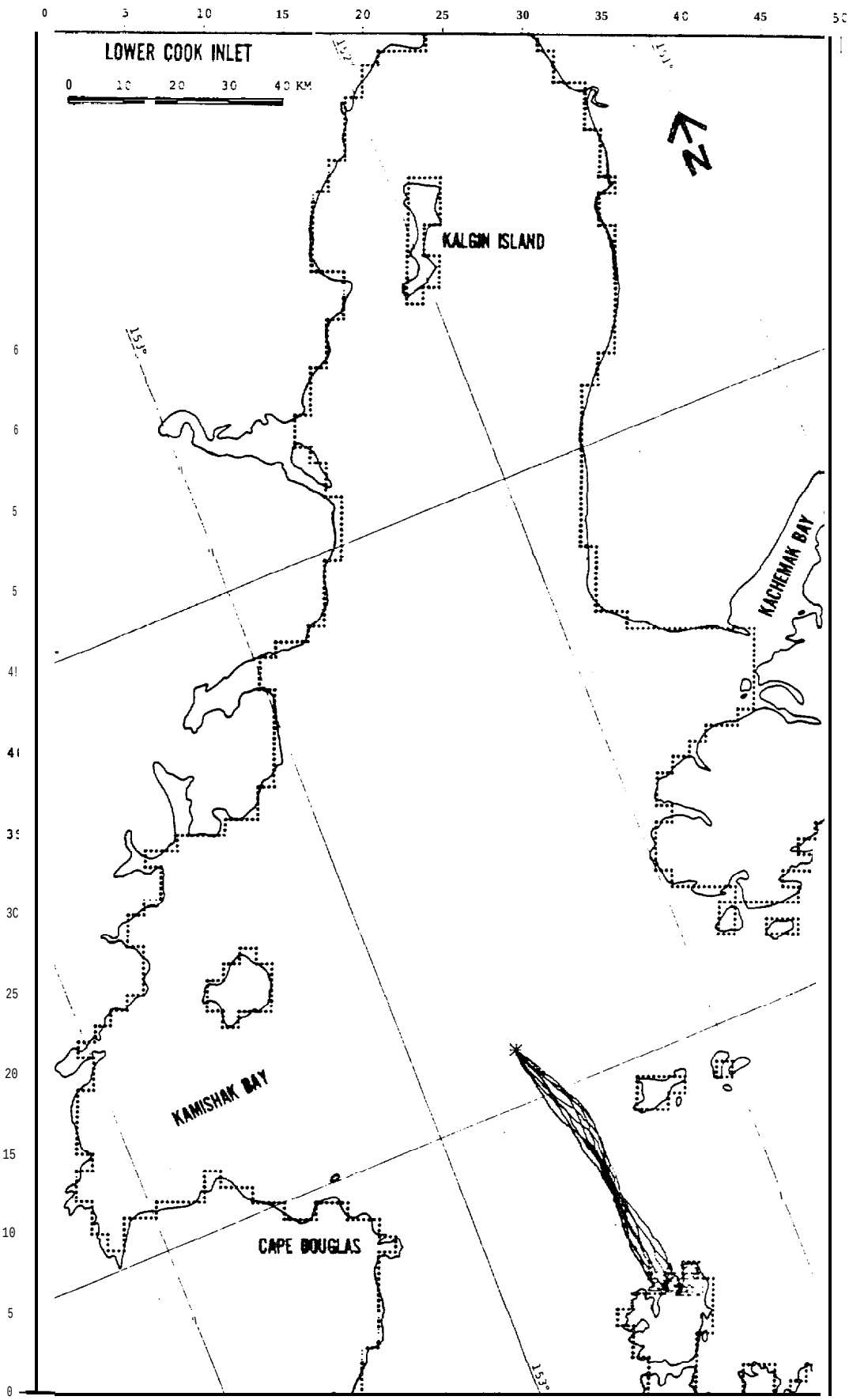

WIND
2

SITE
7

FIGURE C-75: RANDOM PERTURBATION ANALYSIS CASE

WIND
2

SITE
7

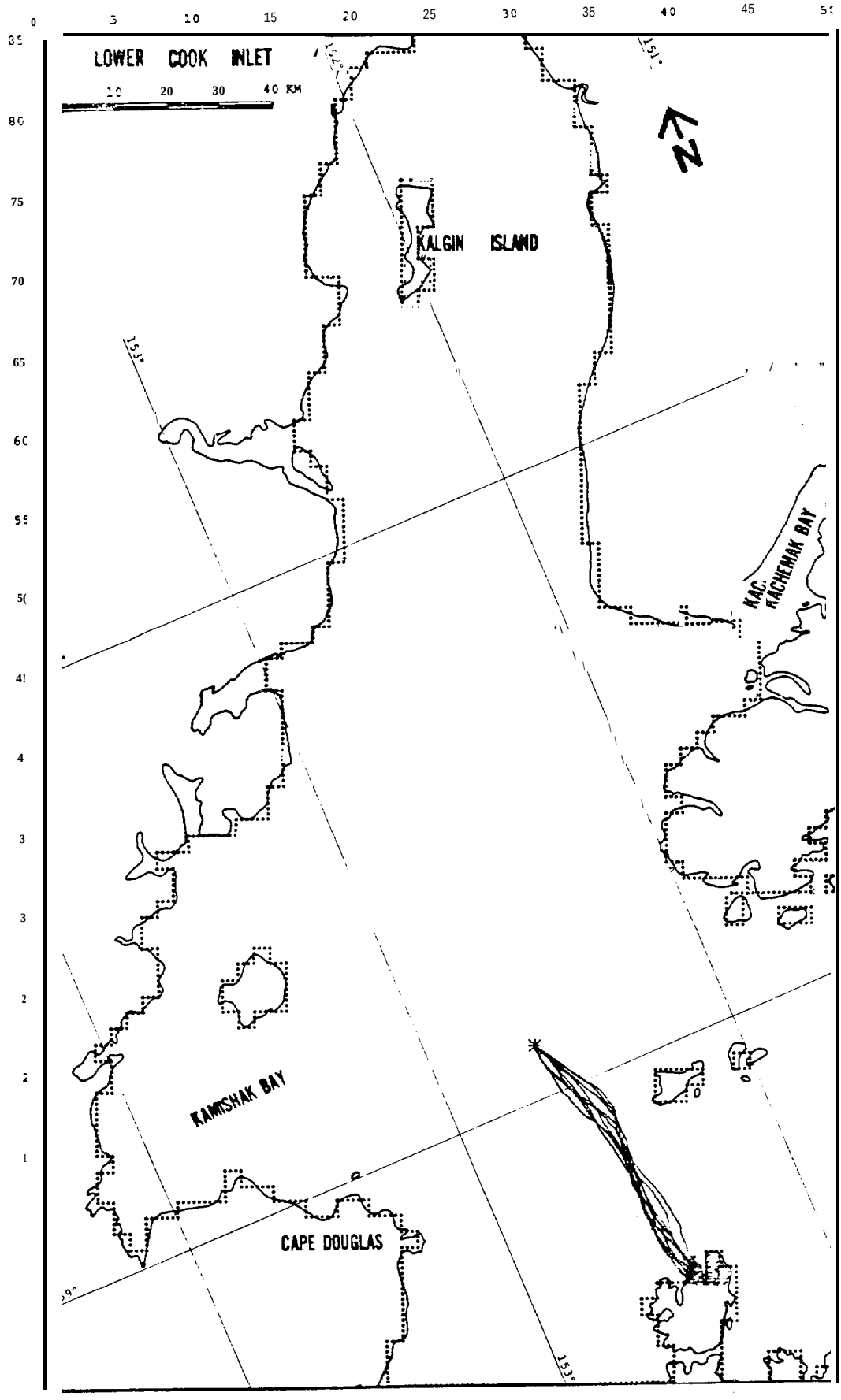

FIGURE C-76: RANDOM PERTURBATION ANALYSIS CASE

WIND
7

SITE
7

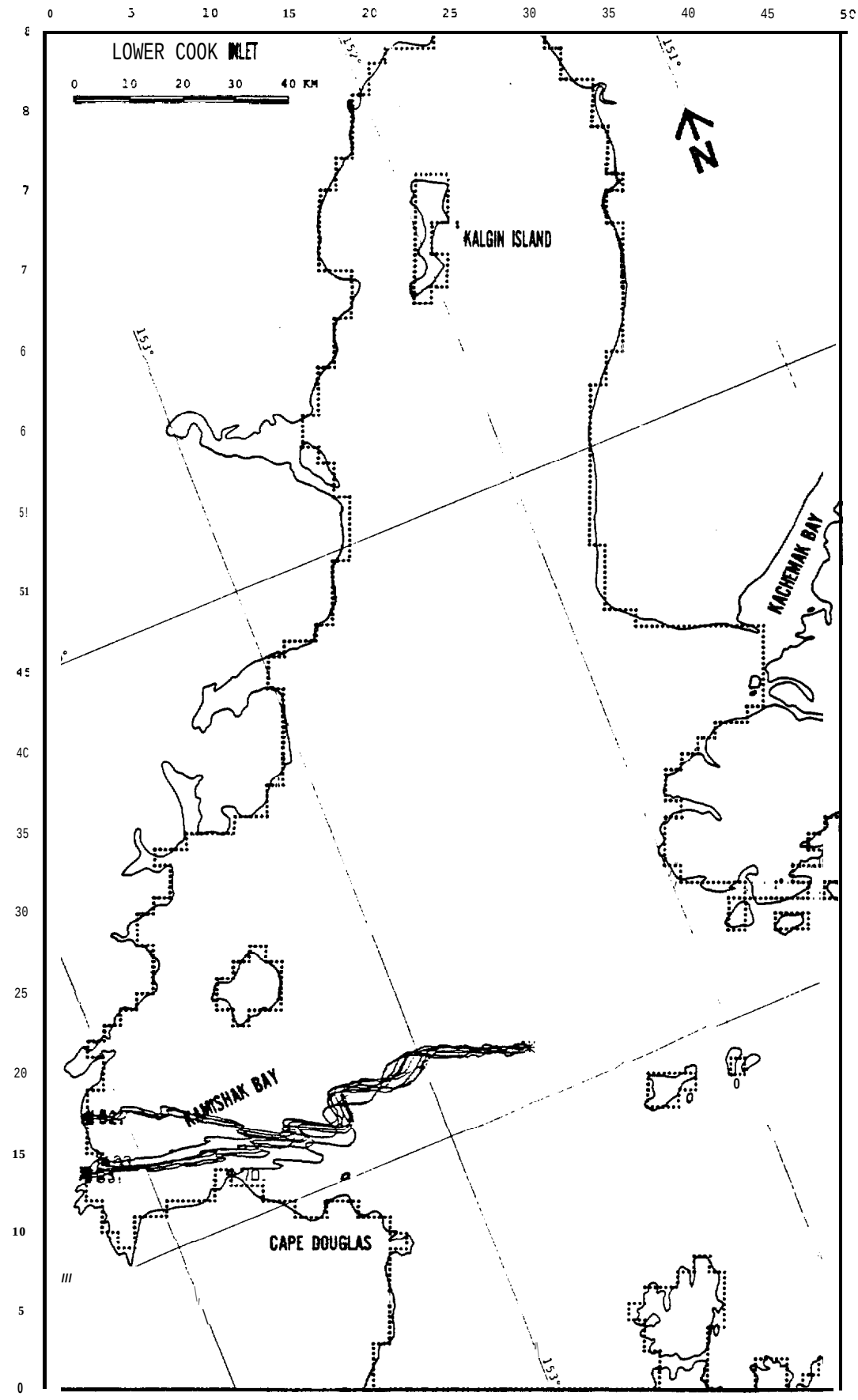

FIGURE C-77: RANDOM PERTURBATION ANALYSIS CASE

WIND
7

SITE
7

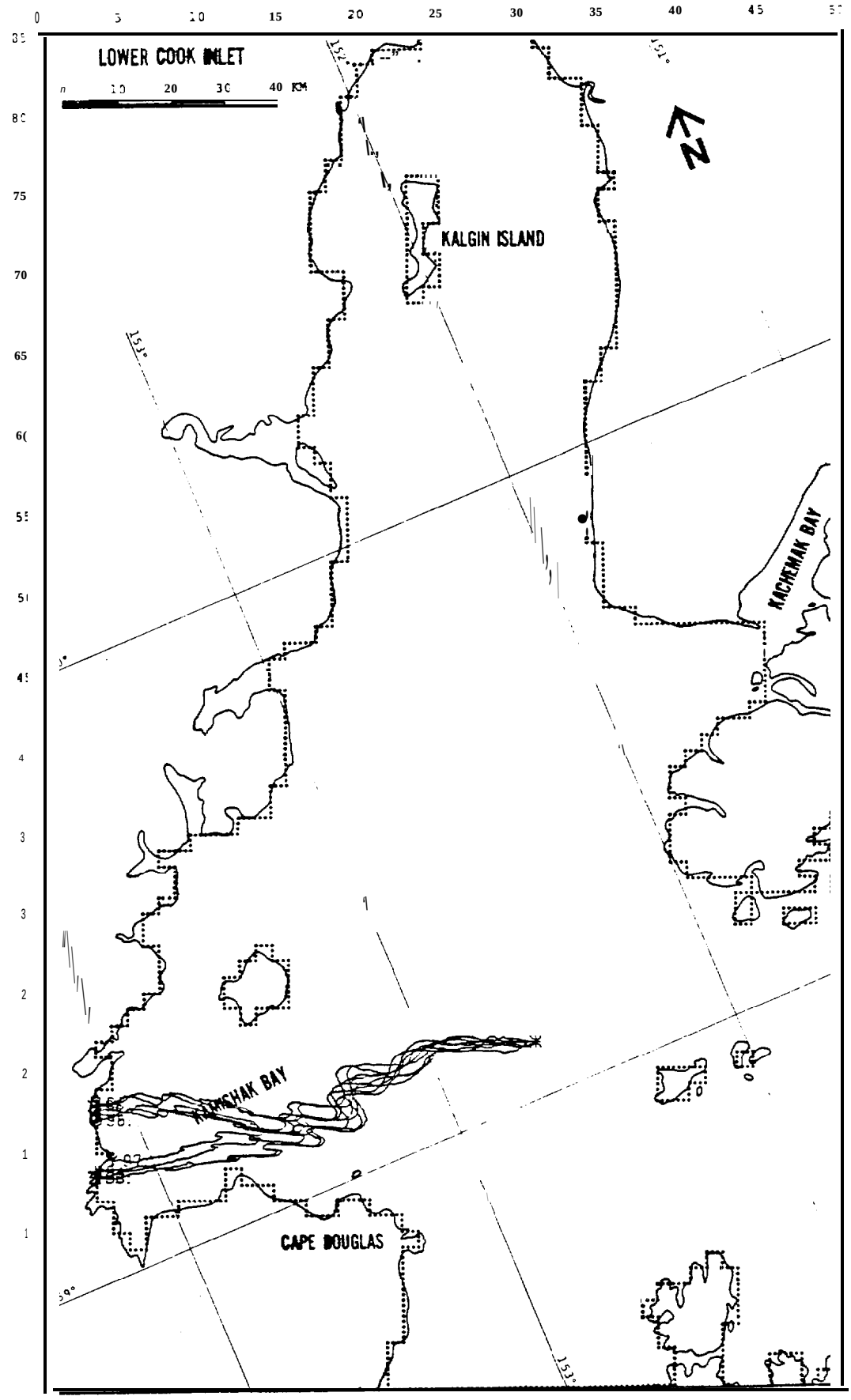

FIGURE C-78: RANDOM PERTURBATION ANALYSIS CASE

APPENDIX D

INPUT DATA FILES

Input Data Files	Input Description
Topo	1 water boundary 2 land 3 “invalid” water 4 “valid” water
Wind	15 wind speed in knots 207 wind direction in degrees clockwise from north
Net Current	0.7 net current speed in km/hr 202 net current direction in degrees clockwise from north
Tidal Current	1.3 tidal current speed in m/s 232 tidal current direction in degrees clockwise from north

INPUT DATA FILE: TOPO

Y-GRID INTERSECTION

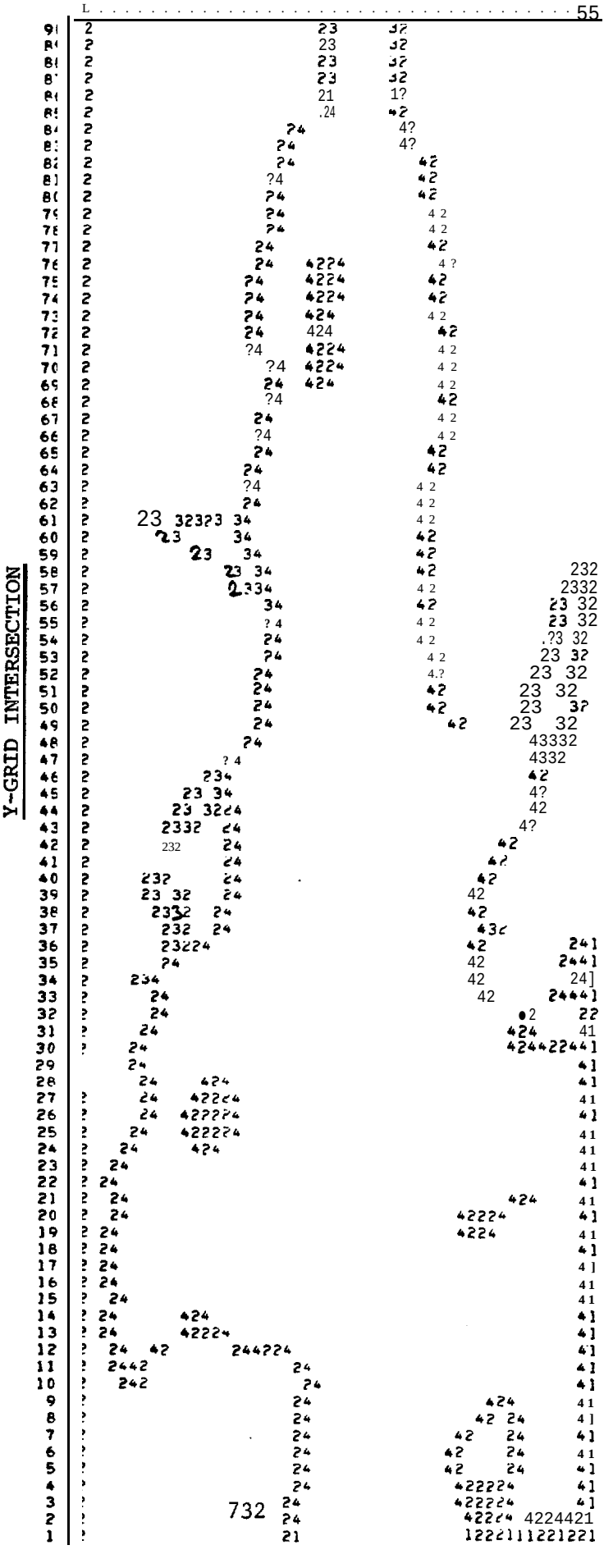

INPUT DATA FILE: WIND PATTERN 1

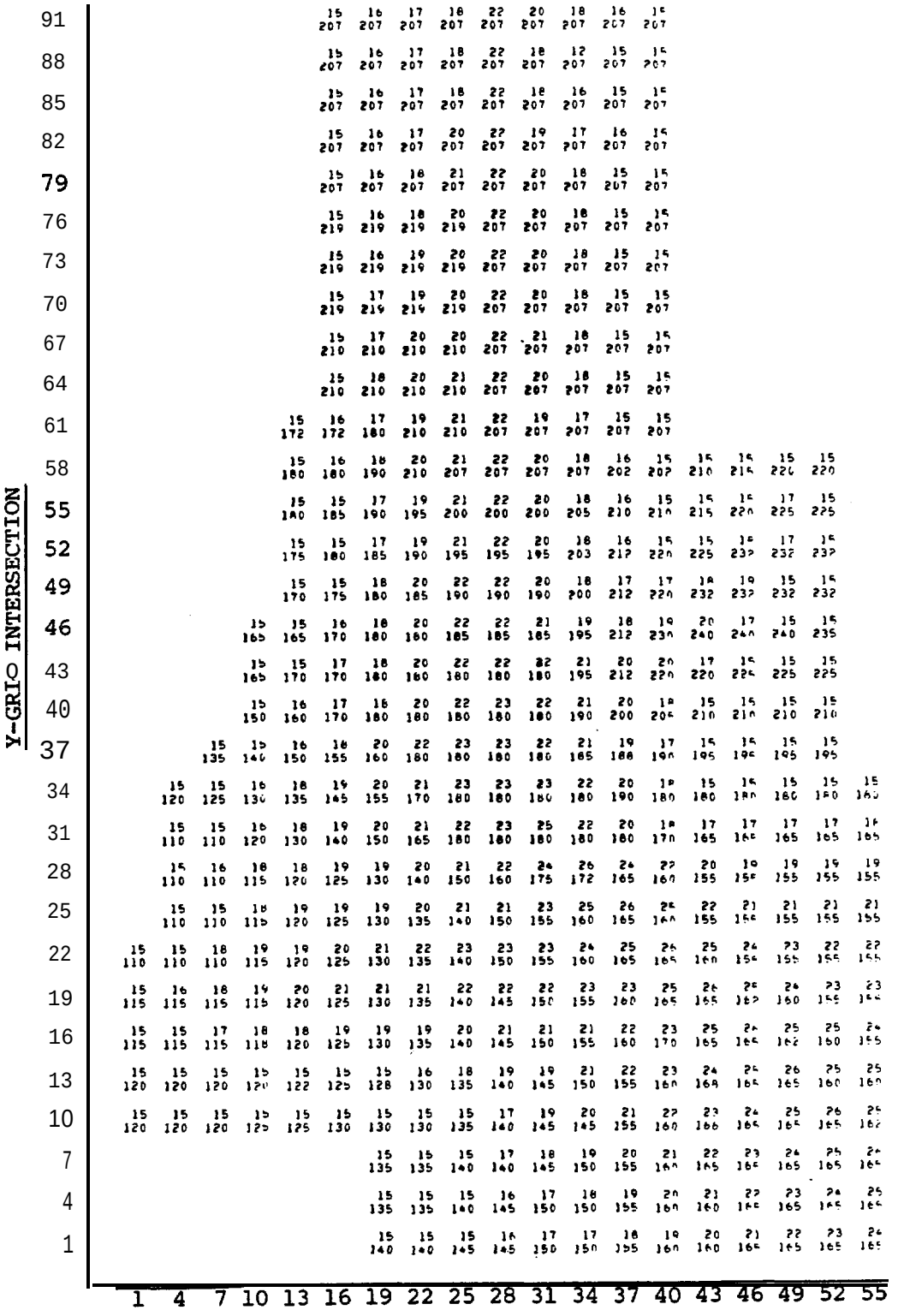

INPUT DATA FILE: WIND PATTERN 2

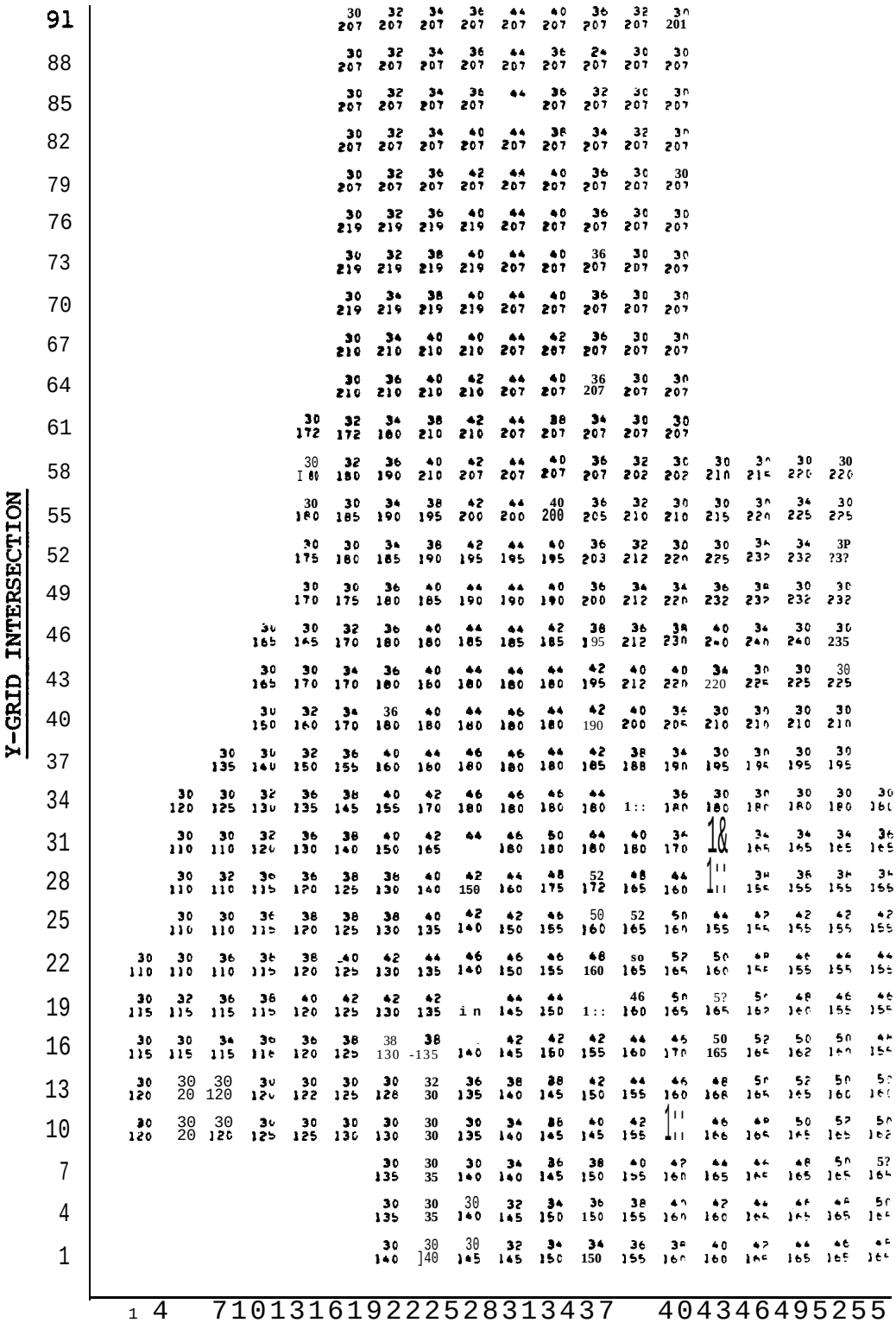

INPUT DATA FILE: WIND PATTERN 3

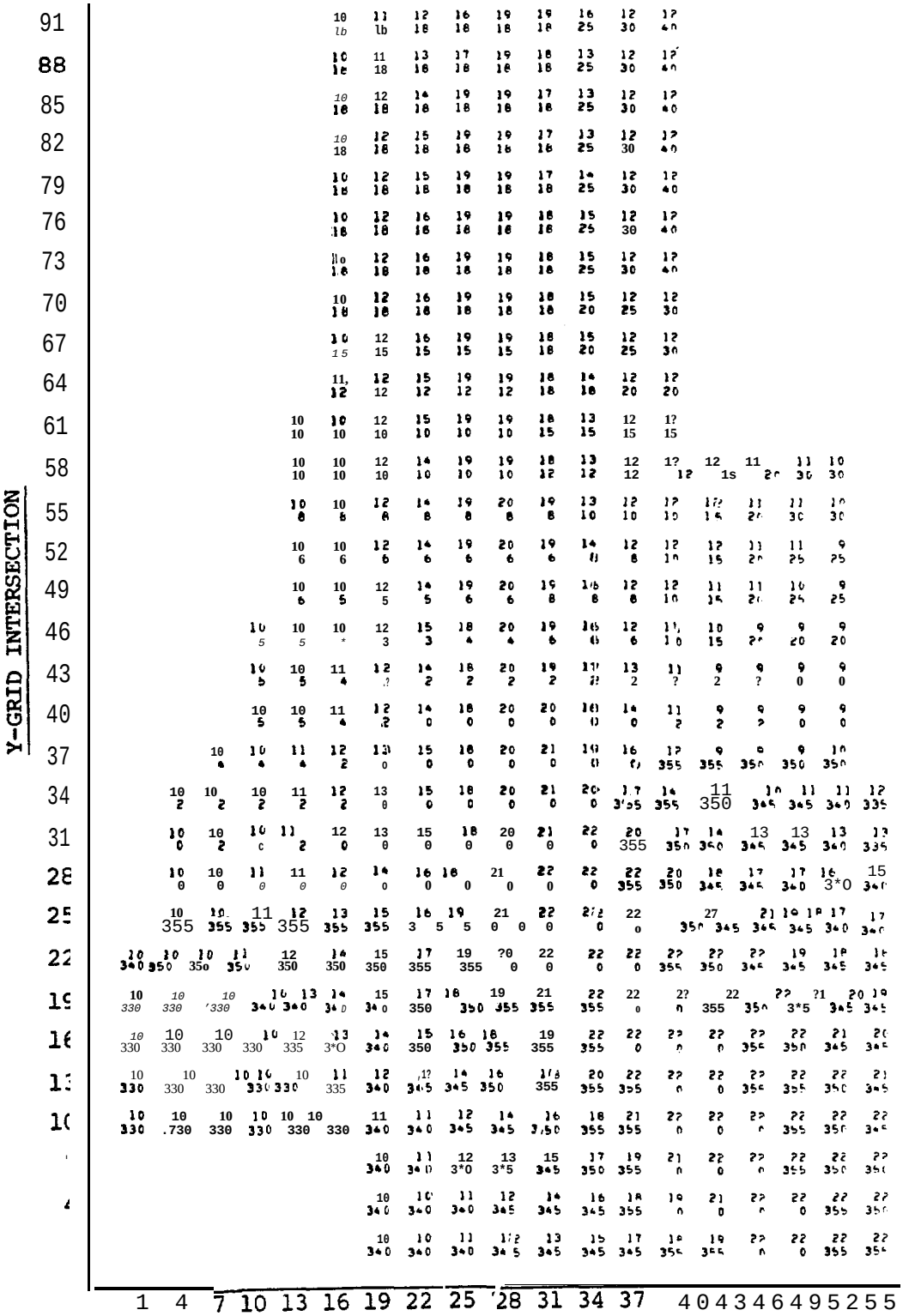

INPUT DATA FILE: WIND PATTERN 4

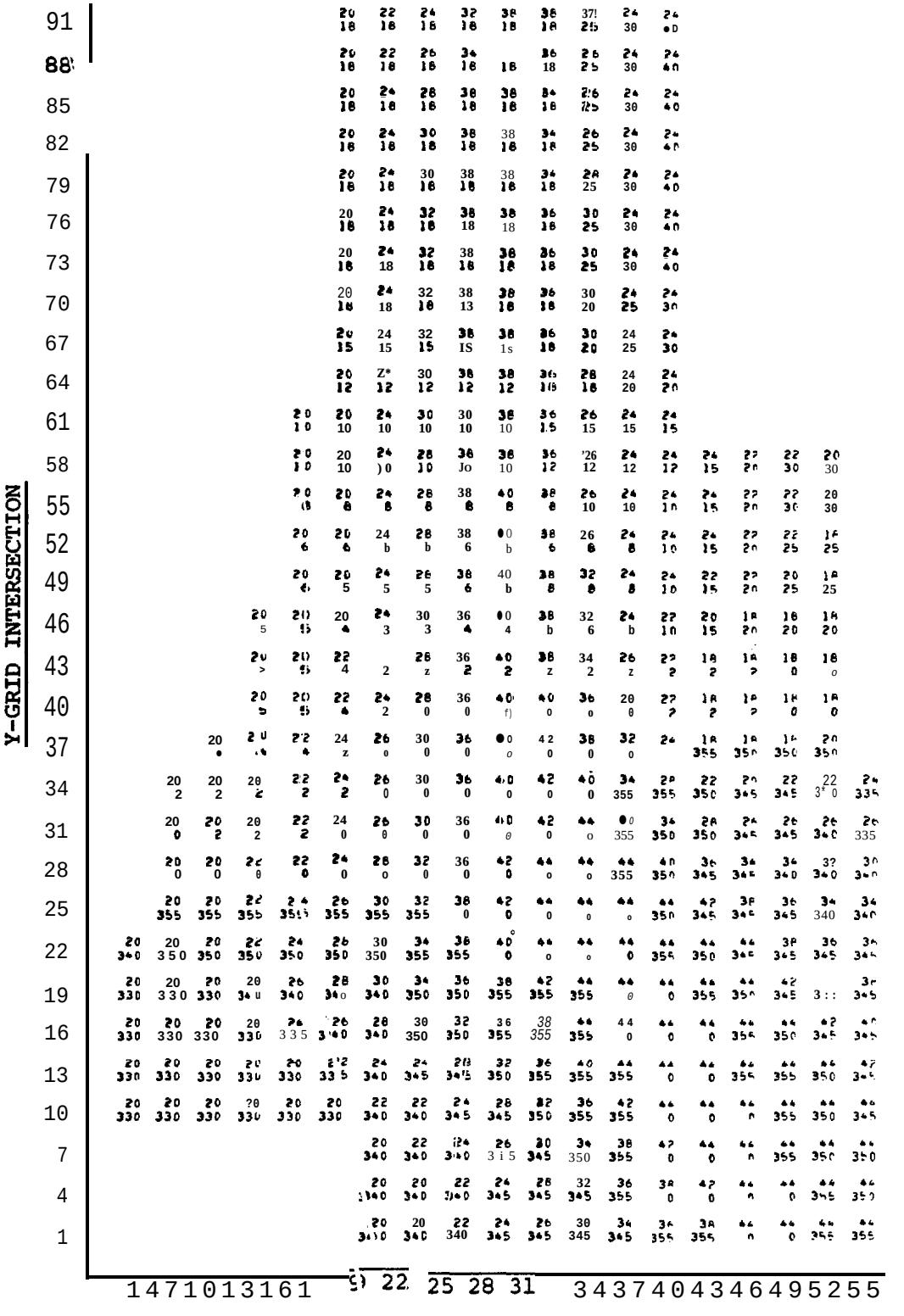

Y-GRID INTERSECTION																			
91						20 18	22 18	24 18	32 18	38 18	38 18	37! 25	24 30	24 •D					
88						20 18	22 18	26 18	34 18	18	36 18	26 25	24 30	24 40					
85						20 18	24 18	28 18	38 18	38 18	34 18	26 25	24 30	24 40					
82						20 18	24 18	30 18	38 18	38 18	34 18	26 25	24 30	24 40					
79						20 18	24 18	30 18	38 18	38 18	34 18	28 25	24 30	24 40					
76						20 18	24 18	32 18	38 18	38 18	36 18	30 25	24 30	24 40					
73						20 18	24 18	32 18	38 18	38 18	36 18	30 25	24 30	24 40					
70						20 18	24 18	32 18	38 13	38 18	36 18	30 20	24 25	24 30					
67						20 15	24 15	32 15	38 IS	38 1s	36 18	30 20	24 25	24 30					
64						20 12	Z* 12	30 12	38 12	38 12	36 18	28 18	24 20	24 20					
61					20 10	20 10	24 10	30 10	30 10	38 10	36 15	26 15	24 15	24 15					
58					20 10	20 10	24)0	28 10	38 Jo	38 10	36 12	'26 12	24 12	24 12	24 15	22 20	22 30	20 30	
55					20 8	20 8	24 8	28 8	38 8	40 8	38 8	26 10	24 10	24 10	24 15	22 20	22 30	20 30	
52					20 6	20 6	24 b	28 b	38 6	•0 b	38 6	26 8	24 8	24 10	24 15	22 20	22 25	18 25	
49					20 6	20 5	24 5	26 5	38 6	40 b	38 8	32 8	24 8	24 10	22 15	22 20	20 25	18 25	
46				20 5	20 5	20 4	24 3	30 3	36 4	•0 4	38 b	32 6	24 b	22 10	20 15	18 20	18 20	18 20	
43				20 >	20 5	22 4	2	28 z	36 2	40 2	38 z	34 2	26 z	22 2	18 2	18 2	18 0	18 o	
40				20 5	20 5	22 4	24 2	28 0	36 0	40 f)	40 0	36 o	20 0	22 2	18 2	18 2	18 0	18 0	
37			20 •	20 4	22 4	24 z	26 o	30 0	36 0	•0 o	42 0	38 0	32 o	24	18 355	18 350	18 350	20 350	
34		20 2	20 2	20 2	22 2	24 2	26 0	30 0	36 0	40 0	42 0	40 0	34 355	28 355	22 350	20 345	22 345	22 3*0	24 335
31		20 0	20 2	20 2	22 2	24 0	26 0	30 0	36 0	40 0	42 0	44 o	•0 355	34 350	28 350	24 345	26 345	26 340	26 335
28		20 0	20 0	22 0	22 0	24 0	28 o	32 0	36 0	42 0	44 o	44 o	44 355	40 350	36 345	34 345	34 340	3? 340	30 340
25		20 355	20 355	22 355	24 355	26 355	30 355	32 355	38 0	42 0	44 0	44 o	44 o	44 350	42 345	38 345	36 345	34 340	34 340
22	20 340	20 350	20 350	22 350	24 350	26 350	30 350	34 355	38 355	40 0	44 o	44 o	44 0	44 355	44 350	44 345	38 345	36 345	36 345
19	20 330	20 330	20 330	20 340	26 340	28 340	30 340	34 350	36 350	38 355	42 355	44 355	44 0	44 0	44 355	44 350	42 345	3::	36 345
16	20 330	20 330	20 330	20 330	24 335	26 340	28 340	30 350	32 350	36 355	38 355	44 355	44 0	44 0	44 0	44 355	44 350	42 345	40 345
13	20 330	20 330	20 330	20 330	20 330	22 335	24 340	24 345	28 345	32 350	36 355	40 355	44 355	44 0	44 0	44 355	44 355	44 350	42 345
10	20 330	20 330	20 330	20 330	20 330	20 330	22 340	22 340	24 345	28 345	32 350	36 355	42 355	44 0	44 0	44 0	44 355	44 350	44 345
7							20 340	22 340	24 340	26 315	30 345	34 350	38 355	42 0	44 0	44 0	44 355	44 350	44 350
4							20 340	20 340	22 340	24 345	28 345	32 345	36 355	38 0	42 0	44 0	44 0	44 355	44 350
1							20 340	20 340	22 340	24 345	26 345	30 345	34 345	36 355	38 355	44 0	44 0	44 355	44 355

1471013161 9 22 25 28 31 3437404346495255

X-GRID INTERSECTION

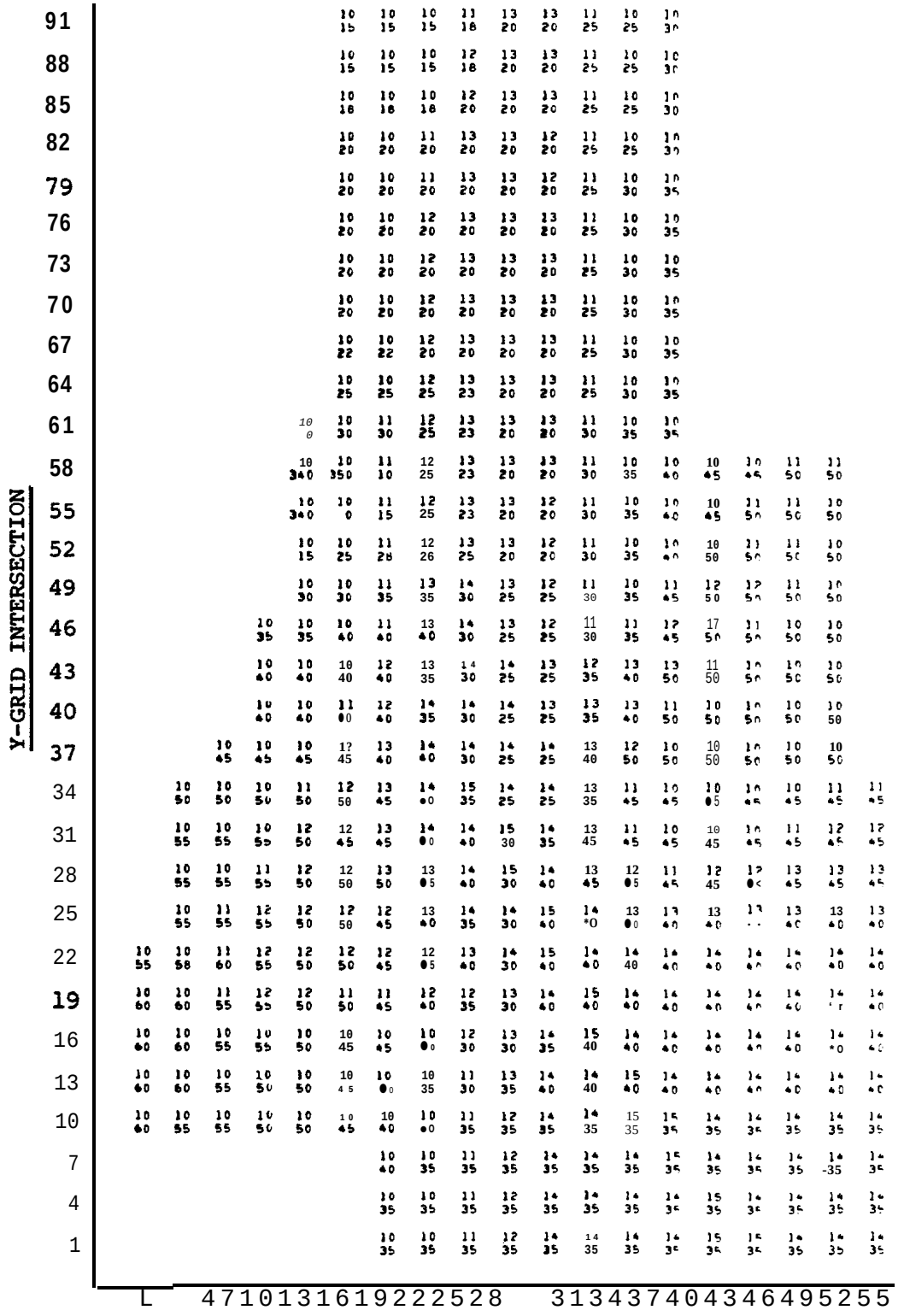
Y-GRID INTERSECTION
91
88
85
82
79
76
73
70
67
64
61
58
55
52
49
46
43
40
37
34
31
28
25
22
19
16
13
10
7
4
1
L 471013161922252 8 3134374043464952 55
X-GRID INTERSECTION

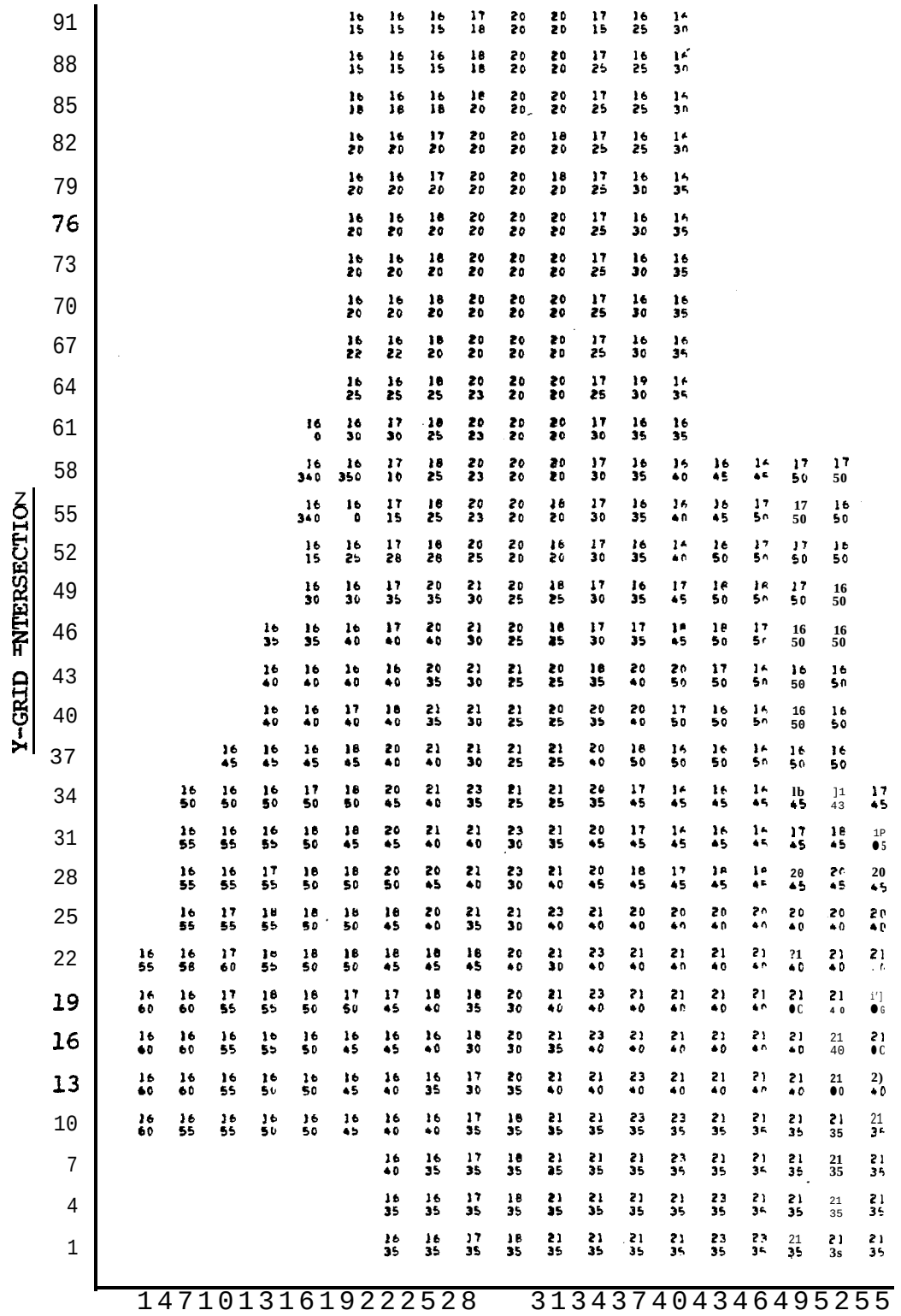
Y-GRID INTERSECTION
X-GRID INTERJECTION
1 4 7 10 13 16 19 22 25 28 31 34 37 40 43 46 49 52 55 58 61 64 67 70 73 76 79 82 85 88 91
1 4 7 10 13 16 19 22 25 28 31 34 37 40 43 46 49 52 55 58 61 64 67 70 73 76 79 82 85 88 91

INPUT DATA FILE: WIND PATTERN 7

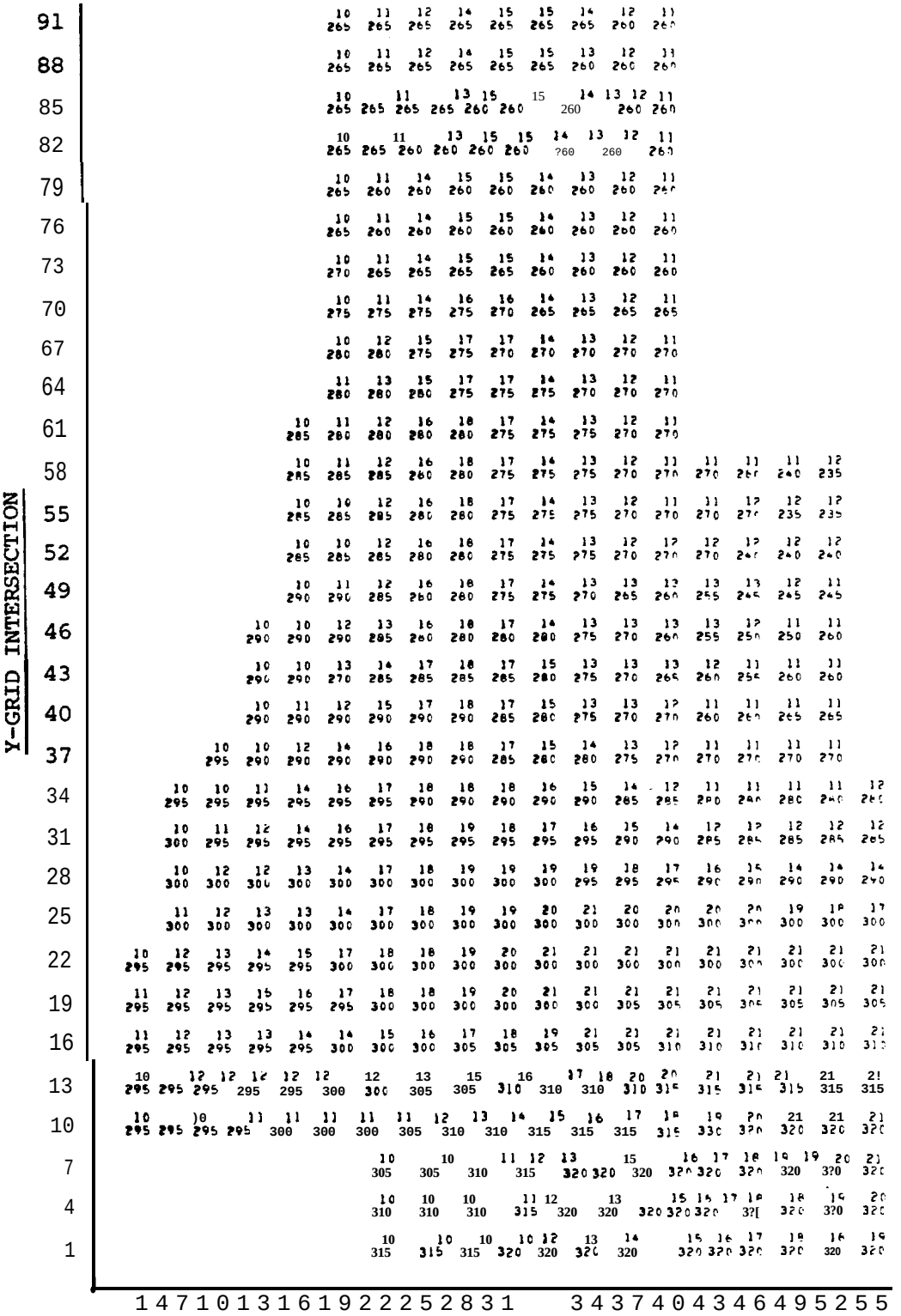

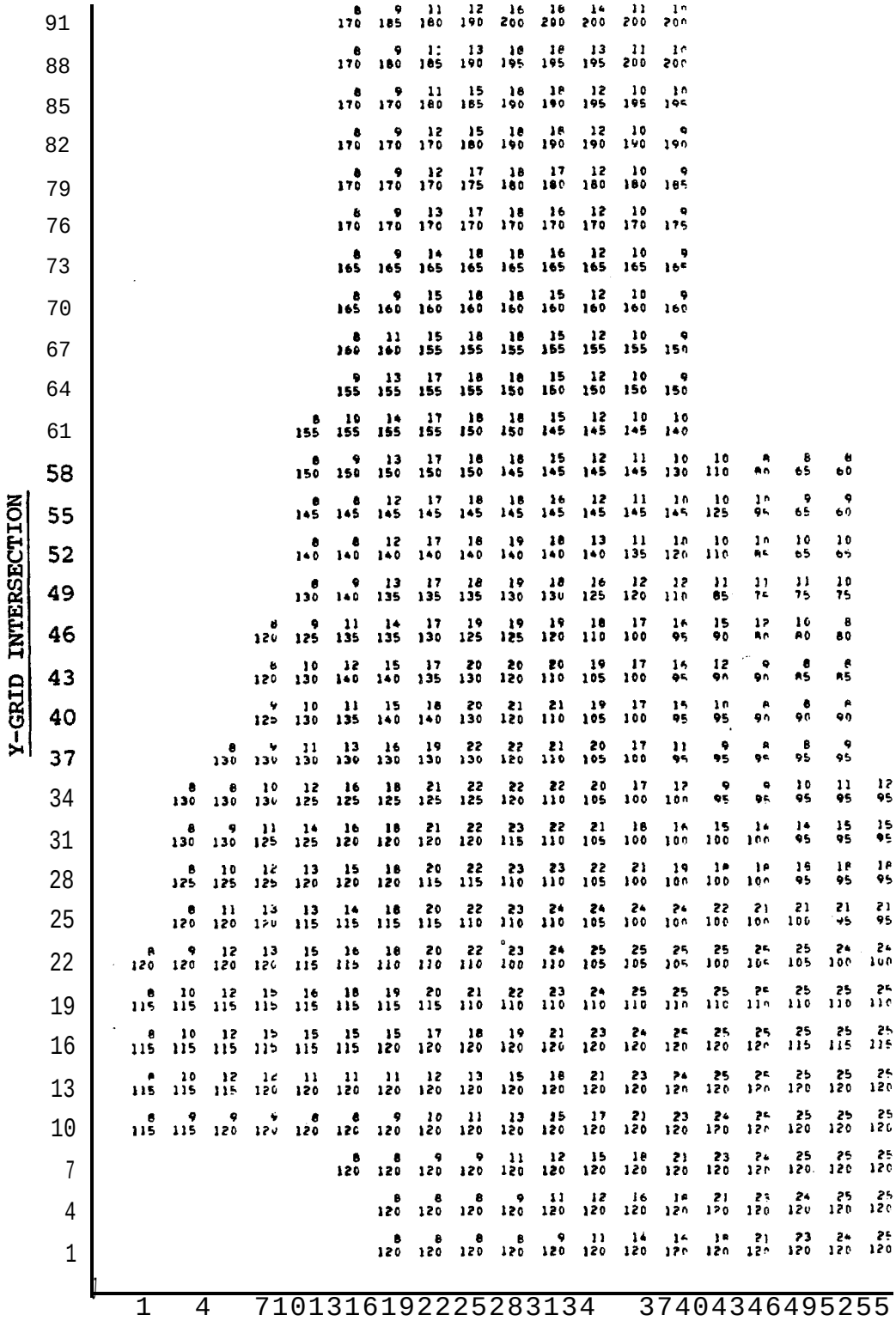
Y-GRID INTERSECTION
X-GRID INTERSECTION
1 4 7 10 13 16 19 22 25 28 31 34 37 40 43 46 49 52 55 58 61 64 67 70 73 76 79 82 85 88 91

INPUT DATA FILE: NET CURRENT PATTERN

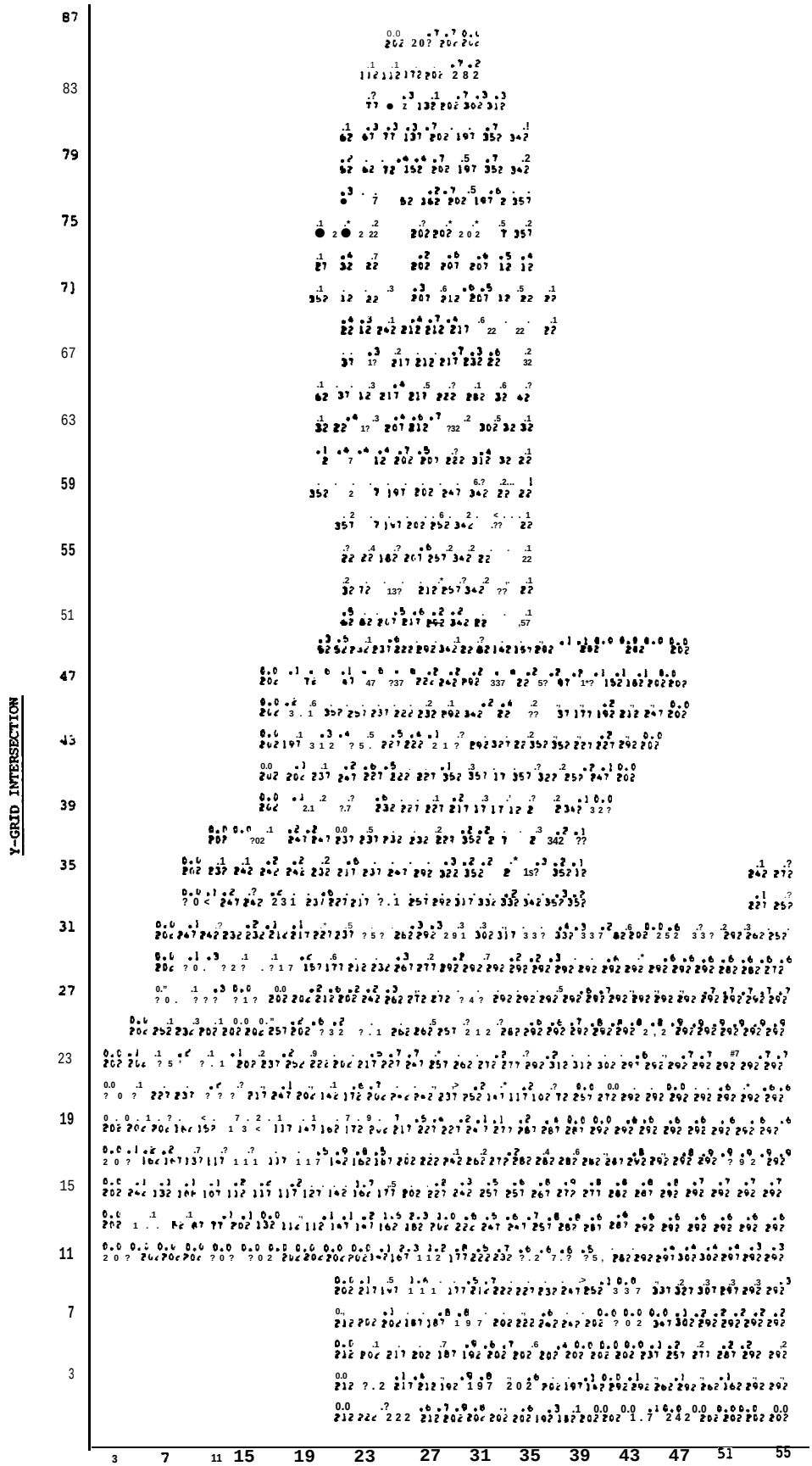

INPUT DATA FILE: TIDAL CURRENT PATTERN
PHASE = 0°
TIME = 0.00 HRS

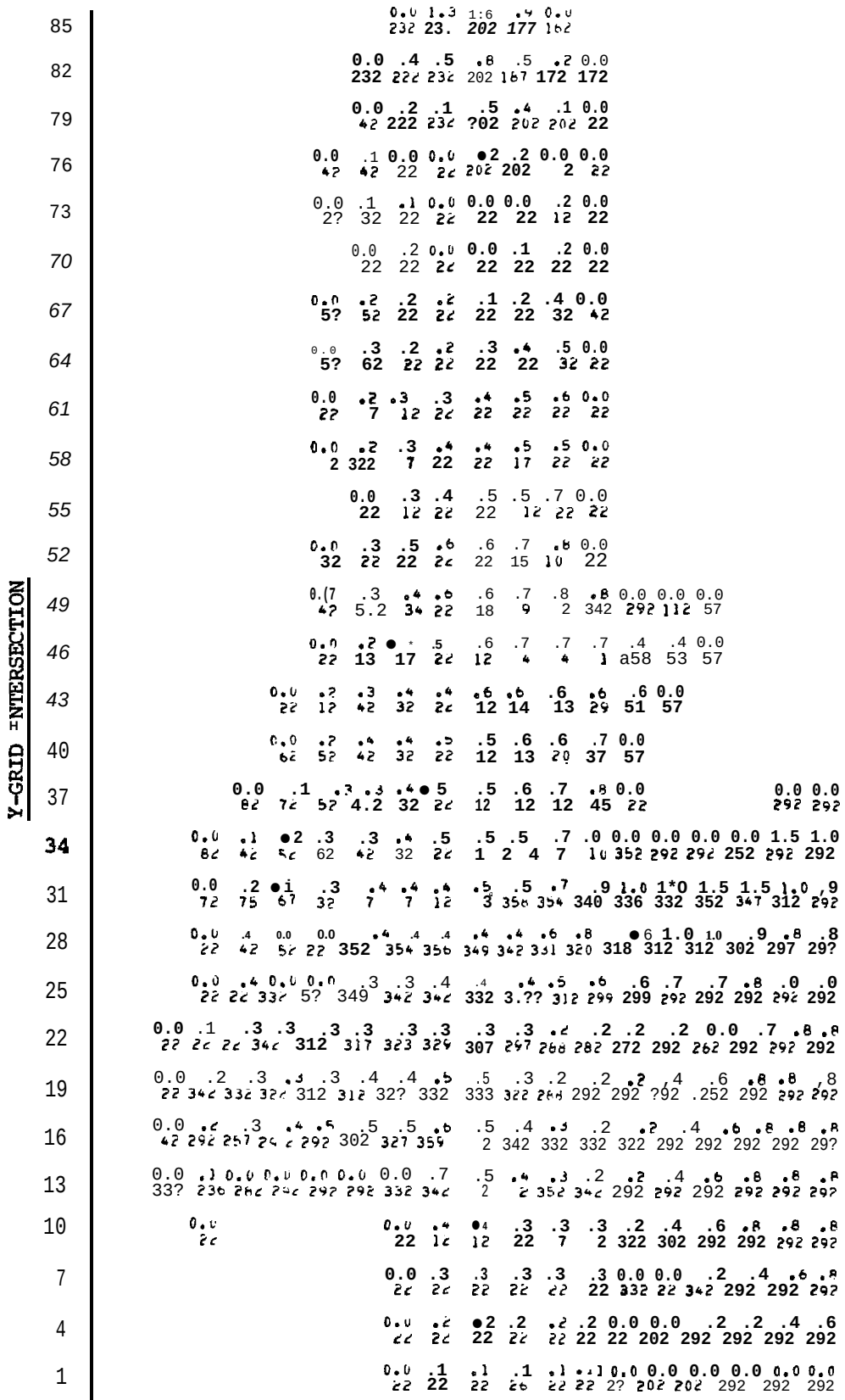

INPUT DATA FILE: TIDAL CURRENT PATTERN
PHASE = 90°
TIME = 3.11 HRS

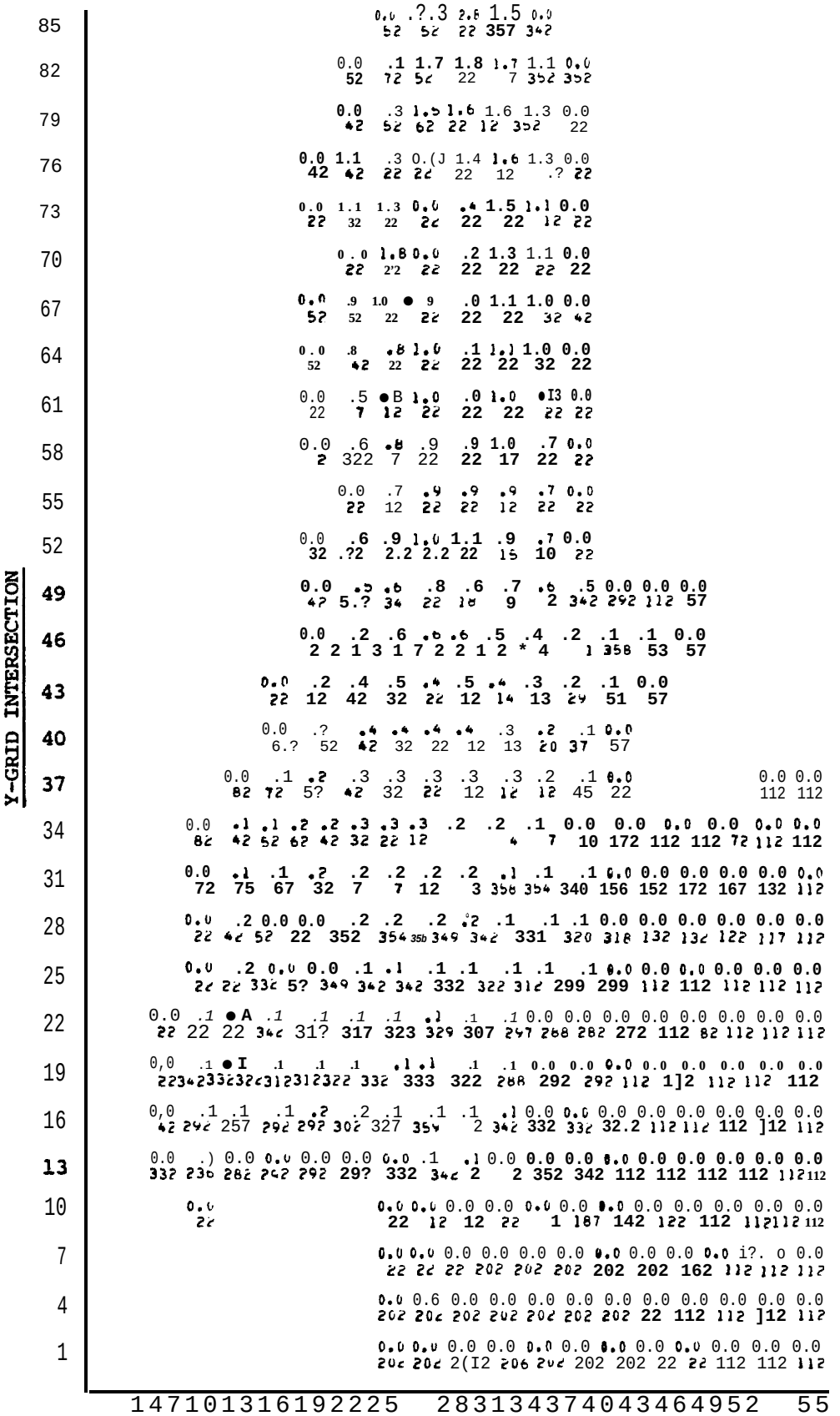

X-GRID INTERSECTION

INPUT DATA FILE: TIDAL CURRENT PATTERN
PHASE = 180°
TIME = 6.21 HRS

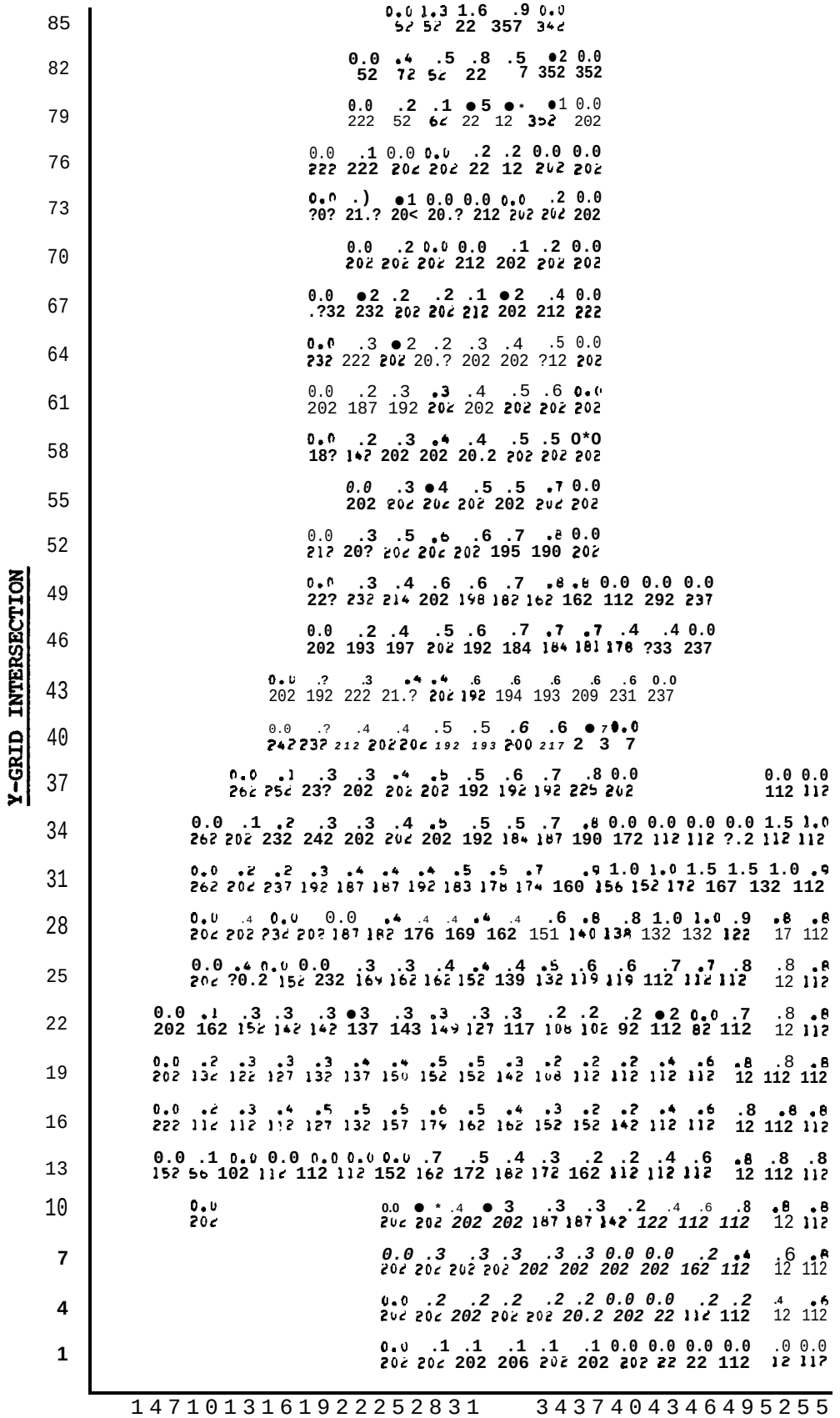

X-GRID INTERSECTION

INPUT DATA FILE: TIDAL CURRENT PATTERN
PHASE = 270°
TIME = 9.32 HRS

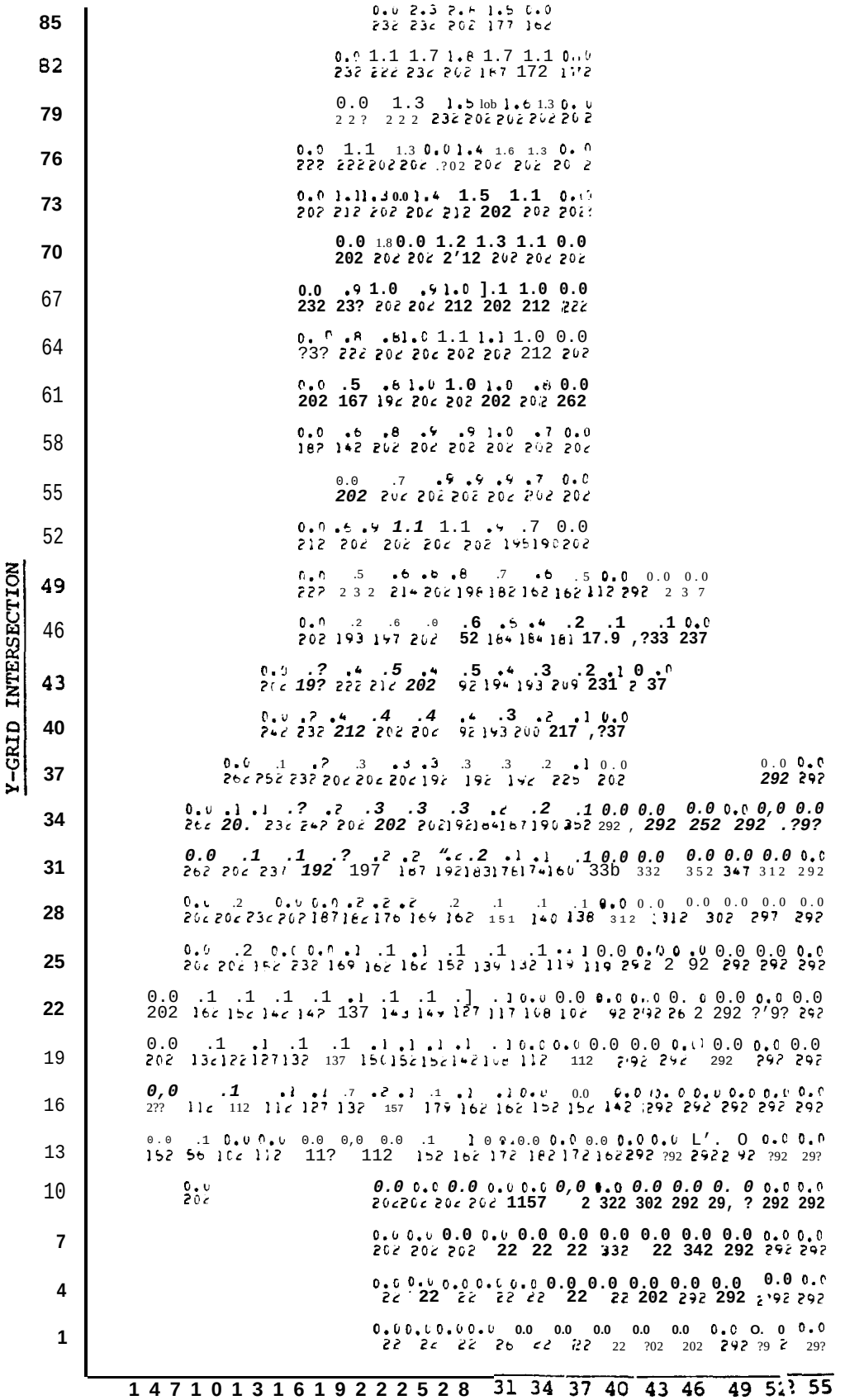

☆ U. S. GOVERNMENT PRINTING OFFICE 1980 - 677-096/1229 Reg. 8